TH 1884

LITHOGEOCHEMISTRY AND GEOTHERMOBAROMETRY OF MINERALIZED CORDIERITE-ORTHOAMPHIBOLE AND RELATED ROCKS AT ATIK LAKE, MANITOBA, NEMISCAU AND MONTAUBAN, QUEBEC

Documents complémentaires

Additional Files

Licence

License

Cette première page a été ajoutée
au document et ne fait pas partie du
rapport tel que soumis par les auteurs.

Énergie et Ressources naturelles
Québec

1H 1884

LITHOGEOCHEMISTRY AND GEOTHERMOBAROMETRY OF MINERALIZED CORDIERITE-ORTHOAMPHIBOLE AND RELATED ROCKS AT ATIK LAKE, MANITOBA, NÉMISCAU AND MONTAUBAN, QUÉBEC.

by Louis R. Bernier

August, 1992

A thesis submitted to the Faculty of Graduate Studies and Research in partial fulfillment of the requirements of the degree of Doctor of Philosophy.

Department of Geological Sciences
McGill University, Montreal

© Louis R. Bernier, 1992

AGP 0191

" ... Science is a human activity strongly influenced by the culture within which it is conducted. Scientists are people who eat and sleep, are timid or bold, are conservative or daring. We think that we understand, and hope that you do also, that no one uses *the* scientific method; that there are significant amounts of ambition, greed, luck, envy ... probably even some sex, underlying the work that gets done and is called science.

To be gained in the bargain is a sense that ideas do not develop neatly. They pick up a bit from one discipline, something else from another, get a big boost from an unexpected direction, perhaps get abandoned for a time. If an idea is valuable enough to survive this tortuous path, it can become, through fortuitous combination with other ideas that have been finding their own irregular way to that moment of combination or discovery, an important part of our cultural way of viewing the world. In combination they sometimes can change perceptions of the world." (Moore, D.M., and Reynolds, R.C., 1989. X-ray identification and analysis of Clay minerals. Oxford press.)

ABSTRACT

Cordierite-orthoamphibole rocks associated with contrasting polymetallic mineralization occur in a wide range of metamorphic conditions in the Atik Lake, Manitoba, and Némiscau and Montauban, Québec, metamorphic terranes.

Lithogeochemistry and geothermobarometry investigations using whole rock major, trace and rare earth elements and mineral chemistries have established the chemical and physical changes that occurred during hydrothermal alteration and subsequent regional metamorphism. The Log(Ratio) method, utilizing ratio profiles of the immobile elements Al_2O_3, TiO_2, Zr, Nb, Y, V and Cr, was designed to identify the protoliths of the metamorphosed altered rocks.

Detailed geothermobarometry and textural evidence indicate that cordierite-orthoamphibole rocks in the three terranes formed at peak P-T conditions of ~2.5 kbar and ~550°C at Atik Lake (andalusite zone), ~4.5 kbar ~650°C at Némiscau (sillimanite zone), and ~6.5 kbar and ~620°C at Montauban (kyanite-sillimanite zone). Cordierite-orthoamphibole rocks in the terranes exhibit a range of bulk chemical compositions with the most Fe-rich occurring in the Atik Lake belt, and the most Mg-rich in the Montauban mine sequence. Mineral assemblages in these rocks were in equilibrium with contrasting sulfide-oxide±arsenide fO_2-fS_2 buffers: pyrrhotite-ilmenite±arsenopyrite± löllingite at Atik Lake, pyrrhotite-pyrite-magnetite at Némiscau, and pyrrhotite-rutile-sphalerite at Montauban.

The partitioning of Fe-Mg between cordierite and anthophyllite was studied for use as a geobarometer. The partitioning coefficient ($K_D^{Fe\text{-}Mg}$) is slightly temperature dependant and strongly pressure dependent. This new geobarometer was empirically calibrated using mineral chemistry from the three terranes and from the literature.

High X_{H_2O} of the metamorphic fluid is required so that the X_{Fe} values of the anthophyllite will be in equilibrium under peak P-T conditions with the appropriate sulfide-oxide±arsenide assemblage. Metamorphic dehydration of chlorite-rich hydrothermally altered rocks in the three terranes is compatible with the generation of such water-rich fluids during the crystallization of the cordierite-orthoamphibole rocks.

RÉSUMÉ

Des roches à cordiérite-orthoamphibole associées à divers gîtes polymétalliques ont cristallisé sous différentes conditions du métamorphisme dans les terrains d'Atik Lake, au Manitoba, et de Némiscau et de Montauban, au Québec.

Le chimisme des éléments majeurs, en traces et des terres rares des analyses roches totales, ainsi que la composition des minéraux furent utilisés lors des investigations lithogéochimiques et géothermobarométriques. Ces dernières permirent de définir les changements chimiques et physiques subis lors de l'altération hydrothermale et du métamorphisme régional subséquent. La méthode Log(Ratio), basée sur les profiles des rapports entre les éléments immobiles Al_2O_3, TiO_2, Zr, Nb, Y, V et Cr, est conçue pour l'identification des protolithes de roches altérées métamorphisées.

La géothermobarométrie de détail et l'évidence texturale indiquent que les roches à cordiérite-orthoamphibole ont cristallisé aux conditions maximales de P-T établies comme ayant été de ~2.5 kbar et de ~550°C à Atik Lake (zone à andalousite), de ~4.5 kbar et de ~650°C à Némiscau (zone à sillimanite), et de ~6.5 kbar et de ~620°C à Montauban (zone à kyanite-sillimanite). Les roches à cordiérite-orthoamphibole montrent une grande variation de composition avec les plus riches en Fe se retrouvant dans la ceinture d'Atik Lake, et celles plus riches en Mg, dans la séquence de la mine à Montauban. Les assemblages minéralogiques dans ces roches étaient en équilibre avec différents assemblages tampons de fO_2-fS_2 à sulfure-oxide±arsenide, soit: pyrrhotine-ilménite±arsénopyrite±löllingite à Atik Lake, pyrrhotine-pyrite-magnétite à Némiscau, et pyrrhotine-sphalérite-rutile à Montauban.

Le partage de Fe et Mg entre la cordiérite et l'anthophyllite a été étudié pour définir un géobaromètre. Le coefficient partage, (K_D^{Fe-Mg}) est sensiblement dépendant de la température, mais fortement de la pression. Ce nouveau géobaromètre a été calibré empiriquement en utilisant le chimisme de ces minéraux dans les trois terrains étudiés ainsi qu'à partir des données de la littérature.

Un fluide métamorphique avec X_{H_2O} élevé est nécessaire pour que les valeurs de X_{Fe} de l'anthophyllite reflètent un équilibre avec les assemblages de sulfure-oxide±arsenide appropriés. La déshydratation métamorphique des roches hydrothermales altérées riches en chlorite est compatible avec la formation de fluides riches en eau durant la cristallisation de roches à cordiérite-orthoamphibole.

ACKNOWLEDGEMENTS

I would like to thank Wallie (W.H. MacLean) for his advices and guidance during the course of this study. I am deeply grateful to R. H. McMillan, D. J. Robinson and C. Rockingham of Westmin Resources Ltd. for the logistical and research support in Manitoba and James Bay, Québec. G. Valiquette, of École Polytechnique de Montréal, kindly provided access to his original sample maps and thin sections from the Némiscau area.

Sincere thanks goes to T.J. Barrett, A. R. Williams-Jones, S.Wood, R.F. Martin, D. N. Ichangi, D. Francis, D. Baker and A.M. Abdel-Raman with whom I had many discussions which were very beneficial. The technical assistance of T. Ahmedali and G. Keating on X-ray fluorescence, of M. McKinnon on the electron microprobe, and of J. Mungall on the scanning electron microscope, was greatly appreciated.

Financial assistance was provided by an FCAR scholarship (La Formation des Chercheurs at de l'Aide à la Recherche).

Finally, I am dedicating this thesis to my wife (Lise) for her constant moral (and financial) support and to my son (Michaël) for all his smiles.

TABLE OF CONTENTS

ABSTRACT i

RÉSUMÉ iii

AKCNOWLEDGEMENTS v

PREFACE ix

CHAPTER 1 Introduction 1

Previous work 5

List of abbreviations and symbols 7

Format of the thesis 9

CHAPTER 2 Geological setting of the three terranes 12

Atik Lake 12

Némiscau 19

Montauban 22

Summary 26

CHAPTER 3 Lithogeochemistry of cordierite-orthoamphibole and associated rocks at Atik Lake Manitoba, Némiscau and Montauban, Québec 28

3A published paper: Auriferous chert, banded iron formation, and related volcanogenic hydrothermal alteration, Atik Lake, Manitoba 29

3B *Addendum* 44

3C A new approach to protolith identification using Log(Ratio) diagram: application to the Atik Lake rocks 50

3D published paper: Vanadiferous zincian-chromian hercynite in a metamorphosed basalt-hosted alteration zone, Atik Lake, Manitoba 60

3E Lithogeochemistry of the Némiscau amphibolites, cordierite-anthophyllite and associated rocks 74

3F manuscript: Geometry and lithogeochemistry of a metamorphosed VMS alteration zone at Montauban, Grenville Provinve, Quebec: a new approach to protolith identification 87

CHAPTER 4 Metamorphic conditions of the three terranes 130

Introduction 130

Mineral assemblages, mineral chemistries and chemographical relations 131

Geothermobarometry in the three terranes 144

Other geothermobarometric methods applicable to the Atik Lake terrane 188

Other geothermobarometric methods applicable to the Némiscau terrane 200

Other geothermobarometric methods applicable to the Montauban terrane 204

Discussion 225

CHAPTER 5 A new empirical geobarometer based on Fe-Mg exchange between cordierite and anthophyllite: calibration and application 233

Introduction 233

Cordierite-anthophyllite Fe-Mg partitioning in the three terranes 234

Empirical calibration 239

Application to other terranes 242

Summary 244

CHAPTER 6 Sulfidation and oxidation of Fe-anthophyllite and metamorphic fluid speciation 245

Introduction 245

Assessment of experimental data 249

Estimation fO_2-fS_2 conditions in the three terranes 253

Fluid equilibria in the system C-O-H-S 260

Conclusions 271

CHAPTER 7 Summary and conclusions 275

Original contributions to knowledge 281

Recommendations for future research 282

REFERENCES 283

APPENDIX I Sample locations maps 312

APPENDIX II Electron microprobe data for the three terranes 319

APPENDIX III Geothermobarometers 364

APPENDIX IV GWBASIC source codes 373

PREFACE

This thesis contains seven chapters. Chapter 3 contains six sections, two of which are reproductions of papers already published and one is in a manuscript format. Section 3A of Chapter 3 was published in Canadian Journal of Earth Sciences (Bernier and MacLean, 1989). Section 3D was published in Canadian Mineralogist (Bernier, 1990), and section 3F has yet to be submitted. The thesis adviser, W.H. MacLean, is a second author in two of these papers. His role in the preparation of the papers consisted of critical evaluation and discussion of my data and interpretations, and of the text writing, particularly, the english grammar, as it is my second language. I have collected all the rock and core samples used in this thesis during my field work completed from 1984 to 1987. I have done some geological mapping for Westmin Resources Limited which was used in this thesis in conjunction with government maps as specified in the text. The rock sample preparation (cutting, crushing and grinding), petrography, electron microprobe analyses, drafting, computer programs, and typing of the thesis were done by myself. The thin and polished thin sections were made by G. Gélinas, at Ecole Polytechnique de Montréal and by Mr. R.Weiss at McGill University. The whole-rock major and trace element analyses were done by T. Ahmedali at McGill University. Ore samples from Westmin Resources Limited were assayed by Chemex Labs Limited. Rare earth element analyses were done by Nuclear Activation Services, Hamilton. Further details on the format of the thesis are given in Chapter 1. The format of this thesis is in agreement with the " Guidelines Concerning Thesis Preparation" from the Faculty of Graduate Studies and Research, at McGill University. The following excerpt is cited in full, in accord with the Guidelines.

Manuscript and Authorship:

The candidate has the option, **subject to the approval of their Department,** of including as part of the thesis the text, or duplicated published text, of an original paper or papers.

- Manuscript-style theses must still conform to all other requirements explained in the Guidelines Concerning Thesis Preparation.

- Additional material (procedural and design data as well as descriptions of equipment) must be provided in sufficient detail (eg. in appendices) to allow clear and precise judgement to be made of the importance and originality of the research reported.

- The thesis should be more than a mere collection of manuscripts published or to be published. It must include a general abstract, a full introduction and literature review and a final overall conclusion. Connecting texts which provide logical bridges between different manuscripts are usually desirable in the interest of cohesion. It is acceptable for theses to include, as chapters, authentic copies of papers already published, provided these are duplicated clearly and bound as an integral part of the thesis. In such instances, connecting texts are mandatory and supplementary explanatory materials is always necessary.

- Photographs or other materials which do not duplicates well must be included in their original form.

- While the inclusion of manuscripts co-authored by the candidate and others is acceptable, the candidate is required to make an explicit statement in the thesis of who contributed to such work and to what extent, and supervisors must attest to the accuracy of the claims at the Ph.D. Oral Defense. Since the task of the Examiners is made more difficult in these cases, it is in the candidate's interest to make the reponsabilities of authors perfectly clear.

CHAPTER 1

INTRODUCTION

This doctoral research deals with the lithogeochemistry, mineralogy and metamorphic petrology of cordierite-orthoamphibole (anthophyllite, gedrite) rocks and associated gneisses hosting base metal and gold deposits. With the advent of the volcanogenic model it was gradually recognized that cordierite-orthoamphibole rocks associated with many massive sulfide deposits in metamorphic terranes were the result of the metamorphism of hydrothermally altered host rocks rather than of the syn-metamorphic alteration of host rocks during mineralization (cf. Appleyard and Guha, 1991). Hydrothermal alteration is generated during the formation of ore deposits by the interaction of ore forming fluid and wall rocks. There may also be interaction of ore components and host rocks, and interaction of both of these with metamorphic fluids during metamorphism and tectonism. The resulting transformation may be so extensive as to obliterate or obscure most primary textural features of the deposits and lead to the formation of unusual metamorphic minerals such as zincian staurolite, gahnite, Mn-garnet, in addition to the more common cordierite, orthoamphibole, biotite and associated minerals. In some deposits, pre-metamorphic primary alteration halos have been recognized (e.g., Riverin and Hogdson, 1980; Casselman and Mioduszewska, 1982; Hall, 1982; Nesbitt, 1986b; Elliot-Meadows and Appleyard, 1991).

Cordierite-orthoamphibole rocks in regionally metamorphic terranes occur through the entire range of amphibolite facies metamorphism (Hudson and Harte, 1985), have widespread distributions, and many are associated with massive sulfide deposits. They formed from the metamorphism of mafic to felsic volcanic rocks that had been hydrothermally altered, largely to chlorite and sericite. The subject of the origin of cordierite-orthoamphibole rocks has

been extensively reviewed by Chinner and Fox (1974), Spear and Schumacher (1982), Hudson and Harte (1985), Arnold and Sandiford (1990), Dymek and Smith (1990), and Schneiderman and Tracy (1991). Establishing a discrimination method that identifies the protolith would be very beneficial in mineral exploration. A new method was designed (Log(Ratio) method) to identify protoliths of cordierite-orthoamphibole rocks based on Al_2O_3, TiO_2, Cr and HFSE (Zr, Y, Nb) inter-element ratio profiles.

A common feature of cordierite-orthoamphibole rocks is their coarse grained nature and lack of preferred orientation of the amphibole. This has been interpreted to represent post peak deformation recrystallization, most likely at or near peak P-T conditions (i.e. Robinson and Jaffe, 1969; Elliot-Meadows and Appleyard, 1991). The systematics of Fe-Mg exchange between cordierite and anthophyllite throughout a wide range of P-T conditions is considered for the first time in this study. Because Zn and Mn are present in most of the mineral deposits, and interfere in calculations for P and T in the standard geothermobarometers, a new geobarometer using cordierite and anthophyllite was developed to overcome the effect of these additional components which are in negligible concentration in these minerals. Also addressed are the controlling effects of varying bulk rock composition on the development of the metamorphic mineral assemblages and the speciation of the metamorphic fluid under peak P-T conditions.

This research project was designed primarily as a field oriented study, with three metamorphic terranes, chosen to cover a wide range of amphibolite facies metamorphism: 1) Atik Lake, Manitoba, 2) Némiscau, James Bay, Québec, and 3) Montauban, Grenville Province, Québec. These three terranes were selected mainly because of logistic as well as geological reasons. I had the opportunity to sample terranes 1 and 2 while conducting mineral exploration

programs for Westmin Resources Ltd. in the summers 1984, 1985 and 1987. During these summers, geological mapping and sampling was carried out on mining properties. The exceptionally good exposures of the cordierite-orthoamphibole rocks in these metamorphic terranes and the availability of drill core for sampling at Atik Lake were also decisive factors. A total of 65 hand specimens and 110 core samples of the lithological units were collected at Atik Lake; 64 samples were analysed for major and trace elements and 122 polished thin sections were made for petrographical analysis. For the Némiscau terrane, 88 hand specimens were collected, 30 were chosen for major and trace element analyses, and 77 polished thin sections were produce for petrographical work. An extensive collection of drill core samples (1100 samples from 56 drill holes; 125 polished thin sections) was already available from my M.Sc. studies on the Montauban deposit. In addition, 24 samples from Montauban were analysed for major and trace elements and 4 samples of regional garnet-bearing amphibolite and 2 of metapelite were selected for geothermobarometry for comparison with results obtained from the mine sequence units. Cordierite-orthoamphibole rocks from the three terranes are associated with contrasting polymetallic mineralization (see Chapter 2), all considered to be volcanogenic in origin.

The Atik Lake cordierite-orthoamphibole zone was recognized by Weber (1974) to be hydrothermal alteration in the footwall basalt hosting Algoma type banded iron formation (BIF) and chert mineralized with gold (auriferous chert). It does, however, have metamorphic mineral assemblages similar to those in metamorphosed altered basalt at the Red Lake gold mine, Ontario, which was interpreted by Mathieson and Hodgson (1984) to be epigenetic in origin. The similarity of the metamorphic assemblages at these two lode gold deposits accentuates the point that cordierite-orthoamphibole rocks associated

with ore deposits may not form exclusively from metamorphosed volcanogenic alteration. There is no general consensus regarding the origin of lode gold deposits in high grade metamorphic terranes as to whether they are metamorphosed deposits or were formed at near peak metamorphic conditions (i.e. Colvine et al., 1988; Robert et al., 1990). As pointed out by Carmichael (1990): "No matter whether Archean lode gold deposits are pre-, syn-, or post-metamorphic, there can be no doubt that metamorphic and metasomatic principles are pertinent to their study."

Cordierite-anthophyllite rocks in the Némiscau belt are associated with Cu-Ni-(Zn-Pb) mineralization in highly deformed and metamorphosed volcano-sedimentary sequences mapped by Valiquette (1975). A rare case of isograd intersection (Andalusite-Sillimanite and Staurolite-out) is documented in this study.

The Montauban terrane has been the object of numerous geological studies, particularly the massive sulfide ore deposits and associated host gneisses and amphibolite. The cordierite-anthophyllite rocks have been interpreted as a metamorphosed volcanogenic hydrothermal alteration zone (Stamatelopoulou-Seymour 1975; Stamatelopoulou-Seymour and MacLean, 1977; Bernier, 1985; Bernier et al, 1987) and also as magnesian metasediments (Prabhu, 1981; Prabhu and Weber, 1984) (c.f., Kamineni, 1975, 1979; Ramsay and Davidson, 1974; Reinhardt, 1987). The exact nature of these rocks forms an integral part of this study. A different approach was used to assess the nature of the protolith and chemical and mass changes that occurred during ore formation.

These three terranes provide a wide range of P-T conditions under which cordierite-orthoamphibole rocks are stable. The range of bulk rock composition as well as P-T allowed the development of a variety of mineral

assemblages that can be used to evaluate the metamorphic evolution of these terranes. They allowed also a study to be made of variation in anthophyllite composition coexisting with sulfide-oxide assemblages to estimate fS_2-fO_2 and fluid composition variations during metamorphism.

PREVIOUS WORK

The approaches of field oriented studies on cordierite-anthophyllite rocks derived from the metamorphism of altered volcanics, many of which are associated with massive sulfide deposits, fall into two categories:

1) bulk rock geochemical studies (Vallance, 1967; Latvalahti, 1979; Riverin and Hogdson, 1980; Hall, 1982; Casselman and Mioduszewska, 1982; Secord and Brown, 1986; Reinhardt, 1987; Beeson, 1988; Schumacher, 1988; Trägårdh, 1988; Dymek and Smith, 1990; Elliot-Meadows and Appleyard, 1991), and

2) metamorphic petrology studies (Eskola, 1914; de Rosen-Spence, 1969; Froese, 1969; Robinson and Jaffe, 1969; Bachinski, 1976; James et al. 1978; Treloar et al., 1981; Spear, 1982; Wolter and Seifert, 1984; Schumacher and Robinson, 1987; Schneiderman and Tracy, 1991).

A few studies have integrated data from the two approaches (e.g. Deb, 1980; Bristol and Froese, 1989).

Paragenetic relations in cordierite-anthophyllite rocks and their petrologic implications and chemography have been investigated by various workers (Froese, 1969; Robinson and Jaffe; 1969; James et al., 1978; Sharma and MacRae, 1981; Spear and Schumacher, 1982). Qualitative and quantitative petrogenetic grids for cordierite-orthoamphibole rocks have been proposed by Froese (1969), Robinson and Jaffe (1969), Spear (1978), Percieval et al. (1982), Hudson and Harte (1985), Spear and Rumble (1986).

Experimental studies on the stability of chlorite + quartz in the system Mg-Fe-Al-Si-H_2O were conducted by Akella and Winkler (1966) and by Fleming and Fawcett (1976), and are pertinent to an understanding of the formation of cordierite-orthoamphibole rocks. The former authors have established the upper stability of aluminous chlorite (X_{Fe}=0.44) to be at T=562±8 °C at P_{H_2O}=2 kbar, and breakdown to cordierite and orthoamphibole; the latter authors have shown that the assemblage orthoamphibole, cordierite, talc and magnetite is stable above 600°C at P_{H_2O}=2 kbar for X_{Fe}=0.5. Field studies on alteration at VMS deposits indicate that chlorite has a wide spectrum of compositions from sheridanite to daphnite (Bachinski, 1976; Kranidiotis and MacLean, 1987; Slack and Coad, 1989), which will be reflected in their metamorphosed equivalents. Other studies have stressed the importance of sulfidation and oxidation reactions during metamorphism on the compositions of chlorite (Nesbitt, 1982; Bryndzia and Scott, 1987), biotite (Tso et al., 1979), anthophyllite (Froese, 1971; Popp et al., 1977a,b; Froese, 1977), cordierite (Froese, 1971; 1973) and gahnite (Spry and Scott, 1986a) .

Pollard (1981) reported on an unusual occurrence of cordierite-anthophyllite rock associated with hydrothermal tin-tungsten mineralization at Tommy Burns mine, Australia, interpreted to have formed during contact metasomatism related to a granitic intrusion.

Previous work in the three terranes

The Atik Lake greenstone belt was mapped by Milligan and Take (1954) and by Weber (1974). A study of the morphology and chemistry of some mafic volcanic flows was made by Hargreaves (1978) and Hargreaves and Ayres (1979). The metamorphic conditions have been briefly and qualitatively outlined by Weber and Scoates (1978) and Weber (1991).

The Némiscau belt was mapped by Valiquette (1964, 1975). A petrographic study of the main occurrence of cordierite-anthophyllite rock was made by Peredery (1966).

The geology of the Montauban area has been described by Bancroft (1915), Smith (1956), Pyke (1966), Rondot (1978) and Morin (1987). The Montauban ore deposits and host rocks have been studied by O'Neil and Osborne (1939), Osborne (1939), Wilson (1939), Stamatelopoulou-Seymour (1975), Prabhu (1981), Stamatelopoulou-Seymour and MacLean (1984), Bernier (1985), and Bernier et al. (1987). Lithogeochemistry studies of the amphibolite and quartzofeldspathic gneisses were done by Stamatelopoulou-Seymour and MacLean (1977), MacLean et al (1982) and Prabhu and Webber (1984).

LIST OF ABBREVIATIONS AND SYMBOLS

Abbreviations and symbols used throughout this thesis are defined below.

Minerals

Whenever possible, the mineral symbols used are those defined by Kretz (1983). However, diagrams produced with the program GEO-CALC and others reproduced from the literature may have different mineral symbols, which will then be defined in the captions.

Act: actinolite	Alm: almandine	An: anorthite
And: andalusite	Apy: arsenopyrite	Ath: anthophyllite
Bt: biotite	Cc: calcite	Chl: chlorite
Cpy: chalcopyrite	Crd: cordierite	Cum: cummingtonite
Di: diopside	Dol: dolomite	Ep: epidote
Fa: fayalite	Gah: gahnite	Ged: gedrite
Gn: galena	Grs: grossular	Grt: garnet
Gru: grunerite	Hd: hedenbergite	Hlb: hornblende

Hrc: hercynite | Ilm: ilmenite | Kfs: K-feldspar

Ky: kyanite | Lö: löllingite | Ms: muscovite

Mt: magnetite | Ol: olivine | Phl: phlogopite

Pl: plagioclase | Pn: pentlandite | Po: pyrrhotite

Prg: pargasite | Prp: pyrope | Qtz: quartz

Rt: rutile | Ser: sericite | Sil: sillimanite

Sph: sphalerite | Spl: spinel | Sps: spessartine

Srp: serpentine | St: staurolite | Tlc: talc

To: tourmaline | Tr: tremolite | Ts: tschermakite

Ttn: titanite

Oxygen and sulfur fugacity buffers:

fO_2: oxygen fugacity fS_2: sulfur fugacity

QFM: quartz-fayalite-magnetite buffer

NNO: nickel-nickel oxide buffer

HM: hematite-magnetite buffer

PPM: pyrite-pyrrhotite-magnetite buffer

PM: pyrrhotite-magnetite buffer

PP: pyrrhotite-pyrite

PL: pyrrhotite-löllingite

PA: pyrrhotite-arsenopyrite

PLA: pyrrhotite-löllingite-arsenopyrite

Chemical systems

CNFMASH: $CaO\text{-}Na_2O\text{-}FeO\text{-}MgO\text{-}Al_2O_3\text{-}SiO_2\text{-}H_2O$

KFMASH: $K_2O\text{-}FeO\text{-}MgO\text{-}Al_2O_3\text{-}SiO_2\text{-}H_2O$

FMASH: $FeO\text{-}MgO\text{-}Al_2O_3\text{-}SiO_2\text{-}H_2O$

Other symbols

BIF: banded iron formation

N-MORB: normal mid-oceanic ridge basalt

VMS: volcanogenic massive sulfides

HFSE: high field strength elements

REE: rare earth elements

P: pressure T: temperature kbar: kilobar

°C: degree centigrade

K_D: partitionning coefficient

X_{Fe}: mole fraction of Fe (Fe/(Fe+Mg+Mn+Zn))

FORMAT OF THE THESIS

Chapter 2 outlines the geological and structural settings of the three terranes and the geological relationship of the cordierite-orthoamphibole rock occurrences.

Chapter 3 deals with the lithogeochemistry of the cordierite-orthoamphibole rocks and associated lithological units; it is subdivided into six sections. Section 3A is a reproduction of a paper published in Canadian Journal of Earth Sciences (Bernier and MacLean, 1989) and reports on the lithogeochemistry of the Atik Lake metamorphosed altered basalt associated with auriferous chert and banded iron formation. Section 3B is an *Addendum* to section 3A. Section 3C describes a new technique, the Log(Ratio) method, designed to help identify protoliths in a metamorphic terrane, and is applied to the Atik Lake rocks. Section 3D is reproduced from a published paper in Canadian Mineralogist (Bernier, 1990) on the petrogenesis of vanadiferous zincian-chromian hercynite found in the Atik Lake metamorphosed altered basalt. The presence of these unusual spinel compositions is the metamorphic expression of the chemical changes recorded by the basalt during hydrothermal alteration. Section 3E presents the geochemical characteristics of the Némiscau rocks; the Log(Ratio) method is used to identify the various protoliths. The final section (3F) is a manuscript to be submitted which deals with the lithogeochemistry of the metamorphosed alteration zone associated with the Montauban massive sulfide

deposit. In this paper, the geometry of the alteration zone, metal zoning, and the Log(Ratio) method are used to identify the protolith of the various rock types; these support a pre-metamorphic volcanogenic origin for the ore deposit and accompaning hydrothermally altered rocks. Overall, Chapter 3 assesses the chemical and mass changes that occur during hydrothermal alteration of mafic and felsic rocks that lead to suitable protoliths for the formation of cordierite-orthoamphibole rocks during regional metamorphism.

Chapter 4 is a major part of this thesis and presents characteristic mineral assemblages in cordierite-orthoamphibole rocks and other units from the three terranes. Chemographical analysis, mineral chemistry and geothermobarometry are used to estimate peak P-T conditions and to delineate the metamorphic evolution of the three terranes. The effect of additional components (Zn, Mn and S) to the FMASH system is assessed for the Montauban cordierite-anthophyllite rocks in which spectacular coronitic textures involving the breakdown of zincian-staurolite and the formation of gahnite rims are observed.

Chapter 5 presents the calibration of a new geobarometer based on Fe-Mg exchange between cordierite and anthophyllite.

Chapter 6 deals with the sulfidation and oxidation of Fe-anthophyllite in the three terranes using the experimental data of Popp et al. (1977b). The compositions of the metamorphic fluids are estimated for the peak P-T conditions for each terrane. Anthophyllite X_{Fe} isopleths were constructed in fO_2-fS_2 space for the determined peak P-T conditions of each terrane (Chapter 4).

The conclusion, original contribution to knowledge, and recommendations for future research are presented in Chapter 7.

The reference list at the end of the thesis includes all the references

quoted in the chapters, except those in the two reproduced published papers (sections 3A, 3D of Chapter 3) which are at the end of each paper.

A series of *Appendices* is presented at the end of this thesis. The sample and drill hole locations are presented in maps in *Appendix I*. Electron microprobe mineral analyses are listed in *Appendix II*. The thermodynamic data, activity models and mathematical expressions of the geothermobarometers used are presented in *Appendix III*. Source code listing of GWBASIC programs written for this thesis are presented in *Appendix IV*.

CHAPTER 2

GEOLOGICAL SETTING OF THE THREE TERRANES

The three terranes containing the metamorphosed hydrothermal alteration zones used for this study lie within the Precambrian Canadian Shield (Fig. 2.1). The first terrane is an Archean greenstone belt from Northern Manitoba (Atik Lake), the second terrane is an Archean volcano-sedimentary belt in northern Québec (Némiscau), and the third one, is a narrow, middle to late Proterozoic supracrustal gneiss segment of the Grenville Province, Québec (Montauban).

Atik Lake

The Atik Lake greenstone belt is located within the western part of the Superior Province of the Canadian Shield in northern Manitoba (Fig. 2.2). It forms part of the Sachigo Subprovince, which is also known as the Cross Lake or God's Lake Subprovince (Weber and Scoates, 1978; Weber, 1991). The geology has been described by Milligan and Take (1954), Weber (1974), Weber and Scoates (1978) and Hargreaves and Ayres (1979). Weber (1990) reports the age of volcanic rocks to be in the range of 2.83-2.7 Ga. The belt is enclosed by massive to foliated granite and granodiorite to the north, and by layered tonalitic and granodioritic gneiss to the south.

The volcano-sedimentary units of the belt form a subvertical, east-west trending and south-facing homoclinal sequence (~35km long) cut by thick gabbro sills. Pillowed, massive and glomeroporphyritic basalts are the dominant volcanic rock types. Hargreaves (1978) studied the morphology, petrography and chemistry of a 400m thick sequence of metabasalts at the base of the

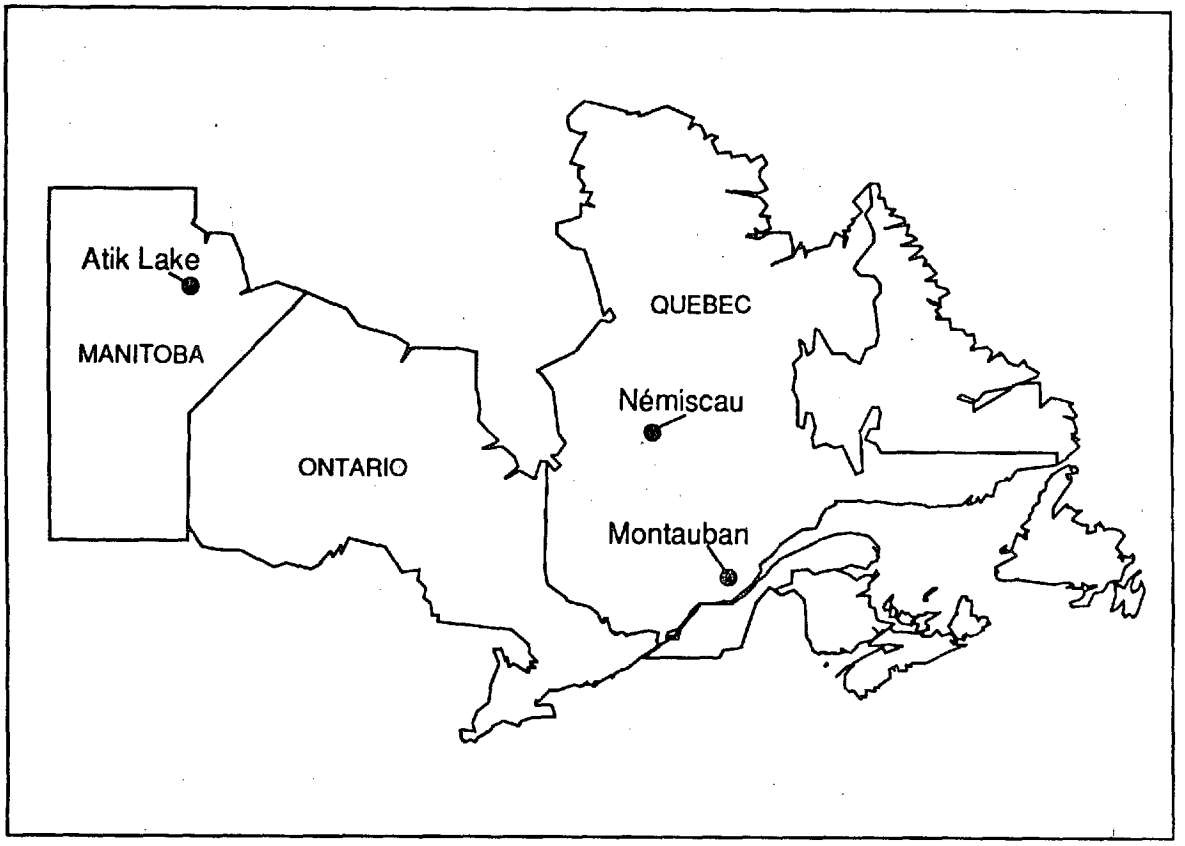

Figure 2.1 Location Map

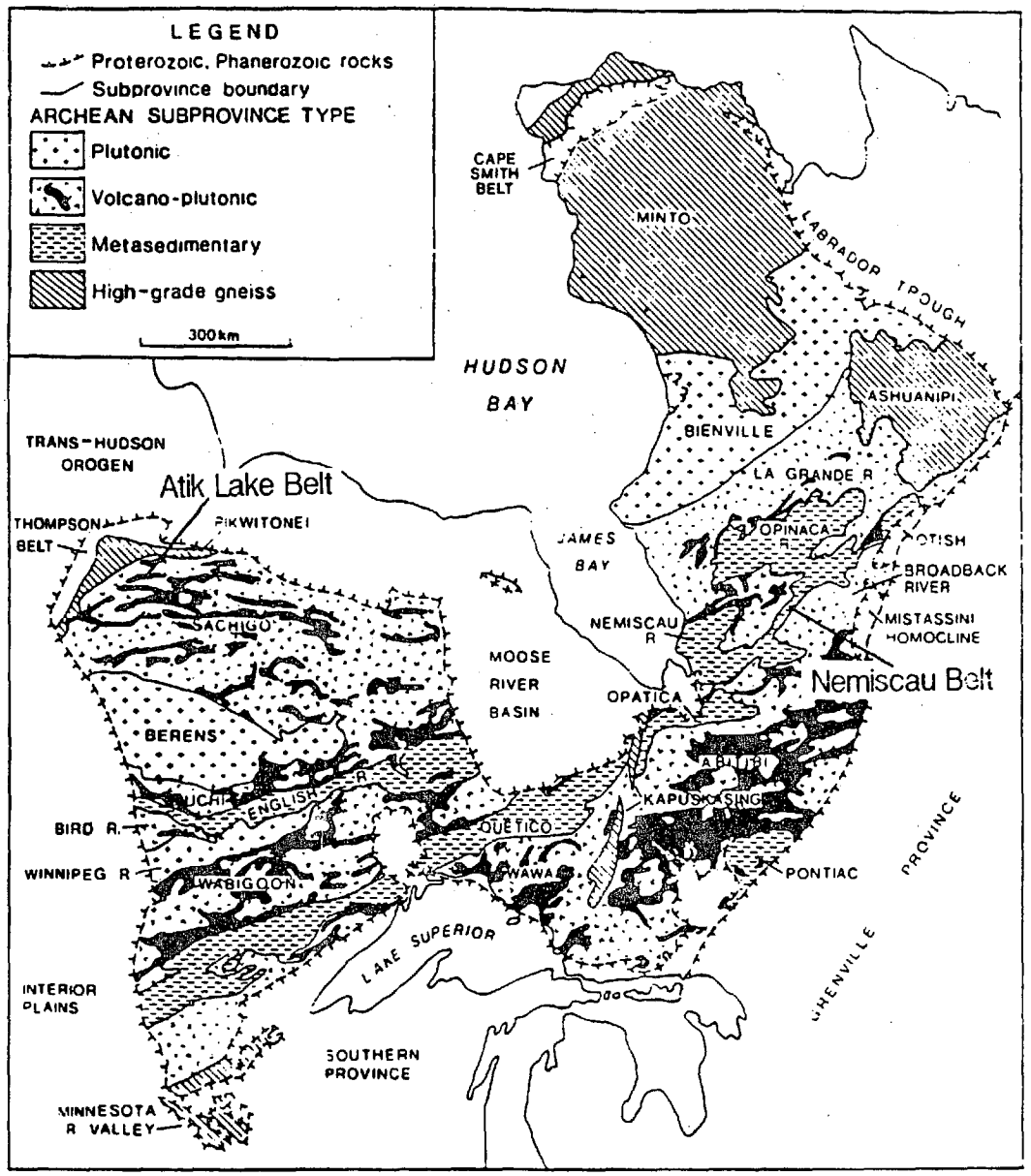

Fig. 2.2. Subprovinces of the Superior Province. From Card (1990), with the addition of the Atik Lake and Némiscau belts.

stratigraphy on Mistuhe island. Phinney et al. (1988) reported on the plagioclase chemistry and bulk REE compositions of the glomeroporphyritic flows and sills.

Metasedimentary units in the stratigraphy are mainly greywackes, but include quartzite, with pelitic interbeds (cordierite-biotite-garnet and cordierite-anthophyllite schists), and polymictic conglomerate. Thin banded iron-formation (BIF) horizons occur between some of the basalt flows (Figs. 2.3A-C) and pyroclastic units. Well preserved metamorphosed hydrothermal alteration pipes and stratiform alteration zones (Figs. 2.3D-G), which were recognized by Weber (1974), are present in a basalt unit at the top of the Mistuhe Island stratigraphic sequence (Figs. 3 and 6 in Bernier and MacLean, 1989). Cordierite-gedrite (±anthophyllite) rocks are well developed in these alteration zones and are the object of this study. Acicular orthoamphibole grains show no preferred orientation, and are presumed to have crystallized after the main deformational event.

The Atik Lake belt is bounded by three major faults (Milligan and Take, 1954; Weber, 1974), giving it a wedge-like shape (Fig. 2.4A). The Atik Lake fault at the southern margin of the belt strikes 070° and intersect the northern fault toward the east, whereas the fault truncating the western margin strikes 050°. Rocks on the NW side of the Atik Lake fault are in the upper amphibolite facies (sillimanite) whereas those on the SE side are in lower amphibolite (andalusite) facies, indicating an upward movement of the NW block (Weber, 1978). Bedding and S1 orientations across the belt (data from Weber, 1974) have been deflected by both the northern and southern (Atik Lake) faults, implying ductile dextral strike slip shearing along these transcurrent faults (Fig. 2.4A).

Ductile shearing was mostly recorded in the interflow oxide and

Fig. 2.3. Field photographs, Atik Lake. A) Magnetite-quartz BIF on top of a pillowed metabasalt flow. B) Sheared grunerite-quartz BIF and a thin bed of auriferous chert (rusty horizon) lying on a metamorphosed altered basalt flow. C) Intrafolial "Z" folds in sheared grunerite-quartz BIF. D) Glomeroporphyritic metabasalt flow with columnar joints from alteration pipe 1. E) Metamorphosed hydrothermally altered equivalent of D. Note the adundance of garnet and gedrite along the columnar joints. F) Outcrop of alteration pipe 2; andalusite-bearing felsic dyke (in white) has displaced BIF on the left against flow-top breccia. G) Close-up of the altered flow-top breccia (in F) below BIF at pipe 2. Arrows indicate stratigraphic tops. Lens cap = 5 cm.

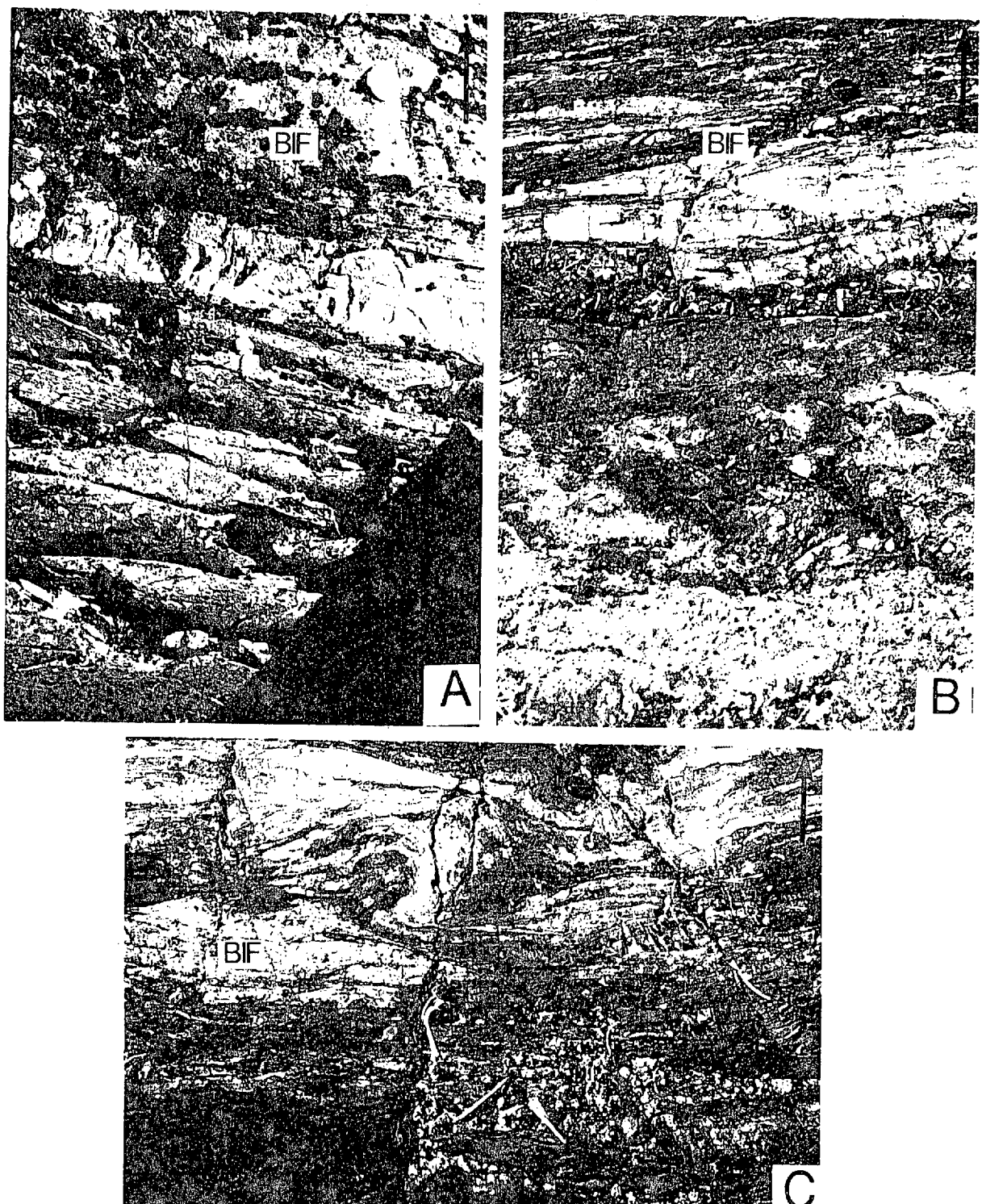
BIF
A
BIF
B
BIF
C

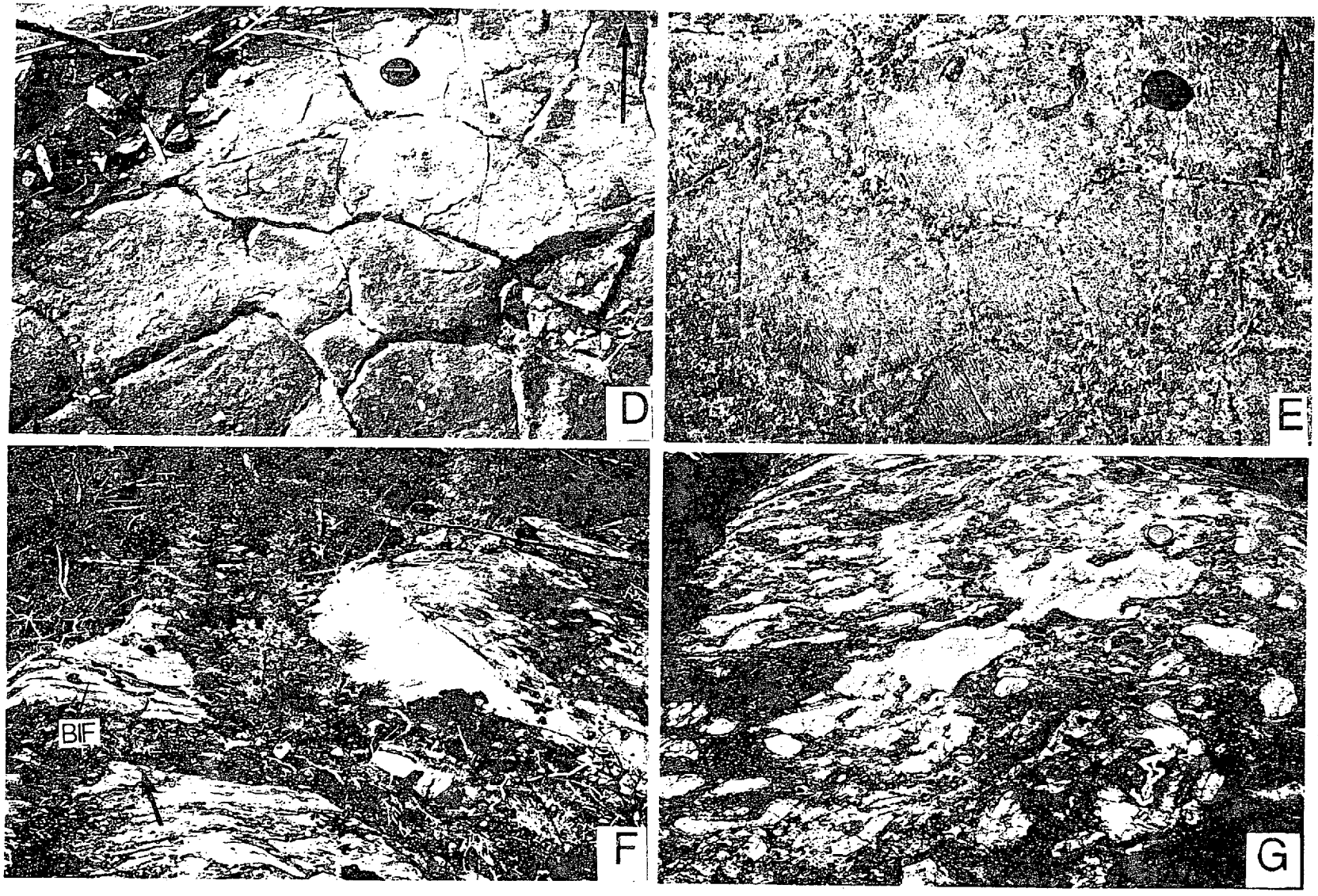
D
E
BIF
F
G

Fig. 2.4. Structural settings of the Three terranes. A) Atik Lake, Manitoba (modified after Weber, 1974). B) Némiscau, Québec, (modified from Valiquette, 1975). C) Montauban, Québec, (modified from Rondot, 1978, and Nadeau and Corrigan, 1991). Filled circle: town, NDA: Notre Dame des Anges, TR: Trois Rivières. MG: Mékimac Group, LPC: Laurentide Parc Complex, SLL: Saint-Lawrence Lowlands, SLR: Saint-Lawrence River; MAG=magnetic.

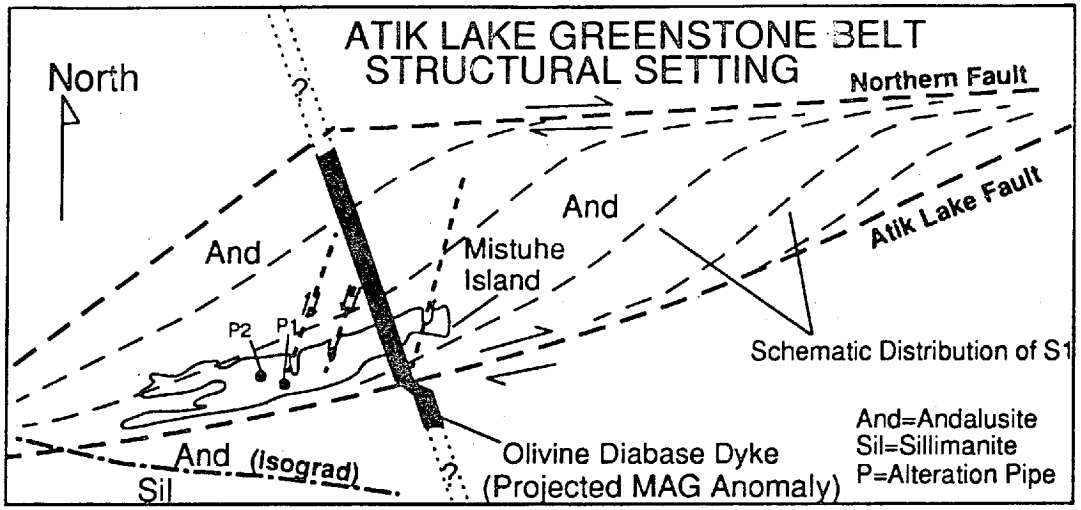
ATIK LAKE GREENSTONE BELT
STRUCTURAL SETTING
North
Northern Fault
Atik Lake Fault
And
And
Mistuhe
Island
P2
P1
Schematic Distribution of S1
And=Andalusite
Sil=Sillimanite
P=Alteration Pipe
And (Isograd)
Sil
Olivine Diabase Dyke
(Projected MAG Anomaly)

A

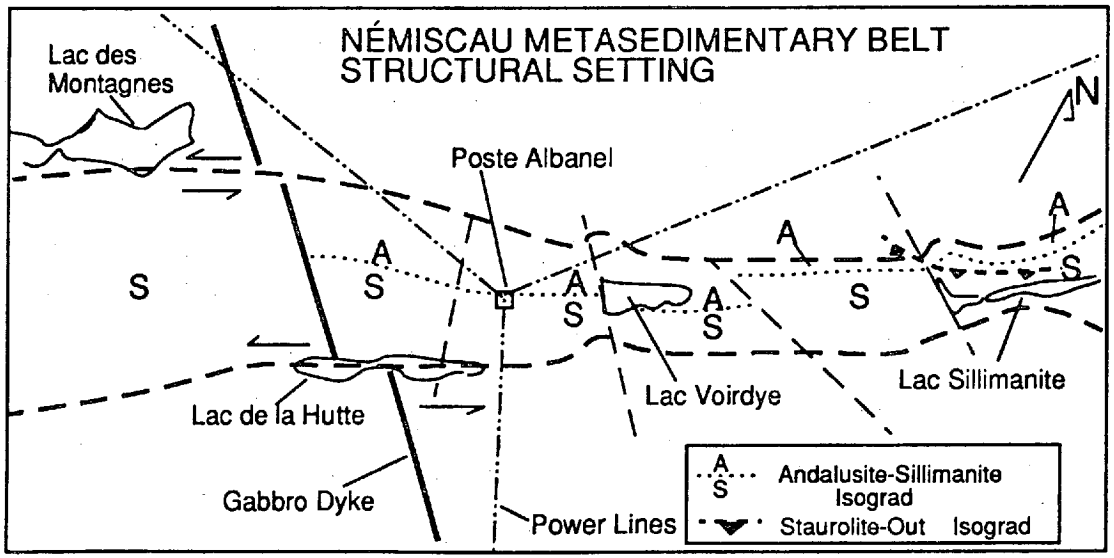
NÉMISCAU METASEDIMENTARY BELT
STRUCTURAL SETTING
Lac des
Montagnes
Poste Albanel
N
S
A
S
Lac de la Hutte
Gabbro Dyke
Power Lines
Lac Voirdye
Lac Sillimanite
Andalusite-Sillimanite
Isograd
Staurolite-Out Isograd

B

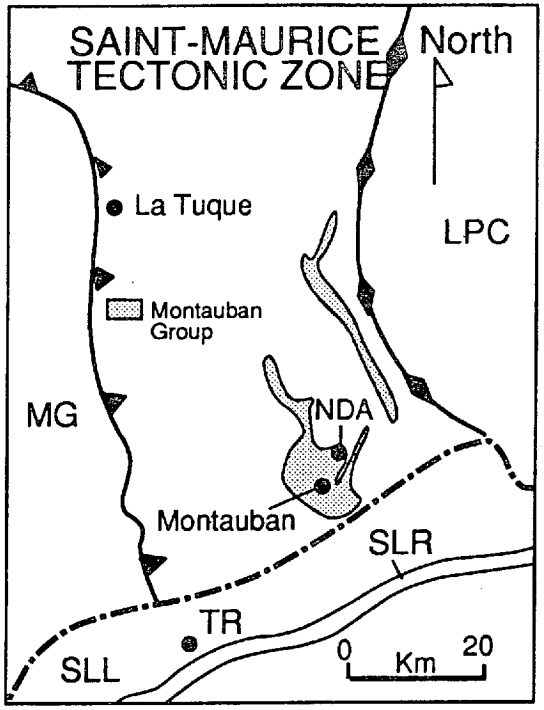
SAINT-MAURICE
TECTONIC ZONE
North
La Tuque
LPC
Montauban
Group
MG
NDA
Montauban
SLR
TR
SLL
0 Km 20

C

sulfide-arsenide iron formation beds (Bernier and MacLean, 1989), and is related to shearing associated with the Atik Lake fault. Highly sheared BIF (U-05) above the alteration pipe 1 conduit contrasts strongly with unsheared equigranular quartz, pyrrhotite and chalcopyrite and clusters of fan-like actinolite-grunerite needles within the pipe 1 conduit. Features indicative of ductile shearing are plentiful on Mistuhe Island:

(1) intrafolial Z-shape folds (cm to m scale; Fig. 2.3C),

(2) flattening of quartz and magnetite grains in moderately deformed BIF,

(3) ribbon quartz grains parallel to the C-foliation in mylonitized BIF and mineralized chert (similar to experimentally sheared quartzite shown by Dell'Angelo and Tullis, 1989),

(4) grains of intensely crushed grunerite with syntectonic garnet porphyroblastic growth, and

(5) pyrite and arsenopyrite porphyroblasts rounded by rotation during shearing.

An aphyric, dark brown olivine diabase dyke having a strong magnetic signature, cuts across the entire belt at 330°, and was intersected by drilling (Fig. 2.4A). It has the proper orientation to be part of the Proterozoic Mackenzie dyke swarm (Douglas, 1979). The dyke appears to have been emplaced in the extensional position for the compression orientation. A series of associated 030° brittle strike-slip faults were interpreted from the offset magnetic anomalies in the iron formations and from mapping (Fig. 2.4A). These brittle faults have the geometry of a propagating wrench fault system, where the dyke occupies the P-plane. This late deformational event pre-dated the emplacement of the diabase dyke and appears unrelated to the mineralization event at Atik Lake.

Némiscau

The Némiscau volcano-sedimentary belt is located in northwestern Québec, 200 km northeast of Matagami (Map Sheets 32N/O), between the Rupert and Eastmain rivers. The belt extends over 150 km along a NE axis with a maximum width of 10 km (Fig. 2.2). Mineral exploration activity has been recorded intermittently for the past 32 years for Ni, Cr, PGE, gold and base metals. The geology of the area was mapped by Valiquette (1964, 1975). Cordierite-anthophyllite rocks at Lac Voirdye (Pike Lake) were the object of a petrographical study by Peredery (1966).

The Némiscau belt connects the Némiscau River and Opinaca River Metasedimentary Subprovinces as defined by Card (1990). Sinistral transcurrent faults bound the belt, which Valiquette (1975) interpreted to be a major synclinal structure overturned to the south. Regional metamorphism in the upper amphibolite facies has affected the rocks in the belt, which are intruded by granite and pegmatite and cross-cut by late NW-SE faults. The dominant aluminosilicate polymorphs are andalusite at the northeast end of the belt and sillimanite at the southwest end. This indicates a relatively low pressure range, suggesting Buchan-type metamorphism (note andalusite-sillimanite isograd on Fig. 2.4B).

Pillowed and massive massive flows of mafic metavolcanic rocks (Figs. 2.5A-C) are exposed along the northern and southern margins of the belt (Figs. 2.4B). Biotite quartzo-feldspathic gneisses are the dominant lithologies in the core of the syncline. Lenses of sulfide and dravite bearing quartzite (meta-chert?) (Fig. 2.5D), iron formation (quartz-grunerite-magnetite and quartz-magnetite), nodular sillimanite and andalusite gneisses, and white quartzite interbedded with cordierite-garnet rock, are closely associated with the mafic metavolcanics. Well preserved pillow structures in blocks of

Fig. 2.5. Field photographs from Némiscau, Québec. A) Elongated pillowed metabasalt flow with epidotized pillow cores. B) Transition from undeformed pillows (right) to highly sheared pillows (left). C) Massive porphyritic matabasalt flow with numerous quartz-epidote veinlets. A-C are from Poste Albanel. D) Sulfide-dravite quartzite from Lac Sillimanite. E) Cordierite-anthophyllite rock from Lac Voirdye.

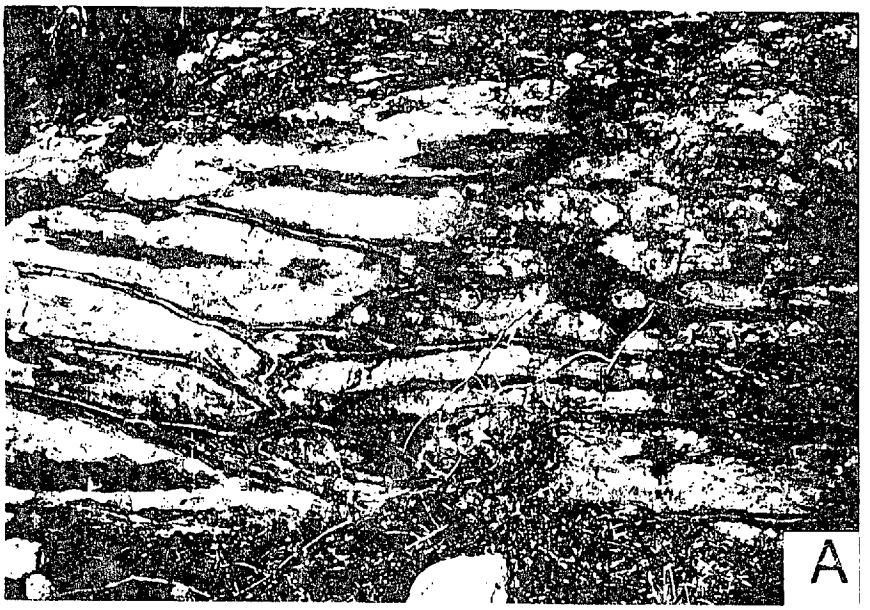
A

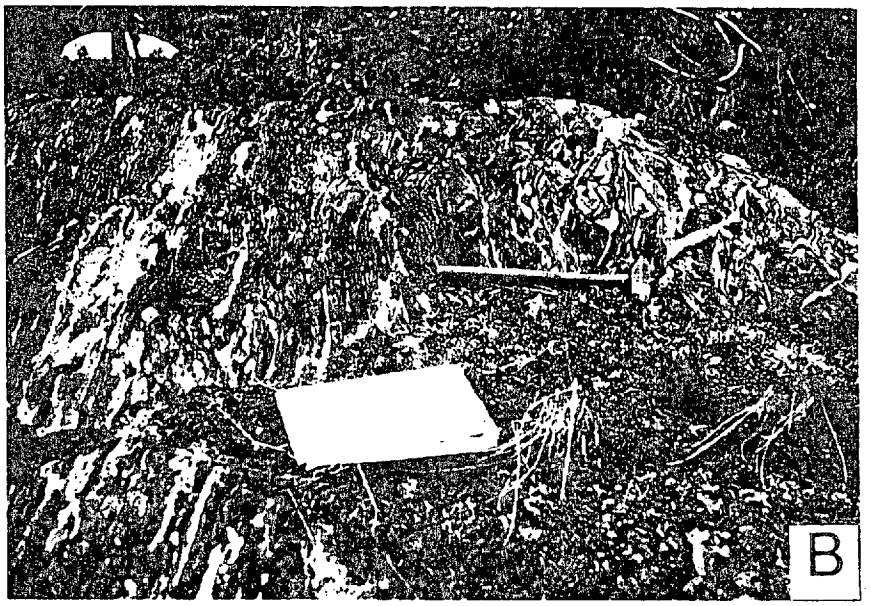
B

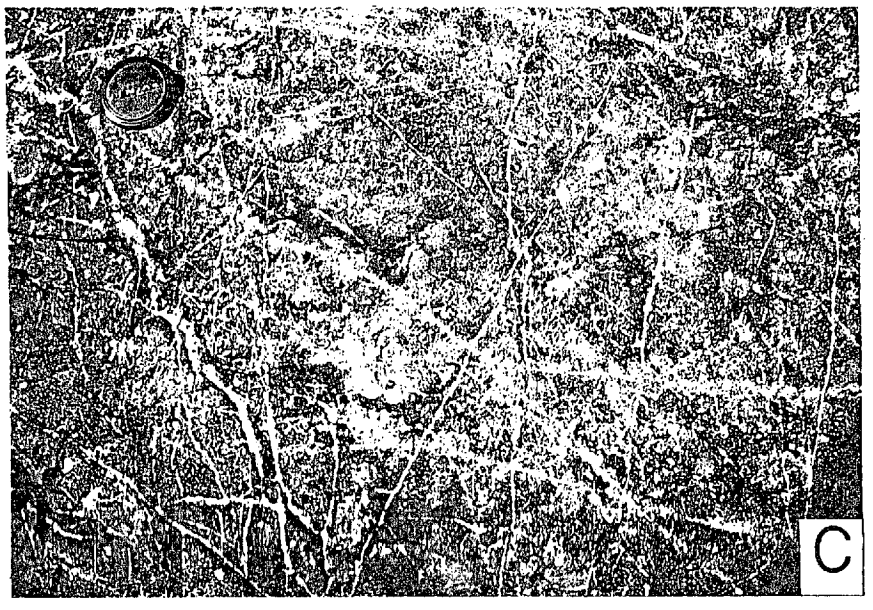
C

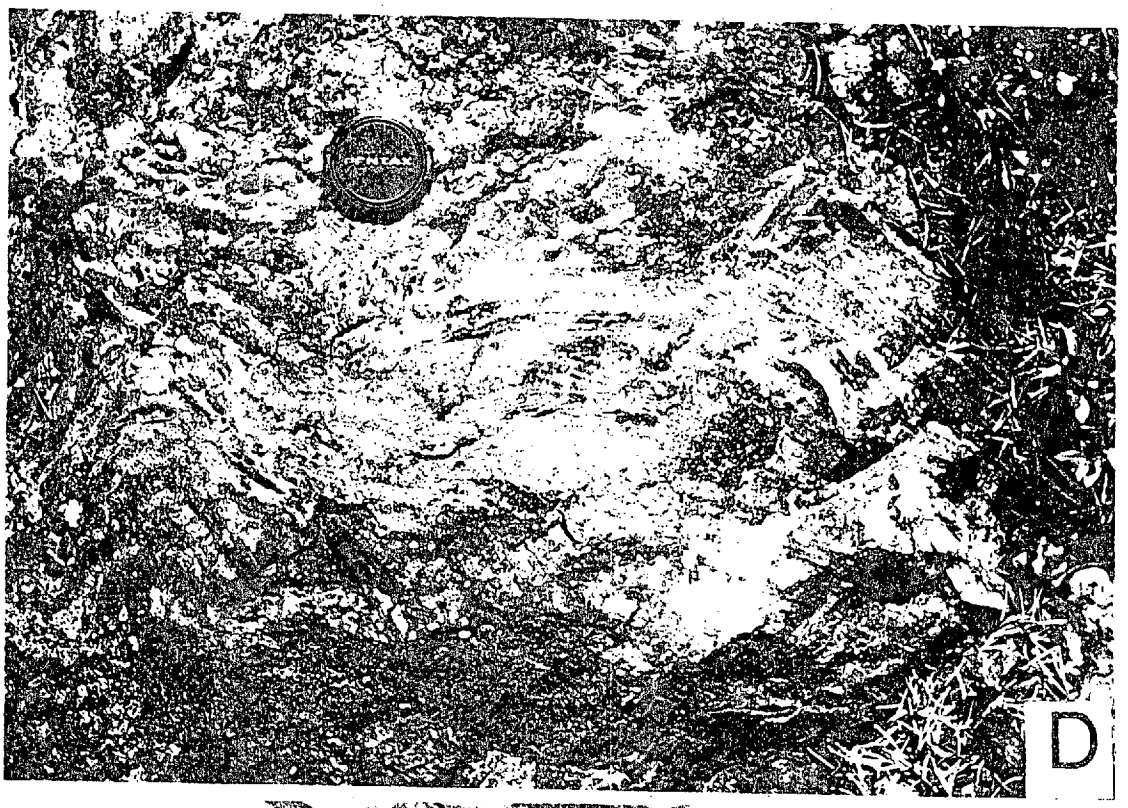
D

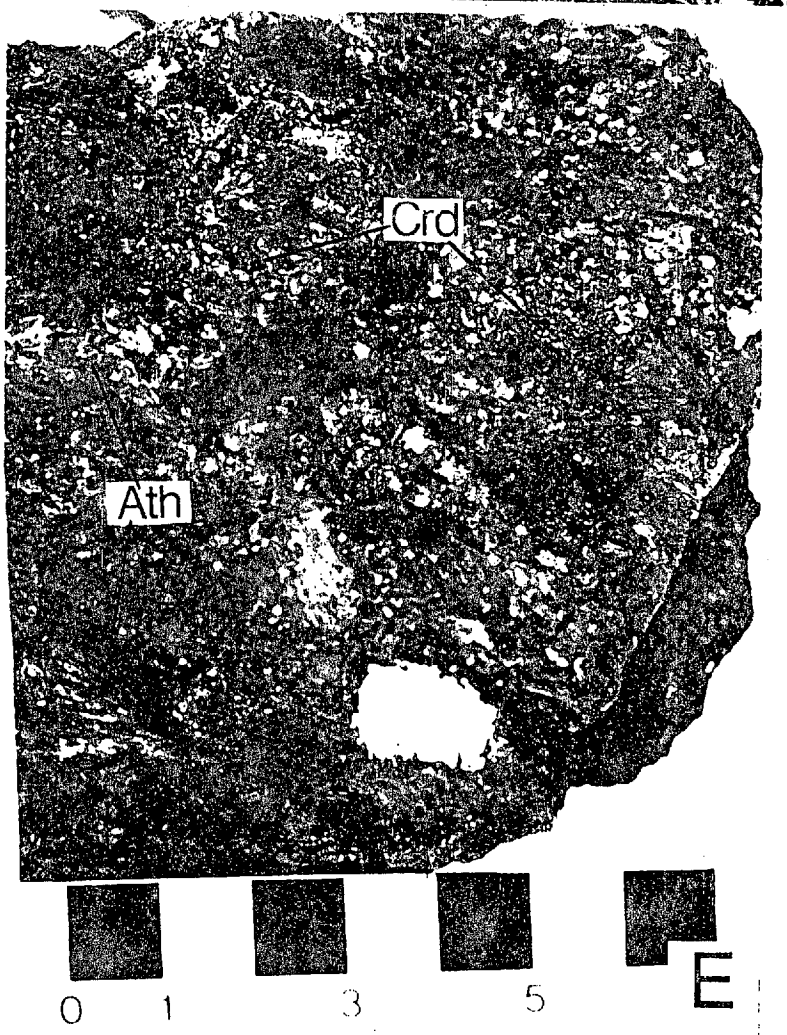
Crd
Ath
0
1
3
5
E

relatively undeformed amphibolite indicate that the stratigraphic tops in these blocks are facing north. However, owing to severe transposition during shearing, lithological contacts may be largely structural. Horizons of cordierite-anthophyllite (Fig. 2.5E), anthophyllite-plagioclase, and cummingtonite-plagioclase rocks, associated with massive sulfide and quartzite lenses, occur mostly within the metabasalts on the southern margin of the belt.

The main occurrence of cordierite-anthophyllite rocks forms a series of elongated lenses which are best exposed in the Lac Voirdye-Lac Senay area (Fig. 2.4B), extending about 10 km along strike with a maximum width of 300m. These rocks contain zones of quartz-chalcopyrite-pyrrhotite stringer mineralization. An S-shape fold, affecting the cordierite-anthophyllite rocks southwest of Lac Voirdye, was mapped by Valiquette (1975), and corroborates the sinistral sense of ductile shearing cited earlier. Other smaller lenses (10 to 200 m long) of cordierite-anthophyllite rocks have been mapped north of Lac de la Hutte and south of Lac des Montagnes. Anthophyllite needles in most of these lenses do not exhibit a preferred orientation, suggesting that post-deformation recrystallization occurred, and that the protolith acquired its unusual chemical composition prior to peak metamorphism.

Numerous bodies of layered and massive ultramafic rocks form discontinuous conformable lenses within the amphibolites and metasediments along the northern and southern margins of the belt. Olivine, tremolite, serpentine, magnetite and talc are the common constituents in these rocks. Massive chromite layers up to 2 m thick are reported south of Lac des Montagnes (Valiquette, 1975).

The Némiscau belt is surrounded by oligoclase gneiss and pink and white granites. Tourmaline-bearing white pegmatite sills and dykes are abundant in

the belt and have extensively invaded the volcano-sedimentary units.

The NE-SW transcurrent faults along the sides of the belt appear to have been mainly ductile strike-slip shears, and were probably syn- to slightly post-peak metamorphism as indicated by the folding of the andalusite-sillimanite isograd (Fig. 2.4B). The fault on the southeastern side has undergone a late major brittle deformation event (Lac de la Hutte Break) (slickensides, S 60° W plunging 35° W), which caused a 5 km sinistral offset of a gabbro dyke in the area (Fig. 2.4.B). A 300 m long mineralized milky-white quartz vein (>1%Zn, >1%Pb, 0.15%Cu, 70 g/t Ag, 0.14 g/t Au) was discovered north of Lac de la Hutte and is related to the fault. Accompanying retrograde sericitization and minor chloritization affected the adjacent amphibolite. Anastomosing shear zones within the belt are typified by intense flattening of some pillows adjacent to relatively undeformed amphibolites (Fig. 2.5A). Intense quartz veining has been observed in enclaves of massive unaltered amphibolite, but not in associated incompetent cummingtonite-anthophyllite rocks (Fig. 2.5F). Many of these veins are deformed (boudinaged, folded), which implies that they formed early in the deformation history. A series of late brittle faults having a general NW-SE orientation cut across the belt (Fig. 2.4B).

Montauban

The Montauban area is located in the Grenville Province, 100 km west of Quebec City (Fig. 2.1). Base metals and gold ore deposits occur in a narrow band of Proterozoic supracrustal rocks, termed the St-Maurice tectonic zone by Nadeau and Corrigan (1991). Regional geological mapping was carried out by Bancroft (1915), Smith (1956), Pyke (1966), Rondot (1978), Morin (1987), Hébert and Nadeau (1990), and Nadeau and Corrigan (1991). The ore deposits

and host rocks were studied by Osborne (1939), O'Neil and Osborne (1939), Wilson (1939), Smith (1956), Stamatelopoulou-Seymour (1975), Prabhu, 1981), Stamatelopoulou-Seymour and MacLean (1984), Bernier (1985), Bernier et al. (1987) and Jourdain et al. (1987). New occurences of polymetallic mineralization have recently been reported in the northeast extension of what is believed to be the equivalent of the Montauban Group (Hébert and Nadeau, 1990). This mineralization is currently the object of intensive exploration drilling by SOQUEM.

Stamatelopoulou-Seymour and MacLean (1977) used major element chemistry to propose a volcanic origin for thick units of quartzofeldspathic gneisses in the mine area. Prahbu and Webber (1984) favored a metasedimentary origin for these gneisses. A trace element geochemical study of the amphibolites and metabasalts by MacLean et al. (1982) indicated a tholeiitic affinity characteristic of island-arc volcanism.

The metamorphism of the ores and associated alteration zones was outlined by Stamatelopoulou-Seymour and MacLean (1984) and Bernier et al. (1987). Bernier (1991, 1992) proposed a metamorphic evolution model, for the area, using mineral equilibria in the cordierite-anthophyllite rocks.

The Montauban ore deposits consist of a Zn-Pb-Cu-Au-Ag massive sulfide lense, and the South, A, and North zones of disseminated or stringer polymetallic mineralization containing economic concentrations of gold and silver. These deposits form stratiform lenses within a narrow sequence of sub-parallel units of calc-silicate rock, cordierite-anthophyllite rock and nodular sillimanite gneiss, which together are referred to as the mine sequence. Details on the geological setting of the mine sequence are given in Chapter 3 (section 3F). The mine sequence is enclosed within much thicker units of quartzofeldspathic gneiss, quartzite and metabasalt (Fig. 2.6A) that

Fig. 2.6. Field photographs, Montauban, Québec. A) Elongated pillows of metabasalt from Mount Tetrault. B) Sheared felsic lapilli tuff. C) Mafic Lapilli tuff.

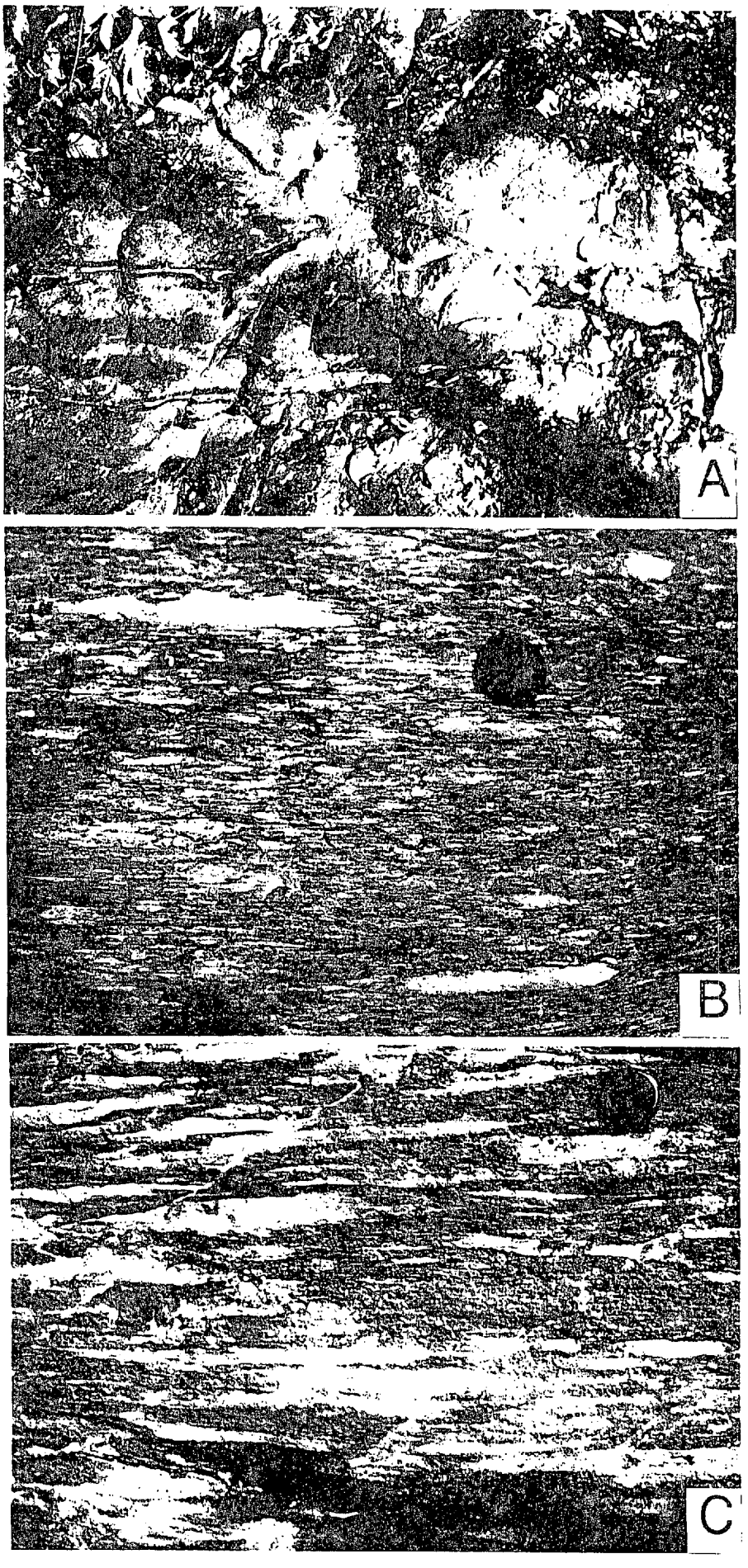
A
B
C

are part of the Proterozoic Montauban Group (Rondot, 1978), which were metamorphosed under middle-amphibolite facies conditions. The presence of relict kyanite and coarse grained to fibrolitic sillimanite at the north gold zone (Bernier et al., 1987) indicates a Barrovian-type of metamorphism.

An outcrop (not previously mapped) of sheared felsic lapilli tuff (Fig. 2.6B) was found during a field trip (1991). It is exposed in the mine tailings pond, about 500m west of the north gold zone, between the pillowed metabasalt ridge and the mine sequence. An outcrop of lapilli tuff with felsic fragments in a more mafic matrix (Fig. 2.6C) and associated with a crystal tuff unit is present in the Lac des Pins area, about 15 km northeast of the Montauban deposits (Nadeau, pers. comm., 1991).

The Montauban Group lies within the St-Maurice tectonic zone. The eastern margin of this zone is bounded by a subvertical sinistral ductile shear zone (Fig. 2.4C). The western boundary is also a ductile shear zone that dips gently to the east and tectonically imbricates the various rock types (Hébert and Nadeau, 1990). It is uncertain whether the St-Maurice tectonic zone is part of the Allochtonous Monocyclic Belt (≤1.3 Ga) as defined by Rivers et al. (1989). Lead-isotope measurements on the Pb-Zn ores yield a minimum age of 1.27 Ga (Fletcher and Farquhar, 1982). However, preliminary zircon U-Pb data on the La Bostanais Complex, which intrudes the Montauban Group, yields an age of ~1.4 Ga (Nadeau pers. Comm. 1991). This latter age would make the St-Maurice tectonic zone at least 0.1 Ga older than the Allochtonous Monocyclic Belt.

The most striking structural feature affecting the mine sequence is a sub-horizontal stretching mineral lineation within the locally crenulated S1 plane. The orebodies are also sub-horizontal and very elongated in he same direction. The surrounding regional gneisses are affected by this strong

lineation, which points to a NNE sub-horizontal (dextral) tectonic transport, possibly thrusting. Ductile shearing and transposition of the Montauban Group probably occurred during this phase of deformation and prior to peak metamorphism, as all the rocks are well recrystallized. This is compatible with microfabric studies indicating that recrystallized minerals, in the absence of a nonhydrostatic stress, commonly show a crystallographic orientation between the new strain-free grains and the older deformed grains (Hobbs et al., 1976).

A second schistosity intersecting S1 at a low angle was observed in the North Gold Zone quartzitic gneiss, but its structural significance is not known. An early interpretation of the deformational history by Pyke (1966) and Morin (1987) involved three phases of deformation, but it is currently being questioned by Nadeau (pers. comm. 1991). The regional tectonic setting of the St-Maurice zone is still a matter of conjecture.

Summary

The three terranes containing cordierite-orthoamphibole rocks that were selected for this study have major dissimilarities in their associated rocks types, and also in their tectonic and metamorphic settings. The Atik terrane is a greenstone belt dominated by mafic volcanic rocks in the lower amphibolite facies (andalusite field), and is bordered by dextral transcurrent faults. The Némiscau terrane is a volcano-sedimentary mobile belt dominated by metasedimentary rocks in the upper amphibolite facies (andalusite-sillimanite field), and is bordered by sinistral transcurrent faults. However, the cordierite-anthophyllite rocks in the Némiscau terrane are associated with mafic volcanic rocks. Both the Atik Lake and Némiscau occurrences of cordierite-orthoamphibole rocks are associated with presently uneconomic

polymetallic mineralization.

The cordierite-anthophyllite rocks at Montauban are hosted by felsic gneisses in the middle-upper amphibolite facies (kyanite-sillimanite field), and are spacially associated with polymetallic massive sulfide ores. The mine sequence and the surrounding gneisses appears to have been subjected to a pre-peak metamorphism NNE tectonic transport (thrusting?).

Cordierite-orthoamphibole rocks from these three terranes are coarse grained and show a knotenschiefer (conspicuous porphyroblastic knots) texture (Spry, 1969). This texture is characteristic of post-tectonic crystallization under fairly static metamorphic conditions, a common feature in other occurrences of similar rocks (Robinson and Jaffe, 1969; Treloar et al., 1981; Elliot-Meadows and Appleyard, 1991).

CHAPTER 3.

LITHOGEOCHEMISTRY OF CORDIERITE-ORTHOAMPHIBOLE AND ASSOCIATED ROCKS AT ATIK LAKE MANITOBA, NÉMISCAU AND MONTAUBAN QUÉBEC.

Auriferous chert, banded iron formation, and related volcanogenic hydrothermal alteration, Atik Lake, Manitoba

LOUIS R. BERNIER AND WALLACE H. MACLEAN
Department of Geological Sciences, McGill University, 3450 University St., Montréal, Que., Canada H3A 2A7

Received January 20, 1989
Revision accepted July 14, 1989

Small-scale alteration pipes and stratiform alteration in Archean glomeroporphyritic tholeiitic basalts at Atik Lake, Manitoba, stratigraphically underlie silicate-oxide banded iron formation (BIF) and auriferous sulfide-bearing chert. The auriferous chert is locally interbedded with graphitic argillite, indicating euxinic conditions during deposition. Cordierite–gedrite rocks formed by recrystallization of alteration assemblages during the lower amphibolite-facies metamorphism (T = 550°C, P = 2.5 kbar). Al_2O_3, TiO_2, Zr, and Nb, which were relatively immobile during alteration, have been used to monitor igneous differentiation and alteration. Volcanogenic hydrothermal alteration resulted in depletion of Ca, Si, Mg, Na, and Sr in the altered basalt and the addition of K, Fe, Rb, and Ba. This was accompanied by mass and volume losses of up to 25%. The mineralizing fluid was reducing and somewhat acidic. Rare-earth-element (REE) profiles of BIF and graphitic argillite, normalized to Archean shale, are less steep ($(La/Lu)_N$ = 0.51 and 0.49 respectively), than those of both mineralized chert ($(La/Lu)_N$ = 0.04) and recent sea-floor, siliceous, gold-enriched massive sulfides ($(La/Lu)_N$ = 0.11). REE profiles and Boström's plot suggest that the auriferous, sulfide-bearing chert formed by mixing of hydrothermal and detrital components. The overall chemical changes in the Atik Lake alteration system are comparable to those in Noranda-type massive-sulfide deposits. The trace-metal association in the auriferous chert is similar to that at some modern sea-floor hydrothermal sites.

Une altération à petite échelle de cheminées et une altération stratiforme dans les basaltes tholéiitiques, glomeroporphyriques, d'âge archéen, au lac Atik, Manitoba, apparaissent en position stratigraphiquement sous-jacentes à une formation ferrugineuse rubanée de silicates et oxydes et à une couche de chert minéralisée en sulfures et or. Ce chert aurifère est localement interlité avec une argilite graphitique, donc un milieu euxénique de dépôt. Les roches à cordiérite–gédrite ont été formées par la recristallisation des assemblages d'altération durant une période d'activité métamorphique dans le faciès des amphibolites de faible degré (T = 550°C, P = 2,5 kbar). Les composantes Al_2O_3, TiO_2, Zr et Nb, relativement immobiles durant l'altération, ont servi de point de repère dans l'étude de la différenciation magmatique et de l'altération. L'altération volcanogénique hydrothermale a créé un appauvrissement en Ca, Si, Mg, Na et Sr dans le basalte altéré et un enrichissement en K, Fe, Rb et Ba. Le tout fut accompagné par des réductions de masse et de volume pouvant atteindre jusqu'à 25%. Le fluide minéralisateur était réducteur et quelque peu acide. Les diagrammes des terres rares de la formation ferrugineuse rubanée et de l'argilite graphitique, normalisés au shale archéen, sont moins abrupts ($(La/Lu)_N$ = 0,51 et 0,49 respectivement) que ceux du chert minéralisé ($(La/Lu)_N$ = 0,04) et également que ceux des sulfures massifs siliceux enrichis en or sur fond océanique récent ($(La/Lu)_N$ = 0,11). Les diagrammes de terres rares et le graphique de Boström suggèrent que le chert minéralisé en sulfures et en or résulte d'un mélange des composantes hydrothermale et détritique. L'ensemble des changements chimiques dans les système d'altération du lac Atik sont comparables à ceux des gîtes de sulfures massifs de type Noranda. L'association des métaux traces dans le chert aurifère est similaire à celle observée dans quelques sites actuels d'activité hydrothermale sur fond océanique.

[Traduit par la revue]

Can. J. Earth Sci. **26**, 2676–2690 (1989)

Introduction

Gold mineralization at Atik Lake, Manitoba (Fig. 1), occurs in poorly banded, sulfide-bearing chert beds associated with banded iron formation (BIF) and basaltic lavas of the Sachigo Subprovince of the Superior Province. Gold values as high as 30 g/t were encountered during an extensive mineral exploration survey by Westmin Resources Limited, but no economic orebody has yet been delineated.

The Atik Lake gold mineralization is different from reported gold occurrences in oxide-bearing BIF. The mineralization occurs within sulfide-bearing iron formation associated with silicate-oxide-bearing BIF that overlies small-scale crosscutting alteration pipes and adjacent stratiform alteration. The pipes are clustered in a circular area about 700 m in diameter within porphyritic basalt. The mineralization appears to have formed in a submarine exhalative or hot-spring setting. In other deposits, gold mineralization in oxide-bearing BIF is commonly reported to be epigenetic and related to late quartz veins and metamorphic sulfidation of iron oxides (Phillips *et al.* 1984; Lhotka and Nesbitt 1989).

This paper describes the geology, geochemistry, and genesis of the Atik Lake auriferous cherts and alteration zones and discusses them in the context of similar Archean and modern sea-floor sulfide deposits.

Regional geology

The Atik Lake belt is within the Archean Superior Province of the Canadian Shield (Fig. 1). It forms part of the Sachigo Subprovince, which is also known as the Cross Lake or God's Lake Subprovince (Weber and Scoates 1978). The geology of the area has been described by Milligan and Take (1954), Weber (1974), Weber and Scoates (1978), and Hargreaves and Ayres (1979).

The volcano-sedimentary units of the belt form a subvertical, south-facing homoclinal sequence that extends ~35 km in an east–west direction. The belt is enclosed by massive to foliated granite and granodiorite to the north and by layered tonalitic and granodioritic gneiss to the south (Fig. 2). Thick gabbro sills crosscut the volcano-sedimentary units at low angles. Pillowed, massive, and glomeroporphyritic basalts are

Printed in Canada / Imprimé au Canada

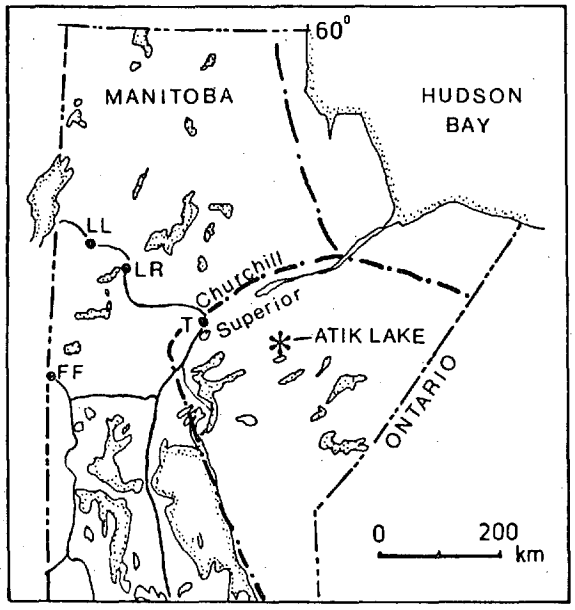

FIG. 1. Location map of the Atik Lake area. FF, Flin Flon; LL, Lynn Lake; LR, Leaf Rapids; T, Thompson.

the dominant volcanic rock types. Metasediments are mainly greywackes but include quartzite, with silty interbeds (cordierite–biotite–garnet schist), and polymictic conglomerate (Figs. 2, 3*a*). Thin BIF's occur between some of the basalt flows and pyroclastic units. Well-preserved hydrothermal alteration pipes and an associated zone of stratiform alteration, which were first recognized by Weber (1974), are present in a basaltic unit at the top of the M4 mafic sequence (Fig. 3*a*).

Northeast-trending strike-slip faults locally displace the volcano-sedimentary sequence. Localized shearing occurs along chert–basalt contacts, as indicated by granulation and deformation bands in chert beds, rotation of silicate and sulfide porphyroblasts, and rare centimetre-scale intrafolial folds.

Metamorphism

Lower amphibolite-facies metamorphism of the sediments and hydrothermally altered volcanics has produced low-variance mineral assemblages. Only one episode of prograde metamorphism has been noted in the area (Weber and Scoates 1978). Microprobe data and the garnet–cordierite geothermometer (five samples; Thompson 1976; Perchuck and Lavrent'eva 1983) have yielded temperature estimates of mineral rims of 523° ± 42°C and cores of 559° ± 29°C. A slightly lower rim temperature of 502° ± 39°C was obtained for 10 samples with the garnet–biotite geothermometer (Thompson 1976; Ferry and Spear 1978), but core temperatures (559° ± 18°C) were identical to those obtained from garnet–cordierite. Temperatures around 550°C may be inferred from the composition of arsenopyrite (34.7% As), which coexists with pyrrhotite (Sharp *et al.* 1985). The peak metamorphic temperature across the belt was fairly uniform except in the north, where it was somewhat higher (T_{rim} = 595°C; T_{core} = 632°C). The presence of andalusite and fibrolitic sillimanite in the rocks at these temperatures indicates a pressure of about 2.5 kbar (1 kbar = 100 MPa) (Holdaway 1971).

Stratigraphy

The oldest unit in the Atik belt is a hornblende gneiss, probably derived from a mafic volcanic rock. It is overlain successively by mafic to felsic agglomerates (M1, Fig. 3*a*) and by sequences of mafic flows (M2–M5) separated by beds of clastic and chemical sediments (Fig. 3*a*). Each mafic sequence is 1–3 km thick and comprises massive and pillowed, aphyric to glomeroporphyritic basalt flows averaging 10 m in thickness (Hargeaves and Ayres 1979). Three types of iron formation occur at three stratigraphic levels (Fig. 3*a*): (1) auriferous sulfide-bearing chert (hereafter referred to as auriferous chert) (Fig. 4*d*) and small massive-sulfide lenses (pyrrhotite, pyrite, sphalerite, and chalcopyrite) containing chert and schist fragments (Fig. 4*a*); (2) banded chert – magnetite (Fig. 4*b*); and (3) banded chert – grunerite–magnetite (Fig. 4*c*).

Beds of graphitic argillite (Fig. 4*e*) containing graphite flakes and anomalous gold values are present between altered footwall basalt and the auriferous chert and locally cap the chert. Pyrrhotite and pyrite form about 5% of the argillite, whereas chalcopyrite and arsenopyrite are minor constituents; gold contents average 105 ppb (5–710 ppb).

Auriferous chert

Gold mineralization is concentrated in two horizons of grey–black sulfide-bearing chert, each about 10 m thick, that lie between basaltic sequences M4 and M5 on Mistuhe Island (Figs. 3*a*–3*c*). The lower auriferous-chert horizon contains more zinc and copper and has lower gold values (20–510 ppb) than the upper horizon (50 – 12 000 ppb); other anomalously enriched elements are Ag, As, and Sb (Table 1). Alternating beds of lower grade mineralization and unmineralized BIF (totalling 40 m in thickness) occur between mafic sequences M2 and M3 (Figs. 3*a*, 3*b*). Pyrrhotite, arsenopyrite (34.7% As), pyrite, and ilmenite are disseminated or form thin to poorly defined beds in the auriferous chert. Second-generation arsenopyrite, characterized by smaller grain size (<0.05 mm) and lower As content (32%), is found in pyrrhotite veinlets, suggesting remobilization after peak matamorphism. Arsenopyrite of the same composition is also present in a thin, 10 m long lens of fuchsite schist at the contact between the altered basalt and auriferous chert. Accessory minerals in the auriferous chert include grunerite hedenbergite, actinolite, albite, carbonate, tourmaline, and apatite.

Gold assays for 10 surface samples of auriferous chert range from 3 to 30 ppm. The samples contain pyrrhotite grains with marcasite coronas, indicative of supergene weathering (Craig and Vaughan 1981). Higher gold concentrations in the near-surface samples may result from a secondary enrichment process. No visible gold was observed in polished sections of ore-zone samples, but electron-microprobe analysis revealed gold contents up to 0.25 wt.% in arsenopyrite and pyrrhotite, which may be as inclusions or in solid solution (cf. Danti *et al.* 1988).

Deformation

Most deformation was concentrated in the iron formation, as indicated by angular to subrounded fragments of wall rock in massive-sulfide lenses (Figs. 3, 4*a*) and by minor shearing in BIF. Deformation bands within chert beds in BIF and grinding, fracturing, and rotation of silicate porphyroblasts denote contrasting competencies of adjacent materials during defor-

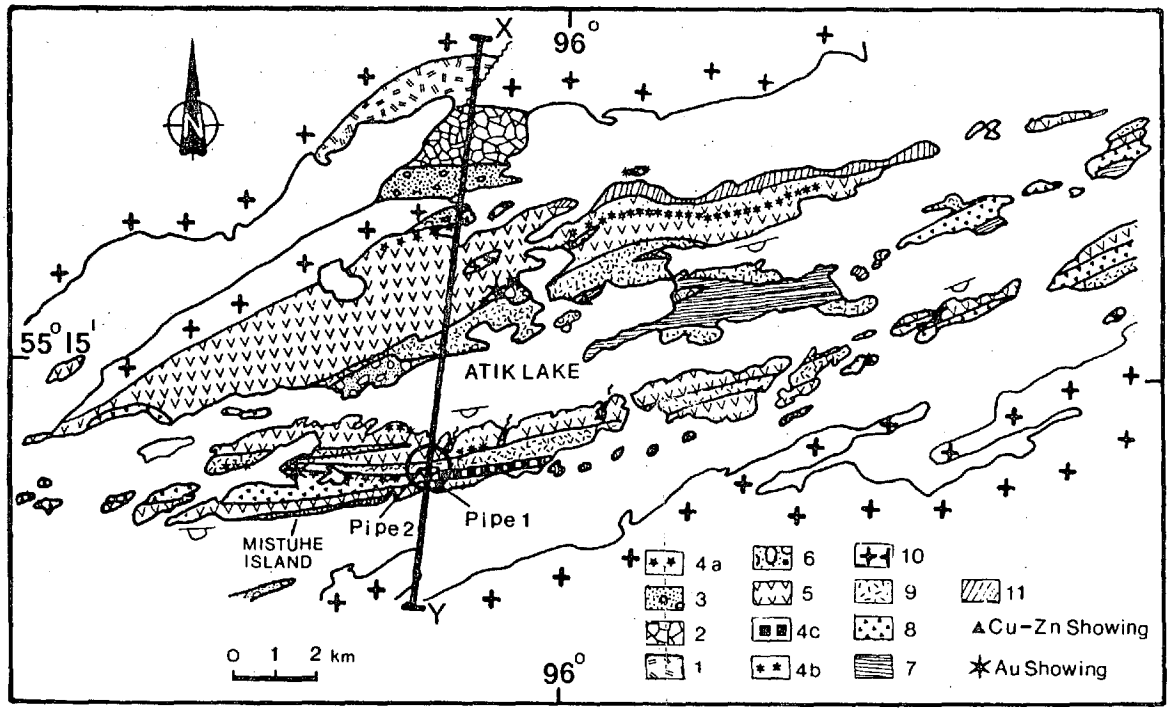

FIG. 2. Geology of the Atik Lake greenstone belt (modified from Weber 1974). (1) Amphibolite; (2) felsic agglomerate and tuff; (3) mafic pyroclastics; (4a) sulfide iron formation (auriferous chert where gold bearing); (4b) oxide BIF; (4c) silicate BIF; (5) basalt; (6) conglomerate; (7) cordierite–biotite gneiss; (8) glomeroporphyritic basalt; (9) gabbro; (10) granitic gneiss (north) and tonalitic gneiss (south); and (11) altered basalt. X–Y, section in Fig. 3.

mation. Pyrite and arsenopyrite porphyroblasts in the auriferous chert are locally fractured and rounded, owing to rotation during shearing. Pyrrhotite exhibits a ductile behaviour and has flowed along late fractures. Sulfides and silicates recrystallized during deformation and metamorphism, as indicated by triple junctions. Observations pertinent to the timing of deformation and metamorphism include the presence of pre- and synkinematic garnet porphyroblasts in deformed grunerite bands, flattened remnant plagioclase, and weak schistosity in the stratiform alteration. These textures suggest continuous minor shearing during and after peak metamorphsim.

Basalt chemistry

Methods

Sixty-four hand and drill-core samples were analyzed for major and trace elements by X-ray fluorescence spectrometry with a Philips PW 1400 instrument at McGill University. Precision is estimated to be within ±2% for major oxides and ±5% for trace elements. Ore samples from Westmin Resources Limited were assayed (inductively coupled plasma-emission spectroscopy, atomic absorption) by Chemex Labs Limited. Rare-earth-element (REE) analyses were made by instrumental neutron activation by Nuclear Activation Services, Hamilton, Ontario. Rock densities (1% reproductibility) were obtained with a Berman density-torsion microbalance (Berman 1939).

Results

The glomeroporphyritic basalt that hosts the alteration zone is composed of a metamorphic assemblage of hornblende, plagioclase (1–5% phenocrysts up to 2 cm), and accessory biotite, sphene, carbonate, and epidote. The least-altered aphyric and glomeroporphyritic basalts form an iron-enrichment trend typical of tholeiitic differenciation (Fig. 5*a*). On Ti–Zr–Sr and Ti–Zr–Y diagrams (Pearce and Cann 1973), both basalts plot within the field of ocean-floor tholeiites (Figs. 5*b*, 5*c*). The REE profile (Fig. 11*a*) is nearly flat ($(La/Lu)_N$ = 1.4), typical of tholeiites. Basalts in the footwall of the ore zone at Mistuhe Island (Figs. 3*a*, 3*c*) are slightly more differentiated (1.2–2.0 wt.% TiO_2) than in the hanging wall (0.7–1.2 wt.% TiO_2).

Alteration zones

The northern end of Mistuhe Island (Fig. 2) offers good exposures of basalt flows (M4) described by Hargreaves and Ayres (1979). The centre of the island is occupied by gabbro sills containing basalt xenoliths; its southern part, by glomeroporphyritic and pillowed-basalt flows that host auriferous chert and BIF. Three basalt flows have stratiform alteration at their contacts with iron formation, but only the glomeroporphyritic unit hosting the auriferous chert contains fracture-controlled alteration pipes.

Two types of alteration geometry are present in the mafic unit hosting the auriferous chert: crosscutting pipes within the flow; and stratiform alteration at the top of the flow below mineralized chert and graphitic argillite. The altered basalt hosting the pipes (group 1, Fig. 5*a*) is enriched in Fe, whereas basalt in the stratiform alteration zone (group 2) is depleted of Fe and enriched in K.

Three pipes, each 15–30 m wide, crosscut the basalt flow

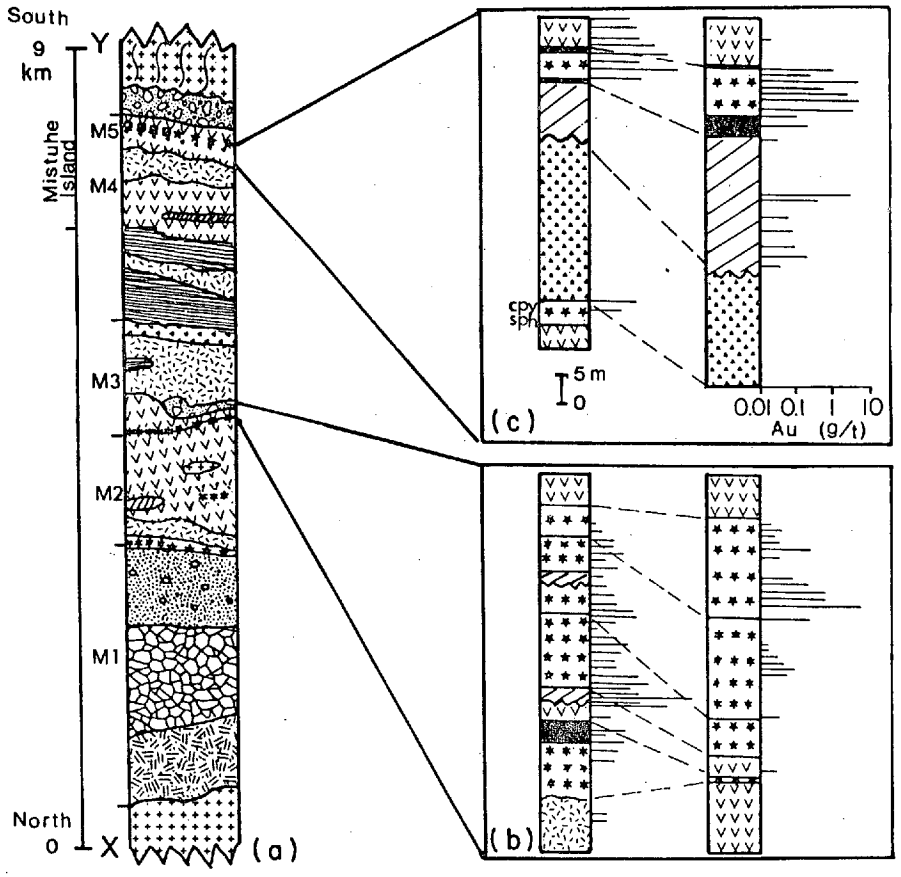

FIG. 3. (*a*) Stratigraphic section (X–Y, Fig. 2). M1–M5 mafic sequences. (*b*, *c*) Detailed sections of the BIF and auriferous cherts. Gold contents are on a logarithmic scale. The hatched symbol in *c* is the stratiform alteration zone. Black areas in *b* and *c* are graphitic argillite; cpy, chalcopyrite; sph, sphalerite. Other symbols as in Fig. 2.

over a surface strike length of 700 m. The two main pipes (1 and 2, Fig. 2) are in the same flow below the silicate-oxide BIF. The auriferous chert occurs along the same horizon as the BIF 1 km west of pipe 1, but it is not clear if this is a separate bed or reflects a facies change. The dimensions of these alteration pipes are similar to those of stockwork zones associated with hot springs on the East Pacific Rise (EPR) (Goldfarb *et al.* 1983) and East Galapagos Rift (Embley *et al.* 1988).

Pipe 1

The three central conduits within pipe 1 (Ut5, Fig. 6) cut perpendicularly across a glomeroporphyritic basalt flow and are filled with chert containing inclusions of pyrrhotite, chalcopyrite, arsenopyrite, Mn-bearing grunerite, and actinolite. The walls of the conduits are 2–5 cm thick crusts composed of Mn-rich grossular, hedenbergite, and plagioclase (An_{95}), which were probably derived from a Ca-rich mineral (carbonate?) and Fe-chlorite. Each conduit is surrounded by an inner alteration zone (Ut3) of cordierite–gedrite–garnet (initially chlorite-rich alteration) and an outer zone of bleached basalt containing quartz, albite, epidote, and hedenbergite (Ut2, Figs. 7*c*, 7*d*; Table 2). The latter grades into the darker, least-altered basalt (Ut1), composed of hornblende and plagioclase (An_{50-70}).

The cordierite–gedrite–garnet zone (Ut3) is the largest of the alteration units (Figs. 6, 7*b*). Cordierite, gedrite, and garnet are preferentially developed along polygonal fractures; traces of tourmaline occur close to the conduits walls. Scattered small grains (5–15 μm) of a chromian (<25 wt.% Cr_2O_3), zincian (<18 wt.% ZnO), and vanadiferous (<6 wt.% V_2O_3) hercynite occur in this zone.

Alteration patches rich in andalusite, quartz, and plagioclase (Ut4) are present in the upper part of the conduit and in the proximal stratiform alteration (Fig. 7*e*). Small amounts of pyrrhotite, loellingite, arsenopyrite, chalcopyrite, and sphalerite also occur in pipe 1.

Pipe 1 is capped by BIF that grades westwardly into auriferous chert and associated graphitic argillite. The BIF was also deposited in the open pipe conduits (Figs. 6, 7*a*).

Pipe 2

This alteration pipe lies 500 m west of pipe 1 at the same stratigraphic level. Alteration zoning, which is not well developed, comprises (*i*) chert in the centre with the same mineralogy as Ut5 in pipe 1, (*b*) andalusite-rich patches on the west wall (Ut4), and (*iii*) an outer cordierite–gedrite–garnet zone (Ut3). Bleached alteration (Ut2) is present only in fragments of the flow-top breccia. Pyrrhotite, loellingite, arsenopyrite, and chalcopyrite are present in the altered rocks.

Stratiform alteration

Stratiform alteration extends 2 km west from pipes 1 and 2 as

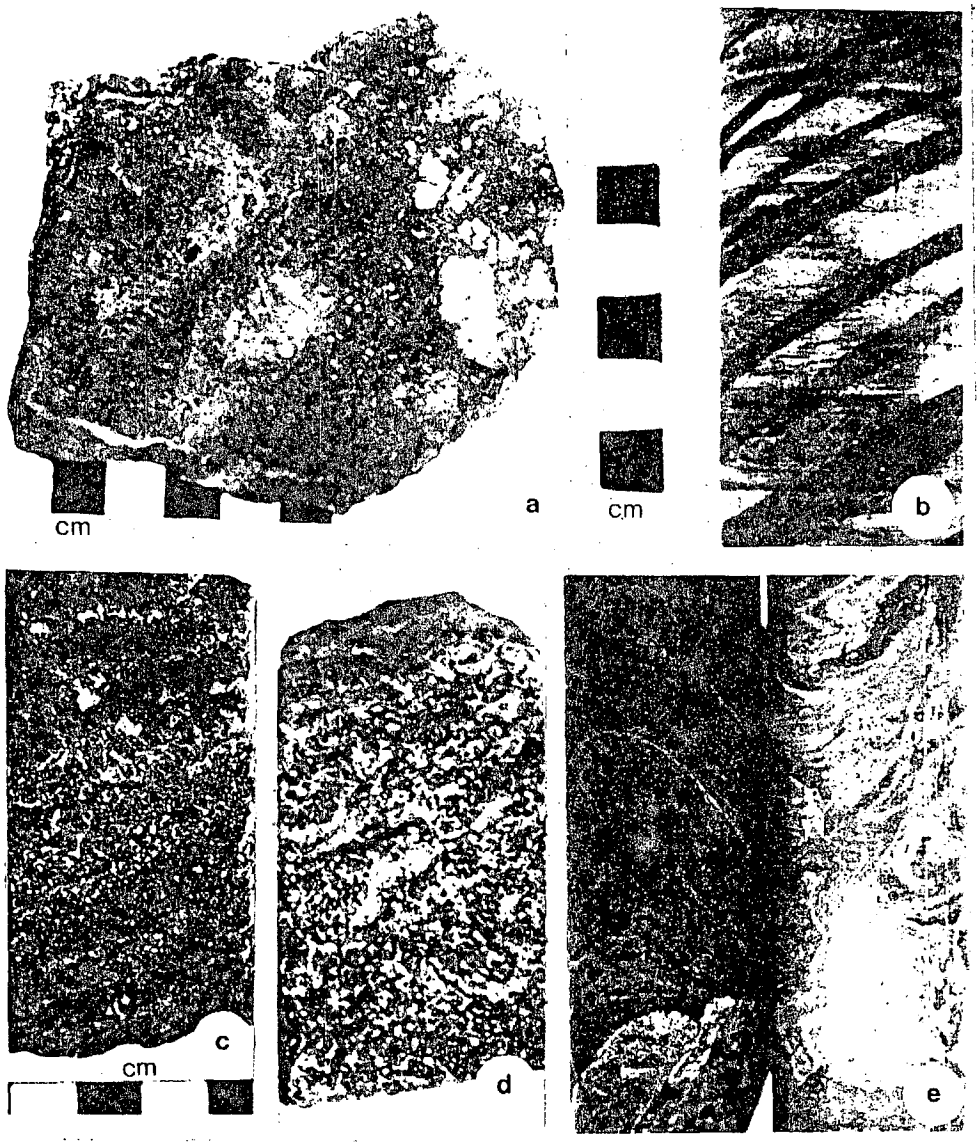

FIG. 4. Photographs of hand specimens. (*a*) Massive sulfides containing chert and schist fragments (durchbewergt texture; Gilligan and Marshall 1987). (*b*) Oxide BIF. (*c*) Silicate-oxide BIF. (*d*) Auriferous chert. (*e*) Graphitic argillite.

a zone that is generally less than 5 m thick but has a maximum thickness of 15 m. Near the pipes, this alteration is an extension of the cordierite–gedrite–garnet zone (Ut3). Within 500 m of the pipes, it grades into more potassic alteration in flow tops, with biotite, cummingtonite, and rims of reddish K-feldspar on plagioclase phenocrysts.

Some high gold values (4 ppm) have been reported in the stratiform zone, as well as disseminated pyrrhotite, chalcopyrite, and arsenopyrite (<5%).

Chemistry of hydrothermally altered basalts

Changes in basalt chemistry resulting from hydrothermal alteration were monitored with analyses of immobile elements and mass-balance calculations. Binary plots such as Al_2O_3-Zr and TiO_2-Zr were used to delineate igneous fractionation and alteration lines (Finlow-Bates and Stumpfl 1981; MacLean and Kranidiotis 1987). For a single parent rock, a linear alteration trend with a high correlation coefficient passes through the precursor rock composition and the origin (Figs. 8*a*–8*c*).

We established an igneous differentiation line for a plot of Al_2O_3-Zr (Fig. 8*a*) using the least-altered basalts of sequences M4 and M5. Samples from altered flows produced three linear alteration trends (Fig. 8*a*) that intersect precursor compositions along the differentiation line. Trend A2 is defined by altered-basalt samples from pipes 1 and 2 and adjacent stratiform alteration, whereas trends A1 and A3 are from underlying altered flows.

The TiO_2-Zr and $Nb-Zr$ plots (Figs. 8*b*, 8*c*) produce linear differentiation lines along which igneous and alteration trends are coincident.

The regression lines for Al_2O_3-Zr, TiO_2-Zr, $Nb-Zr$, and $Al_2O_3-TiO_2$ (Figs. 8*a*–8*c*, 9) have high correlation coefficients (Table 3) and pass through precursor compositions and the origin; these elements have been relatively immobile during alteration. Other element pairs with high correlation coefficients ($V-Zr$, $Cr-Zr$, $Cr-Al_2O_3$, and $Cr-TiO_2$) do not pass through the origin, suggesting some degree of mobility. TiO_2 has the highest correlations with the other elements tested and is taken to be the most immobile.

TABLE 1. Metals and trace elements in auriferous chert

Au (ppb)[a]	10–11 830
Ag[a]	0.6–3.6
As[a]	200 – > 10 000
Ba	<10–200
Cd	<0.5–14.5
Co	15–150
Cr	<1–208
Cu[a]	121 – 1 530
Zn[a]	8 – > 10 000
Mn	213 – 1 800
Pb	<2–70
Ni	50–255
P	<10 – 1 550
Sb[a]	5–580
V	<1–128
Fe (wt.%)	4.1–>15.0
Ca	0.01–1.7
Na	<0.01–0.29
K	<0.01–0.93

NOTES: Ranges based on 32 analyses. Detection limits (inductively coupled plasma spectroscopy): 0.2 ppm for Ag; 5 ppm for As and Sb; 10 ppm for P and Zn; 1 ppm for Ba, Cr, Cu, Mn, Co, Ni, and V; and 0.01 wt.% for Fe, K, Ca, and Na. Gold was analyzed by atomic absorption spectroscopy with a detection limit of 5 ppb.
[a]Anomalously enriched element.

Mass and volume calculations

Using TiO_2 as the immobile element, we made mass-balance calculations for other elements in the altered rock on the basis of 100 g of anhydrous precursor (MacLean and Kranidiotis 1987):

$$[1] \quad M_x^P = C_x^A(C_i^P/C_i^A)$$

where M is the mass in grams of a component, C is the concentration of the component, i is the immobile-element monitor, x is any other component, A is altered rock, and P is precursor rock. Grant (1986) derived a similar equation from Gresens' (1967) equation by assuming constant Al_2O_3. The ratio C_i^P/C_i^A defines an index of total mass gain or loss that can be expressed as

$$[2] \quad \Delta M = [(C_i^P/C_i^A) - 1] \times 100$$

The value of ΔM is negative for mass loss and positive for mass gain. Volume (mass/density) changes are calculated as follows:

$$[3] \quad \Delta V = [(V^A/V^P) - 1] \times 100$$

The ratio V^A/V^P in [3] is equivalent to Gresens' (1967) volume factor when immobile components are used.

A comparison of volume and mass changes for samples from pipe 1 is given in Table 4. Altered samples have volume losses ranging from 1 to 30%. Density changes (2.68–3.23 g/cm^3, Table 4) have only a very small effect on volume losses in the alteration zone, the major factor being mass variation.

Alteration pipes

Bulk-rock analyses for samples from pipes 1 and 2 are listed in Table 5. Mass and volume changes in altered basalts from pipe 1 are summarized in Table 4. Calculated changes in mass

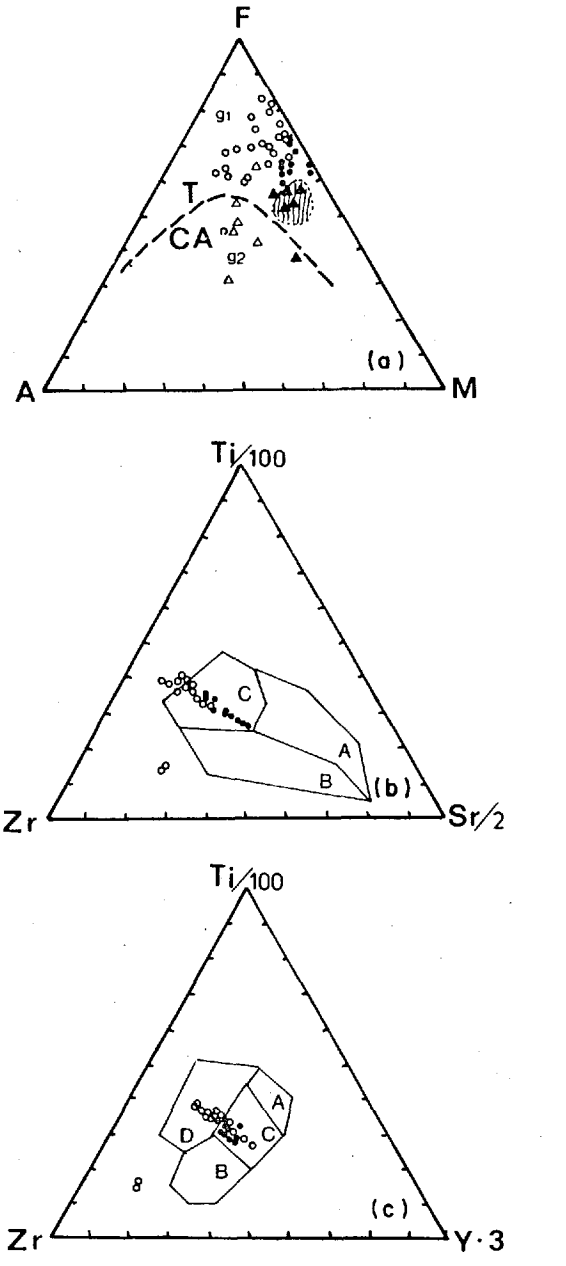

FIG. 5. (*a*) AFM diagram. T, tholeiitic; CA, calc-alkaline. Closed symbols represent least-altered rocks: ●, porphyritic basalt; ▲, aphyric basalts. Open symbols represent altered basalts: ○, pipes 1 and 2 (g1 = group 1); △, stratiform alteration (g2 = group 2). Hatched field is for 10 analyses from Hargreaves (1978). (*b*, *c*) Discriminant diagrams used to distinguish basalt types (Pearce and Cann 1973). A, low-K tholeiite; B, calc-alkaline basalt; C, ocean-floor basalt; D, intraplate basalt.

are similar whether TiO_2, Al_2O_3, or Zr is taken as the immobile component. The major change in pipe 1 is a general loss of mass (up to 24%, Fig. 10). CaO was severely leached, whereas Na_2O, SiO_2, MgO, and Y were only moderately depleted. In contrast, K_2O, Ba, and Rb were added. Fe_2O_3

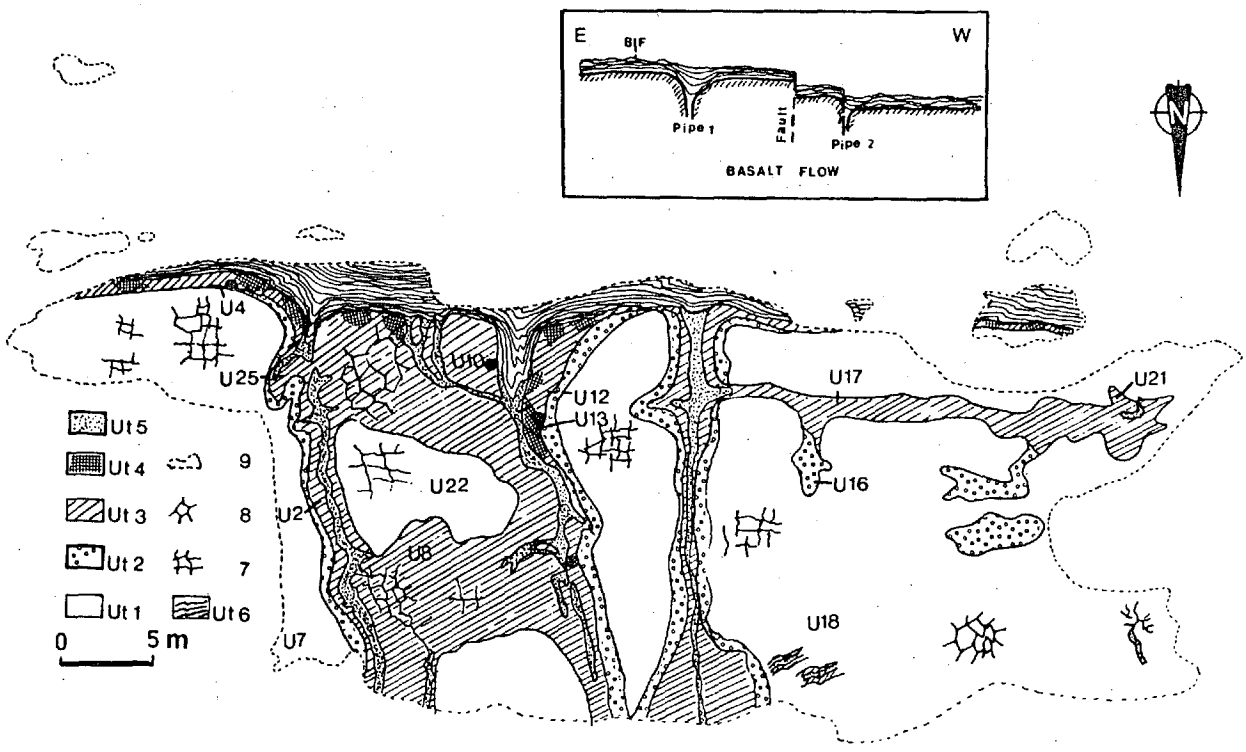

FIG. 6. Outcrop map of pipe 1. Ut1, least-altered glomeroporphyritic basalt; Ut2, bleached zone; Ut3, cordierite–gedrite–garnet zone; Ut4, andalusite-rich zone; Ut5, pipe conduits filled with chert and disseminated sulfides; Ut6, silicate-oxide BIF, showing deposition of BIF into the conduits; 7 and 8, fracture patterns; 9, outcrop limit. ●, Mg-tourmaline. Samples numbers as in Tables 2, 3, 4, and 6. The inset is a schematic diagram showing the relation between pipe 1, pipe 2, stratiform alteration (hatched symbol), and BIF.

(total Fe) was depleted in the lower part of the pipe and enriched as sulfides in the upper part and in the stratiform alteration zone.

Two samples from the andalusite-rich zone at the upper margin of pipe 2 have abnormally low TiO_2 contents; otherwise, changes are similar to those in pipe 1.

Stratiform alteration

Samples from the stratiform alteration zone record a maximum mass loss of 13%, which is about 50% of that calculated for the pipes. K_2O enrichment was greater than in the pipes, and Fe_2O_3 was depleted throughout this zone.

REE geochemistry

REE analyses (Table 6) were used to verify the tholeiitic affinity of the basalts, to compare the chemistry of Atik Lake iron formations with those of other iron formations and of modern sea-floor sulfide accumulations, and to evaluate the detrital and hydrothermal components in the auriferous chert.

The REE pattern of the least-altered basalt is relatively flat (Fig. 11*a*) and similar to those of mid-oceanic-ridge-basalt (MORB) tholeiites. The BIF and graphitic argillite, normalized to Archean shale (Taylor and McLennan 1985), have depleted light- and middle-REE (LREE, MREE) profiles (Fig. 11*b*). Such depletion has also been noted in some other Archean volcanic-hosted BIF's (Barrett *et al.* 1988), but the Atik BIF lacks their positive Eu anomaly. The slopes of the BIF and graphitic argillite profiles ($(La/Lu)_N \simeq 0.50$) are less steep than that of the auriferous chert ($(La/Lu)_N = 0.04$). Au-enriched, siliceous massive sulfides from the Green Seamount, eastern Pacific, also have a steep REE slope ($(La/Lu)_N = 0.11$, Alt 1988), suggesting that they and the auriferous chert may have similar origins.

Iron formation, chert, and argillite contain variable proportions of detrital (volcaniclastic, terrigenous) sediment and chemical precipitate from seawater or hydrothermal fluid (Barrett *et al.* 1988). The REE's in both components may have been modified and residually concentrated during hydrothermal alteration (MacLean 1988). REE mobility in pipe 1 basalts was assessed by normalizing the analytical data (Fig. 11*c*) to immobile Lu ($r_{Lu-Zr} = 0.95$), thereby compensating for mass-change effects (MacLean 1988). From this analysis, it is concluded that there was either a small depletion or enrichment of LREE's and MREE's in each of the altered samples. If it is assumed that the detrital component in the auriferous chert, BIF, and graphitic argillite is derived from the basalts, the changes in their REE patterns can be related to REE mobility. Changes in La compared with changes in mobile REE's form linear plots (Fig. 12) with slopes that are constant for each element: $\Delta REE/\Delta La = 0.70$ for Ce, 0.32 for Nd, 0.19 for Sm, 0.09 for Eu, and -0.04 for Dy. If Dy is excluded, these REE's are depleted in the altered basalts and auriferous chert and enriched in BIF and graphitic argillite. The depletion of mobile REE's in the auriferous chert may reflect the presence of an altered-basalt detrital component. The strong enrichment

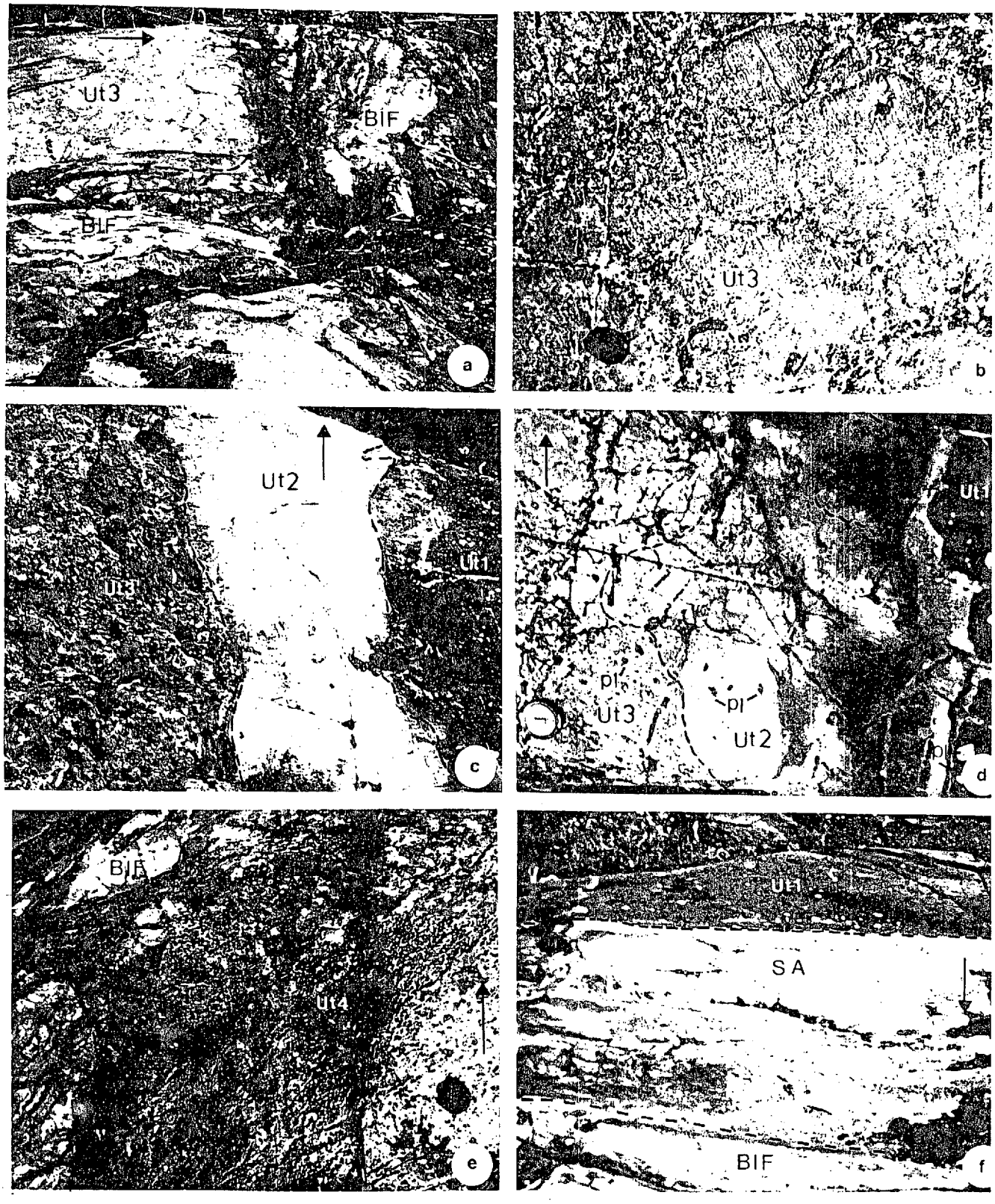

FIG. 7. Photographs of alteration zoning at pipe 1. (*a*) BIF within conduit. (*b*) Polygonal joints in basalt (Ut3, Fig. 6), with concentrations of gedrite needles. (*c*) Alteration zoning from least-altered basalt (Ut1) to bleached basalt (Ut2) and cordierite–gedrite–garnet altered basalt (Ut3). (*d*) Transition from Ut1 to Ut3; pl, plagioclase phenocrysts. (*e*) Andalusite-rich patches (Ut4). (F) Stratiform alteration (S.A.) in flow-top breccia overlying Ut1 and capped by silicate-oxide facies BIF. Arrow indicates stratigraphic top. Lens cap = 5 cm.

TABLE 2. Mineralogy of pipe 1 units (modal percents)

Sample:	U2	U4	U7	U8	U10	U12	U13	U16	U17	U18	U21	U22	U25B
Ut units:	3	3	1	3	3	3	4	2	3	1	2	1	3
Quartz	20	25	5	10	25	10	30	5	10		5		5
Plagioclase	10	15	35	20	10	4	9	45		50	20	50	5
Biotite	10	10		10	tr	5	5				15		10
Chlorite	5	9	tr		25	tr			10		10		10
Andalusite						30	45						
Garnet	5	30		5	15	15					10		15
Cordierite	20			30	20	30			30				30
Gedrite	20			15	5	tr			35		tr		15
Staurolite	tr					5							
Hercynite		tr			tr	2			tr				
Hedenbergite								5					
Epidote										tr		2	
Calcite			tr							tr		tr	
Hornblende			55					30		50	30	45	
Titanite			5									3	
Tourmaline		1					tr						
Ilmenite	10	10		10	tr	3	10	10	8		5		5
Pyrrhotite						1	tr		2		5		3
Sphalerite				tr					tr				
Chalcopyrite				tr			tr		tr				
Arsenides					tr		1	5	5				2

NOTES: See Fig. 6 for identification of Ut units. Arsenides: loellingite and arsenopyrite. Least-altered basalts: U7, U18, and U22.

in mobile REE's in BIF and graphitic argillite is probably a contribution from a hydrothermal plume.

A sea-floor exhalative origin for the Atik Lake mineralization is supported by Fe/Ti and Al/(Al + Fe + Mn) ratios for the auriferous chert; these plot on a mixing line derived by Boström (1973) for EPR-type metalliferous sediments and associated detrital components (Fig. 13.) Ratios for the graphitic argillite form a lower mixing line, indicating different detrital or hydrothermal sources. Comparable mixing lines and interpreted origins have been derived for Jurassic bedded cherts overlying ophiolites (Barrett 1981) and for Appalachian manganiferous metasediments associated with iron formations and massive-sulfide and gold deposits (Wonder *et al.* 1988).

Comparison with other alteration pipes

Archean Noranda-type alteration pipes

Mass and volume calculations have been made for the altered wall rock of the Amulet Upper A (Hall 1982) and Millenbach (Riverin and Hodgson 1980) Cu–Zn deposits in the Noranda district, Quebec. Both deposits lie within the contact-metamorphic aureole of the Dufault granite.

Hall (1982) divided the alteration at the Upper Amulet A, from core outward, into anthophyllite, cordierite, biotite, and stockwork (chlorite–biotite–actinolite) zones. These represent changes from a pre-metamorphic central chlorite zone towards a sericite-rich outer zone. Ca and Na are depleted in all parts of the pipe and are essentially absent in the core (Table 7). Silica is depleted in the core and enriched in the outer cordierite zone. Iron and Mg are enhanced throughout the pipe, but Fe and Mg are more highly concentrated in the core, and K and Ba are more highly concentrated in the biotite and stockwork zones. We calculated that the cordierite zone gained mass (15%) by silicification, whereas the anthophyllite and stockwork zones lost mass (10%). These values are in good agreement with those of Hall (1982), who assumed constant Al_2O_3 in Gresens' (1967) formula. Similar mass and chemical changes were calculated for the alteration at the Millenbach mine.

Alteration below the Helen iron formation

A 2 km wide alteration zone occurs in felsic lavas and pyroclastic flows beneath the siderite and pyrite orebodies at the Helen iron mine in the Wawa greenstone belt, Ontario (Morton and Nebel 1984). Mass and volume losses, according to our calculations, were as high as 30% in the core of the pipe (chlorite, chloritoid–andalusite, iron carbonate) and 15% in the outer quartz–sericite zone. Element changes (Table 7) agree in a general way with those determined by constant-volume calculations by Morton and Nebel (1984) using Gresens' (1967) equations and with element gains and losses listed for Mattabi-type alteration by Morton and Franklin (1987).

The Atik pipe alteration closely resembles the Noranda-type pipe alteration of Morton and Franklin (1987), whereas the stratiform alteration is comparable to their semiconformable type. Although the Atik alteration is associated with Algoma-type iron formation, it contrasts with the alteration at the Helen iron mine (Mattabi type of Morton and Franklin 1987). Morton and Franklin (1987) suggested that the Mattabi-type alteration formed in felsic pyroclastics in a shallow subaqueous or subaerial environment, whereas the Noranda type formed in bimodal volcanic rocks at considerable water depth.

Discussion

Alteration

The Atik pipes are small (30 m wide) compared with many Archean massive-sulfide pipes (200–300 m wide) but are comparable in size to those below EPR sulfide-mound deposits (Goldfarb *et al.* 1983). Basalts host the alteration pipes at Atik

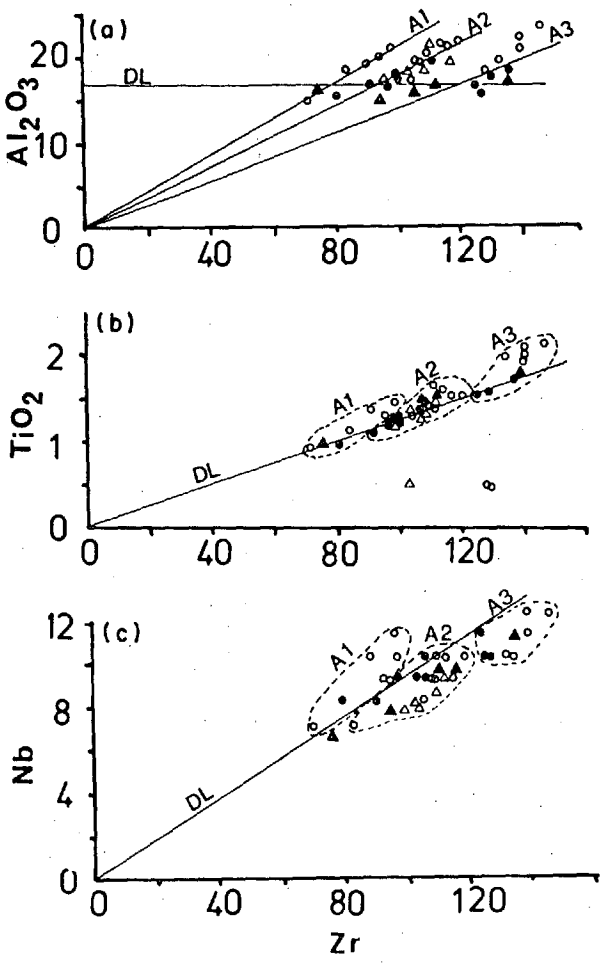

FIG. 8. (*a*) Al_2O_3–Zr diagram. DL, differentiation line; A2, alteration line for pipes 1 and 2 and stratiform alteration; A1 and A3, alteration lines for other flows. (*b*) TiO_2–Zr diagram. Alteration lines A1–A3 coincide with the differentiation line (DL) for all basalt compositions. (*c*) Nb–Zr diagram. Nb shows a distribution similar to that of TiO_2. ●, Glomeroporphyritic basalt; ▲, aphyric basalts; ○, altered basalts; △, stratiform alteration.

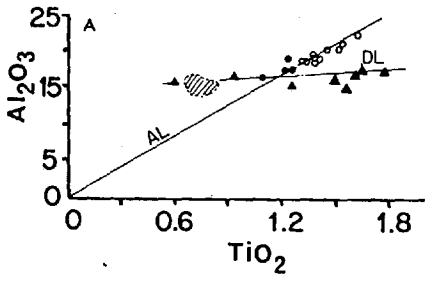

FIG. 9. Al_2O_3–TiO_2 diagram for pipe 1. Symbols as in Fig. 8. AL, alteration line. Hatched field is for 10 analyses from Hargreaves (1978).

TABLE 3. Interelement correlation matrix

	Al_2O_3	TiO_2	Zr	Nb	Y	V	Cr
Al_2O_3	1.00						
TiO_2	0.83	1.00					
Zr	0.72	0.85	1.00				
Nb	0.59	0.20	0.24	1.00			
Y	−0.24	−0.18	0.07	−0.16	1.00		
V	0.72	0.75	0.83	0.00	0.24	1.00	
Cr	0.87	0.80	0.75	0.52	−0.09	0.63	1.00

NOTES: Data from Table 5. Samples anomalously low in TiO_2 not considered.

TABLE 4. Mass and volume changes in altered basalts from pipe 1

Sample:	U4	U7	U12	U13	U17
Density(g/mL):	2.93	2.81	3.23	2.73	2.68
SiO_2 (g)	−7.12	−1.80	−5.17	14.82	−10.26
Al_2O_3	−0.85	1.21	−0.59	−0.17	−0.82
Fe_2O_3*	1.54	0.41	1.50	−7.95	−2.40
MnO	0.03	−0.01	0.00	−0.19	−0.19
MgO	−2.93	0.03	−1.85	−3.76	−1.68
CaO	−9.65	0.17	−11.46	−9.49	−7.63
Na_2O	−0.45	−0.08	−0.99	−0.51	−0.87
K_2O	0.38	0.06	0.15	0.28	−0.06
V (ppm)	−15	5	−7	−59	−46
Cr	37	36	53	64	32
Ni	5	46	−13	24	−29
Ba	204	8	18	489	34
Sr	−70	10	−114	−82	−63
Rb	11	0	4	25	−1
ΔM	−18	−1	−18	−7	−24
ΔV	−22	−1	−29	−4	−21

NOTES: Changes based on 100 g in least-altered basalt U22 (ρ = 2.80 g/mL) at constant TiO_2. Alteration types as in Table 2. ΔM, total mass change; ΔV, total volume change.

Lake and the EPR, whereas felsic volcanics host most Archean massive-sulfide alteration. Iron enrichment in the alteration zones at Atik Lake was moderate to high (Fe/(Fe + Mg) = 0.5–0.8), similar to that in Archean massive-sulfide deposits but slightly lower than in chloritoid-type alteration at the Helen iron mine (0.9). The quartz–chlorite–sericite type of alteration at Atik Lake suggests that the discharging fluids were slightly acidic. Low Fe^{3+}/Fe_{total} ratios in the altered basalt (0.03–0.21) indicate that these fluids were reduced. Overall, chemical changes in the Atik Lake system compare most closely with those in Noranda-type volcanogenic alteration pipes.

Gold in Fe-rich siliceous rocks

Nesbitt *et al.* (1987) showed that gold is leached during subseafloor hydrothermal alteration of basalts. According to Huston and Large (1989), such gold could be deposited in massive sulfides and associated Fe-rich cherts. Massive-sulfide mounds and siliceous zones surrounding the Axial Seamount and the southern Explorer Ridge have gold contents of up to 1500 ppb in association with anomalous Pb, As, Zn, Cu, Ag, and Sb values (Hannington *et al.* 1986). The metal values are similar to those in the auriferous chert at Atik Lake (Table 2). Gold is also concentrated in silica-barite formations close to massive-sulfide deposits in the Nubian Shield (Cottard *et al.* 1986), and siliceous gold-bearing ores occur in association with massive-sulfide deposits at Montauban, Quebec (Bernier *et al.* 1987). According to Huston and Large (1989),

TABLE 5. Geochemical analyses of

	Pipe 1												
	U2	U4	U7	U8	U10	U12	U13	U16	U17	U18	U21	U22	U25
SiO_2 (wt.%)	54.41	52.97	48.74	59.67	47.08	56.03	70.09	54.46	53.12	50.17	51.06	50.55	53.88
TiO_2	1.44	1.51	1.24	1.37	1.41	1.53	1.33	1.38	1.63	1.09	1.34	1.24	1.39
Al_2O_3	19.77	20.19	18.61	19.13	19.01	20.76	18.66	18.70	21.86	16.20	18.67	17.40	18.97
Fe_2O_3*	11.22	15.52	10.78	9.72	23.37	15.65	3.48	11.25	11.58	13.69	14.90	11.18	16.11
MnO	0.19	0.36	0.25	0.17	0.66	0.32	0.08	0.21	0.09	0.17	0.31	0.26	0.42
MgO	3.64	2.60	4.48	3.31	4.37	3.21	0.74	4.49	3.65	6.01	4.98	4.45	2.52
CaO	6.33	4.70	13.67	5.77	3.69	2.53	4.31	9.70	7.75	11.58	9.14	13.50	6.86
Na_2O	2.26	0.78	1.01	0.94	0.05	0.12	0.62	0.52	0.29	1.05	0.50	1.09	0.36
K_2O	0.91	0.69	0.24	0.45	0.17	0.41	0.49	0.24	0.16	0.19	0.19	0.18	0.18
P_2O_5	0.11	0.12	0.11	0.11	0.09	0.11	0.12	0.11	0.09	0.09	0.10	0.10	0.10
LOI	0.20	0.81	0.85	0.37	1.46	0.77	0.24	0.04	0.49	0.86	0.01	0.59	0.01
Total	100.48	100.25	99.98	101.01	101.36	101.44	100.16	101.17	100.71	101.10	101.20	100.54	100.80
CO_2	<0.05	0.64	0.75	<0.05	0.67	1.19	<0.05	<0.05	<0.05	0.50	<0.05	0.50	0.99
S	<0.01	0.05	0.14	0.06	0.06	0.32	0.01	0.04	0.28	0.02	0.10	<0.01	<0.01
Fe^{3+}/Fe_t	0.16	0.11	0.22	0.16	0.03	0.07	0.83	0.19	0.16	0.11	0.09	0.27	0.03
V (ppm)	365	374	327	331	361	389	282	380	364	290	348	322	368
Cr	352	400	307	344	370	399	359	333	398	241	331	270	349
Ni	170	146	161	152	121	126	149	138	113	128	139	116	133
Ba	261	278	31	125	9	51	549	180	76	28	9	23	9
Nb	9	9	10	10	9	10	10	8	19	8	9	9	9
Zr	109	116	99	107	110	120	90	107	121	91	106	99	106
Y	25	26	24	23	34	27	20	24	15	23	25	26	29
Sr	142	103	164	118	53	49	77	136	120	186	109	154	113
Rb	37	19	5	15	5	11	32	7	5	5	5	5	5

NOTES: Total iron as Fe_2O_3*. LOI, loss on ignition. Fe^{3+}/Fe_t, mole ratios of ferric to total iron. Least-altered basalts: U7, U22, P41B, P5, and U105.

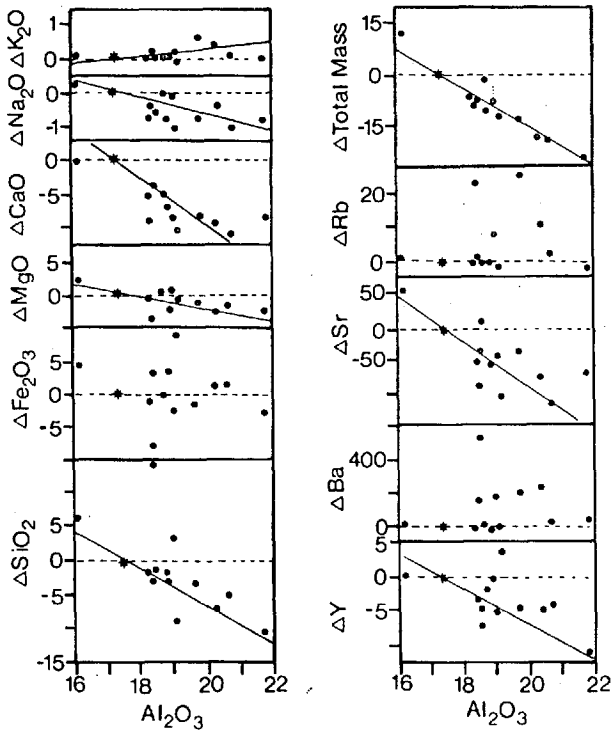

FIG. 10. Element mass changes for pipe 1 (constant TiO_2, Table 4; major elements in grams, trace elements in parts per million). Al_2O_3 is used as the alteration index; it is either concentrated by mass losses or diluted by mass gains. *, Least-altered basalt U22.

gold can be enriched in alteration pipes, in massive-sulfide ores, and in distal sulfides and cherts at different stages of mineralization.

Origin of gold in iron formation

The origin of gold deposits in iron formation is a subject of controversy. The widespread occurrence of primary gold concentrations in Algoma-type iron formation is well established (Crocket *et al.* 1981, up to 0.363 ppm Au; Saager *et al.* 1982, 0.0005–0.667 ppm Au; Gross 1988, 0.001–0.130 ppm Au). However, minable gold deposits have been found only in metamorphosed and deformed iron formation that contains crosscutting quartz veins or sulfide-rich zones in Fe-silicate or oxide layers (Phillips *et al.* 1984; Saager *et al.* 1987; Lhotka and Nesbitt 1989). Phillips *et al.* (1984) suggested that crosscutting fractures (often mineralized quartz veins) with symmetrical alteration and sulfidation fronts are evidence of an epigenetic introduction of gold into BIF. The gold is thought to have been deposited through the reaction of gold bearing, sulfur-rich fluid with an iron-rich mineral:

[4] Fe silicate + $HAu(HS)_2$ = pyrrhotite + quartz + Au + water + O_2

Reaction [4] can lead to a replacement texture involving sulfidation of iron oxides and silicates. However, the texture can also result from *in situ* sulfidation of an auriferous sulfide-bearing iron formation during metamorphism:

[5] pyrite = pyrrhotite + S_2

[6] Fe silicate + S_2 = pyrrhotite + quartz + water + O_2

least-altered and altered basalts

Pipe 2								Stratiform alteration					
P41B	P41C	P41D	P5	P2	P1	P3	P4	U102	U105	U108	U304	U508	U1602
50.44	57.79	70.32	52.37	69.18	47.85	54.25	55.53	48.23	51.78	53.42	51.42	54.23	50.60
1.16	1.29	0.45	0.85	0.42	1.45	1.15	1.26	1.42	1.29	1.38	1.44	0.58	1.25
16.17	16.97	17.41	15.25	17.01	19.96	16.01	17.82	17.33	16.62	16.65	18.04	15.16	14.78
13.14	17.14	3.84	11.19	4.36	15.91	14.66	14.68	17.50	9.06	8.83	8.43	7.77	12.01
0.17	0.29	0.11	0.16	0.12	0.46	0.45	0.36	0.26	0.37	0.26	0.23	0.14	0.23
6.65	3.57	1.71	7.84	1.94	5.16	4.10	3.18	5.48	5.68	4.57	6.21	8.97	6.21
11.29	1.60	3.02	10.52	3.33	7.92	8.57	6.49	4.71	11.69	12.56	8.18	8.98	11.47
0.19	0.32	1.18	1.73	1.53	1.31	0.51	0.77	3.16	0.49	1.18	2.60	3.37	2.62
0.14	1.59	1.24	0.12	1.38	0.21	0.27	0.39	1.11	1.44	0.27	2.18	0.15	0.18
0.09	0.09	0.12	0.09	0.11	0.12	0.10	0.09	0.11	0.10	0.11	0.12	0.14	0.10
0.42	1.08	0.59	0.32	0.65	0.08	0.07	0.12	1.01	1.64	0.60	0.87	0.43	0.12
99.86	101.73	99.99	100.47	100.03	100.43	100.14	100.69	100.32	100.16	99.83	99.72	99.75	99.88
—	—	—	—	—	—	—	—	—	—	—	—	—	—
—	—	—	—	—	—	—	—	—	—	—	—	—	—
—	—	—	—	—	—	—	—	—	—	—	—	—	—
305	383	57	215	48	373	288	317	368	336	328	370	149	342
266	367	40	267	45	308	225	285	302	266	273	347	465	204
162	164	43	111	66	135	108	156	116	126	124	116	291	80
38	81	146	60	119	133	21	70	76	135	110	375	79	104
9	9	10	8	9	8	7	7	6	6	9	7	7	7
96	104	129	101	119	105	95	100	105	98	107	110	107	96
25	36	9	20	8	31	29	29	31	22	25	22	14	26
191	64	91	149	113	113	108	136	78	141	178	100	164	139
5	54	40	7	41	9	13	18	43	66	12	65	9	18

TABLE 6. REE compositions of rocks

	U4	U7	U8	U12	U13	U109	U305	U601	U8505
La (ppm)	4.80	5.40	5.80	6.50	5.00	1.90	1.00	8.50	9.30
Ce	14	15	15	18	18	8	5	20	19
Nd	7	6	7	8	7	4	4	7	6
Sm	2.58	2.72	2.67	3.41	2.58	0.49	0.76	1.53	1.59
Eu	1.12	0.85	0.90	1.00	0.92	0.57	0.48	0.36	0.50
Tb	0.60	0.070	0.60	0.70	0.50	0.50	—	0.10	0.10
Dy	4.00	4.10	4.10	4.00	4.10	—	4.80	1.60	2.50
Ho	1.20	1.10	1.10	1.10	0.90	—	—	—	—
Yb	3.45	2.85	2.91	3.59	2.29	3.20	1.90	1.20	1.30
Lu	0.53	0.40	0.40	0.53	0.34	0.47	0.38	0.21	0.22
La/Lu	0.94	1.40	1.50	1.27	1.52	0.42	0.27	4.20	4.38
Eu/Eu*	1.17	0.89	0.97	0.87	0.95	3.09	1.68	0.62	0.84

NOTES: Detection limits (ppm) were 0.01 for Sm and Lu; 0.05 for Eu and Yb; 0.1 for La and Tb; 0.5 for Dy and Ho; and 1 for Ce, and 3 for Nd.

Both processes lead to replacement textures that cannot be readily distinguished.

Atik Lake mineralization

The gold at Atik Lake is associated with sulfides in poorly banded, sulfide-rich chert units. There are no crosscutting quartz veins or associated alteration haloes. The auriferous chert is a distinct horizon that is associated laterally with Algoma-type BIF. Pipe-like and stratiform alteration zones are prominent and are present only in the stratigraphic footwall to the mineralization (Figs. 3, 6). Basalts directly overlying the mineralization are devoid of alteration. Some samples of the stratiform alteration have elevated gold values (Fig. 3*c*, indicating that the gold mineralization was contemporaneous with the volcanogenic hydrothermal alteration. These features and the association of the gold with a specific suite of trace metals (As, Zn, Cu, Ba, and Sb) are compatible with syngenetic mineralization. The pipe alteration zones in the basalts acted as conduits through which metal-bearing hydrothermal fluids were exhaled onto the sea floor. The fluids accumulated in nearby depressions in the volcanic pile in the manner described by Sato (1972) and interacted with the upper part of the basaltic flow to form the stratiform alteration. The auriferous chert was deposited in these depressions along with graphitic argillite.

The BIF that caps pipes 1 and 2 has infilled the pipe con-

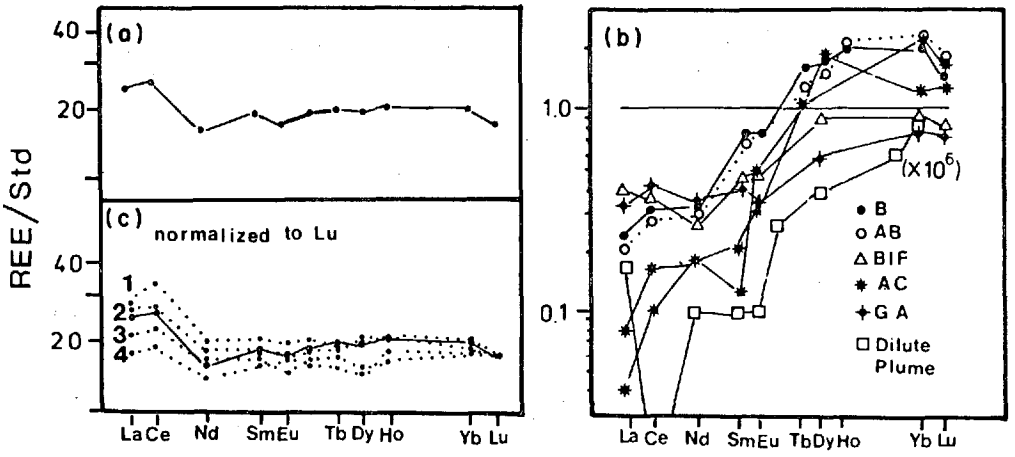

FIG. 11. (*a*) Chondrite-normalized REE profile for least-altered basalt (U7). (*b*) Archean shale-normalized REE profiles: B, basalt (U7); AB, altered basalt (U4); BIF, banded iron formation (U8505); AC, auriferous chert (U305, U109); GA, graphitic argillite (U601); Dilute plume, hydrothermal plume from 2500 m depth, Southeast Pacific Rise (Klinkhammer *et al.* 1983). (*c*) REE profiles normalized to chondrite and to the Lu value of sample U7 (solid line). The dotted profiles are from altered basalts: 1, U13; 2, U8; 3, U12; 4, U4. The normalizing standards used are the chrondrite of Evensen *et al.* (1978) and the Archean shale of Taylor and MacLennan (1985).

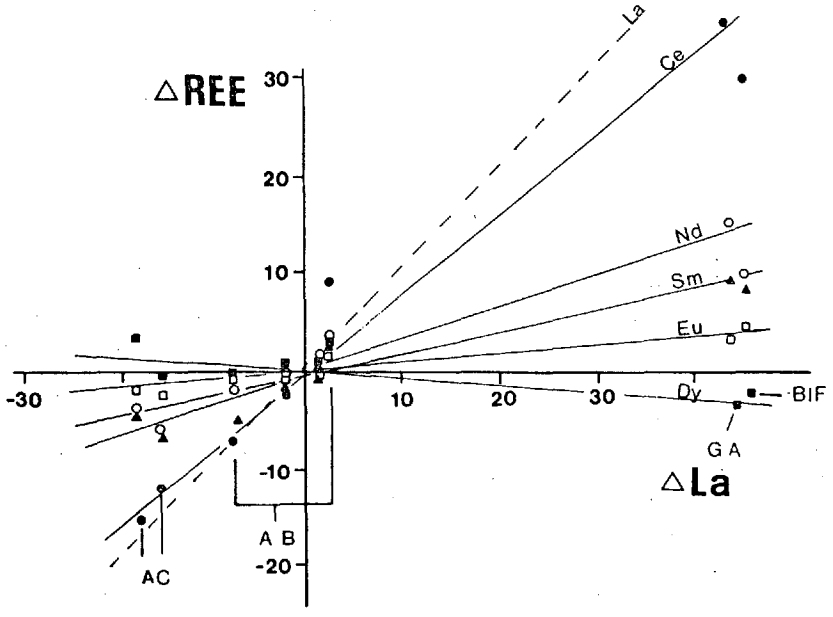

FIG. 12. Changes in chondrite-normalized REE values vs. changes in La. Abbreviations as in Fig. 11. The increase in mobility is indicated by the increase in slope values: Dy = −0.04 (■); Eu = 0.09 (□); Sm = 0.19 (▲); Nd = 0.32 (○); and Ce = 0.70 (●).

duits. Our interpretation favours deposition of BIF during or shortly after the hydrothermal activity, with contemporaneous sagging of the soft-sediment BIF into the open conduits (Figs. 6, 7*a*). The presence of graphite and sulfides in argillite interbedded with the auriferous chert indicates that local euxinic conditions prevailed during deposition. The auriferous chert was probably deposited as colloidal silica with sulfides, gold, and other trace metals. The gold content of the oxide BIF is less than 50 ppb, which is within the limits of background concentrations (Gross 1988); this suggests that gold mineralization was separate from BIF formation. These observations indicate that BIF deposition was a relatively widespread phenomenon associated with basalt volcanism, but associated syngenetic gold mineralization was less common and related to local hydrothermal exhalative centres.

Conclusions

The Atik Lake auriferous chert and associated footwall alteration were formed in a basaltic sequence in a sea-floor exhalative geothermal system and were deposited contemporaneously with Algoma-type BIF. Mass and element changes in the altered rocks are similar to those in alteration associated with Noranda-type massive sulfides. The trace-metal associa-

TABLE 7. Comparison of element gains and losses in alteration zones

Noranda massive-sulfide deposits				Algoma Fe deposit			
Amulet pipe (1)		Millenbach pipe (2)		Helen mine pipe (3)		Atik Lake	
Core	Outer	Core	Outer	Core	Outer	Pipes	Stratiform
				GAINS			
Fe	Fe	Fe	Si	Fe	K	K	K
Mg	Mg	Mg	Fe	CO_2	Fe	Fe	
K	Si	Si	Mg		Mg		
				LOSSES			
Si	Ca	Na	Na	Si	Si	Ca	Si
Ca	Na	K	Ca	Na	Na	Si	Ca
Na		Ca		Ca	Ca	Mg	Fe
				K		Na	Mg
				Mg			Na

NOTES: Elements are in decreasing order of abundance and were calculated at constant TiO_2 using data from (1) Hall (1982), (2) Riverin and Hodgson (1980), and (3) Morton and Nebel (1984).

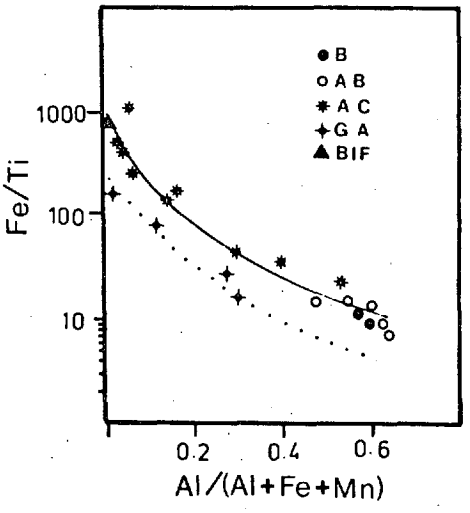

FIG. 13. Fe/Ti vs. Al/(Al + Fe + Mn) diagram (after Boström 1983) illustrating mixing between a pure hydrothermal component (low-Al/(Al + Fe + Mn)) and a detrital or basaltic component (high-Al/(Al + Fe + Mn)). Abbreviations as in Figs. 11 and 12.

tion (As, Zn, Cu, Ag, Ba, and Sb) is identical to that in modern gold-bearing, siliceous sea-floor sulfide deposits. Both BIF and auriferous chert was subjected to minor shearing but not to quartz veining or sulfidation. A syngenetic origin for the auriferous chert and associated hydrothermal alteration is favoured.

Acknowledgments

This paper represents part of a doctoral research study by the senior author at McGill University. We thank Westmin Resources Ltd., Barringer-Magenta Ltd., and Polestar Exploration Inc. for providing access to their property and for research support. Special thanks are extended to C. Rockingham for help in the field. We are indebted to T. J. Barrett for a careful review of a preliminary manuscript. The paper has also benefitted from constructive reviews by R. H. McMillan, W. Weber, P. J. MacGeehan, D. W. Ichangi, and two anonymous reviewers. Financial assistance was provided by a Formation des chercheurs et l'aide à la recherche (FCAR) scholarship to LB and by Natural Sciences and Engineering Research Council of Canada grant A7719 to WHM.

ALT, J. F. 1988. The chemistry and sulfur isotope composition of massive sulfide and associated deposits on Green Seamount, Eastern Pacific. Economic Geology, **80**: 1026–1033.

BARRETT, T. J. 1981. Chemistry and mineralogy of Jurassic bedded chert overlying ophiolites in the North Apennines, Italy. Chemical Geology, **34**: 289–317.

BARRETT, T. J., FRALICK, P. W., and JARVIS, I. 1988. Rare-earth-element geochemistry of some Archean iron formations north of Lake Superior, Ontario. Canadian Journal of Earth Sciences, **25**: 570–580.

BERMAN, H. 1939. A torsion microbalance for the determination of specific gravities of minerals. The American Mineralogist, **24**: 434–440.

BERNIER, L., POULIOT, G., and MACLEAN, W. H. 1987. Geology and metamorphism of the Montauban north gold zone: a metamorphosed polymetallic exhalative deposit, Grenville Province, Quebec. Economic Geology, **82**: 2076–2090.

BOSTRÖM, K. 1973. The origin and fate of ferromanganoan active ridge sediments. Stockholm Contributions to Geology, **27**: 149–243.

COTTARD, F., EL SAMANI, Y., CORTIAL, P., YOUNIS, M. O., DESCHAMPS, Y., HOTTIN, A. M., and VIALLEFOND, L. 1986. A new type of gold deposit: silica-barite formations associated with massive sulfide deposits in the Nubian Shield, Red Sea Hills, Sudan [abstract]. Terra Cognita, **6**: 535.

CRAIG, J. R., and VAUGHAN, D. J. 1981. Ore microscopy and ore petrography. John Wiley & Sons, New York.

CROCKET, J. H., COWAN, P., and KUSMIRSKI, R. T. M. 1981. Gold content of volcanic-hosted interflow sedimentary rocks in the Red Lake area: implications on ore genesis at the Dickenson mine. *In* Genesis of Archean volcanic hosted gold deposits. *Edited by* E. G. Pye and R. G. Roberts. Ontario Geological Survey, Miscellaneous Paper 97, pp. 128–143.

DANTI, K. J., BRIMHALL, G. H., and DONOVAN, J. D. 1988. Gold distribution at the OK Tedi porphyry copper deposit, Papua New Guinea: and electron microprobe investigation [abstract]. Geological Society of America, Abstracts with Programs, **20**: 92.

EMBLEY, R. W., JONASSON, I. R., PERFIT, M. R., FRANKLIN, J. M., TIVEY, M. A., MALAHOFF, A., SMITH, M. F., and FRANCIS, T. J. G. 1988. Submersible investigation of an extinct hydrothermal system of the Galapagos Ridge: sulfide mounds, stockwork zone, and differentiated lavas. *In* Seafloor hydrothermal alteration. *Edited by* T. J. Barrett and J. L. Jambor. The Canadian Mineralogist, **26**: 517–539.

EVENSEN, N. M., HAMILTON, P. J., and O'NIONS, R. K. 1978. Rare-earth abundances in chondritic meteorites. Geochimica et Cosmochimica Acta, **42**: 1199–1212.

FERRY, J. M., and SPEAR, F. S. 1978. Experimental calibration of the partitioning of Fe–Mg between biotite and garnet. Contributions to Mineralogy and Petrology, **66**: 113–117.

FINLOW-BATES, T., and STUMPFL, E. F. 1981. The behavior of the so-called immobile elements in hydrothermally altered rocks associated with volcanogenic submarine-exhalative ore deposits. Mineralium Deposita, **16**: 319–328.

GILLIGAN, L. B., and MARSHALL B. 1987. Textural evidence for remobilization in metamorphic environments. Ore Geology Reveiws, **2**: 205–229.

GOLDFARB, M. S., CONVERSE, D. R., HOLLAND, H. D., and EDMOND, J. M. 1983. The genesis of hot spring deposits on the East Pacific Rise, 21°N. *In* The Kuroko and related volcanogenic massive sulfide deposits. *Edited by* H. Ohmoto and B. J. Skinner. Economic Geology Monograph 5, pp. 184–197.

GRANT, J. A. 1986. The isocon diagram — a simple solution to Gresens' equation for metasomatic alteration. Economic Geology, **81**: 1976–1982.

GRESENS, R. L. 1967. Composition–volume relationships of metasomatism. Chemical Geology, **2**: 47–55.

GROSS, G. A. 1988. Gold content and geochemistry of iron-formation in Canada. Geological Survey of Canada, Paper 66-19.

HALL, B. V. 1982. Geology of the alteration pipe at the Amulet Upper A deposit, Noranda, Quebec. Canadian Journal of Earth Sciences, **19**: 2060–2084.

HANNINGTON, M. D., PETER, J. M., and SCOTT, S. D. 1986. Gold in sea-floor polymetallic sulfide deposits. Economic Geology, **81**: 1867–1883.

HARGREAVES, R. 1978. Morphology and chemistry of early Precambrian metabasalt flows, Utik Lake, Manitoba. M.Sc. thesis, The University of Manitoba, Winnipeg.

HARGREAVES, R., and AYRES, L. D. 1979. Morphology of Archean metabasalt flows, Utik Lake, Manitoba. Canadian Journal of Earth Sciences, **16**: 1452–1466.

HOLDAWAY, M. J. 1971. Stability of andalusite and the aluminum silicate phase diagram. American Journal of Science, **278**: 143–153.

HUSTON, D. L., and LARGE, R. R. 1989. A chemical model for the concentration of gold in volcanogenic massive sulfide deposits. Ore Geology Reviews, **4**: 171–200.

KLINKHAMMER, G., ELDERFIELD, H., and HUDSON, A. 1983. Rare earth elements in seawater and near hydrothermal vents. Nature (London), **305**: 185–188.

LHOTKA, P. G., and NESBITT, B. E. 1989. Geology of unmineralized and gold-bearing iron formation, Contwoyto Lake – Point Lake region, Northwest Territories, Canada. Canadian Journal of Earth Sciences, **26**: 46–64.

MACLEAN, W. H. 1988. Rare earth element mobility at constant inter-Ree ratios in the alteration zone at the Phelps Dodge massive sulphide deposit, Matagami, Quebec. Mineralium Deposita, **23**: 231–238.

MACLEAN, W. H., and KRANIDIOTIS, P. 1987. Immobile elements as monitors of mass transfer in hydrothermal alteration: Phelps Dodge massive sulfide deposit, Matagami, Quebec. Economic Geology, **82**: 951–952.

MILLIGAN, G. C., and TAKE, W. F. 1954. Geology of the eastern Bear Lake area. Manitoba Department of Mines and Natural Resources, Publication 53-1.

MORTON, R. L., and FRANKLIN, J. M. 1987. Two-fold classification of Archean volcanic-associated massive sulfide deposits. Economic Geology, **82**: 1057–1063.

MORTON, R. L., and NEBEL, M. 1984. Hydrothermal alteration of felsic rocks at the Helen siderite deposit. Wawa, Ontario. Economic Geology, **79**: 1319–1333.

NESBITT, B. E., ST. LOUIS, R. M., and MUEHLENBACHS, K. 1987. Distribution of gold in altered basalts of DSDP hole 504B. Canadian Journal of Earth Sciences, **24**: 201–209.

PEARCE, J. A., and CANN, J. R. 1973. Tectonic setting of basic volcanic rocks determined using trace elements analysis. Earth and Planetary Science Letters, **19**: 290–300.

PERCHUCK, L. L., and LAVRENT'EVA, I. V. 1983. Experimental investigation of exchange equilibria in the system cordierite–garnet–biotite. *In* Kinetics and equilibria in mineral reactions. *Edited by* E. D. Saxena. Springer-Verlag, New York, Advances in Geochemistry, Vol. 3, pp. 198–240.

PHILLIPS, G. N., GROVES, D. I., and MARTYN, J. E. 1984. An epigenetic origin for Archean banded iron-formation-hosted gold deposits. Economic Geology, **79**: 162–171.

RIVERIN, G., and HODGSON, C. J. 1980. Wall-rock alteration at the Millenbach Cu–Zn mine, Noranda, Quebec. Economic Geology, **75**: 424–444.

SAAGER, R., MEYER, M., and MUFF, R. 1982. Gold distribution in supracrustal rocks from Archean greenstone belts of southern Africa and from Paleozoic ultramafic complexes of the European Alps: metallogenic and geochemical implications. Economic Geology, **77**: 1–24.

SAAGER, R., OBERTHUR, T., and TOMSCHI, H. P. 1987. Geochemistry and mineralogy of banded iron-formation-hosted gold mineralization in the Gwanda greenstone belt, Zimbabwe. Economic Geology, **82**: 2017–2032.

SATO, T. 1972. Behaviors of ore-forming solutions in seawater. Mining Geology, **22**: 31–42.

SHARP, A. D., ESSENE, E. J., and KELLY, W. C. 1985. A re-examination of the arsenopyrite geothermometer: pressure considerations and applications to natural assemblages. The Canadian Mineralogist, **23**: 517–534.

TAYLOR, S. R., and MCLENNAN, S. M. 1985. The continental crust: its composition and evolution. Geoscience Texts, Blackwell Scientific Publications, Oxford.

THOMPSON, A. B. 1976. Mineral reactions in pelitic rocks: II. Calculations of some $P-T-X(Fe-Mg)$ phase relations. American Journal of Science, **276**: 425–454.

WEBER, W. 1974. Utik Lake – Bear Lake project. *In* Summary of geological field work 1974. *Edited by* R. F. J. Scoates. Manitoba Mineral Resources Division, Exploration and Geological Survey Branch, Geological Paper 2–74, pp. 27–32.

WEBER, W., and SCOATES, R. F. J. 1978. Archean and Proterozoic metamorphism in the northwestern Superior Province and along the Churchill–Superior boundary, Manitoba. *In* Metamorphism in the Canadian Shield. *Edited by* J. A. Fraser and W. W. Heywood. Geological Survey of Canada, Paper 78-10, pp. 516.

WONDER, J. D., SPRY, P. G., and WINDOM, K. E. 1988. Geochemistry and origin of manganese-rich rocks related to iron-formation and sulfide deposits, western Georgia. Economic Geology, **83**: 1070–1081.

3B. ADDENDUM

This *Addendum* contains data on the Atik Lake terrane that were not included in the published paper (Bernier and MacLean, 1989). The data are on the geochemistry and mineral characteristics of the metasedimentary cordierite-anthophyllite rocks, and include information on metal (Au, Cu, Zn, As, Co) distribution in the alteration zones.

CORDIERITE-ORTHOAMPHIBOLE ROCKS OF DUAL ORIGINS

Apart from the cordierite-orthoamphibole rocks formed by metamorphism of the hydrothermally altered basalts, there is an occurrence of cordierite-anthophyllite rocks of sedimentary origin in the Atik Lake belt. Milligan and Take (1954) described a nodular cordierite±anthophyllite gneiss with an unusual chemistry, which they considered to be "The oustanding metamorphic problem of the area, ...". They described this gneiss as being rich in Mg and Fe, poor in the alkalis and Ca, and opted for a sedimentary origin mainly because it was interbedded with quartzite and conglomerate. Weber (1974) used the term volcanogenic metasediment to describe this cordierite gneiss unit.

The presence of two types of cordierite-orthoamphibole rocks at Atik Lake offers an opportunity to compare the petrographic and chemical characteristics of those derived from hydrothermally altered rocks with those from sedimentary rocks. It also allows the possibility of assessing the origin of the sedimentary detrital components.

The most striking petrographic features of the cordierite-anthophyllite rocks from the central sedimentary sequence are the large size of the

cordierite nodules (1-2 cm) and the dominance of cordierite over anthophyllite. In contrast, cordierite-orthoamphibole rocks derived from the altered basalts are characterized by dark green rosettes of gedrite (±anthophyllite) which are more abundant than the fine grained cordierite. Gedrite was not found in the sedimentary-derived rocks. There are also chemical differences between the two types of cordierite-orthoamphibole rocks.

Table 3B.1 Comparison of some chemical components of the two types of cordierite-orthoamphibole rocks.

	Metasediments (n=6)		Altered Basalts (n=12)	
	ave.	σ	ave.	σ
K_2O (wt%)	2.72	0.98	0.50	0.38
Na_2O	0.93	0.40	0.78	0.86
CaO	2.21	1.82	6.31	1.77
$Fe_2O_3^{tot}$	8.70	2.36	13.84	3.41
TiO_2	0.72	0.15	1.49	0.24
Rb (ppm)	70	21	18	15
Y	15	4	26	5

Those derived from altered basalts contains larger concentrations of $Fe_2O_3^{tot}$, CaO, TiO_2 and Y, and less K_2O, Rb and Na_2O than those derived from the metasediments.

Reinhardt (1987) and Beeson (1988) used the AFM diagram to distinguish Mg-rich cordierite-anthophyllite rocks of metasedimentary origin from the generally more Fe-rich metamorphosed altered volcanic rocks. However, the AFM diagram is not always a good discriminant, since altered volcanic rocks can also be Mg-rich owing to the presence of Mg-rich chlorite or talc in the

pre-metamorphic hydrothermal alteration assemblage (c.f., Roberts and Reardon, 1978; Franklin et al., 1981; Urabe et al., 1983; MacLean and Kranidiotis, 1987; Elliot-Meadows and Appleyard, 1991; Montauban, in section 3F).

Cordierite-anthophyllite rocks of sedimentary origin have been studied in other terranes. Those at Mary Kathleen, Queensland are interpreted to be metamorphosed magnesian shale or alkali- and Ca-poor pelites in a carbonate-evaporite-pelite sequence (Ramsay and Davidson, 1974). Kamineni (1975, 1979) interpreted the cordierite-gedrite rocks near Yellownife to be meta-greywacke and meta-argillite. Arnold and Sandiford (1990) proposed a model of synmetamorphic K_2O removal by advecting fluids in semi-pelitic rocks for the origin of cordierite-gedrite rocks from Springton, South Australia.

None of the above studies used HFS trace element signatures to interpret the origin of the rocks, and HFS data is unfortunately not provided by these authors. A new approach to the identification of protolith of cordierite-anthophyllite rocks is presented in the section after this *Addendum*.

METAL DISTRIBUTION IN MISTUHE ISLAND ALTERATION ZONES

The metal concentrations in altered basalts and BIF samples from pipe 1 and pipe 2 on Mistuhe Island are listed in Table 3B.2. Four samples of least altered basalts (U-18, U-22, BI-05, U1602) have comparable metal concentrations averaging (in ppm) 96 Ni, 87 Co, 64 Cu, 83 Zn, 8 As, and 5 ppb Au, which are taken as background values. Altered basalts samples contain an average of 2 ppb gold suggesting that the altering hydrothermal fluid (regardless of origin) was capable of leaching gold. Copper and zinc are also below background values in some altered basalt samples and are enriched in others (Table 3B.2). Arsenic has been added to the altered basalts in the

upper part of pipe 1 and in the altered flow-top breccia at pipe 2.

TABLE 3B.2 Metal Concentrations in Mistuhe Island Rocks.

PIPE 1

Sample	Fe	Mn	Ni	Co	Cu	Zn	As	Au
U-18	9.57	0.04	128	93	87	85	17	5
U-22	7.82	0.14	116	79	39	93	5	5
U-07	7.54	0.17	161	93	166	102	37	6
U-02B	17.83	0.10	170	70	11	82	39	4
U-04	10.91	0.19	146	112	10	166	346	2
U-08	6.80	0.09	152	65	83	183	27	8
U-10	16.35	0.35	121	154	10	151	502	1
U-12	10.95	0.17	126	103	219	184	74	3
U-13	2.43	0.04	149	35	31	20	194	2
U-16	7.87	0.11	138	101	37	104	5	1
U-17	8.10	0.05	113	68	110	104	5	1
U-21	10.42	0.14	139	94	13	108	12	1
U-25B	11.27	0.22	133	103	10	118	350	1

PIPE 2

Sample	Fe	Mn	Ni	Co	Cu	Zn	As	Au
BI-05	7.83	0.09	60	84	45	69	5	5
BI-01	11.13	0.23	135	119	86	131	28	1
BI-02	3.04	0.06	66	15	26	66	6	1
BI-03	10.25	0.24	21	109	10	200	646	3
BI-04	10.27	0.19	156	124	10	171	927	1
U41B	9.19	0.09	162	93	10	75	8	n.a.
U41C	11.99	0.15	164	120	93	171	282	n.a.
U41D	2.69	0.06	43	27	19	64	27	n.a.

STRATIFORM ALTERATION

Sample	Fe	Mn	Ni	Co	Cu	Zn	As	Au
U1602	8.40	0.12	80	93	84	84	5	n.a.
U0102	12.24	0.14	112	122	95	106	2578	29
U0105	6.34	0.20	126	67	107	105	461	n.a.
U0108	6.18	0.14	124	80	100	94	67	n.a.
U0304	5.90	0.12	116	55	164	71	40	n.a.
U0508	5.43	0.07	291	47	41	47	5	14

TABLE 3B.2 (SUITE)

AURIFEROUS CHERT

Sample	Fe	Mn	Ni	Co	Cu	Zn	As	Au
U0109	18.63	0.90	215	216	210	426	24300	2100
U0305	25.42	0.38	334	234	412	104	60100	870
U0125	16.66	0.17	50	18	133	1085	7340	4110
U0346	16.49	0.07	86	41	200	44	9680	3770
U0554	25.35	0.16	110	32	293	1550	2590	2330
U0581	22.16	0.11	110	49	748	3730	1105	550
U1156	9.76	0.65	75	34	448	630	5210	3980

Fe and Mn are in %, Au in ppb and other metals concentrations are in ppm. Least altered basalts: U-18, U-22, BI-05 and U1602; Cordierite-gedrite rocks: U-10, U-17, U-25B, BI-03, BI-04; Gedrite-garnet-rocks: U-08, U-02B, U-21; Aluminous alteration: U-12, U-13, U-41C, U-41D, BI-02; Cordierite-chlorite rock: U-04; Biotite-bearing altered basalt: U0102, U0105, U0108, U0304, U0508

The metal enrichment factors (concentration in altered basalt/concentration in least altered basalt) are low except for arsenic (Table 3B.3). Enrichment factors for most elements are much higher in the mineralized chert.

Table 3B.3 Enrichment Factors in Atik Rocks

	Fe	Mn	Ni	Co	Cu	Zn	As	Au
Pipe 1	1.3	1.4	1.1	1.1	1.0	1.4	18	0.5
(n=11,σ)	0.5	0.7	0.1	0.4	1.1	0.5	21	0.3
Pipe 2	1.0	1.6	1.8	1.4	0.7	2.0	55	0.3
(n=7,σ)	0.5	0.8	0.9	0.6	0.6	0.9	69	0.2

TABLE 3B.3 (Suite)

	Fe	Mn	Ni	Co	Cu	Zn	As	Au
Stratiform	0.9	1.1	1.9	0.8	1.2	1.0	126	4.0
Alteration	0.5	0.4	0.8	0.3	0.5	0.3	198	(2 samples)
(n=5, σ)								
Auriferous	2.3	3.0	1.4	1.0	5.5	13	2147	348
Chert	0.6	0.5	1.0	0.9	3.0	14	2542	168
(n=7, σ)								

Bernier and MacLean (1989) concluded that the hydrothermal fluid responsible for the alteration was slightly acidic and reduced. The fluid apparently leached base metals and gold from the basalts, and also Si, Ca, Mn, Fe, Mg, As, S. These elements were probably exhaled onto the paleoseafloor, and they now occur in metmamorphosed mineralized chert as quartz, Mn-grunerite, actinolite, hedenbergite, Mn-garnet, calcite, sulfides and arsenides. Similar mineral assemblages are reported by Luff et al. (1992) in mineralized and metamorphosed iron formation that caps the Brunswick No. 12 polymetallic massive sulfide deposit.

3C. A NEW APPROACH TO PROTOLITH IDENTIFICATION USING LOG(RATIO) DIAGRAMS: APPLICATION TO THE ATIK LAKE ROCKS.

The problem of protolith identification in metamorphosed terranes is closely related to our ability to determine whether some elements were immobile during metamorphism. Identification of the protoliths of altered rocks by available procedures using immobile elements is complicated by the need to demonstrate that the rocks are derived from an initially chemically homogeneous precursor (Akella, 1966; Kerrich, 1982; MacLean, 1990).

IMMOBILITY OF ELEMENTS IN METAMORPHIC TERRANES.

The immobility of Al, Ti, Cr, V and HFS trace elements (Zr, Y and Nb) during low-grade metamorphism and volcanogenic hydrothermal alteration has largely been inferred by workers on the basis of qualitative interpretation or constant ratios of some of these elements (Finlow-Bates and Stumpfl, 1981; 1982; Costa et al., 1983; Dostal and Strong, 1983; Etheridgeet al., 1983; Robinson, 1984; Howard and Fisk, 1988; Elliot-Meadows and Appleyard, 1991; Tuisku, 1992). Finlow-Bates and Stumpfl (1981) qualitatively outlined a method to identify altered rock protoliths using the intersection point of alteration and magmatic differentiation trends on a TiO_2-Zr diagram (e.g. their Fig. 8). This approach is similar to the quantitative method outlined by MacLean and Kranidiotis (1987) to test for the immobility of Al, Ti and HFS elements. Other workers have used constant element ratios to identify protoliths of altered rocks associated with gold veins and massive sulfide deposits (Kerrich, 1982; Vance and Condie, 1987; Whitford et al. 1989).

Very few studies have been made to assess Al, Ti and trace element immobility in higher metamorphic facies. Carmichael (1969) presented textural

and chemical evidence that the distance of migration of aluminum is small during metamorphic reactions in metapelitic rocks. However, Kerrick (1988) argued that Al can be mobilized as alkali-aluminum complexes during metamorphic segregations. In a different metamorphic system, Galbreath et al, (1988) concluded that Al, Ti and Nb exhibited a consistent behavior, and thus were fairly immobile in alteration associated with a synmetamorphic quartz-graphite vein in low-sillimanite grade quartz-mica schists. More recently, Tuisku (1992) used Al and Cr as immobile elements in a study of chemical diffusion at the contact between amphibolite and metapelite and found low mobility for Mg, Mn, Ni, P, Zr and Hf.

Enrichments in inert components (Al, HSFE) have been reported during syn-metamorphic shearing (Winchester and Max, 1984; Dipple et al., 1990). Similar enrichments in mylonites from Hot Spring Windows, North Carolina and the Fries fault, southern Appalachians have been modelled through volume losses (immobility hypothesis) and a combination of volume losses and partitioning to a metamorphic fluid (O'Hara, 1988; O'Hara and Blackburn, 1989).

It has been established that Al, Ti, V, Cr and HSFE (except Y) were immobile during lower-amphibolite facies metamorphism of the alteration zone in basalt at Atik Lake (Bernier and MacLean, 1989, Bernier, 1990). It was concluded that mass changes were coincident with volume changes during the pre-metamorphic hydrothermal alteration. This contrasts with the results of Riverin and Hodgson (1980) who assumed that volume remained constant and Al was mobile during hydrothermal alteration at the metamorphosed alteration zone of the Millenbach mine, Noranda.

Conflicting interpretations often result from different starting assumptions using Gresens (1967) equations and, it appears necessary to

constrain the mathematics with geological observations (Grauch, 1988). The following Log(Ratio) method was designed to assist in the recognition of the protoliths of a wide variety of rocks in metamorphic terranes.

THE Log(Ratio) METHOD

A technique to assess the nature of the protoliths of cordierite-orthoamphibole rocks and other products of hydrothermal alteration was designed using the whole-rock data from the three terranes examined in this thesis. The technique utilizes inter-element ratios of Al_2O_3, TiO_2, Cr, V and HFSE plotted on a spider-type diagram (Fig. 3C.1). As discussed above, these elements are commonly immobile in hydrothermal alteration associated with massive sulfide deposits and during metamorphism. The technique is a modification of one used by Kerrich (1982) who plotted Log values of absolute abundances of Al, Ti, V, Zr, Sc and Y in decreasing order. Kerrich's plot produced a series of parallel profiles for over-all dilution or residual enrichment of these components during hydrothermal alteration in single precursor rock systems.

In the method presented here, the ratios of the elements are plotted as Log values and arranged in a decreasing order to generate a characteristic sloping profile. Samples of altered rocks derived from a single chemically homogeneous precursor form a consistent single line trend. Hence, the immobility is tested using nine element pairs on one diagram. The smallness of the departures from the single trend is a test for the homogeneity of the precursor. Altered rock profiles can be compared to a variety of precursors profiles to find a suitable match.

Samples of least altered metabasalt flows from Atik Lake have closely identical profiles (Fig. 3C.1A). They are also very similar to profiles of

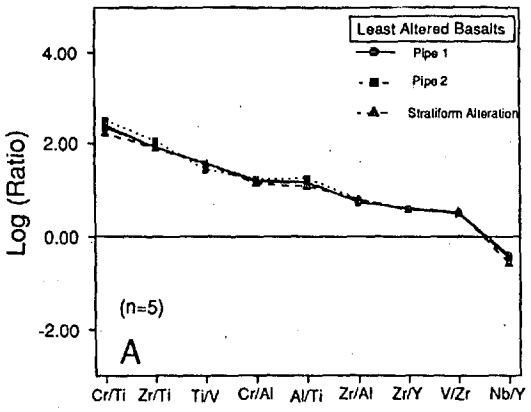
Least Altered Basalts
Pipe 1
Pipe 2
Stratiform Alteration
Log (Ratio)
4.00
2.00
0.00
-2.00
(n=5)
A
Cr/Ti Zr/Ti Ti/V Cr/Al Al/Ti Zr/Al Zr/Y V/Zr Nb/Y

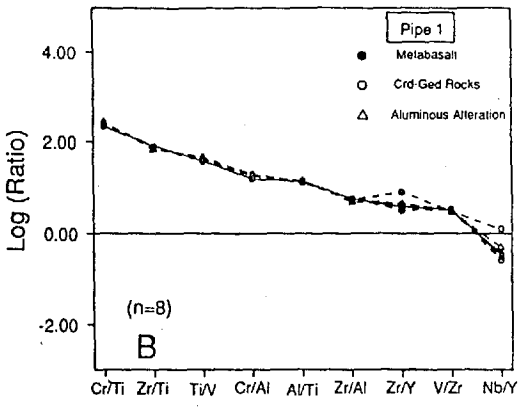
Pipe 1
Metabasalt
Crd-Ged Rocks
Aluminous Alteration
Log (Ratio)
4.00
2.00
0.00
-2.00
(n=8)
B
Cr/Ti Zr/Ti Ti/V Cr/Al Al/Ti Zr/Al Zr/Y V/Zr Nb/Y

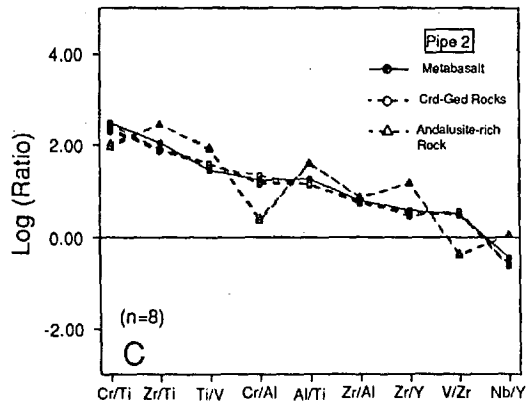
Pipe 2
Metabasalt
Crd-Ged Rocks
Andalusite-rich Rock
Log (Ratio)
4.00
2.00
0.00
-2.00
(n=8)
C
Cr/Ti Zr/Ti Ti/V Cr/Al Al/Ti Zr/Al Zr/Y V/Zr Nb/Y

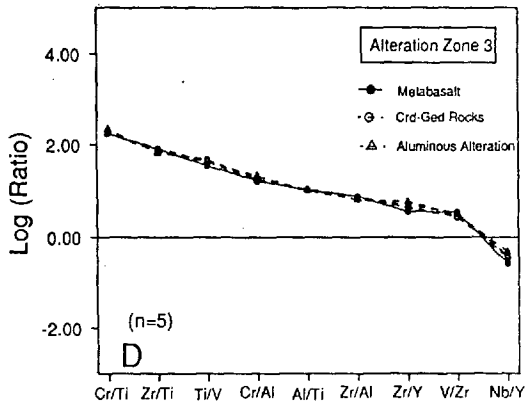
Alteration Zone 3
Metabasalt
Crd-Ged Rocks
Aluminous Alteration
Log (Ratio)
4.00
2.00
0.00
-2.00
(n=5)
D
Cr/Ti Zr/Ti Ti/V Cr/Al Al/Ti Zr/Al Zr/Y V/Zr Nb/Y

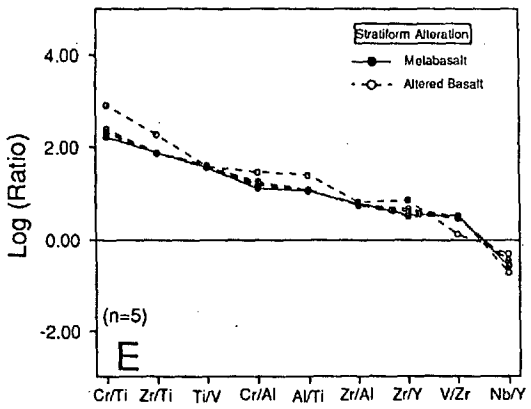
Stratiform Alteration
Metabasalt
Altered Basalt
Log (Ratio)
4.00
2.00
0.00
-2.00
(n=5)
E
Cr/Ti Zr/Ti Ti/V Cr/Al Al/Ti Zr/Al Zr/Y V/Zr Nb/Y

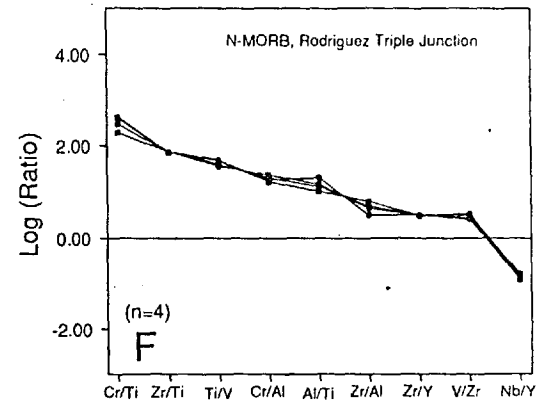
N-MORB, Rodriguez Triple Junction
Log (Ratio)
4.00
2.00
0.00
-2.00
(n=4)
F
Cr/Ti Zr/Ti Ti/V Cr/Al Al/Ti Zr/Al Zr/Y V/Zr Nb/Y

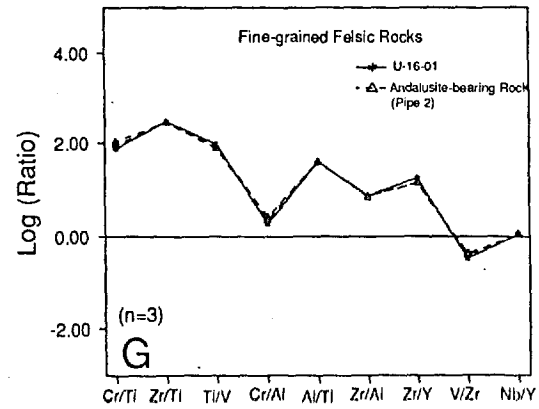
Fine-grained Felsic Rocks
U-16-01
Andalusite-bearing Rock (Pipe 2)
Log (Ratio)
4.00
2.00
0.00
-2.00
(n=3)
G
Cr/Ti Zr/Ti Ti/V Cr/Al Al/Ti Zr/Al Zr/Y V/Zr Nb/Y

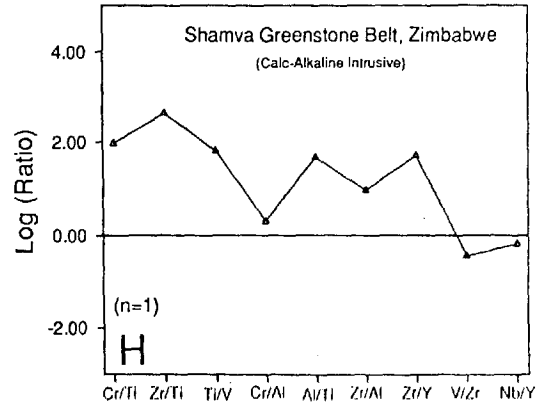
Shamva Greenstone Belt, Zimbabwe
(Calc-Alkaline Intrusive)
Log (Ratio)
4.00
2.00
0.00
-2.00
(n=1)
H
Cr/Ti Zr/Ti Ti/V Cr/Al Al/Ti Zr/Al Zr/Y V/Zr Nb/Y

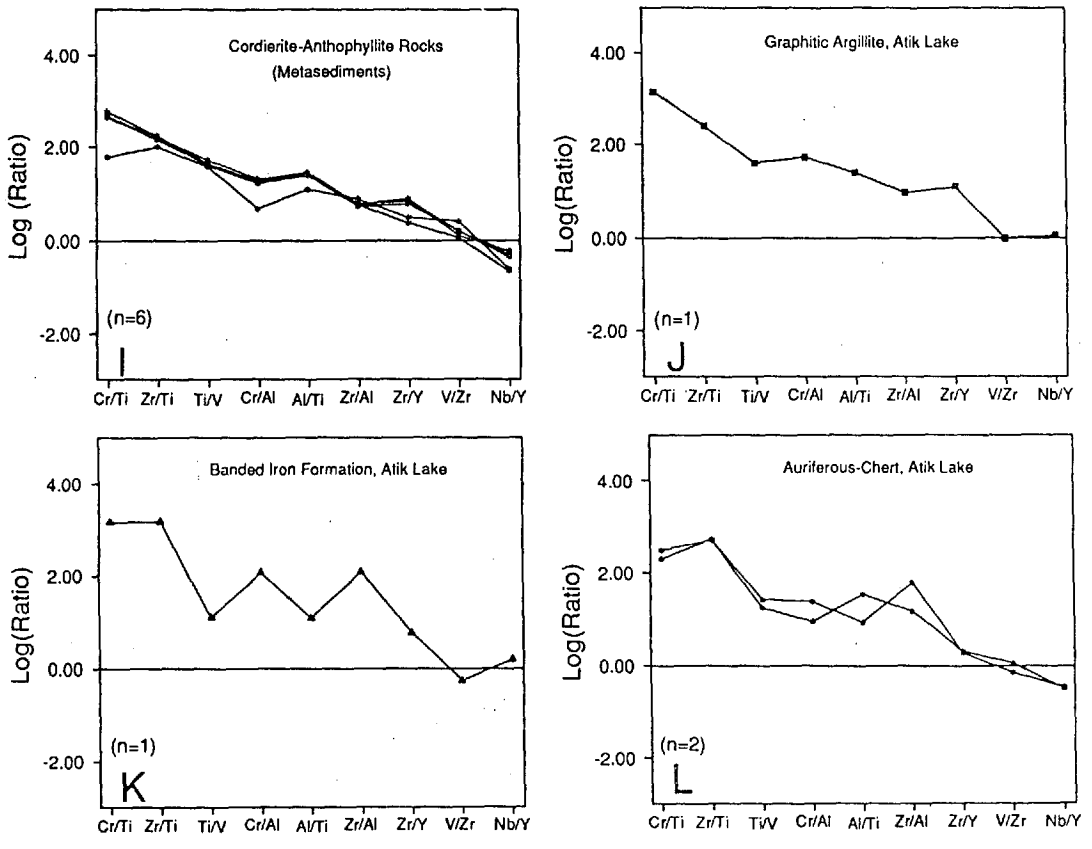

Fig. 3C.1 Log(Ratio) diagrams for the Atik Lake rocks (A-E, G, I-L). Data used in F are from Herzig and Pluger (1988), and those in H from Foster et al. (1986). Al: Al_2O_3 wt%, Ti: TiO_2 wt%. All other elements in the ratios are in ppm. The ratio Ti/V is multiplied by 10000.

modern N-MORB lavas (Fig. 3C.1F). The altered rocks at pipe 1 have the same shape of profiles as their metabasalt protolith (Fig. 3C.1B). Yttrium is the only element that produces a range of ratio values, and this is interpreted as evidence of moderate mobility (compare Zr/Y and Nb/Y ratios). The criteria for mobility is defined by changes in ratios that exceed the range of chemical variations defined by least altered metabasalt profiles.

A slightly larger variation in ratio values is recorded by altered rocks in pipe 2 than in pipe 1. The profiles for the cordierite-gedrite rocks plot within the range of the least altered basalts, so that no mobility is recorded for these elements apart from Y. A striking exception is produced by the very different profiles obtained for the two samples of a fine grained andalusite-bearing felsic rock in a fracture at the center of pipe 2. From an earlier interpretation of the mineralogical and chemical data, it was tentatively concluded that this rock could be a product of intense and unnusual alteration of the surrounding basalt, with some of the commonly immobile elements showing evidence of mobility. However, this hypothesis seems unlikely, as almost every supposedly inert element would have to have been mobile to explain the observed profiles (Figs. 3C.1C, 3C.1G). Furthermore, it is clearly not simply an aluminous alteration, as andalusite-rich altered rocks from pipe 1 and alteration zone 3 (1km west of pipe 2) have profiles identical to their metabasalt protolith (Figs. 3C.1B, D). Because the profiles of the two samples of this felsic rocks are so alike, they indicate a protolith different from the basalt.

A solution to the identity of the protolith was found by comparing the andalusite-bearing felsic rock profiles with those of rocks from the Atik Lake belt. A unit of fine grained biotite-bearing felsic rock (U-16-01) with remnant plagioclase phenocrysts was intersected by exploration drilling along

strike in the stratigraphy, 16 km east of the pipes. The profile for sample (U-16-01) is precisely concordant with that (U41D, P-2) of the altered felsic rock from pipe 2 (Fig. 3C.1G). These three rock samples have a common protolith.

On the $\log(Zr/TiO_2)$-$\log(Nb/Y)$ diagram (Fig. 3C.2), the three felsic samples plot in the alkaline trachyandesite field. The andalusite-bearing spotted felsic rock in the center of pipe 2 is most likely a somewhat hydrothermally altered, silicified (70 wt% SiO_2) and metamorphosed felsic trachyandesite dyke. The felsic dyke in pipe 2 and related felsic rock may be related to the quartz-feldspar porphyritic plutons intruding the volcanic sequence (Hargreaves, 1978). The felsic rocks profiles are very similar to that of a calc-alkaline intrusion (Fig. 3C.1H) from the Shamva greenstone belt, South Africa (data from Foster et al., 1986). The main difference is the higher Nb/Y ratio of the Atik felsic rocks, which is indicative of a more alkaline magma source.

The profiles for altered rocks within alteration zone 3 (Fig. 3C.1D) are very similar to those of the adjacent metabasalt with again, minor fluctuations in ratios involving Y. The stratiform potassic alteration zone profiles (Fig. 3C.1E) are, with the exception of one sample, also compatible with derivation from a basalt protolith. The altered sample with the steeper profile (U-05-08) is from an aphyric metabasalt flow stratigraphically below the first horizon of iron formation (see Fig. 3C in Bernier and MacLean, 1989), and is a different metabasalt protolith having higher Cr and lower Ti and V.

Five of the six samples of cordierite-anthophyllite rocks derived from a metasedimentary protolith have element ratio profiles very similar to the basalts, apart from slightly higher Al/Ti and Zr/Y values. (Fig. 3C.1I).

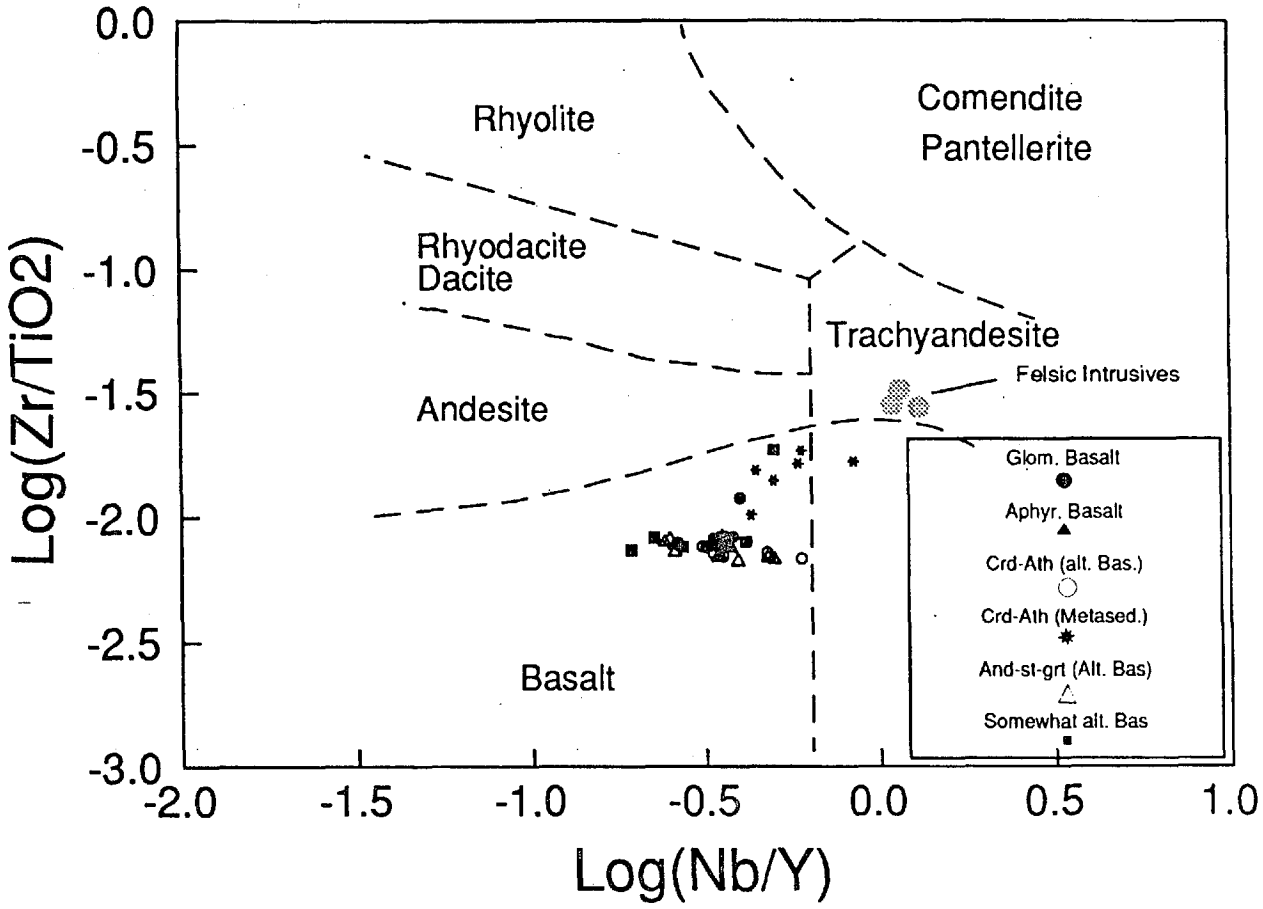

Fig. 3C.2. Plot of the Atik Lake data on a Log(Zr/TiO_2) - Log (Nb/Y) discriminant diagram (Winchester and Floyd, 1977).

These rocks were probably derived from a sedimentary protolith having a dominantly basaltic detrital component.

On a $\log(Zr/TiO_2)$-$\log(Nb/Y)$ diagram (Fig. 3C.2), the metasedimentary cordierite-anthophyllite rocks plot in the basalt field, at slightly higher values than the fresh and altered metabasalt samples. These metasedimentary rocks define a trend between the basalt and trachyandesite fields, which can be explained through sedimentary mixing of two end-members (mafic and felsic) detrital components (Fig. 3C.3). A high proportion of mafic detrital component (Fig. 3C.3B) produces a profile similar to that of the five metasedimentary rock samples (Fig. 3C.1I).

The graphitic argillite (Fig. 3C.1J), BIF (Fig. 3C.1K) and auriferous chert (Fig. 3C.1L) have contrasting Log(Ratio) profiles indicating that they are distinct rock types.

Conclusion

The Atik rocks provide a convincing example of how useful this method of protolith interpretation can be. It appears to be very sensitive to protolith identification in greenstone stratigraphy. The applicability of this technique will be further tested on data from the Némiscau and Montauban terranes.

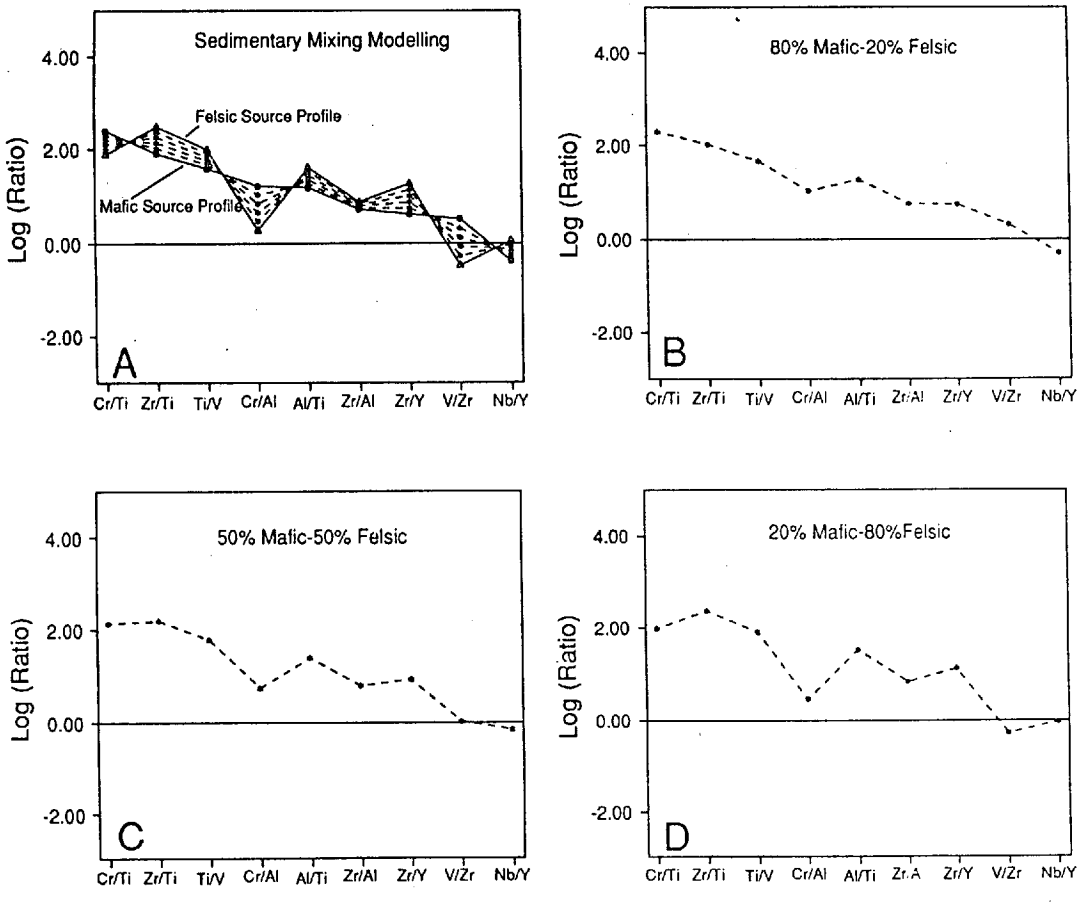

Fig 3C.3. Log(Ratio) profiles modelled by sedimentary mixing of a mafic and a felsic detrital component.

Canadian Mineralogist
Vol. 28, pp. 37-50 (1990)

VANADIFEROUS ZINCIAN–CHROMIAN HERCYNITE IN A METAMORPHOSED BASALT-HOSTED ALTERATION ZONE, ATIK LAKE, MANITOBA

LOUIS R. BERNIER

Department of Geological Sciences, McGill University, 3450 University Street, Montreal, Quebec H3A 2A7

ABSTRACT

Unusual V, Zn and Cr concentrations in hercynite (1.30–5.72 wt.% V_2O_3, 3.32–17.07 wt.% ZnO and 5.05–25.71 wt.% Cr_2O_3) are reported in a metamorphosed, tholeiitic basalt-hosted, cordierite-gedrite-bearing alteration zone associated with Fe-As-Zn-Cu-Au-Ag mineralization in the Atik Lake area, Manitoba. The grains of hercynite are very small (<25 μm) and generally subhedral. In transmitted light, they have a translucent honey-brown color and are isotropic; in reflected light, they show a low-intensity, pale grey reflectance. Single grains show relatively uniform compositions. Cr and V concentrations in the altered basalts were increased by up to 30 % as a result of mass loss due to leaching of mobile cations during hydrothermal alteration; these elements thus were relatively immobile, along with Al, Zr, Ti and Nb. The vanadiferous zincian-chromian hercynite formed during an amphibolite-facies regional metamorphism (550°C, 2.5 kbars) under low $f(O_2)$ and high $f(S_2)$ conditions.

Keywords: hercynite, vanadiferous, zincian, chromian, hydrothermal alteration, metamorphism, cordierite-gedrite, Atik Lake, Manitoba, electron-microprobe data, gold mineralization, arsenopyrite, löllingite, coulsonite.

SOMMAIRE

Des concentrations anomales en V, Zn, et Cr (1.30–5.72% par poids de V_2O_3, 3.32–17.07 % de ZnO et 5.05–25.71% de Cr_2O_3) caractérisent la hercynite des roches à cordiérite-gédrite d'une zone d'altération métamorphisée dans un basalte tholéiitique, associée à une minéralisation de Fe-As-Zn-Cu-Au-Ag dans la région du lac Atik, au Manitoba. Les grains d'hercynite sont très petits (<25 μm) et généralement sub-idiomorphes. En lumière transmise, ils ont une couleur brun-miel et sont isotropes, tandis qu'en lumière réfléchie, ils ont une réflectance gris pâle. Chaque grain possède une composition relativement uniforme. Les concentrations de V et Cr dans les basaltes altérés ont augmenté jusqu'à environ 30%, par la perte de masse due au lessivage des cations mobiles, V et Cr étant particulièrement immobiles durant le processus d'altération hydrothermale, tout comme Al, Zr, Ti et Nb. La formation de l'hercynite vanadifère zincifère et chromifère est liée au métamorphisme régional dans le facies amphibolite (550°C, 2.5 kbars) sous des conditions de faible $f(O_2)$ et de $f(S_2)$ relativement élevée.

Mots-clés: hercynite, vanadifère, zincifère, chromifère, altération hydrothermale, métamorphisme, cordiérite-gédrite, lac Atik, Manitoba, données de microsonde électronique, minéralisation aurifère, arsenopyrite, löllingite, coulsonite.

INTRODUCTION

Vanadiferous zincian-chromian hercynite has only rarely been reported as an accessory phase in metamorphosed hydrothermally mafic and ultramafic altered rocks, sulfide ores and associated metasediments, as well as in some unaltered ultramafic rocks (Table 1). Zincian-chromian spinel has more commonly been reported without data on the vanadium content (Table 1). This paper reports a new occurrence of such spinel in which the hercynite has the highest vanadium content ever reported. Small grains (<25 μm) of vanadiferous zincian-chromian hercynite (up to 5.72 wt.% V_2O_3 and up to 17 wt.% ZnO) were found in cordierite-gedrite rocks in a metamorphosed alteration pipe in the footwall basalt of an auriferous chert and associated quartz-grunerite-magnetite banded iron-formation (BIF) at Atik Lake, Manitoba.

The origin of the reported range of spinel composition is assessed through a study of bulk rock chemical changes related to premetamorphic hydrothermal alteration, and an estimate of tne P–T–$f(O_2)$–$f(S_2)$ conditions of a regional episode of lower amphibolite metamorphism.

PREVIOUS WORK

From previous work, occurrences of vanadiferous zincian-chromian spinel and zincian-chromian spinel in mafic and ultramafic rocks can be grouped into two broad categories: those in metamorphosed altered rocks associated with sulfide mineralization, and adjacent metasediments, and those in unmineralized ultramafic rocks (Table 1).

Mineralized areas

Vanadiferous zincian-aluminian chromite in cordierite-bearing niccolite ores at Málaga, Spain, is considered to have crystallized from a segregated oxide liquid having unusually high V and Zn concentrations (Oen 1973). Groves *et al.* (1977) envisioned direct crystallization of zincian-aluminian chromite from a sulfide-oxide liquid enriched in Al, Ti, Cr, Zn and Mn, to explain the presence of such spinels in Fe-Ni massive sulfide ores, Western Australia.

Zoned spinel grains in mineralized ultramafic

TABLE 1. OCCURRENCES OF (VANADIFEROUS) ZINCIAN-CHROMIAN SPINEL IN MINERALIZED AREAS

AREA	HOST ROCKS	ZNO (wt.%)	V2O3 (wt.%)	Cr/R+3	Al/R+3	ZONING	FACIES	ORIGIN	AUTHORS
Sykesville District Maryland. (close to ore: Fe, Cu, Zn)	Qtz-Mt chemical sediment. Metasomatized Peridotite.	0.88-19.09 (n=20)	-----	0.36-0.54	0.00-0.52	Intense c:Al-Zn r:Mt.	UG to LA	ME	Wylie et al. (1987)
Fe-Ni deposits, Western Australia.	Mineralized UM Altered peridotite.	0.26-5.62 (n=20)	-----	0.54-0.90	0.01-0.30	c:Zn-rich r:Mt.	A	MA ME	Groves et al. (1977)
Klerksdorp Goldfield, Witwatersrand, South Africa.	Detrital chromite in cglt.	0.50-4.71 (n=8)	-----	0.58-0.71	0.20-0.43	no zoning	LG	ME?	Utter (1978)
Cr-Ni-(Cu-As) mineralization, Málaga, Spain.	Crd Rocks and associated Alpine UM.	0.60-1.00 (n=?)	1.80-2.90	-----	-----	-----	UG LA	MA? ME	Oen (1973)
Cu-Co-Zn deposit, Outokumpu, Finland.	Sulfide ore and metasediments.	0.95-14.35 0.50-12.00 (n=14)	0.18-1.76 1.00-3.00	0.31-0.98	0.02-0.58	c:Cr-Fe r:Zn-Al Intense	UA	ME MET	Thayer et al. (1964) Weiser (1967) Treloar (1987) Treloar et al. (1981)
	Crd.-Ath. rocks in stockwork zone	0.95-26.94 (n=24)	0.52-1.06	0.05-0.62	0.33-0.95				
Ni-Fe Thompson deposit, Manitoba.	Selvage between Ore and UM host rocks.	5.00-15.00 (n=2)	-----	0.20-0.50	0.45-0.85	-----	UA to GR	ME ? MET?	Rimsaite & Lachance (1981)
Fe-As-Au-Ag-(Zn-Cu) prospects, Atik Lake, Manitoba.	Altered tholeiitic basalt (crd-ath rock)	2.72-17.20 (n=66)	1.03-5.72	0.06-0.35	0.57-0.92	Weak r:Zn,Al>c	LA	ME MET	This study.
OCCURRENCES of (VANADIFEROUS) ZINCIAN-CHROMIAN SPINEL IN UNMINERALIZED AREAS									
Helgeland area, Norway	Ultramafic rocks	0.13-2.69 (n=8)	----	0.36-0.80	0.01-0.23	-----	-----	-----	Seelinger & Mücke (1969) Moore (1977)
Plan d'Albard, Italy.	Arfvedsonite-bearing Minette.	0.06-8.74 (n=3)	----	0.87	0.06	-----	-----	MA	Wagner & Velde (1985)
Twin Sisters Dunite, Washington.	Alpine UM	0.03-0.27 (n=9)	0.11-0.21	0.57-0.67	0.20-0.39	c:ferrit-chromite	UG	ME	Onyeagocha (1974)

Note: UM: Ultramafic, cglt: conglomerate, Crd.-Ath.: cordierite-anthophyllite, n: number of analyses, c: core, r: rim, UG: upper greenschist, LA: lower amphibolite, A: amphibolite, UA: upper amphibolite, GR: granulite, ME: metasomatism, MA: magmatism, MET: metamorphism. -----: data not available.

rocks, Western Australia, have a zincian–aluminian chromite core and a magnetite rim, and have lower X_{Mg} than chromite from layered ultramafic complexes. These zoned grains of spinel did not crystallize directly from a highly magnesian komatiitic parent magma, but have been affected by metamorphism (Groves *et al.* 1977). Complex zoning is also present in zincian chromite in metamorphosed mineralized ultramafic rocks from Sykesville, Maryland (Wylie *et al.* 1987), and in vanadiferous zincian–chromian spinel in a stockwork zone and adjacent metasediments, serpentinites and Cu–Co–Zn ores, Outokumpu, Finland (Treloar *et al.* 1981, Treloar 1987). According to Groves *et al.* (1977), the complexity of the zoning increases with metamorphic grade. It appears that in these two areas, the original chromite chemistry was modified by metasomatism either during sea-floor hydrothermal alter-

ation or during an overprinted regional metamorphic event. Treloar (1987) interpreted the high levels of Cr, V and Ni in the stockworks to result from their redistribution by hydrothermal ore-forming fluids.

Rimsaite & Lachance (1971) reported an occurence of zincian-chromian hercynite in the chloritized selvage zone between ore and ultramafic rocks at the Thompson Ni–Fe deposit, Manitoba, but did not discuss its origin.

The zincian-aluminian chromite reported in the MB5 zone below the Vaal Reef of the Klerksdorp Goldfield, Witwatersrand, was interpreted to be detrital and derived from the ultramafic rocks in the Archean greenstones (Utter 1978).

Unmineralized areas

Vanadiferous zincian-chromian spinel grains in unmineralized ultramafic rocks (Table 1), such as in the Helgeland area, Norway (Moore 1977), Western Australia (Groves *et al.* 1977), and Twin Sisters dunite complex (Onyeagocha 1974), usually have less than 1 wt.% ZnO and V_2O_3. Zinc generally is considered to be inherited from the magmatic stage, as it tends to concentrate in the silicate liquid and partition into the oxide phase (Groves *et al.* 1977). Anomalous zincian-chromian spinel (up to 8.74 wt.% ZnO) has been reported in minette at Plan D'Albard, Italy; it occurs in altered zones possibly derived from olivine, and also as inclusions in phlogopite grains (Wagner & Velde 1985). The origin of that zincian-chromian spinel is not known; the primary magmatic spinel could have been modified during a metasomatic process indicated by the presence of altered olivine.

Analytical Technique

Electron-microprobe data were obtained with a Cameca Microbeam MB-1 instrument using wavelength dispersion. The analyses were conducted at a voltage of 15 kV, a current beam of 8 nA and counting times on standards and samples of 25 seconds. For ilmenite, V and Ti were determined using a PET (pentaerythritol) crystal and V$K\beta$ and Ti$K\alpha$ peaks, respectively, to avoid an overlap of the V$K\alpha$ and Ti$K\beta$ peaks. This problem was not encountered for the spinel grains, as the Ti concentrations are negligible. The following standards were used: kyanite (Al, Si), magnetite (Fe), willemite (Zn), diopside (Mg), Cr_2O_3 (Cr), spessartine (Mn), rutile (Ti), and vanadinite (V).

X-ray element mapping was done using a JEOL 100 CX TEMSCAN scanning-transmission microscope in conjunction with an energy-dispersion system (PGT System 4). An accelerating voltage of 25 kV and a current of 8 nA were used during X-ray mapping.

Geological Setting

The Atik Lake greenstone belt is located in the Sachigo Subprovince in the Superior Province (Fig. 1) and extends for 35 km along an east-west trend with a maximum width of 10 km. A south-facing, subvertical, homoclinal sequence of volcanosedimentary units characterizes the belt. Breaks in mafic volcanism were marked by deposition of clastic and chemical sediments (BIF and auriferous chert). Periods of quiescence allowed development of hydrothermal systems (Bernier & MacLean 1989).

Small-scale alteration pipes and associated stratiform alteration developed in a tholeiitic basalt unit, footwall to a horizon of auriferous chert with related graphitic argillite and silicate-oxide BIF. Cordierite-gedrite rocks formed during the metamorphism of primary alteration assemblages in the alteration pipes. One of those pipes is well exposed; a detailed map of it (Fig. 2A) also shows the occurrences of the vanadiferous zincian-chromian hercynite.

Mineralogy of Unaltered and Altered Basalts

The least-altered basalt is characterized by a metamorphic assemblage of hornblende and plagioclase (An_{60}) with a minor amount of quartz and titanite. Details on the mineralogy of the metamorphosed altered basalts and their chemistry are presented in Bernier & MacLean (1989). The metamorphism of the altered tholeiitic basalts in the pipe (Fig. 2A) led

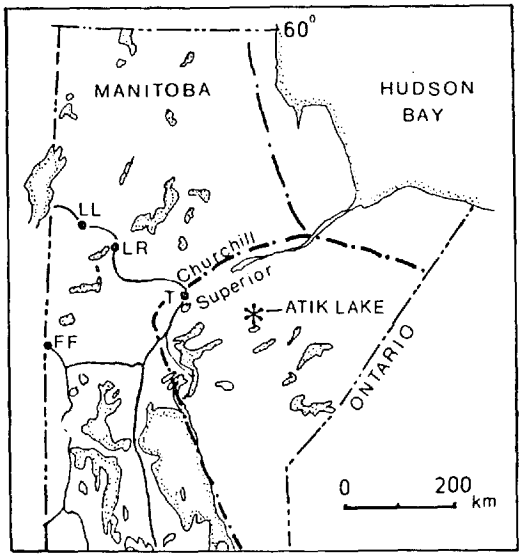

FIG. 1. Location map of the Atik Lake area, Manitoba. Symbols: FF: Flin Flon, LL: Lynn Lake, LR: Leaf Rapids, T: Thompson.

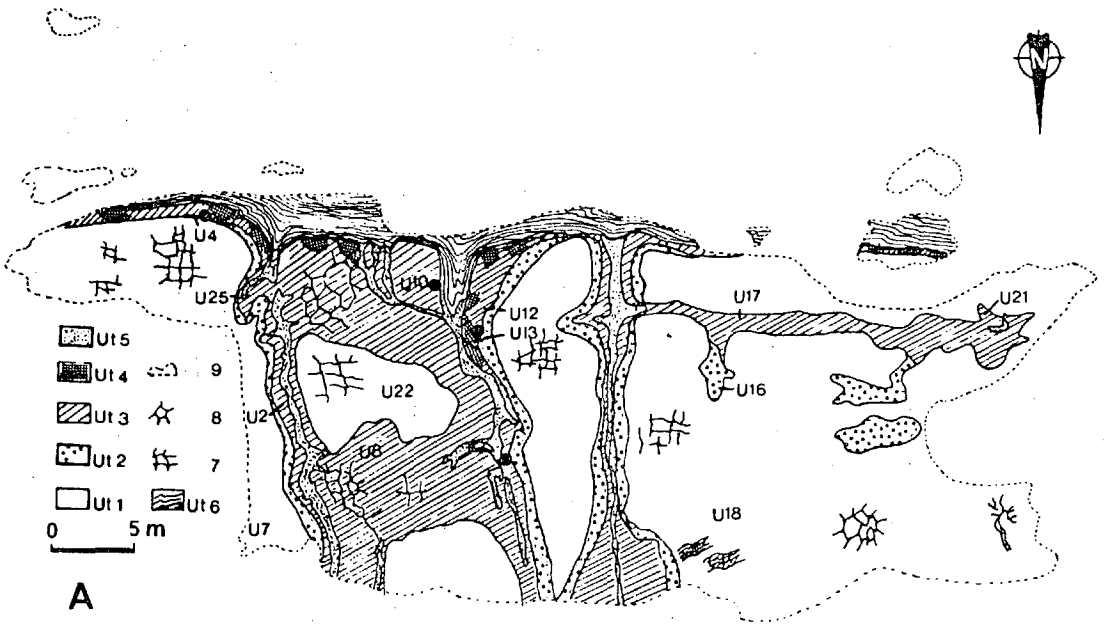

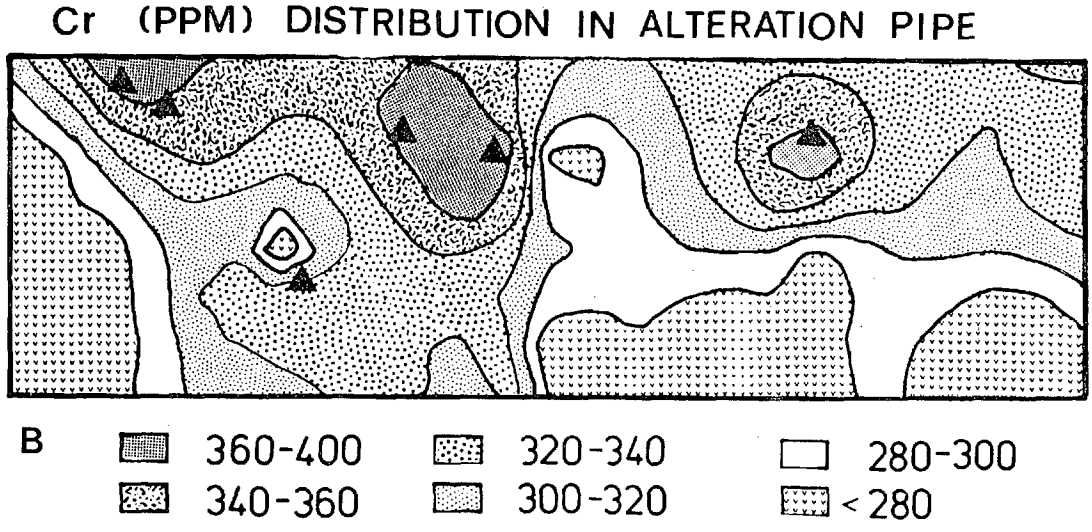

FIG. 2. A. Outcrop map of pipe 1. Symbols: Ut1: least altered glomeroporphyritic basalt, Ut2: bleached zone, Ut3: cordierite–gedrite–garnet zone, Ut4: andalusite-rich zone, Ut5: pipe conduits filled with chert and disseminated sulfides, Ut6: silicate–oxide BIF, showing deposition of BIF into the conduits, 7 and 8: fracture patterns, 9: limit of outcrop. Black dots: magnesian tourmaline. B. Contour map showing chromium concentrations in the alteration pipe. Symbols: triangles: location of samples containing vanadiferous zincian–chromian hercynite.

to the development of variable proportions of cordierite, gedrite, garnet, chlorite, biotite, andalusite, staurolite, quartz and plagioclase (An_7–An_{95}). The main oxide observed in the cordierite–gedrite rocks is a vanadiferous ilmenite (up to 1.76 wt.% V_2O_3: Table 2) with minor vanadiferous zincian–chromian hercynite (Table 3), rare rutile and extremely scarce magnetite rich in the coulsonite (FeV_2O_4) end-

TABLE 2. CHEMICAL COMPOSITIONS* OF ILMENITE AND MAGNETITE IN THE ALTERED BASALT, ATIK LAKE

	ILMENITE							MAGNETITE	
(Wt.%)	U8A	U12C	U12D	U12F	U17A	U17C	U17E	U12A	U12C
TiO_2	51.60	50.79	51.61	50.70	50.58	51.27	51.57	0.82	0.88
Al_2O_3	----	----	----	----	----	----	----	2.39	2.30
Cr_2O_3	0.14	0.18	0.13	0.11	0.15	0.13	0.09	6.94	7.01
V_2O_3*	1.16	1.76	0.43	1.23	1.00	1.43	0.73	16.84	17.12
Fe_2O_3	0.00	1.27	0.66	1.45	1.85	1.25	0.50	39.41	38.62
FeO	44.85	45.51	45.98	45.38	45.20	45.72	45.95	31.81	31.84
MgO	0.30	0.12	0.32	0.03	0.17	0.08	0.11	----	----
MnO	0.52	0.24	0.49	0.28	0.34	0.44	0.43	0.02	0.04
ZnO	----	----	----	----	----	----	----	0.13	0.10
Total	98.36	98.75	99.30	99.14	99.11	100.23	99.23	98.35	97.81
Ti^{4+}	1.89	1.94	1.98	1.84	1.84	1.94	1.86	0.02	0.02
Al^{3+}	----	----	----	----	----	----	----	0.11	0.10
Cr^{3+}	0.00	0.00	0.00	0.00	0.00	0.00	0.00	0.21	0.21
V^{3+}	0.05	0.07	0.02	0.05	0.04	0.06	0.03	0.51	0.52
Fe^{3+}*	0.03	0.05	0.03	0.05	0.07	0.05	0.02	1.13	1.11
Fe	1.91	1.83	1.98	1.83	1.83	1.93	1.98	1.02	1.02
Mg	0.00	0.00	0.00	0.00	0.00	0.00	0.00	0.00	0.00
Mn	0.02	0.01	0.01	0.01	0.02	0.02	0.03	0.00	0.00
Total	4.00	4.00	4.00	3.98	4.00	4.00	4.00	3.00	3.00

Calculations of stoichiometry made on the basis of 4 (magnetite) and 6 (ilmenite) atoms of oxygen respectively. -----: not detected. * Fe_2O_3 calculated from Fe^{3+} determined by stoichiometry. + as determined by microprobe analyses.

member (Table 2). Traces of V and Cr (<1 wt.%) also are present in garnet and staurolite. The cordierite–gedrite rocks contain less than 5 vol.% sulfides (pyrrhotite, arsenopyrite, löllingite, chalcopyrite, sphalerite).

TABLE 3. CHEMICAL COMPOSITIONS* OF HERCYNITE IN ATIK LAKE ALTERED BASALT

(wt.%)	U10A	U10B	U10N	U4A	U4K	U8A	U8C	U12A	U17D	U17H
SiO_2	0.03	0.09	0.06	0.03	0.06	0.13	0.09	0.07	0.03	0.06
TiO_2	---	---	---	0.09	0.04	0.02	0.09	0.10	0.10	0.09
Al_2O_3	45.84	31.58	43.89	44.98	54.44	41.89	38.43	38.74	29.95	33.51
Cr_2O_3	13.62	23.87	14.70	13.43	5.05	18.18	16.72	16.13	25.71	22.42
V_2O_3*	1.56	4.54	1.52	1.56	1.79	1.30	5.72	2.66	2.69	2.02
Fe_2O_3*	0.00	2.08	1.07	0.00	0.00	1.28	2.00	4.14	4.36	3.96
FeO	27.15	29.26	28.18	24.96	19.93	27.06	29.61	33.61	32.14	31.01
MgO	1.38	0.74	1.62	1.25	2.05	1.34	0.75	0.86	0.51	0.60
MnO	0.10	---	0.10	---	0.01	---	---	---	---	---
ZnO	9.83	6.15	8.58	12.94	17.07	10.02	7.19	3.32	3.82	5.56
Total	99.51	98.31	99.52	99.34	100.44	99.02	98.60	99.63	99.41	99.25
Atomic Proportions (Oxygen basis 32)										
Si^{4+}	0.01	0.02	0.01	0.03	0.01	0.03	0.02	0.02	0.01	0.02
Ti^{4+}	---	---	---	0.02	0.01	0.00	0.02	0.02	0.02	0.02
Al^{3+}	13.17	9.74	12.65	13.05	15.00	12.26	11.00	11.45	8.23	10.20
Cr^{3+}	2.63	4.84	2.86	2.61	0.93	3.19	3.39	3.20	5.32	4.58
V^{3+}	0.30	0.95	0.30	0.31	0.34	0.26	1.18	0.53	0.56	0.42
Fe^{3+}	0.00	0.41	0.20	0.00	0.00	0.24	0.39	0.78	0.88	0.77
Fe	5.54	6.41	5.79	5.14	3.80	5.65	6.35	7.05	7.03	6.70
Mg	0.50	0.29	0.59	0.46	0.71	0.50	0.29	0.32	0.20	0.23
Mn	0.02	---	0.02	---	0.00	---	---	---	---	---
Zn	1.77	1.19	1.56	2.35	2.95	1.85	1.36	0.61	0.76	1.06
Total	23.94	23.95	23.98	23.97	23.85	23.89	23.98	23.98	23.99	23.98
End-member Proportions										
Ulvo.	0.00	0.00	0.00	0.25	0.12	0.00	0.25	0.25	0.25	0.25
Spin.	6.21	3.68	7.41	5.75	8.72	6.27	3.63	4.01	2.50	2.88
Gala.	0.25	0.00	0.25	0.00	0.00	0.00	0.00	0.00	0.00	0.00
Chro.	16.34	31.31	17.96	16.30	5.71	20.00	21.19	20.03	33.25	28.63
Gahn.	21.99	13.43	19.03	29.36	36.22	23.20	17.00	7.51	9.44	13.19
Herc.	53.35	42.97	52.20	46.41	47.15	47.40	48.13	60.01	45.69	47.63
Magn.	0.00	0.95	0.68	0.00	0.00	1.50	2.44	4.76	5.31	4.76
Coul.	1.86	6.02	1.88	1.94	2.09	1.63	7.38	3.32	3.50	2.63
Fran.	0.00	1.65	0.57	0.00	0.00	0.00	0.00	0.13	0.06	0.06

The location of the hercynite-bearing samples in the pipe is shown in Figure 2a by the first three digits of the sample number. * Fe_2O_3 calculated from the Fe^{3+} content determined by (Al+Cr+V) deficiencies on the octahedral sites. + as determined by electron-microprobe analysis. --- not detected. Ulvo.: ulvospinel, Spin.: spinel, Gala.: galaxite, Chro.: chromite, Gahn.: gahnite, Herc.: hercynite, Magn.: magnetite, Coul.: coulsonite, Fran.: franklinite.

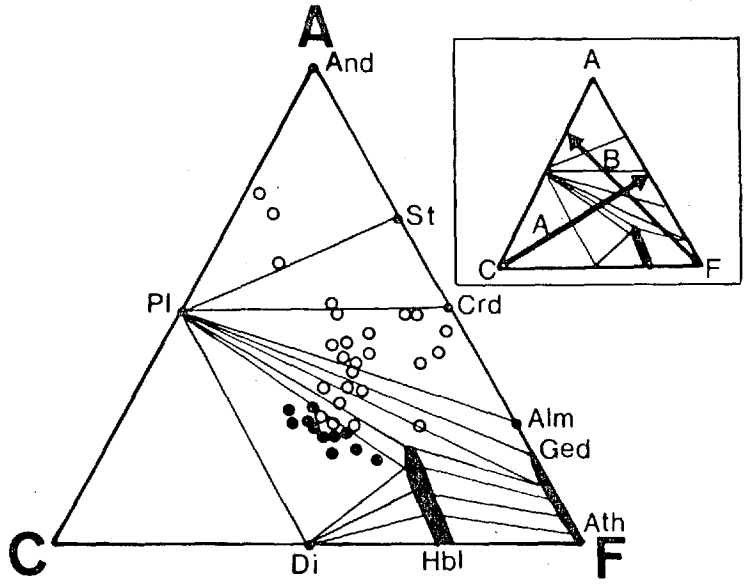

FIG. 3. Bulk-rock compositions plotted onto an ACF diagram. A: $Al_2O_3 + Fe_2O_3 - Na_2O - K_2O$, C: $CaO - 3.3\ P_2O_5$, F: FeO + MgO + MnO. Filled circle: fresh basalt, open circle: altered basalt. And: andalusite, St: staurolite, Crd: cordierite, Alm: almandine, Ged: gedrite, Ath: anthophyllite, Dio: diopside, Hbl: hornblende, Pl: plagioclase. Inset: Trend A: loss of Ca during premetamorphic hydrothermal alteration; trend B: losses of Fe + Mg during hydrothermal alteration.

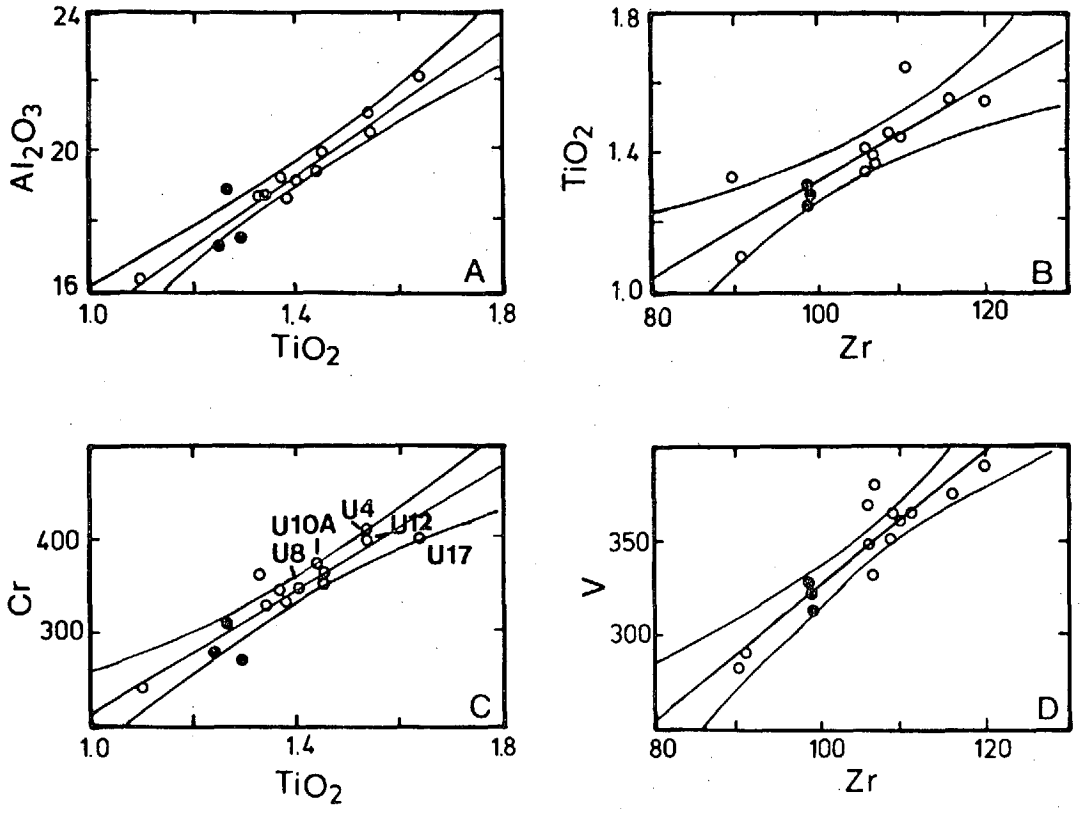

FIG. 4. Plots of element concentrations in rock from pipe 1 (major elements plotted as oxides, expressed in wt.% A. Al_2O_3 - TiO_2, B. TiO_2 - Zr, C. Cr - TiO_2 (the numbers indicate the hercynite-bearing samples of altered basalt), D. V-Zr. Solid lines through data points are derived by linear regression, and the curves reflect a 95% confidence interval. Filled circle: fresh basalt, open circle: altered basalt.

CHEMISTRY OF UNALTERED AND ALTERED BASALTS

At Atik Lake, unaltered basalt has a tholeiitic affinity, with trace-element concentrations typical of ocean-floor basalt (Bernier & MacLean 1989). The absence of titanite in the altered rocks can be explained by a loss of Ca during hydrothermal alteration at vent sites. This loss of Ca is well depicted on an ACF diagram (Fig. 3), assuming isochemical metamorphism of the greenschist alteration-assemblages (apart from losses in volatiles). Leaching of Ca at relatively constant A-F values during alteration appears to be the main trend (A in Fig. 3). Andalusite-rich patches in the pipe (Fig. 2A) can be explained by extreme losses of Fe + Mg, as shown by trend B (Fig. 3), which terminates near the plagioclase–andalusite line. Silicification is responsible for a mass increase of up to 15% in these andalusite patches, thus inducing a dilution of the immobile elements, including Cr and V (Fig. 4). The loss of the more mobile cations, mainly Si, Ca, Na, Mg and Fe, is largely responsible for a total loss of up to 30% of the original mass (Bernier & MacLean 1989); this leaching led to enrichment in immobile components such as Al, and thus favored the appearance of assemblages of aluminous minerals during metamorphism.

TABLE 4. PEARSON CORRELATION MATRIX FOR IMMOBILE ELEMENTS IN THE PIPE

(n=15)	Al_2O_3	TiO_2	Zr	V	Cr
Al_2O_3	1.00				
TiO_2	0.96	1.00			
Zr	0.79	0.84	1.00		
V	0.71	0.77	0.93	1.00	
Cr	0.83	0.93	0.76	0.67	1.00

Correlation coefficients are calculated for 15 rock samples from the alteration pipe. Analyses are presented in Table 3 of Bernier & MacLean (in press).

Figures 4A to D show the effect of alteration on the behavior of the less mobile elements in the altered basalts at Atik Lake. Paired immobile elements have a high correlation-coefficient and plot along an alter-

ation trend passing through the composition of the precursor and origin, which is defined by an increase (mass loss) or a decrease (mass gain) of the immobile elements (MacLean & Kranidiotis 1987). Vanadium and chromium behaved as relatively immobile elements during the alteration of the Atik Lake basalt (Table 4, Figs. 4C, D). Additional evidence for the immobility of V and Cr comes from a study by Seyfried & Mottl (1982), who showed that V and Cr are the most immobile elements among the transition metals during experimental seawater–basalt interaction at 300°C. Furthermore, Howard & Fisk (1988) showed that an alteration crust containing aluminum-rich clays enriched in Ti, V and Cr formed by residual weathering during hydrothermal alteration of basalt on the Gorda Ridge. I have calculated a total mass-loss of up to 75% in the alteration crust from Gorda Ridge, using Al_2O_3 as the immobile component. This mass loss induced an increase in Cr concentration from 411 ppm in the basaltic glass to up to 1060 ppm in the alteration crust. At Atik Lake, background values of 270 ppm Cr and 315 ppm V in the least-altered tholeiite increased by a factor of up to 30% in the cordierite-gedrite rocks. The presence of vanadiferous zincian-chromian hercynite in the altered rocks is the mineralogical expression of these high-Cr and high-V zones in the alteration pipe (Figs. 2A, B). Such spinel grains have been observed only in the metamorphosed altered rocks, and no "primary" igneous chromite is found in the least-altered tholeiitic basalt. The spinel is also absent in the auriferous chert and grunerite–magnetite BIF overlying the alteration zones. The low concentrations of Cr (1–208 ppm) and V (1–128 ppm) in these chemical sediments indicate that Cr and V were not added extensively as hydrothermal components, which suggests that they were relatively immobile during hydrothermal alteration.

Crystal-Chemistry Considerations

Spinels of the TM_2O_4 type have one tetrahedrally (*T*) and two octahedrally (*M*) coordinated sites; these sites can accomodate a large number of cations of different valences (2+, 3+, 4+), allowing complex solid-solutions to occur in nature (O'Neill & Navrotsky 1984). Some elements, such as Fe, V and Mn, may have more than one oxidation state, contributing to possible electron-exchange reactions. A crystal-chemistry study of natural Fe–Mg-rich chromian spinel ($0.15 \leq Cr \leq 1.07$ atoms per formula unit) by Della Giusta *et al.* (1986) shows that: Cr substitutes on both octahedral (*M*) sites, along with Al and some Mg; on the basis of strong site-preference energies, Cr only occupies octahedral (*M*) sites. Della Giusta *et al.* assigned Si^{4+} exclusively to the *T* site, and Ni^{2+} and Ti^{4+} only to the *M* sites. The higher the Cr content, the greater the ordering of Mg in the *T* site and Al in the *M* sites. Zinc has a strong site-preference energy for tetrahedral coordination. Jacob (1976) and Bruckmann-Benke *et al.* (1988) found that the tetrahedrally coordinated site of a binary solid-solution of the type $Zn(Al,Cr)_2O_4$ is almost entirely occupied by Zn, with very small amounts of Al. Vanadium has a strong octahedral site-preference energy and is assigned (both V^{3+} and V^{4+}) to the *M* sites (O'Neill & Navrotsky 1984).

For the Atik Lake spinel, I have assumed that all Mn is divalent and that all V is trivalent. Fe^{3+} has been calculated from atomic proportions based on 32 oxygen atoms (24 cations) and was obtained as the difference between the sum of the octahedrally coordinated cations ($Al + Cr + V^{3+}$) and 16.00. End-member proportions were computed with an algorithm for which all Ti, Cr, V, Mn and Mg were used to form, respectively, ulvöspinel, chromite, coulsonite, galaxite, and spinel. Zn was combined with excess Fe^{3+} after the formation of magnetite to form franklinite. Any remaining Zn was combined with Al to form gahnite, and the leftover Fe and Al were attributed to hercynite (Table 3).

Elements having a strong negative correlation (Table 5) are inferred to substitute for each other in a given site (*e.g.*, Al–Cr, Mg–Cr on the *M* sites; Fe^{2+}–Zn, Fe^{2+}–Mg on the *T* site). Those having a strong positive correlation involve *T*- and *M*-type cations (*e.g.*, Zn–Al, Fe^{2+}–Cr, Fe^{2+}–Fe^{3+}), a reflection of specific end-members. Treloar (1987) found negative correlations between Zn and Cr, and between Fe and Al for spinel at Outokumpu, indicating an inverse relationship between the $FeCr_2O_4$–$ZnAl_2O_4$ components.

Characteristics of the Hercynite

Optical properties

The vanadiferous zincian-chromian hercynite occurs as small subhedral grains (<25 μm) having a honey-brown to dark olive color, strong relief, and low ($R\% \approx 12$) reflectance (grey). The hercynite commonly is found close to garnet porphyroblasts, rarely as inclusions, and usually in a matrix of quartz,

TABLE 5. PEARSON CORRELATION MATRIX FOR CONCENTRATION OF CATIONS IN HERCYNITE FROM ATIK LAKE

(n=66)	Al	Cr	V	Fe^{3+}	Fe^{2+}	Mg	Zn
Al	1.00						
Cr	-0.97	1.00					
V	-0.49	0.41	1.00				
Fe^{3+}	-0.75	0.59	0.19	1.00			
Fe^{2+}	-0.87	0.78	0.42	0.81	1.00		
Mg	0.91	-0.85	-0.45	-0.76	-0.87	1.00	
Zn	0.83	-0.76	-0.41	-0.76	-0.98	0.81	1.00

Correlation coefficients calculated by linear regression on 66 hercynite grains in cordierite-gedrite rocks in the pipe. The complete data-set is available upon request to the author. Representative hercynite compositions are shown in Table 3.

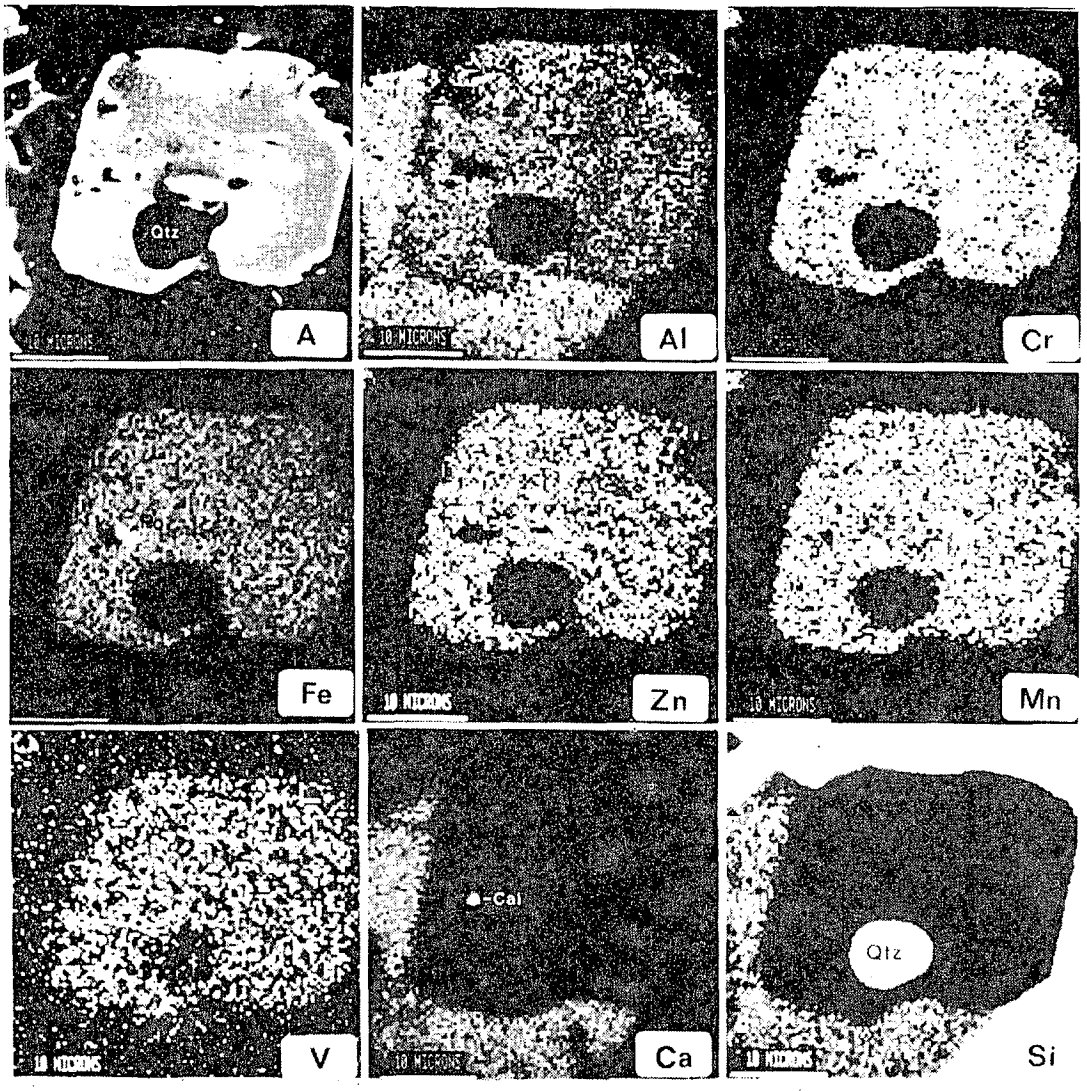

FIG. 5. SEM image of a grain of vanadiferous zincian-chromian hercynite. Others: X-ray element maps: Al, Cr, Fe [white spot corresponds to an inclusion of pyrrhotite (Po)], Zn, Mn, V, Ca (Cal: calcite inclusion beside the sulfide inclusion), Si (Qtz : large quartz inclusion in the hercynite). Bar scale: 10 μm.

plagioclase or cordierite. The hercynite grains may have micrometer-size inclusions of quartz, sulfide and carbonate (Fig. 5).

Chemistry

Electron-microprobe data representative of the compositional range observed are presented in Table 3. The following structural formula expresses the results of 66 microprobe analyses: $(Fe^{2+}_{0.49-0.90}Zn_{0.02-0.37}Mg_{0.02-0.09}Mn_{<0.005})(Al_{1.13-1.87}Cr_{0.12-0.69}Fe^{3+}_{0.00-0.13}V^{3+}_{0.03-0.13})O_4$.

X-ray element mapping shows that single grains of spinel are relatively homogeneous (Fig. 5), but slight increases in Al and Zn from core to rim were detected in some samples. A wide range of spinel compositions is observed within the alteration pipe (Fig. 2) and also at the thin-section scale (Figs. 6, 7). Compositional variations occur among different samples, but also in different grains in the same sample.

When compared to most other occurrences in mineralized areas, the range of spinel compositions at Atik Lake (Table 1, Fig. 6) fills a gap in previ-

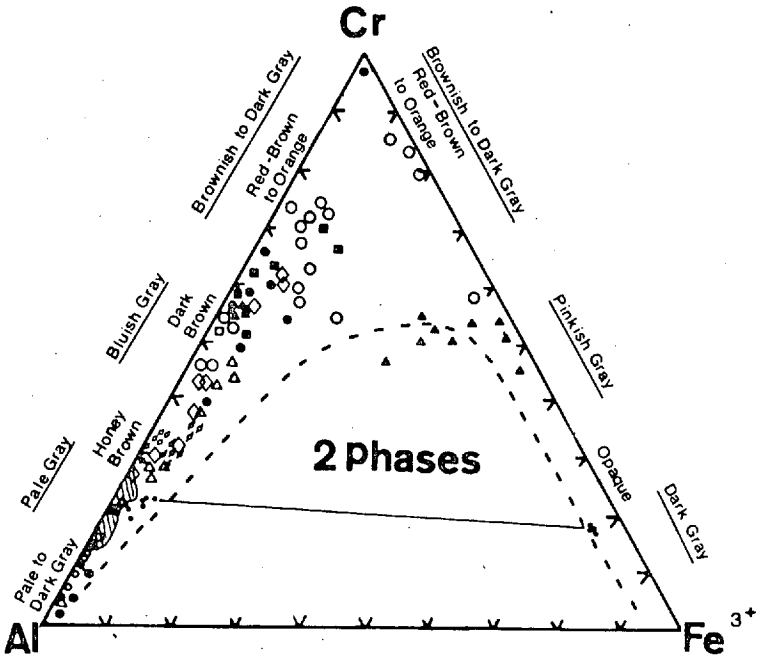

FIG. 6. Al-Cr-Fe^{3+} diagram showing compositional range of (vanadiferous) zincian spinels. Optical characteristics presented on the side of the diagram are compiled from the literature; underlined is the color in reflected light; along Al-Cr and Cr-Fe^{3+} sides are shown color and internal reflection in transmitted light. Dashed line: empirical miscibility gap of Loferski & Lipin (1983). Open circles: Fe-Ni deposit of Western Australia, filled triangles: Fe-Zn-Cu-Co deposits, Sykesville, Maryland, open squares: Thompson mine, Manitoba, filled squares: Klerksdorp Goldfield, Witwatersrand, filled circles: Cu-Co-Zn Outokumpu deposits, Finland. Compositions from Atik Lake: hatched field, represents 36 compositions from U10A, U4, U8, small circle with cross-line: U10B, small open circle with arrow: U17, black dots: U12. Details on location, compositions and references are given in Table 1.

ously reported data for zincian-chromian spinel. The spinel has higher Al/R^{3+} ($R^{3+} = Al + Cr + V^{3+} + Fe^{3+}$) and lower Cr/R^{3+} values than spinel in metamorphosed altered ultramafic rocks. This statement is also valid for compositions of spinel in ultramafic rocks in unmineralized areas (Onyeagocha 1974, Moore 1977, Wagner & Velde 1985; Table 1). A spinel from the selvage zone between Ni-ore and its ultramafic host at the Thompson mine, Manitoba (Rimsaite & Lachance 1971), falls within the compositional range observed at Atik Lake. Core compositions of spinel in the cordierite-anthophyllite rocks from the Outokumpu deposit have much higher Cr/R^{3+} values than their rim, which is more aluminous and falls within the Atik Lake compositional field (Fig. 6; Treloar *et al.* 1981, Treloar 1987). Another striking characteristic of the spinel at Atik Lake is its general lack of intense compositional zoning, as was reported elsewhere for grains of zincian-chromian spinel that reach up to 700 μm across (Weiser 1967, Groves *et al.* 1977, Treloar 1987, Wylie *et al.* 1987).

A continuum of compositions in natural chromium-rich spinel exists between chromian magnetite and "ferritchromit" through Fe^{3+}-poor, low-aluminum chromite through chromian hercynite to pure hercynite, as discussed by Evans & Frost (1975). The zincian-chromian hercynite compositions compiled from the literature also show this continuum (Fig. 6) and plot next to an empirically determined miscibility gap, outlined by Loferski & Lipin (1983).

Interestingly, a euhedral crystal of magnetite containing ~2.5 wt. % Al_2O_3, ~7% Cr_2O_3 and ~17% V_2O_3 was found to coexist with the vanadiferous zincian-chromian hercynite in sample U12 (Tables 2, 3). The slightly low analytical totals for the magnetite (Table 4) could result from the presence of V^{4+}, as all the vanadium was taken to be V^{3+} in the calculations. If this is so, the presence of V^{4+} would lead to overestimation of Fe^{3+} as a conse-

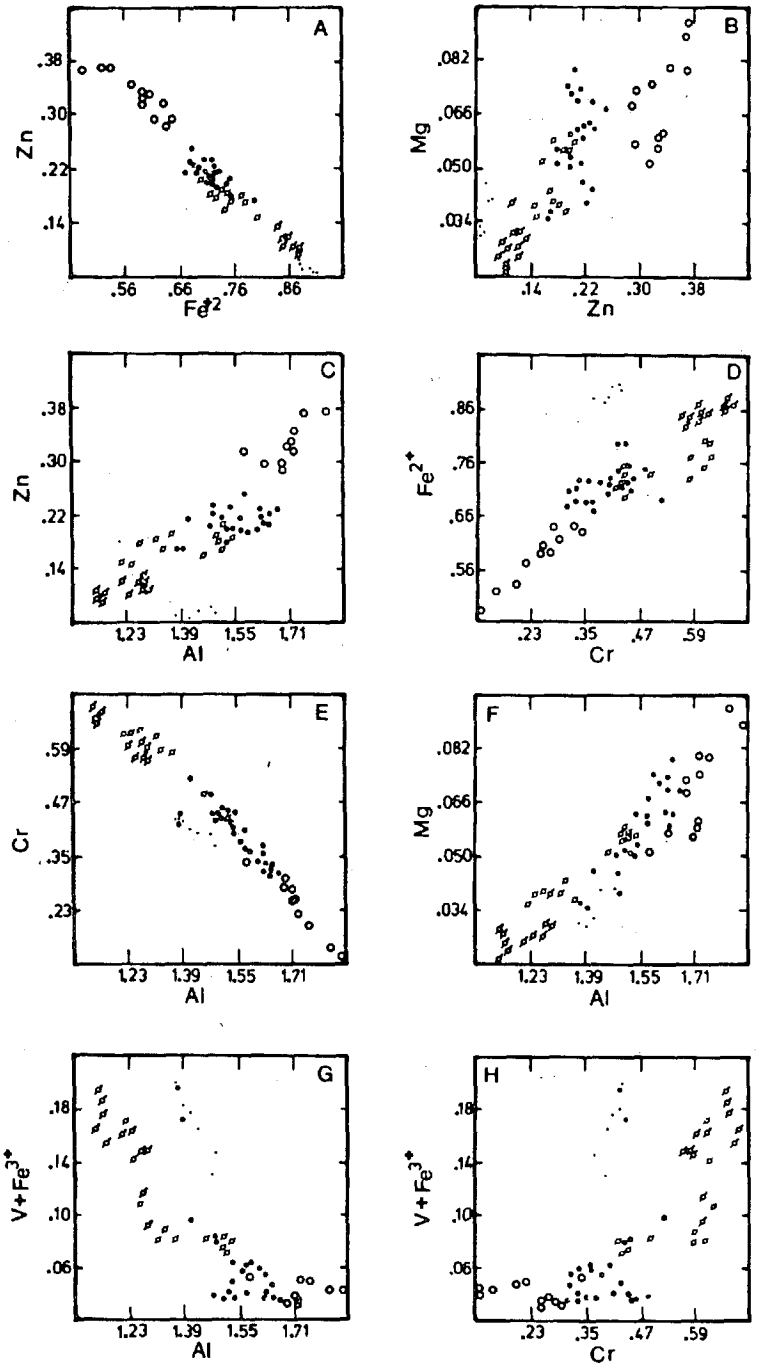

FIG. 7. Binary diagrams showing compositional ranges of hercynite from Atik Lake. Symbols: half-filled circle: U10A, small circle with cross-line: U10B, open circle: U4, filled circle: U8, small dots: U12, open circle with arrow: U17. Correlation coefficients as in Table 5. Concentrations in number of cations.

quence of an electron-exchange reaction such as $Fe^{3+} + V^{3+} = Fe^{2+} + V^{4+}$ (Wakihara *et al.* 1971).

The hercynite grains in sample U12 have high calculated concentrations of Fe^{3+} (Table 3) and plot

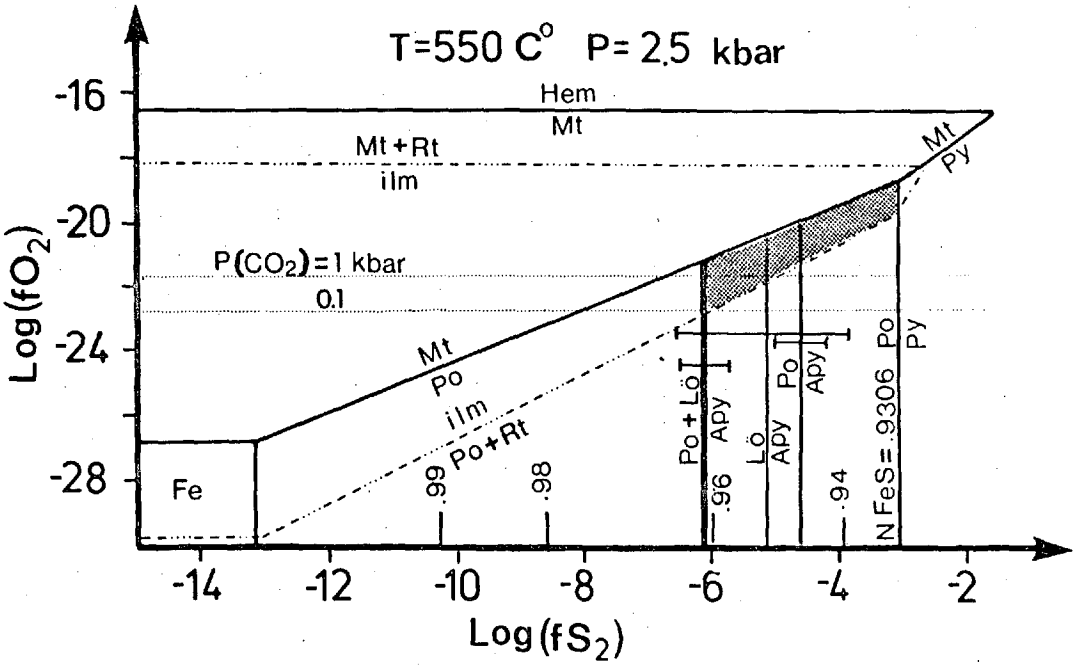

FIG. 8. Log $f(O_2)$ – log $f(S_2)$ diagram. Shaded area shows the stability field of the hercynite at Atik Lake. Symbols: Hem: hematite, Mt: magnetite, Rt: rutile, Ilm: ilmenite, Po: pyrrhotite, Py: pyrite, Lö: löllingite, Apy: arsenopyrite. N_{FeS}^{Po} values shown along the log $f(S_2)$ axis calculated using equations of Froese & Gunter (1976). The error bars for the Apy and Lö boundaries are calculated using the ΔG_f^0 uncertainties of Barton & Skinner (1979). Other sources of thermodynamic data as indicated in the text.

close to one limb of the proposed miscibility gap, whereas the magnetite crystals plot near the opposite limb (Fig. 6). For the vanadiferous spinel, a fourth component has to be considered; the compositional fields and tie line are projected from that fourth component onto the Fe^{3+}–Al–Cr plane. The effect on the solvus of adding V to the system is not known. No evidence of exsolution was found in the Atik Lake spinel. Slightly higher $f(O_2)$ conditions in this part of the alteration pipe (Fig. 2A) led to the formation of the coexisting spinel in local areas of appropriate bulk-compositions. A rare case of unmixing in primary igneous chromite (Loferski & Lipin 1983) was attributed to metamorphic re-equilibration at temperatures around 600°C. As no primary igneous spinel has been identified in the unaltered basalt at Atik Lake, a metamorphic origin for these coexisting spinels is indicated.

CONDITIONS OF METAMORPHISM

Peak conditions of metamorphism at Atik Lake are estimated to have been $T = 550$°C and $P < 3.0$ kbars (Bernier & MacLean 1989). The pressure is not as well constrained as the temperature. The garnet-hornblende geothermometer of Graham & Powell (1984) gives core and rim temperatures of 557°C and 531°C for sample U2C within the pipe. The garnet-hornblende geobarometer of Kohn & Spear (1989) provides core and rim pressures of 3.3 and 2.8 kbars for sample U2C using the activities for the Mg end-members. The core compositions of coexisting garnet–cordierite pairs in the alteration pipe indicates maximum pressures ranging from 2.5 to 3 kbars at the condition $P = P(H_2O)$ using Figure 10 of Aranovich & Podlesskii (1983). The presence of the assemblage cordierite–chlorite–biotite–muscovite in sample U4 indicates a minimum pressure between 1 kbar if $X(H_2O) = 1$ and 2.5 kbar if $X(H_2O) = 0$ at $T = 550$°C using the mineral compositions and the thermodynamic data of Berman (1988). With these pressure considerations and in the absence of a precise estimate of the mole fraction of H_2O, a peak pressure of 2.5 kbars is chosen. The stability field of the vanadiferous zincian-chromian hercynite compositions can be located in $f(S_2)$–$f(O_2)$ space using buffering assemblages and the composition of pyrrhotite in spinel-bearing samples (Table 6). The different phase-boundaries plotted in a log $f(S_2)$–log $f(O_2)$ diagram (Fig. 8) were calculated using the thermodynamic data of Clark (1966), Froese & Gunter (1976), Barton & Skinner (1979), Berman & Brown (1985), Sharp *et al.* (1985) and Berman (1988). Different $f(S_2)$–$f(O_2)$ buffer assemblages observed in

TABLE 8. AVERAGE COMPOSITIONS OF HERCYNITE FROM ATIK LAKE AND $f(O_2)$-$f(S_2)$ BUFFERING ASSEMBLAGES

Sample (n)	X_{Cr}	X_{Al}	Fe^{3+}	V	X_{Zn}	buffering assemblage	Log $f(S_2)^*$
U4 (15)	0.12	0.86	0	0.04	0.34	apy-lo-po-ilm-rt	----
U10A (13)	0.19	0.79	0	0.04	0.22	apy-lo-po-ilm	----
U10B (12)	0.26	0.70	0	0.09	0.17	apy-lo-po-ilm	-4.2
U8 (8)	0.21	0.74	0.02	0.08	0.21	ilm-po-rt	----
U12 (8)	0.20	0.71	0.09	0.08	0.07	ilm-po-mt	-3.9
U17 (12)	0.31	0.61	0.10	0.09	0.11	ilm-po	-3.5

(n) = number of hercynite grains analyzed. * calculated at T = 550°C and P = 2.5 kbar from pyrrhotite compositions N^{Po}_{FeS} = 0.9421, 0.9396, 0.9352 for sample U10B, U12 and U17 respectively using equations of Froese & Gunter (1976). ---- not analyzed. apy: arsenopyrite, lo: löllingite, po: pyrrhotite, ilm: ilmenite, rt: rutile, mt: magnetite. X_{Cr}=Cr/(Al+Cr+V+Fe^{3+}), X_{Al}=Al/(Al+Cr+V+Fe^{3+}), X_{Zn}=Zn/(Fe+Mg+Mn+Zn).

the Atik Lake cordierite-gedrite rocks include arsenopyrite- löllingite-pyrrhotite-ilmenite ± rutile, pyrrhotite-ilmenite-rutile and pyrrhotite-ilmenite-magnetite (Table 6). The magnetite-bearing sample (U12) has a high average X_{Cr} [Cr/(Cr + Al + V^{3+} + Fe^{3+})] and Fe^{3+} content, and the lowest X_{Zn} [Zn/(Fe + Mg + Mn + Zn)]. Calculated log $f(S_2)$ values based on compositions of the pyrrhotite (method of Froese & Gunter 1976) are shown in Table 6. Sample U4 has the highest X_{Zn} and lowest X_{Cr} values and appears to have been buffered at the lowest values of $f(S_2)$ and $f(O_2)$, represented in Figure 8 by the intersection of the arsenopyrite-löllingite-pyrrhotite and ilmenite-pyrrhotite-rutile boundaries. Samples U10A and B were buffered at a similar value of log $f(S_2)$ (= −6.2) as sample U4, but at a higher $f(O_2)$, along the arsenopyrite-löllingite-pyrrhotite boundary within the pyrrhotite-ilmenite field, as indicated by the absence of rutile. A calculated value of X^{Po}_{FeS} = 0.9247 was obtained by solving reactions (1) (Froese & Gunter 1976) and (2) (Barton & Skinner 1979) by iterations, until the two equations are satisfied by a common value of X^{Po}_{FeS}:

(1) □S(in pyrrhotite) = $\frac{1}{2}S_2$ (in vapor)
(2) $2FeAs_2 + 2FeS + S_2 = 4FeAsS$

For reaction (2), the composition of arsenopyrite was used (37.1 As atom%) to calculate an activity aFeAsS = 0.8859, and $a$$FeAs_2$ was taken to be unity. The calculated value of X^{Po}_{FeS} contrasts with the measured value X^{Po}_{FeS} = 0.8905 in sample U10B, which leads to a value of log $f(S_2)$ = -4.12, which is 2 log units higher than that expected from the position of the arsenopyrite-löllingite-pyrrhotite boundary. Although all three minerals are observed within the same thin section, only löllingite-arsenopyrite and pyrrhotite-arsenopyrite pairs are observed in contact. If the pyrrhotite-arsenopyrite boundary is considered instead, a pyrrhotite composition of X^{Po}_{FeS} = 0.8986 is calculated (3).

(3) $2FeAsS + S_2 = 2FeS + 2(As,S)$ liquid
(4) $2FeAs_2 + S_2 = 2FeAsS + 2As$

This value of X^{Po}_{FeS} (0.8986) is much closer to the measured one (0.8905) in sample U10B. The löllingite-arsenopyrite boundary (4) is calculated to occur at log $f(S_2)$ = −5.30. If the maximum uncertainty of 5 kcal on ΔG_T (Barton & Skinner 1979) is applied, the boundary may occur anywhere between −6.4 and −3.9 log $f(S_2)$, a range that overlaps both reaction (2) and (3) boundaries. This suggests that the rare pyrrhotite grains (15 μm) observed in contact with arsenopyrite in sample U10B were in local equilibrium and that reactions 3 and 4 are indicative of the $f(S_2)$ condition rather than reaction 2. The estimated range of $f(O_2)$-$f(S_2)$ values under which the vanadiferous zincian-chromian hercynite formed in the cordierite-gedrite rocks in the Atik Lake alteration zone is indicated by the shaded area in Figure 8. In summary, the assemblage arsenopyrite-löllingite-pyrrhotite-ilmenite fixed the $f(S_2)$ during metamorphism, but allowed variations of up to 2.5 log units in $f(O_2)$ within the pyrrhotite-ilmenite field. The assemblage ilmenite-pyrrhotite-rutile in sample U8 does not allow a precise estimate of $f(S_2)$-$f(O_2)$, but in view of the spinel compositions, it probably has values within the field outlined in Figure 8. The spinel samples having the highest contents of chromite and magnetite components and lowest level of the gahnite component appear to be those buffered at the highest $f(S_2)$-$f(O_2)$ values. Other factors that can influence spinel compositions are: modal amount of spinel formed in the rock and bulk composition of the rock (Fig. 4C).

The $f(O_2)$-$f(S_2)$ conditions prevailing during metamorphism in the alteration pipe contrast with those in the adjacent BIF (magnetite field; Fig. 8), auriferous chert (arsenopyrite-pyrite-pyrrhotite-ilmenite; Fig. 8) and associated graphitic argillite (pyrite-pyrrhotite-graphite-rutile; Fig. 8). None of these sedimentary horizons contain vanadiferous zincian-chromian hercynite.

Discussion and Conclusions

Genesis of the Atik Lake hercynite

Vanadiferous zincian-chromian hercynite occurs in metamorphosed altered basalt (cordierite-gedrite rocks) in an alteration pipe. The alteration zone is overlain by auriferous chert and associated graphitic argillite, and by grunerite-magnetite-bearing BIF (Bernier & MacLean 1989). Primary igneous spinel has not been observed in the fresh tholeiitic basalt.

Primary igneous chromian spinel compositions from deep-sea basalts, as reported by Haggerty (1981), are generally aluminous (up to 49 wt.% Al_2O_3), Mg-rich (up to 19 wt.% MgO) and may be Fe^{3+}-rich (up to 11 wt.% Fe_2O_3). The reported compositions do not show even traces of vanadium

and zinc. Spinel in deep-sea basalt occurs as inclusions in plagioclase, pyroxene, olivine and glass and may show complex zoning as a result of interaction between early-formed crystals and liquid owing to a temperature decrease (Haggerty 1981). The Cr/R^{3+} values found in basalt-hosted spinel are similar to those in Atik Lake metamorphosed altered basalt, and this can readily be attributed to a bulk-composition effect.

At Atik Lake, a premetamorphic stage of hydrothermal alteration enhanced Cr–V concentrations in altered basalts as a result of mass loss (Bernier & MacLean 1989). Cr and V behaved as relatively immobile elements. Cr^{3+} and V^{3+} can substitute for Fe^{3+} and Al^{3+} because of their similar ionic radius; they may have been concentrated in aluminous clays (Howard & Fisk 1988) and chlorite when these minerals formed during the hydrothermal alteration of the basalt. Concentration of Cr in sediment *via* the clay fraction is common (Burns & Burns 1975, Treloar 1987). Regional amphibolite-facies metamorphism induced breakdown of the greenschist-facies assemblages to produce cordierite-gedrite rocks. The grains of vanadiferous zincian–chromian hercynite nucleated under relatively low $f(O_2)$ and high $f(S_2)$ conditions, at sites of available Cr–V–Al–Zn released by breakdown of precursor phases. Apart from the hercynite, which contains a major concentration of Cr, traces of Cr also were found in ilmenite, garnet and staurolite, and it is an important component in magnetite, which is scarce. Vanadium was detected in ilmenite, but is a major component (coulsonite) in magnetite (Table 4). The presence of V and Cr in other minerals of the Atik Lake alteration zone reflects the bulk composition of the rocks, acquired during hydrothermal alteration. The absence of pronounced compositional zoning in these spinel grains could be due to their very small size or may indicate that efficient diffusion occurred at the peak conditions of metamorphism.

Spinel having such unusual compositions in metamorphosed mafic and ultramafic rocks can provide a useful guide for potential mineralization of the Outokumpu type (Cu–Co–Zn), Thompson type (Fe–Ni) or Atik Lake type (Fe–As–Zn–Cu–Au–Ag). Furthermore, the spinel grains are resistant to weathering and can be incorporated into the sedimentary cycle and thus provide useful regional indicators of mineralization.

ACKNOWLEDGEMENTS

This paper represents part of the author's doctoral research at McGill University. I thank Westmin Resources Limited, Barringer–Magenta Limited and Polestar Exploration Inc. for access to their property and for research support. Drs. W.H. MacLean, S. Wood, A.M. Abdel-Rahman and R.F. Martin reviewed a preliminary draft of this manuscript. J.E. Mungall's help on the scanning electron microscope was greatly appreciated. I acknowledge the financial assistance provided by an FCAR scholarship (La Formation des Chercheurs et l'Aide à la Recherche). Research costs were partly covered by Natural Sciences and Engineering Research Council grant A7719 to Dr. W.H. MacLean. The manuscript has also benefitted from the review of two referees.

REFERENCES

ARANOVICH, L.Y. & PODLESSKII, K.K. (1983): The cordierite–garnet–sillimanite–quartz equilibrium: experiments and applications. *In* Kinetics and Equilibrium in Mineral Reactions (S.K. Saxena, ed.). Springer-Verlag, New York.

BARTON, P.B., JR. & SKINNER, B.J. (1979): Sulfide mineral stabilities. *In* Geochemistry of Hydrothermal Ore Deposits (H. L. Barnes, ed.). John Wiley & Sons, New York.

BERMAN, R.G. (1988): Internally-consistent thermodynamic data for minerals in the system Na_2O–K_2O–CaO–MgO–FeO–Fe_2O_3–Al_2O_3–SiO_2–TiO_2–H_2O–CO_2. *J. Petrol.* **29**, 445-522.

_____ & BROWN, T. H. (1985): Heat capacity of minerals in the system Na_2O–K_2O–CaO–MgO–FeO–Fe_2O_3–Al_2O_3–SiO_2–TiO_2–H_2O–CO_2: representation, estimation and high temperature extrapolation. *Contrib. Mineral. Petrol.* **89**, 168-183.

BERNIER, L.R. & MACLEAN, W.H. (1989): Auriferous chert, banded iron-formation and related volcanogenic hydrothermal alteration, Atik Lake, Manitoba. *Can. J. Earth Sci.* **26**, 2676-2690.

BRUCKMANN-BENKE, P., CHATTERJEE, N.D. & AKSYUK, M.A. (1988): Thermodynamic properties of $Zn(Al,Cr)_2O_4$ spinels at high temperatures and pressures. *Contrib. Mineral. Petrol.* **98**, 91-96.

BURNS, V.M. & BURNS, R.G. (1975): Mineralogy of chromium. *Geochim. Cosmochim. Acta* **39**, 903-910.

CLARK, S.P., JR. (1966): High-pressure phase equilibria. *In* Handbook of Physical Constants (S.P. Clark Jr., ed.). *Geol. Soc. Am. Mem.* **97**, 345-370.

DELLA GIUSTA, A., PRINCIVALLE, F. & CARBONIN, S. (1986): Crystal chemistry of a suite of natural Cr-bearing spinels with $0.15 \leq Cr \leq 1.07$. *Neues Jahrb. Mineral. Abh.* **155**, 319-330.

EVANS, B.W. & FROST, B.R. (1975): Chrome-spinel in progressive metamorphism — a preliminary analysis. *Geochim. Cosmochim. Acta* **39**, 959-972.

FROESE, E. & GUNTER, A.E. (1976): A note on the

pyrrhotite-sulfur vapor equilibrium. *Econ. Geol.* **71**, 1589-1594.

GRAHAM, C.M. & POWELL, R. (1984): A garnet-hornblende geothermometer: calibration, testing, and application to the Pelona schist, southern California. *J. Metamorph. Geol.* **2**, 13-31.

GROVES, D.I., BARRETT, F.M., BINNS, R.A. & MCQUEEN, K.G. (1977): Spinel phases associated with metamorphosed volcanic-type iron-nickel sulfide ores from Western Australia. *Econ. Geol.* **72**, 1224-1244.

HAGGERTY, S.E. (1981): Opaque mineral oxides in terrestrial igneous rocks. *In* Oxide Minerals (D. Rumble III, ed.). *Rev. Mineral.* **3**, Hg101-299.

HOWARD, K.J. & FISK, M.R. (1988): Hydrothermal alumina-rich clays and boehmite on the Gorda Ridge. *Geochim. Cosmochim. Acta* **52**, 2269-2279.

JACOB, K.T. (1976): Gibbs free energies of formation of $ZnAl_2O_4$ and $ZnCr_2O_4$. *Thermochim. Acta* **15**, 79-87.

KOHN, M.J. & SPEAR, F.S. (1989): Empirical calibration of geobarometers for the assemblage garnet + hornblende + plagioclase + quartz. *Am. Mineral.* **74**, 77-84.

LOFERSKI, P.J. & LIPIN, B.R. (1983): Exsolution in metamorphosed chromite from the Red Lodge district, Montana. *Am. Mineral.* **68**, 777-789.

MACLEAN, W.H. & KRANIDIOTIS, P. (1987): Immobile elements as monitors of mass transfer in hydrothermal alteration: Phelps Dodge massive sulfide deposits, Matagami, Quebec. *Econ. Geol.* **82**, 951-962.

MOORE, A.C. (1977): Zinc-bearing chromite (donathite?) from Norway: a second look. *Mineral. Mag.* **41**, 351-355.

OEN, I.S. (1973): A peculiar type of Cr-Ni-mineralization; cordierite-chromite-niccolite ores of Màlaga, Spain, and their possible origin by liquid unmixing. *Econ. Geol.* **68**, 831-842.

O'NEILL, H.ST.C. & NAVROTSKY, A. (1984): Cation distributions and thermodynamic properties of binary spinel solid solutions. *Am. Mineral.* **69**, 733-753.

ONYEAGOCHA, A.C. (1974): Alteration of chromite from the Twin Sisters dunite, Washington. *Am. Mineral.* **59**, 608-612.

RIMSAITE, J. & LACHANCE, G.R. (1971): Examples of spinel-mica associations in Canadian ultrabasic rocks and in nickel deposits. *Geol. Surv. Can. Pap.* **71B**, 82-85.

SEELIGER, E. & MÜCKE, A. (1969): Donathit, ein Tetragonaler, Zn-reicher Mischkristall von Magnetit und Chromit. *Neues Jahrb. Mineral., Monatsh.*, 49-57.

SEYFRIED, W.E. & MOTTL, M.J. (1982): Hydrothermal alteration of basalt by seawater under seawater-dominated conditions. *Geochim. Cosmochim. Acta* **46**, 985-1002.

SHARP, Z.D., ESSENE, E.J. & KELLY, W.C. (1985): A re-examination of the arsenopyrite geothermometer: pressure considerations and applications to natural assemblages. *Can. Mineral.* **23**, 517-534.

THAYER, T.P, MILTON, C., DINNIN, J. & ROSE, H., JR. (1964): Zincian chromite from Outokumpu, Finland. *Am. Mineral.* **49**, 1178-1183.

TRELOAR, P.J. (1987): The Cr-minerals of Outokumpu - their chemistry and significance. *J. Petrol.* **28**, 867-886.

_____, KOISTINEN, T.J & BOWES, D.R. (1981): Metamorphic development of cordierite-amphibole rocks and mica schists in the vicinity of the Outokumpu ore deposit, Finland. *Trans. Roy. Soc. Edinb., Earth Sci.* **72**, 201-215.

UTTER, T. (1978): The origin of detrital chromites in the Klerksdorp Goldfield, Witwatersrand, South Africa. *Neues Jahrb. Mineral., Abh.* **133**, 191-209.

WAGNER, C. & VELDE, D. (1985): Mineralogy of two peralkaline, arfvedsonite-bearing minettes. A new occurrence of Zn-rich chromite. *Bull. Minéral.* **108**, 173-187.

WAKIHARA, M., SHIMIZU, Y. & KATSURA, T. (1971): Preparation and magnetic properties of the FeV_2O_4-Fe_3O_4 system. *J. Solid State Chem.* **3**, 478-483.

WEISER, T. (1967): Zink- und Vanadium-Führende Chromite von Outokumpu, Finnland. *Neues Jahrb. Mineral., Monatsh.*, 234-243.

WYLIE, A.G., CANDELA, P.A. & BURKE, T.M. (1987): Compositional zoning in unusual Zn-rich chromite from the Sykesville district of Maryland and its bearing on the origin of "ferritchromit". *Am. Mineral.* **72**, 413-422.

Received August 29, 1989, revised manuscript accepted October 26, 1989.

3E. LITHOGEOCHEMISTRY OF THE NÉMISCAU AMPHIBOLITES, CORDIERITE-ANTHOPHYLLITE AND ASSOCIATED ROCKS.

Introduction

Twenty-nine rock samples from the Albanel, Lac de la Hutte and Lac du Crochet claim blocks were selected for a lithogeochemistry study (Fig. 3E1.). These include eight metabasalts, one ultramafic rock, three sericitized and chloritized amphibolites, twelve cordierite-anthophyllite and anthophyllite-bearing rocks, three sillimanite-bearing gneisses and two K-feldspar bearing felsic gneisses (Table 3E.1). The sample location are shown in *Appendix I*. These samples represent the only chemical analyses reported for rocks of the Némiscau belt. Their mineralogy and mineral chemistry are presented in the section on metamorphism (Chapter 4).

In this section, the major and trace element geochemistry is used to characterize protoliths and their probable origins. The chemical changes resulting from hydrothermal alteration (now cordierite-anthophyllite rocks) are estimated and compared to changes caused by retrograde sericitization and chloritization of some of the amphibolites. The close association of the cordierite-anthophyllite rocks with mafic volcanics permits a comparison to be made with the rocks at Atik Lake. Finally, the Log(Ratio) method is used to identify protoliths in the Némiscau rocks which are at a higher metamorphic grade than those at Atik Lake.

AMPHIBOLITE CHEMISTRY

The least altered amphibolites (N-09, N-30, N-34A, N-15) are composed essentially of hornblende and plagioclase, contain 46 to 52 wt% SiO_2, have

Fig. 3E.1 Geological map of the Némiscau belt, with mineral showings, modified after Valiquette (1975).

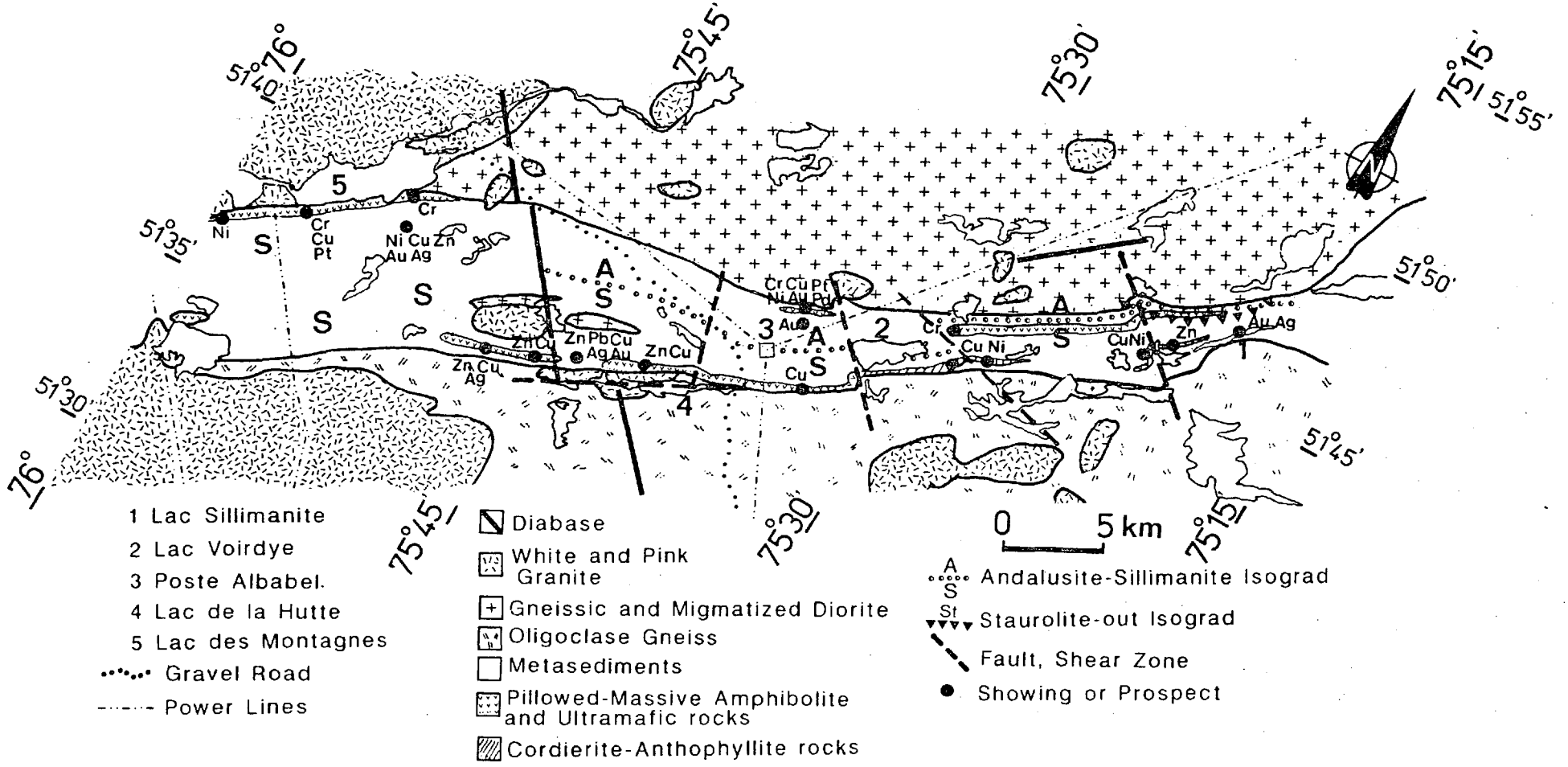
76°
51°40'
75°45'
75°30'
75°15'
51°55'
51°35'
51°50'
51°30'
51°45'
N
5
4
3
2
1
S
A
Ni
Cr
Cu
Pt
Ni Cu Zn
Au Ag
Cr Cu Pt
Ni Au Pd
Au
Zn Cu
Zn Pb Cu
Ag Au
Zn Cu
Ag
Zn Cu
Cu
Cr
Cu Ni
Cu Ni
Zn
Au Ag
0 5 km
1 Lac Sillimanite
2 Lac Voirdye
3 Poste Albabel.
4 Lac de la Hutte
5 Lac des Montagnes
Gravel Road
Power Lines
Diabase
White and Pink Granite
Gneissic and Migmatized Diorite
Oligoclase Gneiss
Metasediments
Pillowed-Massive Amphibolite and Ultramafic rocks
Cordierite-Anthophyllite rocks
Andalusite-Sillimanite Isograd
Staurolite-out Isograd
Fault, Shear Zone
Showing or Prospect

TABLE 3E.1. CHEMICAL ANALYSES OF NÉMISCAU ROCKS

	Amphibolite								UM
	N-09	N-28	N-30	N-34A	N-06	N-12	N-13	N-15	N-08
SiO_2	46.26	53.18	51.91	50.09	50.22	50.12	56.76	50.76	45.35
TiO_2	0.96	0.80	0.85	1.71	0.52	0.52	0.89	0.84	0.16
Al_2O_3	14.25	8.69	15.33	13.93	11.73	14.54	14.99	14.17	4.15
$Fe_2O_3^1$	12.78	12.08	14.06	18.34	10.36	10.86	10.28	12.68	8.72
MnO	0.23	0.40	0.22	0.28	0.21	0.21	0.13	0.19	0.12
MgO	6.88	12.39	8.16	6.21	13.99	9.15	6.55	8.45	29.03
CaO	11.97	11.43	9.04	7.96	9.18	10.69	5.26	11.75	5.30
Na_2O	1.83	0.32	0.59	1.32	0.08	1.58	2.96	1.76	0.01
K_2O	0.84	0.11	0.05	0.17	1.46	0.85	1.04	0.14	0.01
P_2O_5	0.08	0.07	0.07	0.14	0.04	0.14	0.21	0.04	0.02
LOI	1.29	0.69	0.61	0.47	2.02	1.07	1.43	1.76	6.75
Total	100.37	100.16	100.89	100.62	99.81	99.73	100.50	100.51	99.64
V	259	195	305	419	167	158	143	263	63
Cr	290	69	281	84	1270	1100	306	279	2573
Ni	135	38	104	40	529	323	125	70	1772
Ba	38	15	29	92	30	139	195	28	10
Nb	7	5	7	8	5	6	9	6	6
Zr	85	97	78	120	70	101	133	73	45
Y	21	18	21	35	12	12	19	16	5
Sr	126	172	147	150	157	578	254	125	76
Rb	48	77	8	12	78	71	72	113	7
Zr/Y	4.1	5.4	3.7	3.4	5.8	8.4	7.0	4.6	9.0
Nb/Y	0.3	0.3	0.3	0.2	0.4	0.5	0.5	0.4	1.2
X_{Mg}	0.50	0.66	0.52	0.39	0.72	0.61	0.55	0.56	0.86

[1]Total iron as Fe_2O_3. $X_{Mg}=Mg/(Fe^{tot}+Mg)$ on a cation basis.

All oxides and LOI are in weight % and trace elements are in ppm.

	SA			Sillimanite Gneiss					
				felsic			mafic		
	N-18	N-19	N-26	N-07	N-10	N-11	N-27	N-33	N-31
SiO_2	64.49	55.55	50.65	80.04	72.38	76.99	58.48	63.37	47.89
TiO_2	0.59	1.33	1.05	0.12	0.13	0.14	0.77	0.67	0.25
Al_2O_3	20.53	16.71	20.99	13.71	13.32	13.95	20.29	20.43	6.90
$Fe_2O_3^1$	1.48	9.74	10.60	1.06	1.80	1.24	8.69	3.52	10.10
MnO	0.04	0.42	0.29	0.03	0.07	0.05	0.09	0.07	0.14
MgO	1.20	3.11	4.73	1.30	3.03	0.99	3.38	1.32	27.42
CaO	0.78	3.05	3.32	0.97	5.25	1.04	1.12	2.83	2.22
Na_2O	3.32	0.66	2.12	0.23	0.15	0.38	1.16	4.47	0.01
K_2O	2.18	5.34	3.30	1.23	1.83	3.48	4.25	1.98	0.06
P_2O_5	0.20	0.57	0.07	0.04	0.04	0.04	0.14	0.11	0.02
LOI	2.18	3.59	3.40	1.38	2.32	1.75	2.01	1.25	4.87
Total	100.28	100.17	100.52	100.11	100.32	100.05	100.38	99.95	99.88
V	120	160	291	10	10	10	151	108	102
Cr	210	127	491	46	15	15	232	143	2725
Ni	13	80	176	20	15	10	94	113	1279
Ba	461	928	659	287	94	220	766	224	60
Nb	5	14	5	12	12	11	9	10	6
Zr	135	214	97	98	110	110	122	175	47
Y	26	38	18	7	6	12	20	9	5
Sr	191	112	202	144	93	578	145	277	42
Rb	400	306	162	67	77	71	141	68	8
Zr/Y	5.2	5.6	5.4	14.0	15.7	18.3	6.1	19.4	9.4
Nb/Y	0.2	0.4	0.3	1.7	1.7	1.8	0.5	1.1	1.2
X_{Mg}	0.60	0.35	0.46	0.70	0.76	0.60	0.42	0.41	0.84

TABLE 1. (Continued)

	Orthoamphibolite										
	N-14*	N-16*	N-20*	N-21*	N-25	N-29B	N-32	N-34B	N-35	N-36*	N-39
SiO_2	50.76	49.72	46.61	49.74	47.25	51.14	59.33	53.02	53.45	51.14	52.25
TiO_2	1.00	1.07	2.08	1.49	0.79	1.63	0.95	0.84	0.82	0.87	1.06
Al_2O_3	20.30	21.37	16.75	13.73	14.16	13.48	16.43	15.27	15.22	15.99	19.46
$Fe_2O_3^t$	11.34	10.83	15.43	14.39	14.35	17.62	14.42	18.68	18.84	13.62	12.79
MnO	0.17	0.21	0.15	0.27	0.14	0.33	0.34	0.45	0.45	0.20	0.21
MgO	4.97	4.61	10.27	13.39	15.10	10.55	5.59	10.58	10.58	9.91	6.96
CaO	6.98	7.82	6.98	6.23	2.40	0.67	1.13	0.50	0.58	7.50	4.13
Na_2O	2.47	1.76	0.69	0.43	0.50	0.25	0.63	0.26	0.26	1.19	1.19
K_2O	1.10	0.88	0.51	0.33	2.48	0.17	1.42	0.40	0.40	0.04	0.85
P_2O_5	0.07	0.06	0.14	0.18	0.06	0.12	0.09	0.04	0.03	0.07	0.05
LOI	1.43	2.17	1.21	0.74	3.06	4.79	1.11	1.09	1.03	0.21	2.05
Total	100.59	100.50	100.82	100.82	100.29	100.75	101.44	101.20	101.66	100.74	101.00
V	281	292	342	248	216	330	255	236	240	248	319
Cr	487	523	171	56	306	119	279	348	334	328	600
Ni	163	172	101	58	122	68	72	166	156	156	169
Ba	86	198	43	116	192	11	268	49	40	43	187
Nb	5	6	6	10	5	7	6	6	6	7	6
Zr	96	96	124	121	69	116	81	72	72	76	83
Y	16	15	16	22	22	25	14	13	18	17	12
Sr	169	155	103	95	67	37	103	38	40	107	120
Rb	76	53	59	40	92	25	58	20	28	10	31
Zr/Y	6.0	6.4	7.8	5.5	3.1	4.6	5.8	5.5	4.0	4.5	6.9
Nb/Y	0.3	0.4	0.4	0.9	0.2	0.3	0.4	0.5	0.3	0.4	0.5
X_{Mg}	0.56	0.45	0.56	0.64	0.67	0.53	0.39	0.52	0.52	0.58	0.51

* cordierite is absent.

generally less than 1 wt% TiO_2, and are low in K_2O (0.05-0.84 wt%) (Table 3E.1). One sample (N-28) has low Al_2O_3 content (8.69 wt%) and higher MgO than the others. Three groups of the amphibolites can be defined on the basis of Cr content: 1) low-Cr (<100 ppm; N-28, N-34A), 2) intermediate-Cr basaltic range (~200-300 ppm; N-09, N-13, N-15, N-30, N-34), and 3) high-Cr (>1000 ppm; N-06, N-12). Three samples (N-13, N-06, N-12) showing evidence of moderate to strong shearing are cummingtonite-bearing and more potassic (0.85-1.46 wt% K_2O) than their unsheared counterparts.

The compositional homogeneity of the three amphibolite types can be tested with the immobile element Log(Ratio) diagram (Fig. 3E.2). Samples of intermediate-Cr amphibolites have very similar ratios (Fig. 3E.2A), although the sheared sample N-13 shows minor differences. The low- and high-Cr amphibolites have substantially different (Figs. 3E.2B, C) profiles. The high-Cr amphibolite profile is transitional with the intermediate-Cr amphibolite and the ultramafic unit (Fig. 3E.2D). The two high-Cr samples from Lac de la Hutte may represent metamorphosed sills, or more primitive Mg-basalt flows.

For comparison, Log(Ratio) profiles are shown for a series of basalts, komatiites, and boninites from well known areas (Fig. 3E.3). From these diagrams, it is clear that mafic magmas have distinctive Log (Ratio) profiles. The intermediate-Cr amphibolites at Némiscau have profiles similar to MORB (Figs. 3E.2A, 3E.3A). The low-Cr amphibolite profile (Fig. 3E.2B) is transitional with that of Andean calc-alkaline basalts (Fig. 3E.3B) and MORB (Fig. 3E.3A). The high-Cr amphibolites profiles (Figs. 3E.2C) are clearly distinct from those of island arc calc-alkaline Mg-rich basalts at Vanuatu (Fig. 3E.3C), and basaltic komatiite and peridotitic komatiite at the Barbeton Belt (Fig. 3E.3D. However, they are very similar to olivine boninites from

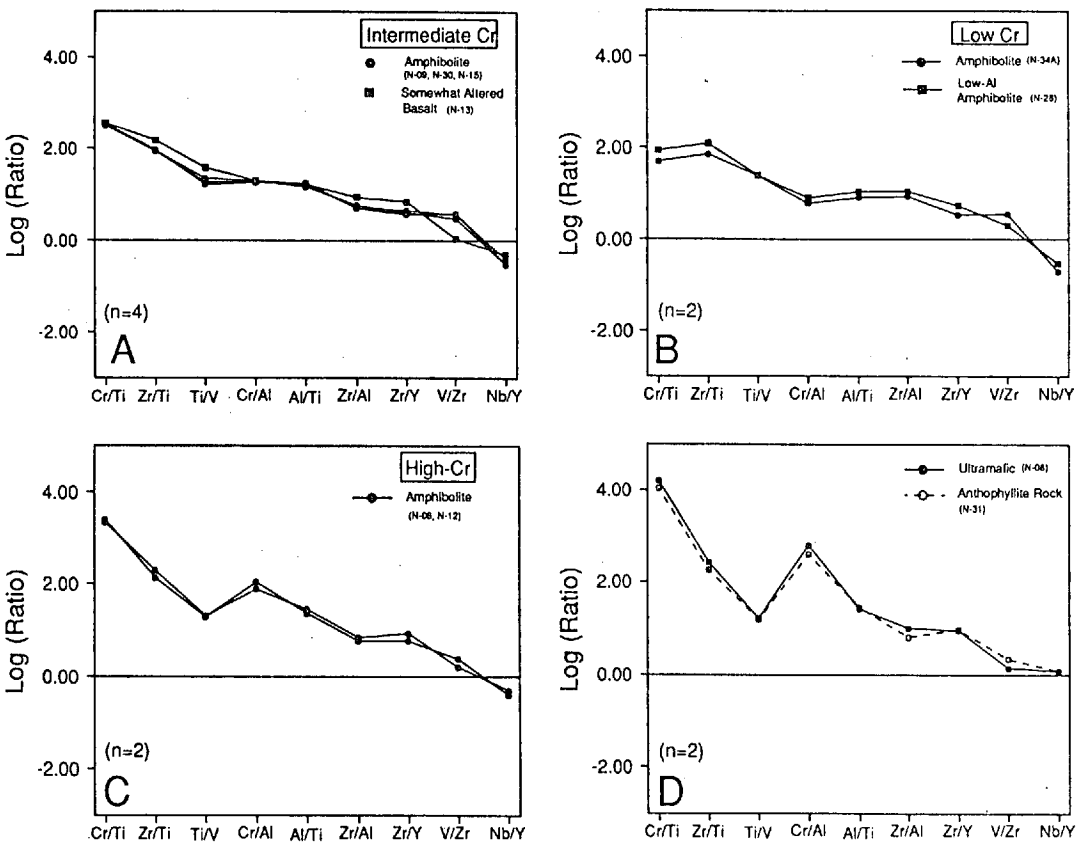

Fig. 3E.2 Log(Ratio) diagrams for Némiscau amphibolites and ultramafic rocks.

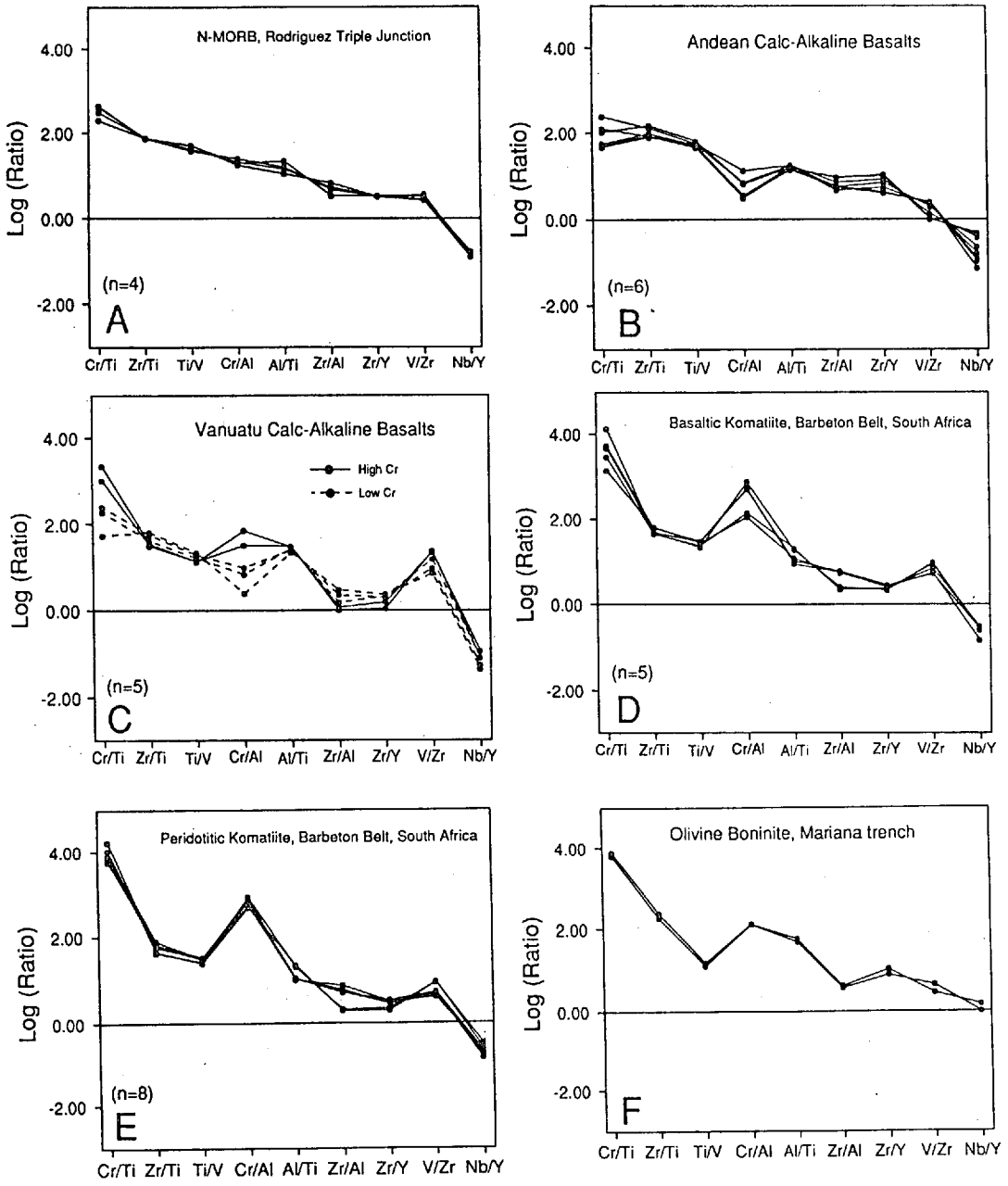

Fig. 3E.3 Log(Ratio) diagrams for mafic and ultramafic rocks using data from the literature. A) Data from Herzig and Plüger (1988), B) Hickey et al. (1986), C) Barsdell and Berry (1990), D) Nesbitt et al. (1979), and E) Bloomer and Hawkins (1987).

the Mariana trough (Fig. 3E.3F), apart from a slightly lower Al/Ti ratio. Boninites are generated during arc volcanism and have the chemical characteristics of primitive mantle-derived magmas (X_{Mg}>0.7, Ni=100-450 ppm, Cr=300-900 ppm; Bloomer and Hawkins, 1987) as do the high-Cr amphibolites from Némiscau (Table 3E.1).

ULTRAMAFIC ROCK CHEMISTRY

Two samples of ultramafic rocks were analysed, one (N-08) being typical of a tremolite-olivine-magnetite-serpentine ultramafic lens, and the other (N-31) of an anthophyllite-rich body transitional with another ultramafic lens, 10 km northeast of sample N-08. Both samples are characterized by low TiO_2 (0.16, 0.25 wt%), Al_2O_3 (4.15, 6.90 wt%), and Zr (45, 47 ppm), but high Cr (2573, 2725 ppm) and MgO (27.42, 29.05 wt%), typical of a peridotitic composition (e.g. Nesbitt et al., 1979). They have very similar log(Ratio) profiles (Fig. 3E.2D) which closely resemble that of the olivine boninite, compared with that of the peridotitic komatiite (Figs. 3E.3E, 3E.3F). Primary boninitic magmas are thought to result from hydrous melting of a mixture of a depleted peridotitic mantle and a LREE, Zr, Ba and Sr-rich fluid or melt. The reader is referred to the work of Bloomer and Hawkins (1987) for additional references. The anthophyllite-rich rocks is most likely derived from the metamorphism of a serpentinized ultramafic body.

The recognition of bonititic rocks in the Némiscau belt has important implications on the nature of the paleotectonic setting. More detailed petrological work will be required to further resolved the exact nature of these rocks.

ALTERED ROCKS

Cordierite-anthophyllite rocks

The metamorphosed altered mafic rocks have anthophyllite as the dominant amphibole and can be termed orthoamphibolite. Two sub-groups of orthoamphibolites are recognized in the Némiscau belt on the basis of mineralogy: 1) cordierite-anthophyllite ± garnet rocks, and 2) anthophyllite ± cummingtonite plagioclase rocks. Biotite is present in all samples. Peredery (1966) reported staurolite inclusions in garnets from some of the cordierite-anthophyllite rocks. In his detailed mapping of part of the Lac Senay cordierite-anthophyllite zone, Perydery clearly showed the transitional nature of hornblende-bearing metabasalt with cummingtonite-bearing amphibolite and cordierite-anthophyllite rocks, which is most likely an alteration feature. These cummingtonite-bearing rocks are similar to those in the Flin Flon belt interpreted by Froese and Ashton (1990) as altered rocks derived from moderate Fe-Mg metasomatism.

The nature of the altered rock protoliths was assessed with the Log(Ratio) profiles (Figs. 3E.4A, B). The orthoamphibolites are clearly derived from both the intermediate-Cr (compare Figs. 3E.2A and 3E.4A), and the low-Cr basaltic amphibolites (Figs. 3E.2B, 3E.6B). In both, there is a range in the ratios involving Y, which was probably mobile and leached. The range in Cr/Ti and Cr/Al ratios are likely due to igneous fractionation (c.f. Carmichael, 1974).

Zincian-chromian hercynite grains were analysed in a cordierite-anthophyllite sample (N-39) with the highest Cr/Al ratio (31). The grains are very small (≈10 μm) and composed of 36% chromite, 33% hercynite, 22% gahnite, 8% spinel, 1% coulsonite, comparable to those in the Atik Lake rocks (Bernier, 1990). Zincian-chromian spinel of metamorphic origin has also

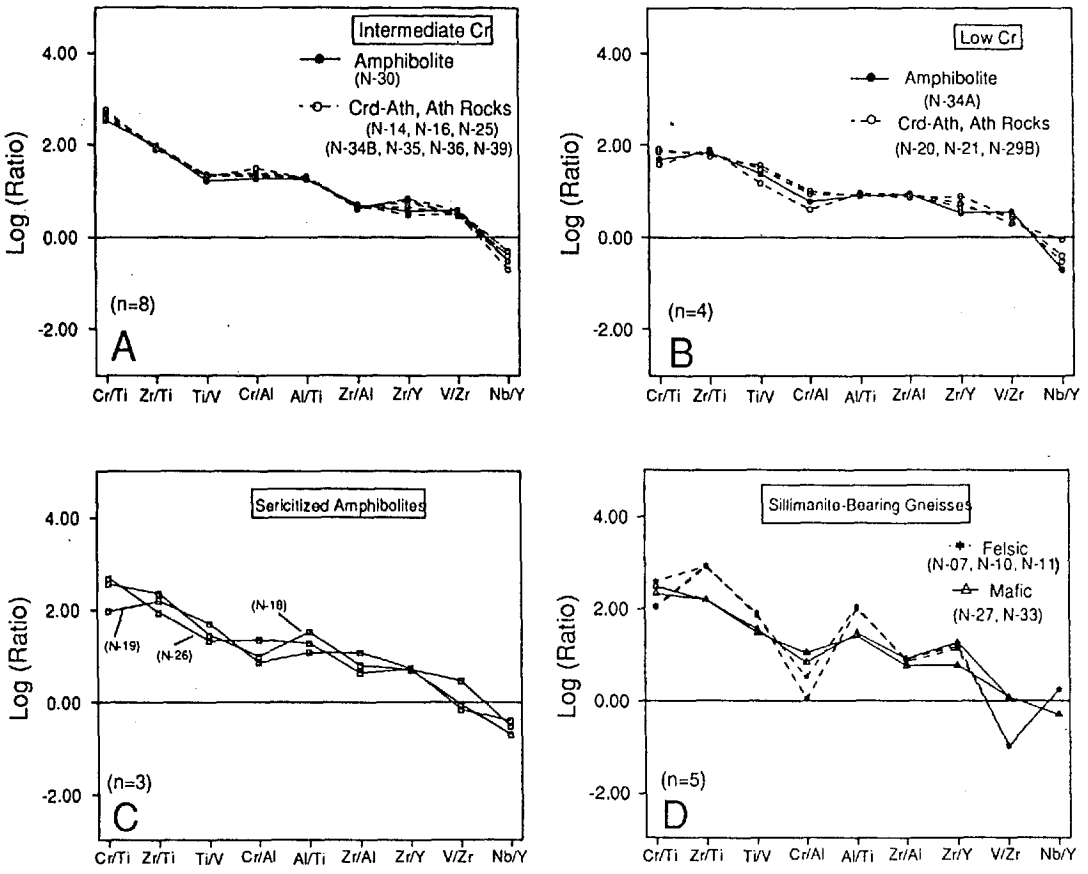

Fig. 3E.4. Log (Ratio) diagrams for altered rocks in the Némiscau belt.

been reported by Pan and Fleet (1991).

Most of the amphibolite and orthoamphibolite samples plot within the basalt field in a Zr/TiO_2-Nb/Y (Fig. 3E.5). The scatter of the Nb/Y data is most likely related to the Y mobility.

On the metamorphic ACF diagram (Fig. 3E.6), altered samples (orthoamphibolites) plot within fields of aluminous metamorphic phases as a result of loss of CaO during hydrothermal alteration. The alteration pattern is very similar to that observed at Atik Lake (Bernier, 1990).

Sericitized amphibolites

Three samples of sericitized amphibolites from Lac de la Hutte fault zone have been analysed. Two (N-18, N-19) are from an outcrop hosting a mineralized quartz vein (Fig. 3E.1), and the other (N-26) near a pegmatite body 800 m to the east. These samples are highly sheared, and remnants of garnet porphyroblasts were extensively rotated and chloritized. The sericite laths define an anastamosing schistosity superimposed on a flaser fabric.

These sericitized amphibolites have distinct Log(Ratio) profiles (Fig. 3E.4C) that are readily comparable to the intermediate- and low-Cr basaltic amphibolites (Figs. 3E.2A,B; 3E.4C). Chemical changes are characterized by large increases in K_2O (2.18-5.34 wt%), LOI (2.18-3.59 wt%), Ba (461-928) and Rb (162-400) and mainly reflect sericitization.

Sillimanite-bearing gneisses

Sillimanite-bearing gneisses form felsic (N-07, N-10) and mafic (N-27, N-31) groups on the basis of chemistry (Table 3E.1). The mafic gneiss has log (Ratio) profiles very similar to the most sericitized amphibolite sample (N-18, igs. 3E.4C, D) and could be a metamorphosed counterpart. The profile

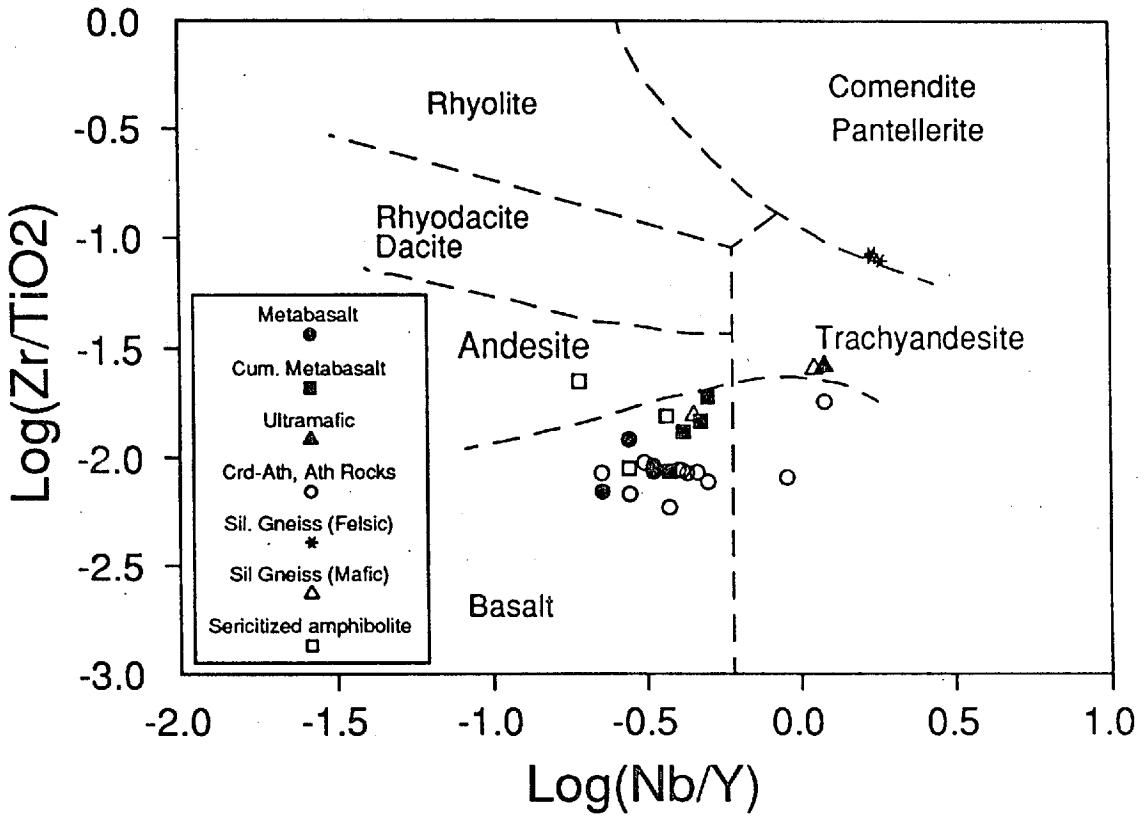

Fig. 3E.5 Log(Zr/TiO_2) - Log(Nb/Y) discriminant diagram (Winchester and Floyd, 1977) for rocks in the Némiscau belt.

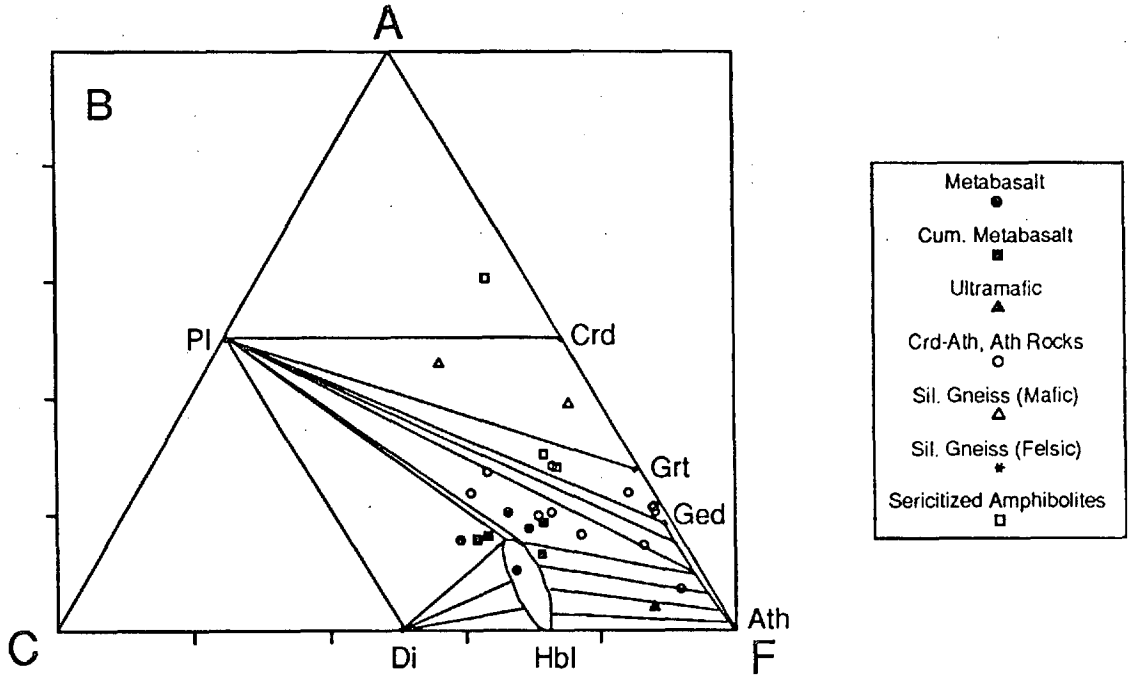

Fig. 3E.6 Bulk rock compositions plotted on an ACF diagram. A: Al_2O_3 + Fe_2O_3 - Na_2O - K_2O, C: CaO - 3.3 P_2O_5, F: FeO + MgO + MnO.

for the felsic gneiss is identical to that of the felsic intrusive rocks at Atik Lake (Fig. 3C.1G in section 3C) and fall in the comendite-pantellerite field in a Log(Zr/TiO_2)-Log(Nb/Y) diagram (Fig. 3E.5).

CONCLUSION

Freshest intermediate- and low-Cr amphibolites in the Némiscau belt are metamorphosed equivalents of basaltic protoliths (MORB and calc-alkaline). The high-Cr amphibolites and ultramafic rocks protoliths were not derived from typical komatiitic magma but have Log(Ratio) profiles similar to olivine boninite and may reflect arc volcanism. The orthoamphibolite rocks were most likely derived by metamorphism of chloritized basalts and serpentinised ultramafic bodies formed during sea-floor and volcanogenic hydrothermal alteration. Sericitized amphibolite formed during retrograde alteration associated with the emplacement of a mineralized quartz vein during brittle faulting related to the Lac de la Hutte fault. Mafic sillimanite-bearing gneisses probably represent the metamorphosed equivalents of sericitized amphibolites. The felsic sillimanite-bearing gneiss has a felsic intrusive rock protolith.

The Log(Ratio) diagram is useful in locating irregularities in the geochemistry of a suite of metamorphosed volcanic rocks. It can help to identify the most probable protoliths. It has proved to be capable of relating specific rock types to one another within the stratigraphy of the Némiscau terrane, even though samples may by highly altered and separated by large distances from each other (see location map in *Appendix I*).

3F. GEOMETRY AND LITHOGEOCHEMISTRY OF A METAMORPHOSED VMS ALTERATION ZONE AT MONTAUBAN, GRENVILLE PROVINCE, QUEBEC: A NEW APPROACH TO PROTOLITH IDENTIFICATION.

(to be submitted)

ABSTRACT

The Montauban stratiform polymetallic (Zn-Pb-Cu-Ag-Au) deposits form part of the Montauban Group, which is east of the Allochtonous Monocyclic Belt in the Proterozoic Grenville Province. Two main types of ore have been mined: Ag-rich Zn-Pb-Cu massive sulfide ore in calc-silicate rocks, and disseminated gold ore in quartzitic gneiss. Metal zoning is prominent at the North Gold Zone and outlines a Au-Cu-rich core plunging to the south, and parallel to the mineral lineation.

The mine sequence consists of massive sulfide ores, marble, calc-silicate rocks, biotite-muscovite quartzofeldspathic gneiss, cordierite-anthophyllite gneiss, nodular sillimanite gneiss, and polymetallic mineralization and gold and silver ores in quartzitic gneiss. The Log(Ratio) immobile element method indicates these gneisses are derived from intermediate to felsic volcanic rocks or related volcaniclastic sediments. The mine sequence at the North Gold Zone represents a metamorphosed alteration zone that has been transposed during ductile shearing.

The cordierite-anthophyllite rocks and associated gneisses are the metamorphosed equivalents of hydrothermally altered protoliths dominated by Mg-rich chlorite ± talc ± sericite ± quartz. Log(Ratio) profiles and mass balance calculations show that the rocks of the mine sequence were derived

from surrounding biotite-muscovite quartzofeldspathic gneiss. During alteration some rocks gained mass by addition of Si, Mg and Fe, whereas others lost mass by leaching of Si, Ca and Na, which resulted in the residual concentration of immobile elements (Al, Ti, Zr, Y). The calc-silicate rocks were probably derived from Mg-Ca carbonates and marl deposited coevally with the ores or from a carbonatization during hydrothermal alteration.

The Montauban ores and alteration resemble Kuroko-type massive sulfide deposits and were likely formed in a volcanic arc environment in a dominantly sedimentary and felsic volcanic terrane. Intense deformation and upper-amphibolite metamorphism (T=620°C, P=6.5 kbars) occurred during the Grenvillian orogeny.

INTRODUCTION

Two principal genetic models have been proposed to explain the formation of the base-metal and gold deposits in high grade metamorphic gneisses at Montauban, Quebec. Early workers (O'Neil and Osborne, 1939; Wilson, 1939; Smith, 1956) postulated a replacement pyrometasomatic origin during metamorphism. Later, King (1958) compared the Montauban and Broken Hill (Australia) deposits and proposed that both formed prior to metamorphism and deformation. The discovery of pillowed metabasalt (Pyke, 1966) in the Montauban Group, combined with the stratiform nature of the sulfide lenses, led to the classification of the Montauban ores as volcanogenic massive sulfide deposits, of pre-metamorphic origin (Sangster, 1972; Stamatelopoulou-Seymour and MacLean, 1977; MacLean et al., 1982; Bernier et al., 1987; Morin, 1987). Associated cordierite-anthophyllite rocks have been interpreted as either a metamorphosed hydrothermal alteration zone coeval with

ore formation, or a Mg-rich chemical sediment.

This paper provides new information on the distribution of lithological units in the Montauban mine sequence. The relationship of cordierite-anthophyllite rocks and associated nodular sillimanite and quartzitic gneisses to more widespread biotite-muscovite quartzofeldspathic gneiss is examined using major and trace element geochemistry. The Log(Ratio) method based on immobile elements ratio profiles indicates that the biotite-muscovite quartzofeldspathic gneisses are the metamorphosed equivalent of dacitic-rhyodacitic volcanic rocks, and are also the protolith of the cordierite-anthophyllite, biotite-cordierite, nodular sillimanite and mineralized quartzitic gneisses. Mass balance calculations reveal gains and losses of chemical components that are characteristic of volcanogenic hydrothermal alteration. The geometry of the altered rocks and metal zoning reflect a footwall alteration zone that was inverted, transposed and recrystallized during deformation and metamorphism. These data, in conjunction with structural information and estimates of conditions of metamorphism, are used to interpret the origin and paleo-tectonic setting of the deposits.

PREVIOUS GEOLOGICAL STUDIES

Regional geological mapping in the Montauban area was carried out by Bancroft (1915), Smith (1956), Pyke (1966), Rondot (1978) and Morin (1987). The ore deposits and host rocks were studied by Osborne (1939), O'Neil and Osborne (1939), Wilson (1939), Smith (1956), Prabhu and Webber (1984), Stamatelopoulou-Seymour and MacLean (1984), Bernier (1985), and Bernier et al. (1987).

Stamatelopoulou-Seymour and MacLean (1977) used major element chemistry to propose a volcanic origin for the quartzofeldspathic gneisses of the region, whereas Prahbu and Webber (1984) favored a metasedimentary origin for the rocks. A trace element geochemical study of the amphibolites and metabasalts in the area (MacLean et al., 1982) indicated that these rocks are metamorphosed island-arc tholeiites. Recent discoveries of polymetallic mineralization 40 km north of Montauban (Hébert and Nadeau, 1990) have contributed to a reactivation of mineral exploration in the area.

The metamorphism of the orebodies and alteration zone was outlined by Stamatelopoulou-Seymour and MacLean (1984) and Bernier et al. (1987). More recently, Bernier (1991) proposed a metamorphic evolution model based on mineral equilibria in the cordierite-anthophyllite rocks.

GEOLOGIC SETTING

The Montauban Group, which includes the Montauban ore bodies, lies within the St-Maurice tectonic zone (Fig. 1) (Nadeau and Hébert, 1990). The western margin of this zone is a ductile shear zone that dips gently to the east, whereas the eastern margin is bounded by a subvertical sinistral ductile shear zone (Nadeau and Corrigan, 1991).

The Montauban massive sulfides and North Gold Zone (NGZ) ore bodies (Figs. 2, 3) are stratiform lenses within calc-silicate, cordierite-anthophyllite and nodular sillimanite gneisses. This group of rocks is locally referred to as the mine sequence, which is enclosed within quartzofeldspathic gneisses, quartzite and metabasalt (Fig. 4A) that are part of the Proterozoic amphibolite-facies Montauban Group (Rondot, 1978) in the Grenville Province (Fig. 1). Lead-isotope measurements on the Pb-Zn ores

Fig. 1. A. Geology of the Montauban area (modified from Pyke, 1966 and Morin, 1987). The location of Montauban (M) is shown in the regional inset map. B. Regional tectonic setting after Rondot (1978) and Nadeau and Corrigan (1991). The Montauban Group (hatched area) is in the St-Maurice tectonic zone (SMTZ) west of the Mékinac Group (MG), and east of the Laurentides Park Complex (LPC). The southeast portion of the area is occupied by the St-Lawrence lowlands (SLL). Symbols: LT = La Tuque, NDA = Notre Dame des Anges., M = Montauban, TR = Trois Rivières. SLR = St-Lawrence River.

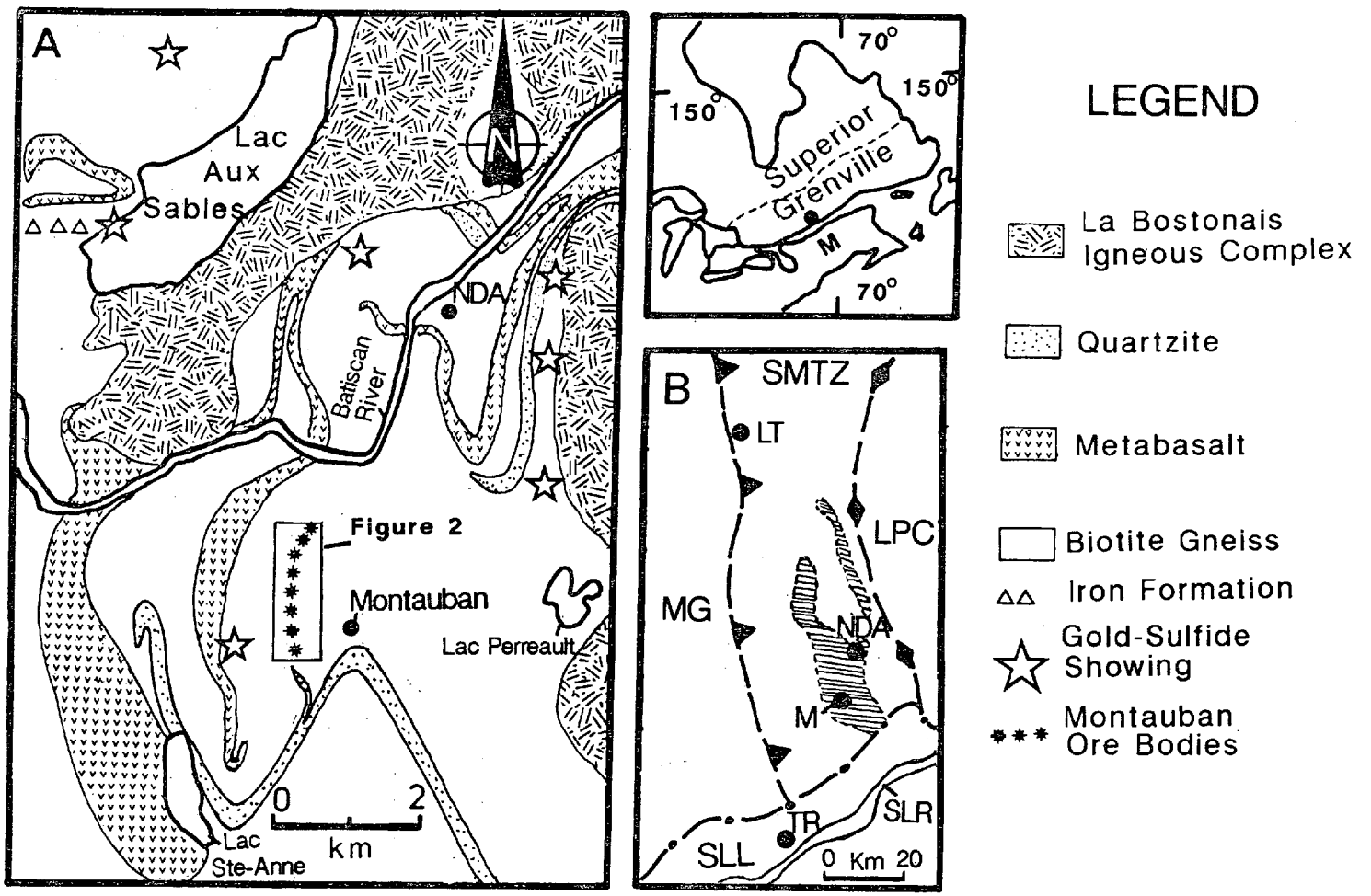
A
Lac
Aux
Sables
N
NDA
Batiscan
River
Figure 2
Montauban
Lac Perreault
0
2
km
Lac
Ste-Anne
70°
150°
150°
Superior
Grenville
M
4
70°
B
SMTZ
LT
LPC
MG
NDA
M
JR
SLR
SLL
0 Km 20
LEGEND
La Bostonais
Igneous Complex
Quartzite
Metabasalt
Biotite Gneiss
Iron Formation
Gold-Sulfide
Showing
Montauban
Ore Bodies

yield a minimum age of 1.27 Ga (Fletcher and Farquhar, 1982).

MINE SEQUENCE

The mine sequence is enclosed to the east by a hornblende-plagioclase grey gneiss (Figs. 2, 4B) and to the west by biotite-muscovite quartzofeldspathic gneiss (Fig. 4C). A recently discovered unit of felsic lapilli tuff lies between the pillowed metabasalt ridge and the NGZ. An age of 1.45 Ga was recently obtained with zircon from that tuff (Nadeau, pers. comm.). The biotite-muscovite quartzofeldspathic gneiss at the NGZ is composed of alternating orthoclase-biotite-muscovite, orthoclase-biotite-muscovite-quartz and quartz-rich layers, each 1-3 cm thick (Fig. 4C). The mine sequence (Table 1) consists of calc-silicate gneiss, biotite-muscovite quartzofeldspathic gneiss (Fig. 4C), mineralized garnet-gahnite quartzitic gneiss (Figs. 4D, E), cordierite-anthophyllite rock (Figs. 4F-I), and nodular sillimanite gneiss (Figs. 4J, K). Metamorphic mineral assemblages for chemically analysed samples of these units are listed in the *Appendix*.

Mafic sills intersect the mine sequence at low angles and are deformed, foliated and metamorphosed to garnet-bearing amphibolite (Fig. 4L). Undulating pegmatite dykes are abundant in the grey gneiss and locally crosscut the mine sequence and mineralization.

The most striking structural feature affecting the mine sequence is a sub-horizontal stretching mineral lineation within locally crenulated S1 planes. The orebodies are also sub-horizontal and very elongated. The surrounding regional gneisses are affected by this strong lineation, which points to a NNE sub-horizontal tectonic transport. Ductile shearing and transposition of the Montauban Group probably occurred during this early phase

Fig. 2. Geological map (A), longitudinal section (B), and cross sections (C) of the Montauban orebodies. Map A is modified after O'Neil and Osborne (1939) and Bernier (1985). The longitudinal section is from a survey plan provided by Muscocho Exploration Limited. Numbers 4a to 4l and 5a to 5d refer to photographs in figures 4 and 5.

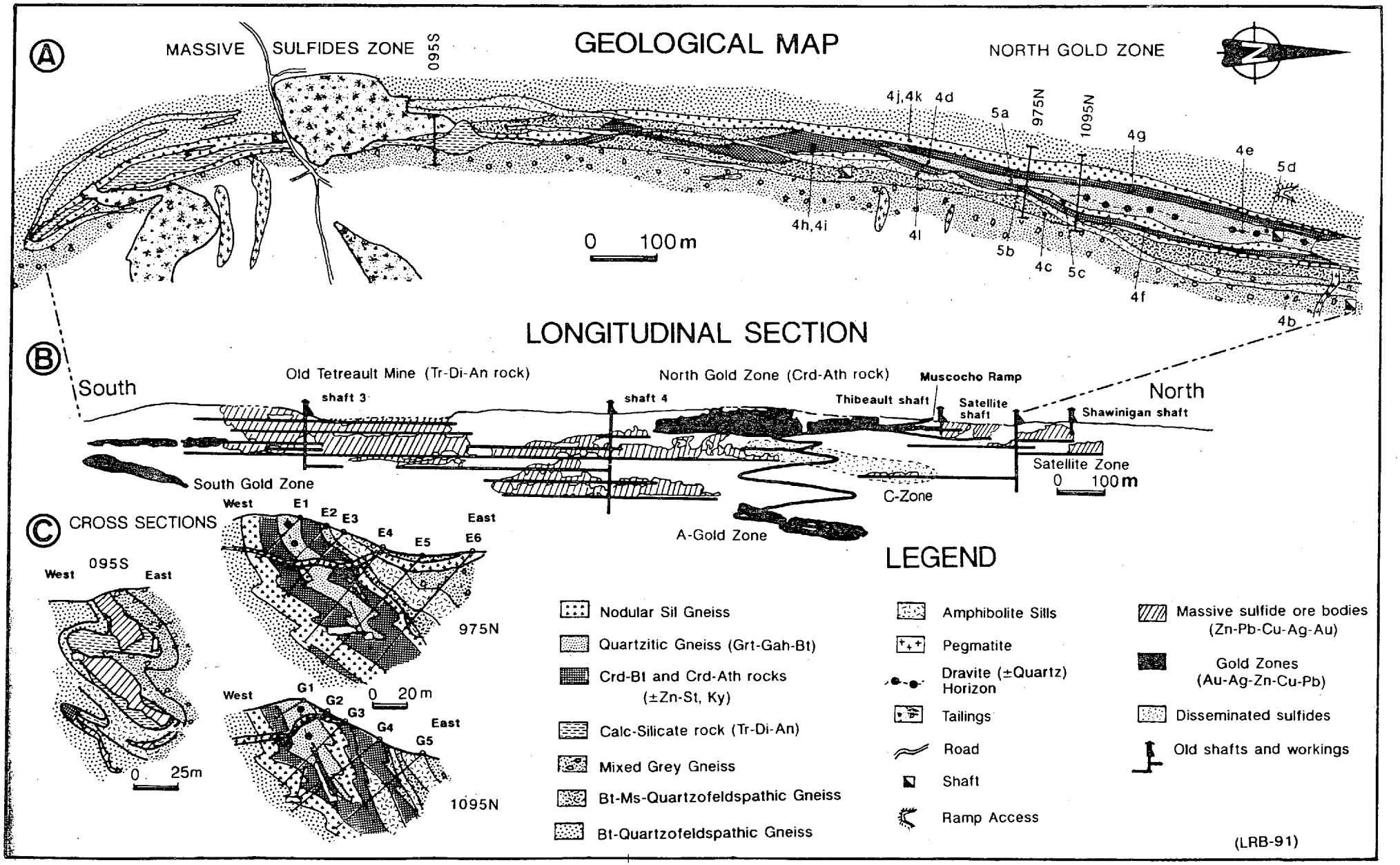
A
MASSIVE SULFIDES ZONE
095S
GEOLOGICAL MAP
NORTH GOLD ZONE
N
4j,4k
4d
5a
975N
1095N
4g
4e
5d
4h,4i
4l
5b
4c
5c
4f
4b
0 100m
B
LONGITUDINAL SECTION
South
Old Tetreault Mine (Tr-Di-An rock)
shaft 3
shaft 4
North Gold Zone (Crd-Ath rock)
Muscocho Ramp
Thibeault shaft
Satellite shaft
Shawinigan shaft
North
Satellite Zone
0 100m
South Gold Zone
C-Zone
A-Gold Zone
C
CROSS SECTIONS
West
E1
E2
E3
E4
E5
E6
East
975N
0 20m
095S
West
East
0 25m
West
G1
G2
G3
G4
G5
East
1095N
LEGEND
Nodular Sil Gneiss
Quartzitic Gneiss (Grt-Gah-Bt)
Crd-Bt and Crd-Ath rocks (±Zn-St, Ky)
Calc-Silicate rock (Tr-Di-An)
Mixed Grey Gneiss
Bt-Ms-Quartzofeldspathic Gneiss
Bt-Quartzofeldspathic Gneiss
Amphibolite Sills
Pegmatite
Dravite (±Quartz) Horizon
Tailings
Road
Shaft
Ramp Access
Massive sulfide ore bodies (Zn-Pb-Cu-Ag-Au)
Gold Zones (Au-Ag-Zn-Cu-Pb)
Disseminated sulfides
Old shafts and workings
(LRB-91)

Fig. 3. Metal distributions and geology at section 975N in the NGZ zone. The stars denote assayed samples in drill holes E1 to E6. The first contour value is shown for each elements. Contour intervals are: 0.1% for Cu, 0.25% for Zn, 0.3% for Pb, and 3 g/t for Au and Ag. Symbols as in Figure 2.

Cu DISTRIBUTION, SECTION 975N

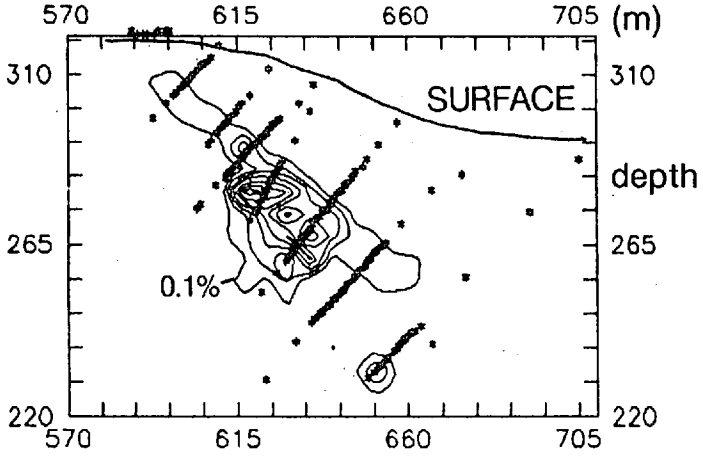

Zn DISTRIBUTION, SECTION 975N

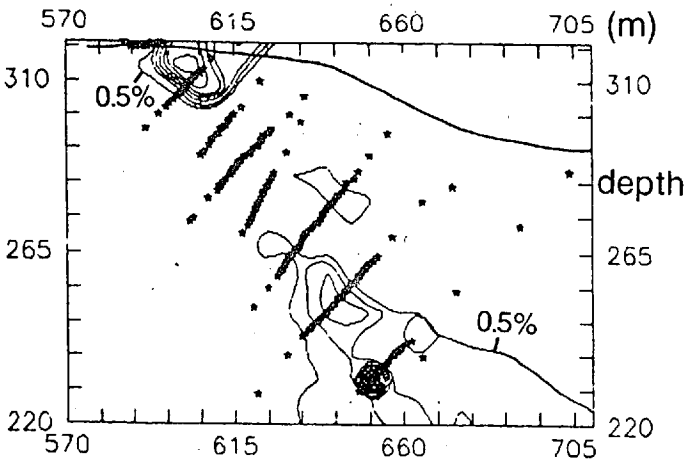

Au DISTRIBUTION, SECTION 975N

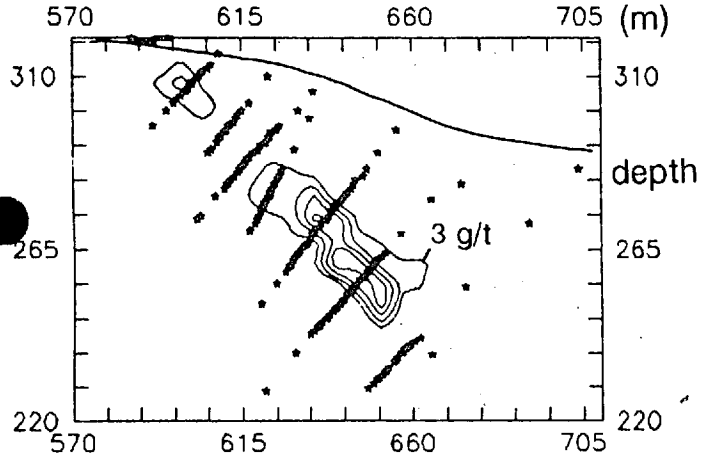

Pb DISTRIBUTION, SECTION 975N

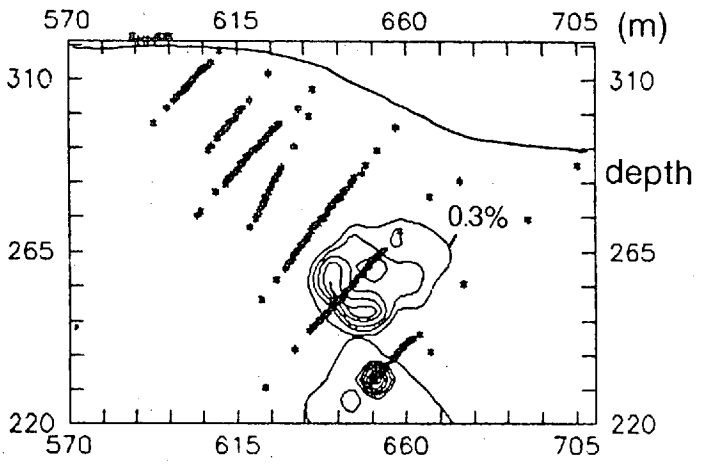

Ag DISTRIBUTION, SECTION 975N

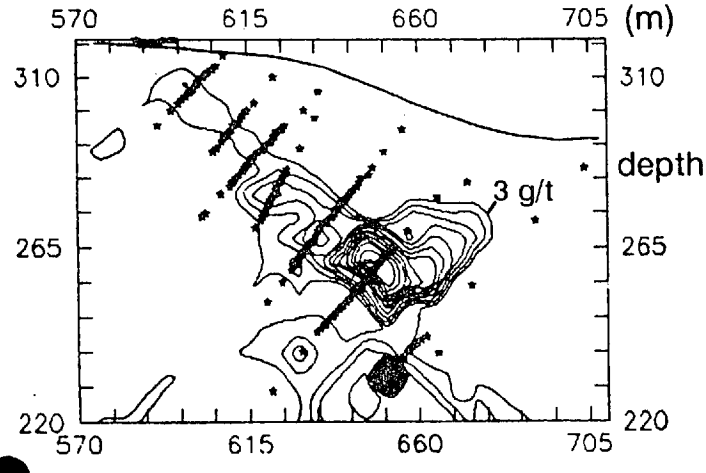

GEOLOGY SECTION 975N

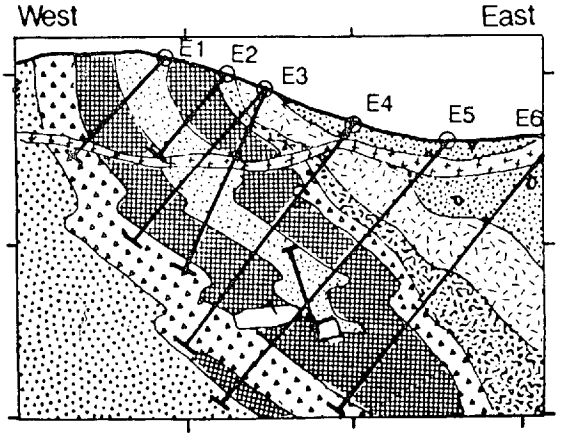

of deformation.

Montauban Orebodies

The elongated tabular ore bodies are of two main types: 1) massive sulfide bodies in calc-silicate rocks, and 2) the NGZ in cordierite-anthophyllite rocks (Table 1, Figs. 2, 3). Intermittent mining activities between 1914 and 1965 produced 2.5 million tons of massive sulfide ore grading 6.8% zinc, 2.3% lead, 1.3 g/t Au and 131 g/t Ag. Mining of the gold zones between 1983 and 1989 produced 2571 kg of gold and 8068 kg of silver (Hébert and Gobeil, 1991).

Prominent metal zoning occurs within and between the orebodies. Sphalerite, galena, pyrrhotite and pyrite are the main constituents of the massive ores, whereas chalcopyrite and pyrrhotite form veinlets confined to the quartzitic gneiss and cordierite-anthophyllite rocks in the NGZ. Silver/gold ratios vary from 125 in the massive sulfides to 11 in the South Gold Zone and to 3.5 in the NGZ (Bernier et al., 1987). The NGZ is characterized by (1) high Au concentrations in the Cu-rich core of the zone, (2) increasing Zn concentrations outward from the center of the zone, and (3) antithetic variation of Cu versus Zn and Pb (Fig. 3).

The mine sequence and associated ores are affected by Z-type dextral folds ranging in amplitudes from 1 to 100 m (Smith, 1956; Bernier, 1985). The massive sulfide lenses occupy the flanks and hinges of a major Z-fold plunging gently north (Fig. 2C). In contrast, fold axes in the quartzitic gneiss at the NGZ (Fig. 5A), and a stretching lineation in the surrounding gneisses (Fig. 4F, J), plunge gently south. The Cu-Au rich core of the mineralized quartzitic gneiss also plunges gently south.

of deformation.

Montauban Orebodies

The elongated tabular ore bodies are of two main types: 1) massive sulfide bodies in calc-silicate rocks, and 2) the NGZ in cordierite-anthophyllite rocks (Table 1, Figs. 2, 3). Intermittent mining activities between 1914 and 1965 produced 2.5 million tons of massive sulfide ore grading 6.8% zinc, 2.3% lead, 1.3 g/t Au and 131 g/t Ag. Mining of the gold zones between 1983 and 1989 produced 2571 kg of gold and 8068 kg of silver (Hébert and Gobeil, 1991).

Prominent metal zoning occurs within and between the orebodies. Sphalerite, galena, pyrrhotite and pyrite are the main constituents of the massive ores, whereas chalcopyrite and pyrrhotite form veinlets confined to the quartzitic gneiss and cordierite-anthophyllite rocks in the NGZ. Silver/gold ratios vary from 125 in the massive sulfides to 11 in the South Gold Zone and to 3.5 in the NGZ (Bernier et al., 1987). The NGZ is characterized by (1) high Au concentrations in the Cu-rich core of the zone, (2) increasing Zn concentrations outward from the center of the zone, and (3) antithetic variation of Cu versus Zn and Pb (Fig. 3).

The mine sequence and associated ores are affected by Z-type dextral folds ranging in amplitudes from 1 to 100 m (Smith, 1956; Bernier, 1985). The massive sulfide lenses occupy the flanks and hinges of a major Z-fold plunging gently north (Fig. 2C). In contrast, fold axes in the quartzitic gneiss at the NGZ (Fig. 5A), and a stretching lineation in the surrounding gneisses (Fig. 4F, J), plunge gently south. The Cu-Au rich core of the mineralized quartzitic gneiss also plunges gently south.

Fig.4. Photographs of the main rock types. Bar scale is 1 cm. Lens cap and magnifier = 5 cm. A. Pillow lava from the metabasalt outcrop west of the ore zone (from Pyke, 1966). B. Grey gneiss with mafic (M) and felsic (F) zones. C. Banded biotite-quartzofeldspathic gneiss. D. Garnet-gahnite quartzitic gneiss. E. Quartz-tourmaline (dravite) boudinaged vein in (D). F. Cordierite-biotite gneiss: cordierite porphyroblasts (Crd) form a mineral lineation with C-axes at a high angle to the plane of the photograph. G. Coarse grained cordierite(Crd) -anthophyllite (Ath) rock with zincian-staurolite porphyroblasts (St). H. Chalcopyrite- pyrrhotite veinlet (Cp-Po) in cordierite-anthophyllite rock. I. Equigranular cordierite-anthophyllite rock. J. Nodular sillimanite gneiss: white nodules of quartz-fibrolitic sillimanite (Sil) form a mineral lineation plunging gently to the left (south). K. Nodular sillimanite (Sil) gneiss cut perpendicular to the nodules axes. L. Garnetiferous (Grt=garnet) amphibolite sill. Hornblende (Hb) forms a mineral lineation. Photograph locations (except 3a) are in Figure 2A.

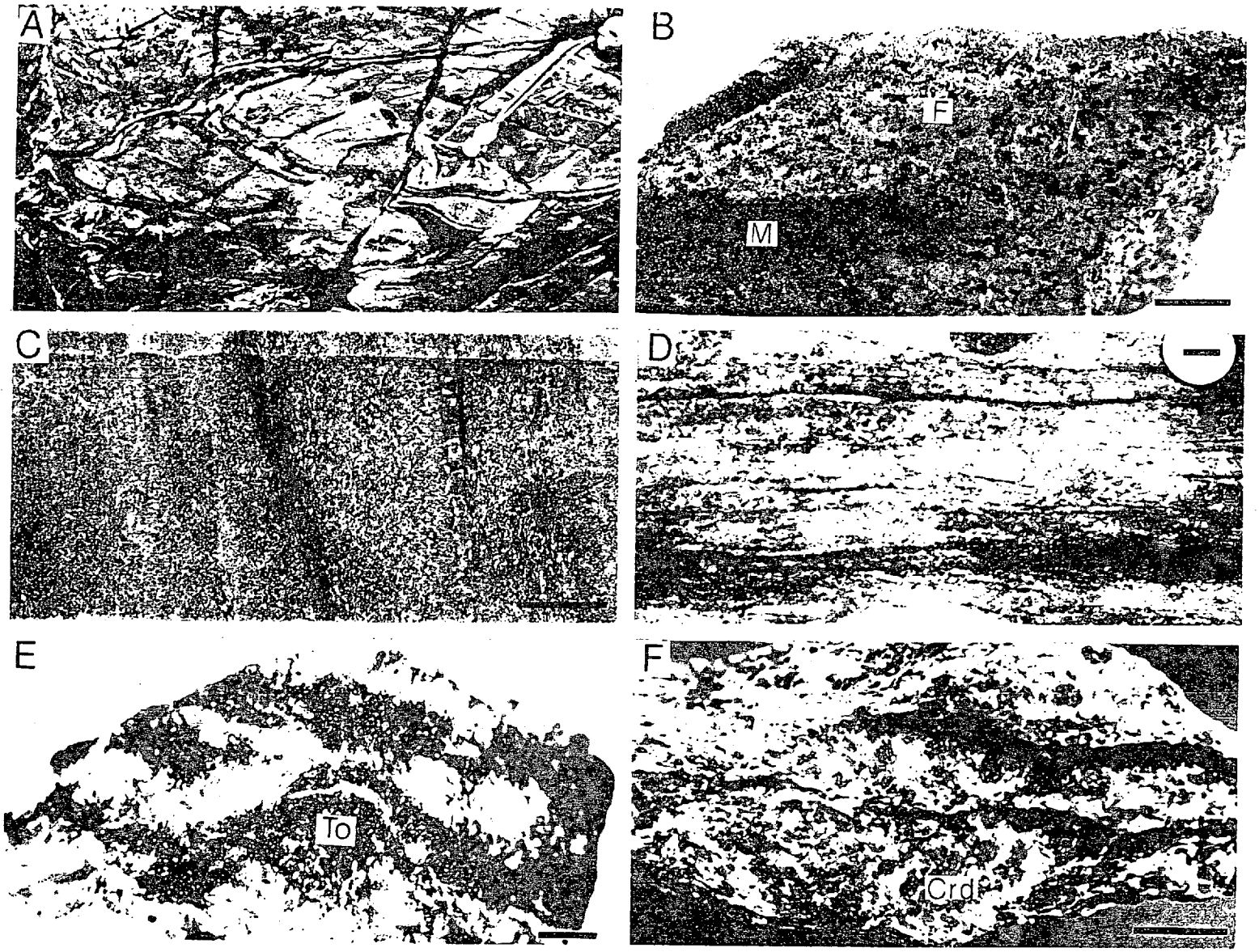
A
B
F
M
C
D
E
To
F
Crd

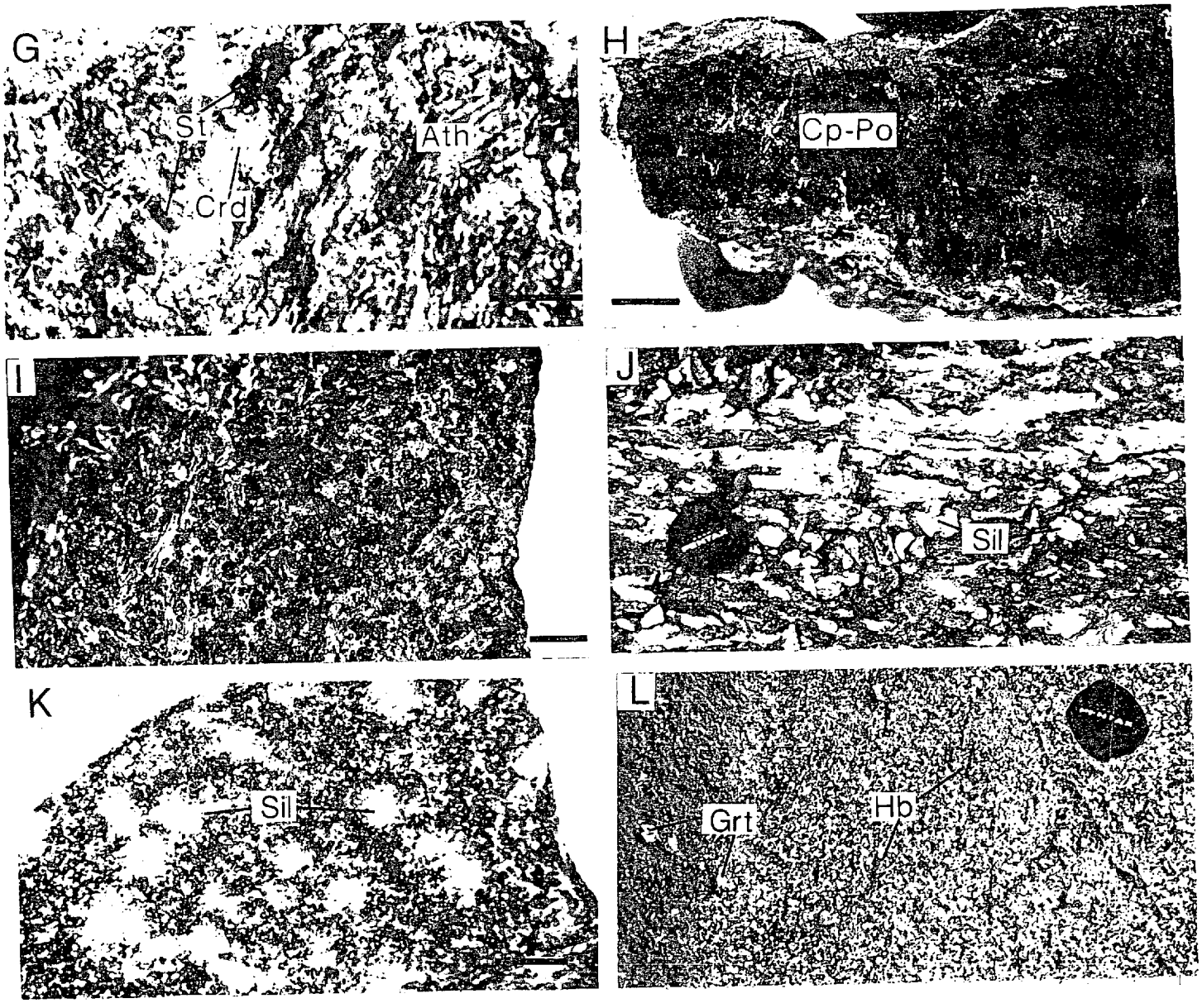
G
St
Ath
Crd
H
Cp-Po
I
J
Sil
K
Sil
L
Grt
Hb

TABLE 1. PRINCIPAL GANGUE AND ORE MINERALS AT MONTAUBAN

Massive sulfide zone (Calc-silicate rocks)	North gold zone (Altered rocks)
GANGUE MINERALS[1]	
Diopside, tremolite, phlogopite, anorthite, calcite, dolomite, scapolite, titanite, apatite, dravite, zircon	Cordierite, anthophyllite, zincian-staurolite, gahnite, phengite, phlogopite, quartz, plagioclase, garnet, kyanite, sillimanite, rutile, dravite, zircon, apatite, corundum[2]
ORE MINERALS	
Sphalerite, galena, pyrite, chalcopyrite, pyrrhotite, tetrahedrite, electrum, silver, gold, molybdenite[3] arsenopyrite[3]	Pyrrhotite, chalcopyrite, sphalerite, galena, pyrite, electrum, gold arsenopyrite[3]
SECONDARY RETROGRADE MINERALS[4]	
Chlorite, talc, brucite, laumontite, prehnite, gypsum, jarosite, brochantite, hisingerite, hematite	

[1]Minerals formed during prograde metamorphism
[2]In silica undersaturated rocks
[3]Rarely observed
[4]Minerals formed in veinlets during retrograde metamorphism

A variety of meso- and microscale features suggest a complex deformational history. A folded, dextrally-verging S-1 schistosity (Fig. 5B), crenulation of a fibrolite nodule schistosity (Fig. 5C), and dextral folds in the cordierite-anthophyllite gneiss (Fig. 5D) indicate ductile dextral shearing parallel to contrasting lithological contacts. Folded fibrolite mats (Fig. 5E) and rotated inclusion trails in garnet (Fig. 5F) also indicate intrafolial ductile shearing. Schistosities intersect at low angles in the mineralized quartzitic gneiss (Fig. 4D); this reflects a regional overprinting by an S-2 fabric. The isoclinal folding observed in the mine sequence is thus related to dextral ductile shearing.

Distribution and Mineralogy of the Altered Rocks

Cordierite-anthophyllite, cordierite-biotite and nodular sillimanite gneisses lie on either side of the gold ore in the quartzitic gneiss. They are best developed over a strike length of 800 m in the NGZ (Fig. 2). Pyrrhotite-chalcopyrite veinlets occur locally in the cordierite-anthophyllite and cordierite-biotite rocks (Fig. 4H). The quartzitic gneiss contains variable amounts of disseminated pyrrhotite, chalcopyrite, sphalerite, galena, and minor gold and electrum. The nodular sillimanite gneiss lies outward from the cordierite-anthophyllite rock and also outward from the calc-silicate rocks hosting the massive sulfide ores (Fig. 2).

The ferromagnesian minerals in the cordierite-anthophyllite rocks have fairly homogeneous compositions (Bernier et al., 1987). Anthophyllite contains 1.9-5.3 wt% Al_2O_3, 0.2-2.8 wt% MnO, and has X_{Mg} (Mg/(Mg+Fe)) values ranging from 0.66 to 0.72. Values of X_{Mg} for cordierite range from 0.84 to 0.90, and for biotite from 0.76 to 0.84. The X_{Mg} values decrease in the

Fig. 5. Structural features in the mine sequence. A. Section perpendicular to the axis of a minor fold in mineralized quartzitic gneiss. B. Minor fold in mineralized quartzitic gneiss showing dextral vergence. C. Crenulated S1 schistosity in nodular sillimanite (Sil) gneiss, crosscut by a late quartz veinlet (QV). D. Z-Fold in cordierite-anthophyllite rock. E. Photomicrograph of a folded mat of fibrolitic sillimanite. F. Photomicrograph of garnet porphyroblast containing inclusion trails indicative of rotation during growth. Figures 5a-d are located on figure 2A.

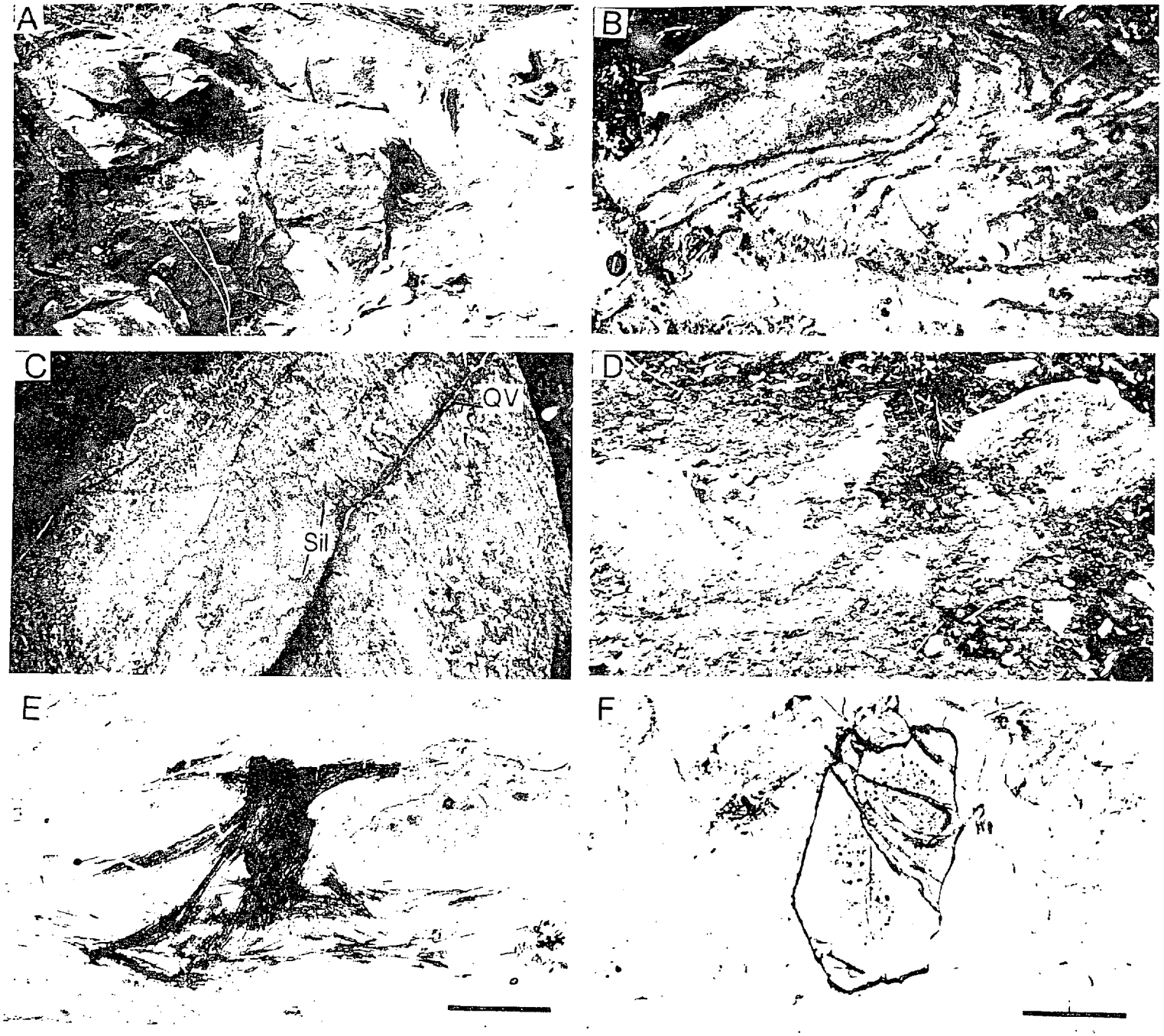
A
B
C
QV
Sil
D
E
F

order: cordierite > biotite > anthophyllite > staurolite > garnet. Anthophyllite is not observed in contact with zincian staurolite, which is frequently rimmed by gahnite, bytownite (An_{80}), cordierite and quartz. This texture suggests that anthophyllite was not stable with zincian staurolite (Bernier et al., 1987). In other aluminous enclaves, bytownite surrounds gahnite, zincian staurolite and kyanite grains in cordierite.

The nodular sillimanite gneiss is composed of quartz, biotite, fibrolitic sillimanite mats, plagioclase, minor amounts of cordierite, garnet and gahnite, and relict grains of zincian staurolite and kyanite. Disseminated sphalerite and pyrrhotite are present in a few samples. Plagioclase is more sodic (An_{30}) and the biotite more aluminous and iron-rich (X_{Mg}=0.66-0.73) than in the cordierite-anthophyllite rocks.

The mineralized quartzitic gneiss is composed chiefly of quartz with subordinate Mn-rich garnet, gahnite, biotite, sodic-plagioclase and 5-20% sulfides.

GEOCHEMISTRY

Analytical Techniques

Drill-core and hand samples of rocks were analysed for major and trace elements by wavelenght-dispersive X-ray fluorescence spectrometry with a Philips PW 1400 instrument at McGill University. Precision is estimated at ±2% for major element oxides and ±5% for trace elements.

Electron microprobe data were obtained by wavelength dispersive spectrometry at McGill University using a Cameca Microbeam MB-1 instrument, operated at a voltage of 15 kV, a current beam of 8 nA, and counting times on standards and samples of 25 seconds.

NGZ Mine Sequence

Quartzofeldspathic gneiss

Biotite quartzofeldspathic gneisses in the Montauban area (data from Morin, 1987) plot mainly in the andesite field in a Zr/TiO_2-Nb/Y diagram (Fig. 6A), whose components are normally highly immobile in water-rock interactions (Winchester and Floyd, 1977; Kerrich, 1982; Robinson, 1984; Maclean and Kranidiotis, 1987; Bernier and MacLean, 1989; O'Hara and Blackburn, 1989). The biotite ± muscovite quartzofeldspathic gneisses that surround the altered rocks at the NGZ are peraluminous and plot in the sub-alkaline andesite-rhyodacite fields (Fig. 6B). Two samples of the gneiss from section 975N (Fig.2) average 73.9 wt% SiO_2, 2.8% CaO, 2.6% Na_2O, 1.9% K_2O, and have a Zr/Y ratio of 6.1 (Table 2). Stamatelopoulou-Seymour and MacLean (1977) and Morin (1987) report a range of 65 to 77 wt% SiO_2 for biotite quartzofeldspathic gneisses in the district.

Nodular sillimanite gneiss

This peraluminous unit differs from the quartzofeldspathic gneisses only in its low content of CaO (0.40 wt%) and Na_2O (0.01 wt%), and slightly higher FeO and MgO (Table 2). It has a Zr/Y ratio of 6.1, and also plots in a sub-alkaline andesite-rhyodacite fields of figure 6B.

Cordierite-anthophyllite gneiss

The cordierite-anthophyllite and cordierite-biotite gneisses differ from the other peraluminous gneisses in their high MgO (4.5-27.1 wt%), FeO (3.4-13.1 wt%), MnO (0.1-0.6 wt%) and LOI contents, and low CaO (0.4-1.4 wt%), Na_2O (0.01-0.3 wt%) and SiO_2 (43-65 wt%) contents (Table 2). Their average

TABLE 2. CHEMICAL ANALYSES OF MINE SEQUENCE ROCKS FROM THE NORTH GOLD ZONE

	BMQ gneiss		BG	NS gneiss				CBG gneiss	
	E-6-6	E-6-4	E-5-4	E-2-1	E-4-34	MT01	E9504	E-4-5	E-6-15
SiO_2	77.76	70.41	71.13	86.31	70.37	71.67	66.11	50.12	64.82
TiO_2	0.34	0.36	0.31	0.39	0.39	0.29	0.34	0.65	0.48
Al_2O_3	11.94	13.05	12.45	6.39	13.65	12.44	12.37	19.71	15.48
Fe_2O_3	0.01	4.31[1]	3.82[1]	0.01	0.62	0.68	8.34[1]	0.01	0.01
FeO	1.94	-----	-----	3.92	2.63	3.64	-----	8.55	5.70
MnO	0.05	0.06	0.10	0.06	0.16	0.17	0.15	0.35	0.11
MgO	1.45	2.71	2.96	1.27	6.34	6.48	4.57	10.06	4.48
CaO	1.94	3.65	0.35	0.71	0.14	0.37	0.87	0.52	0.76
Na_2O	2.84	2.41	0.44	0.01	0.01	0.01	0.39	0.15	0.02
K_2O	1.40	2.37	8.00	0.62	3.78	2.84	2.73	4.86	5.43
LOI	0.50	0.44	0.73	0.61	1.47	1.33	2.92	3.83	1.90
Total	100.17	99.77	100.29	100.30	99.56	99.92	98.79	98.81	99.19
V	11	68	12	16	10	10	30	113	60
Cr	14	38	10	28	10	10	65	23	14
Ni	56	10	10	10	10	10	10	30	11
Ba	278	435	951	93	304	248	127	414	649
Nb	13	5	8	5	9	10	7	10	8
Zr	160	106	190	114	213	185	98	226	211
Y	35	14	27	12	35	31	24	39	30
Sr	212	656	88	12	23	52	82	33	55
Rb	48	61	123	13	114	72	80	113	122
Pb	14	6	11	409	253	25	1722	78	13
Zr/Y	4.6	7.6	7.0	9.5	6.1	6.0	4.1	5.8	7.0
X_{Mg}[2]	0.57	0.56	0.61	0.46	0.78	0.73	0.52	0.68	0.58

	Cordierite-anthophyllite gneiss								Quartzitic gneiss (Ore zone)					
	E9508	E-2-9	E-5-39	E-4-7	E-6-24 *	E-6-32	MT02	LB-1	E9501	MT03	E-1-2	F-1-7	E-1-13	E9502	E9506
SiO_2	38.46	59.56	60.72	62.69	42.87	51.66	52.86	49.87	44.35	87.07	69.53	62.36	81.27	55.16	52.22
TiO_2	0.67	0.63	0.48	0.26	0.37	0.30	0.87	0.18	0.56	0.10	0.15	0.10	0.25	0.36	0.19
Al_2O_3	24.41	13.23	13.00	14.79	12.56	8.12	16.94	16.50	17.52	4.93	7.97	5.04	8.29	10.15	9.43
Fe_2O_3	12.70[1]	1.73	0.66	0.16	0.01	0.97	0.96	13.84[1]	12.85[1]	3.56[1]	6.59[1]	7.94[1]	5.12[1]	14.52[1]	20.48[1]
FeO	-----	5.58	3.37	4.06	13.12	3.69	4.87	-----	-----	-----	-----	-----	-----	-----	-----
MnO	0.26	0.24	0.49	0.26	0.49	0.60	0.41	1.06	0.56	0.12	0.78	0.13	0.23	0.22	0.14
MgO	12.89	11.36	16.28	11.34	12.20	27.06	19.29	16.46	16.18	2.27	4.79	1.31	1.53	8.32	8.13
CaO	0.46	1.38	0.83	0.42	0.42	0.51	0.60	0.29	0.37	0.48	0.21	0.07	0.26	1.47	0.55
Na_2O	0.76	0.01	0.01	0.01	0.26	0.01	0.01	0.57	0.39	0.10	0.16	3.52	0.11	0.43	0.27
K_2O	5.85	2.40	0.23	1.76	1.40	3.02	0.16	0.28	2.49	1.12	2.53	0.88	2.60	2.36	2.70
LOI	2.71	3.13	3.41	3.80	14.39	2.37	2.87	1.31	4.10	0.72	1.58	3.86	1.06	3.39	4.39
Total	99.17	99.25	99.48	99.55	98.09	98.31	99.84	100.36	99.37	100.47	96.61[3]	102.06[4]	100.72	96.38	98.50
V	74	72	26	10	47	36	87	23	66	10	11	10	37	42	12
Cr	63	14	10	20	30	10	13	39	15	51	53	21	10	50	76
Ni	10	15	10	51	10	20	10	10	10	10	10	10	10	14	10
Ba	168	212	44	131	31	76	28	10	267	10	10	10	951	194	107
Nb	11	9	11	7	7	5	18	5	6	5	5	5	8	9	7
Zr	214	145	183	213	141	88	189	170	235	78	110	74	190	127	81
Y	44	31	25	44	20	25	33	32	58	6	12	5	27	16	31
Sr	57	42	70	32	38	13	47	10	43	66	9	6	88	90	44
Rb	196	65	11	47	36	232	5	8	89	32	75	5	123	93	96
Pb	1254	44	227	193	268	673	8	2589	10200	531	663	3498	111	444	1677
Zr/Y	4.9	4.7	7.3	4.8	7.0	3.5	5.7	5.3	6.2	13	9.2	15	7.8	7.9	2.6
X_{Mg}[2]	0.67	0.74	0.88	0.83	0.62	0.91	0.88	0.70	0.71	0.56	0.59	0.25	0.37	0.53	0.44

[1]Total iron as Fe_2O_3. [2]$X_{Mg}=Mg/(Fe^{tot}+Mg)$ on a cation basis.

All oxides and LOI are in weight % and trace elements are in ppm.
BMQ = biotite-muscovite quartzofeldspathic gneiss, BG = biotite gneiss, CGB = cordierite-biotite±garnet, NS = nodular sillimanite.
* = chlorite-talc pseudomorphs after anthophyllite and cordierite.
[3]Total includes 1.06 %ZnO, 1.26% CuO. [4]Total includes 16.85% ZnO.

Fig. 6. Log (Zr/TiO_2)-Log (Nb/Y) diagrams (Winchester and Floyd, 1977). A. Data for the regional biotite quartzofeldspathic gneiss are from (Morin, 1987); the amphibolites are from data used by MacLean et al. (1982). B. Gneisses from the NGZ mine sequence. Zr/Y ratio is 5.8, and they also plot within the sub-alkaline andesite-rhyodacite fields of figure 6B.

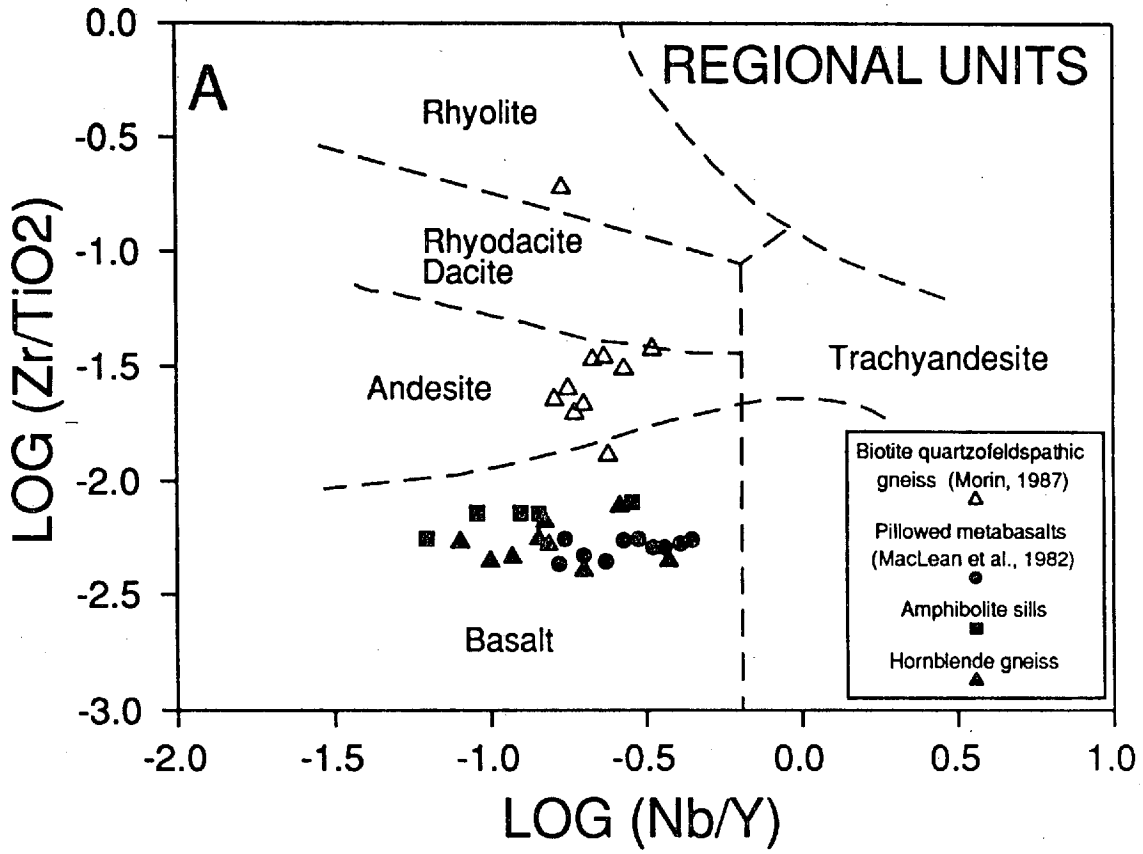
A
REGIONAL UNITS
Rhyolite
Rhyodacite
Dacite
Andesite
Trachyandesite
Basalt
Biotite quartzofeldspathic gneiss (Morin, 1987)
Pillowed metabasalts (MacLean et al., 1982)
Amphibolite sills
Hornblende gneiss
LOG (Zr/TiO2)
LOG (Nb/Y)
0.0
-0.5
-1.0
-1.5
-2.0
-2.5
-3.0
-2.0
-1.5
-1.0
-0.5
0.0
0.5
1.0

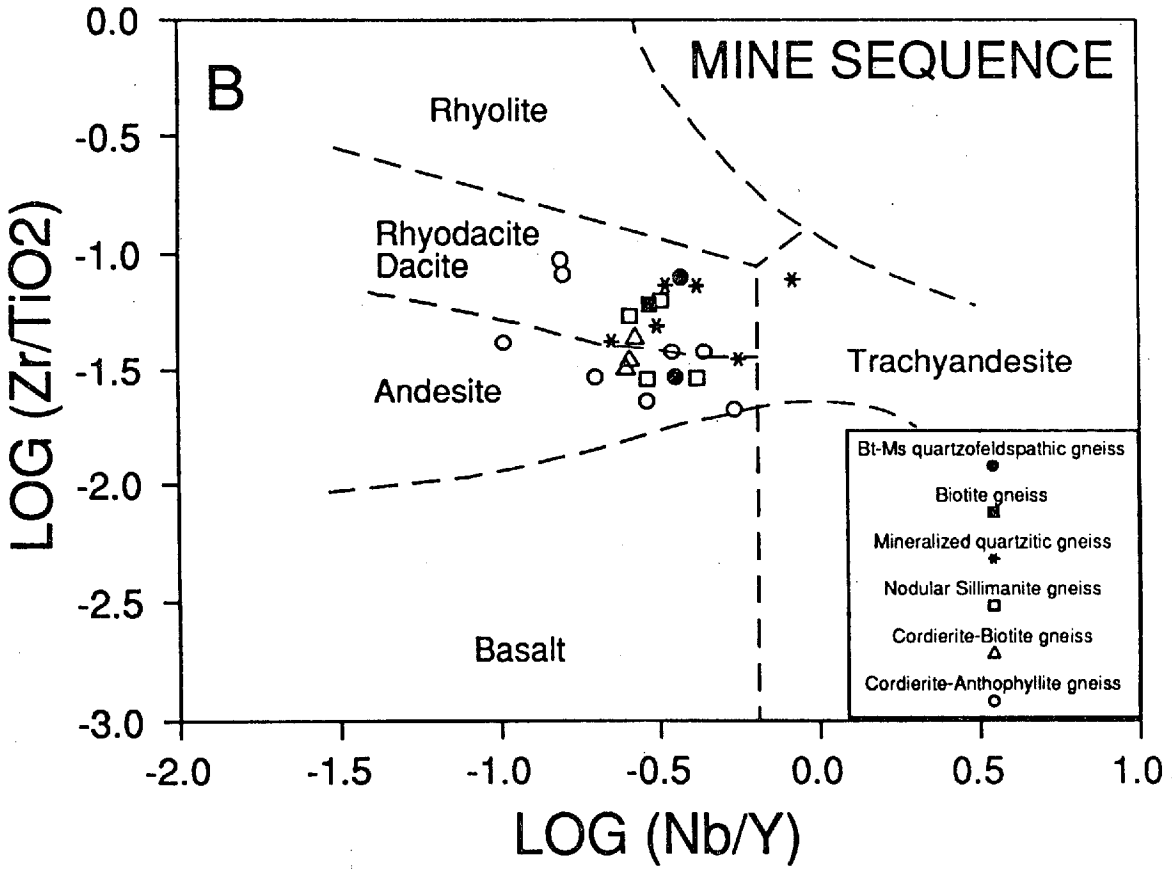
B
MINE SEQUENCE
Rhyolite
Rhyodacite
Dacite
Andesite
Trachyandesite
Basalt
Bt-Ms quartzofeldspathic gneiss
Biotite gneiss
Mineralized quartzitic gneiss
Nodular Sillimanite gneiss
Cordierite-Biotite gneiss
Cordierite-Anthophyllite gneiss
LOG (Zr/TiO2)
LOG (Nb/Y)
0.0
-0.5
-1.0
-1.5
-2.0
-2.5
-3.0
-2.0
-1.5
-1.0
-0.5
0.0
0.5
1.0

Zr/Y ratio is 5.8, and they also plot within the sub-alkaline andesite-rhyodacite fields of figure 6B.

Mineralized quartzitic gneiss

This unit is host to most of the ore in the NGZ. Overall, it is low in Al_2O_3 (5-10 wt%), Na_2O (0.1-0.5 wt%) and CaO (0.1-1.5 wt%). It has a wider range of Zr/Y ratios (3-15) than the surrounding gneisses of the mine sequence, but plots with these gneisses in the sub-alkaline andesite-rhyodacite fields of figure 6B.

Protolith Identification

Although the lithological units of the mine sequence have very different mineralogical and bulk chemical compositions, their trace element geochemistry (Fig. 6) suggests they were derived from the same protolith. The Log(Ratio) diagrams (Chapter 3, section 3C) are used successfully in these comparisons. Units of the surrounding gneisses are also identified by this method.

On such diagrams, the Montauban pillowed metabasalts and hornblende gneiss have the same type of profiles as Mid-Ocean Ridge basalts (MORB), and compare closely with those of the Tudor and Turriff metabasalts from the Grenville Central Metasedimentary Belt (Figs. 7A, 8A, 8E). The amphibolitic gneisses have somewhat different profiles, with lower Cr/Al ratios (Fig. 7B), and compare better with the Turriff intermediate metavolcanic (Fig. 8F).

The regional and mine sequence biotite quartzofeldspathic gneisses have distinct profiles (Figs. 7C, D). Matching profiles are found in the Tudor and Turriff felsic metavolcanic rocks (Fig. 8G), the felsic metavolcanic rocks of the Farnacht Formation, Ireland (Fig. 8B), the modern island arc

Fig. 7. Log(Ratio) diagrams for the Montauban lithological units. A-D: least altered rocks. Data in A are those used by MacLean et al. (1982). Data in B and C are from Morin (1987). E-F: metamorphosed altered rocks from the North Gold Zone mine sequence.

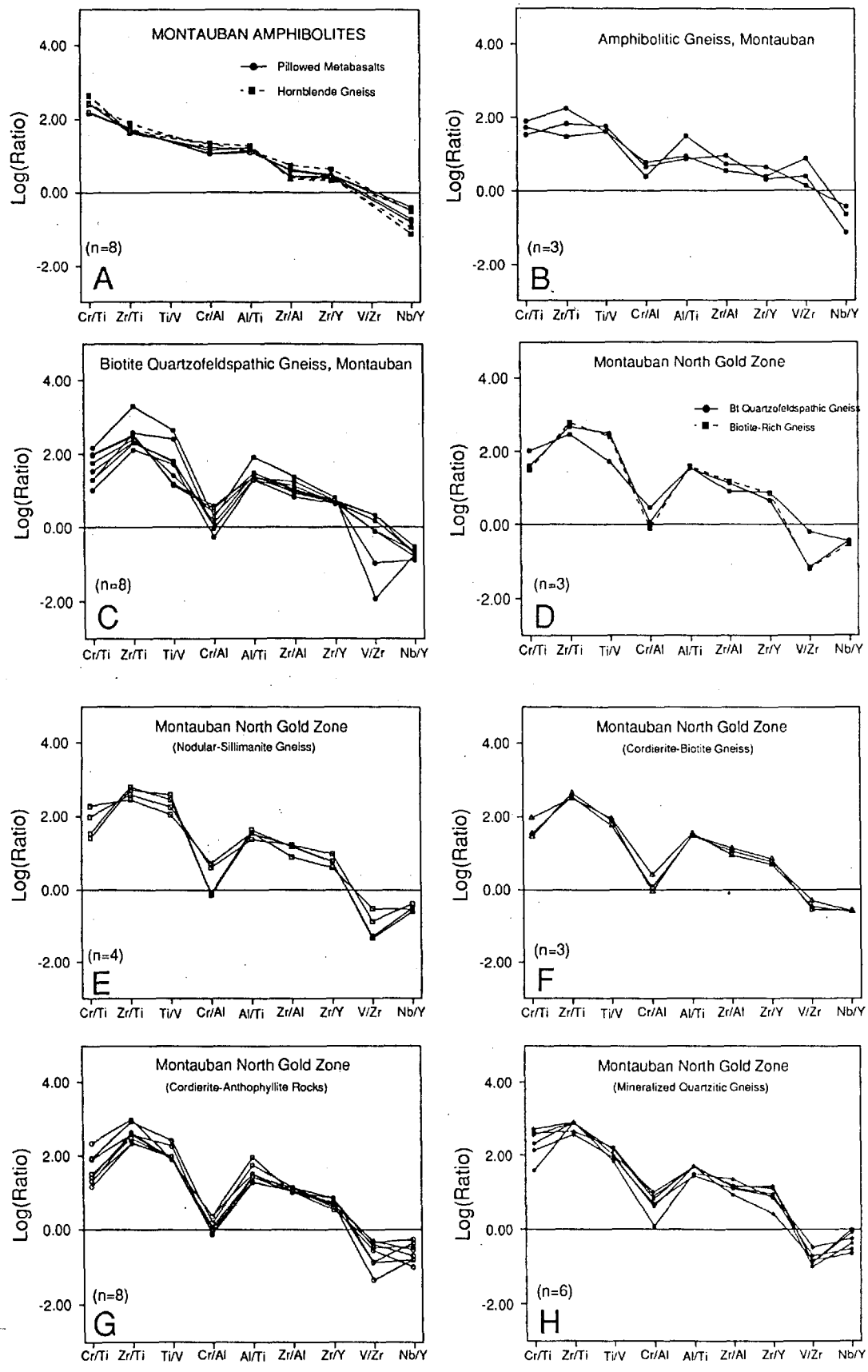
MONTAUBAN AMPHIBOLITES
Pillowed Metabasalts
Hornblende Gneiss
Log(Ratio)
4.00
2.00
0.00
-2.00
(n=8)
A
Cr/Ti Zr/Ti Ti/V Cr/Al Al/Ti Zr/Al Zr/Y V/Zr Nb/Y
Amphibolitic Gneiss, Montauban
(n=3)
B
Biotite Quartzofeldspathic Gneiss, Montauban
(n=8)
C
Montauban North Gold Zone
Bt Quartzofeldspathic Gneiss
Biotite-Rich Gneiss
(n=3)
D
Montauban North Gold Zone
(Nodular-Sillimanite Gneiss)
(n=4)
E
Montauban North Gold Zone
(Cordierite-Biotite Gneiss)
(n=3)
F
Montauban North Gold Zone
(Cordierite-Anthophyllite Rocks)
(n=8)
G
Montauban North Gold Zone
(Mineralized Quartzitic Gneiss)
(n=6)
H

Fig. 8. Log(Ratio) diagrams for mafic, intermediate and felsic volcanic rocks. A) data from Herzig and Pluger (1988), B) data from Max et al. (1988), C) data from Barsdell and Berry (1990), D) data used by MacLean et al.(1982), E-G) data from Smith et al. (1986).

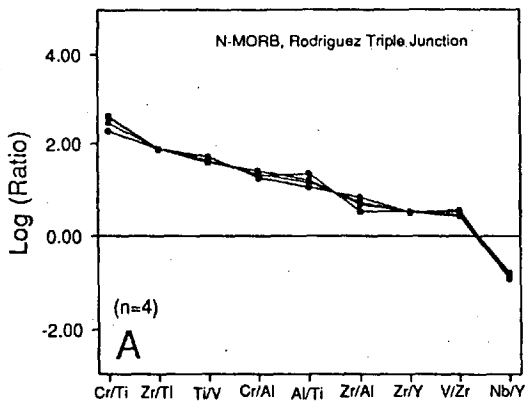
N-MORB, Rodriguez Triple Junction
Log (Ratio)
4.00
2.00
0.00
-2.00
(n=4)
A
Cr/Ti Zr/Tl Ti/V Cr/Al Al/Ti Zr/Al Zr/Y V/Zr Nb/Y

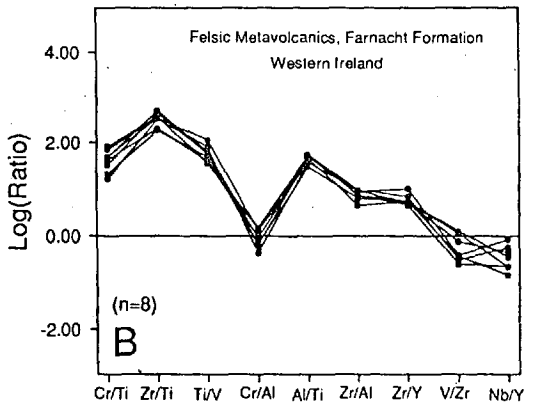
Felsic Metavolcanics, Farnacht Formation
Western Ireland
Log(Ratio)
4.00
2.00
0.00
-2.00
(n=8)
B
Cr/Ti Zr/Ti Ti/V Cr/Al Al/Ti Zr/Al Zr/Y V/Zr Nb/Y

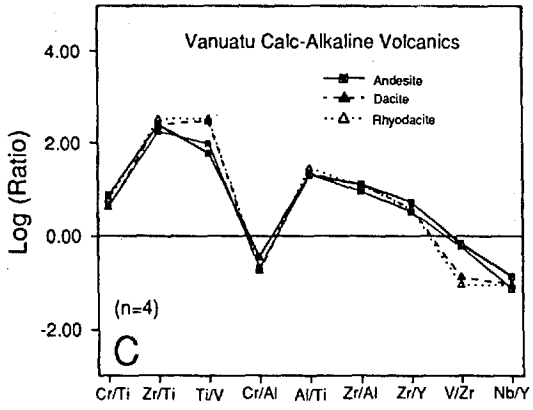
Vanuatu Calc-Alkaline Volcanics
Andesite
Dacite
Rhyodacite
Log (Ratio)
4.00
2.00
0.00
-2.00
(n=4)
C
Cr/Ti Zr/Ti Ti/V Cr/Al Al/Ti Zr/Al Zr/Y V/Zr Nb/Y

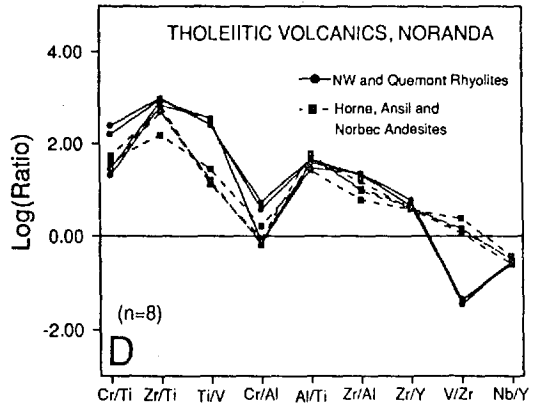
THOLEIITIC VOLCANICS, NORANDA
NW and Quemont Rhyolites
Horne, Ansil and
Norbec Andesites
Log(Ratio)
4.00
2.00
0.00
-2.00
(n=8)
D
Cr/Ti Zr/Ti Ti/V Cr/Al Al/Ti Zr/Al Zr/Y V/Zr Nb/Y

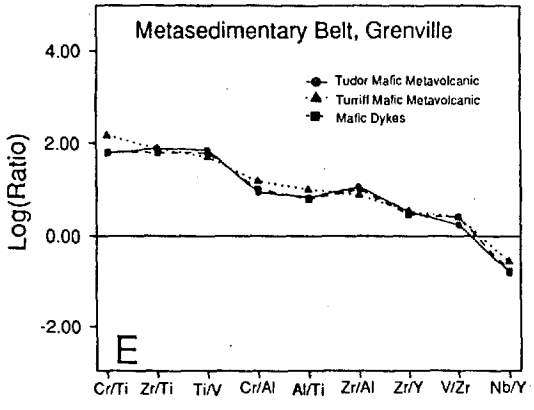
Metasedimentary Belt, Grenville
Tudor Mafic Metavolcanic
Turriff Mafic Metavolcanic
Mafic Dykes
Log(Ratio)
4.00
2.00
0.00
-2.00
E
Cr/Ti Zr/Ti Ti/V Cr/Al Al/Ti Zr/Al Zr/Y V/Zr Nb/Y

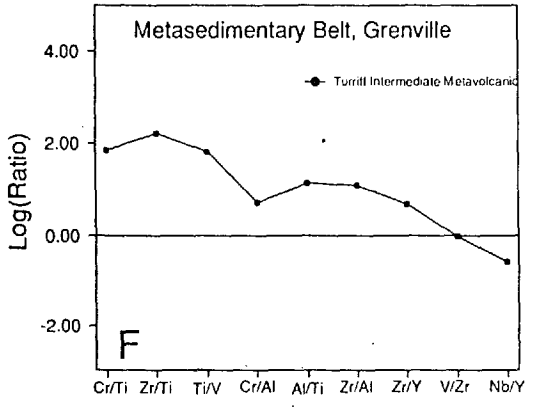
Metasedimentary Belt, Grenville
Turriff Intermediate Metavolcanic
Log(Ratio)
4.00
2.00
0.00
-2.00
F
Cr/Ti Zr/Ti Ti/V Cr/Al Al/Ti Zr/Al Zr/Y V/Zr Nb/Y

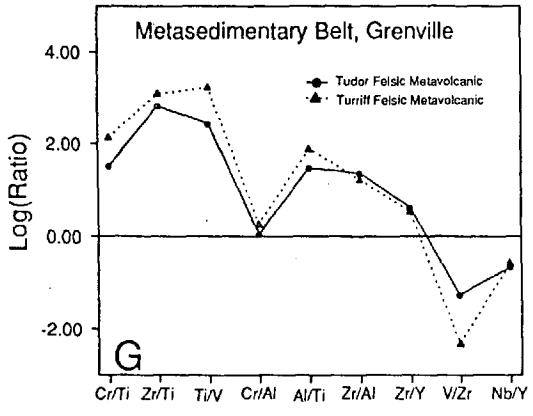
Metasedimentary Belt, Grenville
Tudor Felsic Metavolcanic
Turriff Felsic Metavolcanic
Log(Ratio)
4.00
2.00
0.00
-2.00
G
Cr/Ti Zr/Ti Ti/V Cr/Al Al/Ti Zr/Al Zr/Y V/Zr Nb/Y

calc-alkaline andesites-rhyodacites from Vanuatu (Fig. 8C), and the Archean tholeiitic andesites and rhyolites from Noranda (Fig. 8D). The variations in the profiles of these comparative volcanic suites are most likely related to igneous differentiation. The Montauban regional biotite quartzofeldspathic gneisses and the mine sequence gneisses have profiles typical of andesites to rhyodacites (Figs. 7, 8).

All of the cordierite-anthophyllite (altered) rocks from the mine sequence also have profiles identical to those of the biotite quartzofeldspathic gneisses, which strongly indicates that these are altered and metamorphosed equivalents. The protoliths of these rocks were intermediate to felsic volcanic or volcaniclastic rocks.

Mass Changes

Other tests can be applied with the immobile elements to determine whether the cordierite-anthophyllite and associated gneisses were derived from the surrounding quartzofeldspathic gneiss. The altered rocks in the mine sequence at the NGZ define an Al_2O_3-Zr alteration line (r=0.85; Fig. 9) with a F-test ratio (26) indicating a 99% confidence interval. The average alteration line intersects the compositional field (e.g. MacLean and Kranidiotis, 1987) of the biotite±muscovite quartzofeldspathic gneiss, and corroborates the Log(Ratio) results that this unit is the precursor of the altered rocks. The alteration line is derived by mass gains and losses of mobile components owing to pre-metamorphic hydrothermal alteration of the precursor. Inter-element correlation coefficients for other commonly immobile elements are somewhat lower than for Al_2O_3-Zr (Table 3). Part of the scatter in the data defining the alteration line is probably an effect of a

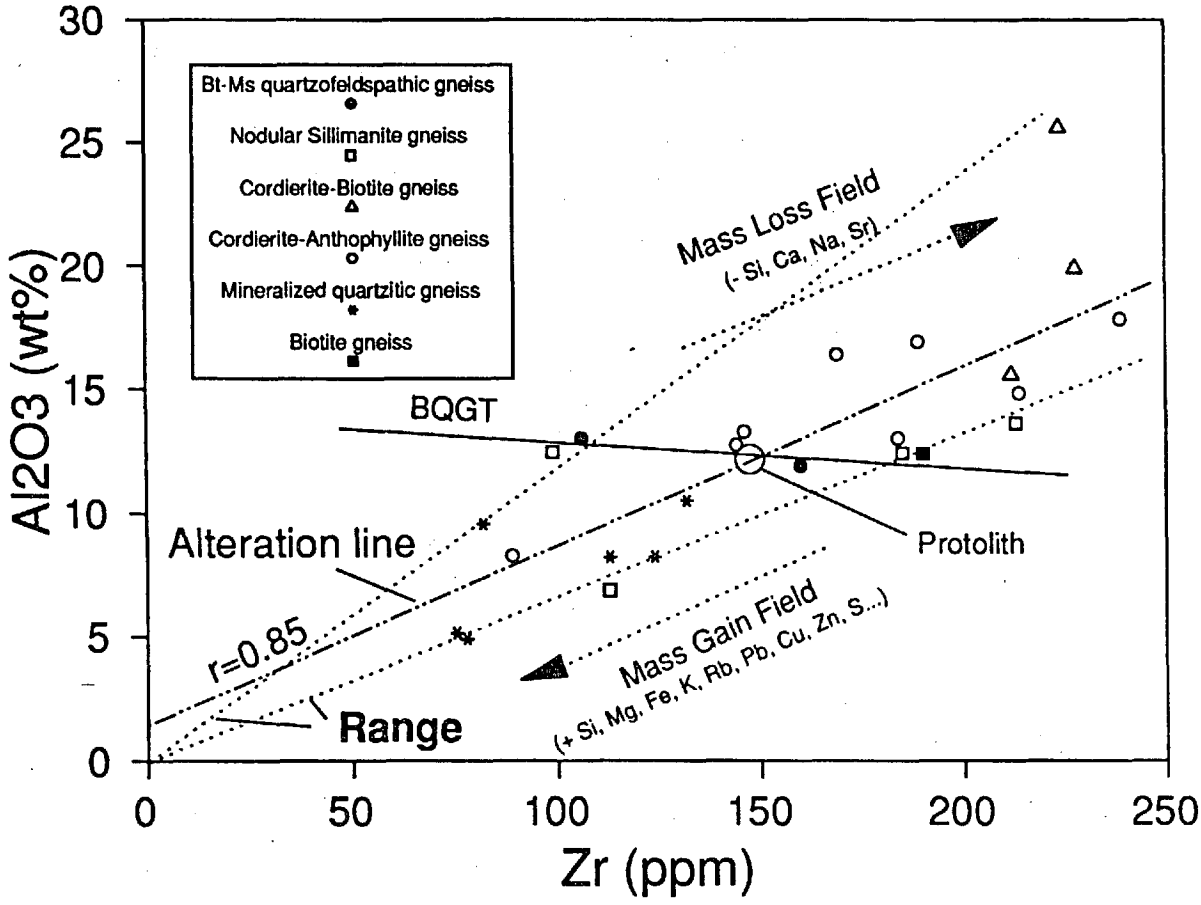

Fig. 9. Al_2O_3-Zr diagram. The metamorphosed altered rocks from the NGZ mine sequence define an alteration line (regressed line). The compositional field of the felsic gneisses (BQGT) is intersected by the alteration line indicating a felsic gneiss protolith precursor for the altered rocks. The protolith precursor composition is schematically shown.

TABLE 3. INTERELEMENT CORRELATION COEFFICIENTS

Alteration trend (n=22)						
	Ti	Al	V	Nb	Zr	Y
Ti	1.00					
Al	0.69	1.00				
V	0.85	0.71	1.00			
Nb	0.78	0.57	0.58	1.00		
Zr	0.61	0.85	0.53	0.50	1.00	
Y	0.53	0.83	0.51	0.37	0.81	1.00

compositional range (Fig. 9) in the quartzofeldspathic gneiss protolith at the mine. However, for simplicity, the data is considered as a single precursor system.

The precursor composition used in the mass change calculations is the average of samples E-6-4, E-6-6 (Table 2) of the biotite quartzofeldspathic gneiss from the NGZ. The mass change calculations were made at constant Al_2O_3 (MacLean and Kranidiotis, 1987; Bernier and MacLean, 1989), and shown in Figure 10. Most samples of the cordierite-anthophyllite and cordierite-biotite gneisses have experienced mass loss (residual concentration of immobile elements) (Fig. 9). In greenschist facies metamorphic terranes, altered rock associated with volcanogenic ores that plot within the mass loss field are invariably chloritized and sericitized and have lost silica (MacLean and Kranidiotis, 1987; Barrett and MacLean 1991). At Montauban, samples that plot below the precursor in the mass gain field are mostly mineralized quartzitic gneiss, but one is a cordierite-anthophyllite gneiss that has gained mass through addition of Mg, probably as talc, and another is a silicified nodular sillimanite gneiss.

The overall mass changes in the altered rocks are marked by large losses of Si except in the central quartzitic gneiss, which gains silica (Fig. 10).

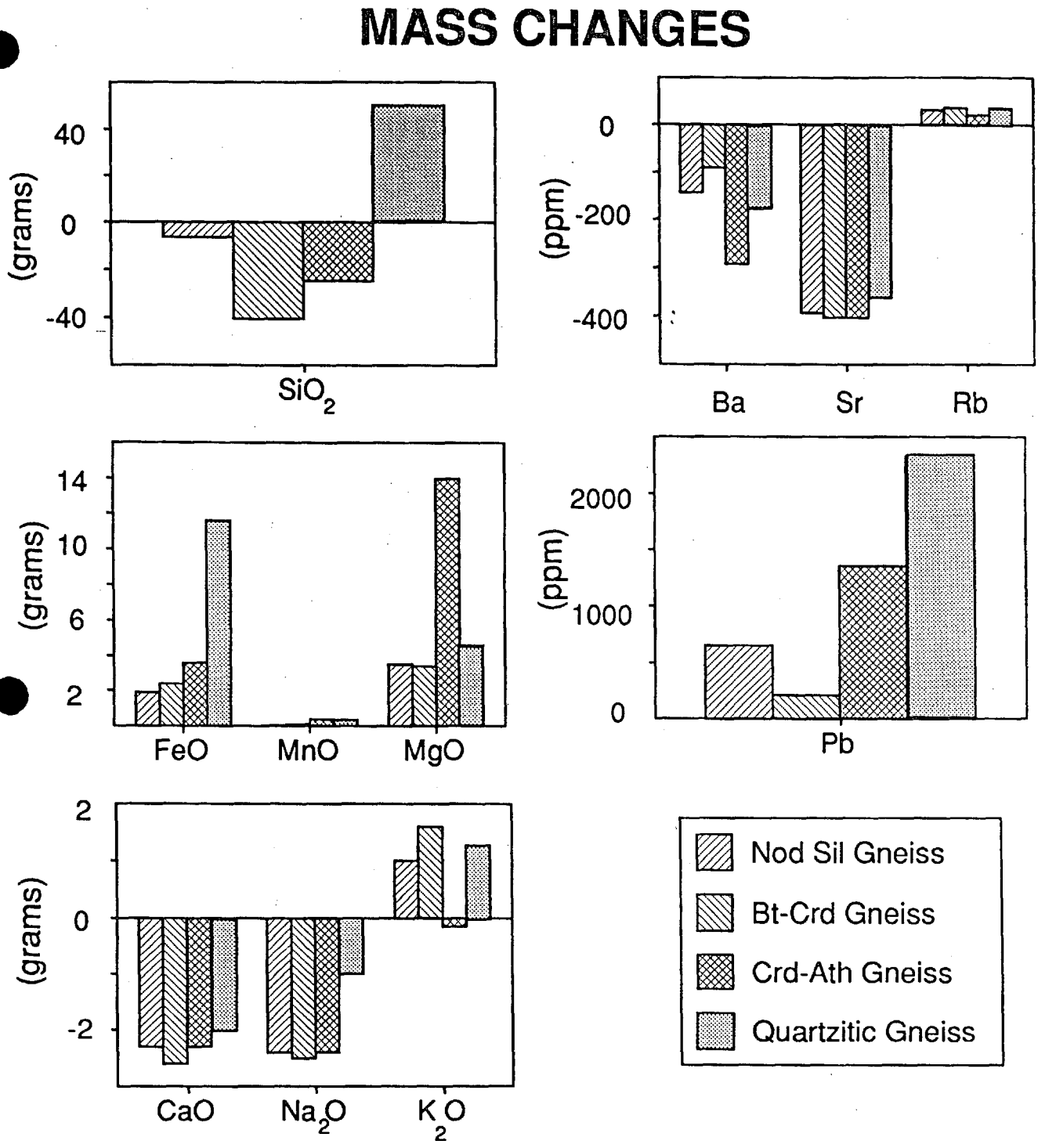

Fig. 10. Bar diagrams illustrating average mass changes for the North Gold Zone altered rocks.

Fig. 11. Cation alteration diagrams. A. Al-Si: the altered rocks are residually enriched in Al (immobile) and depleted in Si and other mobile cations during hydrothermal alteration; Al is diluted by silicification (Si addition). B. Si-(Fe+Mg): the altered rocks define a trend towards Si depletion and Fe-Mg enrichment towards chlorite. C. K-(Fe+Mg): the cordierite-anthophyllite rocks and mineralized quartzitic gneiss samples have lower K contents (less sericite) than the cordierite-biotite and nodular sillimanite gneisses at the margin of the alteration zone. Bt Qtz-feld = Biotite quartzofeldspathic.

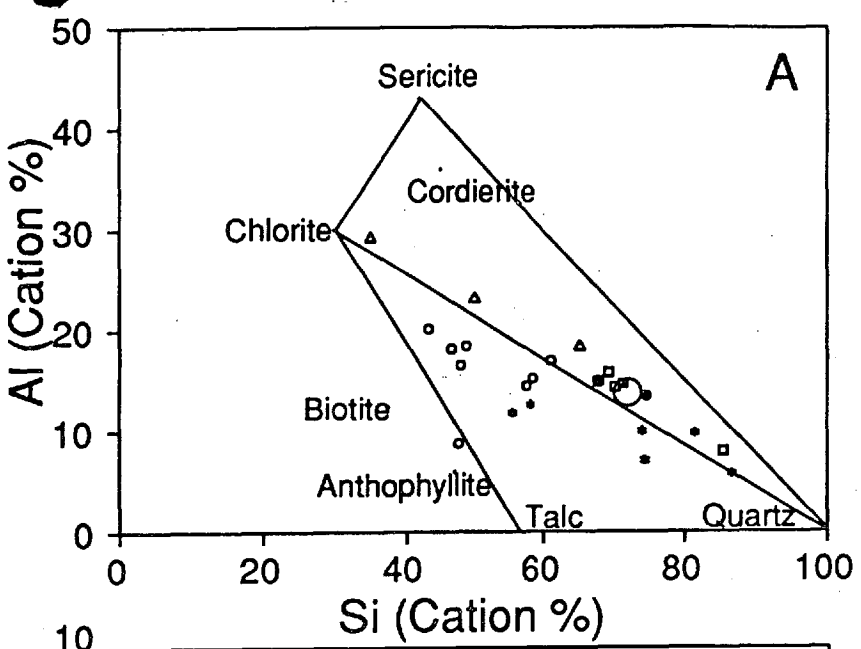
A
Sericite
Cordierite
Chlorite
Biotite
Anthophyllite
Talc
Quartz
Al (Cation %)
Si (Cation %)
0
10
20
30
40
50
0
20
40
60
80
100

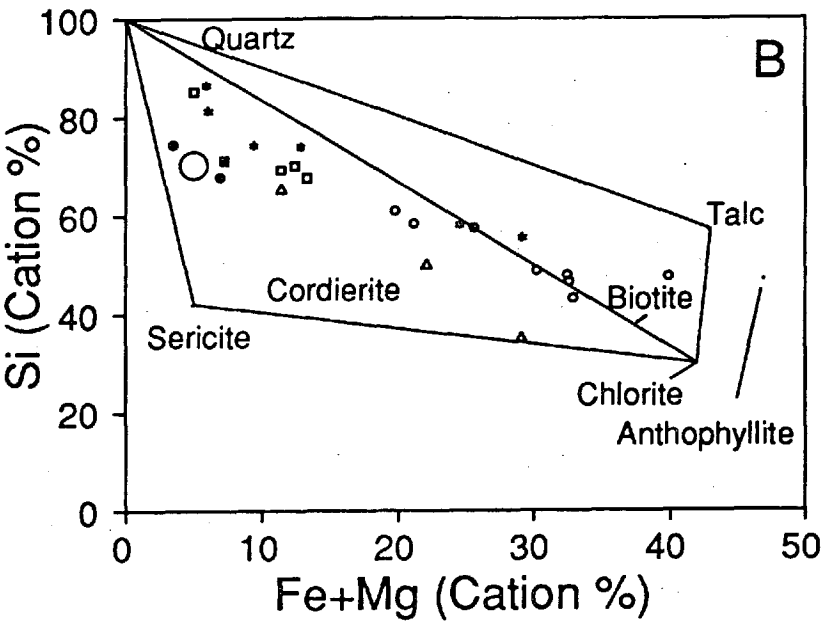
B
Quartz
Talc
Cordierite
Biotite
Sericite
Chlorite
Anthophyllite
Si (Cation %)
Fe+Mg (Cation %)
0
20
40
60
80
100
0
10
20
30
40
50

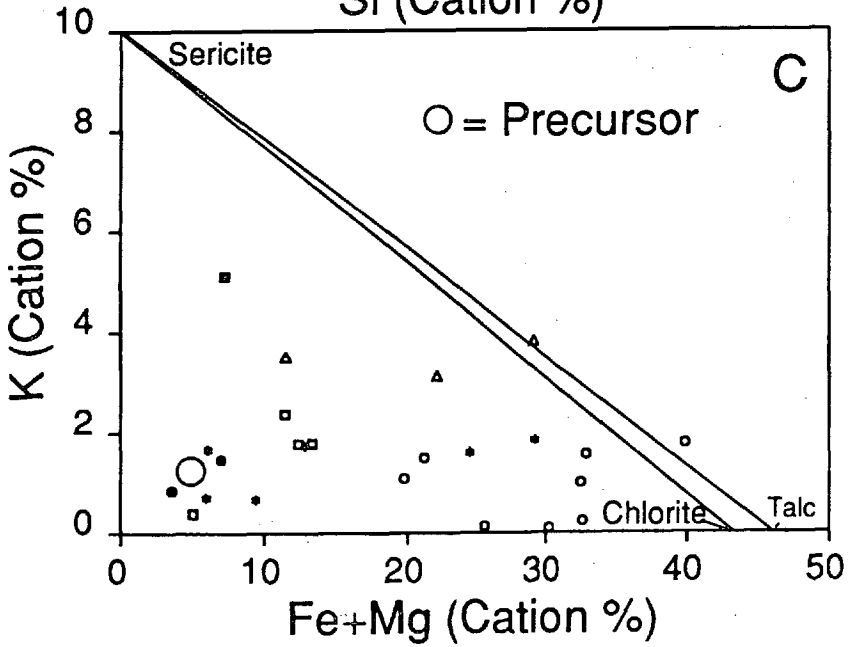
C
Sericite
O = Precursor
Chlorite
Talc
K (Cation %)
Fe+Mg (Cation %)
0
2
4
6
8
10
0
10
20
30
40
50

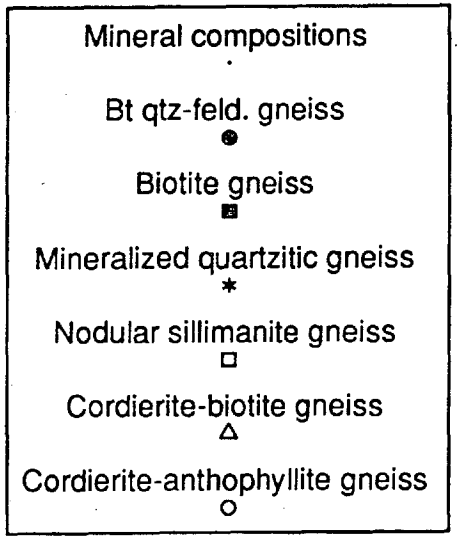
Mineral compositions
Bt qtz-feld. gneiss
Biotite gneiss
Mineralized quartzitic gneiss
Nodular sillimanite gneiss
Cordierite-biotite gneiss
Cordierite-anthophyllite gneiss

Potassium was added to most altered rocks but was leached in the cordierite-anthophyllite rock. All altered units have lost Ca, Na, Ba, and Sr, and gained Mg, Fe, Mn, Pb and Rb (Fig. 10). The gain in FeO is highest in the central quartzitic gneiss, wheareas MgO was enriched in the surrounding altered rocks.

The alteration changes are well depicted on Si-(Fe+Mg) and Al-Si cation diagrams (Figs. 11A, B). The systematic decrease in Si and increase in Fe+Mg observed in the cordierite-biotite and cordierite-anthophyllite rocks are probably related to a primary chlorite-sericite-talc alteration accompanied by leaching of silica. Most nodular sillimanite gneiss samples plot close to the precursor, indicating little mass change, but one is moderately silicified. Sericitic alteration was, in general, less intense than chloritization (Fig. 11C). The cordierite-anthophyllite rock and the mineralized quartzitic gneiss represent the core of the alteration zone and had the highest chlorite/sericite ratios. The surrounding cordierite-biotite and nodular sillimanite gneisses had lower ratios, reflecting the higher abundances of sericite at the margin of the alteration zone.

Changes in the bulk rock chemistry illustrated on an A -K-F diagram (Fig. 12) correlate with changes in the metamorphic assemblages. The biotite quartzofeldspathic gneiss samples plot within the field defined by K-feldspar-muscovite-biotite. With enrichment in (Fe-Mg)±K and loss in Ca-Na-Si, they move into the biotite-sillimanite-muscovite, biotite-cordierite-sillimanite and biotite-cordierite-anthophyllite fields. Gahnite and staurolite (not shown) are additional phases stabilized by zinc, a metal related to the ore mineralization.

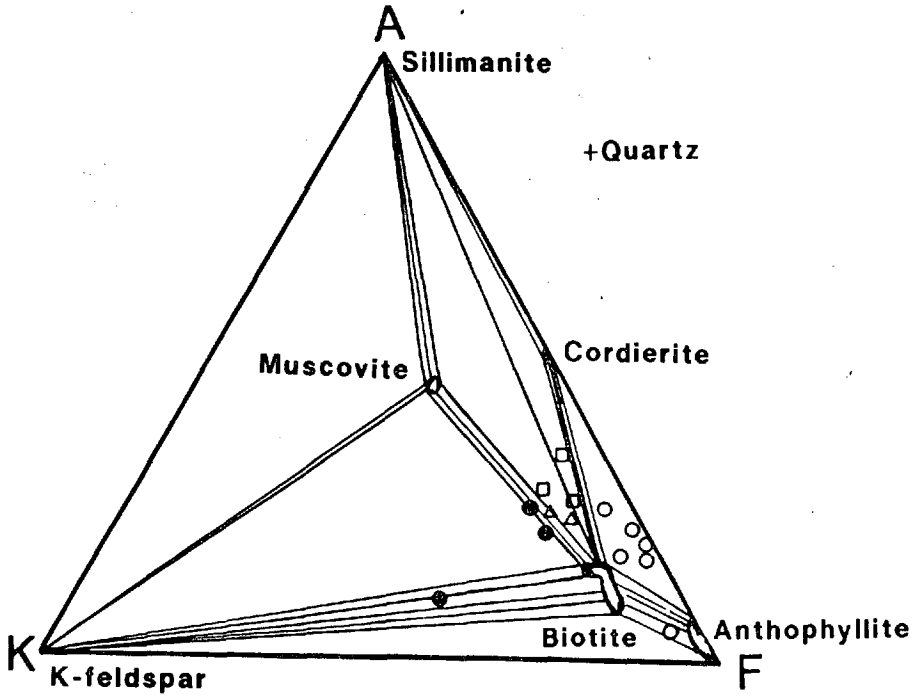

Fig. 12. A-K-F diagram. A = Al_2O_3 + Fe_2O_3 - Na_2O - K_2O - CaO, K = K_2O, F = FeO + MgO + MnO. Symbols as in Figure 6. The analysed muscovite contains up to 6.5 wt% MgO and 0.5 wt% FeO.

Origin of the Mine Sequence

Quartzofeldspathic gneiss

The biotite quartzofeldspathic gneiss is undoubtedly the metamorphosed equivalent of felsic volcanic rock, as indicated by the Log(Ratio) diagrams (Figs. 7, 8), and is the protolith of the altered rocks at the NGZ.

Calc-silicates

Calc-silicate rocks in the mine sequence are probably metamorphosed calcareous and dolomitic rocks (Prahbu and Webber, 1984) formed by sedimentary mixing of marine carbonate and detrital components (clay, fresh or altered volcaniclastic) deposited coevally with the massive sulfide ores. An alternate origin could have involved carbonatization of volcaniclastic rocks or Mg metasomatism of impure limestone during hydrothermal alteration (e.g. Latvalahti, 1979; Large and Both, 1980).

Nodular sillimanite gneiss

The nodular sillimanite gneiss is particularly well developed adjacent to the cordierite-anthophyllite rocks in the NGZ, and locally surrounds the calc-silicate rocks (Fig. 2). The fibrolitic sillimanite nodules (Figs. 4J, K, 5C) form a lineation within locally crenulated S1 planes, suggesting syn-S1 nodule formation. The gneiss was probably derived from the quartzofeldspathic gneiss by depletion of Ca and Na and minor addition of K, Fe and Mg (Fig. 10), implying minor chloritization and sericitization during hydrothermal alteration.

The genesis of nodular sillimanite gneiss has been reviewed by Kerrick

(1990). These gneisses are reported from metapelitic and metarhyolitic rocks in various metamorphic terranes (Kerrick, 1990), as well as from metamorphosed alteration zones associated with massive sulfide deposits (Casselman and Mioduszewska, 1982; Studer, 1982). The main mechanisms proposed for the sillimanite-biotite association are: 1) prograde metamorphic reaction (Kerrick, 1990),

$$St + Ms + Qtz = Bt + Sil + H_2O \qquad (1)$$

2) leaching of base cations from pre-existing biotite (Vernon, 1979),
3) fibrolitization of biotite by influx of acidic volatiles released during crystallization of granite (Kerrick, 1990), and 4) deformation-induced fibrolitization (Vernon, 1987).

Another reaction involves quartz-biotite-fibrolite formation by prograde breakdown of chlorite and muscovite:

$$1.5Chl + 2.5Ms = 1Qtz + 2.5Bt + 8Sil + H_2O \qquad (2)$$

This reaction was experimentally calibrated for the system $MgO\text{-}SiO_2\text{-}Al_2O_3\text{-}H_2O$ by Bird and Fawcett (1973). The breakdown of Mg-chlorite and muscovite will occur at T=635°C for P=6.5 Kbars. This reaction most likely led to the formation of the nodular sillimanite gneiss at the NGZ as well as at other metamorphosed alteration zones associated with massive sulfide ores (e.g. Casselman and Mioduszewska, 1982; Studer, 1982).

Cordierite-anthophyllite rocks

Cordierite-anthophyllite rocks are frequently associated with metamorphosed massive-sulfide deposits (e.g. Froese, 1969; Bachinski, 1976; Latvalahti, 1979; Deb, 1980 Riverin and Hodgson, 1980; Hall, 1982; Bernier and MacLean, 1989; Bristol and Froese, 1989). The formation of these

metamorphism of chlorite-rich alteration zones.

The relationship between cordierite-anthophyllite rocks and hydrothermal alteration zones can also be evaluated on Si-(Fe+Mg), Al-Si and K-(Fe+Mg) diagrams (Fig. 11). These diagrams are used to assess the alteration of felsic volcanics associated with massive sulfide deposits (e.g. MacLean and Kranidiotis, 1987; Barrett and MacLean, 1991). The cordierite-anthophyllite rocks from NGZ fall within fields of the alteration assemblages quartz-chlorite-sericite and quartz-chlorite-talc. Bulk compositions of these rocks at the NGZ have high X_{Mg} (0.6-0.9; Table 2) and extremely low CaO and Na_2O. This is probably due to hydrothermal leaching of Ca and Na and formation of Mg-rich chlorite and talc, commonly reported at other massive sulfide deposits (Roberts and Reardon, 1978; Costa et al., 1983), and interpreted to involve addition of Mg from seawater into the upper part of an alteration zone.

Geometry of the Alteration Zone and Orebodies

The length/breadth ratios of the massive sulfide lenses (8) and the NGZ (11) are appreciably higher than for most unmetamorphosed massive sulfide deposits (<4) (Marshall and Gilligan, 1987). This suggests a severe stretching distortion from the original ore geometry. The parallelism between the elongation of the orebodies and the stretching mineral lineation is attributed to dextral shearing during ductile deformation. Deformation during amphibolite-facies metamorphism may have generated, or at least enhanced, the parallelism between the cordierite-anthophyllite alteration zone, the calc-silicate bodies, and the massive sulfide lenses.

Metal distribution

Metal distributions in the NGZ (Fig. 3) can be related to the volcanogenic alteration model. On cross-sections a cone-shaped Cu-Au anomaly plunges gently south, parallel to the stretching lineation (Fig.13). The occurrence of most of the gold as sub-microscopic inclusions in chalcopyrite and cubanite (Bérubé, 1982) explains the overlapping Cu and Au distributions. The disseminated gold ore is contained in a quartzitic gneiss which is interpreted as the metamorphosed silicified core of an alteration pipe with Zn- and Pb-rich zones at its outer margins (Figs 2, 3, 13). The mineralized quartzitic gneiss and surrounding cordierite-anthophyllite and nodular sillimanite rocks (Figs. 2, 11, 13) were derived from the same protolith (Figs. 6, 7, 9). Prior to metamorphism, the siliceous core was probably surrounded successively by concentric zones of chloritite, quartz-chlorite and sericite ± chlorite ± quartz ± talc.

Alteration Zone

The geometry of the altered rocks with the siliceous ore in the NGZ (Figs. 2, 13) resembles the alteration zonation around Tertiary Kuroko-type deposits. Alteration zones at some Kuroko-type deposits (Franklin et al. 1981; Urabe et al., 1983) have a mineralized siliceous core and successive outward haloes of quartz-sericite, Mg-chlorite-sericite, and aluminous clay-sericite ± chlorite ± quartz ± albite.

Peak metamorphic conditions for the Montauban mine sequence are estimated using various geothermobarometric techniques (Chapter 4) to have been T=620±50°C and P=6.5±1 Kbar (Fig. 14A). These conditions are compatible with the presence of relicts of kyanite rimmed by muscovite and Mg-rich cordierite,

Fig. 13. Schematic longitudinal section of the Montauban orebodies and alteration zone. The inferred fault is a late brittle structure. The block diagram is a longitudinal section showing the deformed alteration zone. The Cu-Au-rich core and siliceous zone plunge gently south.

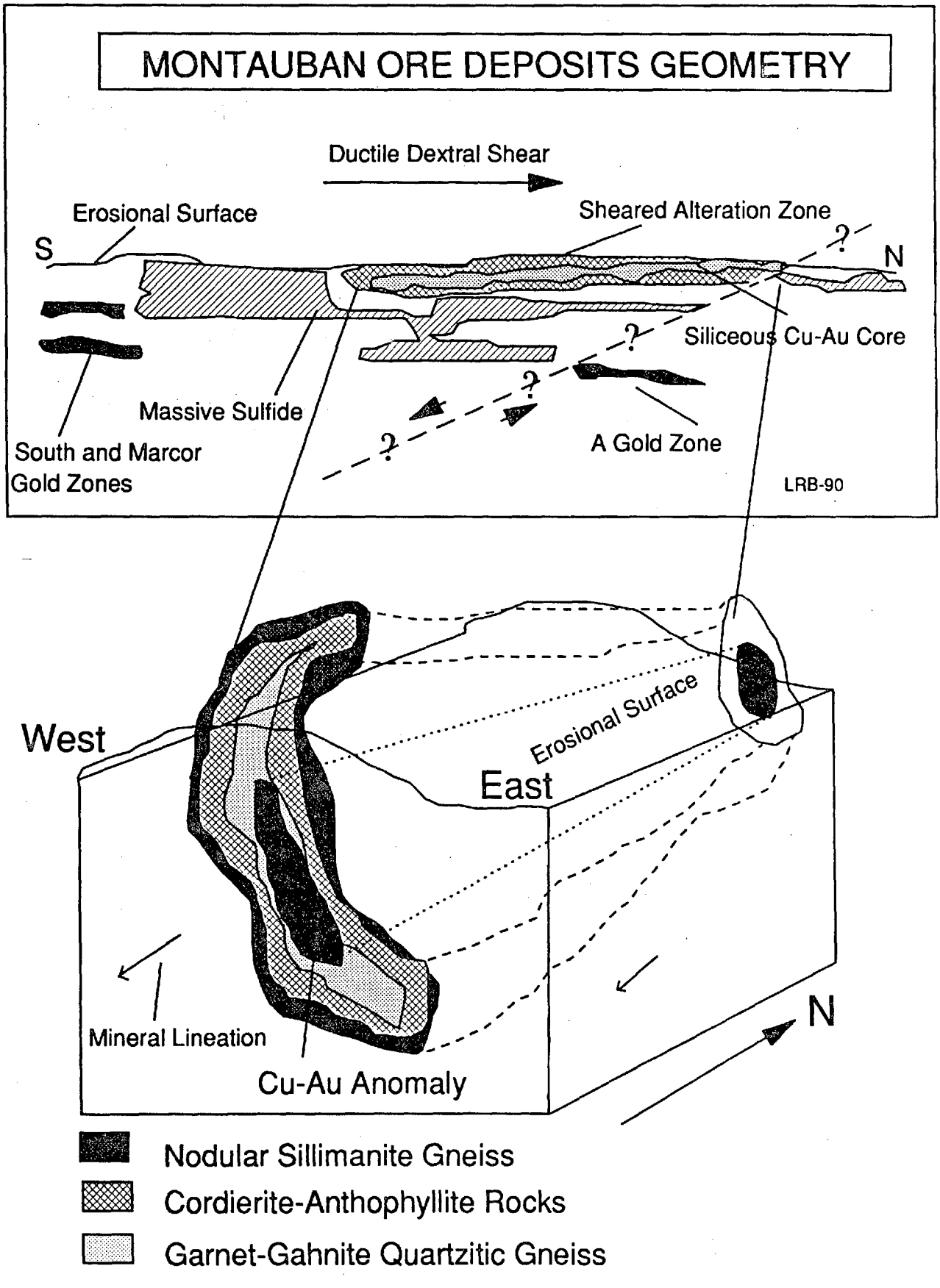
MONTAUBAN ORE DEPOSITS GEOMETRY
Ductile Dextral Shear
Erosional Surface
Sheared Alteration Zone
S
N
?
?
?
?
Siliceous Cu-Au Core
Massive Sulfide
South and Marcor
Gold Zones
A Gold Zone
LRB-90
West
Erosional Surface
East
Mineral Lineation
Cu-Au Anomaly
N
Nodular Sillimanite Gneiss
Cordierite-Anthophyllite Rocks
Garnet-Gahnite Quartzitic Gneiss

Fig. 14. A) Diagram showing the range of P-T conditions for the Montauban mine sequence. B) Schematic Schreinemakers P-T diagram (in the system F=FeO, M=MgO, A=Al_2O_3, S=SiO_2, H=H_2O) showing the probable P-T path recorded by the cordierite-anthophyllite rocks. The retrograde metamorphism was mainly due to decompression during isostatic uplift. Each univariant reactions is labeled with the absent phase.

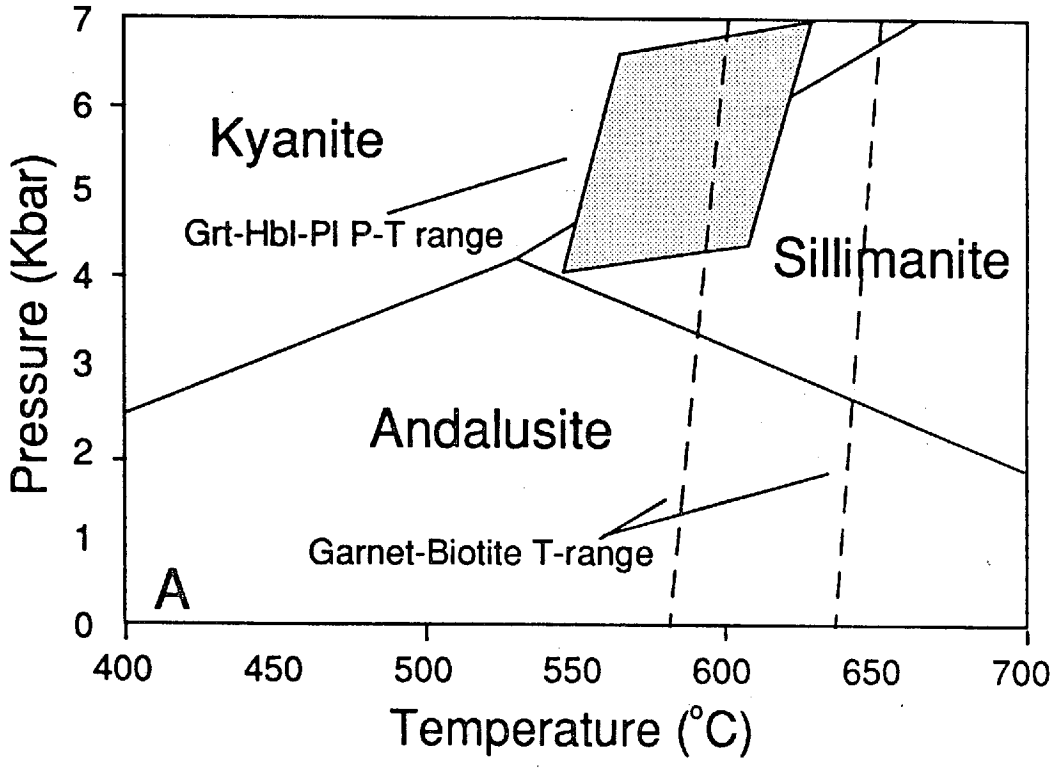
Kyanite
Grt-Hbl-Pl P-T range
Sillimanite
Andalusite
Garnet-Biotite T-range
A
Pressure (Kbar)
Temperature (°C)
0
1
2
3
4
5
6
7
400
450
500
550
600
650
700

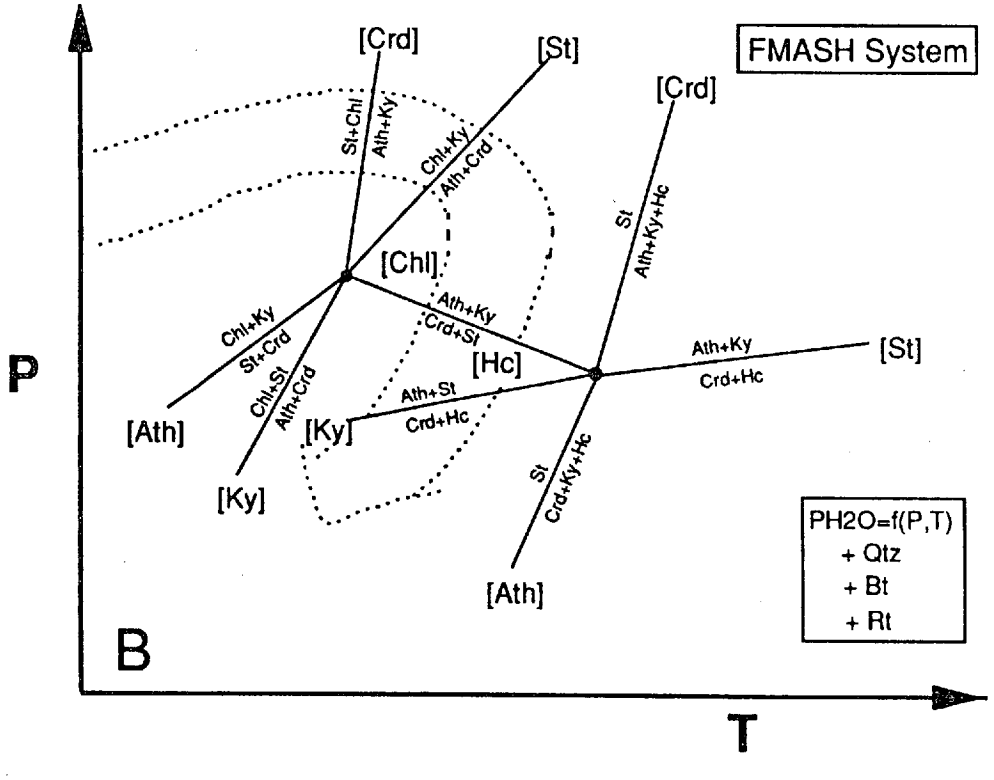
FMASH System
[Crd]
[St]
[Crd]
St+Chl
Ath+Ky
Chl+Ky
Ath+Crd
St
Ath+Ky+Hc
[Chl]
Ath+Ky
Crd+Si
Chl+Ky
St+Crd
[Hc]
Ath+Ky
[St]
Crd+Hc
Chl+St
Ath+Crd
Ath+St
Crd+Hc
[Ath]
[Ky]
[Ky]
St
Crd+Ky+Hc
[Ath]
PH2O=f(P,T)
+ Qtz
+ Bt
+ Rt
P
T
B

and with the breakdown of Fe-rich staurolite to almandine and Al-silicate (Bernier et al., 1987). High-grade metamorphism, such as at NGZ, converted alteration haloes composed of quartz, chlorite, sericite, ± talc to cordierite-anthophyllite ± biotite and cordierite-biotite ± sillimanite rocks according to reactions (3) to (7).

$$Chl + 9.5\ Qtz = 1.5\ Crd + Ath + 8\ H_2O\ (\Delta V_s = -15\%) \quad (3)$$

$$Chl + Ser + 4.25\ Qtz = 1.75\ Crd + Bt + Sil + 6.25\ H_2O\ (\Delta V_s = -16\%) \quad (4)$$

$$7\ Tlc = 3\ Ath + 4\ Qtz + 4\ H_2O\ (\Delta Vs = -7\%) \quad (5)$$

$$2.7\ Chl + 1.2\ Ser + 20.1\ Qtz = Ath + 5.2\ Crd + 1.2\ Bt + 15.5\ H_2O$$

$$(\Delta V_s = -16\%) \quad (6)$$

Volume losses for the solids (ΔV_s) calculated at constant Al are substantial in all the reactions. The water liberated in the reactions may have played a role in the intense shearing in the mine sequence and fibrolite formation in the nodular sillimanite gneiss (c.f. Kerrick, 1990). Dehydration reactions during metamorphism and tectonic deformation can induce pore pressures greater than hydrostatic, thus favoring shearing (Hobbs et al., 1976). A sericite-chlorite-clay alteration envelope would be weaker than the mineralized siliceous core and act as a strain sink and partially cushion the mineralized core and associates orebody (Cox, 1987). Hence, the altered rocks being a zone of intense strain could focus the flow of metamorphic fluids around the orebody and minimize chemical remobilization (Marshall and Gilligan, 1987).

An AFM diagram (Fig. 15) is used to compare compositions of bulk rocks and coexisting cordierite and anthophyllite, and relate them to chlorite compositions from alteration zones in mafic (Bachinski, 1976) and felsic

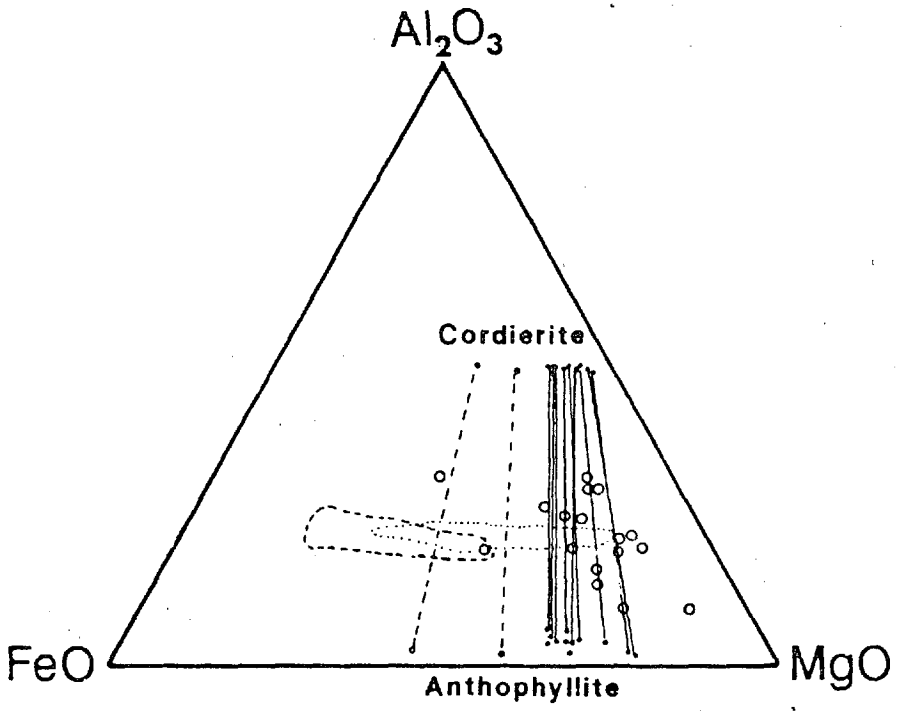

Fig. 15. Al_2O_3-FeO-MgO molecular diagram. Open circles are data for cordierite-anthophyllite rocks from Prahbu (1981) and this study. Solid tie-lines between cordierite and anthophyllite compositions are from this study; the dashed tie-lines and dashed field of chlorite compositions are from Bachinski (1976). The dotted field of chlorite compositions is from Kranidiotis and MacLean (1987).

(Kranidiotis and MacLean, 1987) volcanic rocks. The high X_{Mg} of the Montauban cordierite-anthophyllite pairs indicates Mg-rich chlorite precursors. The X_{Mg} of the cordierite (0.84-0.90) and anthophyllite (0.67-0.76) plot within the range of X_{Mg} (0.62-0.91) of the bulk rocks (Fig. 15). The average X_{Mg} of the cordierite-anthophyllite rocks (0.77 ± 0.11) is much higher than for the quartzofeldspathic gneiss protolith (0.58, Table 2) indicating, as with mass balance calculations (Fig. 10), that substantial Mg enrichment occurred during hydrothermal alteration. These data are consistent with the experimental results of Akella and Winkler (1966) which showed that cordierite-anthophyllite ± talc (reaction 3) is formed from Mg-chlorite (X_{Fe}=0.14) + quartz at 580°C and P_{H_2O}=2 kbars.

Other high grade metamorphic reactions relating to the petrology of the cordierite-anthophyllite rocks in the simplified FMASH system (Fig. 14B) are:

$$St + 3.2\ Chl + 29.1\ Qtz = 5.4\ Ath + 14.2\ Ky + 22.3\ H_2O \quad (8)$$

$$Chl + 1.2\ Ky + 8.3\ Qtz = 1.1\ Ath + 1.5\ Crd + 5.5\ H_2O \quad (9)$$

$$St + 4.8\ Crd + 2.0\ Qtz = 2.0\ Ath + 18.2\ Ky + 4.6\ H_2O \quad (10)$$

$$2.5\ Ath + 3.3\ St = 7.3\ Crd + 15.1\ Hrc + 9.3\ Qtz + H_2O \quad (11)$$

Reactions (8) and (9) are prograde and may have contributed to the formation of cordierite-anthophyllite and anthophyllite-kyanite assemblages, whereas reactions (10) and (11) are retrograde and mainly pressure dependent (Fig. 14B). A reaction similar to (11), but for quartz-absent rocks, has been experimentally calibrated in the system $FeO\text{-}SiO_2\text{-}Al_2O_3\text{-}H_2O$ and shown to be pressure sensitive (Grieve and Fawcett, 1974). The formation of gahnite coronas on zincian staurolite enclosed with garnet in cordierite and set in a matrix of quartz and anthophyllite is related to a similar reaction but in the expanded system Fe-Mg-Mn-Zn-Al-Si-H-O-S (Bernier, 1992):

$$5.7\ St + 4.6\ Ath + 7.5\ Sph + 0.2\ S_2 =$$

$$22.1\ Gah + Grt + 13.9\ Crd(0.73H_2O) + 3.4\ Qtz + 8.1\ Po + 2.1\ O_2 \quad (12)$$

These coronas most likely formed by decompression during isostatic uplift or by changes in oxidation state. The coronas are very similar to the aluminous enclaves formed by diffusion-controlled reactions during decompression in cordierite-gedrite rocks of the Ammonoosuc volcanics (Schumacher and Robinson, 1987).

Comparison With Other Deposits

Polymetallic massive sulfide deposits similar to the Montauban ores have formed through a wide span of geologic time. Metamorphosed deposits of this type (Table 4) are characterized by the common association of massive sulfide ores with calc-silicate (hanging wall) and cordierite-anthophyllite rocks (footwall) containing the chalcopyrite stringer mineralization. They are typically hosted by calc-alkaline felsic volcanic and volcaniclastic rocks, and tholeiitic metabasalts are present in the stratigraphic sequence.

The 1.1 Ga Ambaji-Deri stratiform Zn-Pb-Cu deposits (Deb, 1980), for example, strongly resemble the Montauban orebodies and host rocks. At both deposits, massive sulfide lenses are enclosed in sheared and isoclinally folded calc-silicate rocks, which are intimately associated with chalcopyrite-bearing "quartzite" and cordierite-anthophyllite rocks. Deb and Sarkar (1990), contend that the cordierite-anthophyllite rocks could be metamorphosed hydrothermal alteration haloes coeval with ore formation, and that some of the quartzofeldspathic gneisses were metamorphosed felsic volcanic rocks.

The 1.8 Ga Metsämonttu Zn-Pb-Cu-Ag-Au deposit at Orijarvi, Finland

TABLE 4. POLYMETALLIC MASSIVE SULFIDE DEPOSITS

(METAMORPHOSED)

DEPOSIT	AGE	ALTERATION	VOLCANIC ROCKS	TONNAGE
Bathurst-Norsemines (N.W.T.) P=?, T=? (Amphibolite facies) (Casselman and Miodesuska, 1982)	>2.5	di-act-bt-grt ms-qtz, crd-ath sil-bt-grt, (gah)	tuff and-rhy basalt	tot. res. 14 mt 5-9%Zn, 1-1.4% Pb, 0.25-0.45% Cu, 183-239 g/t Ag 0.5 g/t Au
Garpenberg (sweden) T=550°C P=3.5 kb (Gaàl, 1990)	1.8?	tr-tlc-chl-phl marble, dol. crd-ath, and-st-grt, ms-bt, (gah)	basalt dac-rhy	Minig district of Bergslagen 75 mt 5.5% zn, 1.8% pb, 0.65% cu, 46g/t ag, 0.4 g/t au
Metsämonttu (Finland) T=550-600°C P=3 kb (Gaàl, 1990)	1.8	tr-di crd-ath, crd-bt and-crd-ms, gah	fels tuff volc. fels basalt	3.5 mt 3.5% Zn, 0.79% Pb, 0.21% Cu 1.4g/t Au, 25 Ag
Montauban T=550-620°C P=4.5-6.5 kb (this study)	>1.4	marble di-dol tr-di-cc-dol crd-bt-ky, nod.sil, crd-ath-st Mn-grt, gah	and-dac. tuff basalt	2.5 mt 6.8% Zn, 2.3% Pb, 131 g/t Ag, 1.3 Au NGZ (0.9 mt) 3.6 Au, 17.7 Ag g/t
Ambaji-Deri (India) T=525-625°C P=2-4 kb (Deb and Sarkar, 1990)	1.1	chl-tr qtz, crd-ath-chl gah	basalt fels. volc.	9.2 mt 12.1-14.7% Zn-Pb-Cu
Ore Hill (N.H. U.S.) T=550-620°C, P=4.5-6.5 kb (brown and secord, 1986)	0.45	tr-phl crd-ky-phl-ms gah	basalt tuf fels.	Zn-Pb-Cu 0.05-0.1 mt (Mount Chase 2-3 mt) (Ledge Ridge 5 mt) Cu-Zn-Au (Bald Mountain 40 mt)

(UNMETAMORPHOSED)

Brunswick-12 (N.B. Can) (Luff et al., 1992)	0.50	sid-mt-grun fe-, mg-chl, ms-qtz-alb	crystal tuff fels volc basalt	83.9 mt 8.9% Zn, 3.6% Pb, 0.31% Cu, 101.6 g/t Ag
Harborside Maine (Stephens et al., 1984)	0.40	mg-chl-tlc tlc-cc-dol	bas, and, dac, rhy	1 mt 5.5% Zn, 1.25% Cu, 0.5% Pb
Mount Chalmers (Queensland aust) (Large and Both, 1980)	0.25	dol-cc-tlc-py qtz-chl-ser	lapilli tuff and - rhyol. epiclas sed.	3.9 mt 3.5% Zn, 1.7% Cu 1% Pb, 3g/t Au, 40 Ag
Lau basin (back-arc) (Fouquet et al., 1991)	modern	(Mn-oxides)	bas-and a rhyodacite thol. basalt	MS mounds 10-26% Zn, 0.2-0.6% Pb, 3-7% Cu, 0.6-2 g/t Au, 107-517 Ag.

di=diopside, act=actinolite. tr=tremolite, bt=biotite, phl=phlogopite, grt=garnet, gah=gahnite, ms=muscovite, qtz=quartz, crd=cordierite, ath=anthophyllite, and=andalusite, nod=nodular, sil=sillimanite, ky=kyanite, st=staurolite, cc=calcite, dol=dolomite, tlc=talc, chl=chlorite, and=andesite, dac=dacite, rhy=rhyolite, bas=basalt, volc=volcaniclastic, epiclas=epiclastic, sed=sediment, fels=felsique.

(Latvalahti, 1979), also has a geological setting comparable to Montauban. Latvalahti (1979) interpreted the cordierite-anthophyllite rocks as a metamorphosed footwall alteration zone derived from felsic volcanic rocks. Calc-silicate rock and dolomitic limestone interlayered with the massive sulfide lenses above the alteration zone are attributed to Mg-Fe metasomatism and silicification of impure limestone during hydrothermal alteration.

The alteration pipe and ores at the Mount Chalmers polymetallic massive sulfide deposit of Permian age, Australia, provide a model for pre-metamorphic conditions at Montauban. A chloritic alteration pipe is developed in relatively fresh rhyodacitic pyroclastics, and the massive sulfide ores grade laterally into dolomite-pyrite rocks (Huston and Large, 1989). Large and Both (1980) classified this deposit as a Kuroko-type, and concluded that the bedded dolomite-pyrite rock is a facies variant of the massive ore, both having formed during hydrothermal activity in the volcanic pile.

The Devonian Harborside (Zn-Cu-Pb) deposit, Maine, is characterised by talc-rich, Mg-chlorite-talc and talc carbonates alteration zones associated with the massive sulfide lenses (Stephens et al., 1984). It also appears to be quite similar to Mount Chalmers.

Luff et al. (1992) have recently presented evidence for the presence of a complex hydrothermal feeder zone to the Brunswick No. 12 massive sulfide deposit (Table 4). An inner zone is characterized by Fe-rich chlorite, muscovite, quartz and ferroan carbonate, and an outer zone by Mg-rich chlorite, muscovite, quartz and albite. The alteration zone and associated orebody are hosted by felsic volcanic rocks. A horizon of carbonate-silicate-oxide layered iron formation caps the massive sulfide body. The stringer sulfides are surrounded by hydrothermal alteration zones similar

to those at Kuroko deposits (Luff et al., 1992).

The siliceous Cu-Au ore at the NGZ has higher gold (3.6 g/t) than the Zn-Pb massive ore (1.3 g/t). Gold is enriched in footwall alteration pipes at other massive sulfide deposits. At Mount Chalmers most of the Au occurs in a Cu-rich stringer zone (>3 g/t), which was the hottest part of the alteration pipe during the formation of the overlying massive ores (Huston and Large, 1989). According to Huston and Large (1989), Au and Cu were transported as chloride complexes in high-temperature, high-salinity fluids for the stringer ore, and Au as an $Au(HS)_2^-$ complex in low-temperature fluids for the massive ore. Mineralogical evidence such as the presence of scapolite (O'Neil and Osborne, 1939) and phlogopite with up to 0.55 wt% Cl (Bernier, 1985) suggests that hydrothermal brines at Montauban were saline and may account for the Au enrichment in the NGZ alteration zone.

Paleotectonic Setting and Ore Genesis

Geochemical evidence suggests that the Montauban biotite-quartzofeldspathic gneisses were derived from intermediate to felsic volcanic rocks and related volcaniclastic sediments. The Zr/Y ratio (~6) indicates a calc-alkaline affinity. The mine sequence gneisses and regional biotite quartzofeldspathic gneiss plot in the volcanic arc field on the Rb-(Y+Nb) and Nb-Y diagrams (Figs. 16A, B) used to assess the tectonic setting of granites (Pearce et al., 1984) and felsic metavolcanic rocks (Schumacher, 1988). The wider distribution of analyses of NGZ altered rocks compared to the biotite quartzofeldspathic gneiss protolith (Fig. 16A) is mostly due to the mobility of Rb which follows the behavior of K. The clustering of the altered samples with the biotite quartzofeldspathic gneiss (Fig. 16B)

Fig. 16. Discriminant diagrams (Pearce et al., 1984) for felsic magmas. A. Log (Rb-(Y+Nb)) diagram. B. Log (Nb-Y) diagram.

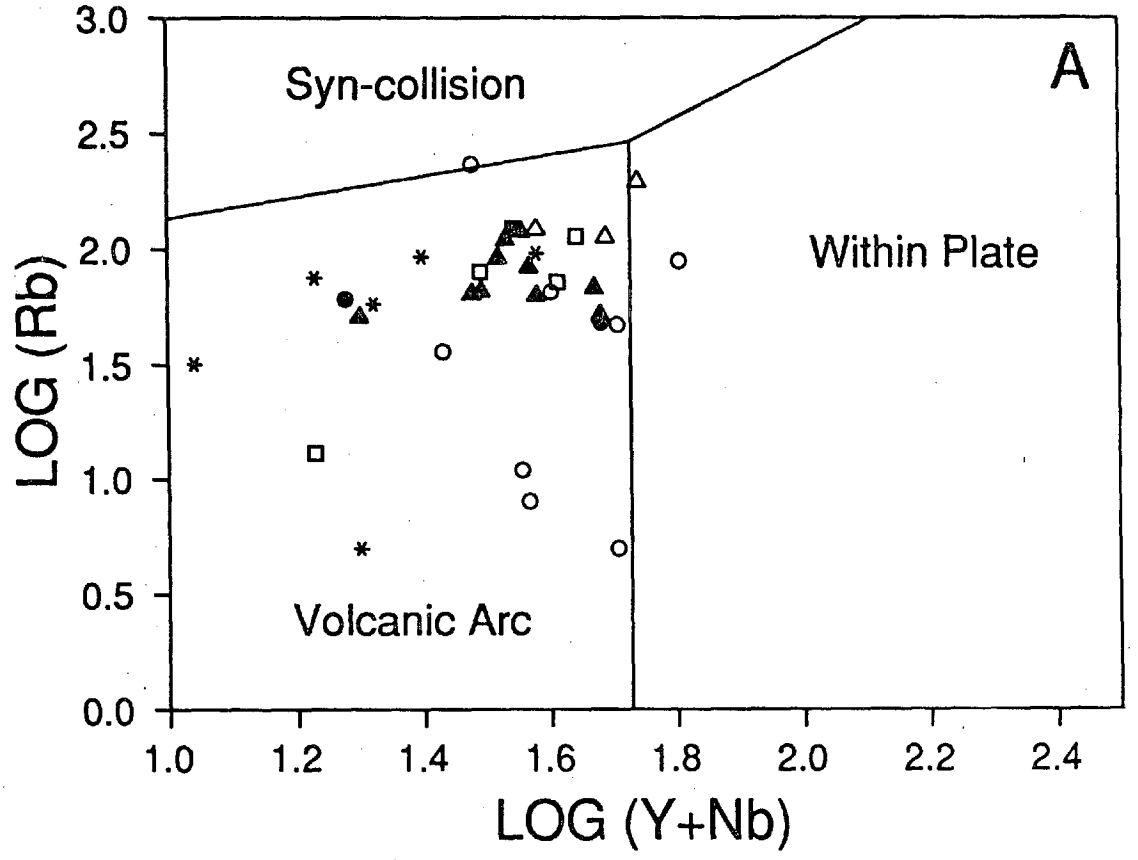
A
Syn-collision
Within Plate
Volcanic Arc
LOG (Rb)
LOG (Y+Nb)
3.0
2.5
2.0
1.5
1.0
0.5
0.0
1.0
1.2
1.4
1.6
1.8
2.0
2.2
2.4

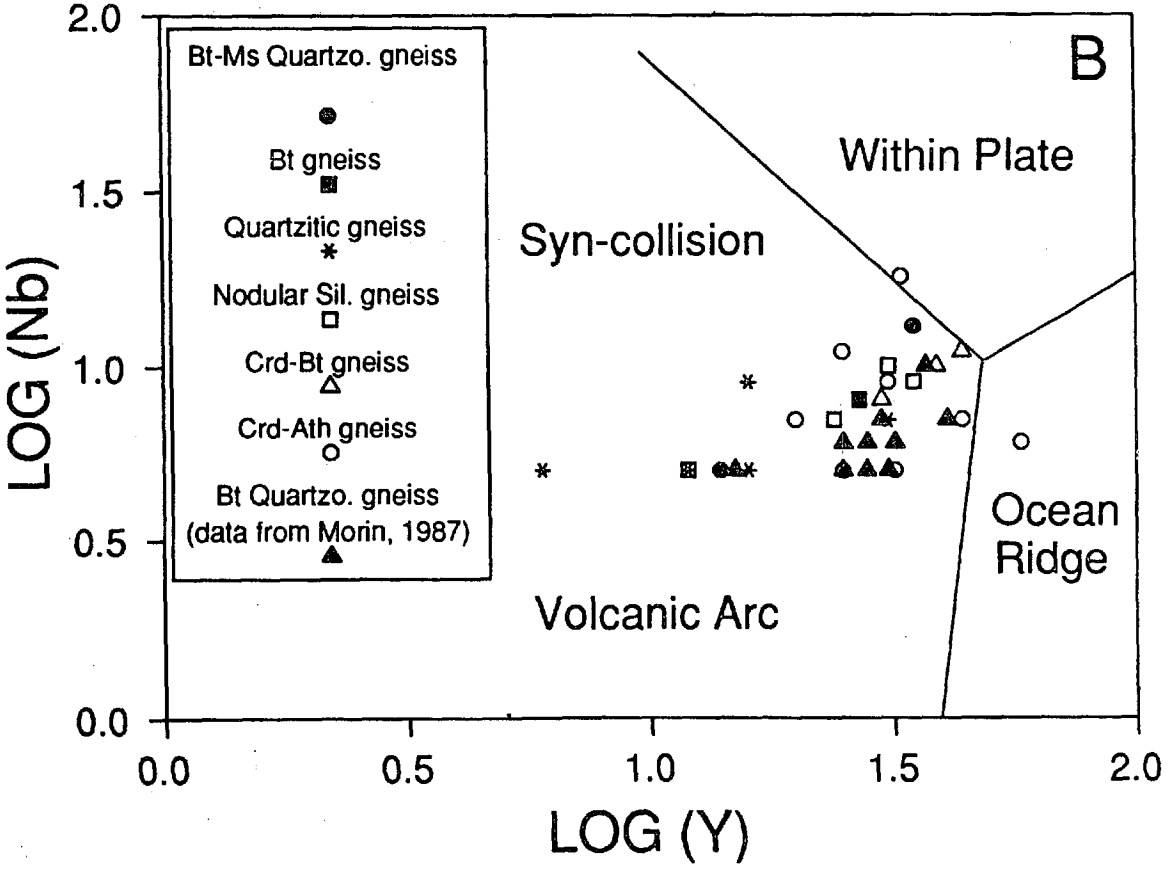
B
Bt-Ms Quartzo. gneiss
Bt gneiss
Quartzitic gneiss
Nodular Sil. gneiss
Crd-Bt gneiss
Crd-Ath gneiss
Bt Quartzo. gneiss
(data from Morin, 1987)
Within Plate
Syn-collision
Ocean
Ridge
Volcanic Arc
LOG (Nb)
LOG (Y)
2.0
1.5
1.0
0.5
0.0
0.0
0.5
1.0
1.5
2.0

corroborates that the latter is the protolith. The above evidence, combined with trace element data for the metabasalts (MacLean et al., 1982), suggests an island arc or back-arc setting for the volcanism and associated polymetallic massive sulfide deposits.

The Montauban ores resemble the unmetamorphosed Kuroko-type Mount Chalmers polymetallic deposit, which formed in an island-arc setting (Large and Both, 1980), and also the metamorphosed Zn-Pb-Cu Ambaji-Deri deposit which formed in a graben-like basin in a back-arc environment (Deb and Sarkar, 1990). The older Orijarvi deposits have also been interpreted to have formed in an island-arc structure (Latvalahti, 1979). Visible gold (0.6-2 g/t Au) was reported from modern Zn-Pb-rich polymetallic massive sulfide mounds near hydrothermally active vents in the Lau back-arc basin (Fouquet et al., 1991). The basin is characterized by andesite and rhyodacite, whereas theoleiitic basalt are forming in the portion of the basin under extensional rifting. These ores and volcanic rocks are very similar to those at Montauban. Carbonates and impure limestone are part of the stratigraphy of most modern back-arc basins of the Western Pacific Ocean, except the sea of Japan (Klein and Lee, 1984). They are also intimately associated with andesitic volcanics that formed in the Coastal Range island-arc, Taiwan (Teng and Lo, 1985). Hence, the presence of marbles and calc-silicate rocks in metamorphic terranes is not incompatible with an island-arc, back-arc paleotectonic setting.

It appears that polymetallic massive sulfide deposits resembling those at Montauban have been forming since Archean time, in island arc settings, and are probably equivalent to modern Kuroko-type deposits. The paleotectonism of ancient basins in metamorphic terranes is quite complex. The preservation and incorporation of these deposits into continents is most likely related to

collision tectonics (Cornell et al., 1990).

CONCLUSIONS

Based on major and trace element geochemistry, the Montauban quartzofeldspathic gneisses are most likely metamorphosed equivalents of andesitic to rhyodacitic volcaniclastic rocks formed in a back-arc tectonic environment. The cordierite-anthophyllite rocks, nodular sillimanite gneiss and quartzitic gneiss represent a regionally metamorphosed hydrothermal alteration zone associated with massive sulfide deposits. The orebodies, calc-silicate rocks and alteration zone acquired their sub-parallel structural relationship during deformation and metamorphism. Immobile element geochemistry shows that the altered rocks were derived from the protolith of the adjacent quartzofeldspathic gneiss. The cordierite-anthophyllite and associated rocks formed from chlorite ± sericite ± talc ± quartz alteration assemblages associated with ore formation. The Montauban ores resemble Kuroko-type deposits, and probably formed in an island-arc setting.

ACKNOWLEDGEMENTS

This paper is part of the doctoral research of LRB at McGill University. We thank Muscocho Explorations Limited for access to their property and for providing the longitudinal section. T.J. Barrett is thanked for a thorough review of a preliminary draft of the manuscript. Financial assistance was provided by a La Formation des Chercheurs et l'Aide à la Recherche (FCAR) scholarship to LRB and by Natural Sciences and Engineering Research Council of Canada grant A7719 to WHM.

CHAPTER 4.

METAMORPHIC CONDITIONS OF THE THREE TERRANES

Introduction

Chapters 2 and 3 dealt with the geological setting of the Atik Lake, Némiscau and Montauban metamorphic terranes in which metamorphosed alterated rocks (cordierite-orthoamphiboles) are associated with various types of mineralization. The lithogeochemistry of the hydrothermal alteration zones in the three terranes was used to estimate mass changes, and a new technique, the Log (Ratio) method, was outlined and applied to the identification of cordierite-orthoamphibole and associated gneiss protoliths.

In this chapter, mineral assemblages and chemistries are defined and used in conjunction with geothermobarometry, multi-equilibrium calculations using GEO-CALC (Brown et al., 1988) and THERMOCALC (Holland and Powell, 1990), phase equilibria and Schreinemakers analyses, to delineate the metamorphic evolution of each terrane. More particularly, peak P-T conditions and P-T paths are estimated for each terrane to characterize the metamorphic conditions under which the cordierite-orthoamphibole rocks evolved. The effect of additional components such as Mn and Zn on mineral stabilities are evaluated, particularly for the Montauban terrane. The study of Fe-Mg partitioning between cordierite and anthophyllite led to the calibration of a new geobarometer, which will be presented in chapter 5 and applied to other occurrences reported in the literature.

A knowledge of peak P-T conditions and mineral compositions is used to quantitatively evaluate sulfide-silicate-oxide equilibria. The experimental data of Popp et al. (1977b) is used to extrapolate the free energy of reactions involving Fe-anthophyllite and to model fO_2-fS_2 equilibria under

peak P-T conditions (Chapter 6). These data, combined with ideal mixing modelling of metamorphic fluids in the system C-O-H-S, are used to evaluate the buffering capacity of various compositional systems (alterated basalts, altered felsic rocks, BIF, graphitic argillite and auriferous chert) in the three terranes (Chapter 6). Furthermore, this analysis will be helpful in establishing the timing of the hydrothermal alteration and mineralization with respect to metamorphism.

Mineral Assemblages, Mineral Chemistries and Chemographical Relations

"The partial replacement of one P-T sensitive mineral assemblage by another can provide valuable information on the P-T path of metamorphism. Although it may be considered to be "old-hat" by some metamorphic petrologists, the data are relatively easy to obtain and require nothing more than a petrographic microscope." Ghent et al. (1988), MAC, v. 14, p.160

The minerals were analysed by electron microprobe (Chapter 3, 3D) and the results for the three terranes are presented in *Appendix II*. Stoichiometries were calculated for most of the minerals with the computer program MINFILE (Afifi and Essene, 1988). Recasting of the staurolite analyses into structural formulae followed the scheme proposed by Holdaway et al. (1986, 1988); cations were normalized to (Si+Al)=25.53 for reduced metamorphic conditions, and excess anion charges were balanced by H^+ on the assumption that the total oxygen is 48. The cation assignment to structural sites is based on the presence of 0.25 Fe^{+3} at the octahedral Al(3A) sites, $(Mn+Fe^{+2})=0.25$ at the U(1) site and Mg, Zn, Ti and the remaining Fe at the tetrahedral (Fe) site (Holdaway et al., 1986; Zaleski et al., 1991). Weight percent H_2O, Fe_2O_3, and FeO were then back-calculated.

Atik Lake terrane

The rock types of importance in establishing metamorphic conditions are altered basalts, altered intermediate felsic volcanics and metasediments. These units have developed low variance mineral assemblages useful to geothermobarometric study. Sample locations are shown on the maps in *Appendix 1*. Their mineral assemblages are summarized in Table 4.1A. The alteration zones are best developed in the basalt forming the footwall to BIF and mineralized chert at Mistuhe Island. The zones are subdivided according to characteristic metamorphic mineral assemblages (Table 4.1A):

1) bleached basalt,
2) cordierite-orthoamphibole rock,
3) orthoamphibole-garnet rock,
4) cordierite-chlorite rock,
5) aluminous alteration patches,
6) transitional alteration,
7) Fe-rich calc-silicate alteration,
8) fuchsite schist.

The fuchsite schist was observed only as a sheared contact between basalt and mineralized chert. It is the only rock type to contain rare ullmanite (NiSbS) coronas on pyrrhotite and arsenopyrite.

Contrasting metamorphic mineral assemblages (except fuchsite schist) were observed in one outcrop (Chapter 3, 3A), and reflect rapid changes in bulk rock compositions. Accordingly, various metamorphic reactions proceded under the same P-T conditions in rocks with contrasting compositions. The occurrence of Fe-rich cordierite or andalusite in some of the assemblages is indicative of low pressure metamorphism (Winkler, 1979; Best, 1982). Weber and Scoates (1978) draw an andalusite-sillimanite isograd parallel to the Atik

TABLE 4.1A MINERAL ASSEMBLAGES, ATIK LAKE

Assemblages	Opaques	Samples
LEAST ALTERED BASALTS		
Hbl-Pl (±Qtz, Cc[1], Chl[1], Ep, Tnt)	Ilm±Rt	U-07, U-22, U-18
FELSIC ROCKS		
Qtz-Pl-Bt (Cc, Ep)		U161
Qtz-Pl-Bt-And	Ilm	U-41D
BLEACHED BASALT		
Hlb-Pl-Hd-Qtz-Ep-Tnt (Cc)	Ilm±Apy	U-25A, U-19, U-20 U-16
STRATIFORM ALTERATION		
Hlb/Cum-Pl-Qtz-Bt-Tnt (±Grt, Ep, Cal, Kfs)	Ilm±Po±Apy	U102, U108, U034, U058, U086, U112
CORDIERITE-ORTHOAMPHIBOLE ROCKS		
Ged-Crd-Chl (Qtz, Pl, Hrc)	Ilm-Po-Apy-Cpy-Sph	U-17B
Ged-Crd-Grt (Qtz, Pl, Bt)	Ilm-Po-Apy-Cpy-Sph	U-24, U39
Ath-Crd-Chl (Qtz, Bt)	NDO	U-31A, U-31B
Ged-Crd-Grt-Chl (Qtz, Bt)	Po-Apy	U-25B
Ged-Ath-Crd-Grt (Qtz, Pl, Bt)	Ilm-Po-Cpy	U-29B
Ath-Crd-Grt-Chl (Qtz, Pl, Bt, Hrc, To)	Ilm-Apy-Po-Lö	U-10A, U10B
ORTHOAMPHIBOLE-GARNET ROCKS		
Ged-Grt (Qtz, Pl)	NDO	U-28
Ged-Ath-Grt (Qtz, Pl, Bt, Hrc)	Ilm-Po-Sph-Rt	U-08
Ged-Grt-Chl (Qtz, Pl, Bt, To)	Ilm-Po-Apy-Lö	U-01, U-14, U-27
Ath-Grt-Chl (Qtz, Bt)	Ilm	U-02B, U-21
CORDIERITE-CHLORITE ROCKS		
Crd-Chl-Grt-Bt-Ms (Qtz, To, Hrc)	Ilm-Po-Apy-Lö-Rt?	U-04
ALUMINOUS ALTERATION		
And (Qtz, Pl, Bt, To)	Ilm-Po-Apy-Lö	U-13, U-40D
And-Grt (Qtz, Pl, Bt)	Ilm-Apy-Po-Cpy	U-06, U-31C
And-St-Grt (Qtz, Pl, Bt)	Ilm-Po-Apy	U-35B
And-St-Crd (Qtz, Bt)	NDO	U-40A
And-St-Grt-Crd (Qtz, Bt)	Ilm±Apy-Po	U-26
St-Grt-Crd-Chl (Qtz, Bt)	Ilm-Po-Apy-Lö-Cpy	U-41C1

Assemblages	Opaques	Samples
TRANSITIONAL ALTERATION		
And-St-Grt-Ged-Crd (Qtz, Bt)	Ilm-Po-Apy-Lö	U-41C2
And-St-Grt-Crd-Ged-Chl (Qtz, Bt, Hrc)	Ilm-Po-Mt	U-12B
CALC-SILICATE CRUST		
Hd-Grt-Cc-Ep-Hlb	Ilm	U-2C
FUCHSITE SCHIST		
Green Ms-Bt (Qtz, Pl, To)	Ilm-Po-Apy-Ulm	UBI1A
CORDIERITE-ANTHOPHYLLITE ROCKS (METASEDIMENTS)		
Ath-Chl (Qtz, Pl, Bt)	Ilm-Po-Cpy	U84-5B
Crd-Ath (Qtz, Pl, Bt)	Ilm-Po-Cpy	U84-1, U2401
Crd-Ath-Chl (Qtz, Pl, Bt)	Ilm-Po-Py-Cpy	U84-7
Crd-Grt-Ath (Qtz, Pl, Bt)	Ilm-Po-Cpy	U84-5A
GRAPHITIC ARGILLITE		
Bt, Ms, Qtz, Pl	Gr-Po-Py-Apy-Rt	U0506, U0601
PIPE-1 CONDUIT		
Gru-Act-Qtz	Po-Py-Cpy	U-2C
AURIFEROUS CHERT		
Gru-Qtz	Po-Apy-Cpy	UBI1B, U0505
Act-Grt-Qtz	Po-Apy-Cpy	U0109
Gru-Act-Qtz-Cc-To-	Po-Py	U1902
Gru-Act-Hd-Qtz	Po-Apy	U-32
Hd-Act-Grt-Qtz	Po-Apy	U3103, U3105
BANDED IRON FORMATION		
Qtz	Mt	
Gru-Qtz	Mt	U34, U2803
Gru-Grt-Qtz	Mt	U-05
Gru-Hd-Qtz	Mt	U-41A
Gru-Fa-Qtz	Mt	U1804
Gru-Act-Qtz	Mt-Po	U2301

TABLE 4.1 (continued)

TABLE 4.1B MINERAL ASSEMBLAGES, NÉMISCAU

Assemblages	Opaques	Samples
LEAST ALTERED AMPHIBOLITE		
Hlb-Pl (±Qtz, ±Ep)	Ilm	S27, S28, N09, N37, N40 N17
Hlb-Cum-Pl (±Qtz, ±Bt)	Ilm±Py±Po	N15, N28, N30, N34A
Cum-Pl (±Qtz, ±Bt)	Ilm±Py±Po	S12, N12, N13, N31, N41, N42
FELSIC ROCKS		
Ms-Kfs (Qtz, Pl)	None	N11
Ms-Bt-Sil (Qtz, Pl)	None	N-07, N10
ULTRAMAFIC		
Tr-Ol-Tlc-Srp	Mt	N08
Tr-Ol-Srp-Tlc-Spl-Cc-Ep	Ilm-Po-Py-Apy-Cpy	S31
Ath	None	N31
ANTHOPHYLLITE-CUMMINGTONITE ROCKS		
Ath-Cum (Qtz, Pl, Bt)	Ilm-Po±Mt	N16, N20, N21, N36, N44
Ath-Grt (Qtz, Pl, Bt, To)	Ilm-Po	S36-N14
Ath-Cum-Grt (Qtz, Pl, Bt)	Ilm-Po-Apy-Cpy	S32, N22, N26
CORDIERITE-ANTHOPHYLLITE ROCKS		
Ath-Crd (Qtz, Bt, Chl[r])	Mt-Ilm-Po-Cpy-Pn-Py[r]	SE1, SE2, SE3
Ath-Crd-Bt-Ms	Ilm-Po	N25
Ath-Crd-Grt (Qtz, Pl, Bt, Hrc)	Ilm-Po-Cpy	N39
Ath-Ged-Crd-Grt (Qtz, Pl, Bt)	Ilm-Po-Cpy	N-32
Ath-Cum-Crd-Grt (Qtz, Pl, Bt)	Ilm±Rt	N34B, N35
SILLIMANITE GNEISS (MAFIC)		
Sil-Bt (Qtz, Pl, ±To)	None	N27, N33
CALC-SILICATE ROCK		
Hd-Grt-Cc-Ep	Po-Py-Apy	N02
METAPELITES		
And-St-Grt-Bt-Ms (Qtz, Pl)	Ilm	V4811, V4814
Sil (Qtz, Pl, Bt)	Po-Sph	S29
Grt (Qtz, Pl, Bt)	Ilm	S14, N38
Grt-Sil (Qtz, Pl, Bt, To)	Ilm±Po±Rt	S5, S21
Ms-Kfs-Bt-Grt (Qtz, Pl)	Ilm-Rt-Apy	S26
Grt-Crd-Sil-Bt (Ms-St-Gah-Crd-Chl[f]	Ilm	S30
SULFIDE-RICH QUARTZITE		
Qtz-Bt-Grt-Sil (To)	Po-Pn-Rt	S03
Qtz-Bt-Ms	Po-Py-Pn-Sph	S15
Qtz-Bt-Sil-Crd (To)	Po-Sph-Apy	S25A, B

TABLE 4.1. (continued)

TABLE 4.1C MINERAL ASSEMBLAGES, MONTAUBAN

Assemblages	Opaques	Samples
BIOTITE QUARTZOFELDSPATHIC GNEISS (NGZ)		
Bt-Kfs-Qtz-Pl±Ms	None	E66, E64, E54 B55, B511, I230
GREY MIXED GNEISS (NGZ)		
Hlb-Kfs-Pl-Di-Bt±Ms	None	B22, B510, D710
REGIONAL AND NGZ GARNET-AMPHIBOLITE		
Hlb-Pl-Grt±Qtz	Ilm±Po±Cpy	B401, G511, G513 I305, I307
Hlb-Pl-Grt-Bt±Qtz	Ilm±Po±Cpy	MQ4, MQ6, E302
REGIONAL METAPELITES		
Bt-Grt (Qtz, Pl)	Ilm	MQ1
Bt-Ms-Grt (Qtz, Pl)	Ilm	MQ7
Bt-Sil-Kfs (Qtz, Pl, Tnt)	Ilm	MQ13, 17, 20
Bt-Kfs-Ms-Grt-Sil (Qtz, Pl)	Ilm	MQ10
BIOTITE-CORDIERITE GNEISS (NGZ)		
Crd-Ky/Sil (Bt, Qtz)	Po	C106
Crd-Grt-Sil (Bt, Qtz, Pl)	Po	E333, N204
Crd-St-Ky/Sil (Bt, Qtz)	±Po	G522, I230
Crd-Grt-St-Ky (Bt, Qtz, Pl)	Po-Cpy±Sph±Rt	C207, D312
Crd-Grt-St-Gah (Bt, Qtz Pl)	Py-Sph-Rt-Gn	I204
Crd-St-Gah-Ky (Bt, Qtz, Pl)	Po-Sph-Rt-Cpy-Gn	A106, J123
Crd-Grt-Gah-Ky (Bt, Qtz, Pl)	Po-Sph-Rt-Gn	B421, D207, D319
Crd-Grt-St-Gah-Ky (Bt, Qtz, ±Pl)	Po-Sph-Rt±Cpy±Gn	E326, I108, I109, I203, J209
CORDIERITE-ANTHOPHYLLITE ROCKS (NGZ)		
Ath-Crd (Bt, Qtz)	Po-Rt±Sph±Cpy±Gn	C620, F322, J21
Ath-Crd-Grt (Bt, Qtz)	Rt	D608
Ath-Crd-St (Bt, Qtz)	±Po±Sph±Cpy±Gn±Rt	C522, D617, E204, J303
Ath-Crd-Grt (Bt, Qtz, ±Pl)	Po-Rt-Sph-Cpy-Gn	E525
Ath-Crd-Gah (Bt, Qtz, Pl)	Po-Rt-Sph±Cpy±Gn	D305, D723, G312,
CORDIERITE-ANTHOPHYLLITE ROCKS		
Ath-Crd-Grt-Gah (Bt, Qtz, Pl)	Po-Sph-Rt±Cpy±Gn	C406, D514, I323, MQ12,
Ath-Crd-St-Gah (Bt, Qtz, Pl)	Po-Rt	D211
Ath-Crd-Grt-St-Gah (Bt, Qtz, ±Pl)	Po-Rt-Sph±Cpy±Gn	C322, F307, F319, G315, E519, E524, N202
NODULAR SILLIMANITE GNEISS (NGZ)		
Sil-Ms-Bt (Qtz, Pl)	Po-Cpy-Sph	D318
Sil-Crd (Qtz, Bt, Pl)	Po	B523, G325, I302
Sil-Ky-Crd-St (Bt-Qtz, Pl)	Po±Rt	A109, B211, C108. E321, E436, E214
Sil-Grt-Gah-Ms-Bt (Qtz, Pl)	Po-Sph±Rt±Cpy±Gn	C332, G325, E216
MINERALIZED QUARTZITIC GNEISS (NGZ)		
(Qtz, Pl, Bt)	Po-Sph-Rt-Cpy-Gn	E-4-28
Gah (Qtz, Bt, ±Pl)	Po-Sph±Cpy±Gn	C514, D407, E311
Grt (Qtz, Bt, Pl)	Po±Sph±Cpy±Gn	C416, C211, D517 F205
Grt-Gah (Qtz, Bt,)	Po-Sph±Cpy±Gb	B419, B205, E225 F104, H204, J103 K102, K106
Grt-Gah-Ath (Qtz, Bt, Pl)	Po-Sph-Cpy-Gn	D110
Bt-Ms-Sil (Qtz, Pl)	Po-Sph-Rt	D319
Bt-Ms-Grt (Qtz, Pl)	Po-Sph-Cpy-Gn	E419
Bt-Ms-Grt-Gah (Qtz, Pl)	Po-Cpy-Sph±Rt±Gn	C419, D519, E313, E219, E104, H201
Bt-Ms-Gah-Ath (Qtz, Pl)	Po-Sph-Cpy-Gn	D108

Lake fault on the southern margin of the belt, but Weber (1974) restricts sillimanite to the outermost southwest extremity of the belt. In the present study, andalusite is shown to be the stable aluminosilicate across the entire belt.

The system SiO_2, Al_2O_3, TiO_2, Fe_2O_3, V_2O_3, Cr_2O_3, MgO, FeO, ZnO, MnO, CaO, Na_2O, K_2O, H_2O describes the major element chemistry of Atik Lake cordierite-orthoamphibole rocks. Biotite is the only phase to contain important concentrations of K_2O, and thus K_2O can be omitted. Muscovite is rare and was only found in two samples of altered basalt. As V_2O_3 and Cr_2O_3 are components only of spinel, TiO_2 of ilmenite and rutile, and ZnO of spinel and staurolite, these oxides can, to a first approximation, also be omitted. Sulfide-arsenide assemblages in these rocks indicate relatively reducing conditions during metamorphism and stoichiometric calculations indicate that Fe_2O_3 is unimportant in garnet and gedrite and can thus be neglected. MnO is a minor constituent in most Fe-Mg silicates, ilmenite and spinels and can be omitted. These assumptions reduce the system to SiO_2, Al_2O_3, MgO, FeO, CaO, Na_2O, H_2O (CNFMASH). However, part of the alteration zone contains muscovite and biotite without plagioclase and is best represented by the KFMASH system. Cordierite-anthophyllite rocks with no gedrite and plagioclase can be represented adequately in the FMASH system.

The mineral assemblages of the cordierite-orthoamphibole rocks and the small patches of aluminous alteration can be adequately described and compared with bulk rock compositions in an AFM diagram (Robinson et al., 1982). Figure 4.1A shows ranges in bulk rock and mineral compositions in altered basalts and cordierite-anthophyllite metasediments. The projection is that of Robinson and Jaffe (1969) and Spear and Rumble 1986) who used plagioclase, quartz and water as the projecting phases. It should be noted that even if Ca and Na

have been leached during hydrothermal alteration, plagioclase destruction was not complete as it is a common contstituent of the cordierite-gedrite rocks. Furthermore, all analysed gedrites, except one sample (U-14D) which has a nearly pure gedrite rim composition, have an important pargasitic component (0.5-1.8 wt% Na_2O), a common phenomenon of natural occurrences (Spear, 1980; Treloar and Putnis, 1982; Stoddard and Miller, 1990; Schneiderman and Tracy, 1991). This requires that Na was available either through the fluid phase or by exchange with plagioclase, the chief source of sodium. Schneiderman and Tracy (1991) used the Al_2O_3-MgO-FeO-$NaAlO_2$ tetrahedron to illustrate chemographic relationships of cordierite-gedrite rocks from Orijarvi, Finland, but their method offers little advantage over the AFM projection through plagioclase. Because most of the cordierite-orthoamphibole rocks have less than 1.5 Wt% K_2O, a correction for the Al, Fe and Mg contained in biotite is minimal, and projecting the bulk rock compositions onto the AFM plane does not result in discernable changes in chemography.

The aluminous and cordierite-gedrite alterations in the basalts form transitional trends toward the A apex (Fig. 4.1A). The metasedimentary cordierite-anthophyllite rocks are more magnesian than the altered basalts and plot to the right of that trend. Cordierite, chlorite, gedrite, anthophyllite and garnet show a wide range of Fe-Mg solid solution, whereas staurolite is exclusively Fe-rich. Staurolite is rare at Atik Lake; it occurs as relict grains within garnet and cordierite in altered intermediate volcanic rocks (U-84-2), and within a few samples of altered basalt. Some staurolite grains are visible ($\leq$2 mm) in hand specimen, and have a brown-orange color. Staurolite in sample U-12 is very Fe-rich (12.2 wt%) and contains 0.73 wt% ZnO, which might have contribute to stabilize it.

The mole fraction of Mg (X_{Mg}) decreases in the following order for

Fig. 4.1. AFM diagrams for the Atik Lake cordierite-orthoamphibole rocks and aluminous alteration patches. A=Al_2O_3 + Fe_2O_3 + 2 TiO_2 - Na_2O - CaO, F=FeO + MnO - TiO_2, M=MgO. A) Bulk rock and mineral compositions projected through plagioclase, quartz and water. B) Stable (solid lines) and unstable (dashed lines) mineral assemblages in sample U-12 from a Fe-rich transitional alteration patch. The staurolite and gedrite are metastable. C) Mineral assemblage in sample U-29B indicating the breakdown of gedrite (tie-lines suggesting a terminal reaction) to form garnet, anthophyllite and cordierite. D) Mineral assemblages in Fe-rich (cordierite-garnet-anthophyllite) and Mg-rich (cordierite-anthophyllite±chlorite) cordierite-anthophyllite rocks of sedimentary origin.

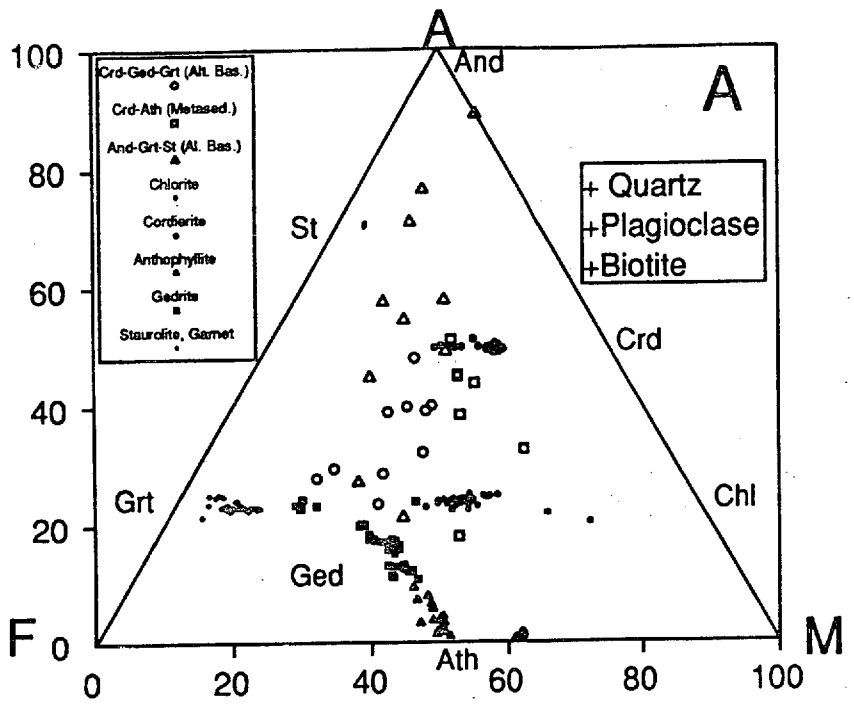
A
And
A
Crd-Ged-Grt (Alt. Bas.)
Crd-Ath (Metased.)
And-Grt-St (Alt. Bas.)
Chlorite
Cordierite
Anthophyllite
Gedrite
Staurolite, Garnet
+ Quartz
+Plagioclase
+Biotite
St
Crd
Chl
Grt
Ged
Ath
F
M
0
20
40
60
80
100

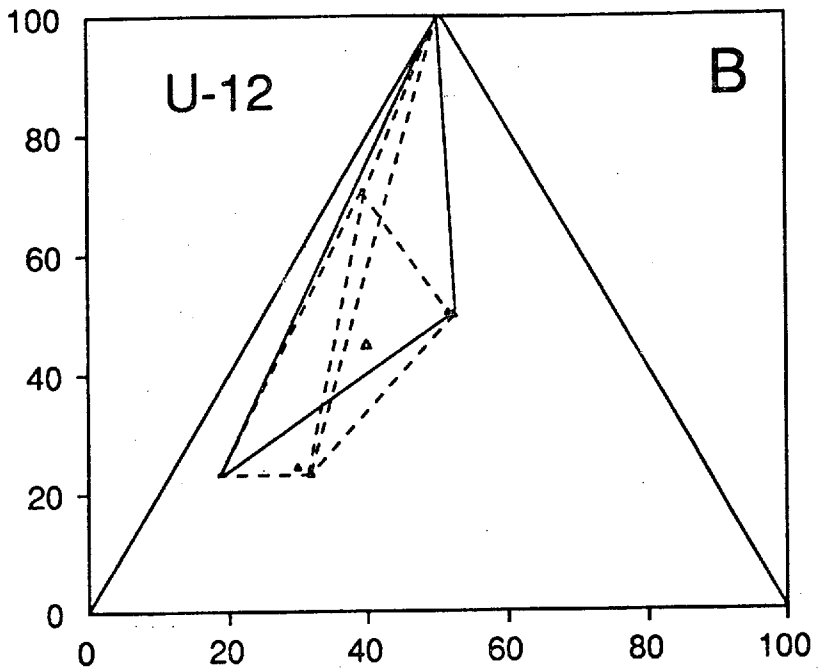
U-12
B
0
20
40
60
80
100

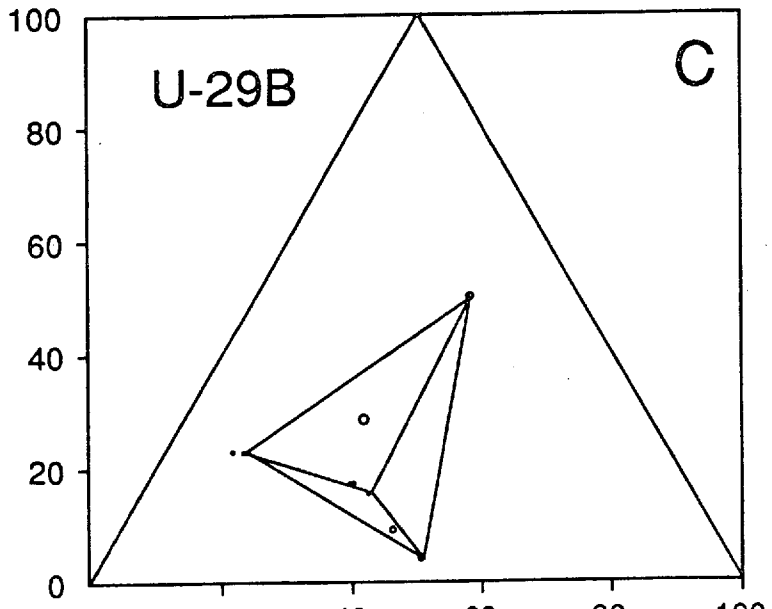
U-29B
C
0
20
40
60
80
100

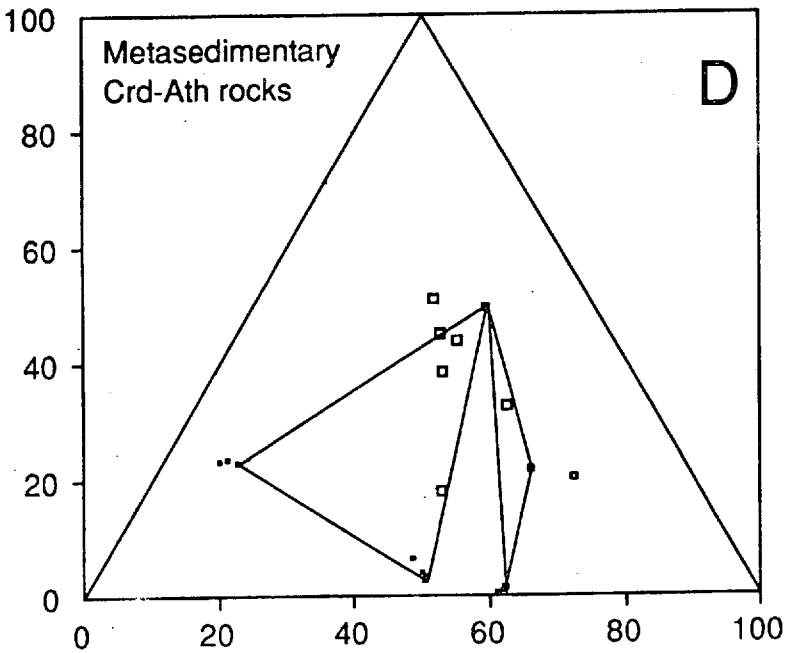
Metasedimentary
Crd-Ath rocks
D
0
20
40
60
80
100

coexisting Atik Lake AFM phases: $X_{Mg}^{Crd} \geq X_{Mg}^{Chl} > X_{Mg}^{Bt} > X_{Mg}^{Ath} > X_{Mg}^{Ged} > X_{Mg}^{St} > X_{Mg}^{Grt}$. This is in agreement with the findings of Thompson (1976) and Spear (1982) and consistent with the petrographic observation that chlorite in the alteration zones is prograde. Chlorite, arsenopyrite, pyrrhotite, and loëllingite inclusions in garnet are common and indicate that the timing of the emplacement of the sulfide-arsenide mineralization is pre-metamorphic. Some garnets in alteration pipe 1 samples close to the sheared BIF, show evidence of retrograde metamorphism, as they are cut by chlorite veinlets.

The various mineral assemblages described in Table 4.1A and the AFM chemography allow prediction of the metamorphic reactions that occurred in rocks of different bulk compositions during peak metamorphic conditions (Fig. 4.1B-D). Metastable mineral assemblages are present in some altered basalt samples (Fig. 4.1B): staurolite and gedrite relicts are preserved in sample U-12 with the stable assemblage andalusite, Fe-cordierite and garnet; gedrite appears metastable in the assemblage cordierite, anthophyllite and garnet (Fig. 4.1C). The common stable assemblage in metasedimentary cordierite-anthophyllite rock is cordierite, anthophyllite and garnet (Fig. 4.1D). Cordierite-gedrite-garnet is a common assemblage of the altered basalts and the displacement of the compositional field is linked to changes in bulk composition rather than to changes in intensive parameters. This chemographic analysis is useful in predicting metamorphic reactions that can be used (in combination with standard geothermobarometric techniques discussed in an upcoming section) to model the metamorphic P-T path.

Némiscau terrane

The altered basalts, ultramafic, calc-silicate and metapelitic rocks are of importance in establishing the metamorphic conditions in the Némiscau belt.

The altered basalts are subdivided into:

1) cordierite-anthophyllite gneiss,

2) anthophyllite-cummingtonite gneiss,

3) sillimanite-bearing gneiss.

Two isograds were mapped in the Némiscau belt (Fig. 4.2) by combining field data gathered in this study with field observations made by Valiquette (1975). The most extensive isograd is andalusite-sillimanite which more or less parallels the long axis of the belt and abruptly disappears against a late diabase dyke toward the southwest. All of the cordierite-anthophyllite rocks occur in the sillimanite-zone (Fig. 4.2). The staurolite-out isograd is restricted to the northeast end of the belt. Its intersection with the andalusite-sillimanite isograd constitutes an important indicator of metamorphic conditions. Its location is consistent with the presence of staurolite inclusions in garnets (Peredery, 1966; Valiquette, 1975; this study) south of the isograd, mostly in the Lac Sillimanite and Lac Voirdye areas.

The same considerations outlined for the Atik Lake cordierite-orthoamphibole rocks with respect to the chemical system applies to Némiscau. An exception at Némiscau is the presence of anthophyllite as the main orthoamphibole with gedrite being rare and only encountered as a reaction rim on anthophyllite in one sample (N-32). The mineral assemblages characteristic of the main rock types are listed in Table 4.1B. Sample locations are presented in *Appendix I*.

As at Atik Lake, biotite is ubiquitous in cordierite-anthophyllite and metapelite rocks. The chemographic relationships of the stable mineral assemblages constituting the cordierite-anthophyllite rocks and mafic sillimanite gneiss are shown in an AFM diagram (Fig. 4.3), along with bulk

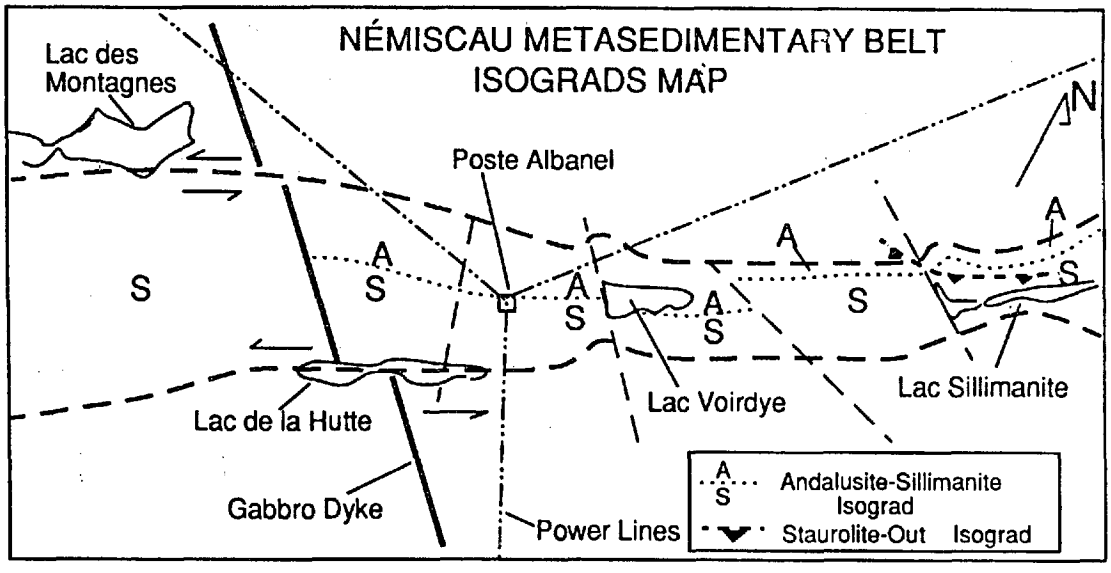

Fig. 4.2. Isograd map of the Némiscau belt. The cordierite-anthophyllite rocks (hatched symbol) are in the sillimanite zone (S). Also shown are the crossing staurolite-out and andalusite-sillimanite isograds.

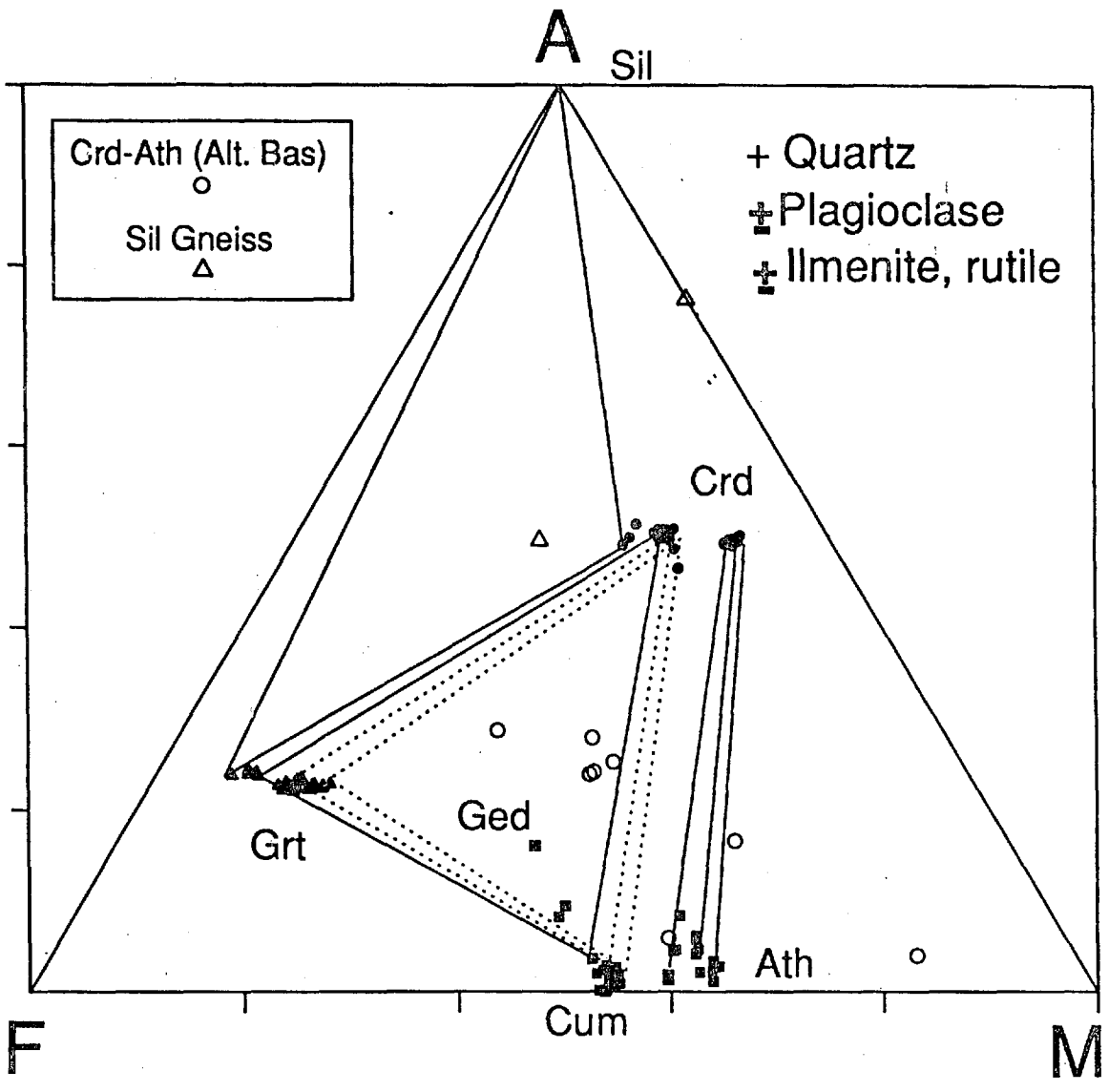

Fig. 4.3. AFM diagram showing the projected bulk rock and mineral compositions for cordierite-anthophyllite rocks and a sample of sillimanite gneiss in the Némiscau belt.

rock compositions. Cordierite-anthophyllite rocks, where Fe-rich, contain garnet. Cummingtonite generally contains less than 1 wt% Al_2O_3 but, as it was virtually impossible to distinguish from anthophyllite under the microprobe, the two minerals are not distinguished in the AFM diagram. Anthophyllite-cummingtonite rocks have garnet in Fe-rich bulk composition. A common assemblage in the metapelitic gneiss and sillimanite-gneiss is cordierite-garnet-sillimanite. The least altered amphibolites contain hornblende or cummingtonite, or both minerals (Table 4.1B).

The anthophyllite-cummingtonite rocks are marked by the absence of hornblende and are interpreted to represent a somewhat altered amphibolite. These cummingtonite-bearing rocks are similar to those of the Flin Flon belt, which have been interpreted by Froese and Ashton (1990) to be metamorphosed rocks that underwent moderate Fe-Mg metasomatism during hydrothermal alteration. Overall, the stable mineral assemblages in the Némiscau cordierite-anthophyllite rocks are fairly simple and are identical to those reported by Elliot-Meadows and Appleyard (1991) for the metamorphosed Mg-rich alteration zone of the Lar Cu-Zn deposit at Lynn Lake Area, Manitoba.

Coronitic gahnite and cordierite around zincian staurolite relicts were observed in a metapelite sample (S-30). This texture and its metamorphic significance will be discussed later in reference to coronitic textures in cordierite-anthophyllite rocks at Montauban.

Montauban Mine Sequence

The rock types in the NGZ alteration zone have been defined as:

1) central garnet-gahnite quartzitic gneiss

2) cordierite-biotite gneiss

3) cordierite-anthophyllite rocks

4) nodular sillimanite gneiss

The mineral assemblages from the Montauban alteration zone rocks units are presented in Table 4.1C. Sphalerite-absent altered rocks contain the simplest mineral assemblages. Gahnite is absent from these rocks, staurolite has the lowest zinc content of all the assemblages (<2 wt%), and garnet is less manganiferous than in their sphalerite-bearing conterparts. This has an important bearing on the chemical system that should be used to characterize the chemographic relationships in these rocks.

To a first approximation, the chemography of sulfide absent assemblages can be modeled in the system FMASH where biotite is stabilized by K_2O. The resulting AFM diagrams are shown in Figure 4.4 for bulk rock compositions and a few mineral assemblages from cordierite-biotite and cordierite-anthophyllite rocks. Relict "grains and sprays" of kyanite are present in a few samples of cordierite-biotite and nodular sillimanite gneiss, and these constitute an important pressure indicator. As in the previous two terranes, mineral compositions are highly dependent on bulk rock compositions. Surprisingly, the nodular sillimanite bulk rock compositions plot near those of cordierite-biotite in the AFM diagram (Fig. 4.4A). This may be an artifact of the projection used because these rocks, in contrast to the cordierite-anthophyllite rocks, were subjected to substantial K-enrichment during hydrothermal alteration. Thus the AFM components require a correction for biotite composition which will shift the projected bulk compositions toward the A apex.

The chemographic relationships of the sulfide bearing assemblages cannot be adequately described in the FMASH system. Because zinc is a major constituant of sphalerite, gahnite and staurolite (up to 5.31 wt%) and a minor component in biotite and anthophyllite, and manganese is an important

Fig. 4.4 AFM diagrams for the Montauban mine sequence. A) Bulk rock compositions. B, C) Mineral compositions and assemblages in sulfide-poor cordierite-biotite and cordierite-anthophyllite gneisses.

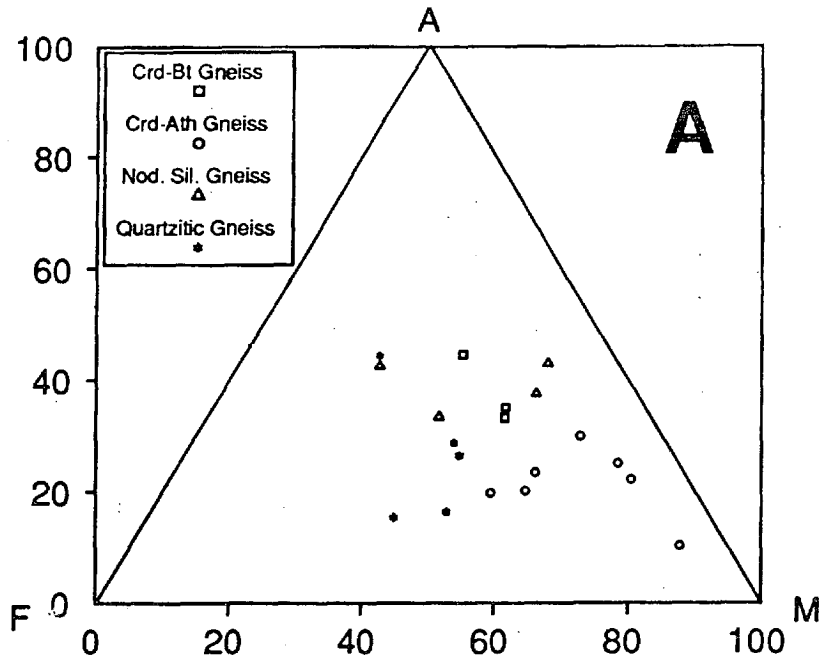

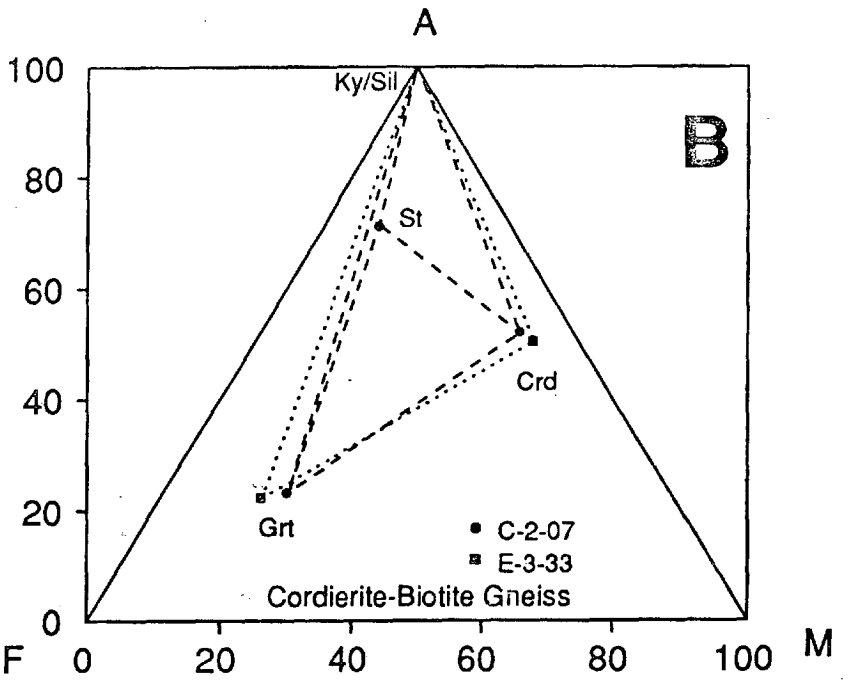

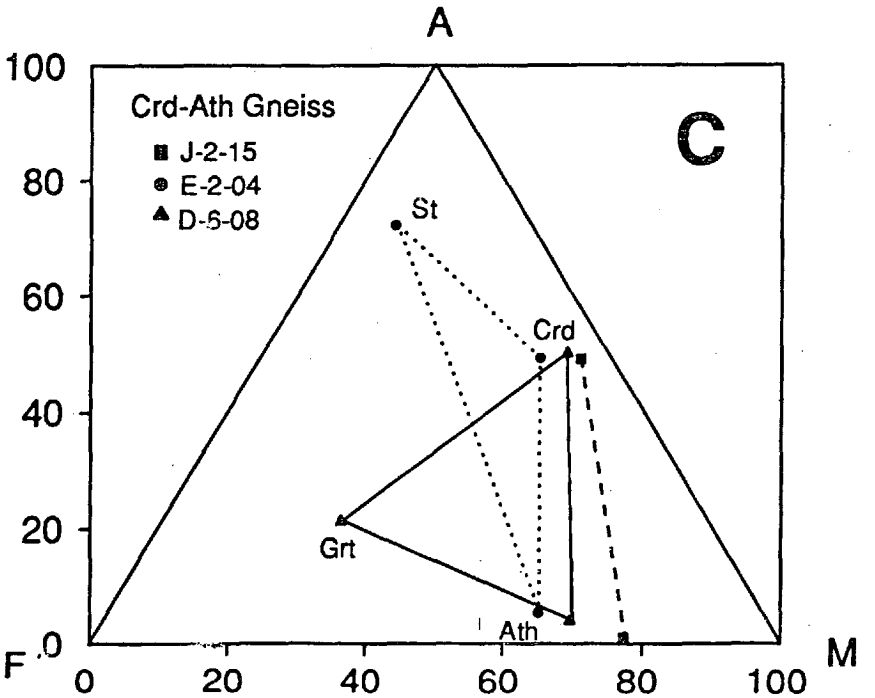

+ Quartz

+ Biotite

±Plagioclase

+ Rutile

constituent of garnet and is present in anthophyllite (up to 2.86 wt% MnO) and staurolite (up to 0,88 wt%), these minerals must be treated as quaternary Fe-Mg-Zn-Mn phases. Thus, the chemographic relationships of the mineralized altered rocks must be described by the nine component Fe-Mg-Mn-Zn-Al-Si-H-O-S system. Calcium is a minor component of garnet and anthophyllite and when substantially abundant, it is stabilized in plagioclase. Sodium is neglected but again, is mainly present as a minor constituent in biotite and anthophyllite and as a major constituent in plagioclase. Potassium is essentially restricted to biotite and does not appear to have participated in most of the metamorphic reactions experienced by these rocks. A few samples of mineralized quartzitic and nodular sillimanite gneiss contain both muscovite and biotite (Table 4.1C), and K has to be treated as an additional component in these minerals. The breakdown of zincian staurolite and the formation of coronitic gahnite and cordierite will be discussed in the section on other geothermobarometric techniques.

Geothermobarometry in the Three Terranes

"In a real attempt at geothermobarometry, one would have uncertainty in the activities introduced by analytical error, by inadequate solid-solution models, and by imperfect equilibration among the minerals of the rock under study. When multiple equilibria of this sort fail to pass through a single point in a real attempt at barometry using an internally consistent data-set, one is forced to turn to analytical error and imperfect equilibrium in an attempt to rationalize the results. Perhaps it should be noted, however, that an incorrect but thermodynamically consistent data-set will give a perfect intersection that passes through the wrong coordinates."

Hugh J. Greenwood (1989), Can. Min., 27, p.11.

Geothermobarometric techniques applicable to amphibolite facies rocks have been critically reviewed by Essene (1989), who also outlined potential abuses and pitfalls. As this author points out, a serious limitation is that

activity-X relations involving Fe/Mg as well as Mn and Zn remain unknown for many ferromagnesian minerals occurring in amphibolite facies rocks. In addition, simplified experimental systems are very restrictives except perhaps for Mg-rich whiteschist and Fe-rich iron formations (Essene, 1989).

Petrogenetic grids constructed for metapelitic rocks (Albee, 1965; Hess, 1969; Thompson, 1976; Pattison and Harte, 1985; Pattison, 1989; Spear and Cheney, 1989; Powell and Holland, 1990; Tuisku and Laajoki, 1990); metacarbonate and calc-silicate rocks (Baker et al, 1991, Connolly and Trommsdorff, 1991; Carmichael, 1991); and for metabasites and amphibolites (Abbott, 1982; Percival et al., 1982; Hudson and Harte, 1985; Spear and Rumble, 1986) provide useful guides in estimating metamorphic conditions. However, petrogenetic grids derived for Fe-Mg metapelitic and amphibolitic compositions may not be directly applicable to metamorphosed altered rocks showing similar mineral assemblages without considering the possible effect of additional components (Zn, Mn, F, Cl etc.) on mineral equilibria (Thompson, 1976; Spear, 1988; Spear and Cheney, 1989; Tuisku and Laajoki, 1990; Zaleski et al., 1991). Other factors that ought to be considered are the oxidation state of natural assemblages and metamorphic fluid composition that may differ from those of the experimental calibrations and affect estimates of P-T space stability relationships among the minerals (see Pattison, 1989).

Recent advances in microcomputer technology and the availability of internally consistent thermodynamic databases (Berman, 1988; Holland and Powell, 1990) and the development of related software (THERMO, Perkins et al., 1987; GEO-CALC, Brown et al, 1988; THERMOCALC, Holland and Powell, 1990; TWEEQU, Berman, 1991) offer powerful tools for modelling P-T-X equilibria (multi-equilibrium calculcations technique). The program METPET (Ball and Robin, 1990) was used for balancing independent reactions.

The samples used for geothermobarometry are located on the maps in *Appendix I.* Aluminosilicate polymorphs (andalusite, sillimanite, kyanite), garnet-biotite geothermometry, garnet-cordierite-aluminosilicate geothermobarometry are used to estimate peak P-T conditions and as a comparison basis between the three terranes. Other methods were applied to specific mineral assemblages in each terrane and are presented in the following sections.

Aluminosilicate geothermobarometry

Revised experimental determination of the aluminosilicate polymorphs triple point by Bohlen et al. (1991) constrains its location at 4.2±0.3 Kbars and 530±20 °C.

According to Kerrick and Speer (1988) the presence of Fe^{3+} (and probably Mn^{3+} in Mn-rich rocks) in the aluminosilicates under oxidizing conditions may significantly affect the location of the polymorphic transition boundary in P-T space (mainly andalusite-sillimanite, their Fig. 2). Fe^{3+} concentrations increase in the order And > Sil > Ky (Grambling and Williams, 1985; Kerrick and Speer, 1988). The addition of Fe^{3+} lowers the Al_2SiO_5 activities thus enlarging the stability field of andalusite and to a lesser extent kyanite, to higher T and P. Fibrolite (fine grained fibrous sillimanite) has been inferred to have the same P-T stability as sillimanite by many petrologists (see chapter 7 in Kerrick, 1990). However, it has been reported in all alumino-sillicate zones and may be a metastable phase. The problem of probable fibrolite metastability during regional metamorphism is addressed in detail by Kerrick (1990).

Atik Lake

Andalusite occurs as greyish-white poikiloblastic knots up to 2 cm in altered basalts (Bernier and MacLean, 1989), is the stable aluminosilicate in the Atik Lake belt, and indicates a low pressure metamorphism (P≤ 4.2 Kbars). Andalusite knots in aluminous alteration patches formed under fairly reducing conditions as indicated by sulfide-arsenide-oxide assemblages (Table 4.1A). The presence of andalusite knots in the felsic dyke from the central conduit of pipe 2 suggests that the dyke intrusion was early and pre-metamorphism. Minor fibrolite was observed as needles nucleated on biotite in a sample from the lower stratigraphy, and is probably metastable. However, sillimanite was reported by Weber (1974) in the southwest margin of the belt in biotite-plagioclase gneiss injected by alaskite and granitic material. Weber and Scoates (1978) interpreted the sillimanite isograd in this part of the belt (see maps in *Appendix I*) to be related to vertical displacement along the Atik Lake fault, subparallel to the belt margin.

Némiscau

The andalusite-sillimanite isograd is located more or less at the centre of the belt, parallel to its long axis, and disappears at the diabase dyke toward the southwest end. The andalusite forms knobs (up to 3cm wide) in metapelite and is poekiloblastic in thin section. Valiquette (1975) reported fibrolite in andalusite bearing samples. There is, however, no evidence of replacement of andalusite by sillimanite. The isograd is based on the absence of andalusite and the presence of coarse grained sillimanite in metapelitic rocks. Fibrolite which nucleated on biotite is ubiquitous in sillimanite-bearing metapelites south of the isograd. It has been suggested by Kerrick (1990) that fibrolite within the andalusite zone could be

attributed to progradation into the sillimanite zone and metastable persistence of the andalusite during regional metamorphism. The lack of andalusite replacement by sillimanite may reflect kinetic barriers (Kerrick, 1991).

Montauban

Sprays of kyanite blades (Fig. 4.5A) as well as scarce prismatic sillimanite, have been observed within cordierite bearing rocks but the two aluminosilicate were never observed in contact. Kyanite, rimmed by muscovite (Fig. 4.5B) cordierite and biotite, was found in one sample indicating a retrograde replacement. The petrologic significance of this texture will be discussed below in the section dealing with other geothermobarometric methods applicable to the Montauban terrane. Fibrolitic sillimanite (fibrolite) overgrowing Mg-rich biotite (Figs. 4.5C, D) in a triangular arrangement, and coexisting with quartz, is characteristic of the nodular sillimanite gneiss. The fibrolite does not replace kyanite or prismatic sillimanite and is found also as inclusions in a variety of minerals including quartz, gahnite, garnet and cordierite. Fibrolite was also observed along grain boundaries of some silicates.

The presence of the common assemblage pyrrhotite-rutile in the Montauban host rocks indicates fairly reduced metamorphic conditions implying that Fe^{3+} and Mn^{3+} substitutions were not important. Microprobe analyses of kyanite and sillimanite show that the total of Mn and Fe concentrations are always lower than 0.08 wt% (MnO+FeO), which would have little effect on the position of the kyanite-sillimanite boundary in P-T space.

Fig. 4.5. Photomicrographs of aluminosilicates from the Montauban gneisses. A) Kyanite (Ky) blades and vermicular gahnite (Gah) surrounded by cordierite (Crd) and biotite (B). B) Coronitic texture of kyanite (Ky) surrounded by muscovite (Ms), cordierite (Crd), biotite (Bt) and quartz (Qtz). C) Fibrolite mat (Fib) replacing biotite (Bt). D) Triangular arrangement of sillimanite (Sil) on biotite (Bt). Field view for A-C is 2.6 mm across and 0.85 mm across for D.

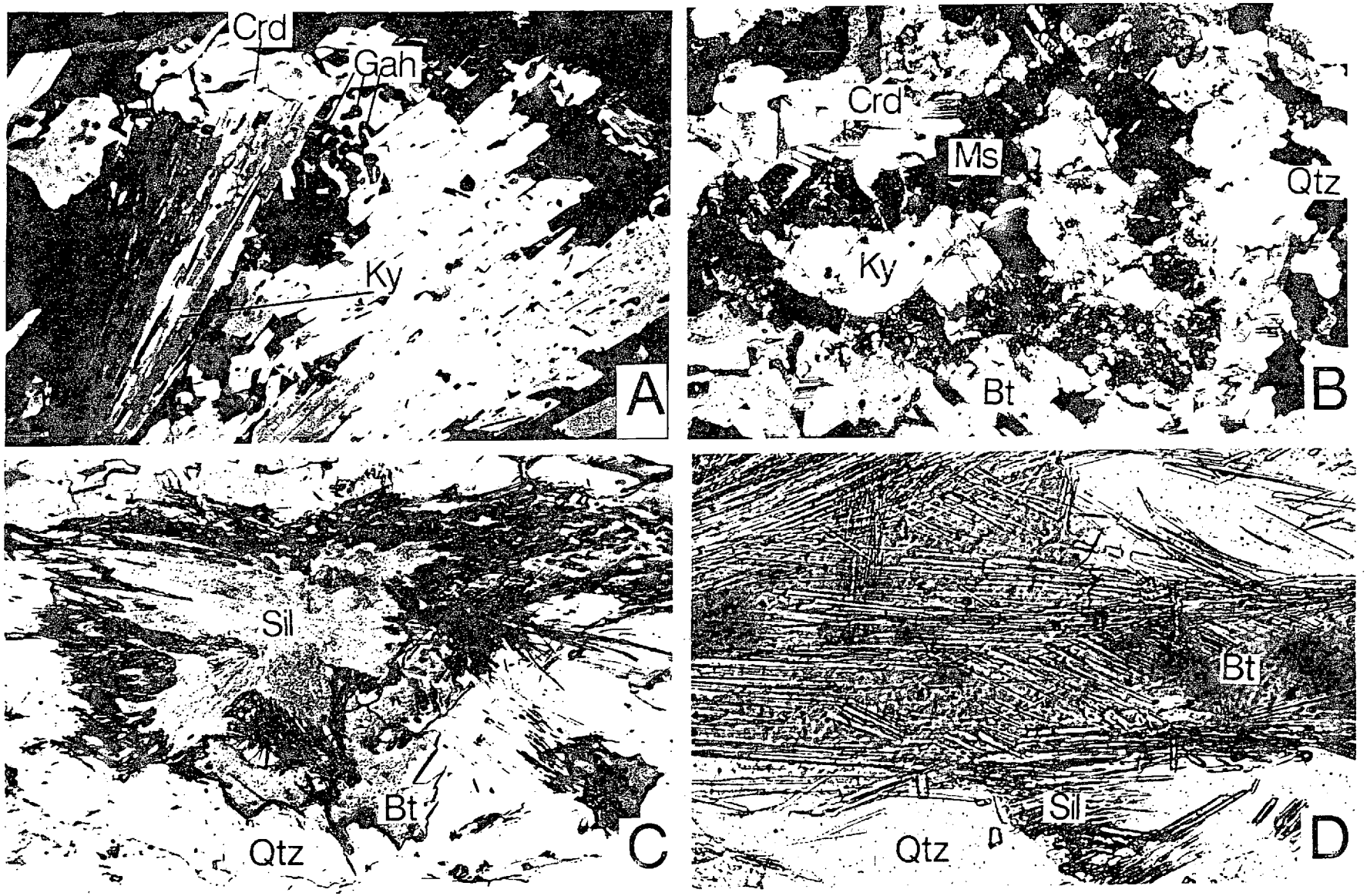
Crd
Gah
Ky
A
Crd
Ms
Qtz
Ky
Bt
B
Sil
Bt
Qtz
C
Bt
Sil
Qtz
D

Garnet-cordierite geothermobarometry

It has been demonstrated that the Fe-Mg exchange between cordierite and garnet is temperature dependent:

$$\text{Fe-Crd} + \text{Prp} = \text{Mg-Crd} + \text{Alm} \quad (1)$$

Reaction (1) has been calibrated empirically by Thompson (1976) and Perchuck (1977) and experimentally by Perchuck and Lavrent'eva (1983). The assemblage quartz-garnet-cordierite-sillimanite (kyanite) has been proposed as a geobarometer and water fugacity indicator and it has been established that the hydration of cordierite as well as high Mg content can stabilize cordierite to pressures of up to 11 kbar (Hutcheon et al. 1974, Thompson 1976, Holdaway and Lee 1977, Newton and Wood 1979, Lonker 1981, Martignole and Sissi 1981, Aranovich and Podlesskii 1983). The following reaction (2) was used in experimental calibrations of the barometer:

$$3\text{Crd}^{\circ}n\text{H}_2\text{O} = 2\text{Grt} + 4\text{Sil} + 5\text{Qtz} + 3n\text{H}_2\text{O} \quad (2)$$

where $n\text{H}_2\text{O}$ is the hydration number in mol pfu (per formula unit). The discrepancies observed in the dP/dT slopes (positive vs negative) of the various Mg-Fe end-member calibrations of reaction (2) are reviewed in Martignole and Sissi (1981). The actual amount of water (and other volatiles) that can be incorporated into cordierite and ferrocordierite (sekaninaite) is still a topic under debate. In their hydration model, Newton and Wood (1979) used a value of $n\text{H}_2\text{O}=1.2$, Martignole and Sissi (1981) assumed a standard state of $n\text{H}_2\text{O}=1$, Johannes and Schreyer (1981) assigned a maximum of 1 mol of gas per formula unit (pfu), Boberski and Schreyer (1990) found a maximum value of $n\text{H}_2\text{O}=0.8$ in hydration of synthetic cordierite experiments, whereas Berman (1988) and McPhail et al. (1990) used $n\text{H}_2\text{O}=2$ in their hydration of cordierite model. The problem of cordierite volatile content is reviewed in recent studies by Vry et al. (1990) and Boberski and Schreyer (1990).

Cordierite compositions

Atik Lake: Garnet-cordierite±andalusite are present in altered basalt and metasediments. Cordierite is fine grained in the altered basalts, and poikiloblastic nodules up to 2cm in diameter were observed in the central metasediments (nodular cordierite and cordierite-anthophyllite rocks). Cordierite in altered basalt has X_{Mg}=0.49-0.68 and in the metasediments, X_{Mg}=0.67-0.69.

Némiscau: Cordierite compositions range from XMg=0.61-0.68 in metapelites and from 0.69-0.84 in cordierite-anthophyllite rocks (altered basalts).

Montauban: The cordierite is a highly ordered (Al-Si) low cordierite (distortion index Δ=0.270±0.005), is biaxial negative ($2V_x$=85°), has a mean refractive index n=1.5418±0.0002, and has X_{Mg} values ranging from 0.75 to 0.92 (Bernier, 1985). The mean refractive index value for this cordierite is comparable to that of the synthetic hydrous cordierite having similar X_{Mg}, which was used by Boberski and Schreyer (1990) in their hydration experiments.

Cordierites from the three terranes have high total (Na+Ca+K): 0.02-0.10 mol pfu for Atik Lake, 0.03-0.27 mol pfu for Némiscau and 0.03-0.09 mol pfu for Montauban. Vry et al. (1990) have shown that the type-II H_2O in cordierite channels correlates with total alkali content where two molecules of water are combined with each alkali cation. These authors found that cordierite having high total alkali contents (>0.05 mol pfu) are the most hydrated, which suggests that the cordierites from the three terranes were highly hydrated. The Mg/Fe ratios increase in the following order Atik Lake < Némiscau < Montauban and reflect variation in bulk rock compositions (Table 4.2).

Garnet compositions

The compositions of garnets coexisting with cordierite are summarized in Table 4.2. Garnet compositions will be discussed in detail in the section of biotite-garnet geothermometry.

Application to the three terranes

The program GRCDTP (*Appendix)* was written to simultaneously solve: 1) the garnet-cordierite empirical geothermometer and barometer equations of Thompson (1976), and 2) the experimental thermometric calibration of Perchuck and Lavrenteva (1983) with the experimental geobarometric calibration for fully hydrated cordierite of Aranovich and Podlesskii (1983). The Mg/Fe partitioning coefficient and compositional characteristics of garnets and cordierites from the three terranes are summarized in Table 4.2. It was assumed, as a first approximation, that the cordierites from the three terranes were fully hydrated during peak metamorphic conditions.

The rocks from the Montauban NGZ are characterized by high-Mn garnets. The substitution of Mn for Fe in garnet appears to affect the Fe-Mg partitioning (K_D) between garnet and cordierite (Thompson, 1976) in the same way as it affects garnet-biotite Fe-Mg exchange (see next section). Because these calibrations do not correct for Mn contents, erroneously low-T-P estimates will result for Mn-rich garnet.

Garnetiferous cordierite-anthophyllite rocks from the three terranes do not contain an aluminosilicate phase ($a<1$) and thus the calculated pressures are maximum values. However, the calculated pressures do not differ greatly from those calculated for aluminosilicate-bearing rocks (Table 4.2).

Temperature and pressure data for the three terranes are shown in Table 2 and displayed in figure 4.6. Core-rim P-T estimates obtained by solving

TABLE 4.2A CORDIERITE-GARNET GEOTHERMOBAROMETRY, ATIK LAKE

Samples		Garnet Gr	An	Sp	Mg/Fe	Crd Mg/Fe	Kd	Th T(°C)	BER P(Kb)	PL & AP T(°C)	P(Kb)
U842	C	0.06	0.01	0.06	0.137	1.534	11.16	577	3.4	558	2.9
	C	0.06	0.01	0.07	0.134	1.340	10.01	604	3.5	583	3.0
	R	0.05	0.01	0.04	0.123	1.627	13.17	537	3.3	520	2.5
U845*	C	0.06	0	0.04	0.181	2.203	12.16	558	3.8	541	3.3
	R	0.05	0	0.05	0.151	2.101	13.90	527	3.7	511	2.9
U04*	C	0.06	0	0.01	0.173	2.079	12.09	560	3.8	542	3.4
	R	0.05	0	0.03	0.109	2.016	16.84	486	3.3	472	2.3
U12	C	0.03	0.02	0.03	0.105	1.148	10.93	581	3.1	561	2.7
	R	0.03	0.02	0.03	0.105	1.225	11.67	565	3.1	546	2.6
U29B*	C	0.05	0.01	0.02	0.189	2.014	10.65	591	4.0	572	3.8
	R	0.05	0	0.02	0.189	1.987	12.53	551	3.5	534	3.2
						Average C:		579	3.6	560	3.2
							(1σ)	16	0.3	15	0.4
						Average R:		533	3.4	517	2.7
							(1σ)	27	0.2	25	0.3

Note: the aluminosilicate is andalusite.

TABLE 4.2B CORDIERITE-GARNET GEOTHERMOBAROMETRY, NÉMISCAU

Samples		Garnet Gr	An	Sp	Mg/Fe	Crd Mg/Fe	Kd	Th T(°C)	BER P(Kb)	PL & AP T(°C)	P(Kb)
S30	C	0.03	0	0.04	0.217	1.843	8.51	654	4.7	631	4.4
	R	0.03	0	0.04	0.202	2.118	10.49	595	4.0	577	4.0
	R	0.03	0	0.04	0.182	2.118	11.61	570	3.9	552	3.6
N32*	C	0.06	0	0.02	0.212	2.436	10.51	595	4.4	577	4.1
	C	0.06	0	0.03	0.277	2.375	8.56	652	5.0	632	4.8
	R	0.06	0	0.03	0.220	2.269	10.34	600	4.3	581	4.0
	R	0.06	0	0.03	0.256	2.367	9.24	631	4.4	611	4.5
N35	C	0.06	0	0.05	0.280	2.215	7.91	676	5.1	654	4.9
	C	0.06	0	0.05	0.260	2.319	8.82	643	4.8	623	4.6
	R	0.06	0	0.06	0.232	2.304	9.97	608	4.2	589	4.1
	R	0.06	0	0.05	0.228	2.595	11.37	576	4.1	558	3.9
N39*	C	0.06	0	0.06	0.258	2.259	8.73	646	4.7	625	4.5
	C	0.06	0	0.05	0.244	2.352	9.63	619	4.5	600	4.3
	R	0.06	0	0.05	0.243	2.432	10.02	608	4.0	589	4.2
	R	0.06	0	0.05	0.214	2.389	11.17	579	4.0	561	3.8
						Average C:		641	4.7	620	4.5
							(1σ)	24	0.2	23	0.3
						Average R:		596	4.1	577	4.0
							(1σ)	19	0.2	18	0.3

Note: the aluminosilicate is sillimanite.

TABLE 4.2C CORDIERITE-GARNET GEOTHERMOBAROMETRY, MONTAUBAN

Samples		Garnet Gr	An	Sp	Mg/Fe	Crd Mg/Fe	Kd	Th T(°C)	BER P(Kb)	PL & AP T(°C)	P(Kb)
855N											
C207	C	0.07	0	0.04	0.342	3.198	9.35	629	5.7	610	5.1
	R	0.06	0	0.09	0.320	3.198	10.01	610	5.1	591	4.7
885N											
D617*	C	0.07	0	0.20	0.438	5.468	12.47	555	5.1	541	4.5
	R	0.07	0	0.18	0.484	5.467	11.29	580	4.9	564	4.8
D312	C	0.07	0	0.20	0.431	4.719	10.96	586	4.9	570	4.5
	R	0.07	0	0.19	0.433	4.719	10.91	588	5.0	570	4.6
D514*	C	0.07	0	0.15	0.518	5.182	10.00	612	5.7	595	5.3
	R	0.06	0	0.13	0.519	5.183	9.98	613	5.7	596	5.3
D207	C	0.05	0	0.15	0.590	5.467	9.26	633	5.8	615	5.6
	R	0.05	0	0.18	0.543	5.467	10.06	610	5.5	593	5.3
885N											
D608*	C	0.08	0	0.24	0.778	9.125	11.69	573	5.4	560	5.4
	R	0.07	0	0.23	0.782	9.125	11.66	573	5.4	560	5.4
975N											
E519*	C	0.06	0	0.15	0.464	5.063	10.92	588	5.5	573	5.0
	R	0.07	0	0.15	0.481	5.063	10.53	598	5.7	581	5.1
E525*	C	0.08	0	0.21	0.484	5.254	10.86	572	4.9	572	4.6
	R	0.08	0	0.15	0.526	5.256	9.99	612	5.5	595	5.2
MQ12*	C	0.06	0	0.09	0.605	5.709	9.43	630	6.1	613	6.0
	R	0.07	0	0.12	0.426	5.260	12.36	558	4.9	544	4.7
						Average Peak T-P for Sp<0.15:		620	5.8	602	5.4
							(1σ)	13	0.2	12	0.3

Note: The aluminosilicates are kyanite and fibrolitic sillimanite

Gr=grossular, An=andradite, Sp=sperssatite, C=core, R=rim, Crd=cordierite, Kd=[(Mg/Fe)^{Crd}/(Mg/Fe)^{Grt}] for geothermometry, Grt=garnet, Th=Thompson (1976), Ber=Berman (1988, 1990), Pl=Perchuck and Lavrent'eva (1983), AP=Aranovich and Podleskii (1983).
*=no aluminosilicate present and the pressure estimates is maximum. See text for explanation and effect of Mn in Montauban garnets.

Fig. 4.6. Pressure-temperature conditions for the three terranes obtained from cordierite-garnet-aluminosilicate geothermobarometry. A) Results obtained with the Perchuck and Lavrent'eva (1983) thermometer and Aranovich and Podleskii (1983) barometer. Filled and open symbols are for core and rim data. B) P-$\dot{T}$ boxes are outlined from results obtained with GEO-CALC for core data only.

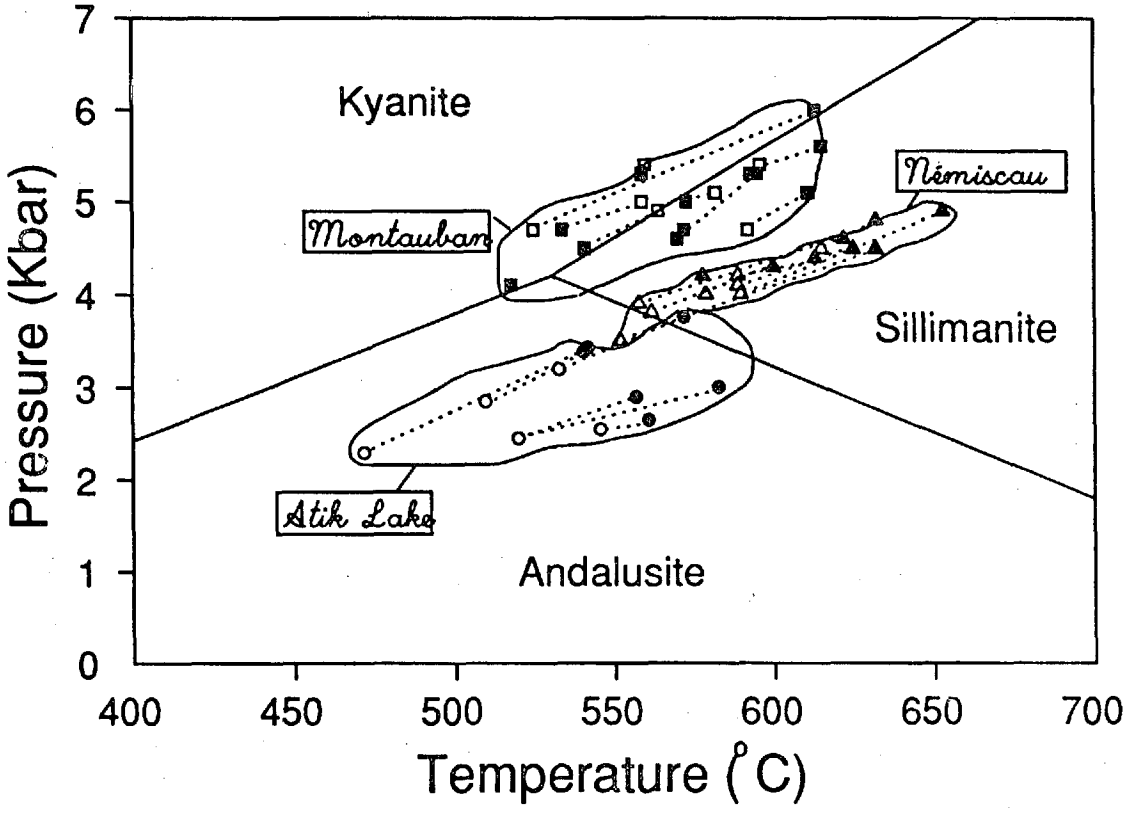
Kyanite
Némiscau
Montauban
Sillimanite
Atik Lake
Andalusite
Pressure (Kbar)
Temperature (°C)
0
1
2
3
4
5
6
7
400
450
500
550
600
650
700

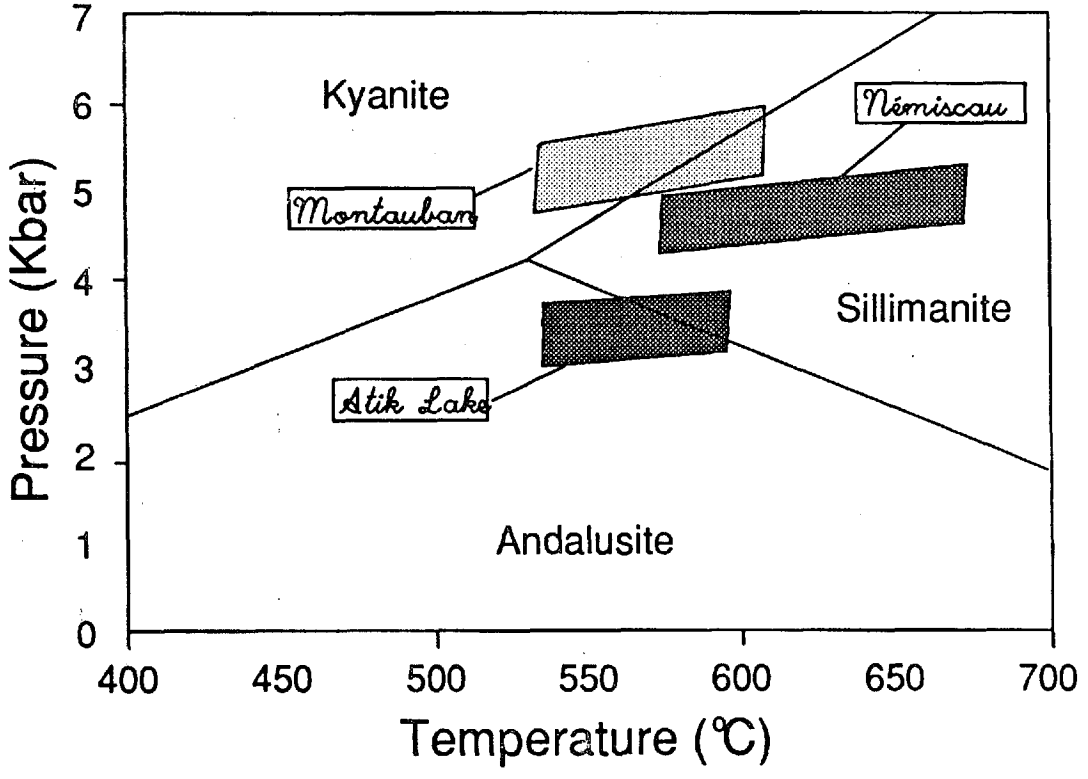
Kyanite
Némiscau
Montauban
Sillimanite
Atik Lake
Andalusite
Pressure (Kbar)
Temperature (°C)
0
1
2
3
4
5
6
7
400
450
500
550
600
650
700

simultaneously for garnet-cordierite thermometry (Perchuck and Lavrent'eva, 1983) and barometry (Aranovich and Podlesskii, 1983) for the three terranes are summarized in figure 4.6A. The data have also been processed with GEO-CALC (Brown et al., 1988; Berman, 1988) using ideal mixing activities for the Mg-end members of garnet and a fully hydrated cordierite. The resulting calculations are shown in figure 4.6B. The P-T boxes are delineated from the intersection of garnet-biotite thermometry and garnet-cordierite barometry and are in excellent agreement with the previous estimates (Fig. 4.6A). The resulting garnet-cordierite P-T conditions are consistent with the stability fields of the corresponding aluminosilicates observed in the three terranes, supporting the revised determination of the aluminosilicates triple point by Bohlen et al. (1991). If a dry-cordierite model is used, pressures estimates are about 1.5 kbar lower and predict aluminosilicate phases different from those observed.

In summary, garnet-cordierite geothermobarometry provides a range of peak P-T conditions for Atik Lake (T=564±15°C, P=3.2±0.3 kbar), Némiscau (T=634±23°C, P=4.7±0.2 kbar), and Montauban (T=614±13°C, P=5.62±0.3 kbar), that are compatible with the observed aluminosilicate minerals. Because of the high Mn content of the garnet at Montauban, the pressure estimate is a minimum, and it is shown later that a peak pressure 6.5 kbar is more appropriate.

Garnet-biotite geothermometry

Garnet-biotite pairs are ubiquitous in a variety of rock types in the three terranes. Each of the terranes offers a range of bulk rock compositions that have equilibrated under characteristic regional P-T conditions (different

for each terrane). This provides a good opportunity to test various calibrations of the geothermometer.

The various calibrations are all based on the Fe-Mg exchange:

$$Alm + Phl = Prp + Ann \quad (3)$$

They can be grouped as follows: 1) Fe-Mg (low Ca-Mn) empirical (Thompson, 1976; Goldman and Albee, 1977) and experimental (Ferry and Spear, 1978; Perchuck, 1981; Perchuck and Lavrent'eva, 1983); 2) ternary (Fe-Mg-Ca) garnet calibrations which incorporate a correction for Ca mixing non-ideally with Fe and Mg (Newton and Haselton, 1981; Hoinkes, 1986); and 3) quaternary (Fe-Mg-Mn-Ca) garnet calibrations (Hodges and Spear, 1982; Ganguly and Saxena, 1984, 1985; Williams and Grambling, 1990; Berman, 1990).

Calibrations 2 and 3 are derived from the Ferry and Spear (1978) experimental calibration, modified to account for non-ideal mixing in garnet or biotite (Indares and Martignole, 1985) and natural garnet compositional deviation from that of garnets (Alm_{90}) used in the calibration. Perchuk and Lavrent'eva (1983) used natural garnets averaging Fe/(Fe+Mg)=0.6 in their experiments. Chipera and Perkins (1988) evaluated many of the above calibrations and found that the most precise and accurate one was that of Perchuk and Lavrent'eva (1983) for Fe-rich (Fe/Fe+Mg>0.7) garnets in metapelites. Factors that are not well constrained but may have a profound effect on garnet-biotite thermometry are:

1) The treatment of all Fe in biotite as Fe^{+2} may yield an overestimation of T (Dallmeyer, 1974; Dyar, 1990; Kretz, 1990);

2) Owing to the inverse relationship between increases in Mn and Ca in garnet and $\ln K_D$, Mn- or Ca-rich garnets may produce low temperature estimates (Goldman and Albee, 1977; Hoinkes, 1986; Bernier et al., 1987; William and Grambling, 1990); and

3) The use of activity models which are based on different assumptions regarding cation mixing in garnet octahedral sites, mainly ideal or symmetric and asymmetric non-ideal mixing and statistically derived excess energies of mixing (Margules parameters), may yield over- or underestimation of the true T (cf., Edwards and Essene, 1988).

Mixing properties in ternary and quaternary garnets have been reviewed recently and discussed by Berman (1990) and Williams and Grambling (1990). Discrepancies between Fe-Mg mixing models exist. Ferry and Spear (1978) suggested ideal mixing based on their experimental data, whereas Ganguly and Saxena proposed that Fe-Mg mixing is significantly non-ideal and asymmetric. Recent work by Hackler and Wood (1989), however, suggests that Fe-Mg mixing is nearly ideal, and this is in agreement with the statistical analysis of Williams and Grambling (1990).

In their experimental garnet-biotite calibration, Ferry and Spear (1978) used two garnet compositions, with most runs having a starting garnet composition Alm_{90}-Prp_{10} and four runs with a starting garnet composition Alm_{80}-Prp_{20}. The experimental brackets of lnK as a function of 1/T were found to be much larger for runs with the Alm_{80}- than for Alm_{90}-garnets. The latter data set was used by Ferry and Spear (1978) to obtain their linear least-squares fit of lnK vs. 1/T. They concluded that Fe-Mg mixed ideally in biotite and garnet owing to the consistency of the final compositions of Alm_{80}-garnet runs with the regressed equation based on Alm_{90}-garnets. Nevertheless, if a linear least square fit is calculated for the Alm_{80}-garnet runs (Fig. 4.7), a thermometric expression leading to higher temperature estimates, is derived for low-Mn and Ca garnets:

$$T\ (K) = [(2597 + 0.057P(bars)) / (1.3983 - \ln K_D)] \quad (4)$$

More problematic is the behavior of Mn when mixed with Fe and Mg in

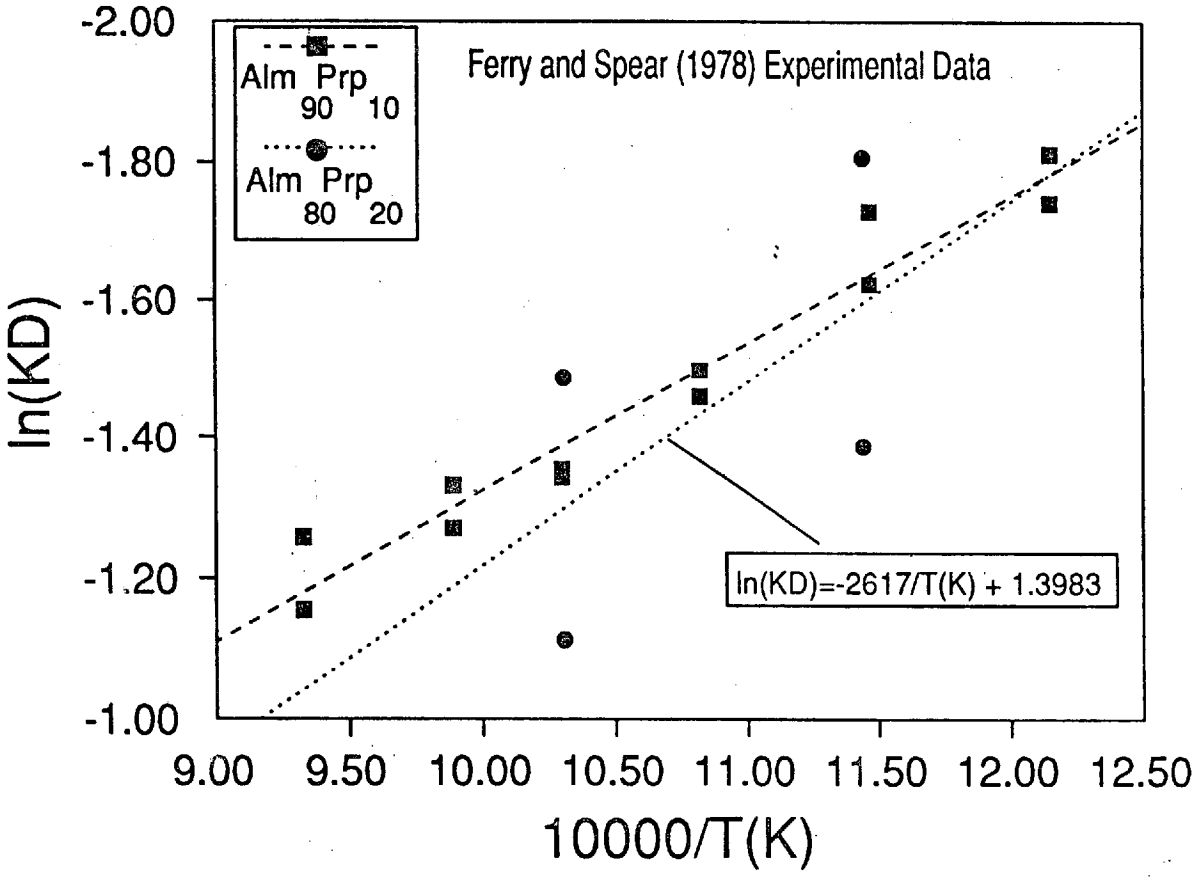

Fig. 4.7. Ln(K_D)-1000/T diagram showing the Ferry and Spear (1988) experimental data. The equation for the least squares regression line is for the Alm_{80} garnet runs.

low-Ca garnet. It has been demonstrated that Mn-Fe mixing is nearly ideal, but mixing properties pertaining to Mn-Mg exchanges are more controversial. Hodges and Spear (1982) tested values of W_{MnMg} ranging from 0 to 10468 J/mol (where W_{MnMg} is the free energy interaction for the binary bounding solutions in the quaternary system) and, like Berman (1990), favored a value of W_{MnMg}=0. Ganguly and Saxena (1984) derived a value of W_{MnMg}= 12561 j/mol whereas Williams and Grambling (1990) favored a value of W_{MnMg}= 6431 j/mol (their model 3).

Biotite Compositions

Ranges of biotite compositions for the various rock types in the three terranes are shown on a Al^{IV}-X_{Fe} diagram (Fig. 4.8) and in Table 4.3. Single biotite grains are not compositionally zoned.

Atik Lake: Biotite at Atik Lake (Fig. 4.8A) has a composition in the range X_{Fe}=0.33-0.61, with the most Fe-rich samples occuring in the metamorphosed hydrothermally altered volcanics. The most magnesian biotites are in the metasedimentary cordierite-anthophyllite rocks. In general, biotites cluster at about X_{Fe}=0.48 and have X_{Ti}+ $X_{Al^{vi}}$=0.12-0.23.

Némiscau: The range of X_{Fe} in Némiscau biotites is 0.26-0.62 (Fig. 4.8B). The Fe-rich biotites are in the metapelites and the Mg-rich ones in cordierite-anthophyllite rocks (altered basalts). Most of the biotites cluster around X_{Fe}=0.45 and have X_{Ti}+ $X_{Al^{vi}}$=0.10-0.21.

Montauban: Biotites at Montauban show the largest range of X_{Fe} (0.10=0.68). The most Fe-rich ones are in regional metapelite and amphibolite. Biotites from the mine sequence rocks are very Mg-rich and form a distinct cluster

TABLE 4.3. GARNET-BIOTITE COMPOSITIONS

TABLE 4.3A GARNET-BIOTITE COMPOSITIONS, ATIK LAKE

Samples		Garnet				Biotite			Kd
		Gr	An	Sp	Mg/Fe	X_{Ti}	$X_{Al^{VI}}$	Mg/Fe	
LOWER STRATIGRAPHY									
U842	C	0.065	0.004	0.063	0.137	0.046	0.145	0.636	0.216
	C	0.068	0.004	0.068	0.134	0.046	0.046	0.636	0.210
	R	0.064	0.007	0.066	0.123	0.042	0.149	0.638	0.194
CENTRAL METASEDIMENTS									
U845	C	0.061	0.000	0.041	0.181	0.033	0.167	1.085	0.167
	R	0.053	0.000	0.048	0.151	0.035	0.147	1.149	0.132
	C	0.050	0.002	0.044	0.180	0.031	0.128	1.113	0.162
	R	0.053	0.000	0.049	0.152	0.037	0.143	1.146	0.132
MISTUHE ISLAND (UPPER STRATIGRAPHY)									
U02	C	0.057	0.011	0.029	0.190	0.023	0.110	1.131	0.168
	R	0.057	0.005	0.035	0.178	0.032	0.118	1.110	0.160
	C	0.053	0.004	0.033	0.159	0.035	0.130	0.976	0.163
	R	0.058	0.000	0.037	0.115	0.035	0.112	0.950	0.121
U04	C	0.059	0.000	0.013	0.173	0.020	0.104	1.121	0.154
	R	0.056	0.001	0.038	0.109	0.037	0.131	1.142	0.095
U06	C	0.046	0.000	0.146	0.126	0.039	0.151	0.710	0.178
	R	0.045	0.002	0.125	0.119	0.038	0.157	0.663	0.180
U10A	C	0.069	0.000	0.003	0.159	0.036	0.104	1.111	0.143
	R	0.059	0.000	0.014	0.198	0.039	0.105	1.069	0.185
U10B	C	0.057	0.004	0.057	0.121	0.032	0.184	1.338	0.091
	R	0.064	0.001	0.010	0.171	0.025	0.203	1.261	0.135
U12	R	0.047	0.012	0.028	0.105	0.031	0.151	0.685	0.153
U14	C	0.054	0.004	0.019	0.150	0.030	0.118	0.936	0.160
	R	0.052	0.000	0.021	0.114	0.033	0.116	0.960	0.118
U25B	C	0.102	0.009	0.097	0.078	0.034	0.108	0.940	0.083
	R	0.059	0.008	0.016	0.162	0.036	0.111	0.959	0.169
U29B	C	0.053	0.004	0.002	0.189	0.036	0.142	1.130	0.167
	R	0.052	0.004	0.024	0.189	0.028	0.110	1.118	0.169
U31A	C	0.065	0.000	0.040	0.135	0.028	0.109	1.150	0.117
	R	0.060	0.004	0.022	0.163	0.031	0.121	1.125	0.145

Rock Types:

Altered felsic: U842
Cordierite-anthophyllite (metasediment): U845
Cordierite-chlorite-muscovite (altered basalt): U04
Cordierite-gedrite (altered basalt): U02, U10A, U10B, U25B, U29B, U31A
Gedrite-garnet (altered basalt): U14
Aluminous alteration (altered basalt): U06, U12

TABLE 4.3B GARNET-BIOTITE COMPOSITIONS, NÉMISCAU

Samples		Garnet				Biotite			Kd
		Gr	An	Sp	Mg/Fe	X_{Ti}	$X_{Al^{VI}}$	Mg/Fe	
GRID S-1 (LAC SILLIMANITE)									
S14	C	0.077	0.000	0.019	0.224	0.040	0.096	1.211	0.185
	R	0.076	0.000	0.069	0.219	0.041	0.097	1.253	0.175
	C	0.095	0.016	0.063	0.215	0.038	0.077	1.368	0.157
	R	0.085	0.014	0.087	0.197	0.038	0.087	1.371	0.144
S16	C	0.039	0.007	0.034	0.186	0.046	0.184	0.737	0.253
	R	0.045	0.007	0.039	0.148	0.041	0.183	0.731	0.203
	C	0.034	0.000	0.036	0.165	0.053	0.153	0.791	0.209
	R	0.037	0.008	0.042	0.124	0.055	0.162	0.792	0.157
	C	0.036	0.003	0.038	0.169	0.029	0.174	0.835	0.202
	R	0.044	0.003	0.042	0.137	0.028	0.204	0.744	0.184
S30	C	0.024	0.009	0.039	0.198	0.043	0.157	1.079	0.184
	R	0.033	0.000	0.039	0.173	0.044	0.159	1.073	0.161
	C	0.026	0.000	0.039	0.217	0.031	0.206	1.124	0.193
	R	0.028	0.000	0.035	0.202	0.027	0.166	1.180	0.171
S32	C	0.100	0.000	0.075	0.298	0.041	0.098	1.362	0.219
	R	0.100	0.000	0.086	0.203	0.040	0.100	1.322	0.154
	I	0.112	0.000	0.092	0.178	0.033	0.097	1.115	0.159
	C	0.095	0.006	0.075	0.255	0.045	0.093	1.322	0.193
	R	0.103	0.008	0.101	0.203	0.044	0.094	1.320	0.154
GRID A-1 (POSTE ALBANEL)									
N22	C	0.065	0.001	0.078	0.230	0.035	0.109	1.268	0.184
	R	0.063	0.000	0.050	0.195	0.034	0.101	1.233	0.158
	C	0.063	0.000	0.045	0.222	0.046	0.103	1.193	0.103
	R	0.064	0.000	0.049	0.207	0.042	0.124	1.294	0.160
	I	0.059	0.000	0.049	0.226	0.034	0.094	1.235	0.183
N32	C	0.069	0.006	0.021	0.240	0.026	0.126	1.283	0.187
	R	0.062	0.000	0.027	0.242	0.029	0.116	1.362	0.178
	C	0.060	0.005	0.023	0.254	0.024	0.113	1.261	0.202
	R	0.059	0.003	0.027	0.245	0.031	0.111	1.263	0.194
N35	C	0.061	0.000	0.051	0.263	0.033	0.115	1.145	0.230
	R	0.057	0.000	0.050	0.244	0.032	0.125	1.384	0.177
	C	0.061	0.000	0.051	0.263	0.027	0.129	1.253	0.210
	R	0.059	0.000	0.057	0.232	0.032	0.125	1.384	0.167
GRID H-3 (LAC DE LA HUTTE)									
N14	C	0.057	0.006	0.060	0.268	0.028	0.095	1.450	0.185
	R	0.063	0.003	0.044	0.281	0.015	0.075	1.427	0.197
	C	0.056	0.004	0.037	0.292	0.034	0.088	1.360	0.214
	R	0.061	0.013	0.040	0.267	0.038	0.096	1.343	0.191
N39	C	0.057	0.003	0.060	0.259	0.031	0.106	1.260	0.205
	R	0.059	0.000	0.049	0.227	0.034	0.102	1.275	0.178
	C	0.057	0.009	0.050	0.254	0.044	0.118	1.396	0.182
	R	0.057	0.001	0.049	0.218	0.034	0.103	1.358	0.163
GRID C-1 (LAC DU CROCHET)									
N38	C	0.036	0.000	0.024	0.147	0.017	0.145	0.710	0.207
	R	0.038	0.000	0.026	0.143	0.015	0.221	0.761	0.188
	C	0.039	0.000	0.025	0.142	0.027	0.158	0.719	0.197
	R	0.032	0.000	0.033	0.108	0.040	0.144	0.730	0.147
ANDALUSITE-STAUROLITE ZONE									
V4811	C	0.035	0.000	0.022	0.132	0.031	0.106	0.746	0.177
	R	0.032	0.000	0.021	0.122	0.034	0.105	0.651	0.187
V4814	C	0.031	0.000	0.019	0.140	0.037	0.127	0.753	0.185
	R	0.028	0.000	0.018	0.127	0.043	0.114	0.745	0.170
	C	0.028	0.000	0.019	0.134	0.034	0.158	0.676	0.198
	R	0.030	0.000	0.019	0.035	0.143	0.128	0.736	0.174

Rock Types:
Metapelites (andalusite zone): V4811, V4814
Metapelites (sillimanite zone): S14, S16, S30, N38
Anthophyllite-garnet (altered basalt): S32, N22, N14
Cordierite-anthophyllite (altered basalt): N-32, N-35, N39.

TABLE 4.3C GARNET-BIOTITE COMPOSITIONS, MONTAUBAN

Samples		Garnet Gr	An	Sp	Mg/Fe	Biotite X_{Ti}	$X_{Al^{VI}}$	Mg/Fe	Kd
REGIONAL METAPELITES									
MQ1	R	0.105	0.006	0.038	0.189	0.045	0.106	1.115	0.170
	R	0.085	0.005	0.038	0.217	0.044	0.108	1.101	0.197
	R	0.088	0.011	0.035	0.228	0.043	0.111	1.102	0.207
	I	0.074	0.002	0.035	0.249	0.045	0.098	1.385	0.180
MQ10	C	0.033	0.000	0.078	0.109	0.081	0.115	0.503	0.217
	R	0.023	0.000	0.060	0.089	0.081	0.116	0.503	0.177
	C	0.035	0.000	0.079	0.108	0.076	0.164	0.493	0.219
	R	0.033	0.000	0.078	0.109	0.091	0.128	0.735	0.148
	I	0.035	0.001	0.078	0.104	0.096	0.097	0.611	0.171
	I	0.038	0.000	0.073	0.111	0.084	0.144	0.602	0.184
NORTH OF MINE SEQUENCE (Crd-Ath)									
MQ12	C	0.069	0.001	0.115	0.497	0.016	0.120	3.521	0.141
	R	0.068	0.000	0.116	0.403	0.017	0.120	3.444	0.117
	C	0.071	0.002	0.122	0.513	0.022	0.113	3.298	0.156
	R	0.068	0.000	0.122	0.408	0.022	0.113	3.198	0.124
MINE SEQUENCE, NORTH GOLD ZONE MINERALIZED QUARTZITIC GNEISS									
B205	C	0.059	0.000	0.212	0.428	0.010	0.148	4.104	0.104
	R	0.057	0.000	0.198	0.478	0.089	0.148	3.834	0.125
C211	C	0.057	0.000	0.149	0.336	0.006	0.117	2.000	0.168
	R	0.061	0.000	0.136	0.346	0.006	0.117	1.999	0.173
C416	C	0.057	0.000	0.186	0.386	0.004	0.152	2.724	0.142
	R	0.007	0.000	0.176	0.446	0.004	0.152	2.724	0.164
D517	C	0.068	0.000	0.196	0.438	0.010	0.144	3.262	0.134
	R	0.068	0.000	0.181	0.484	0.010	0.144	3.262	0.148
E219	C	0.036	0.000	0.250	0.266	0.030	0.148	1.680	0.158
	R	0.036	0.000	0.242	0.266	0.030	0.148	1.677	0.159
E313	C	0.073	0.000	0.204	0.272	0.009	0.137	2.403	0.113
	R	0.064	0.000	0.271	0.297	0.009	0.137	2.403	0.123
E419	C	0.050	0.000	0.296	0.396	0.034	0.168	3.951	0.168
	R	0.046	0.000	0.304	0.416	0.034	0.168	3.951	0.105
CORDIERITE-BIOTITE ROCK									
B421	C	0.065	0.000	0.386	0.422	0.026	0.124	5.011	0.084
	R	0.068	0.000	0.353	0.496	0.026	0.124	5.010	0.099
C207	C	0.045	0.000	0.064	0.324	0.026	0.146	2.208	0.147
	R	0.045	0.000	0.065	0.340	0.027	0.142	2.265	0.150
D312	C	0.089	0.000	0.024	0.430	0.048	0.160	3.197	0.135
	R	0.062	0.000	0.191	0.433	0.048	0.160	3.197	0.135
D207	C	0.052	0.000	0.180	0.590	0.016	0.123	3.990	0.148
	R	0.053	0.000	0.181	0.543	0.015	0.123	3.990	0.136
E326	C	0.062	0.000	0.403	0.482	0.011	0.099	4.692	0.103
	R	0.056	0.000	0.418	0.434	0.011	0.066	4.692	0.099
CORDIERITE-ANTHOPHYLLITE ROCK									
D608	C	0.079	0.000	0.240	0.781	0.027	0.140	5.367	0.145
	R	0.072	0.000	0.233	0.782	0.027	0.141	5.366	0.146
D514	C	0.069	0.000	0.145	0.519	0.021	0.133	3.628	0.143
	R	0.061	0.000	0.129	0.519	0.021	0.133	3.628	0.143
E519	C	0.063	0.000	0.147	0.434	0.026	0.119	3.254	0.142
	R	0.066	0.000	0.147	0.481	0.026	0.119	3.254	0.148
E525	C	0.081	0.000	0.208	0.484	0.021	0.115	4.203	0.115
	R	0.085	0.000	0.148	0.526	0.021	0.115	4.206	0.125
F319	C	0.059	0.000	0.173	0.548	0.022	0.121	3.084	0.178
	R	0.064	0.000	0.169	0.569	0.022	0.121	3.084	0.185
I323	C	0.071	0.000	0.207	0.586	0.020	0.126	4.222	0.139
	R	0.076	0.000	0.209	0.463	0.020	0.126	4.222	0.110
N202	C	0.068	0.000	0.125	0.417	0.015	0.135	3.670	0.114
	R	0.076	0.000	0.119	0.465	0.015	0.135	3.670	0.127
NODULAR SILLIMANITE GNEISS									
C332	C	0.040	0.000	0.531	0.486	0.024	0.169	4.346	0.112
	R	0.028	0.000	0.527	0.481	0.024	0.169	4.346	0.111
	C	0.054	0.000	0.463	0.543	0.023	0.131	6.682	0.081
	R	0.063	0.000	0.482	0.580	0.023	0.131	6.682	0.087
AMPHIBOLITES									
MQ4	C	0.269	0.006	0.151	0.016	0.065	0.075	0.135	0.115
	R	0.297	0.016	0.144	0.017	0.065	0.075	0.135	0.126
	C	0.272	0.014	0.149	0.018	0.067	0.077	0.145	0.123
	R	0.259	0.011	0.154	0.016	0.067	0.077	0.145	0.109
MQ6	C	0.179	0.001	0.145	0.115	0.060	0.075	0.713	0.162
	R	0.181	0.007	0.150	0.108	0.060	0.069	0.721	0.150
	C	0.182	0.007	0.144	0.119	0.061	0.071	0.729	0.163
	R	0.191	0.000	0.147	0.106	0.061	0.071	0.729	0.146
G202	C	0.153	0.014	0.084	0.182	0.032	0.098	1.365	0.133
	R	0.137	0.021	0.035	0.225	0.032	0.097	1.317	0.171

Gr=grossular, An=andradite, Sp=sperssatite
$Kd=[(Mg/Fe)^{Grt}/(Mg/Fe)^{Bt}]$
C=Core, R=bim, I=biotite inclusion in garnet.

Fig. 4.8 Biotite compositions plotted in Al^{IV}-X_{Fe} diagrams.

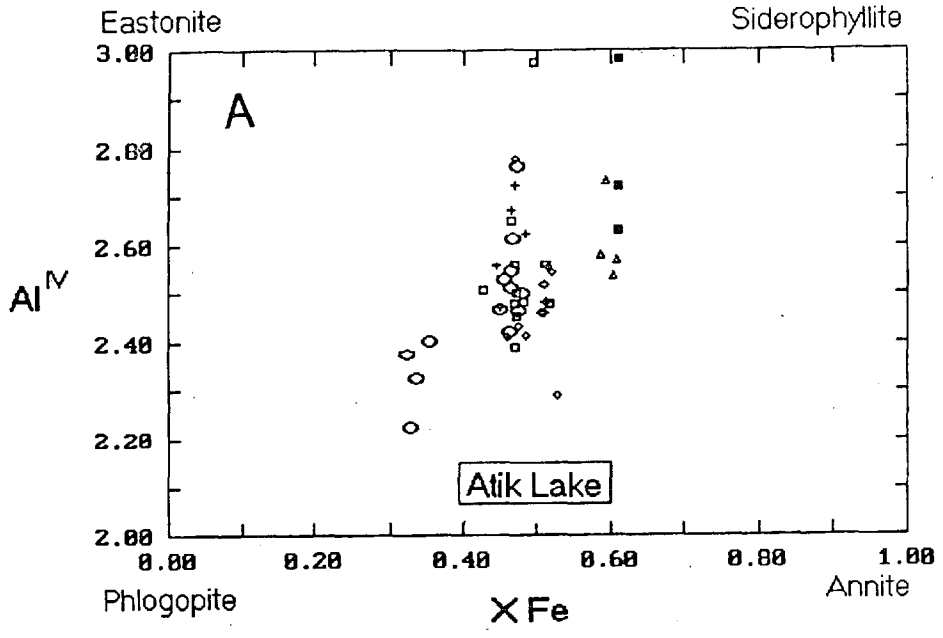

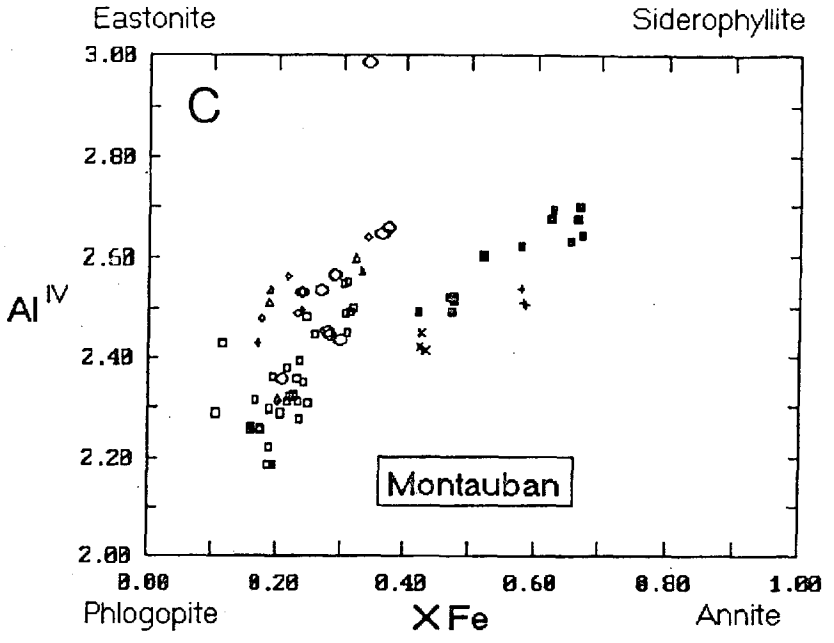

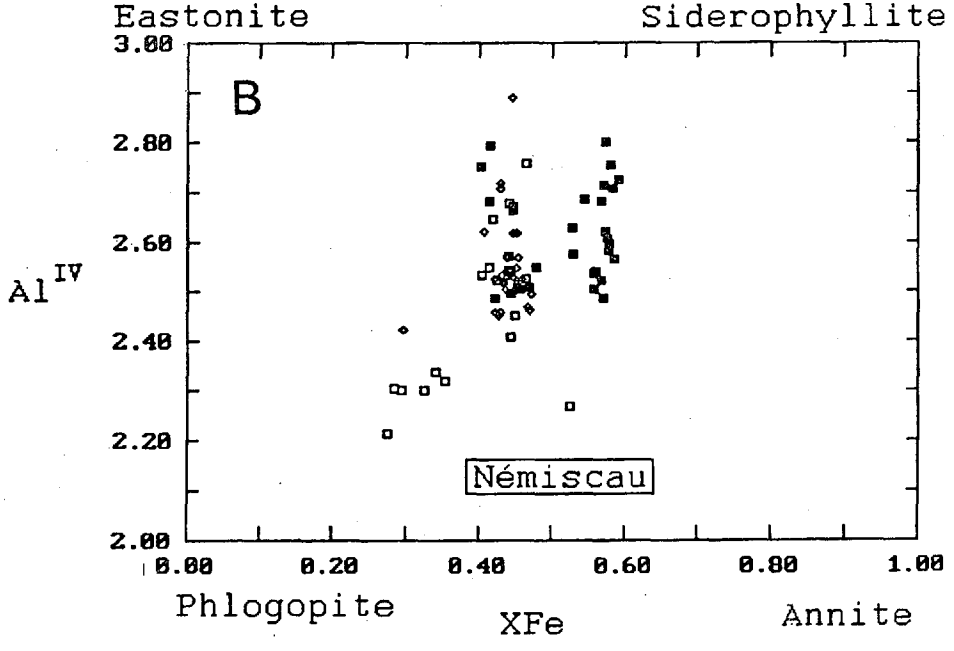

LEGEND

	Atik Lake	Némiscau	Montauban
□	Crd-Ged-Ath	Crd-Ath	Crd-Ath
■	Alt. felsic volc.	Metapelite	Metapelite
x			Amphibolite sills
○	Crd-Ath (Sed)		Quartzitic gneiss
+	Crd-Chl-Ms		Regional amphibolite
△	Aluminous alt.		Nodular sillimanite gneiss
◇		Ath-Cum-Pl	Crd-Bt

(Fig. 4.8C). The most Fe-rich biotites from the mine sequence rocks are in mineralized quartzitic gneiss and nodular sillimanite gneiss: the Mg-rich ones are from cordierite-anthophyllite and cordierite-biotite rocks. They have a range of $X_{Ti}+ X_{Al^{vi}}$=0.13-0.20.

As can be seen from Figure 4.8, variation of biotite compositions with rock types suggest a bulk rock composition dependency on biotite compositions.

Garnet Compositions

Atik Lake: Two garnet morphologies were observed in the garnetiferous rock units. 1) Syn-kinematic garnets ≤0.5 cm with snowball textures are characteristic of the altered intermediate volcanic at the base of the stratigraphic sequence; very small (≤1mm) syn-kinematic garnets also occur in crushed grunerite bands of mylonitized BIF above alteration pipe 1. 2) Euhedral post-kinematic idioblastic garnets are common in altered basalts (<1.5cm) and in the metasedimentary cordierite-anthophyllite rocks (0.5-3mm). The predominance of post-kinematic garnet indicates that peak metamorphic temperatures were reached after peak deformation. An alternative explanation could be that the two types formed coevally, as ductile deformation was very localized along incompetent metasedimentary horizons in the vicinity of the sheared margins of the belt, where the synkinematic garnets were observed.

The garnets fall into three compositional groups (Fig. 4.9A)

1) almandine garnets from altered basalts, intermediate volcanic and cordierite-anthophyllite metasediments,

2) grossular-andradite garnets from calc-silicate rocks, and

3) spessartite-rich garnets in sulfide-arsenopyrite- bearing iron formation

Only group 1 garnet coexists with biotite.

A comparison of core and rim analyses indicates that single garnet grains

Fig. 4.9. Garnet compositions shown on X_{Sps}-(X_{Alm}-X_{Prp}) diagrams for rock types in the three terranes.

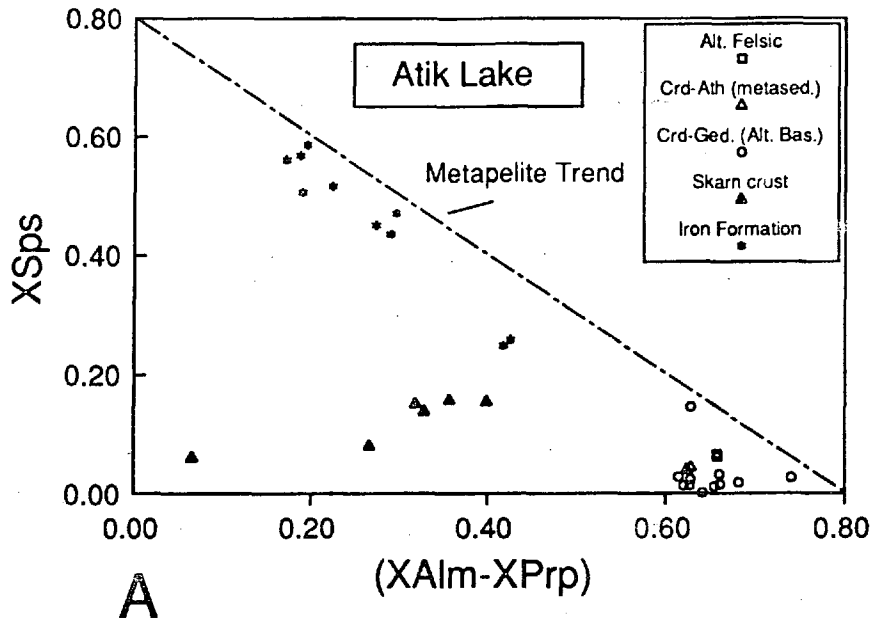
Atik Lake
Metapelite Trend
Alt. Felsic
Crd-Ath (metased.)
Crd-Ged. (Alt. Bas.)
Skarn crust
Iron Formation
XSps
(XAlm-XPrp)
0.00
0.20
0.40
0.60
0.80

A

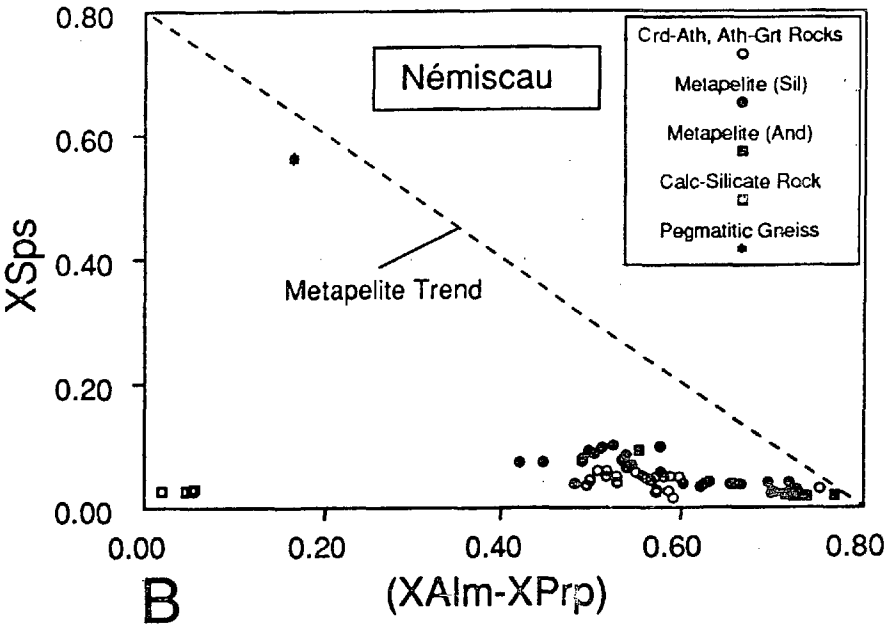
Némiscau
Metapelite Trend
Crd-Ath, Ath-Grt Rocks
Metapelite (Sil)
Metapelite (And)
Calc-Silicate Rock
Pegmatitic Gneiss
XSps
(XAlm-XPrp)
0.00
0.20
0.40
0.60
0.80

B

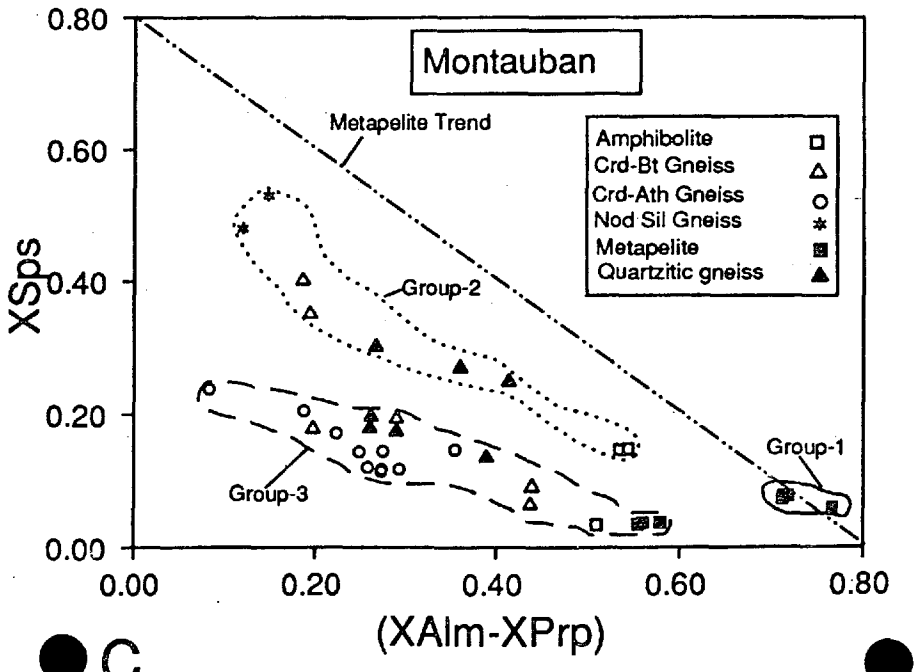
Montauban
Metapelite Trend
Amphibolite
Crd-Bt Gneiss
Crd-Ath Gneiss
Nod Sil Gneiss
Metapelite
Quartzitic gneiss
Group-1
Group-2
Group-3
XSps
(XAlm-XPrp)
0.00
0.20
0.40
0.60
0.80

C

are fairly homogeneous. Minor zoning and core to rim variations are mainly: 1) X_{Fe} and X_{Mn} increase with decrease in X_{Mg}(reverse zoning), and 2) X_{Fe} and X_{Mg} increase with decreases in X_{Mn} and X_{Ca} (prograde zoning). The most common zoning is type (1), but both types are observed for garnet in contact with biotite, suggesting prograde and retrograde diffusion for different metamorphic reactions.

Némiscau: Both snowball textured syn-tectonic garnet and idioblastic post-tectonic garnet have been observed in Némiscau rocks. Most of the garnets are fairly homogeneous. Moderately flat normal compositional profiles were found for a large garnet porphyroblast in a cordierite-anthophyllite rock (Fig. 4.10A).

Three garnet composition types are present, each in different rock lithological units (Fig. 4.9B). The most almandine-rich garnets are in andalusite and sillimanite bearing metapelites: those having the lowest almandine contents are from the cordierite-bearing metapelites and cordierite-anthophyllite rocks. Only one sample of metapelite (S-26) had Mn-rich garnet. Grossular-rich garnets are from a skarn sample (N-02) in Lac de la Hutte area.

Montauban: Garnets from the metapelites (MQ1 and MQ10) have low X_{Ca} and X_{Mn} (Table 4.3). Garnets from the north gold zone gneisses also have low X_{Ca}, but a wide range of X_{Mn} (0.04-0.53). Garnets in biotite-bearing amphibolite have high X_{Ca} and moderate X_{Mn} (Table 4.3).

Two patterns of garnet zoning are observed, 1) a bell shape normal zoning with Mn-Ca-rich and Mg-Fe-depleted core relative to rim compositions (prograde

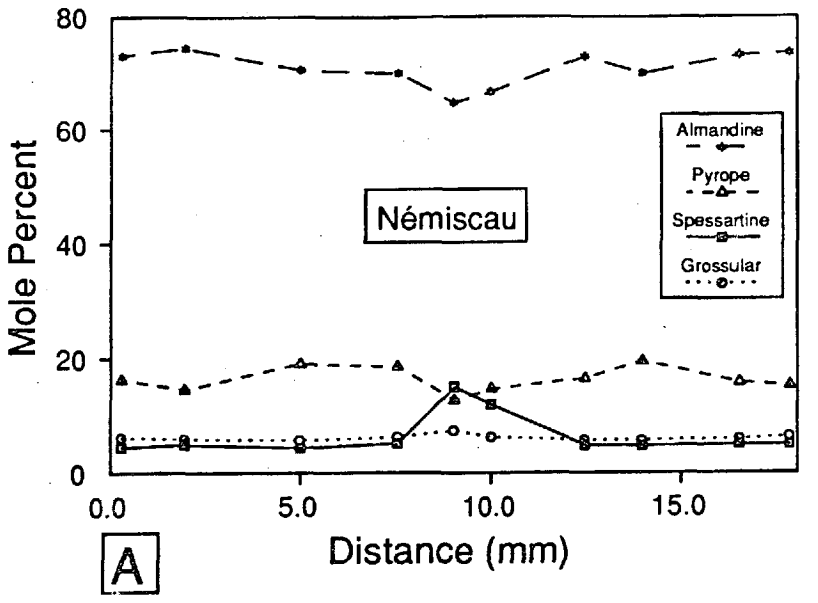

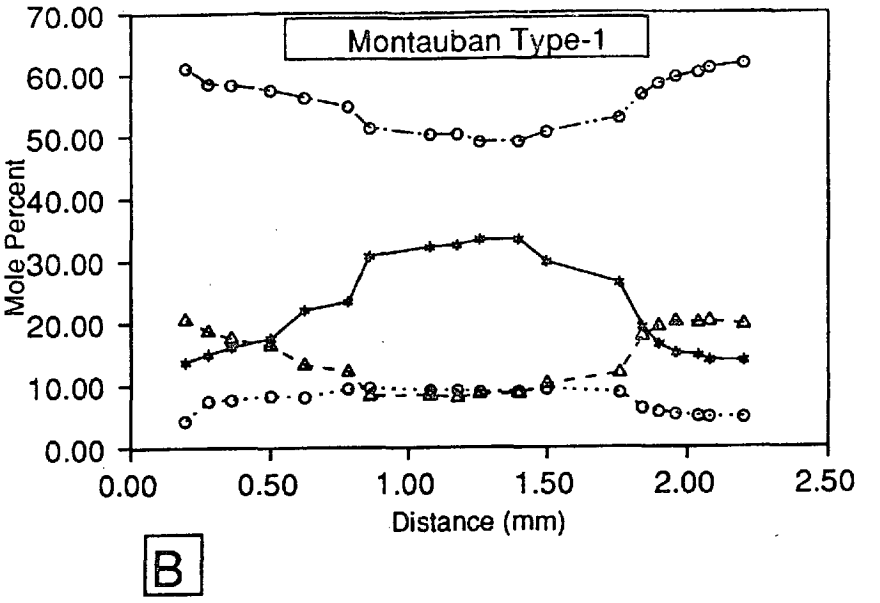

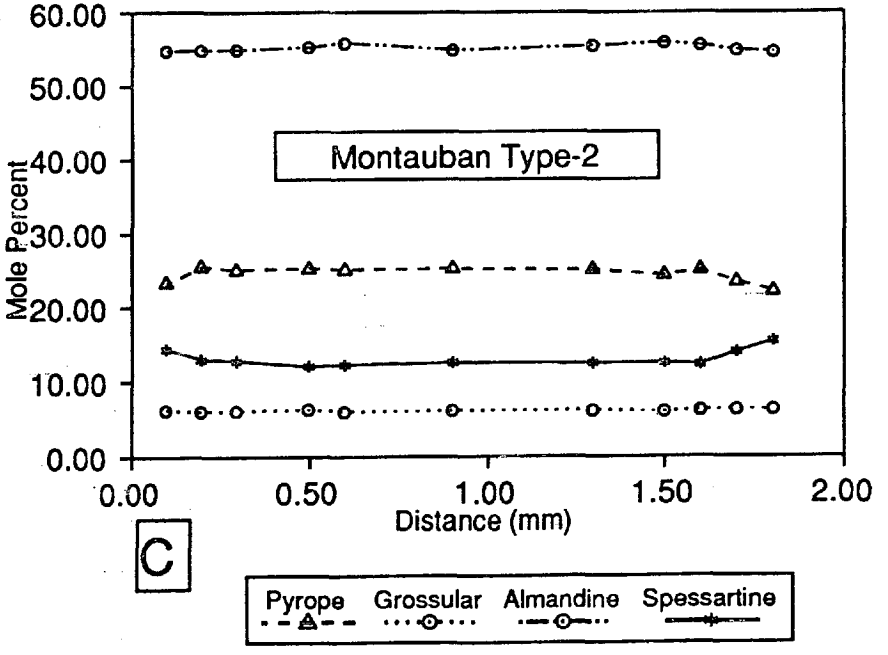

Fig. 4.10. Garnet zoning profiles.

zoning; cf. Atherton, 1968; Tracy, 1982; Holdaway et al., 1988), and 2) a flat normal zoning with or without retrograde Mn-increases toward the rim (Fig. 4.10B-C). Most Mn-rich garnets have a fairly flat prograde zoning profile, suggesting a continuous availability of Mn during garnet growth and a Mn-rich bulk composition, probably acquired during hydrothermal alteration.

On a ternary Mn-Fe-Mg cation diagram (Fig. 4.11) the coexisting biotite-garnet pairs (X_{Ca}^{Grt}=0.06±0.02) exhibit an array of tie-lines where Mn-rich garnet coexists with Mg-rich biotite in sulfides-bearing samples, an equilibrium relationship also described by Miyashiro (1953), Mohr and Newton (1983), Spear (1988), Williams and Grambling (1990). On this diagram, three groups of garnet compositions are apparent: 1) low Mg and Mn garnet from regional metapelite, 2) low Mg and intermediate to high Mn garnet from the north gold zone quartzitic and nodular sillimanite gneiss, and 3) high-Mg and intermediate Mn garnet from cordierite-biotite and cordierite-anthophyllite rocks. Both groups 2 and 3 form linear trends that parallel the Fe-Mn side of the triangle (Fig. 4.11) and have differently sloping tie-lines.

A similar array of garnet-biotite compositional tie-lines has been documented by Nesbitt (1982) at the Ducktown massive sulfide deposit. Changes in X_{Fe} of the ferromagnesian silicates in metapelites were attributed by Nesbitt (1982) to sulfidation reactions as a result of sulfur diffusion during metamorphism or sulfur enrichment during the pre-metamorphic emplacement of the ore. Mohr and Newton have reported Mn-rich garnet and Mg-rich biotite in graphitic and sulfidic kyanite-bearing schists from great Smoky Mountains. They have attributed these enrichments in Mn and Mg to internally buffered sulfidation reactions related to the prograde formation of pyrrhotite:

$$\text{Fe-silicates} + \text{Py} + \text{carbon} = \text{Fe-poorer silicates} + \text{Po} + CO_2$$

At Montauban, the garnet-biotite pairs having the lowest Mn and Mg contents

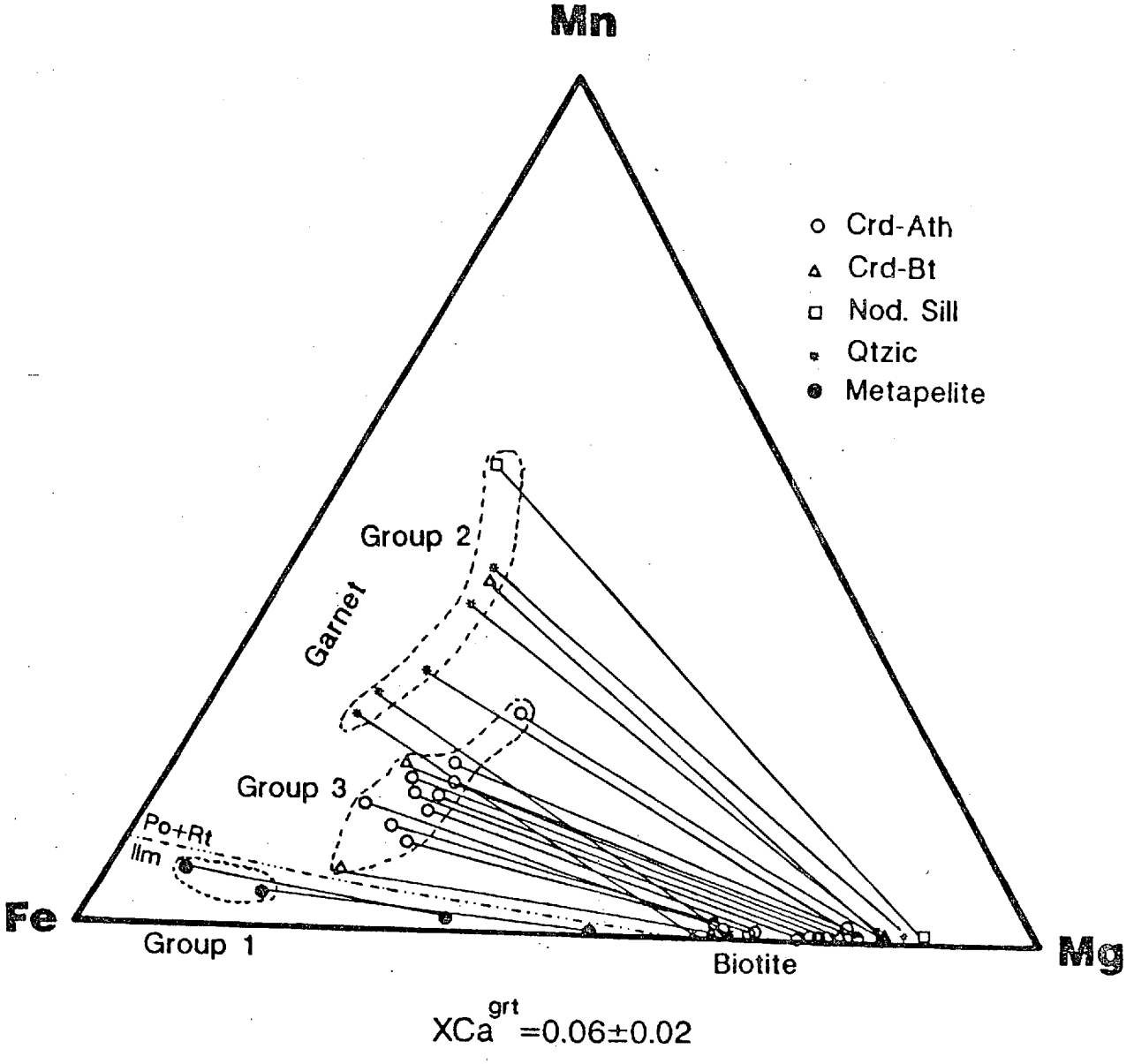

Fig. 4.11. Mn-Fe-Mg ternary diagram (cation basis) showing garnet-biotite tie-lines relationships for the Montauban rocks. The outlined garnet groups are described in the text.

are from the regional metapelite (15 km NE of the mine sequence) which contains ilmenite. In contrast, sulfide-bearing gneisses of the metamorphosed alteration zone contain Mn- and Mg-rich garnet and biotite coexisting with pyrrhotite and rutile. Internally controlled sulfidation reactions during metamorphism may indeed have contributed to lowering the $K_D^{Grt\text{-}Bt}$ by extracting iron from the silicates and thus increasing the proportion of Mn and Mg.

Williams and Grambling (1990) used a binary X_{Sps}-(X_{Alm}-X_{Prp}) diagram to illustrate ranges in garnet compositions from Mn-rich metapelites. This diagram is derived by projecting low-Ca ternary garnet compositions in the Mn-Fe-Mg system (Fig. 4.11) perpendicularly to the Fe-Mg boundary (the least squares solution; see Spear, 1988). Group 1 garnets, as defined above project to the lowest Mg contents (X_{Prp}=0.08±0.01); group 2 garnets have intermediate pyrope contents (X_{Prp}=0.17±0.02) and the highest spessartite contents (Fig. 4.9C); and group 3 garnets are the most magnesian (X_{Prp}=0.25±0.04). Rocks containing group 3 garnets are Mg-rich (bulk rock X_{Mg}=0.77±0.13) compared to the quartzitic and nodular-sillimanite gneisses (bulk rock X_{Mg}=0.56±0.19). It is apparent that the higher pyrope components in group 3 garnets reflect the effects of bulk rock compositions. The effect of varying bulk composition on garnet-biotite K_D is discussed below.

Geothermometry in the Three Terranes

Compositional characteristics of garnet and biotite for the three terranes are summarized in Table 4.3. The garnet-biotite geothermometry calculations were processed with the BTGRTEM program (written by LRB, *Appendix IV)* and with GEO-CALC using Berman's (1990) garnet activity model. Matrix biotite grains were used as they are likely to best preserve the peak metamorphic compositions (Barber and Yardley, 1985; Chipera and Perkins,

1988). The peak temperature estimates for each terrane are compiled on a bar-diagram (Fig. 4.12) and summarized in Table 4.4. Pressures of 2.5, 4.5 and 6.5 Kbars were used, respectively for the Atik Lake, Némiscau and Montauban temperature calculations. These are prefered pressures based on garnet-cordierite and estimates obtained from other geobarometers presented in upcoming sections. Nevertheless, pressure is not a critical parameter for T determination as a change of 1 kbar induces a T increase of ~7°C. Berman's (1990) calibration provides the highest T estimate. The Atik Lake and Némiscau garnets have low Mn-contents and the various garnet-biotite geothermometers provided very consistent estimates of T=559±20 °C and T=645±23°C, respectively. The Ganguly and Saxena (1984) calibration overcorrected for the high Mg-contents in the garnets, and produces lower T estimates (cf., Edwards and Essene, 1988). Application of garnet-biotite geothermometry to the Montauban mine sequence rocks is more problematic as the garnets are Mg and Mn rich.

The effect of increasing Mn substitution in garnet on the $K_D^{Bt\text{-}Grt}$ $((Mg/Fe)^{Grt}/(Mg/Fe)^{Bt})$ is illustrated in Figure 4.13. There is a large decrease of $\ln K_D$ with increasing X_{Mn}, regardless of rock type. This relationship has also been reported by Ganguly and Kennedy (1974), Newton and Haselton (1981) and Vivallo (1985) and is discussed by Williams and Grambling (1990). This negative correlation can result from the substitution of larger cations (Ca, Mn) for Fe^{2+} and Mg which induces localized structural expansions, favoring the inclusion of Fe^{2+} over Mg to minimise local intracrystalline strains (Dallmeyer 1974). Williams and Grambling (1990) suggested that the negative correlation incorporates the effects of non-ideal mixing of Mn and other components in garnet and biotite because of multicolinearity between compositional variables in garnet and biotite.

TABLE 4.4 GARNET-BIOTITE GEOTHERMOMETRY

ATIK LAKE

ROCK TYPE	(n)	PEAK TEMPERATURE FOR P=2.5 KBARS FS	TH	P	PL	GS	HS	BER
LOWER STRATIGRAPHY								
ALT. FELSIC METASEDIMENTS	1	640	632	624	634	678	666	720
CRD-ATH MISTUHE ISLAND	1	548	562	565	584	548	572	608
CRD-CHL-MS	1	524	543	544	570	522	547	584
CRD-GED	7	537	553	553	577	534	560	582
(1σ)		23	19	29	14	32	24	18
AL. ALT.	2	536	553	560	577	558	557	594
(1σ)		30	24	19	18	26	30	26

NÉMISCAU

ROCK TYPE	(n)	PEAK TEMPERATURE FOR P=4.5 KBARS FS	TH	P	PL	GS	HS	BER
METAP. (AND)	2	591	596	589	611	589	589	641
(1σ)		14	11	8	8	2	28	14
METAP. (SIL)	4	614	614	606	623	608	639	664
(1σ)		45	34	25	25	50	45	18
ATH-GRT	3	611	617	609	617	557	639	653
(1σ)		23	16	14	16	23	27	17
CRD-ATH	3	617	617	608	625	567	642	679
(1σ)		36	28	22	20	30	37	6

MONTAUBAN

ROCK TYPE	(n)	PEAK TEMRATURE FOR P=6.5 KBARS FSB	TH	P	PL	WG	HS	BER
REGIONAL METAP.	2	740	655	617	620	732	705	692
		5	11	13	10	21	19	22
(Bt-Incl.)	2	663	597	576	577	651	620	634
		20	13	13	10	21	19	14
NGZ QUARTZITIC	8	612	550	580	544	613	632	619
		51	44	42	30	25	41	9
BT-CRD	6	631	534	566	535	587	608	616
		26	50	12	40	25	21	13
CRD-ATH	9	623	550	567	547	600	618	612
		28	35	25	22	38	42	16
NOD SIL	2	553	474	592	537	625	618	548
		40	35	34	45	45	55	18

FS: Ferry and Spear (1978); Th: Thompson (1976); P: Perchuck (1981); PL: Perchuck and Lavrent'eva (1983); GS: Ganguly and Saxena (1984); HS: Hodge and Spear (1982); BER: Berman (1990); WG: William and Grambling (1990). Other abbreviations as in Table 4.1

Fig. 4.12. Temperature histograms for the three terranes showing the results obtained with various garnet-biotite geothermometers. FS78=Ferry and Spear (1978), TH76=Thompson (1976), P81=Perchuck (1981), PL83=Perchuck and Lavrent'eva (1983), GS84=Ganguly and Saxena (1984), HS82=Hodges and Spear (1982), BER91=Berman (1991), WG90=Willimans and Grambling (1990). E=number of samples, n=number of points analysed.

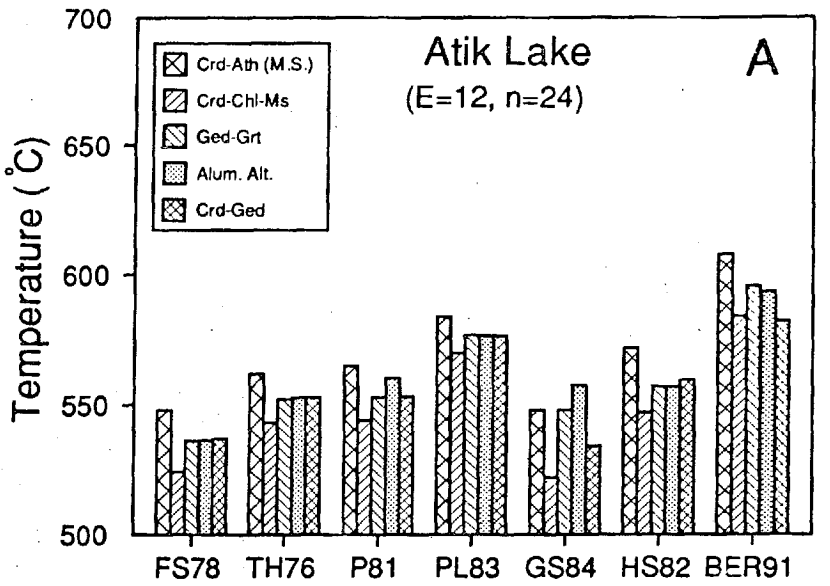
Atik Lake
(E=12, n=24)
A
Crd-Ath (M.S.)
Crd-Chl-Ms
Ged-Grt
Alum. Alt.
Crd-Ged
Temperature (°C)
700
650
600
550
500
FS78
TH76
P81
PL83
GS84
HS82
BER91

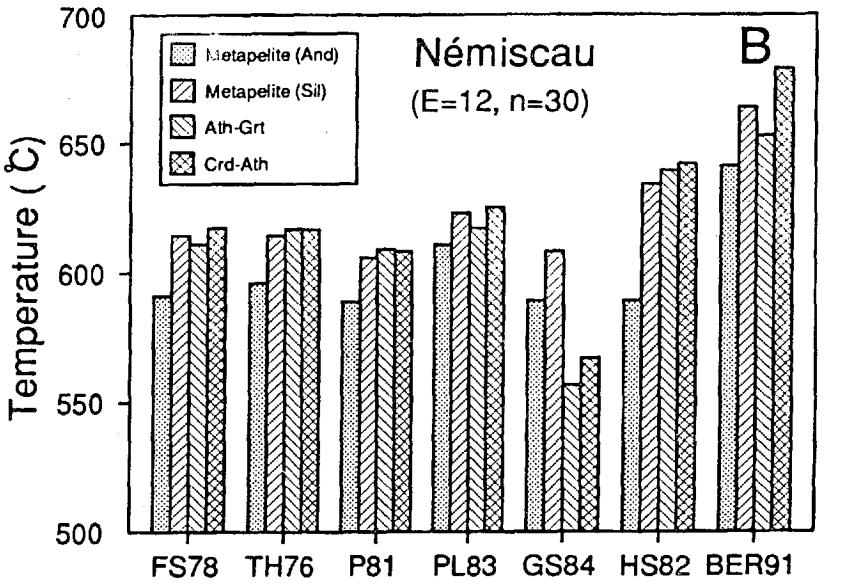
Némiscau
(E=12, n=30)
B
Metapelite (And)
Metapelite (Sil)
Ath-Grt
Crd-Ath
Temperature (°C)
700
650
600
550
500
FS78
TH76
P81
PL83
GS84
HS82
BER91

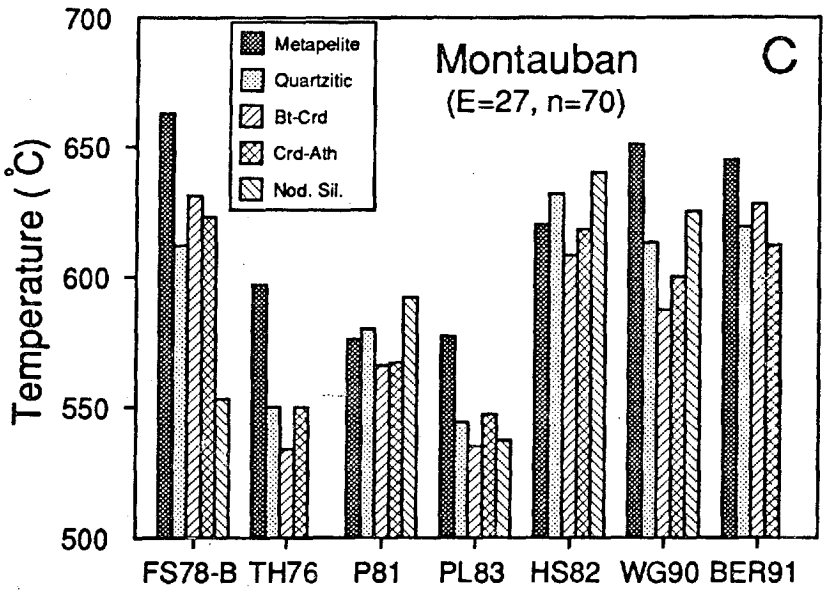
Montauban
(E=27, n=70)
C
Metapelite
Quartzitic
Bt-Crd
Crd-Ath
Nod. Sil.
Temperature (°C)
700
650
600
550
500
FS78-B
TH76
P81
PL83
HS82
WG90
BER91

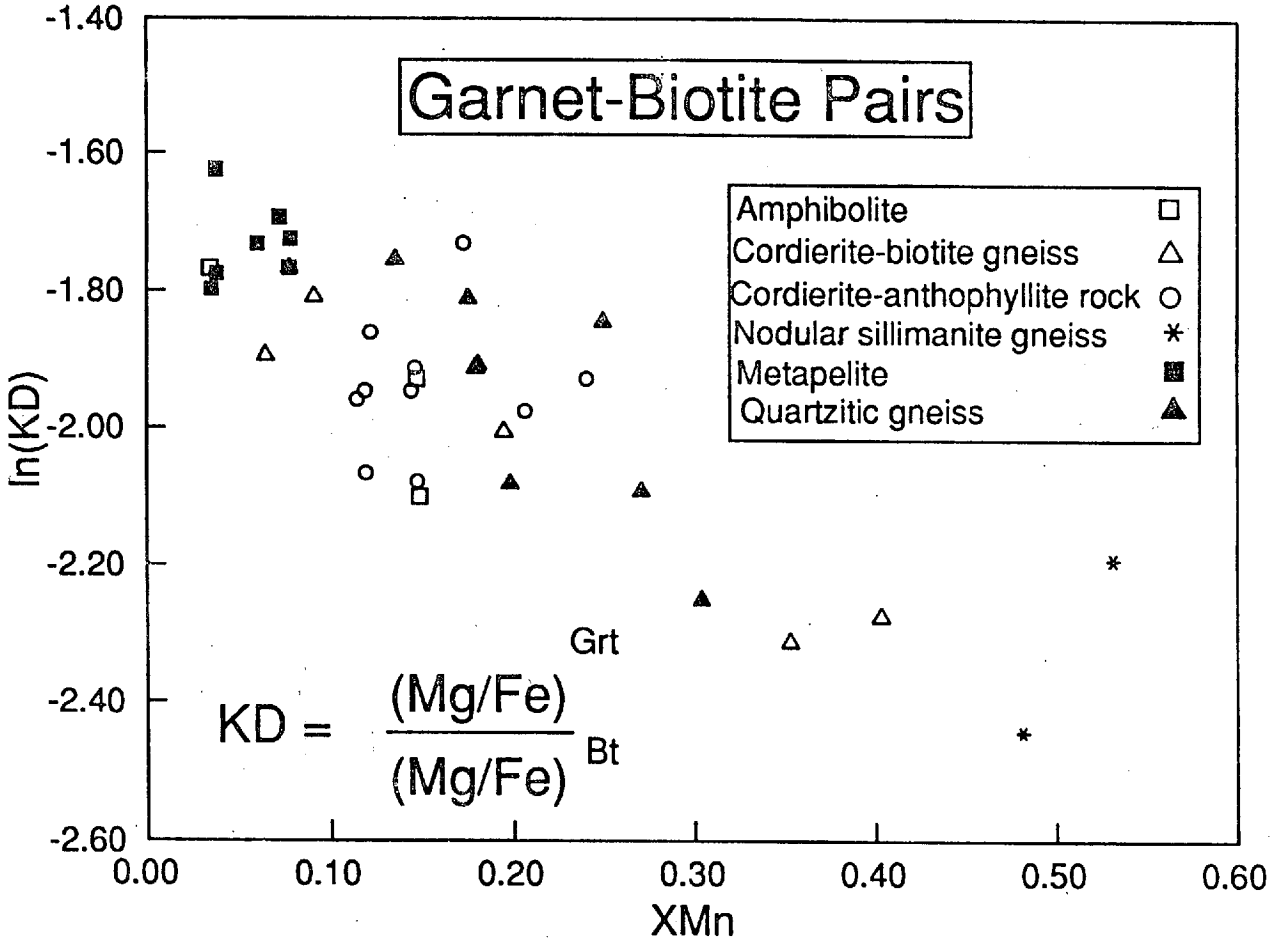

Fig. 4.13. $Ln(K_D)$-X_{Mn} diagram for garnet-biotite pairs in rock types from Montauban.

The effect of high Mn-content in garnet is well depicted by the erroneously low T obtained using GEO-CALC (Fig. 4.14) in which Berman's (1990) quaternary garnet mixing model assumed W_{MgMn}=0. This is also true for all versions of the geothermometers that do not include a correction factor for Mg-Mn mixing (Fig. 4.12). Only low-Mn garnets were used with Berman's (1990) calibrations for Figure 4.12. Whith Hodges and Spear's (1982) calibration, their maximum value of W_{Mn-Mg}= 10468 j/mol had to be used in order to obtain consistent temperature estimates between rock types (Table 4.4). The Williams and Grambling (1990) model 3 geothermometer also provided consistent results. It should be pointed out that Williams and Grambling's metric conversion of the Ferry and Spear's geothermometer expression is in error. Their ΔH=17042 J value has been corrected twice [(12454 cal x 4.184 J/cal / 3) - (0.057 cal/bar x 2070 bar x 4.184 J/cal x 1.987 $calmol^{-1}K^{-1}$ / 3)] to account for the Ferry and Spear (1978) experimental pressure of 2.07 Kbar. The correct number is ΔH=17369 J, which is already pressure corrected (see Ferry and Spear, 1978, equation 6, p. 116). The preferred peak temperature estimate for Montauban is that derived from biotite inclusions in metapelite garnets and low-Mn garnets from the north gold zone altered rocks. The modified Ferry and Spear (1978) (equation 4), Williams and Grambling (1990), Hodge and Spear (1982) and Berman (1990) calibrations yield T=621±17°C.

Summary

The peak temperatures for the three regionally metamorphosed terranes are: Atik Lake, T=559±20 °C for P=2.5 Kbar; Némiscau, T=645±23°C for P=4.5 Kbar; and Montauban, T=621±17 °C for P=6.5 Kbar.

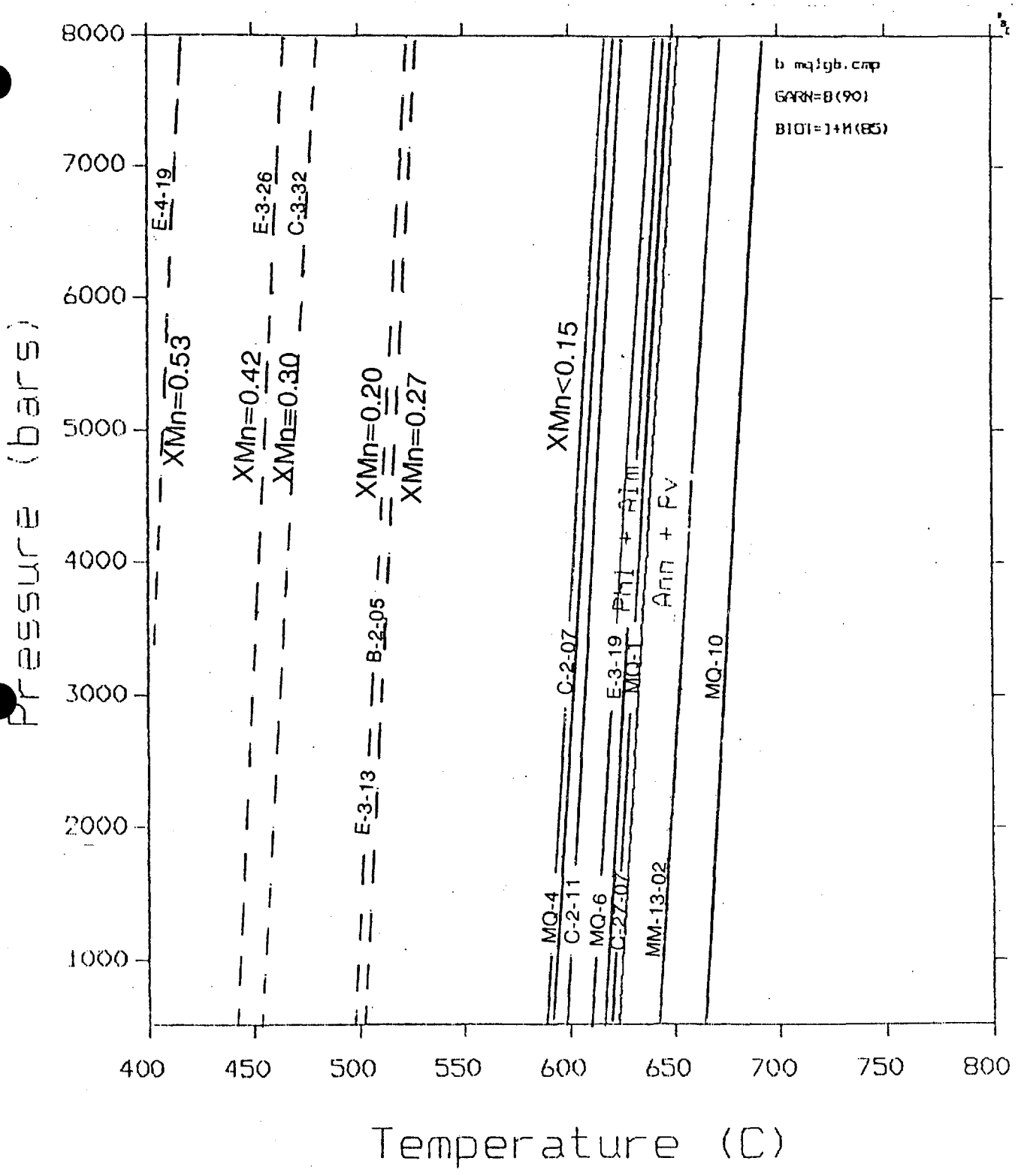

Fig. 4.14. Pressure-temperature diagram showing the garnet-biotite equilibria calculated for the Montauban rocks using GEO-CALC and Berman's (1991) garnet activity model. The equilibrium boundary is displaced toward lower T with increasing mole fraction of spessartine (X_{Mn}) in garnet.

Anthophyllite-gedrites solvus thermometry

A solvus involving A-site occupancy (the site of alkalies in amphiboles) and Al (both tetrahedral and octahedral) in the coexisting orthoamphiboles (anthophyllite and gedrite) was schematically outlined by Robinson et al. (1971), and empirically calibrated against T by Spear (1980) at bulk $X_{Fe} \approx 0.4$. According to Spear, the crest of the solvus lies at about 600±25°C for $Al^{IV}=0.75$, $Al^{VI}=0.3$ and A-site=0.15 (Fig. 4.15A). The width of the solvus expressed as A-site occupancy is a function of X_{Fe} with Fe-rich samples showing the widest gap. However, the effect of varying bulk composition on the solvus loci is not precisely known. Because coexisting orthoamphiboles have been reported for a wide range of pressure conditions at T=500-600°C, pressure probably has very little effect on the width of the solvus: e.g. 535°C, 5-6 Kbars for Post-Pound volcanics, Spear (1980); 600°C , 3.5 Kbars for Outokumpu, Treloar and Putnis (1982); 500-600°C, Pmax=6 Kbars for Old Woman Mountains, Stoddard and Miller (1990); 550-600°C, 3 Kbars for Orijärvi area, Schneiderman and Tracy (1991). The location of the solvus in P-T space has been calculated by Spear and Rumble (1986) and shown on their petrogenetic grid for amphibolites (Fig. 4.15B).

Orthoamphiboles in the three terranes studied in this thesis are elongated, bladed and commonly form rosettes or fan like arrays. Gedrite, which is dominant in Atik Lake altered basalts, is medium green, whereas anthophyllite is pale-beige in all the terranes. They are compositionnally classified using the relation between alkalies and Al^{IV} (Fig. 4.16) according to the scheme of Leake (1978). Trends of Fe and Mg versus Al^{VI} (not shown) are also present, and are identical to those observed by Spear (1980). Iron varies little with Al^{VI} between anthophyllite and coexisting gedrite, and Mg varies inversely with Al^{VI} implying that the tschermak exchange

Fig. 4.15. A) Hypothetical T-X solvus for gedrite-anthophyllite at $X_{Fe} \approx 0.4$, from Spear (1980). B) Petrogenetic grid for orthoamphibolite constructed by Spear and Rumble (1986). Note the position of the orthoamphibole solvus in P-T space. [For this figure, Ga=garnet, Cin=cummingtonite, An=anthophyllite, Gd=gedrite, Oam=orthoamphibole (supersolvus), Ch=chlorite, Cd=cordierite, St=staurolite, Ky=kyanite, Si=sillimanite, And=anddalusite, Qz=quartz, Pyroph=pyrophyllite.]

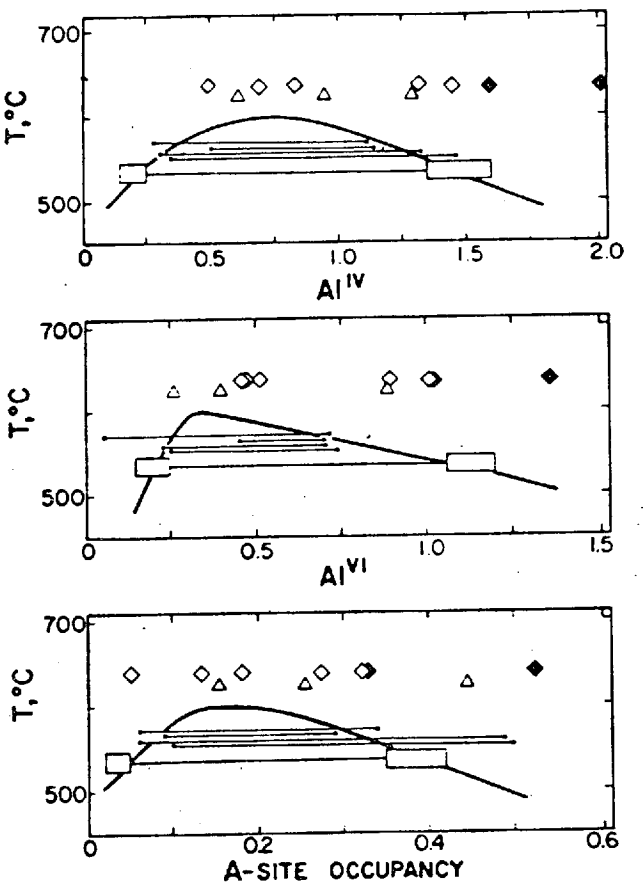
T,°C
700
500
0
0.5
1.0
1.5
2.0
Al^{IV}
T,°C
700
500
0
0.5
1.0
1.5
Al^{VI}
T,°C
700
500
0
0.2
0.4
0.6
A-SITE OCCUPANCY

A

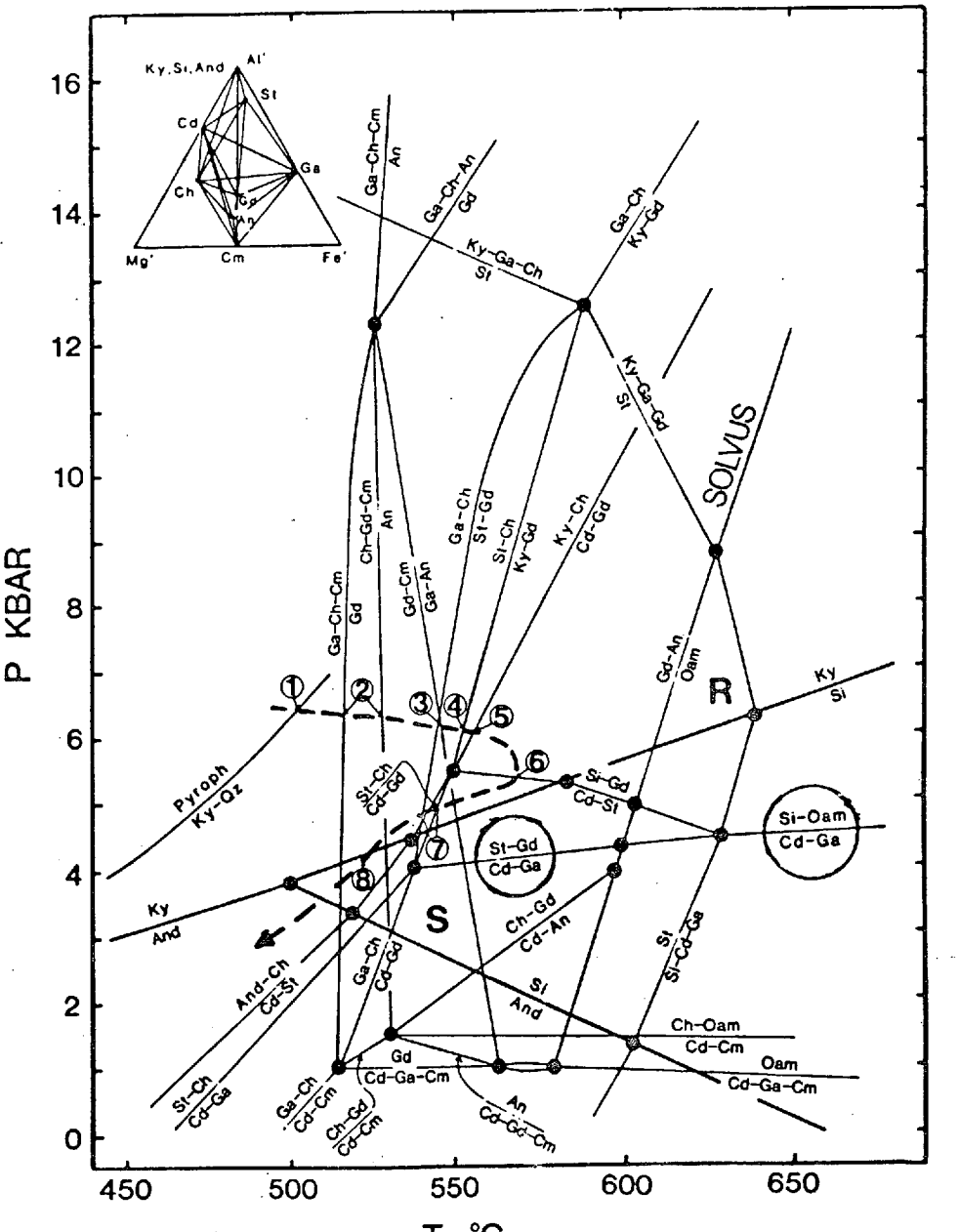
Ky, Si, And
Al'
St
Cd
Ga
Ch
Mg'
Cm
Fe'
P KBAR
16
14
12
10
8
6
4
2
0
450
500
550
600
650
T °C
SOLVUS
R
S
St-Gd
Cd-Ga
Si-Oam
Cd-Ga
Pyroph
Ky-Qz
Ky
And
Ky
Si
Ch-Oam
Cd-Cm
Oam
Cd-Ga-Cm
Gd
Cd-Ga-Cm

B

($Al^{VI}Al^{IV}$=MgSi) involved only the Mg component. Similar relationships have been reported by Abraham and Schreyer (1973), Kamineni (1975), Damman (1989) and Schneiderman and Tracy (1991).

Atik Lake

The Atik Lake orthoamphiboles fall within the range 0.16 to 0.37 edenite/tschermakite (Ed/Ts) values (Fig. 4.16A), but one gedrite sample has a vacant A-site. Individual grains range from X_{Fe}= 0.37-0.75, but coexisting gedrite-anthophyllite occur only in the range X_{Fe}=0.5 to 0.65. Textures indicate that these coexisting grains formed at sub-solvus conditions (Fig. 4.16A). Anthophyllite is the sole orthoamphibole (X_{Fe}=0.37-0.49) in Mg-rich cordierite-orthoamphibole rocks from the central metasedimentary sequence. Stoddard and Miller (1990) also reported that anthophyllite was the only orthoamphibole in Mg-rich rocks at Old Woman Mountains. Three compositional sub-groups can be defined: (1) Mg-rich, Fe-Al-alkali-poor (X_{Fe}=0.37) anthophyllite from the central metasedimentary rocks, (2) Fe-Al-alkali-rich (X_{Fe}=0.75) gedrite from Fe-rich altered basalts, (3) coexisting anthophyllite and gedrite forming a compositional continuum from X_{Fe}=0.50-0.65. In contrast, Spear, (1980) reported the coexisting pair of orthoamphiboles in Post Pond Volcanics for three ranges of X_{Fe}, 0.25-0.30, 0.35-0.45, and 0.45-0.55.

In orthoamphiboles coexiting with ilmenite in this terrane, gedrite (0.05-0.49 wt% TiO_2) is always more titaniferous than anthophyllite (0-0.08 wt% TiO_2). Tie-lines for coexisting anthophyllite-gedrite pairs have positive slopes in Ti-X_{Fe}, Al^{IV}-X_{Fe}, A_{site}-X_{Fe} and (Mg-Si^{IV}) diagrams (not shown). These positive slopes and tie-lines are similar to those obtained from the orthoamphiboles in the Post Pond metavolcanics by Spear (1980, 1982). Spear,

Fig. 4.16. A-site occupancy (Na+K)-Al^{IV} diagrams showing orthoamphibole compositions from the three terranes. The amphibole nomanclature if from Leake (1978).

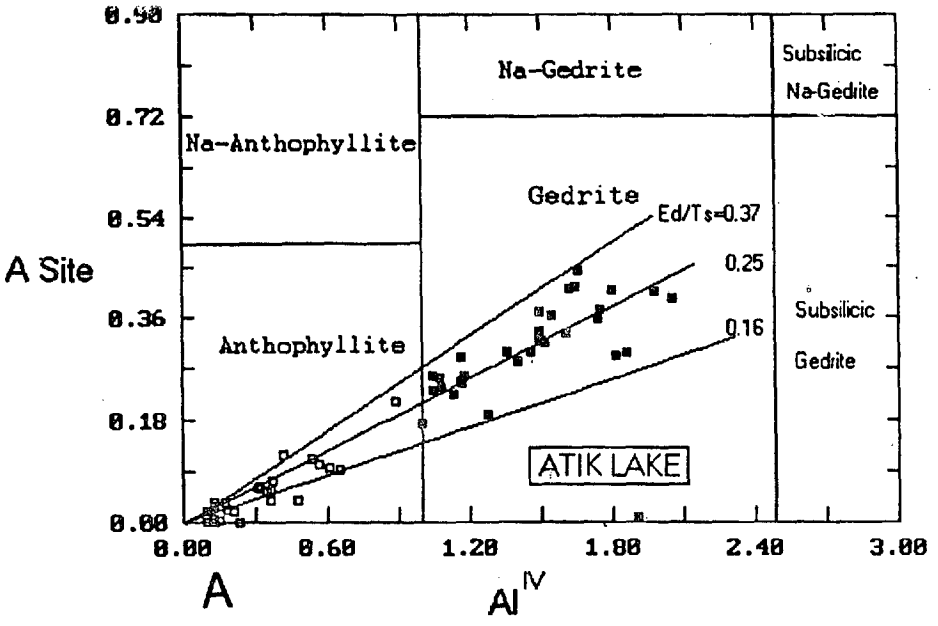
Na-Gedrite
Subsilicic
Na-Gedrite
Na-Anthophyllite
Gedrite
Ed/Ts=0.37
0.25
0.16
Subsilicic
Gedrite
Anthophyllite
ATIK LAKE
A Site
0.90
0.72
0.54
0.36
0.18
0.00
0.00
0.60
1.20
1.80
2.40
3.00
A
Al IV

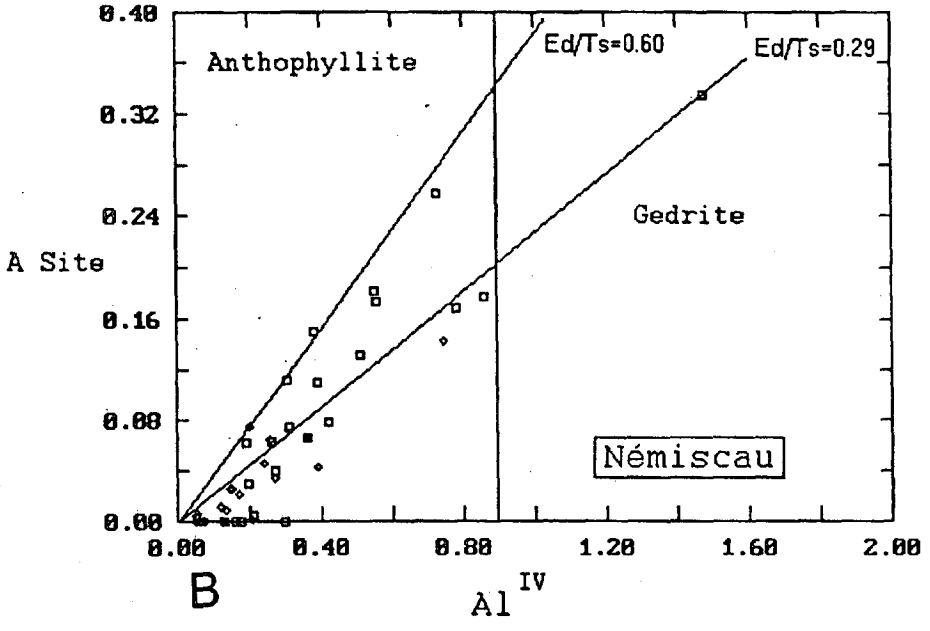
Anthophyllite
Ed/Ts=0.60
Ed/Ts=0.29
Gedrite
Némiscau
A Site
0.40
0.32
0.24
0.16
0.08
0.00
0.00
0.40
0.80
1.20
1.60
2.00
B
Al IV

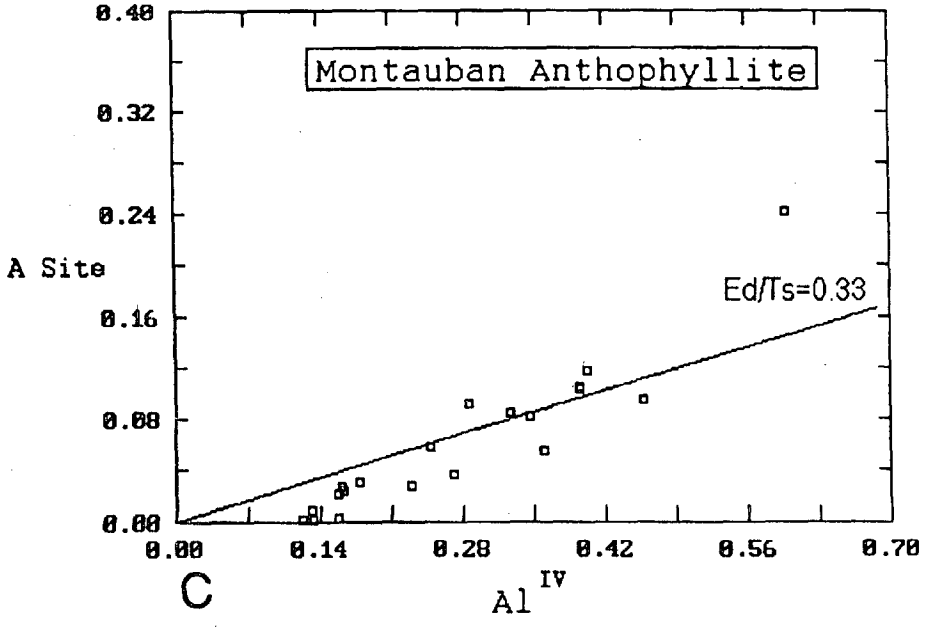
Montauban Anthophyllite
Ed/Ts=0.33
A Site
0.40
0.32
0.24
0.16
0.08
0.00
0.00
0.14
0.28
0.42
0.56
0.70
C
Al IV

however, did not find such a continuum in orthoamphibole compositions, but Treloar and Putnis (1982) and Stoddard and Miller (1990) show a similar continuum at Outokumpu and Old Woman Mountains, respectively.

The peak temperature condition, ≈550-600°C, at Atik Lake is close to that of the crest of the solvus. Some orthoamphibole analyses fall within the solvus zone (Fig. 4.15A), and are probably finely exsolved supersolvus grains.

Némiscau

The orthoamphiboles at Némiscau are dominantly anthophyllites and only one sample contains gedrite (Fig. 4.16B) which rims cummingtonite, a texture interpreted by Schneiderman and Tracy (1991) to have a retrograde origin in Orijarvi rocks. Most of the anthophyllites are distributed along the Ed/Ts=0.29 trend but may range up to Ed/Ts=0.60 (Fig. 4.16B). Anthophyllite in the range X_{Fe}=0.38-0.53 coexists with garnet and cordierite, whereas that coexisting with cordierite has X_{Fe}=0.34-0.38 (Fig. 4.3). The previously determined peak T (≈650°C) and P (≈4.5 kbar) conditions for this terrane are consistent with the formation of super-solvus orthoamphiboles (see reaction Gd-An=Oa, Fig. 4.15B).

Montauban

The orthoamphibole at Montauban is exclusively anthophyllite (X_{Fe}=0.19-0.34) which is distributed along Ed/Ts=0.33 trend (Fig. 4.16C). As at Némiscau, there are no exsolution textures, which is consistent with the formation of a super-solvus orthoamphibole at peak T (≈620°C), P (≈6.5 kbar) conditions.

Discussion

Overall, the position of the orthoamphibole solvus (Spear, 1980) is consistent with observed relationships and peak P-T estimates for the three terranes. The Atik Lake orthoamphibole compositions are the most Fe-rich of the three, and coexist with ilmenite-pyrrhotite-arsenides. At Némiscau, the most Fe-rich anthophyllites are in ilmenite-pyrrhotite bearing rocks, and the most Mg-rich ones coexist with magnetite-pyrrhotite. At Montauban, the anthophyllites are the most Mg-rich of the three, and are in pyrrhotite-rutile bearing rocks. Under similar peak P-T conditions, Spear (1980, 1982) found that Mg-rich orthoamphiboles coexisted with rutile, wheareas the most Fe-rich ones are in ilmenite-bearing rocks. This may indicate the lower oxidation state (or lower fS_2) for Fe-rich bulk-rock compositions.

Damman (1989) suggested that the edenite/tschermakite ratio could be pressure sensitive with the highest ratio formed at the lowest pressures. However, as P, T, bulk rock composition, and oxidation states varied, it is difficult to quantify this assumption.

Garnet-plagioclase-hornblende geothermobarometry

Montauban

The garnet-plagioclase-hornblende geobarometers of Kohn and Spear (1989, 1990) have been applied to regional garnet bearing amphibolites and on amphibolite sills from the north gold zone. The temperature data used to solve Kohn and Spear expressions was obtained from garnet-hornblende compositions using the Graham and Powell (1984) geothermometer:

$$1/4\ \text{Fe-Prg} + 1/3\ \text{Prp} = 1/4\ \text{Prg} + 1/3\ \text{Alm} \quad (5)$$

This geothermometer does not include a pressure correction, which should be minimal (Graham and Powell, 1984), and its application is restricted to amphibolite with Mn-poor garnet (X_{Mn}<0.1). The garnets in the amphibolite have X_{Ca}= 0.14-0.30 and X_{Mn}=0.03-0.15; the calculated temperatures for those with X_{Mn}>0.1 are considered to be minimum values. The results are listed in Table 4.5 and illustrated on a P-T diagram (Fig. 4.17).

The initial calibrations of Kohn and Spear (1989) were based on the following reactions:

$$6\text{An} + 3\text{Ab} + 3\text{Tr} = 2\text{Grs} + \text{Py} + 3\text{Prg} + 18\text{Qtz} \quad (6)$$

$$6\text{An} + 3\text{Ab} + 3\text{Fe-Act} = 2\ \text{Grs} + \text{Alm} + 3\text{Fe-Prg} + 18\text{Qtz} \quad (7)$$

The Kohn and Spear (1990) calibrations which yield more constrained pressure estimates were based on:

$$6\text{An} + 3\text{Tr} = 2\text{Grs} + \text{Py} + 3\text{Tsch} + 6\text{Qtz} \quad (8)$$

$$6\text{An} + 3\text{Fe-Act} = 2\text{Grs} + \text{Alm} + 3\text{Fe-Tsch} + 6\text{Qtz} \quad (9)$$

The program GRHBPLTP was written (by LRB) to calculate mineral activities and T and P (*Appendix*). Kohn and Spear (1990) cautioned the use of pressure estimates obtained from mineral compositions falling outside their empirical calibration range (see *Appendix*). The peak temperature from core compositions is 607 ± 12°C with an average pressure of 6.7 ± 0.4 Kbar (670 MPa) using

TABLE 4.5. GARNET-HORNBLENDE-PLAGIOCLASE GEOTHERMO-BAROMETRY

Sample	(n)	T (°C)	1989 models				1990 model		(kb)
			P^1_{Mg}	P^2_{Mg}	P^1_{Fe}	P^2_{Fe}	P_{Mg}	P_{Fe}	
Atik Lake									
U-02	C (1)	557	3.3	5.5	3.4	5.6	2.6	4.5	
	R (1)	531	3.0	5.6	2.7	5.3	2.1	4.4	
Montauban									
					Regional				
MQ-6	C (3)	594±8	6.6±.3	6.6±.6	7.7±.6	6.8±.6	6.9±.1	7.1±.1	
	R (3)	587±6	6.3±.1	5.9±.5	7.3±.1	6.3±.1	7.0±.2	7.2±.2	
MQ-4	C (3)	623±24	9.4±1	12.1±2	12.1±2	12.9±2	9.2±.3	9.7±.2	
	R (3)	561±14	7.6±1	10.6±1	13.4±1	11.6±1	9.2±.8	9.8±.6	
					Mine Sequence Sills				
Sill-1									
1095N									
G511	C (4)	604±16	6.3±.2	6.3±.3	6.6±.4	6.7±.3	7.1±.4	7.4±.4	
	R (4)	562±20	6.0±.6	5.5±.8	6.4±.8	6.0±.9	6.5±.6	6.8±.7	
G513	C (4)	608±23	5.4±.2	5.2±.3	5.6±.4	5.9±.3	5.4±.2	6.0±.1	
	R (2)	565±9	4.4±.3	3.4±.3	4.1±.3	3.9±.4	4.2±.3	4.7±.4	
Sill-2									
805N									
B401	C (3)	580±7	4.8±.5	4.5±.4	4.4±.6	5.1±.3	3.5±.3	4.1±.3	
	R (3)	535±19	4.3±.5	3.4±.8	3.8±.5	3.8±.8	2.7±.1	3.2±.1	
975N									
E302	C (2)	572±8	5.0±.6	4.4±.8	4.3±.9	4.8±.8	5.8±.8	6.1±.7	
	R (4)	539±17	4.2±.3	3.0±.5	3.6±.5	3.4±.5	4.7±.7	5.0±.6	
1160N									
I305	C (2)	568±11	4.5±.5	4.1±1.4	4.0±.9	4.2±1	5.5±.3	5.8±.3	
	R (1)	546	4.3	3.5	3.9	3.8	5.0	5.3	
I307	C (4)	560±9	4.6±.3	3.7±.2	4.0±.4	4.1±.2	5.2±.2	5.5±.2	
	R (4)	536±11	4.3±.4	3.3±.4	3.8±.5	3.7±.5	4.0±.1	4.3±.1	

T calculated with the Graham and Powell (1984) geothermometer, and P with the Kohn and Spear (1989, 1990) geobarometers.

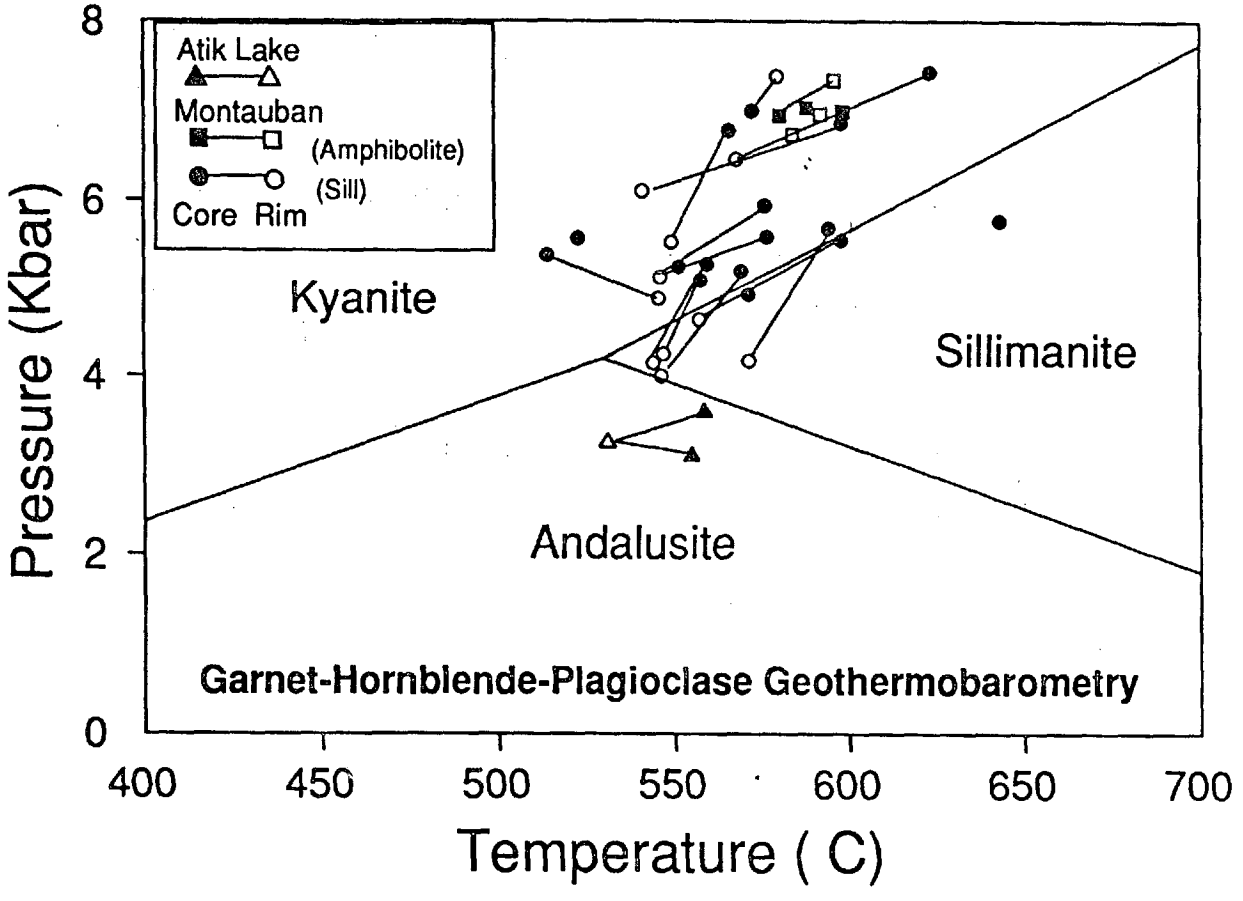

Fig. 4.17. Pressure-temperature diagram showing core-rim P-T estimates for Atik Lake and Montauban from garnet-hornblende-plagioclase geothermobarometry.

reactions activity models and Mg-Fe end-members reactions (6) and (7). When reactions (8) and (9) are used, an average core pressure of 7.1 ± 0.2 kbar is obtained. Rim T=569 ± 12°C with an average P=6.2 ± 0.5 Kbar with reactions (6) and (7) and P=6.9 ± 0.5 Kbar with reactions (8) and (9). One sample (MQ-4) gave unrealistic high pressures (Table 4.5), probably because the amphibole is very Fe-rich, and its composition falls outside the range of Kohn and Spear's (1989, 1990) calibrations (Appendices A, B); it does however, yield a reasonable peak T=620°C.

One of the amphibolite sills in the north gold zone, (sill-1; Table 4.5) yielded P-T estimates similar to the regional sample (MQ-6). Samples from another amphibolite sill (sill-2; Table 4.5) appears to have equilibrated at lower core and rim temperatures and pressures T_{core} = 570 ± 8°C, T_{rim} = 539 ± 5°C; P_{core} = 4.4 ± 0.4 Kbar, P_{rim} = 3.8 ± 0.4 Kbar for reactions (5) and (6) and P_{core} = 5.7 ± 0.3 Kbar, P_{rim} = 4.7 ± 0.5 Kbar for reactions (7) and (8). Plagioclase in one sample (B401, Table 4.5) from sill-2 is very calcic (An_{89}) and falls outside the calibration range; this may have led to the unrealistically lower calculated pressure.

Atik Lake

The wallrock calc-silicate assemblage of garnet, hornblende and plagioclase allows T and P determinations using the above geothermobarometers. The Atik garnets and hornblendes compositions fall well within the calibration compositional limits (*Appendix*), but the plagioclase is very calcic (XAn=0.91) and outside the prescribed range of 0.2≤XAn≤0.7. The core P=2.6 Kbar estimate for the Mg-endmember, at core T=559°C, is lower than that obtained for the Fe-endmember (4.5 Kbar). However, the resulting average P and the core-rim P-T paths are in excellent agreement with those obtained from

garnet-cordierite-andalusite data (Figs. 4.6, 4.17).

Garnet-plagioclase-Al_2SiO_5-quartz barometry

The calibration of Koziol and Newton (1988) employing the activity models of Newton and Haselton (1981), use the barometer reaction (10). Pressure and temperature estimates for Némiscau and Montauban terranes were obtained by solving simultaneously for equilibrium (10) and the biotite-garnet exchange reaction calibration of Hodges and Spear (1982) (Table 4.6; Fig. 4.18).

$$3An = Grs + 2Ky\ (Sil) + Qtz \quad (10)$$

The program GBPALTP was written (by LRB) to perform these calculations (*Appendices III, IV*).

Némiscau

The andalusite-bearing metapelite sample (V-48-11) has core values within the sillimanite field, whereas rim P-T estimates are well within the andalusite field (Fig. 4.18) at T≈510°C, P≈3 Kbar. Owing to the lack of sillimanite in the assemblage, the latter most likely represent the equilibrium situation. Calculated P-T values for a sample of sillimanite-bearing metapelite fall well within the sillimanite field (Fig. 4.18) but at higher values than those for the garnet-cordierite geothermobarometry (Fig. 4.6).

Montauban

I have used a value of 2500 cal (10460 J) for the W_{MnMg} Margules parameter, which is the maximum value tested by Hodges and Spear (1982). An average core T=602 ± 46°C and rim T=622 ± 35°C, with corresponding P_{core}=6.1 ± 0.8 Kbar and P_{rim}=6.7 ± 0.8 Kbar are obtained, when Kyanite is used in the

TABLE 4.6 GARNET-PLAGIOCLASE-Al_2SiO_5 GEOBAROMETRY

Sample	X_{Ca}^{Grt}	X_{Mn}^{Grt}	X_{An}^{Pl}	X_{Ab}^{Pl}	T (°C)	P (kb)
Némiscau						
V4811C	.034	.022	.278	.717	591	4.6
R	.031	.019	.267	.731	509	2.8
V4811C	.034	.019	.273	.723	589	4.7
R	.033	.021	.271	.726	617	3.0
V4814C	.029	.195	.251	.747	618	4.9
R	.028	.020	.243	.753	597	4.5
Montauban						
MQ-1 I	.085	.035	.545	.452	610	7.0
R	.105	.038	.549	.449	615	8.2
B421 C	.065	.386	.910	.088	566	5.6
R	.068	.353	.894	.086	598	6.3
E313 C	.073	.204	.358	.622	571	6.5
R	.064	.271	.325	.633	627	7.1
E219 C	.036	.250	.258	.741	690	7.2
R	.036	.242	.258	.741	687	7.2
I108 C	.054	.235	.797	.183	554	5.1
R	.059	.219	.798	.183	574	5.6
E326 C	.056	.418	.788	.200	620	6.1
R	.062	.403	.781	.198	629	6.7

Note: T is calculated with the Hodges and Spear (1982) garnet-biotite thermometer using W_{Mn-Mg}=2500 cal for Montauban and W_{Mn-Mg}=0 for Némiscau.

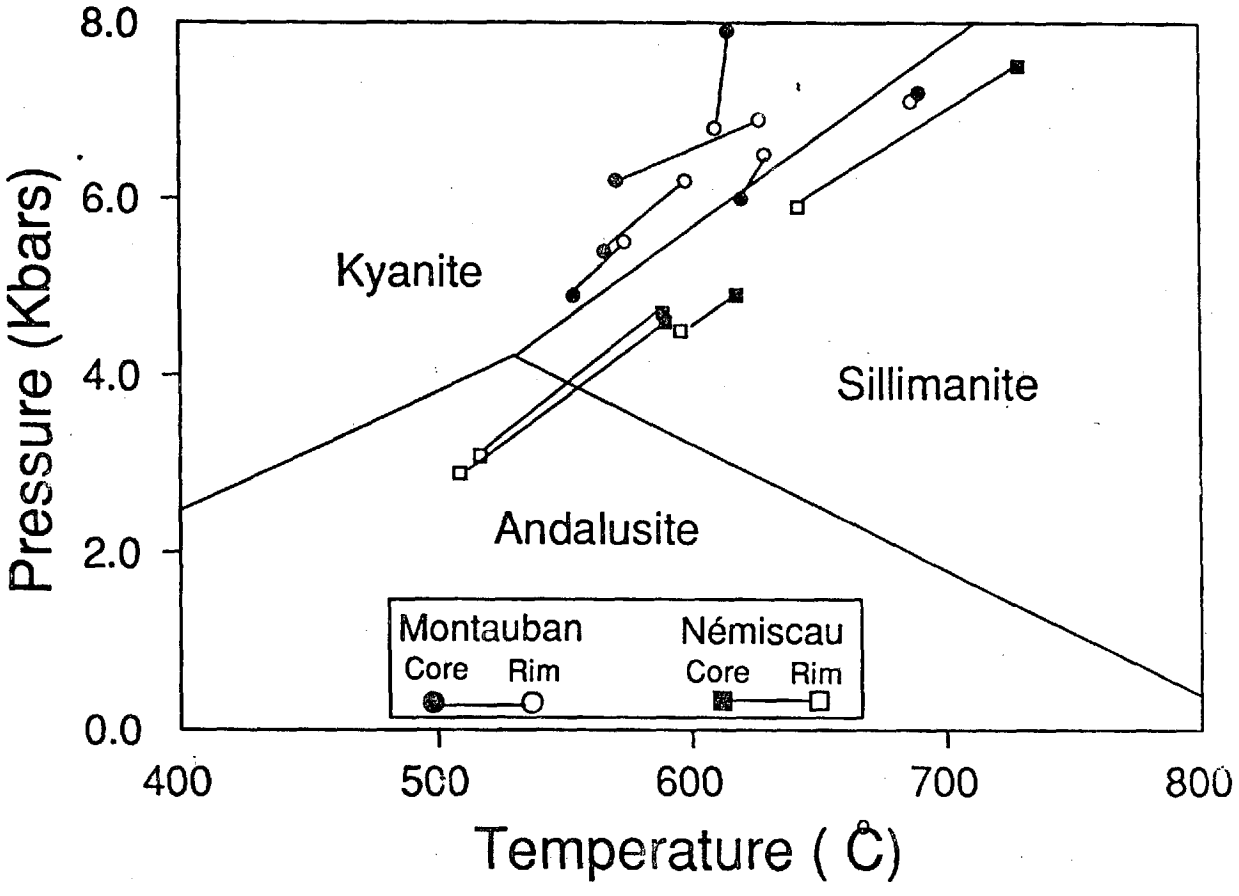

Fig. 4.18. Pressure-temperature diagram showing the core-rim P-T estimates for Némiscau and Montauban obtained from the garnet-plagioclase-biotite-aluminosilicate geothermobarometry.

calculations (Fig. 4.18). Sample I-1-08 gives a lower values, T=579 °C and P=5.5 Kbars, which probably reflect post-peak metamorphic re-equilibration. These conditions are similar to those derived for the late emplacement of the amphibolite sill at the North gold zone. The garnet zoning in the north gold zone reflects prograde garnet growth with peak P-T values obtained from rim compositions. This observation is consistent with garnet-biotite (Tables 4.3,4.4) and garnet-cordierite (Table 4.2) results.

Other Geothermobarometric Methods Applicable to the Atik Lake Terrane

Garnet-chlorite geothermometry

Garnet-chlorite pairs are present in some samples of the altered basalt. Matrix chlorite is pale green with a greenish-brown birefringence (X_{Mg}=0.47-0.71) and appears to be in textural equilibrium with the adjacent garnet and other silicates. Inclusions of chlorite in garnet cores have similar optical characteristics suggesting a prograde replacement of chlorite by garnet. The garnet-chorite geothermometer of Patrick and Evans (1989) based on Fe-Mg partitioning (*Appendix III*) yields an average T=553±36°C (Table 4.7), which is consistent with the garnet-biotite estimates.

Ferroactinolite - hedenbergite transition

Ferroactinolite and hedenbergite are common gangue minerals in the sulfide-arsenopyrite-bearing auriferous chert. This association suggests that actinolite was converted to hedenbergite during prograde dehydration reactions. Increases in modal amounts of hedenbergite in mineralized chert horizons down stratigraphy also favors this hypothesis.

The stability of ferroactinolite and tremolite were studied experimentaly by Ernst (1966). The breakdown of ferroactinolite to

TABLE 4.7 GARNET-CHLORITE GEOTHERMOMETRY

Sample		X_{Gr}	X_{Alm}	X_{Prp}	X_{Sps}	Grt Mg/Fe	Chl Mg/Fe	K_D	T (°C)
U-04	C	.058	.792	.137	.013	.173	1.243	.1391	530
	R	.054	.817	.089	.038	.109	1.039	.1044	444
	R	.054	.821	.098	.028	.119	1.168	.1022	438
U-10	C	.067	.802	.127	.003	.159	1.177	.1258	496
	R	.058	.774	.151	.014	.195	1.263	.1652	593
U-11	C	.046	.805	.113	.033	.140	1.130	.1239	494
	C	.046	.790	.096	.057	.121	1.115	.1088	456
	R	.056	.797	.137	.008	.172	1.097	.1564	572
	R	.057	.791	.135	.010	.171	1.097	.1557	570
U-14	C	.047	.806	.121	.019	.150	1.222	.1232	493
	R	.051	.833	.095	.021	.114	0.988	.1150	471
U-25	C	.046	.796	.129	.016	.162	0.988	.1644	593
	R	.089	.742	.058	.098	.078	0.899	.0863	393
U-31	C	.063	.789	.106	.040	.135	1.214	.1110	459
	R	.052	.790	.129	.022	.163	1.198	.1359	523

$K_D = (Mg/Fe)^{Grt} / (Mg/Fe)^{Chl}$

hedenbergite, fayalite and quartz ± magnetite, occurs at 543±10°C for PH_2O= 3.0±0.2 kbar under the QFM and WM fO_2 buffers, and that of pure Mg-endmember tremolite, at 890°C under similar conditions (Ernst, 1966). This reaction is somewhat pressure sensitive (dP/dT≈0.027 kbar/°C) and occurs at T=475°C for P= 1 kbar. The effect of Mn in this system was not investigated by Ernst. Since only Fe-rich hedenbergite was observed in the Kay Lake iron formation (between M2 and M3 in Fig. 3a, Bernier and MacLean (1989; chapter 3), the temperature (for a water-rich fluid) would probably has been higher than 543°C at P=3 Kbars toward the northern part of the belt. The preferred peak P-T estimates for the central and southern part of the belt are T=550°C, P=2.5 kbar.

The association hedenbergite, pyrrhotite and quartz at Kay Lake may have resulted from prograde dehyration and sulfidation of ferro-actinolite:

$$\text{Fe-Act} + 3/2\ S_2 = 2\ \text{Hd} + 4\ \text{Qtz} + 3\ \text{Po} + H_2O + 3/2\ O_2 \quad (11)$$

Sulfur diffusion probably occurred during prograde desulfidation of pyrite from adjacent mineralized chert.

Another hedenbergite reaction could have been (Haase, 1982):

$$\text{Gru} + 7\ \text{Cc} + 6\ \text{Qtz} = 7\ \text{Hd} + H_2O + 7\ CO_2 \quad (12)$$

The equilibrium T at P=2.5 kbar calculated with THERMOCALC (Holland and Powell, 1990) varies between 454°C (X_{H_2O}=0.9) and 530°C (X_{H_2O}=0.1). The addition of Mg to the system induces a displacement of the equilibrium towards lower T values. Calcite is an accessory phase in samples of both Mistuhe Island (U-32) and Kay Lake auriferous chert (U-31-03). In both, it coexists with hedenbergite, but grunerite is absent and was probably completely consumed, so that equilibrium T are minimum estimates and depend on fluid composition.

hedenbergite, fayalite and quartz ± magnetite, occurs at 543±10°C for PH_2O= 3.0±0.2 kbar under the QFM and WM fO_2 buffers, and that of pure Mg-endmember tremolite, at 890°C under similar conditions (Ernst, 1966). This reaction is somewhat pressure sensitive (dP/dT≈0.027 kbar/°C) and occurs at T=475°C for P= 1 kbar. The effect of Mn in this system was not investigated by Ernst. Since only Fe-rich hedenbergite was observed in the Kay Lake iron formation (between M2 and M3 in Fig. 3a, Bernier and MacLean (1989; chapter 3), the temperature (for a water-rich fluid) would probably has been higher than 543°C at P=3 Kbars toward the northern part of the belt. The preferred peak P-T estimates for the central and southern part of the belt are T=550°C, P=2.5 kbar.

The association hedenbergite, pyrrhotite and quartz at Kay Lake may have resulted from prograde dehyration and sulfidation of ferro-actinolite:

$$\text{Fe-Act} + 3/2\ S_2 = 2\ \text{Hd} + 4\ \text{Qtz} + 3\ \text{Po} + H_2O + 3/2\ O_2 \quad (11)$$

Sulfur diffusion probably occurred during prograde desulfidation of pyrite from adjacent mineralized chert.

Another hedenbergite reaction could have been (Haase, 1982):

$$\text{Gru} + 7\ \text{Cc} + 6\ \text{Qtz} = 7\ \text{Hd} + H_2O + 7\ CO_2 \quad (12)$$

The equilibrium T at P=2.5 kbar calculated with THERMOCALC (Holland and Powell, 1990) varies between 454°C (X_{H_2O}=0.9) and 530°C (X_{H_2O}=0.1). The addition of Mg to the system induces a displacement of the equilibrium towards lower T values. Calcite is an accessory phase in samples of both Mistuhe Island (U-32) and Kay Lake auriferous chert (U-31-03). In both, it coexists with hedenbergite, but grunerite is absent and was probably completely consumed, so that equilibrium T are minimum estimates and depend on fluid composition.

Dehydration of grunerite

The assemblage grunerite, fayalite, quartz, magnetite from BIF (U1804) in the central sedimentary sequence, is indicative of the breakdown of grunerite during prograde metamorphism. Because magnetite occurs essentially in quartz-grunerite bands, and fayalite forms distinct bands with quartz and grunerite, two simultaneous breakdown reactions of grunerite occurred at slightly different fO_2 conditions but close to QFM, i.e. that the assemblages reflect P-T conditions on both side of the invariant point. This suggests bed to bed variation in fO_2.

$$[Mt]\ 2\ Gru = 7\ Fa + 9\ Qtz + 2\ H_2O \quad (13)$$

$$[Fa]\ 3\ Gru + 7/2\ O_2 = 7\ Mt + 24\ Qtz + 3\ H_2O \quad (14)$$

Other reactions of interest are:

$$[W, Gru]\ 3\ Fa + O_2 = 2\ Mt + 3\ Qtz \quad (15)$$

$$[Qtz]\ 2\ Gru + 6\ Mt = 16\ Fa + 2\ H_2O + 3\ O_2 \quad (16)$$

A schematic Schreinemakers P-T (or P-μH_2O) diagram (Fig. 4.19A) was constructed for these reactions, which includes a degeneracy (reaction 15). Reaction (13) was modeled with THERMOCALC using sample U1804 mineral compositions which are very close to the Fe-end members. The univariant reaction (Fig. 4.19A) indicates that for $XH_2O=1$, the breakdown of grunerite occurs at 578°C for P=3 Kbars, which is in very good agreement with the previous P-T estimates. If $XH_2O=0.8$, the breakdown temperature for P=3 Kbars will be lowered to 559°C. These results agree with the experimental data of Fonarev et al. (1976, 1979), but not with those of Forbes (1977) and the calculations of Miyano and Klein (1986) who found a higher breakdown T=650-700°C. The discrepancy between these experimental data sets was reviewed by Gilbert et al., (1982) who concluded that it could not be easily resolved. However, the Atik Lake data and field evidence strongly favor those

Fig. 4.19. A) Pressure-temperature diagram for Atik Lake showing the dehydration eqilibrium of grunerite calculated in the FASH system using THERMOCALC (Powell and Holland, 1990). A schematic Schreinemakers diagram drawn for magnetite, quartz, fayalite and grunerite is shown in the inset. B) T-X section of phase relations on the Mg_7-Fe_7 join at fO_2 defined by QFM, from Popp et al. (1977a).

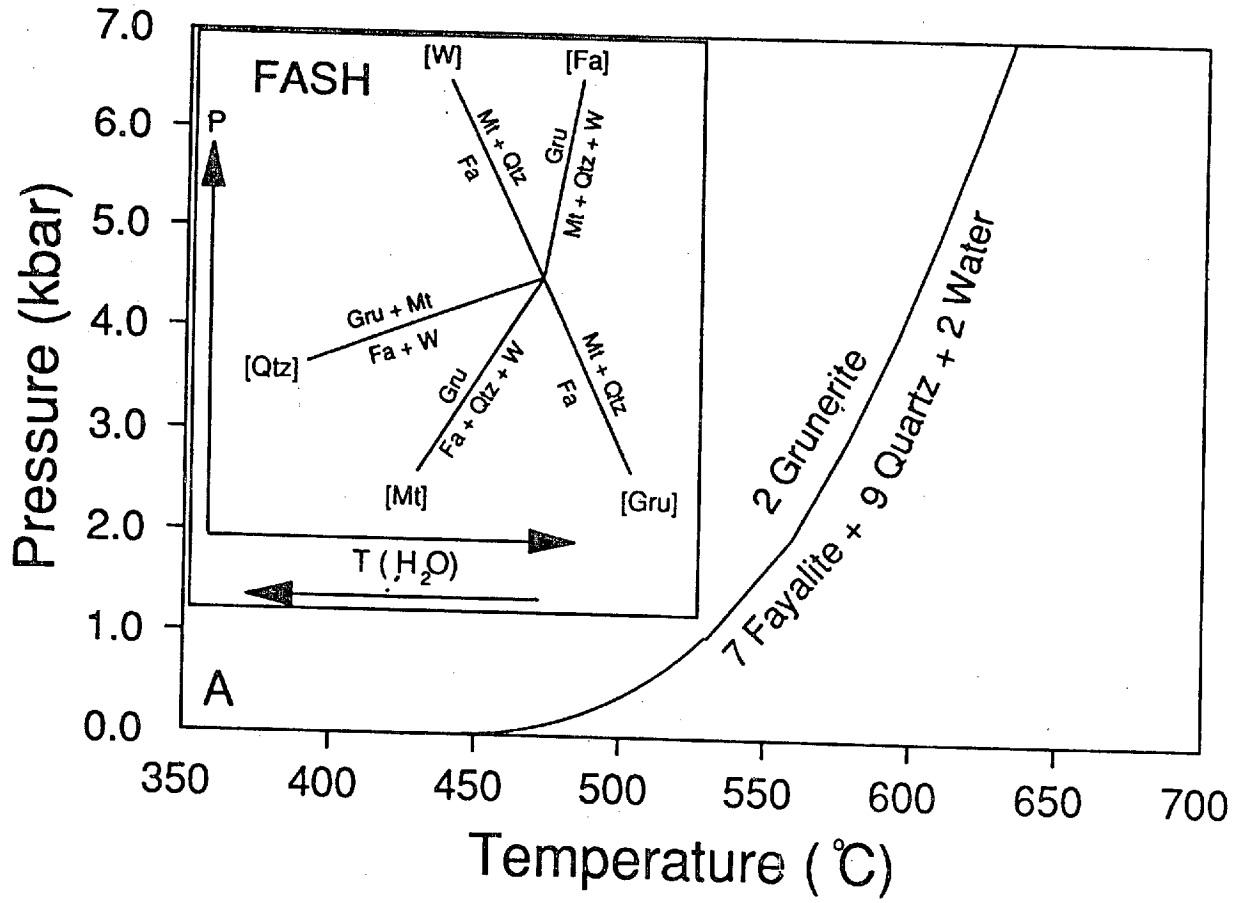
FASH
[W]
[Fa]
[Qtz]
[Mt]
[Gru]
P
T (H_2O)
Mt + Qtz
Fa
Gru
Mt + Qtz + W
Gru + Mt
Fa + W
Gru
Fa + Qtz + W
Mt + Qtz
Fa
2 Grunerite
7 Fayalite + 9 Quartz + 2 Water
A
Pressure (kbar)
Temperature (°C)
7.0
6.0
5.0
4.0
3.0
2.0
1.0
0.0
350
400
450
500
550
600
650
700

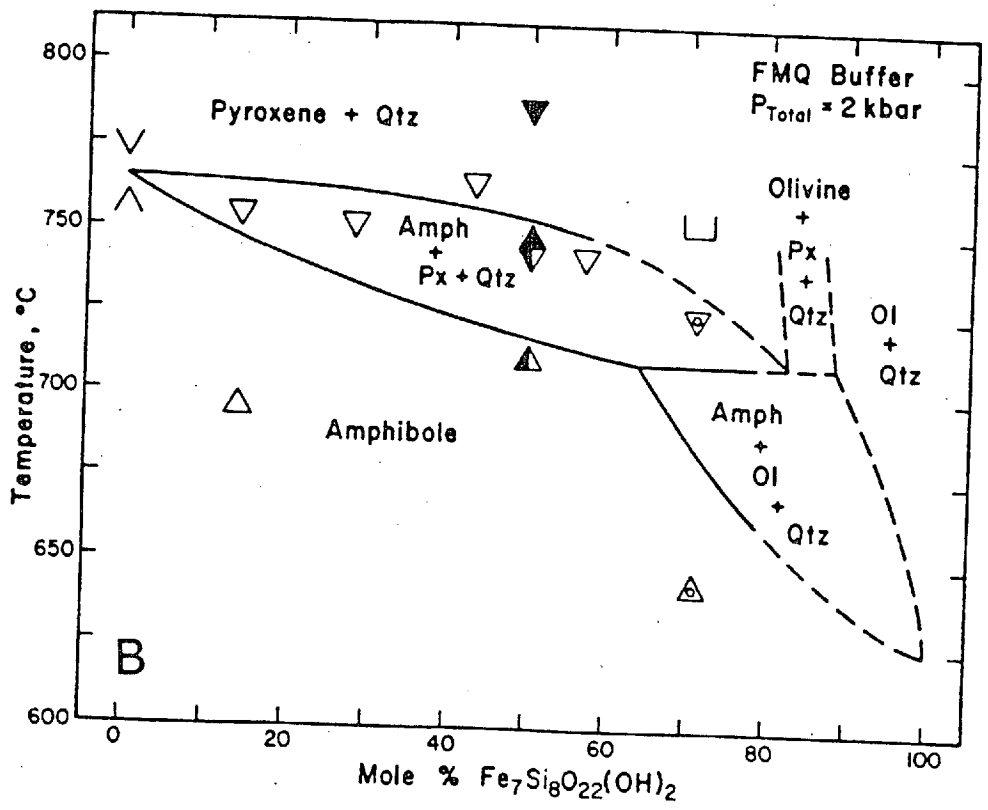
FMQ Buffer
P_{Total} = 2 kbar
Pyroxene + Qtz
Olivine + Px + Qtz
Ol + Qtz
Amph + Px + Qtz
Amphibole
Amph + Ol + Qtz
B
Temperature, °C
Mole % $Fe_7Si_8O_{22}(OH)_2$
800
750
700
650
600
0
20
40
60
80
100

of Fonarev et al. (1976, 1979).

Popp et al. (1977a) studied the stability of grunerite-anthophyllite compositions with the QFM, HM and NNO fO_2 buffers at P=2 Kbar. Their lower limit for the stability of amphibole, olivine and quartz is poorly constrained and estimated at about 625°C for the pure Fe-end members (Fig. 4.19B). The data from Atik BIF suggests the limit lies at a lower T.

A sample of BIF (U1805) with quartz, fayalite and pyrrhotite, from drill hole U18, occurs 3 m from sample U1804 (Qtz, Fa, Gru, Mt), suggesting that the grunerite-out isograd was crossed. The presence of pyrrhotite suggests bed to bed variations of fO_2-fS_2 conditions. A combined sulfidation-devolatilisation reaction may explain the mineral assemblage in U1805.

$$Gru + 1/2\ S_2 = 3\ Fa + 1\ Po + 5\ Qtz + H_2O + 1/2\ O_2 \quad (4.17)$$

Local variations in oxidation state and speciation of metamorphic fluid over distances of centimetre(s) to metre(s) scale have frequently been reported in metamorphosed BIF (Popp et al., 1977; Haase, 1982; Miyano and Klein, 1986). The role of metamorphic fluids is addressed later in chapter 6.

Diarsenide, sulpharsenides and antimonide geothermometry

Arsenopyrite and Löllingite

Arsenopyrite is disseminated in altered basalts on Mistuhe Island and forms porphyroblasts in mineralized chert (≤5mm). Large arsenopyrite crystals contain inclusions of actinolite, hedenbergite and quartz. Arsenopyrite has a wide compositional range (Fig. 4.20) that covers the experimentally studied range of Kretschmar and Scott (1976) who proposed a geothermometer based on its As contents and the fS_2 buffering assemblage. Some arsenopyrite grains in the altered basalts are As-rich (Type 1) and coexist with löllingite ($FeAs_2$), pyrrhotite and rare gersdorffite (NiAsS); the arsenopyrite contains up to 4%

Fig. 4.20. Atik Lake arsenopyrite and löllingite compositions in at%. A) (Fe+Ni+Co)-As-S ternary diagram. B) Close-up on the arsenopyrite compositional field in A. C) Arsenopyrite compositions on an As-S diagram.

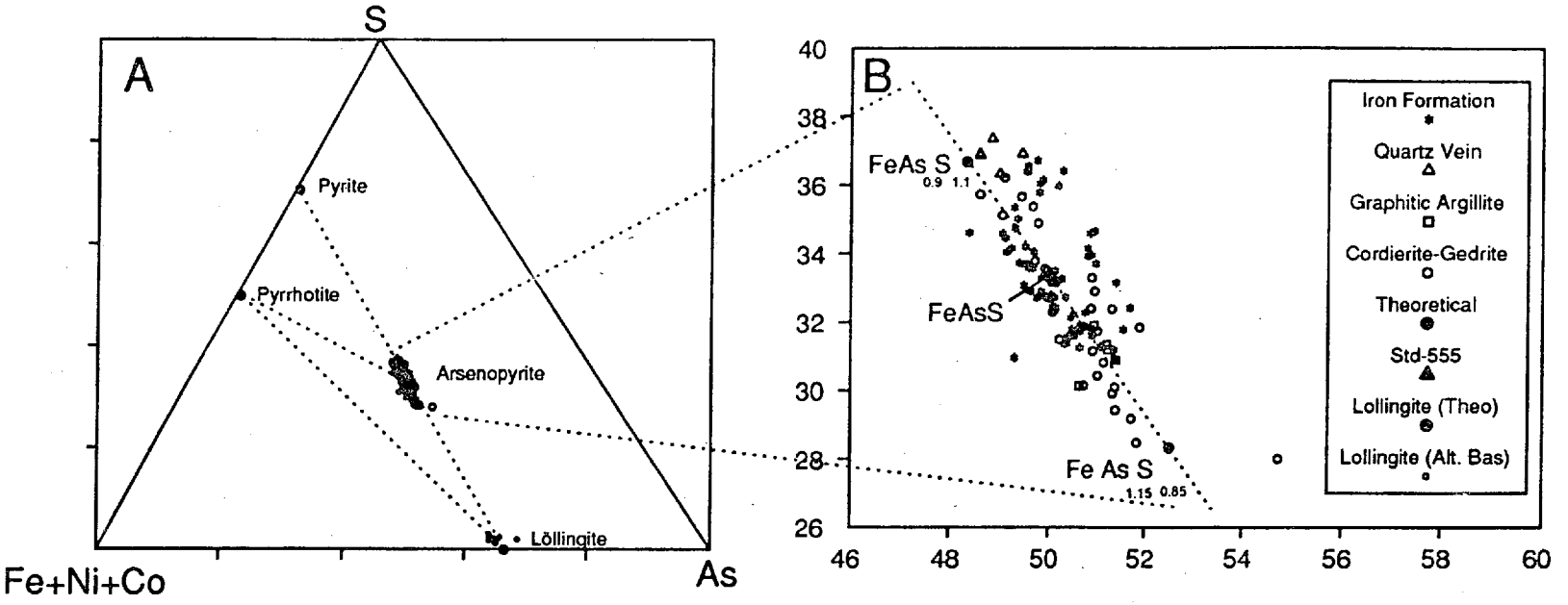
A
S
Fe+Ni+Co
As
Pyrite
Pyrrhotite
Arsenopyrite
Löllingite
B
FeAs S
0.9 1.1
FeAsS
Fe As S
1.15 0.85
Iron Formation
Quartz Vein
Graphitic Argillite
Cordierite-Gedrite
Theoretical
Std-555
Lollingite (Theo)
Lollingite (Alt. Bas)
40
38
36
34
32
30
28
26
46
48
50
52
54
56
58
60

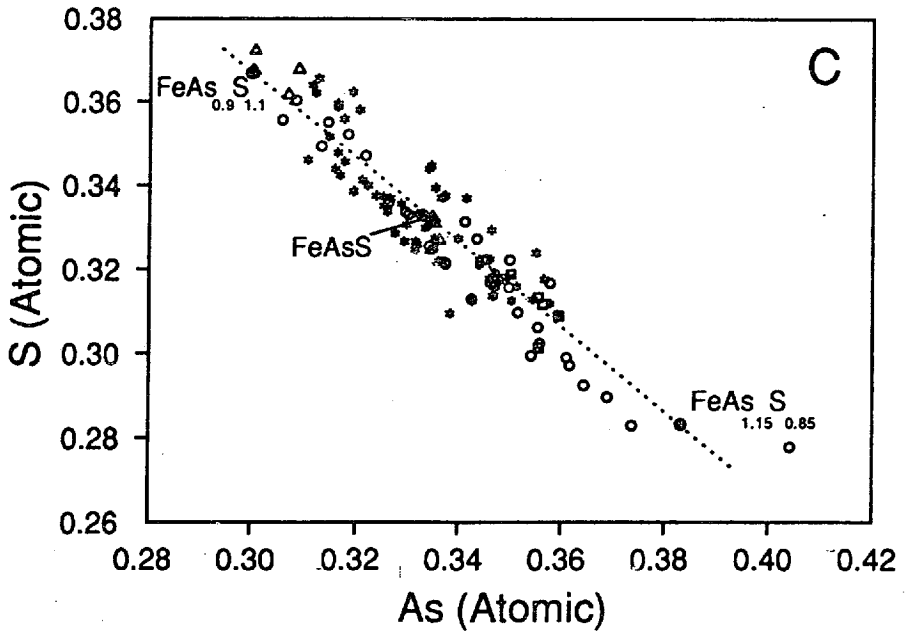
C
FeAs S
0.9 1.1
FeAsS
FeAs S
1.15 0.85
S (Atomic)
As (Atomic)
0.38
0.36
0.34
0.32
0.30
0.28
0.26
0.28
0.30
0.32
0.34
0.36
0.38
0.40
0.42

Co, 2.5% Ni and 0.5% Sb. This constrasts with arsenopyrite (Type 2) in mineralized chert and graphitic argillite which coexists with pyrrhotite ± pyrite. This arsenopyrite is As-poor and does not contain detectable Co, Ni and Sb. In order for the arsenopyrite compositions to plot along the pyrite-löllingite join, Ni and Co in the analyses must be added to Fe (Fig. 4.20). Antimony concentrations are low and the effect of its substitution for As is minimal.

Löllingite is exclusively observed in altered basalts as euhedral crystals and elongated laths ≤2mm (Plate 3.6). It contains 3.0-6.6% Co, 6.8-11.9 %Ni, <0.5% Sb and 1.1-3.3% S, and plots on the löllingite-pyrrhotite tie-line (Figs. 3.7A, C).

Sharp et al. (1985) have re-evaluated the arsenopyrite geothermometer and estimated the effect of pressure. They concluded that its application is valid for greenschist and amphibolite facies conditions. However, independent P-T estimates are necessary to properly interpret arsenopyrite compositions. Sharp et al. (1985) have calculated that arsenopyrite (As=33.3%) may coexist with pyrrhotite and pyrite up to 550°C at 5 kbar, a shift up temperature from T=491°C for P=1bar (Fig. 4.21).

Arsenopyrite coexisting with löllingite and pyrrhotite (U43B) inclusions in garnet has an average As%=37.5 which yields a maximum T=600°C. Altered basalt sample U-04 contains arsenopyrite, löllingite and pyrrhotite for which independent garnet-biotite and garnet-chlorite temperatures are available (543 and 530°C respectively). The arsenopyrite composition, As%=36 indicates a slightly lower T=500°C (Fig. 4.21). The wide range of arsenopyrite compositions (Figs. 4.20, 4.21) for identical sulfide-arsenide assemblages may be attributed in part to local variations in fS_2 or re-equilibration during cooling. The effect of Co-Ni-Sb substitution in arsenopyrite and löllingite

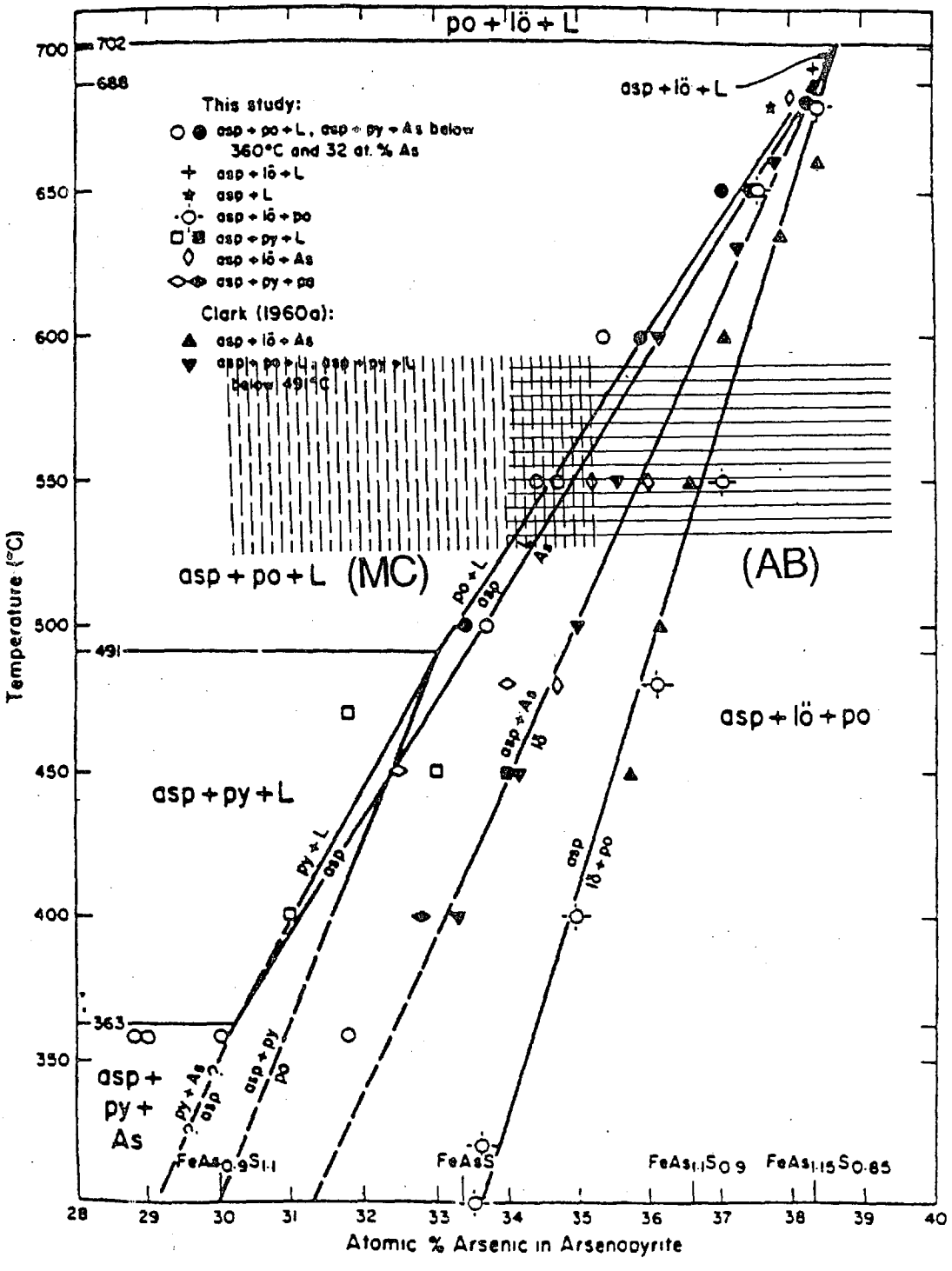

Fig. 4.21. Temperature-composition diagram with arsenopyrite-buffered boundaries, from Kretchmar and Scott (1976). The ranges of arsenopyrite compositions in the mineralized chert (MC) and the altered basalt (AB) are shown in the two hatched boxes.

is not well known and could affect the stability fields of these minerals. Two contrasting arsenopyrite compositions (As, Co, Ni-rich and As-Co-Ni poor) in altered basalts suggest two episodes of arsenopyrite crystallisation.

The presence of chlorite, pyrrhotite, pyrrhotite-löllingite, pyrrhotite-arsenopyrite and löllingite-arsenopyrite inclusions in garnet from altered basalts indicate that at least some of the sulfide-arsenide are pre-metamorphic in origin.

Gersdorffite and Ullmanite

Gersdorffite (NiAsS) is rare and was only identified as small (≤0.05mm) euhedral grains in a sample of altered basalt (U10B). It coexists with löllingite, pyrrhotite and arsenopyrite, and has the formula ($Ni_{.52}Fe_{.27}Co_{.21}As_{1.1}S_{.9}$) with S-As substitution within the limits defined by Yund (1962). Very little is known about substitution in the Co-Ni-Fe-As-S system. A miscibility gap between gersdorffite (NiAsS) and cobaltite (CoAsS) was outlined experimentally by Klemm (1965) with complete miscibility above 550°C for 35% NiAsS. The effect of pressure on the solvus is not known. The Atik Lake gersdorffite has a homogenous composition, indicating crystallisation above the solvus but effect of Fe-substitution is not known.

Ullmanite (NiSbS) is very rare at Atik Lake and is clearly exotic to the gold-sulfide-arsenide mineralization, as it forms coronas on arsenopyrite and pyrrhotite and only occurs in the fuchsite schist on Mistuhe Island. It contains 1.1% Fe, 0.5% Co and 2% As and can be termed arsenian ullmanite (Bayliss, 1969). Ullmanite is the only reported mineral belonging to the Ni-Sb-S system (Williams and Kullerud, 1968). A miscibility gap between ullmanite and wylliamite (CoSbS) has been recently proposed by Dobbe (1991) to occur at T<550°C, where ullmanite would be on the high temperature side of the

phase diagram. Ullmanite formation at Atik Lake is interpreted to be retrograde and related to shearing and formation of the fuchsite schist.

Multi-equilibrium P-T calculations

Internally consistent thermodynamic databases such as those of Berman (1988), Powell and Holland (1988), and Holland and Powell (1990), and their respective computer software packages (PTAXSS and THERMOCALC), provide means to quantitatively model P-T using mineral assemblages compositions. Thermodynamic data for Fe and Mg end-members are not available for all phases of interest (e.g., gedrite), nor do these databases contain Mn and Zn end-members. Thus full modelling for the multicomponent system is not possible; modelling in the FMASH system will be used as a first approximation. The method for multi-equilibrium calculations using GEO-CALC is outlined by Berman (1991). The P-T estimates are obtained by considering mineral equilibrium intersections in P-T space calculated for all possible end-members minerals forming an asssemblage. Under ideal conditions, (perfect thermodynamic data, no analytical errors, all minerals equilibrated under the same P-T conditions) all equilibria should intersect as one point in P-T space. This method provides more realistic but less constrained P-T estimates than arbitrary single geothermobarometer pairs (Lieberman and Petrakakis, 1991).

Two samples (U04 and U12; Table 4.1A) from the same outcrop have contrasting bulk rock compositions and mineral assemblages and are suitable for use of the multi-equilibrium method. The resulting P-T diagrams are shown in Figure 4.22. The activity models used are shown in the *Appendix III*. Both samples have comparable zones of intersecting equilibrium (outlined by the dark triangles) in P-T space. The scatter is most likely related to

Fig. 4.22. Multi-equilibrium P-T diagrams calculated using GEO-CALC (Brown et al., 1988) for two contrasting rock compositions at Atik Lake. A) P-T diagram calculated among the components of garnet, chlorite, biotite, cordierite, muscovite and quartz in the system CKFMASH adjusted for mineral compositions in sample U-04. B) P-T diagram calculated among the components of garnet, andalusite, biotite, staurolite, cordierite, and quartz in the system CKFMASH adjusted for mineral compositions in sample U-12. Both stable and metastable equilibria are shown.

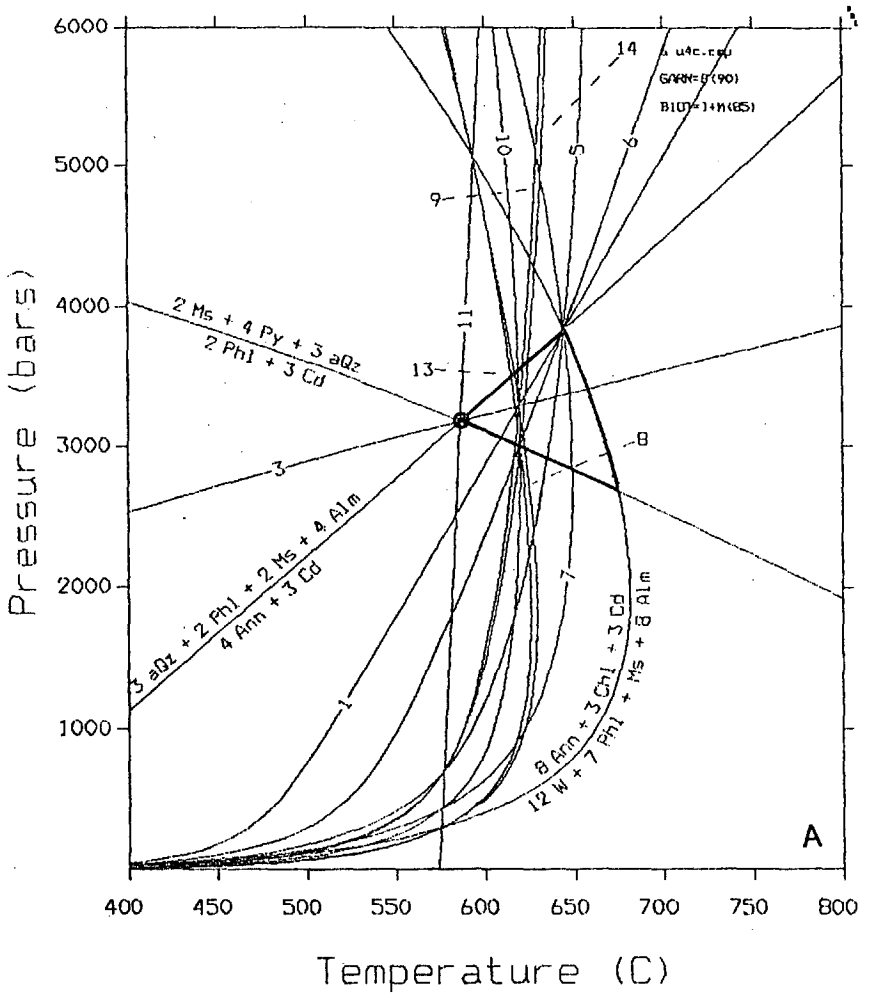

REACTION LIST (U-04)
Assemblages on the left are stable on the:
high side of the Y-axis variable, or the
high side of the X-axis variable for vertical reactions

1): 7 aQz + 4 Ms + 2 Chl + 4 Alm = 4 Ann + 5 Cd + 8 W

2): 3 aQz + 2 Phl + 2 Ms + 4 Alm = 4 Ann + 3 Cd

3): 3 aQz + 2 Py + 2 Ms + 2 Alm = 2 Ann + 3 Cd

4): 12 W + 7 Phl + Ms + 8 Alm = 8 Ann + 3 Chl + 3 Cd

5): 3 aQz + Ms + 3 Chl + 4 Ann = 4 Alm + 5 Phl + 12 W

6): Chl + Ms + 2 aQz = 4 W + Phl + Cd

7): 4 Alm + 4 Phl + 8 W = aQz + Cd + 2 Chl + 4 Ann

8): 12 W + 7 Py + Ms + Alm = Ann + 3 Chl + 3 Cd

9): 3 aQz + Ms + 3 Chl + Alm = Ann + 5 Py + 12 W

10): 8 W + 4 Py = 2 Chl + Cd + aQz

11): Alm + Phl = Py + Ann

12): 2 Ms + 4 Py + 3 aQz = 2 Phl + 3 Cd

13): Ms + 8 Py + 12 W = Phl + 3 Cd + 3 Chl

14): 3 Chl + Ms + 3 aQz = 12 W + 4 Py + Phl

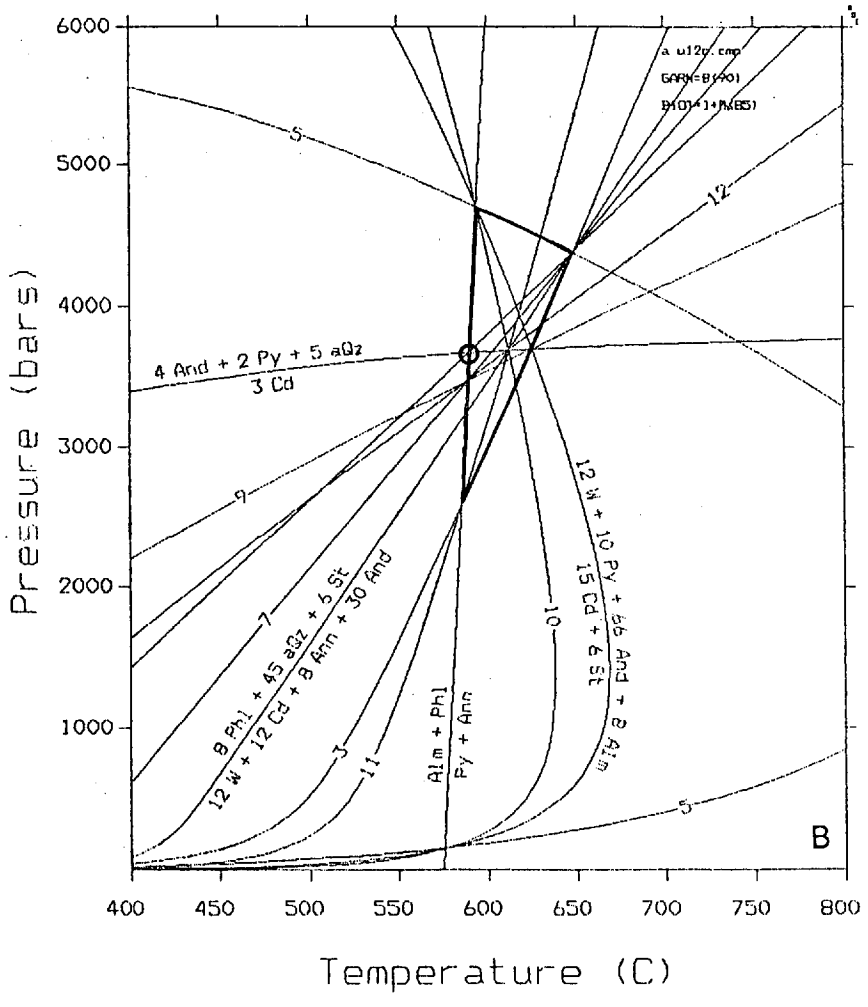

REACTION LIST (U-12)
Assemblages on the left are stable on the:
high side of the Y-axis variable, or the
high side of the X-axis variable for vertical reactions

1): 2 Alm + 4 And + 2 Phl + 5 aQz = 3 Cd + 2 Ann

2): 4 And + 2 Py + 5 aQz = 3 Cd

3): 6 St + 25 aQz = 8 Alm + 46 And + 12 W

4): Alm + Phl = Py + Ann

5): 10 Ann + 15 Cd + 6 St = 12 W + 10 Phl + 66 And + 18 Alm

6): 8 Phl + 45 aQz + 6 St = 12 W + 12 Cd + 8 Ann + 30 And

7): 12 St + 165 aQz + 46 Phl + 30 Alm = 46 Ann + 69 Cd + 24 W

8): 12 W + 10 Py + 66 And + 8 Alm = 15 Cd + 6 St

9): 12 St + 165 aQz + 46 Py = 16 Alm + 69 Cd + 24 W

10): 66 And + 8 Ann + 18 Py + 12 W = 6 St + 8 Phl + 15 Cd

11): 6 St + 25 aQz + 8 Phl = 46 And + 8 Ann + 8 Py + 12 W

12): 12 St + 165 aQz + 30 Py + 16 Phl = 16 Ann + 69 Cd + 24 W

analytical error and the activity models used. Another explanation may reside in different closing temperatures of thermometers and sloped barometers involving different mineral exchanges in a common assemblage (Ghent et al., 1988). The preferred P-T for sample U04 is from the intersection of equilibria 2, 3, 11, and 13 (Fig. 4.22A) which yields T=584°C, P=3.1 Kbar. For sample U12, the intersection of equilibria 2 and 4 yields T=590°C, P=3.4 Kbar (Fig. 4.22B), and the intersection of equilibria 4, 7, 9 and 12 produces a similar T and slighly lower P=3.2 Kbar. These peak P-T estimates are in excellent agreement with previous P-T estimates for Atik Lake.

The following reaction implying the breakdown of gedrite and staurolite is pressure sensitive and of particular interest for Atik Lake altered basalts (see assemblages for samples U24, U26, U39, U12B, U41C1, U41C2 in Table 4.1A):

$$2.5\ St + 3.0\ Ged + 10.2\ Qtz = Pl + 5.5\ Crd + 3.1\ Grt + 5.5\ H_2O \quad (4.18)$$

This reaction occurs at a pressure of about 4 kbars at T=550°C which is about 1 Kbar higher than the peak P estimates and results in differences between Atik Lake mineral compositions and those used by Spear and Rumble (1986) for their petrogenetic grid (Fig. 4.15B).

Other geothermobarometric methods applicable to the Némiscau Terrane

Isograds intersection

A rare case of intersecting isograds (And-Sil, St-out) is present in the northeast part of the Némiscau belt (Fig. 4.2). The staurolite-out isograd is only definable east of a NW-SE fault in Lac Sillimanite area. Staurolite porphyroblasts are found in Fe-rich metapelite coexisting with garnet, staurolite, biotite, muscovite, quartz and plagioclase, north of the staurolite-out isograd. South of it, muscovite is virtually absent and only staurolite occurs as inclusions in garnet. The divariant assemblages

cordierite-biotite-garnet and garnet-biotite-sillimanite are the most common south of the isograds where cordierite occurs in more Mg-rich bulk rock compositions. There are two possible reaction mechanisms to explain the breakdown of staurolite:

1) a terminal discontinuous reaction for standard Fe-rich metapelite (from Spear and Cheney, 1989):

1.0 St + 0.40 Ms + 3.8 Qtz = 0.9 Grt + 8.4 AS + 0.40 Bt + 2.0 H_2O

where AS=andalusite or sillimanite (4.19)

This reaction corresponds to the staurolite-out isograd (Fig. 4.2) and is valid for metapelite assemblages containing excess quartz and muscovite.

2) a terminal discontinuous reaction for more Mg-rich pelitic rocks without muscovite (Winkler, 1979):

$$St + Qtz = Grt + Crd(nH_2O) + AS + (X-n)\ H_2O \quad (4.20)$$

Reaction (4.20) is not balanced because all the phases were not found in a single thin section. Biotite in these Mg-rich rocks would be stabilized by the additional component K_2O. Note that, after the disappearance of one phase, these reactions become continuous in producing divariant three phase field AFM assemblages.

A petrogenetic grid for metapelites in the system KFMASH has been recently calibrated by Spear and Cheney (1989). The originality of their grid relies in their calculated garnet compositions along KFMASH univariant equilibria and intervening divariant regions (Fig. 4.23A). According to their grid, the intersection of reaction (4.19) with the andalusite-sillimanite boundary (Fig. 4.23) gives values of T and P equal to 590°C and 2.5 kbar respectively. However, the andalusite-sillimanite boundary is the most uncertain in P-T space owing to the very small ΔV, ΔS and ΔG of the reaction (Powell and Holland, 1990). As emphasized by Salje (1986), Kerrick, (1987) and by Powell

Fig. 4.23. Petrogenetic grids for metapelite (A) from Spear and Cheney (1989) and orthoamphibolite (B) from Hudson and Harte (1985). A) The P-T conditions inferred from the intersection of the staurolite-out and andalusite-sillimanite isograds in the Némiscau belt are shown in the stippled circle (T≈590°C, P≈ 2.5 kbar). B) P-T diagram showing the stability field (stippled area) outlined for the assemblage garnet-cordierite-anthophyllite common in Fe-rich cordierite-anthophyllite rocks at Némiscau.

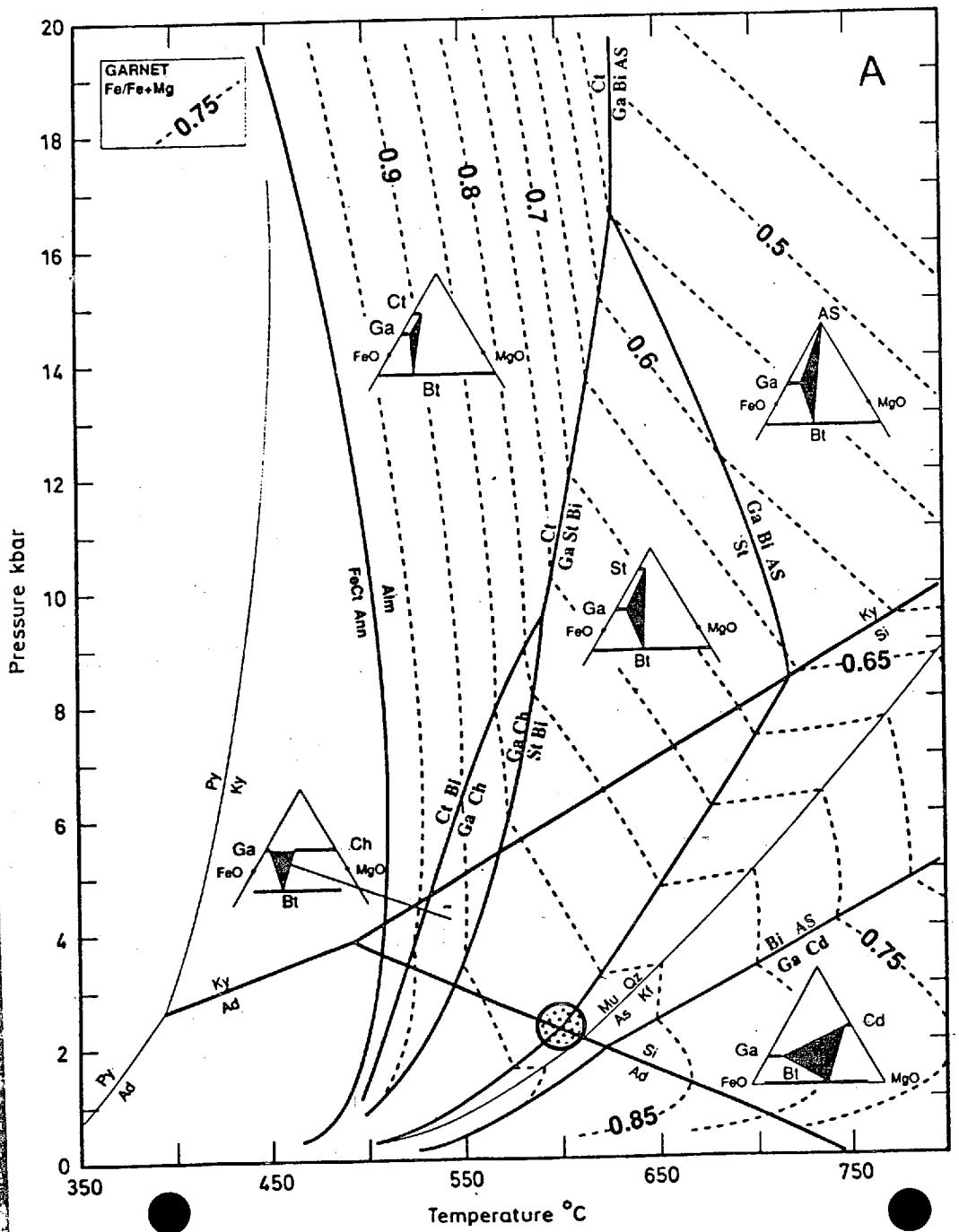
A
GARNET
Fe/Fe+Mg
0.75
0.9
0.8
0.7
0.6
0.5
0.65
0.75
0.85
Ct Ga Bi AS
Ct Ga St Bi
St Ga Bi AS
Ct Bi Ga Ch
Ga Ch St Bi
Bi AS Ga Cd
Fe Ct Ann
Alm
Py Ky
Py Ad
Ky Ad
Ky Si
St Si
Ad Si
Mu Qz As Ky
Ct Ga Bt
AS Ga FeO MgO Bt
St Ga FeO MgO Bt
Ga Ch FeO MgO Bt
Cd Ga FeO MgO Bt
Pressure kbar
Temperature °C
350
450
550
650
750
0
2
4
6
8
10
12
14
16
18
20

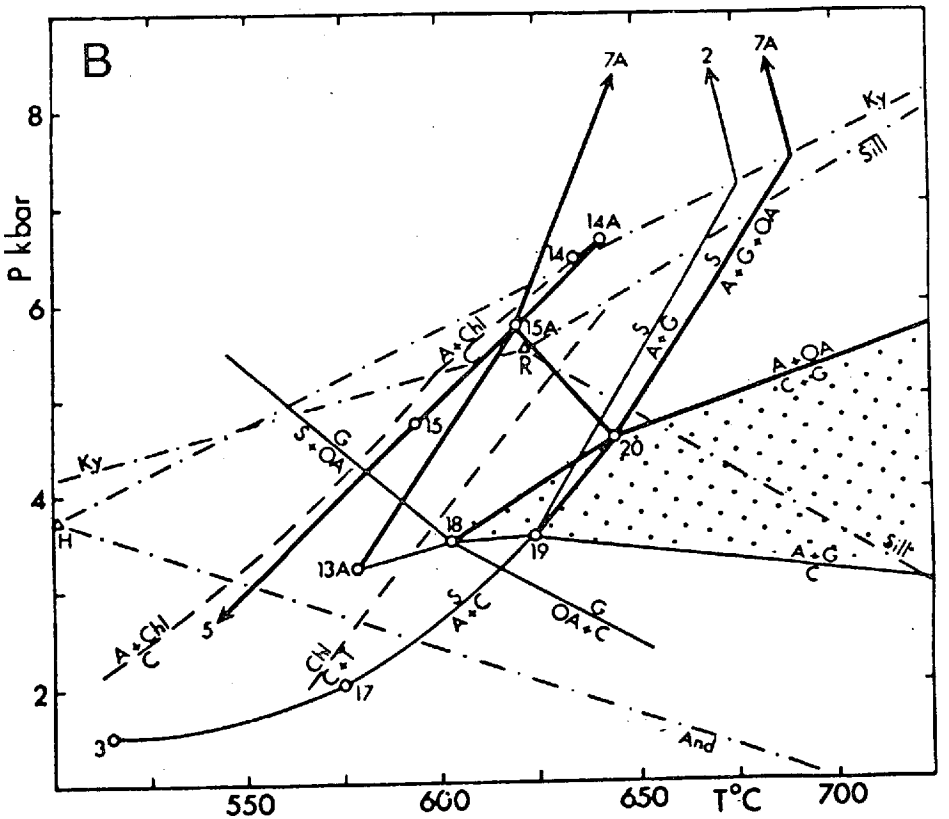
B
P kbar
T°C
550
600
650
700
2
4
6
8
7A
2
7A
Ky
Sill
14A
14
15A
R
A+Chl
S A+G+OA
S A+G
A+OA
C G
15
20
S+OA
G
Ky
18
19
13A
A+G
C
5
S A+C
G OA+C
A+Chl C
Chl A+C
17
3
And

and Holland (1990), there are likely to be many triple points that result from the differences in the energetics of coarse grained sillimanite and fibrolite. The Némiscau isograds are based on coarse grained andalusite and sillimanite, as fibrolite is present in both zones and is probably metastable. If the triple point of Bohlen et al. (1991) is used, the intersection would be at about T=620°C, P=3.2 Kbar, which is more consistent with the garnet-biotite temperatures for the andalusite and sillimanite bearing metapelites (Table 4.4).

One sample (S-30) of metapelite contains zincian staurolite relicts surrounded by gahnite, muscovite, cordierite and chlorite. This coronitic texture most likely implies the breakdown of zincian staurolite, which probably reacted with Mg-rich biotite in a more complex chemical system involving additional components (Zn and Mn). Local availability of zinc may have stabilized staurolite to higher T and P than the Fe-rich conterpart. The breakdown of zincian staurolite will be discussed in the Montauban section.

The FMASH divariant assemblage anthophyllite-garnet-cordierite observed in samples N-34B, N-35 and N-39 is compatible with the peak P-T estimates (650°C, 4.5 kbar) as deduced from the petrogenetic grid of Hudson and Harte (1985). This divariant assamblage occurs on both side of the univariant reaction St = Sil + Grt + Crd (Fig. 4.23B).

Multi-equilibrium P-T calculations

The multi-equilibrium technique (Berman, 1991) has been applied to two samples of metapelites from the Lac Sillimanite area. One sample is from the staurolite-andalusite zone (V4811) and another from the staurolite-out sillimanite zone (S-30) which contains staurolite relicts. The resulting P-T diagrams are shown in figure 4.24. Interestingly, the series of reactions

involve the SGAM (Quartz=S, Garnet, Aluminosilicate, Mica) thermobarometer, proposed by McMullin et al. (1991). The SGAM intersecting point occurs along the upper side of the triangle enclosing the reactions intersections (Fig. 4.24). The P-T values defined by the centre of the triangle of intersections for the andalusite zone are T=575°C and P=2.5 Kbar (Fig. 4.24A), whereas for the sillimanite zone, they are T=650°C and P=4.5 Kbar (Fig. 4.24B). These values are in excellent agreement with those obtained from the other geothermobarometer and are close to the andalusite-sillimanite boundary (Fig. 4.24) of Bohlen et al. (1991). The almandine content of garnet coexisting with biotite in the andalusite zone is 0.86 (V4811) and 0.78 (S30) for the sillimanite zone. These values are also in good agreement with the garnet X_{Fe} contours in P-T space (Fig. 4.23) proposed by Spear and Cheney (1989) In summary, the peak metamorphic conditions for the Némiscau belt range from T≈600°C at P≈2.5 Kbars for the andalusite-staurolite zone to T≈650°C at P≈4.5 Kbar for the sillimanite zone. The cordierite-anthophyllite rocks were formed under the metamorphic conditions of the sillimanite zone.

Other Geothermobarometric Methods Applicable to the Montauban Terrane

Sphalerite geobarometry

A corrected version of the sphalerite-hexagonal pyrrotite geobarometer (Bryndzia et al., 1990) has been applied on sphalerite bearing ore samples from the north gold zone (Table 4.8). Their geobarometric expression is a linear regression of P (Kbar) versus $\log(\gamma_{FeS}^{Sph})$, where $\gamma_{FeS}^{Sph}=(a_{FeS}^{Po}/X_{FeS}^{Sph})$ which is not a true activity coefficient. This pseudo-activity coefficient is temperature dependent, as is a_{FeS}^{Po}, but independent of pressure (Froese and Gunter, 1976; Bryndzia et al., 1990). Thus, independent temperature estimates

Fig. 4.24. Multi-equilibrium P-T diagrams calculated using GEO-CALC (Brown et al., 1988) for two metapelites at Némiscau. A) P-T diagram calculated among the components of garnet, biotite, staurolite, andalusite, muscovite and quartz in the system CKFMASH adjusted for mineral compositions in sample V4811 (andalusite zone). B) P-T diagram calculated among the components from the same minerals as in A, except that sillimanite is present instead of andalusite; adjusted for mineral compositions in sample S-30 (sillimanite zone). Both stable and metasable equilibria are shown.

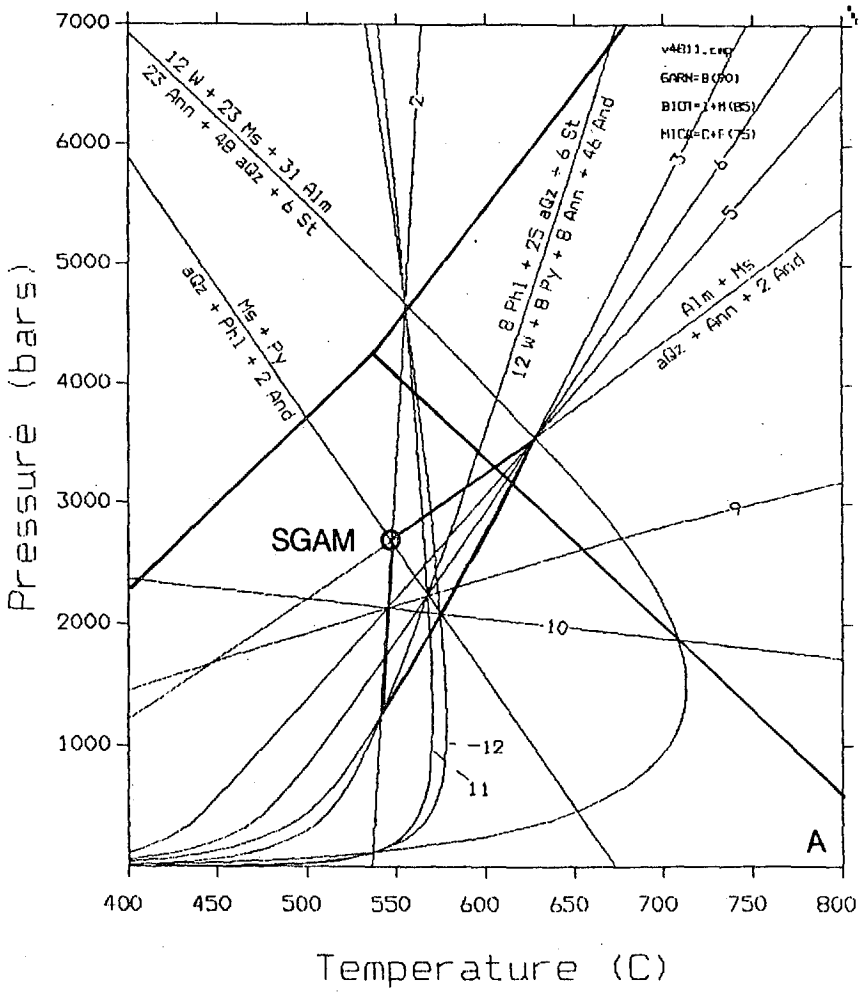

REACTION LIST (V4811)
Assemblages on the left are stable on the:
high side of the Y-axis variable, or the
high side of the X-axis variable for vertical reactions

1): Alm + Ms = aQz + Ann + 2 And

2): Phl + Alm = Ann + Py

3): 25 aQz + 6 St = 12 W + 46 And + 8 Alm

4): Ms + Py = aQz + Phl + 2 And

5): 17 Alm + 25 Ms + 6 St = 12 W + 25 Ann + 96 And

6): 8 Ms + 17 aQz + 6 St = 12 W + 8 Ann + 62 And

7): 12 W + 23 Ms + 31 Alm = 23 Ann + 48 aQz + 6 St

8): 8 Phl + 25 aQz + 6 St = 12 W + 8 Py + 8 Ann + 46 And

9): 25 Ms + 17 Py + 6 St = 12 W + 17 Phl + 8 Ann + 96 And

10): 25 Ms + 25 Py + 6 St = 12 W + 25 Phl + 96 And + 8 Alm

11): 12 W + 31 Py + 23 Ms + 8 Ann = 31 Phl + 48 aQz + 6 St

12): 12 W + 23 Py + 23 Ms + 8 Alm = 23 Phl + 48 aQz + 6 St

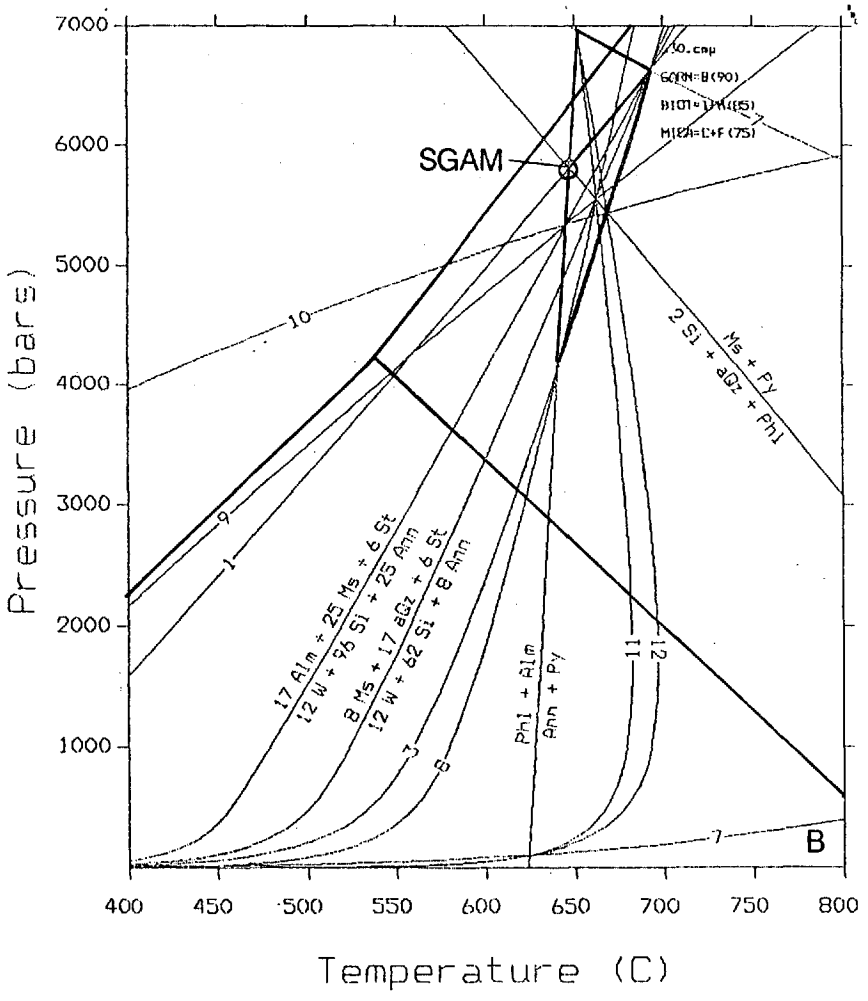

REACTION LIST (S-30)
Assemblages on the left are stable on the:
high side of the Y-axis variable, or the
high side of the X-axis variable for vertical reactions

1): Alm + Ms = 2 Si + aQz + Ann

2): Phl + Alm = Ann + Py

3): 25 aQz + 6 St = 12 W + 46 Si + 8 Alm

4): Ms + Py = 2 Si + aQz + Phl

5): 17 Alm + 25 Ms + 6 St = 12 W + 96 Si + 25 Ann

6): 8 Ms + 17 aQz + 6 St = 12 W + 62 Si + 8 Ann

7): 23 Ann + 48 aQz + 6 St = 12 W + 23 Ms + 31 Alm

8): 8 Phl + 25 aQz + 6 St = 12 W + 46 Si + 8 Py + 8 Ann

9): 25 Ms + 17 Py + 6 St = 12 W + 96 Si + 17 Phl + 8 Ann

10): 25 Ms + 25 Py + 6 St = 12 W + 96 Si + 25 Phl + 8 Alm

11): 12 W + 31 Py + 23 Ms + 8 Ann = 31 Phl + 48 aQz + 6 St

12): 12 W + 23 Py + 23 Ms + 8 Alm = 23 Phl + 48 aQz + 6 St

are needed to use the geobarometer. The preferred peak T=620°C was used to calculate a_{FeS}^{Po} from pyrrhotite microprobe data using the Froese and Gunter (1976) FeS activity formulation (see below). An average core pressure of 7.3 ± 0.5 Kbars at T=620°C and rim pressure of 6.5 ± 0.5 Kbars (assuming rims re-equilibrated at T=550°C) were obtained (Table 4.8) and are somewhat higher than previous pressure determinations (Tables 4.2, 4.5, 4.6).

The range of sphalerite compositions coexisting with pyrrhotite and pyrrhotite + pyrite ± chalcopyrite in the north gold zone is shown in figure 4.25A. The equilibrium sphalerite composition for the assemblage sphalerite + pyrrhotite + pyrite was modeled at P=6.5 kbar and T=620°C. Froese and Gunter's (1976) thermodynamic expressions were used to calculate a_{FeS}^{Po} (0.5268) and $\log fS_2$ (-1.306) for pyrrhotite coexisting with sulfur vapor and pyrite. The activity of FeS in sphalerite (a_{Fes}^{Sph} =0.1926) was solved by using the free energy expression of Hutcheon (1978) for equilibrium (4.21) and the thermal expansions and compressibilities data of Scott (1973) (see *Appendix III*for details on calculations) to solve for the pressure integral ($\int_1^p \Delta Vs$).

$$FeS^{Po} = FeS^{Sp} \quad (4.21)$$

The values of a_{FeS}^{Sp} were calculated as a function of X_{FeS}^{Sp} (Fig. 4.25B) using the program ACTCOEF (written by LRB) derived from Hutcheon's (1978) equations. This yields a value of X_{FeS}^{Sp}=0.1252. Where pyrite is absent (the most general situation), sphalerite and pyrrhotite compositions will vary as a function of $f(S_2)$ under fixed P-T. Sphalerite compositions coexisting with pyrrhotite and rutile have been calculated. The average composition (X_{FeS}^{Sph}=0.145±0.007) indicates a $\log fS_2$ value of -2.20 at T=620°C, P=6.5 Kbar (see Fig. 6.2C, Chapter 6).

TABLE 4.8 SPHALERITE-PYRRHOTITE GEOBAROMETRY
(Montauban North Gold Zone)

Samples		X_{FeS}^{Po}	X_{FeS}^{Sph}	a_{FeS}^{Po}	$\dot{\gamma}_{FeS}^{Sph}$	P (kb)
E-5-25	C	.878	.148	.573	3.872	7.9
	C	.871	.148	.541	3.663	7.2
	R	.863	.138	.507	3.670	7.2
	R	.866	.138	.519	3.766	7.6
	R	.867	.148	.509	3.438	6.5
	R	.876	.155	.545	3.512	6.7
E-6-29	C	.873	.149	.552	3.719	7.4
	C	.867	.151	.528	3.505	6.7
	R	.869	.144	.536	3.725	7.4
	R	.867	.150	.525	3.493	6.6
	R	.865	.150	.518	3.465	6.5
	R	.869	.145	.537	3.713	7.4
F-3-19	C	.855	.130	.473	3.633	7.1
	R	.859	.131	.490	3.723	7.4
	R	.856	.130	.479	3.692	7.3

Fig. 4.25. Sphalerite compositions at Montauban. A) Histogram of sphalerite compositions at the north gold zone. B) Mole fraction (X_{FeS}, X_{ZnS}) versus AFeS in sphalerite diagram. Note the deviation from ideal mixing. The calculated value of X_{FeS}^{Sph} (0.1252) is for sphalerite coexisting with pyrrhotite and pyrite at T=620°C and P=6.5 kbar.

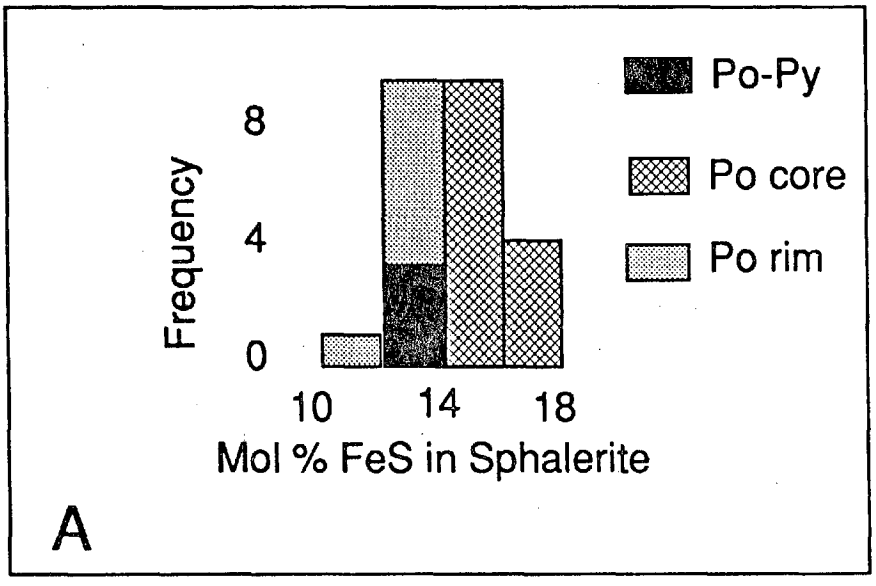
Po-Py
Po core
Po rim
Frequency
8
4
0
10
14
18
Mol % FeS in Sphalerite
A

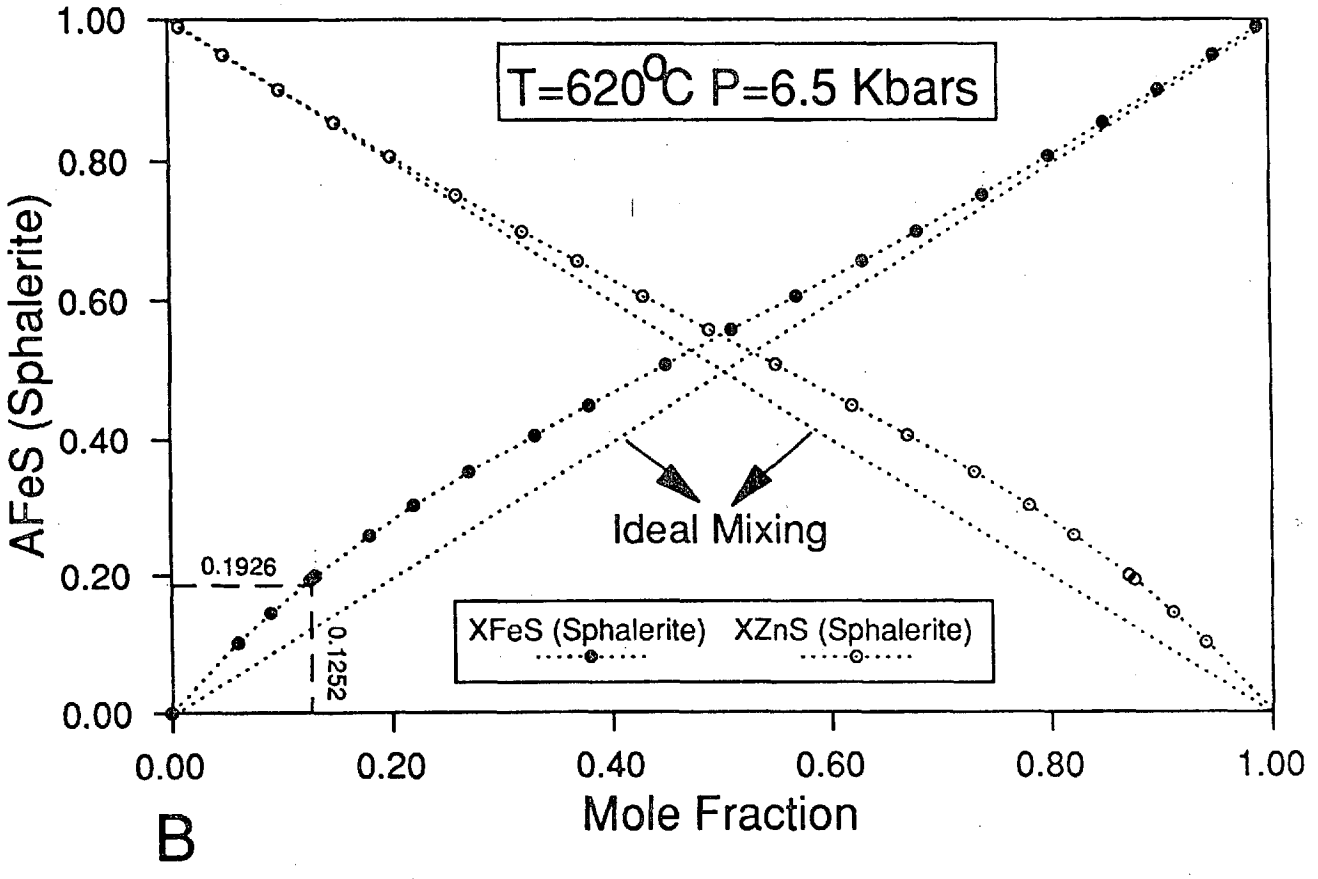
T=620°C P=6.5 Kbars
AFeS (Sphalerite)
1.00
0.80
0.60
0.40
0.20
0.00
0.1926
0.1252
Ideal Mixing
XFeS (Sphalerite)
XZnS (Sphalerite)
0.00
0.20
0.40
0.60
0.80
1.00
Mole Fraction
B

Multi-equilibrium P-T calculations

Metapelites

A sample of metapelite (MQ-10) from the Notre-Dame-des-Anges area contain garnet, biotite, fibrolite, K-feldspar, quartz and muscovite. The biotite flakes and fibrolite define a crenulated S-1 schistosity crosscut by late muscovite. Euhedral garnet porphyroblasts (2-4 mm) have overgrown the biotite. The sample is from a small band of metasediment squeezed between granodiorite and granite intrusions. The application of the multi-equilibrium technique using rim mineral compositions from sample MQ-10 produced a zone of equilibria intersections restricted by a lozenge shaped box (Fig. 4.26A) with T=660 ± 50 °C and P=4 ± 1 Kbar. The SGAM thermobarometer intersection lies along the low-P boundary of the P-T box (Fig. 4.26A).

The garnet-hornblende-plagioclase P-T lozenge shaped box is shown for comparison. The highest T-estimates for the Montauban area are from these metapelites close to felsic intrusions. The higher T and lower P are best explained in terms of a superimposed contact metamorphism. Contact metamorphic effects on metapelites regionally metamorphosed to the amphibolite facies might not be readily recognizable in the field and require detailed geothermobarometry and structural analysis around the intrusions, which has never been done and is outside the scope of this thesis.

Mine Sequence Rocks

The rocks from the mine sequence are characterized by a complex mineralogy that relates mainly to a wide range of bulk rock compositions. The additional components Zn and Mn complicate the chemographic analysis and introduce multivariancy by increasing mineral solid-solutions and stabilizing certain phases (gahnite, staurolite). The presence of coronitic textures,

Fig. 4.26. Multi-equilibrium P-T diagrams calculated using GEO-CALC (Brown et al., 1988) for Montauban rocks. A) P-T diagram calculated among the components of garnet, biotite, sillimanite, K-feldspar, muscovite and quartz in the system CKFMASH adjusted for mineral compositions in sample MQ-10 (regional metapelite). SGAM is the quartz, garnet, aluminosilicate, and muscovite geothermobarometer of McMullin et al. (1991). B) P-T diagram calculated among the components of anthophyllite, staurolite, spinel, hydrated cordierite, biotite and quartz in the system CKFMASH adjusted for mineral compositions in sample D211 (cordierite-anthophyllite rock). The garnet-plagioclase-hornblende P-T box is shown for comparison. C) P-T diagram for the same mineral assemblage as in B, except that a dry cordierite was used. Note that the cordierite-spinel-quartz barometers fall outside the Grt-Pl-Hlb box. Both stable and metasable equilibria are shown.

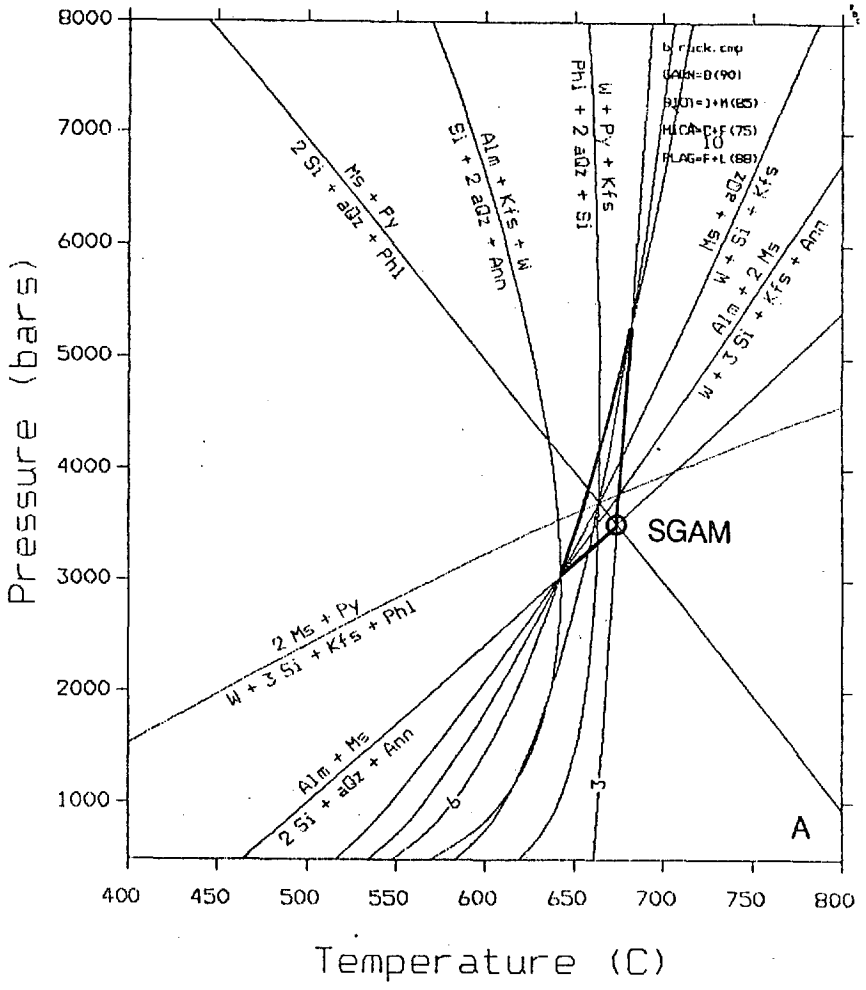

REACTION LIST (MQ-10)
Assemblages on the left are stable on the:
high side of the Y-axis variable, or the
high side of the X-axis variable for vertical reactions

1): Alm + Ms = 2 Si + aQz + Ann

2): Alm + Kfs + W = Si + 2 aQz + Ann

3): Phl + Alm = Ann + Py

4): Alm + 2 Ms = W + 3 Si + Kfs + Ann

5): Ms + aQz = W + Si + Kfs

6): 3 aQz + Ms + Ann = Alm + 2 Kfs + 2 W

7): Ms + Py = 2 Si + aQz + Phl

8): W + Py + Kfs = Phl + 2 aQz + Si

9): 2 Ms + Py = W + 3 Si + Kfs + Phl

10): Ms + Phl + 3 aQz = 2 W + Py + 2 Kfs

REACTION LIST (MD211)

Assemblages on the left are stable on the:
high side of the Y-axis variable, or the
high side of the X-axis variable for vertical reactions

1): 10 Ath + 14 St = 38 W + 70 Sp + 185 aQz + 56 Hc

2): 2 Sp + 5 aQz = Cd

3): 5 aQz + 2 Hc = fCd

4): 10 Ath + 4 Sp + 14 St = 38 W + 56 Hc + 37 Cd

5): 10 Ath + 14 St = 38 W + 10 aQz + 56 Hc + 35 Cd

6): 10 Ath + 18 Hc + 14 St = 38 W + 70 Sp + 37 fCd

7): 10 Ath + 14 St = 38 W + 70 Sp + 45 aQz + 28 fCd

8): 70 Ann + 30 Ath + 42 St = 114 W + 555 aQz + 70 Phl + 378 Hc

9): 42 St + 56 Phl + 30 Ath = 56 Ann + 555 aQz + 378 Sp + 114 W

10): 6 Hc + 2 Phl + 15 aQz = 3 Cd + 2 Ann

11): 2 Ann + 15 aQz + 6 Sp = 2 Phl + 3 fCd

12): 10 Ath + 14 St = 38 W + 52 Hc + 2 fCd + 35 Cd

13): 10 Ath + 14 St = 38 W + 52 Sp + 28 fCd + 9 Cd

14): 10 Ath + 130 aQz + 14 St = 38 W + 28 fCd + 35 Cd

15): 30 Ath + 4 Phl + 42 St = 114 W + 156 Hc + 111 Cd + 4 Ann

16): 30 Ath + 56 Phl + 42 St = 114 W + 156 Sp + 111 Cd + 56 Ann

17): 42 St + 390 aQz + 56 Phl + 30 Ath = 56 Ann + 189 Cd + 114 W

18): 70 Ann + 30 Ath + 42 St = 114 W + 70 Phl + 156 Hc + 111 fCd

19): 6 Ann + 10 Ath + 14 St = 38 W + 52 Sp + 6 Phl + 37 fCd

20): 70 Ann + 30 Ath + 390 aQz + 42 St = 114 W + 70 Phl + 189 fCd

21): 3 Cd + 2 Ann = 3 fCd + 2 Phl

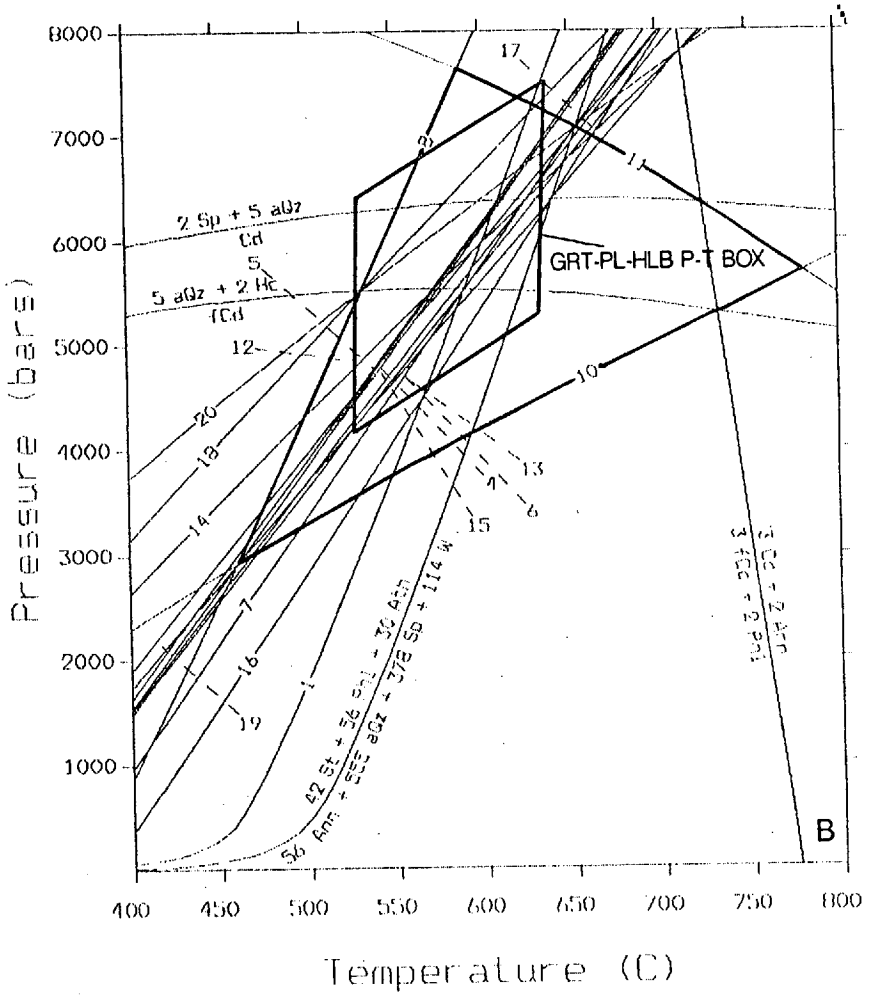
Pressure (bars)
Temperature (C)
GRT-PL-HLB P-T BOX
2 Sp + 5 aQz
Cd
5
5 aQz + 2 Hc
fCd
12
10
20
18
14
13
15
6
7
16
19
1
17
11
B
8000
7000
6000
5000
4000
3000
2000
1000
400
450
500
550
600
650
700
750
800

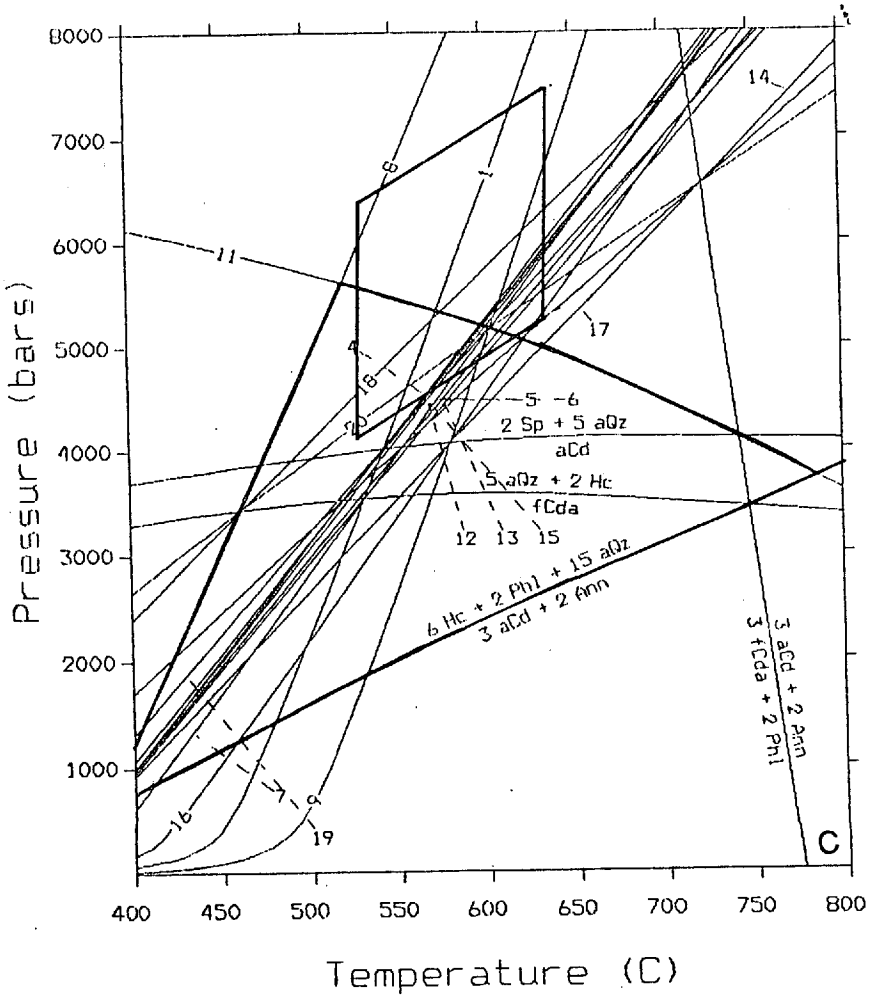
Pressure (bars)
Temperature (C)
14
8
1
11
17
18
20
5
6
2 Sp + 5 aQz
aCd
5 aQz + 2 Hc
fCda
12
13
15
6 Hc + 2 Phl + 15 aQz
3 aCd + 2 Ann
3 aCd + 2 Ann
3 fCda + 2 Phl
16
19
C
8000
7000
6000
5000
4000
3000
2000
1000
400
450
500
550
600
650
700
750
800

implying the breakdown of zincian staurolite, will be discussed below.

A sample of cordierite-anthophyllite rock (D211) containing zincian staurolite, gahnite, cordierite, biotite, anthophyllite and quartz was used to estimate the P-T conditions of the corona formation by using rim compositions and reduced Fe-Mg end-members mineral activities. The resulting multi-equilibrium analysis for X_{H_2O}=1 and a fully hydrated cordierite is presented in figure 4.26B. Most equilibria intersections are within a large triangle defined by reactions 8, 10 and 11 (see reaction list, Fig. 4.26B). Most intersections occur near the center of the triangle at T=625°C and P=6 Kbar, where reactions 1 and 9 have the steepest dP/dT slopes and intersect the cordierite-spinel-quartz barometers. Note that the intersections occur within the garnet-hornblende-plagioclase P-T box. However, when a dry cordierite model is used, the triangle defined by reactions 8, 9 and 10 increases dramatically and equilibria intersection occur outside the Grt-Hlb-Pl box (Fig. 4.26C). Thus, equilibria involving a highly hydrated cordierite yield P-T results that are consistent with Grt-Hlb-Pl geothermobarometry.

Coronitic muscovite around kyanite

The coronitic texture involving muscovite rimming kyanite (previously described, Fig. 4.5D) most likely formed as a result of a continuous reaction between Mg-rich biotite and kyanite to produce muscovite and cordierite:

$$8\ Ky + 7\ Qtz + 2\ Bt + 3nH_2O = 3\ Crd\text{-}(nH_2O) + 2\ Ms \quad (4.22)$$

The invariant point and univariant equilibria involving biotite, aluminosilicate, hydrous cordierite, muscovite, quartz and water has been computed for the endmember KFASH and KMASH systems using the program THERMOCALC (Holland and Powell, 1990), and is shown in figure 4.27. The

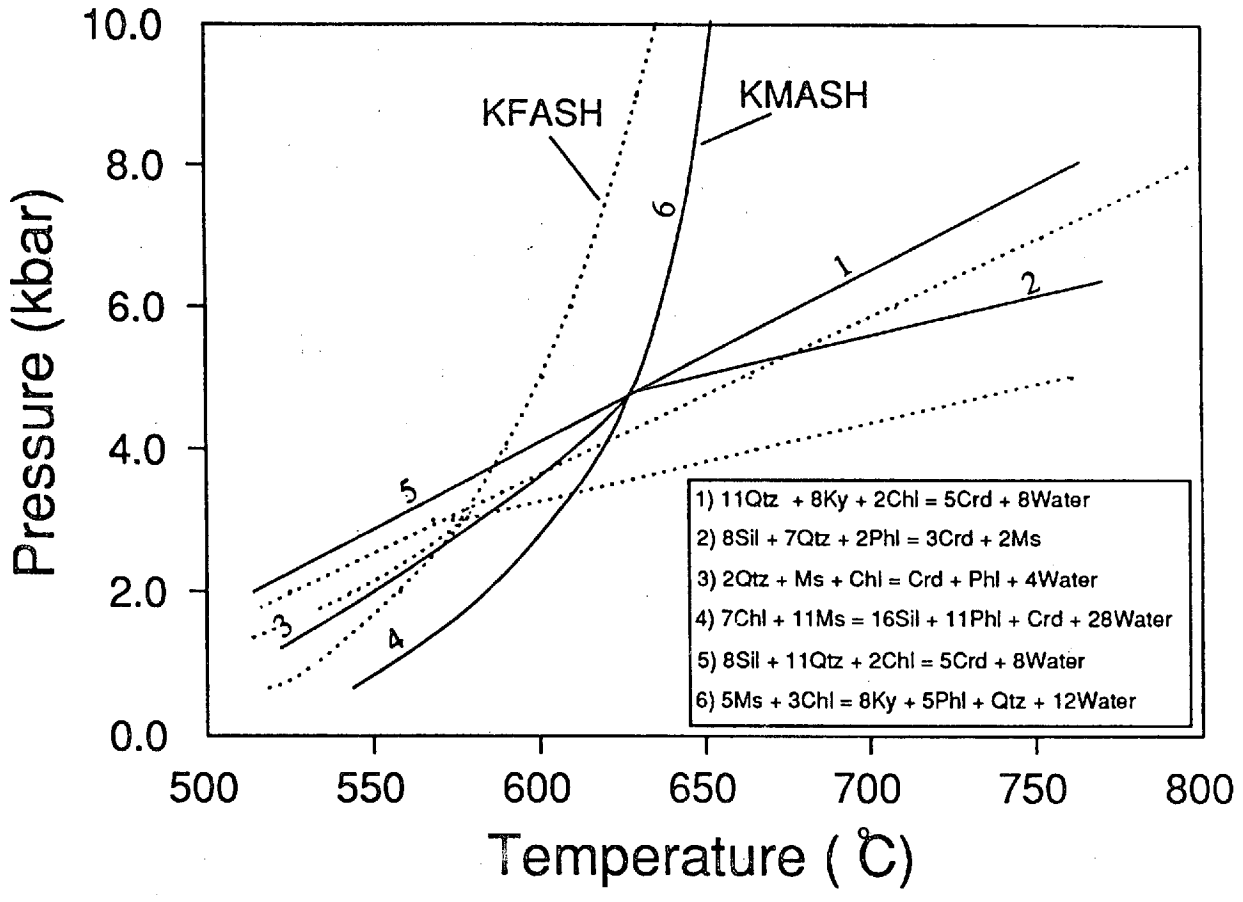

Fig. 4.27. Pressure-temperature diagram calculated using THERMOCALC (Powell and Holland, 1990) for equilibria involving chlorite, biotite, muscovite, cordierite, kyanite and quartz in the KFASH and KMASH systems.

invariant point for the KMASH system occurs at T=627°C and P=4.6 Kbar. If the program GEO-CALC (Brown et al, 1988; Berman, 1988) is used to compute mineral equilibria in the KMASH, system a pressure of P=5.8 Kbar is obtained for the invariant point. This difference may be attributable to the different thermodynamic model used for the hydration of cordierite (model of Kurepin, 1985 in THERMO; model of McPhail et al., 1990 in GEO-CALC).

Reaction (4.22) is strongly pressure dependent. The coronitic texture suggests attainment of the reaction boundary during decompression when P became lower than 6 Kbar at T≈625°C, which agrees with the previous P-T estimates. Because the rocks of the north gold zone are very Mg-rich, the reaction in the KFMASH system will occur close to the KMASH endmember reaction, but still within the area outlined by the KFASH and KMASH endmember reactions.

Coronitic textures and the breakdown of zincian-staurolite

Zincian staurolite- and sulfide- bearing cordierite-anthophyllite rocks at the north gold zone (Table 4.1C) are characterized by a ubiquitous coronitic texture involving gahnite and cordierite rimming staurolite which is never observed in contact with anthophyllite (Figs. 4.28 A, B) (Bernier, 1985; Bernier et al., 1987). A rim of bytownite is sometimes present between the zincian-staurolite, gahnite and cordierite (Fig. 4.28C, D). Euhedral Mn-bearing garnet porphyroblasts are frequently observed in cordierite replacing staurolite (Fig. 4.28E). In advanced stages of breakdown, the zincian staurolite may form a symplectitic texture with gahnite in cordierite, whereas in some extreme cases, the zincian staurolite has completely disappeared, leaving vermicular gahnite intergrowths with cordierite (Fig. 4.28F).

Fig. 4.28. Photographs of coronitic textures in cordierite-anthophyllite rocks from the Montauban north gold zone. A) Hand specimen of cordierite-anthophyllite rock with orange-brown zincian staurolite (St). Note that the staurolite is armoured with cordierite (Crd) and is not in contact with anthophyllite (Ath). B) Zincian staurolite (St) rimmed by gahnite (Gah) and cordierite (Crd), in transmitted light (left) and crossed nicols (right) C) Vermicular gahnite (Gah) and staurolite (St) surrounded by plagioclase (Pl) and cordierite (Crd). Note the partial replacement of plagioclase by sericite (Ser) and cordierite by chlorite (Chl). D) Zincian staurolite rimmed by gahnite, sericitized plagioclase and cordierite. Note the garnet (Grt) in cordierite. The opaque mineral is pyrrhotite. E) Garnet (Grt) and cordierite (Crd) in zincian staurolite (St) armoured by a thin rim of gahnite (Gah). F) Vermicular gahnite (Gah) with relict grains of zincian staurolite and pyrrhotite in cordierite adjacent to anthophyllite (Ath) and biotite (Bt). The fields of view are: 0.85 mm for B, 3.3 mm for C, D, and 2.6 mm for E, F.

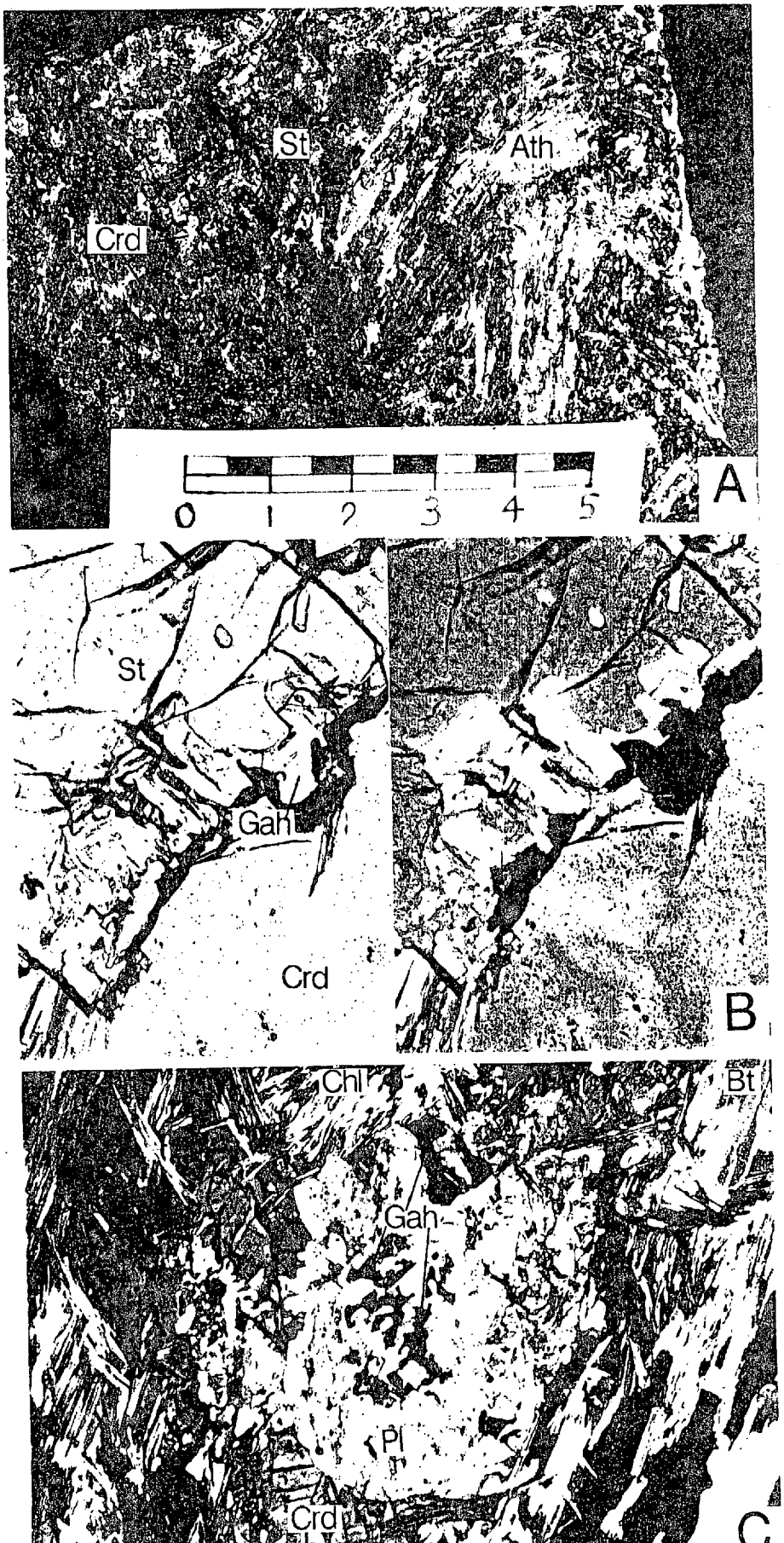
St
Ath
Crd
0 1 2 3 4 5
A
St
Gah
Crd
B
Chl
Bt
Gah
Pl
Crd
C

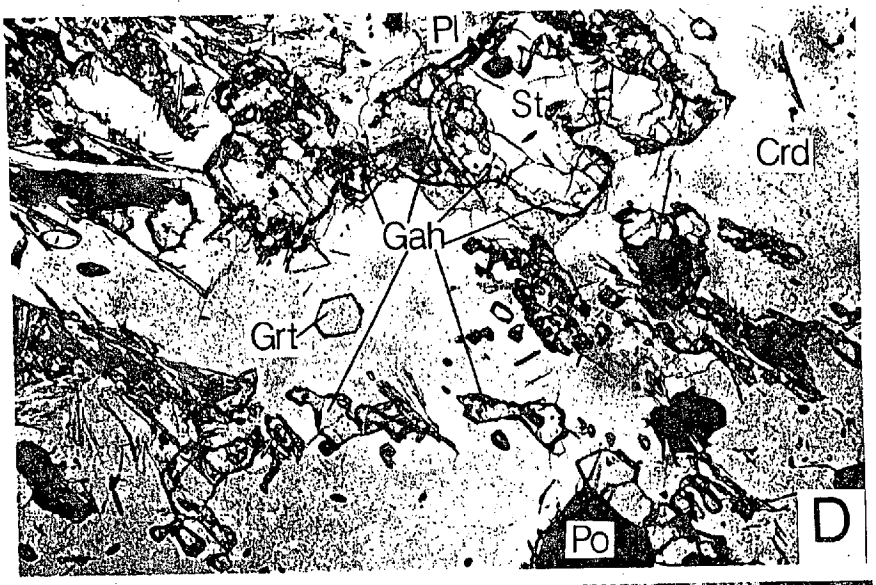
Pl
St
Crd
Gah
Grt
Po
D

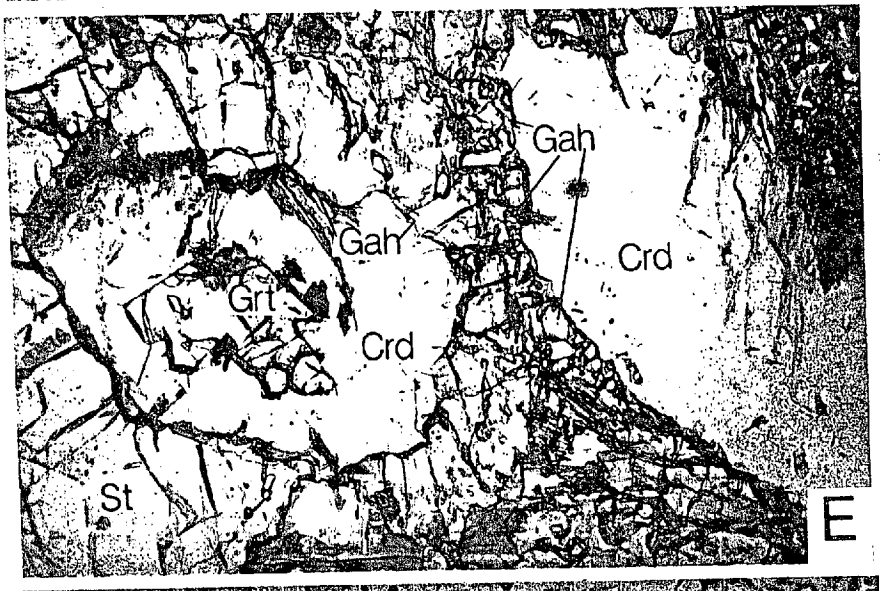
Gah
Gah
Crd
Grt
Crd
St
E

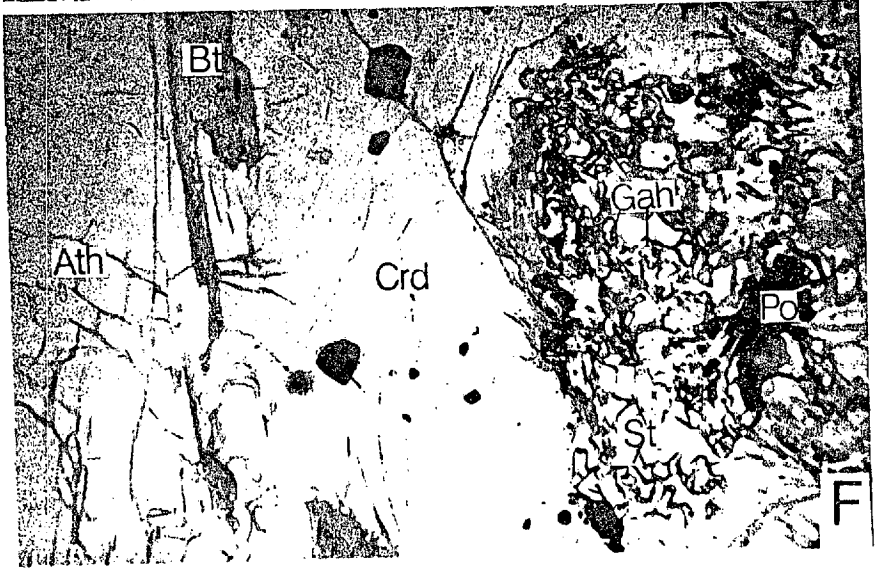
Bt
Gah
Ath
Crd
Po
St
F

Similar textures involving gahnite and zincian staurolite have been described in other cordierite-anthophyllite (gedrite) rocks (Robinson and Jaffe, 1969; Atkin, 1978; James et al, 1978; Stoddard, 1979; Treloar et al., 1981; Schumacher and Robinson, 1987). Froese (1969) may have been dealing with similar textures for the cordierite-gedrite rocks of the Coronation Mine as he reports: " *Staurolite occurs in some cordierite-anthophyllite rocks* (the anthophyllite is actually a gedrite, his Table 1) *as corroded grains by cordierite, or more rarely by garnet. These grains are interpreted as armored relics, implying that staurolite is not compatible with anthophyllite. ... Green spinel is a common accessory mineral.*" Schumacher and Robinson (1987) have interpreted zincian staurolite to have overgrown gahnite grains in the aluminous enclaves of the cordierite-gedrite rocks of the Ammonoosuc volcanics. Zincian staurolite riming gahnite has also been reported by Moore and Reid (1989) as resulting from a retrograde hydration of the granulitic assemblage quartz-gahnite-sillimanite, in rocks from the Namaqualand Metamorphic Complex, South Africa.

Zincian staurolite and gahnite porphyroblasts in apparent textural equilibrium have been reported by Spry and Scott (1986) and Zaleski et al. (1991), but they are not in cordierite-anthophyllite rocks. Zaleski et al. (1991) have attributed the presence of the assemblage anthophyllite-staurolite-gahnite at the Linda deposit, Snow-Lake, Manitoba, to the stabilizing effect of zinc. Harley (1985) explained the presence of staurolite coexisting with quartz under granulite facies conditions as an effect of the presence of zinc. It is well known that residual staurolite concentrates Zn (Guidotti, 1970; Albee, 1972; Ashworth, 1975; Griffen and Ribbe, 1973).

Zinc shows a strong preference for tetrahedrally-coordinated cation sites

available in hercynite and staurolite (Albee, 1972; Stoddard, 1979; Griffen, 1981; Miyake, 1985; Holdaway et al. 1986; Bruckmann-Benke et al., 1988). In a bulk rock composition study of metapelites from Central Finland, Tuisku et al. (1987) concluded that zinc is immobile under amphibolite facies conditions, despite the evidence for considerable fluid flow through the rock during certain stages of metamorphism. The preservation of large zinc-rich massive sulfide/oxides deposit in metamorphic terranes (cf. Geco, Suffel et al., 1971; Ducktown, Nesbitt, 1982; Broken Hill, Spry, 1987; Franklin Hill, Johnson et al., 1990) also suggests that zinc is not being massively leached during metamorphism.

At Montauban, samples of cordierite-anthophyllite rock having low modal amounts of sphalerite and pyrrhotite exhibit the stable assemblage anthophyllite, zincian-staurolite (<3.00 wt% ZnO) and cordierite (Table 4.1C, Fig. 4.4). Powell and Holland (1990) contended that staurolite and cordierite are only rarely seen to coexist because the assemblage requires rather reducing conditions.

Zincian staurolite rimmed by gahnite always has more than 3.00 wt% ZnO, and occurs within or in the proximity of sphalerite-rich zones. Porphyroblastic gahnite is restricted to the central mineralized quartzitic gneiss and is distributed within the zinc anomalous zone (see metal distribution in NGZ, Chapter 3), whereas vermicular gahnite occurs in staurolite-bearing cordierite-anthophyllite rocks near the sphalerite-rich zones in the mineralized quartzitic gneiss (Bernier, 1985).

The Némiscau and Montauban gahnite and zincian staurolite relationships are shown in a Zn-Mg-Fe ternary diagram (Fig. 4.29) for comparison. The Mn-content of both minerals is low and can be disregarded. In both areas, gahnite rims zincian staurolite. The Némiscau gahnite and zincian staurolite

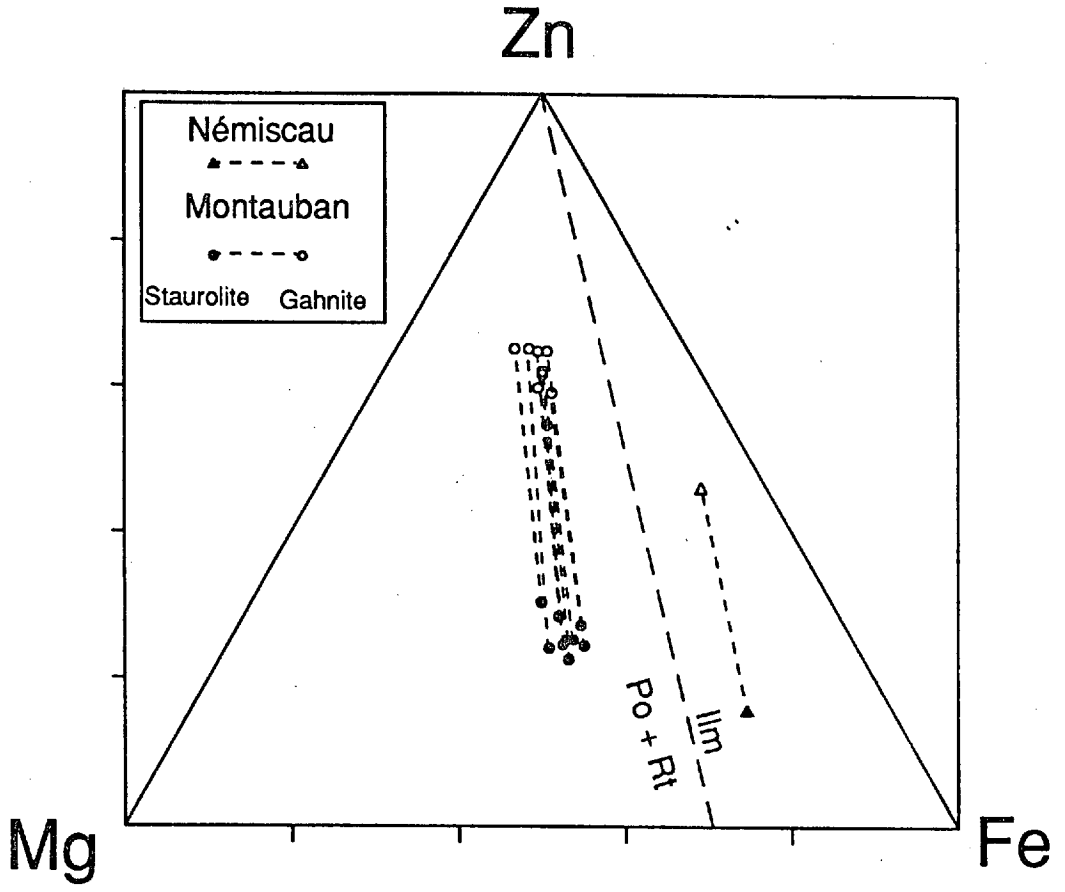

Fig. 4.29. Compositions of zincian staurolite and gahnite in a Zn-Fe-Mg ternary diagram (cation %) for the Némiscau and Montauban terranes. The Ilm = Po + Rt boundary is schematic.

coexist with ilmenite and are much more Fe-rich and have less zinc than those from Montauban which coexist with pyrrhotite and rutile. However, the slopes of the tie-lines are similar and are consistent with the data of Schumacher and Robinson (1987), and Zaleski et al. (1991). The boundary Ilm-(Po+Rt) shown in figure 4.29 is schematic because the metamorphic conditions for the two areas differ.

FASH System: The petrologic significance of the coronitic texture involving the breakdown of zincian staurolite can be evaluated by looking at the simple FASH system, for which reaction (4.23) was experimentally calibrated by Grieve and Fawcett (1974).

$$5\ \text{Fe-Ath} + 3\text{St} = 10.8\ \text{Fe-Crd-}(0.7\ H_2O) + 15.4\text{Hrc} + 0.44\ H_2O \qquad (4.23)$$

Note that their anthophyllite is a ferro-aluminous variety and that balancing the reaction is dependent on the hydration of cordierite.

The P-T location of reaction (4.23) was defined experimentally for the Fe-endmember system under Ni-NiO and QFM fO_2 buffers by Grieve and Fawcett (1974). Their experimental data indicate that the equilibrium boundary for reaction (4.23) was poorly constrained and its location can vary up to 1 kbar from the proposed location.

A schematic P-T grid for the FMASH system was proposed by Grieve and Fawcett (1974). Reaction 4.23 is tied to an invariant point for quartz-absent rocks and at higher temperature, almandine is stable instead of hercynite. For quartz-saturated rocks, hercynite is not formed and the reaction Ath + St + Qtz = Crd will occur. The chemography of reaction 4.23 is shown in figure 4.30.

Reaction (4.23) is relatively independent of temperature and fO_2 and thus constitutes a potential geobarometer. LnK curves for diluted Fe-endmember activities were calculated for reaction (4.23) and mapped in P-T space using

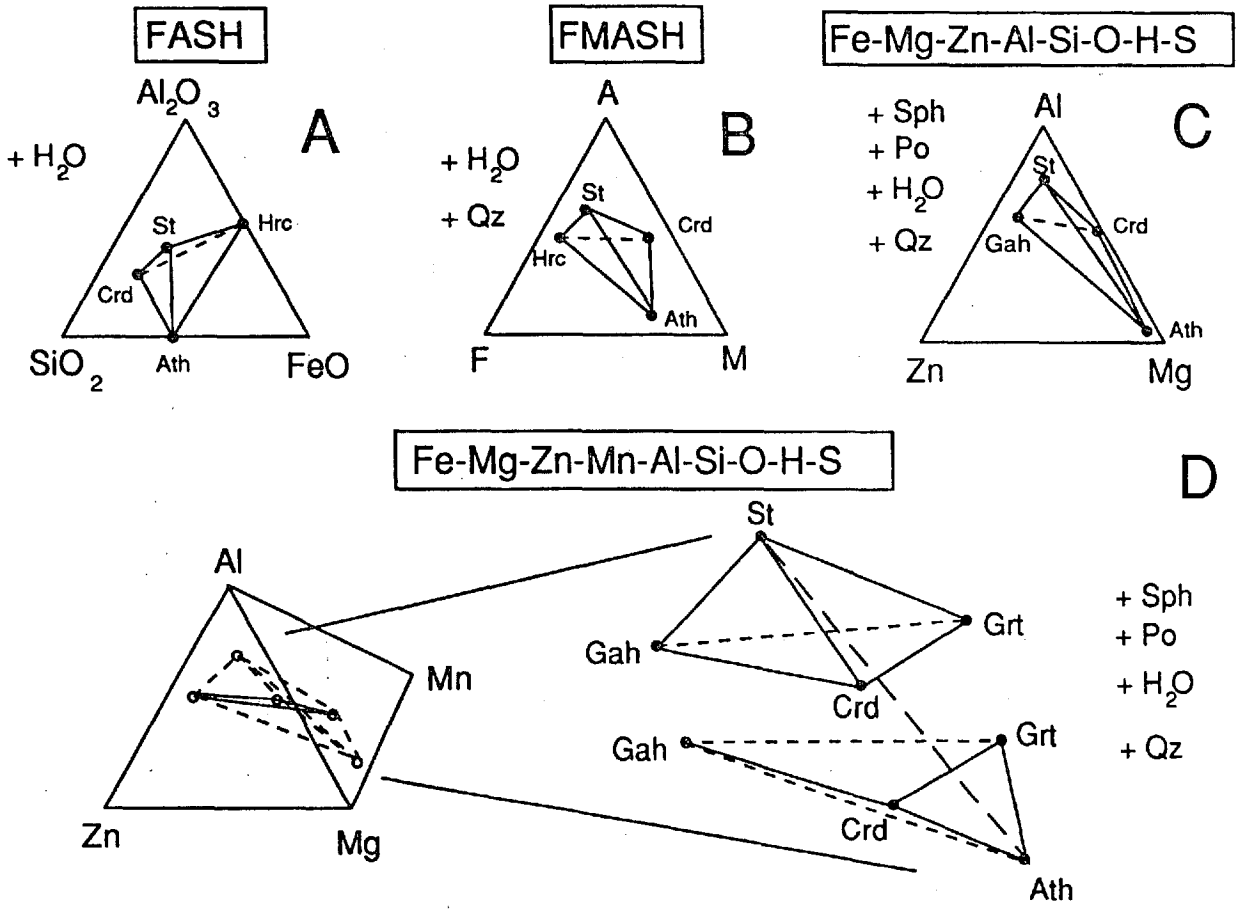

Fig. 4.30. Chemography involving anthophyllite, hercynite, cordierite and staurolite for various chemical systems increasing in components from A to D. The addition of Zn, Mn and S stabilized gahnite, garnet and sulfides respectively.

equation (4.24) and the water fugacity table of Burnham et al. (1969).

$$\ln K_{4.23} = (P-P_o)\Delta V_s/(-RT) - 0.44\ln(f^P_{H_2O}/f^{P_o}_{H_2O}) \quad (4.24)$$

The molar volume change for reaction (4.23) (-49.7 j/bar) was calculated using Berman's (1988) thermodynamic database; P_o is the pressure for $\ln K_{4.23}=0$ at T of interest and P is the pressure of interest at T. Three starting (T,P,fH_2O) datasets [(550°C, 2500 bars, 1079 bars); (600°C, 3000 bars, 1535 bars); (650°C, 3500 bars, 1998 bars)] defining equilibrium (4.23) for the condition lnK=0 were extracted from Grieve and Fawcett's (1974; their Fig. 2) diagram and Burnham et al.'s (1969) water table. $\mathrm{Ln}K_{4.23}$ values for varying pressures at 550°, 600° and 650°C have been calculated using equation (4.24). Linear least squares regression equations of lnK versus P (4.31A) were obtained for each temperature and solved to locate fixed values of $\ln K_{4.23}$ in P-T space (4.31B). Calculated lnK values for three samples of cordierite-anthophyllite rocks range from $\ln K_{4.23}=16$ to 22, indicating pressures between 5-6 Kbar; this is comparable to the multi-equilibrium results (Fig. 4.26B).

The chemography involving anthophyllite, spinel, cordierite and staurolite is shown in figures 4.30B-D for more complex chemical systems.

At Montauban, the presence of Zn (4.30C) and Mn (4.30D) adds complexity to the system, as they substitute for Fe in hercynite, staurolite, garnet, and anthophyllite. The spectacular coronitic textures involving the assemblage zincian-staurolite, gahnite, cordierite, garnet, and anthophyllite, with excess quartz, pyrrhotite and sphalerite, can be modelled in the system Fe-Mg-Mn-Zn-Al-Si-O-S. Phlogopite and rutile are ubiquitous and are stabilized by K_2O and TiO_2 respectively. In this system, a seven-phase assemblage defines a univariant reaction in fO_2-fS_2 space under fixed P-T and fH_2O (Fig. 4.32A). Two reactions involving MgO metasomatism have been

Fig. 4.31. Calculated ln(K) values for changes in P and T for the reaction involving the breakdown of ferro-anthophyllite and staurolite using the experimental data of Grieve and Fawcett (1974). A) P versus ln(K) diagram. B) Calculated ln(K) values displayed in P-T space.

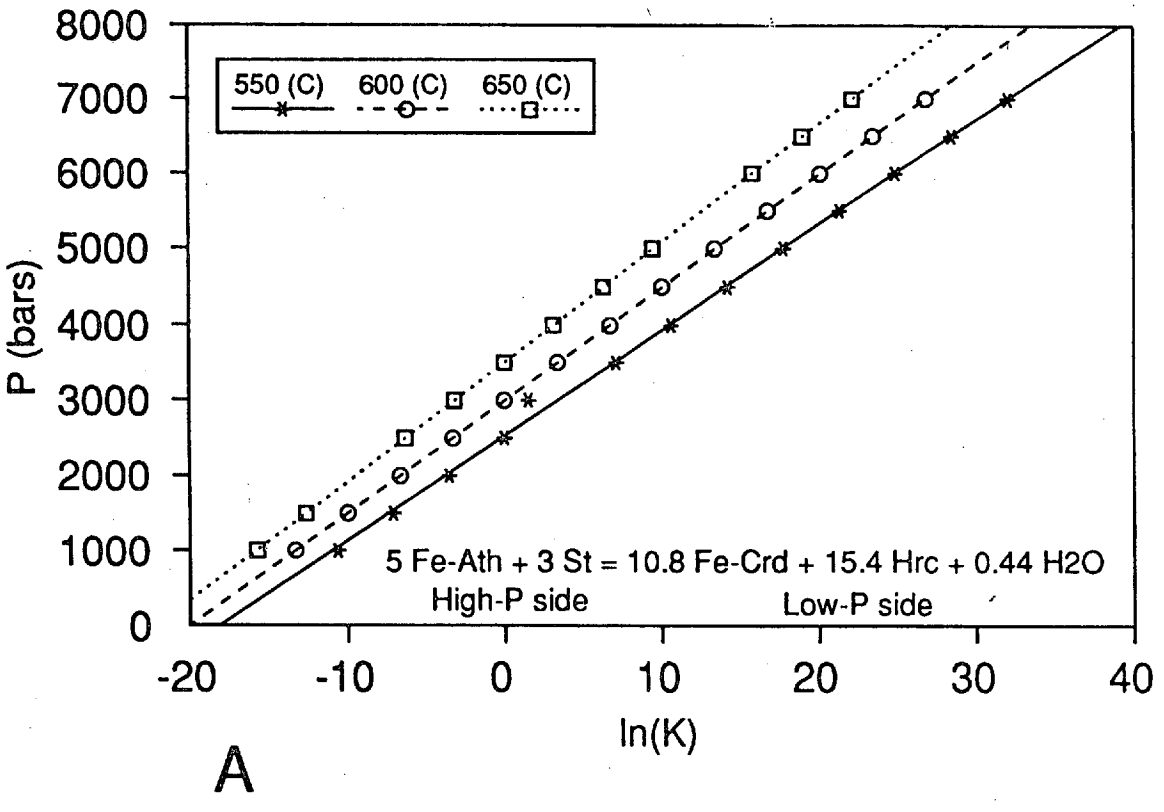
8000
7000
6000
5000
4000
3000
2000
1000
0
P (bars)
550 (C)
600 (C)
650 (C)
5 Fe-Ath + 3 St = 10.8 Fe-Crd + 15.4 Hrc + 0.44 H2O
High-P side
Low-P side
-20
-10
0
10
20
30
40
ln(K)

A

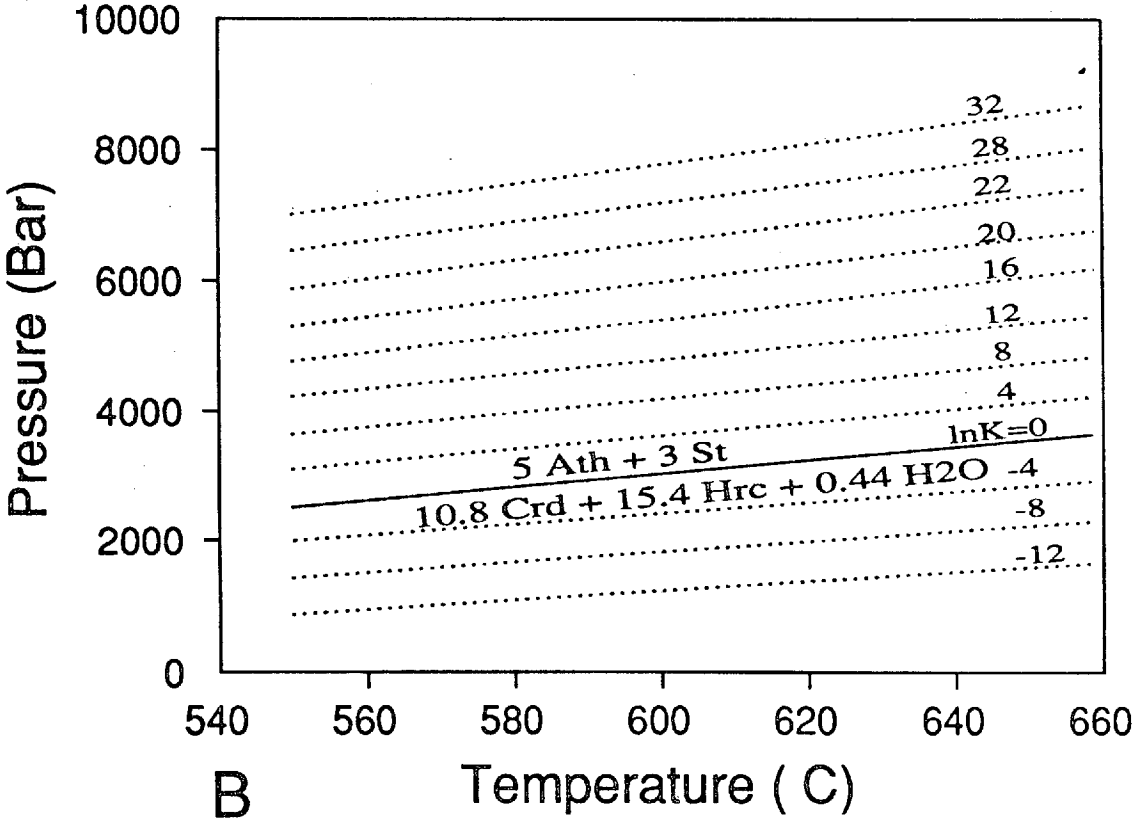
10000
8000
6000
4000
2000
0
Pressure (Bar)
32
28
22
20
16
12
8
4
lnK=0
5 Ath + 3 St
10.8 Crd + 15.4 Hrc + 0.44 H2O
-4
-8
-12
540
560
580
600
620
640
660
Temperature (C)

B

Fig. 4.32. Modelling of the breakdown of zincian staurolite and in the Montauban cordierite-anthophyllite rocks and the formation of gahnite in the quartzitic gneiss. A) Breakdown of zincian staurolite and formation of coronitic textures. B) Oxidation mechanism to model the formation of porphyroblastic gahnite in quartzitic gneiss and gahnite rims on zincian staurolite in cordierite-anthophyllite rocks. The sulfur released by the gahnite-forming reaction is diffused into the cordierite-anthophyllite wallrocks and contributes to the reaction in (A).

BREAKDOWN OF ZINCIAN-STAUROLITE

A

SYSTEM Fe-Mg-Mn-Zn-Al-Si-H-O-S (C-3-22)

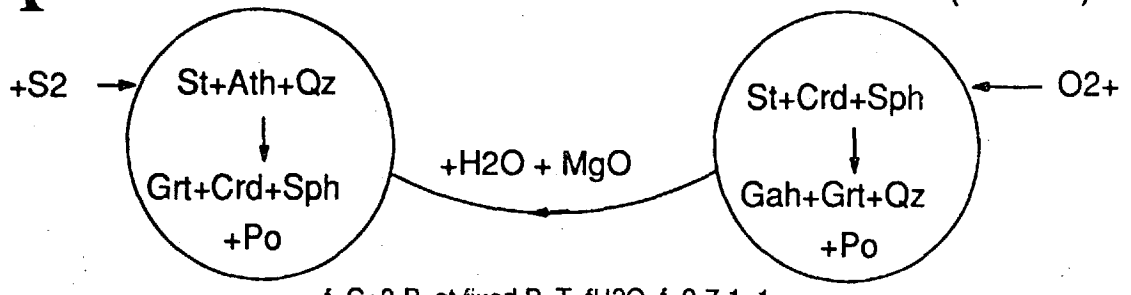

f=C+2-P, at fixed P, T, fH2O, f=9-7-1=1

(4.25) Univariant in fO2-fS2 space (4.26)

Overall Reaction

(4.27) 5.73 Zn-St + 4.61 Ath + 7.54 Sph + 0.22 S2 =

22.13 Gah + Mn-Grt + 13.91 Crd(0.73 H2O) + 3.44 Qz + 8.06 Po +2.13 O2

f=9-8=1 at fixed P, T

MONTAUBAN ALTERATION ZONE

B

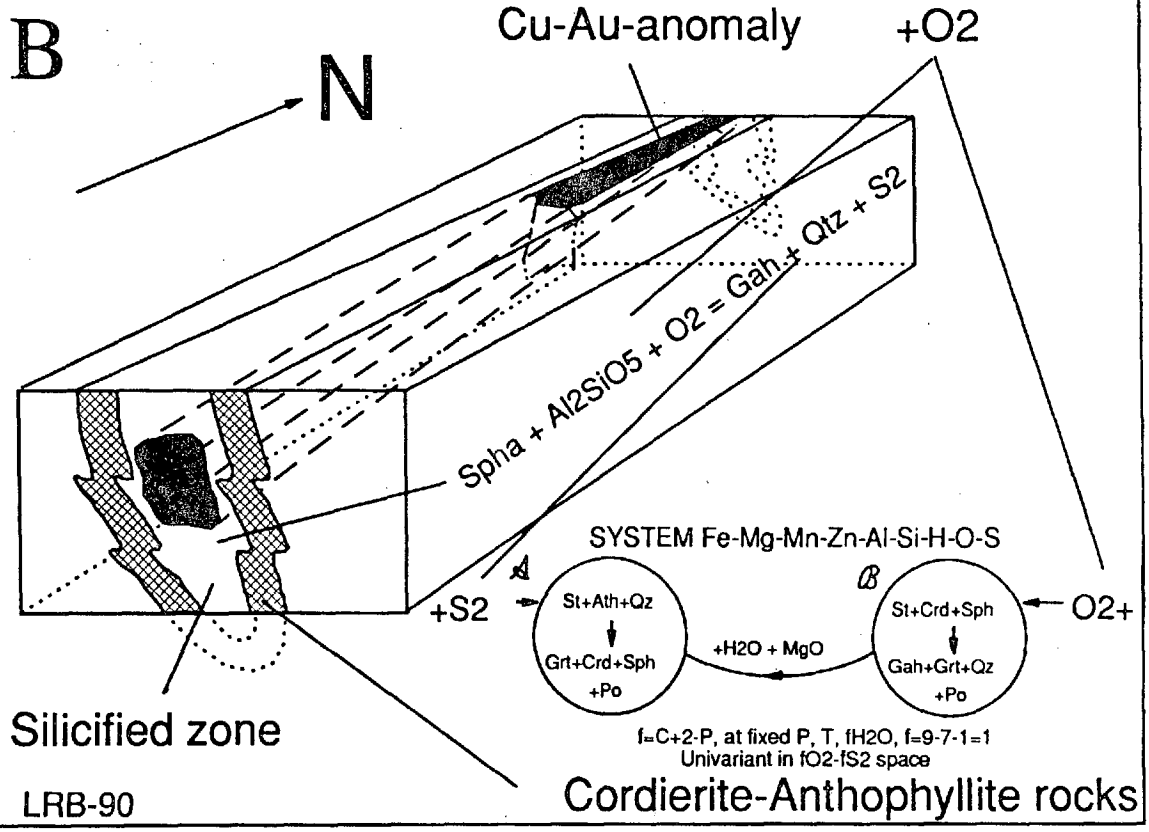

LRB-90

balanced from mineral compositions in sample (C-3-22) using the program METPET (Ball and Robin, 1990):

$$83.47\ St + 69.77\ Ath + 772.13\ Qtz + 219.48\ H_2O + 205.78\ MgO + 105.9\ S_2 = 14.12\ Grt + 370.18\ Crd(1\ H_2O) + 105.34\ Sph + 106.61\ Po + 158.71\ O_2 \quad (4.25)$$

$$3.17\ St + 159.89\ Crd(1\ H_2O) + 220.08\ Sph + 126.44\ O_2 = 334.56\ Gah + Grt + 824.18\ Qtz + 162.89\ H_2O + 205.78\ MgO + 15.21\ Po + 102.44\ S_2 \quad (4.26)$$

These are believed to represent thin section scale reaction domains exchanging chemical components (similar to Carmichael's (1969) reaction domains model) that produced the overall reaction (4.27), with simplified stoichiometric numbers:

$$5.73\ St + 4.61\ Ath + 7.54\ Sph + 0.22\ S_2 = 22.13\ Gah + Grt + 3.44\ Qtz + 13.91\ Crd(0.73\ H_2O) + 8.06\ Po + 2.13\ O_2 \quad (4.27)$$

Reaction (4.27) is univariant in fS_2-fO_2 space if the hydration number of cordierite allows water to be balanced, otherwise, an invariant situation would occur with fH_2O being externally controlled (Fig. 4.32A). This provides a realistic hydration number of 0.73 for the Montauban cordierite. Reaction (4.23) has a flat slope (nS_2/nO_2=0.1) in fO_2-fS_2 space, and thus is sensitive to changes in oxidation state. Coexisting sphalerite and pyrrhotite buffer fS_2 during metamorphism. However, balancing the reaction is dependent on the pyrrhotite composition. Pyrrhotite is known to reequilibrate upon cooling and a back-calculated pyrrhotite composition N^{FeS}=0.94 was used for a sphalerite composition of X^{FeS}=0.15. The balancing with METPET required the used of exchange components ($FeMn_{-1}$, $FeMg_{-1}$, $FeZn_{-1}$). The balancing of the resulting independent reaction was a stepwise process which involved replacement and

adjustment of the exchange component $FeZn_{-1}$ stoichiometric number for sphalerite and pyrrhotite compositions, and finally, balancing for O_2 and S_2.

Reaction (4.27) requires an input of sulfur. This sulfurization is interpreted to have been produced by the gahnite-forming reactions in the central quartzitic gneiss involving desulfurization of sphalerite owing to an increase in oxidation state. A probable reaction is (Spry and Scott, 1986):

$$Sph + Sil + O_2 = Gah + Qtz + S_2 \quad (4.28)$$

Moore and Reid (1988) explained the formation of gahnite in the metamorphosed Aggeneys and Gamsberg massive sulfide deposits South Africa, from the interaction of sulfides with high-fO_2 metamorphic fluids infiltrated along grain boundaries such as:

$$2H_3AlO_3 + Sph = Gah + 2H_2O + H_2S \quad (4.29)$$

$$2KH_2AlO_3 + Sph = Gah + 2KOH + H_2S \quad (4.30)$$

The presence of gahnite rims on sphalerite at Montauban (Bernier et al., 1987) implies local mobility of aluminum, perhaps as in reaction (4.29). However, the Log(Ratio) profiles for the Montauban altered rocks displayed in chapter 3 (3F) suggest that Al was fairly immobile at the hand specimen scale. The overall reaction mechanism needed to explain the presence of Mg in gahnite solid-solution, which must have been present in a reacting phase or brought in from another reaction site via an intergranular fluid. The only Mg-bearing mineral in the central quartzitic gneiss is biotite. As shown in figure 4.8C, there is an increase in Al^{IV} with X_{Fe} in biotite. A possible reaction could have been:

$$\overset{Al\text{-}rich}{Sph + Fe\text{-}Bt} + Qtz = \overset{Al\text{-}poor}{Gah + Mg\text{-}Bt} + H_2O + S_2 \quad (4.31)$$

in which case, no externally controlled oxidation would have been necessary. The exact gahnite forming reaction is difficult to identify, and more than one

mechanism might have been active. As a first approximation, reaction (4.28) is used in the model proposed. The oxidation would have also induced reaction (4.27). The gahnite-forming reaction (Spry and Scott, 1986) involves production of sulfur that could have diffused toward the surrounding cordierite-anthophyllite rocks, thus completing the reaction cycle schematically illustrated in figure 4.32B. This oxidation may have occured during decompressional uplift.

The tight clustering of rim gahnite and zincian staurolite compositions (Fig. 4.29) suggests that, although there is an apparent textural desequilibrium, there was local achievement of chemical equilibrium, which is compatible with a diffusion-controlled reaction (Schumacher and Robinson, 1987).

It appears that zinc stabilized staurolite to higher pressures and that the coronitic texture observed in the Montauban cordierite-anthophyllite rocks formed during decompression and are best explained as a result of an increase in the oxidation state.

In summary, peak metamorphic conditions at the Montauban deposits are established to have been around 6.5 kbar pressure at a temperature of 620°C. The wide range of bulk rock compositions at the mine sequence allowed the metamorphic history to be recorded through various reaction mechanisms.

DISCUSSION

"The presently exposed features of a metamorphosed deformed belt do not represent a snapshot of the terrain at any particular time in its development, but rather are a composite picture of events occurring through much of the evolutionary history of the mountain belt."

Tracy and Robinson, (1979), IGCP, P.189

Peak P-T Conditions and P-T Paths

From the geothermobarometric study, it is clear that the cordierite-orthoamphibole rocks formed in very contrasting metamorphic regimes in the three terranes. The Atik Lake terrane is characterized by peak P-T within the andalusite field, whereas peak P-T conditions in the Némiscau terrane recorded the andalusite-sillimanite transition which is typical of Buchan type metamorphism (Tracy and Robinson, 1979). This suggests that P-T paths for these two terranes were below the aluminosilicate triple point. In both terranes metabasalts were the precursor of the cordierite-orthoamphibole rocks.

In chapter 3 (3F) it was established that the Montauban cordierite-anthophyllite rocks and associated gneisses had a felsic volcanic protolith. The preservation of kyanite relics in the Mg-rich cordierite-biotite rocks, and fibrolite and sillimanite in the north gold zone mine sequence suggests a P-T path above the aluminosilicate triple point indicatives of Barrovian type metamorphism (Miyashiro, 1973; Tracy and Robinson, 1979). Sillimanite, however, is the aluminosilicate in the regional metapelites. The presence of kyanite relics in the mine sequence rocks is best explained by the anomalous bulk rock compositions and different metamorphic reactions occuring at different P-T conditions along the P-T-t path. In the mine sequence, kyanite most likely formed from the breakdown of muscovite and Mg-rich chlorite while sillimanite most likely formed at higher T in the Fe-rich metapelites from the breakdown of Fe-staurolite.

Coronitic textures (gahnite-cordierite riming Zn-staurolite) in the mine sequence cordierite-anthophyllite rocks, and retrograde muscovite in the metapelites suggests a near isothermal decompression P-T path for the Montauban terrane, probably during uplift and gneiss doming. The higher

temperatures recorded in the metapelites may be an effect of contact metamorphism caused by the intrusion of the La Bostonais Complex.

Only speculative inferences can be made on the possible tectono-metamorphic history and paleo-tectonic environment of these three terranes, owing to the lack of available detailed structural analysis and age-dating pertinent to each terrane, which was beyond the scope of this thesis. It should be pointed out that the geothermobarometry study of the three terranes was oriented to established peak P-T from mineral equilibria in order to bracket the metamorphic conditions for the formation of the cordierite-orthoamphibole rocks. Thus, the delineation of a complete and precise P-T-t path for each terrane would have required the application of several other techniques such as age dating, study of mineral inclusions in porphyroblasts, fluid inclusion study, etc. However, it was possible to gather some information on P-T path trajectories in the three terranes by using mineral assemblages, crossing isograds and coronitic textures.

The origin of low-pressure regional metamorphism such in the Atik Lake (T=550°C, P=2.5 Kbar) and Némiscau terranes (T=650°C, P=4.5 Kbar), is somewhat uncertain. Some workers regard low-pressure metamorphism as regional-scale contact metamorphism (Thompson, 1981; Kerrick, 1990). Belts affected by regional metamorphism typically contain numerous intrusive bodies (Kerrick, 1990). Intrusive heat sources have been proposed for low-pressure regional metamorphism because of the required abnormally high geothermal gradients (dP/dT>40°C/km), but this remains controversial (Thompson, 1981; Fowler and Nisbet, 1988; Kerrick, 1990). The peak P-T conditions at Montauban (T=620°C, P=6.5 Kbar) requires a lower geothermal gradient (dP/dT<40°C/km).

Peak P-T conditions for the three terranes are plotted in a P(depth)-T diagram (Fig. 4.33 A). Modern tectonic settings generating metamorphism

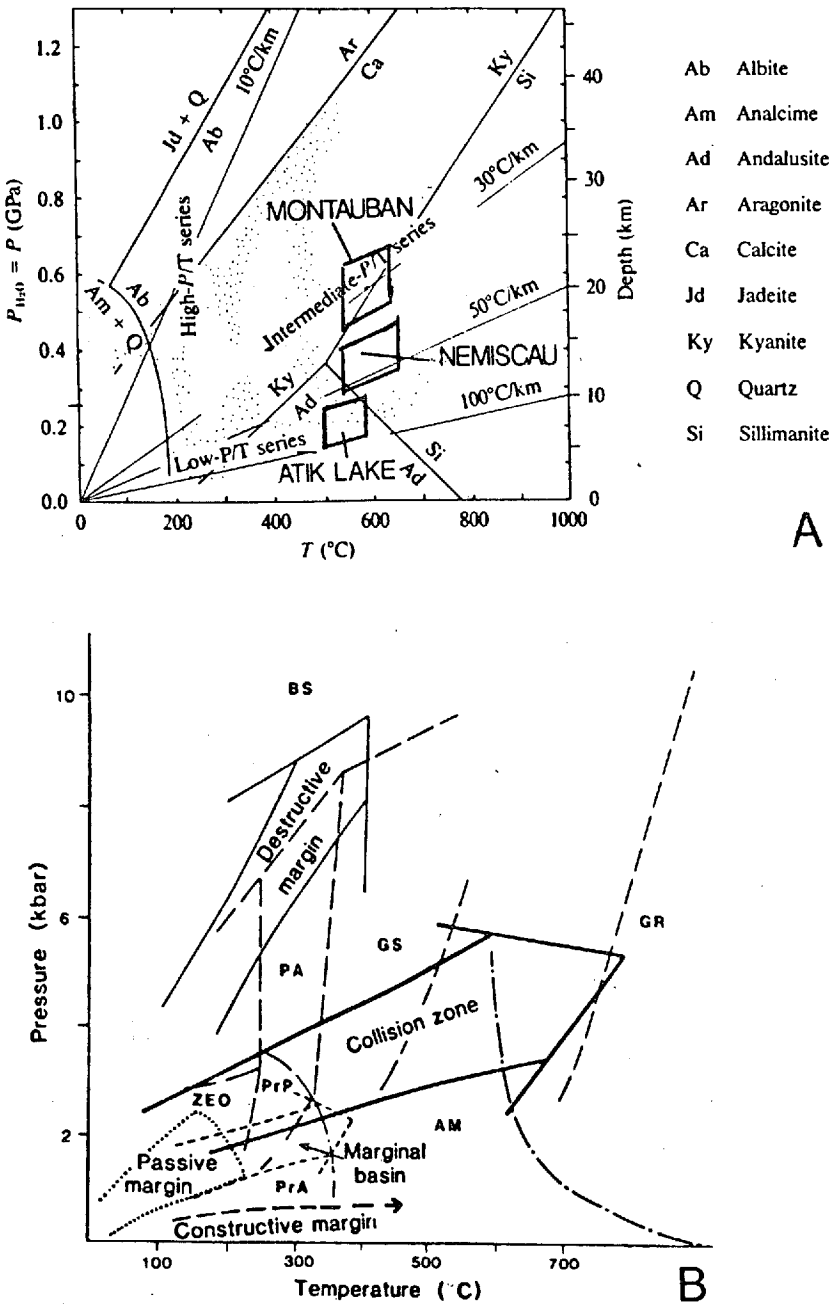

Fig. 4.33. Schematic diagrams of P-T ranges for the metamorphic facies series (A) from Best (1982), and for major tectonic settings (B) from Robinson (1987). The range of peak P-T conditions estimated for the Atik Lake, Némiscau and Montauban terranes are outlined on these P-T diagrams. A) Geotherms are drawn for 10, 30, 50, 100°C/Km. B) ZEO=zeolite facies, PrA=prehnite-actinolite facies, BS=blueschist facies, GS=greenschist facies; AM=amphibolite facies, GR=granulite facies.

(Robinson, 1987) are shown in figure 4.33B. An overlying crustal thickness of less than 10 km is required at Atik lake, between 15 and 20 km at Némiscau, and about 25 km at Montauban, to explain the metamorphic regimes in these terranes. The peak P-T conditions in the Atik Lake terrane are along the prolongation of the marginal basin P-T trend (Fig. 4.33B), those for Némiscau are transitional between the marginal basin and collision zone trends, and those for Montauban are within the collision zone trend. However, it is clear that the P-T-t path for a particular volume of rock may have crossed more than one geotherm (Thompson, 1981; Fowler and Nisbet, 1988), and the above figures only relate to "peak" metamorphic conditions and not to the overall P-T-t paths (metamorphic geotherms or metamorphic field gradients).

Tectonic Evolution

The tectonic evolution of greenstone belts has been a subject of controversy, and many of the relevant questions are reviewed by deWit and Ashwal (1986), Barley and Groves (1990), Card (1990), Thurston and Chivers (1990), and Hoffman (1990). Recently, it has been proposed that granite-greenstone terranes may be amalgamated island arcs, collapsed continental rifts, or back-arc basins, as summarized by Thurston and Chivers (1990). However, they most likely represent a variety of tectonic environments (deWit and Ashwal, 1986), although Hoffman (1990) favored a process of arc-trench propagation.

Atik Lake

MORB-type tholeiitic mafic volcanism was repetitive in the Atik Lake stratigraphy, and was associated with numerous interflow BIF. Major breaks in the mafic volcanism were marked by the deposition of clastic sediments,

mainly polymictic conglomerates (with granitic blocs), quartzitic sandstone and pelitic rocks in the middle and upper stratigraphy of the belt, which suggests a marginal basin model. However, metamorphism in modern marginal and back-arc basins is restricted to zeolite and lower greenschist facies (Robinson, 1987). The higher regional metamorphic temperatures required at Atik Lake may have been generated by surrounding and underlying felsic intrusions (c.f., Thompson, 1981). However, the general increase in metamorphic grade in the Sachigo Subprovince greenstone belts toward the Pikwitonei Subprovince (Weber and Scoates, 1978) has been attributed by Card (1990) to the exposure of progressively deeper crustal levels; consequently, the regional metamorphism in the Atik Lake belt could be related to depth as well as plutonism.

Némiscau

The mafic volcanism in the Némiscau metasedimentary belt (Chapter 3) is transitional between MORB (or back arc) and arc tholeiites, and was restricted to the lower stratigraphy, where it is intimately associated with podiform ultramafic bodies. Regional metamorphism was low-pressure, high temperature upper-amphibolite facies. There is a lack of conglomerate in the stratigraphy, and the paleotectonic setting is uncertain. Early rifting may have initiated the mafic volcanism and favored upward transposition of hotter geotherms (c.f. Thompson, 1981). The belt is narrower than the Atik Lake belt, and has been invaded by numerous granitic intrusions. The presence of a staurolite-andalusite zone in the NE part of the belt (lower T and P) suggests a prograde increase in metamorphism toward the southwest. The disappearance at NW faults boundaries of the staurolite-out and of the andalusite-sillimanite isograds suggests faults movements. However, the peak

metamorphic condition in the central part of the belt, where cordierite-anthophyllite rocks occur, was fairly homogeneous.

Montauban

The Montauban terrane is part of the St-Maurice tectonic zone in the Grenville Province. Problems relating to Grenvillian tectonics are reviewed by Moore (1986) and Rivers et al. (1989). The peak metamorphic conditions at Montauban are typical of the regional metamorphism kyanite-sillimanite facies series characteristic of orogenic belts (plate collision zone) (Robinson, 1987). Recent mapping and structural analysis of the St-Maurice tectonic zone by Nadeau and Hébert (1990) indicates that the tectonic style of the boundary faults (shear zones) is incompatible with the intracontinental rift model. Furthermore, the St-Maurice tectonic zone appears to be a distinct entity (Nadeau et al., 1992), and not the eastern continuation of the Allochtonous Monocyclic Belt overthrusting the Allochthnonous Polycyclic Belt as proposed by Rivers et al. (1989). It has been established in chapter 3 that the mine sequence, biotite ± muscovite quartzofeldspathic gneiss, cordierite-anthophyllite rocks and associated gneisses, were derived from a common felsic volcanic protolith of calc-alkaline affinity. These "felsic" gneisses and the metabasalts have trace element signatures compatible with a volcanic arc paleotectonic environment. An island arc (including back arc) setting is also favored to explain the formation of the polymetallic massive sulfide deposits. The metamorphism, incorporation and preservation of the Montauban massive sulfide deposits at a continental margin is best explained by collision tectonics (e.g., Cornell et al., 1990).

Summary

The metamorphic study of these three terranes, has established that cordierite-orthoamphibole rocks can be generated in very contrasting tectono-metamorphic regimes. The coarse-grained and undeformed nature of these rocks suggests that they formed at or near peak metamorphism after the main deformational events. Cordierite-orthoamphibole rocks can develop from the metamorphism of a variety of sedimentary rocks and, importantly in mineral exploration, from both hydrothermally altered felsic or mafic volcanic protoliths.

Cordierite-anthophyllite rocks from the three terranes have equilibrated with contrasting sulfide-oxide assemblages (Table 4.1). The well constrained peak P-T conditions established for these terranes can be used to model orthoamphibole-sulfide-oxide equilibria (Chapter 6) using the Popp et al. (1977b) experimental data. The data collected here also allows the Fe-Mg exchange between cordierite and anthophyllite to be studied and assessed in terms of a new geothermobarometer (Chapter 5).

CHAPTER 5

A NEW EMPIRICAL GEOBAROMETER BASED ON Fe-Mg EXCHANGE BETWEEN CORDIERITE AND ANTHOPHYLLITE: CALIBRATION AND APPLICATION.

Introduction

Cordierite and anthophyllite are the most common minerals formed from the metamorphism of chlorite-rich alteration zones around massive sulfide deposits. They are also common products of regionally metamorphosed sedimentary rocks (chlorite schists, magnesian pelites). There has been no geothermobarometer calibration made for these two minerals, based on Fe-Mg or other exchanges. The most common FMASH assemblage is cordierite-anthophyllite-biotite but other minerals can be present such as garnet, staurolite, and gahnite; these minerals are generally stabilized by additional components (Mn, Zn), particularly in metamorphosed alteration zones, which render P-T estimates from standard geothermobarometers inapplicable. Cordierite and anthophyllite have low distribution coefficients for Mn, Zn exchange with Fe and Mg. There are currently no available geothermobarometers directly applicable to these alteration zone rocks and one has to rely on surrounding metasediments to find mineral assemblages suitable for geothermobarometry. An independant geobarometer based on cordierite and anthophyllite will be very valuable in establishing independant pressure estimates for metamorphosed altered rocks around mineral deposits or Mg-rich metasediments.

A number of workers (Kamineni, 1975; Froese, 1976; Beeson, 1978; Sharma and MacRae, 1981; Spear, 1982; Wolter and Seifert, 1984; Schneiderman and Tracy, 1991) have calculated K_D^{Fe-Mg} between cordierite and orthoamphibole

(gedrite or anthophyllite) for specific regional P-T conditions. Metamorphic conditions reported in these studies were estimated by applying various geothermobarometers to metasedimentary rocks mineral assemblages. Spear (1982) demonstrated that K_D^{Fe-Mg} is lower for cordierite-anthophyllite than for cordierite-gedrite pairs; this has been confirmed recently by Schneiderman and Tracy (1991). Gedrite (Al-rich) and anthophyllite (Al-poor) are very similar mineralogically, and unfortunately, are often not distinguished in hand specimen or in thin section. Beeson (1978) did not separate gedrites from anthophyllites in his K_D^{Fe-Mg} calculations. Schneiderman and Tracy (1991) attributed the higher values of the cordierite-anthophyllite K_D^{Fe-Mg} for the Orijärvi area (T=550-600°C, P=3 Kbar) compared to those for the Post Pond volcanics (T=535°C, P=5-6 Kbar; Spear, 1982), to an increase in temperature. However, there is up to a 2-3 kbar pressure difference between these metamorphic terranes to be accounted for. As gedrite is restricted to the Atik Lake terrane in this study, only Fe-Mg exchange between cordierite and anthophyllite will be considered.

The well constrained peak P-T conditions (Chapter 4) and chemical composition data for cordierite-anthophyllite pairs for the Atik Lake, Némiscau and Montauban terranes will be combined with data from the literature to identify the controlling parameter on K_D^{Fe-Mg}. This treatment has led to the calibration of a new empirical geobarometer, applicable to a variety of metamorphosed alteration zones as well as in regionally metamorphosed Mg-rich metasediments.

Cordierite-Anthophyllite Fe-Mg Partitioning in the Three Terranes

Values of X_{Mg} for coexisting AFM phases in cordierite-anthophyllite rocks from the three terranes decrease in the order Crd > Bi > Ath > St > Grt

(Chapter 4). This is the normal equilibrium sequence for AFM phases (Thompson 1976). Values of X_{Mg}^{Ath} obtained from this study and others are always smaller than for biotite and cordierite (c.f. Kamineni, 1975; Beeson, 1978; Sharma and MacRae, 1981). Values of the distribution coefficient ($K_D^{Fe-Mg}=(Mg/Fe)^{Ath}/(Mg/Fe)^{Crd}$) have been calculated (Table 1). The average cordierite-anthophyllite K_D^{Fe-Mg} is 0.50 ± 0.03 (1σ) for Atik Lake, 0.44 ± 0.07 for Némiscau, and 0.37 ± 0.04 for Montauban.

The K_D^{Fe-Mg} values for cordierite and anthophyllite from the three terranes are plotted against corresponding mineral X_{Fe} in figure 5.1A. This diagram is somewhat similar to the T-X_{Fe} and P-X_{Fe} loop diagrams used by Thompson (1976) to represent minerals compositional changes involved in continuous reactions, as K_D^{Fe-Mg} most likely relates to changes in T and P. Coexisting cordierite-anthophyllite from other metamorphic terranes (Sondeled-Tvedestrand, South Norway, Beeson, 1978; Outokumpu, Finland, Treloar et al. 1981; Limpopo belt, South Africa, van Reenen, 1986; Orijärvi, Finland, Schneiderman and Tracy, 1991) are plotted in figure 5.1B for comparison. The aluminosilicate polymorphs and sulfide-oxide assemblage are shown as a guide to P-T and oxidation conditions.

There are four main observations to be made from figure 5.1A:

1) K_D^{Fe-Mg} versus X_{Fe} values for cordierite-anthophyllite pairs for a specific terrane define a loop;

2) the loops are displaced along the X_{Fe} axis according to bulk rock composition, which is different for each terrane:
$X_{Fe}^{Atik} > X_{Fe}^{Nemiscau} \geq X_{Fe}^{Montauban}$, (Fig. 5.2);

3) there is a general decrease in K_D^{Fe-Mg} with increasing metamorphic grade (P, T), which is different in each terrane;

4) the most reduced assemblages coexist with pyrrhotite-rutile at

TABLE 5.1 CORDIERITE-ANTHOPHYLLITE COMPOSITION DATA, CALCULATED K_D^{Fe-Mg}, PRESSURES AND TEMPERATURES USED IN CALIBRATION

Sample no.	Crd Mg/Fe	Ath Mg/Fe	K_D^{Fe-Mg}	P-T DATA
ATIK LAKE (AL)				
U845	2.101	1.023	0.484	T=560±50°C
	2.209	0.975	0.447	P=2.5±1 Kbar
U8401	2.030	0.923	0.464	Andalusite zone
	1.941	1.041	0.514	
	2.030	1.000	0.504	
U24	1.857	0.999	0.537	
U29B	2.030	1.068	0.526	
U40C	1.941	1.000	0.515	
NÉMISCAU (N)				
N32	2.358	1.197	0.508	T=650±50°C
N35	2.184	0.996	0.456	P=4.5±1 Kbar
	2.241	1.195	0.533	Sillimanite zone
	2.215	1.199	0.541	
N39	2.394	1.207	0.504	
SE1	4.452	1.629	0.366	
	4.328	1.708	0.395	
	4.289	1.761	0.410	
SE2	5.300	1.879	0.355	
	4.552	1.783	0.392	
SE3	4.553	1.876	0.412	
	5.018	1.882	0.375	
MONTAUBAN (M)				
C322	6.250	2.125	0.340	T=620±50°C
D218	5.810	2.060	0.354	P=6±1 Kbar
D514	5.182	2.034	0.393	Kyanite-Sillimanite
D608	9.146	2.433	0.266	zone
D211	6.928	2.612	0.377	
E519	5.063	1.902	0.376	
E525	5.255	1.964	0.374	
G315	8.513	3.170	0.372	
I323	5.372	2.375	0.442	
J215	11.609	3.927	0.338	
N202	5.408	1.897	0.351	
MQ12	5.487	2.120	0.386	
WEST UUSIMAA (WU)				
FK291	3.032	1.320	0.435	T=600±50°C
RH17	2.401	0.894	0.372	P=4±1 Kbar
MS150	1.941	1.012	0.521	Andalusite-
MS166	3.292	1.646	0.500	Sillimanite zone
(Schreurs and Westra, 1985)				
ORIJARVI (Or)				
OR8A	2.774	1.296	0.467	T=550-600°C
OR12A	4.780	2.198	0.460	P=3±1? Kbar
OR26A	1.941	0.951	0.490	Andalusite zone
OR27D	2.268	1.075	0.474	
OR40B	1.740	0.929	0.534	
OR40C	1.703	0.931	0.548	
PN2B	2.003	1.066	0.532	
PN3C	3.167	1.514	0.478	
O215	3.444	1.541	0.447	
O218A	4.556	1.954	0.429	
(Schneiderman and Tracy, 1991)				
NOTRE DAME BAY (NDB)				
NB201	1.500	0.852	0.568	T=500-550°C
NB202	1.564	0.818	0.523	P≈2 Kbar
NB203	2.704	1.326	0.490	Andalusite-
(Bachinski, 1976)				chlorite zone
OUTOKUMPU (O)				
O1	3.476	1.488	0.428	T=600±50°C
O2	3.619	1.363	0.377	P=3.5±1 Kbar
O3	5.435	2.020	0.372	Andalusite-
O4	4.817	1.928	0.400	Sillimanite relics
O5	3.708	1.568	0.423	
O6	3.824	1.639	0.428	
O7	3.619	1.516	0.419	
(Treloar et al., 1981)				
LIMPOPO BELT (LB)				
DR157	6.731	2.251	0.334	T=625-650°C
DV3	5.000	2.185	0.437	P=6±1 Kbar
DV1	8.227	2.714	0.330	Kyanite zone
(van Reenen, 1986)				
POST POND VOLCANICS (PP)				
68432G	6.747	2.672	0.396	T=530±20°C
68432M	5.642	1.965	0.348	P=5-6 Kbar
(Spear, 1982)				Kyanite zone

Fig. 5.1. X_{Fe} (Fe/Fe+Mg) versus the Fe-Mg partitioning coefficient (K_D) for cordierite and anthophyllite: A) the three terranes in this study; B) other occurrences reported in the literature. The alunimosilicate polymorphs and oxide-sulfide-arsenide assemblages are shown in rectangles for comparison, and as an indication of metamorphic grade and oxidation state.

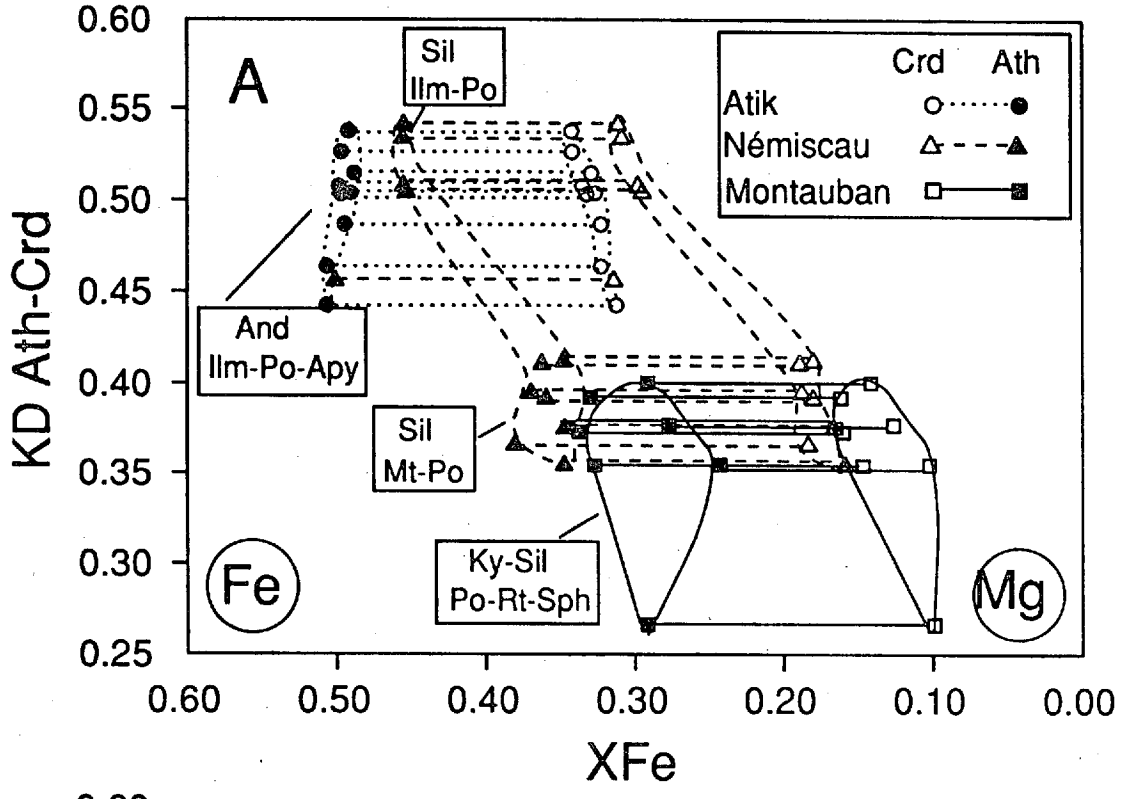
A
Sil
Ilm-Po
Crd
Ath
Atik
Némiscau
Montauban
And
Ilm-Po-Apy
Sil
Mt-Po
Ky-Sil
Po-Rt-Sph
Fe
Mg
KD Ath-Crd
XFe
0.60
0.55
0.50
0.45
0.40
0.35
0.30
0.25
0.60
0.50
0.40
0.30
0.20
0.10
0.00

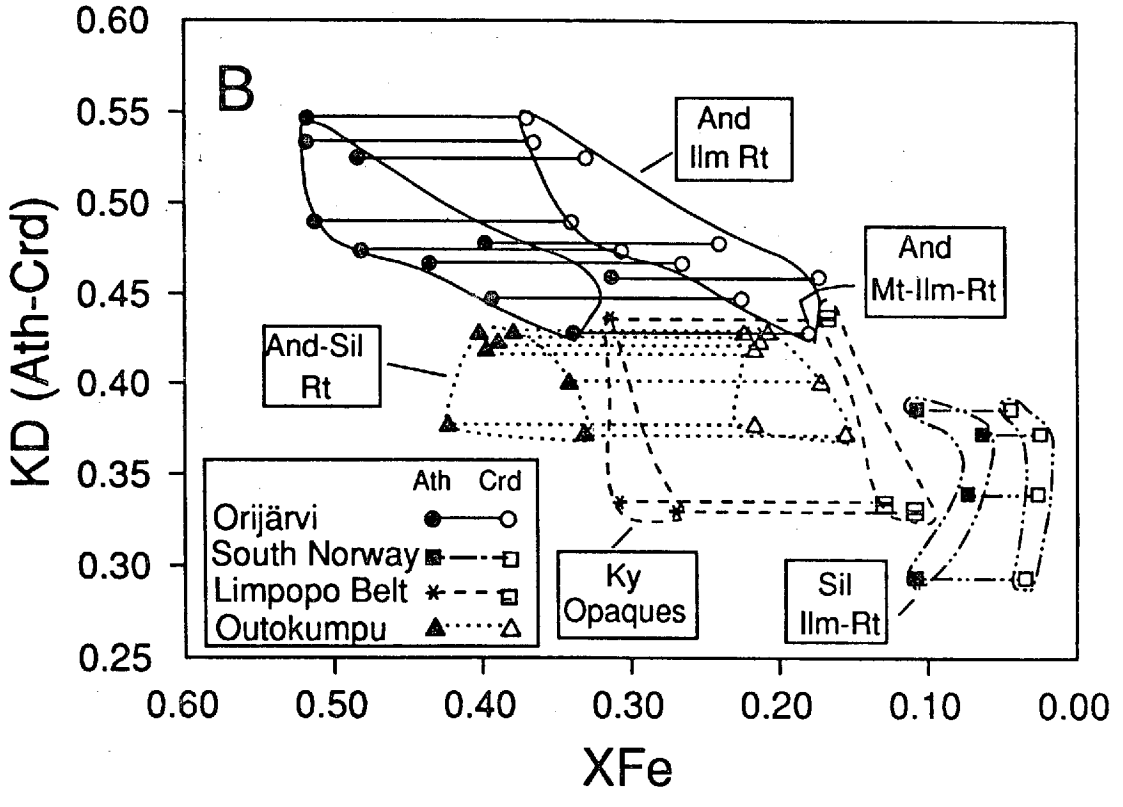
B
And
Ilm Rt
And
Mt-Ilm-Rt
And-Sil
Rt
Ath
Crd
Orijärvi
South Norway
Limpopo Belt
Outokumpu
Ky
Opaques
Sil
Ilm-Rt
KD (Ath-Crd)
XFe
0.60
0.55
0.50
0.45
0.40
0.35
0.30
0.25
0.60
0.50
0.40
0.30
0.20
0.10
0.00

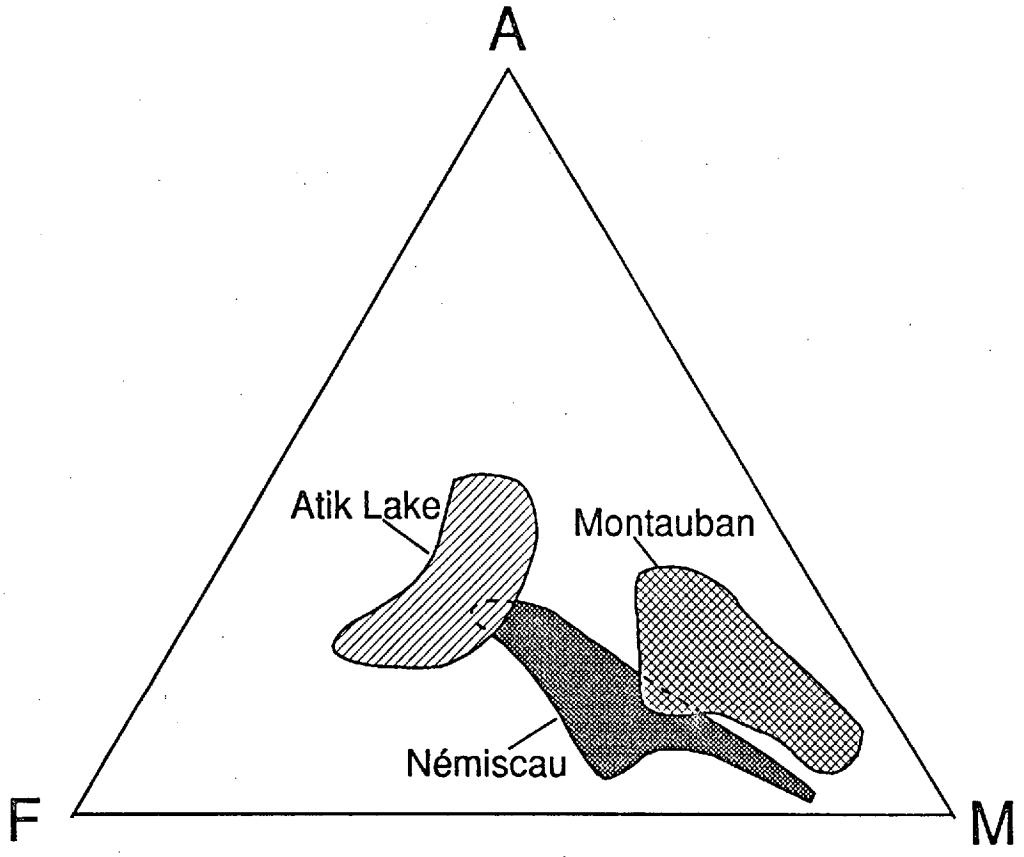

Fig 5.2. Ranges of cordierite-orthoamphibole rocks compositions for the three terranes shown in an AFM diagram (molecular proportion).

Montauban) have the lowest K_D^{Fe-Mg} and X_{Fe} values. Cordierite and anthophyllite at Némiscau that coexist with ilmenite-pyrrhotite have higher K_D^{Fe-Mg} and X_{Fe} values than those coexisting with magnetite-pyrrhotite; both appear to have formed under similar peak P-T conditions.

These observations also apply to Fe-Mg cordierite-anthophyllite partitioning in other metamorphic terranes (Fig. 5.1B), although the data for the very Mg-rich rocks from South Norway appear to define a reverse loop. Unfortunately, none of these studies provide bulk rock compositional data. Hence, as a first approximation, it will be assumed that K_D^{Fe-Mg} is independant of bulk rock composition and varies only with metamorphic conditions. The cordierite-anthophyllite pair from Orijärvi having the lowest X_{Fe} and K_D^{Fe-Mg} values coexists with ilmenite-magnetite-rutile, which indicates the highest fO_2 condition of all samples studied by Schneiderman and Tracy (1991). It appears from figure 5.1 that K_D^{Fe-Mg} is dependant mainly of the metamorphic grade and perhaps to some extent to the oxidation state. Higher oxidation states reduce X_{Fe} in Fe-Mg bearing minerals. Because fO_2 increases with T, it is difficult to assess the effect of varying oxidation state in cordierite-anthophyllite rocks on the basis of oxide-sulfide buffering assemblages, for terranes of differing P-T conditions. The identified loops are consistent with continuous Fe-Mg exchange during metamorphism (Thompson, 1976), however, the exact reaction mechanism is uncertain.

Empirical Calibration

In an attempt to determine whether K_D^{Fe-Mg} is more T or P dependant, $T\text{-}K_D^{Fe-Mg}$ (Fig. 5.3A) and $P\text{-}K_D^{Fe-Mg}$ (Fig. 5.3B) plots were made using the data from the three terranes and other appropriate data from the literature (Bachinski, 1976; Treloar et al. 1981; Spear, 1982; Schreurs and Westra, 1985;

Fig. 5.3. Temperature (A) and pressure (B) versus Fe-Mg partitioning coefficient (K_D) between cordierite and anthophyllite for the three terranes and other occurrences. Abbreviations as in Table 5.1. C) $Tln(K_D)$-P diagram for the dataset in Table 5.1. Equations for the least squares regressions are shown on the diagrams.

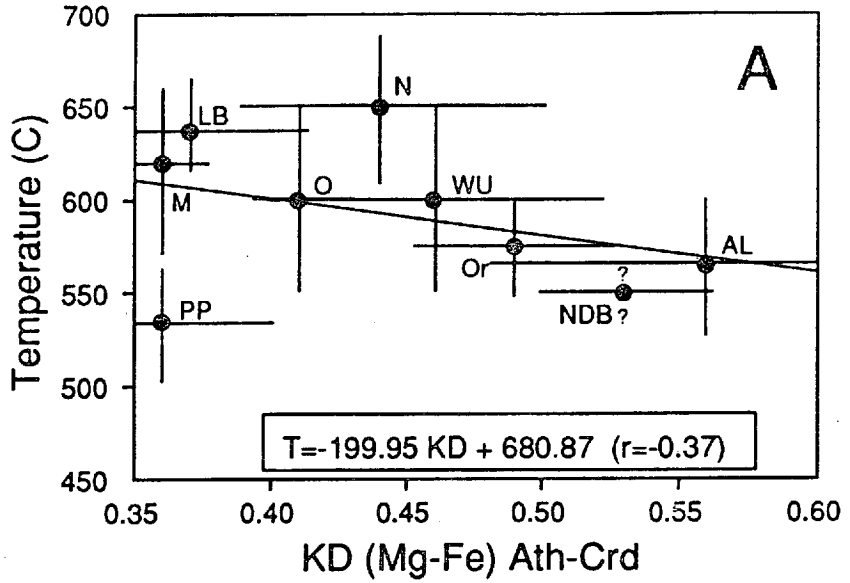
A
Temperature (C)
KD (Mg-Fe) Ath-Crd
T=-199.95 KD + 680.87 (r=-0.37)
700
650
600
550
500
450
0.35
0.40
0.45
0.50
0.55
0.60
N
LB
M
O
WU
Or
AL
PP
?
NDB?

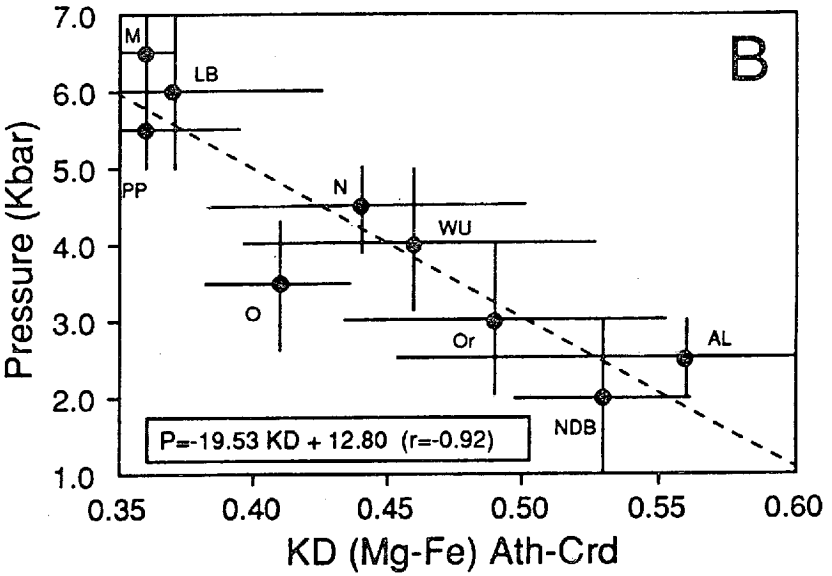
B
Pressure (Kbar)
KD (Mg-Fe) Ath-Crd
P=-19.53 KD + 12.80 (r=-0.92)
7.0
6.0
5.0
4.0
3.0
2.0
1.0
0.35
0.40
0.45
0.50
0.55
0.60
M
LB
PP
N
WU
O
Or
AL
NDB

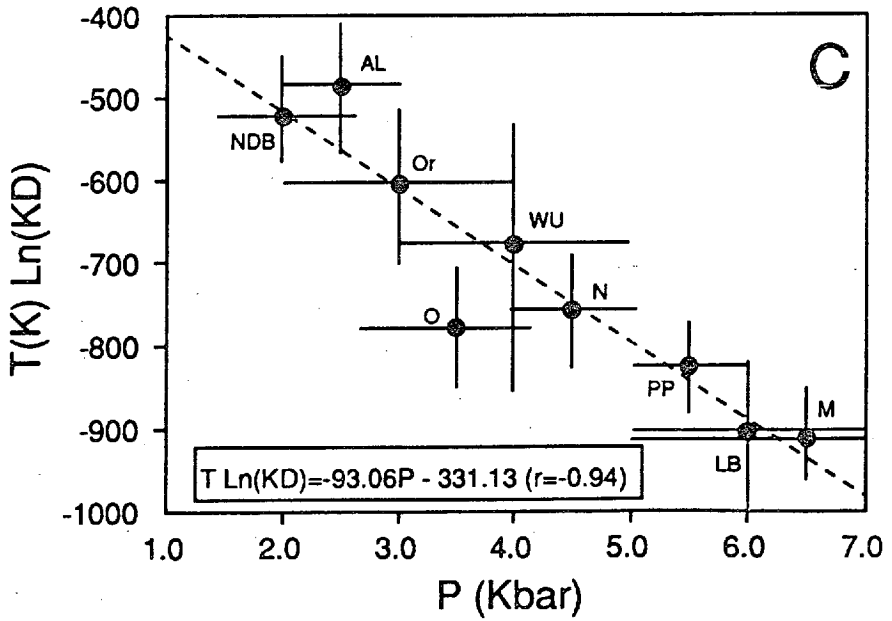
C
T(K) Ln(KD)
P (Kbar)
T Ln(KD)=-93.06P - 331.13 (r=-0.94)
-400
-500
-600
-700
-800
-900
-1000
1.0
2.0
3.0
4.0
5.0
6.0
7.0
AL
NDB
Or
WU
N
O
PP
M
LB

van Reenen, 1986; Schneiderman and Tracy, 1991) for which reasonably good P-T estimates were available (Table 5.1). Owing to the lack of independant P-T estimates for individual samples used in this study and in the literature data, K_D^{Fe-Mg} values were averaged for each terrane and calibrated against the peak regional P-T values. A potential pitfall with this method is possible re-equilibration among the minerals during post-peak metamorphic cooling. For this reason, only core-core data were used.

It appears from figures 5.3A and 5.3B that K_D^{Fe-Mg} is much more dependant on pressure (r=-0.94) than temperature (r=-0.37). This is somewhat surprising because of a steep dP/dT ($\Delta S/\Delta V$) slope (150) calculated for the Fe-Mg exchange between cordierite and anthophyllite using the thermodynamic data of Powell and Holland (1990). For comparison, the dP/dT slope for the Fe-Mg exchange between garnet and biotite is 44 (Ferry and Spear, 1978), and K_D^{Fe-Mg} (Grt-Bt) is highly temperature dependant.

The lack of good correlation of K_D^{Fe-Mg} cordierite-anthophyllite with T is difficult to explain. However, if the Post Pond data point is excluded from the regressed data set, a correlation coefficient of r=-0.79 is calculated. The correlation with temperature could be somewhat masked by effects of varying pressure and oxidation states included in the calculated K_D^{Fe-Mg} values. The calculated slope could be in error owing to poorly constrained thermodynamic data on Fe-cordierite and Fe-anthophyllite. Also, the degree of hydration of cordierite will affect molar volume values. McPhail et al. (1990) found that the hydrous Mg-cordierite molar volume is 2.3066 J/bar higher than that of anhydrous Mg-cordierite. The effect of hydration on the Fe-cordierite molar volume is not known. However, Boberski and Schreyer (1990) found that the water content of both Fe- and Mg-cordierite increases with increasing pressure and decreases with increasing temperature.

It is difficult to precisely evaluate the effects of the varying oxidation states, which are included in the averaged K_D^{Fe-Mg} values. The effect of minor Mn substitution is unknown but could be a contributing factor. Alternatively. the Fe-Mg exchange between cordierite and anthophyllite could be controlled by a continuous reaction that is pressure dependant. It is clear that experimental data are needed to better assess the factors controlling the Fe-Mg exchange between these minerals. Pressure appears to be a definite major factor.

The best correlation (r=-0.94) was obtained by plotting $TLn(K_D^{Fe-Mg})$ versus P (Fig. 5.3C). The derived expression is the cordierite-anthophyllite Fe-Mg exchange geobarometer (T is in K):

$$P=-[(TLn(K_D^{Fe-Mg}) + 331.13) / 93.06] \text{ Kbar} \quad (5.1)$$

The application of this geobarometer should be restricted to low-Al-anthophyllites (<7wt% Al_2O_3) coexisting with cordierite, where peak temperature is known. However, in the absence of an estimate for T, the equation given in figure 5.3.B (inset) can be used to calculate P. The error on the calculated pressure is difficult to evaluate but is, at best, in the order of ±1 kbar. This geobarometer can yield useful pressure estimate, and can be applied with other geobarometers in many metamorphic terranes.

Application to Other Terranes

The cordierite-anthophyllite geobarometer (eqn. 5.1) has been applied to data sets from the literature for which some knowledge of metamorphic conditions are provided (range or T, P or presence of an aluminosilicate polymorph). The results are presented in Table 5.2. In the absence of T information, the pressure was calculated for two T values. The estimates appear to be consistent with inferred metamorphic grades.

TABLE 5.2 CALCULATED PRESSURES FOR OTHER TERRANES

Area	K_D^{Fe-Mg}	Oxide-Sulfide	T,P Data Al-Sil	Calculated P (± 1 Kbar)
1) Gullbridge Newfoundland	0.495 (n=1)	?	And	(T=500) 2.3 (T=600) 3.0
2) Old Woman Montains SE California	0.443 (n=1)	Ilm±Rt	Ky-Sil-And	(T=500) 3.2 (T=600) 4.0
3) Garon Lake Matagami	0.453 (n=1)	Po-Mt-Py	low Amph. facies	(T=500) 2.9 (T=600) 3.9
4)-Lar Deposit Lynn Lake	0.441±0.069 (n=6)	Po-Mt±Rt	Sil	(T=500) 3.2 (T=600) 4.1
5) Geco Manitouwadge	0.485 (n=1)	Ilm+ Sulfides	Sil	T=625 3.4
6) Bamble Sector South Norway (two localities)	0.333 (A) 0.463 (B) (n=2)	Ilm-Rt Ilm-Rt	Ky-Sil Ky-And	T=685 7.6 4.0
7) Tvedestrand South Norway	0.348±0.036 (n=4)	Ilm-Rt?	Sil	(T=600) 6.2 (T=700) 7.5

Temperatures in brackets were used for pressure calculations with equation (1) when no T°C were provided. Amph=amphibolite. 1) MacRae (1973), 2) Stoddard and Miller (1990), 3) Aftabi (1980), 4) Elliott-Meadows and Appleyard (1991), 5) James et al. (1978); 6) Vissor and Senior (1990), 7) Beeson (1978).

Summary

In summary, this empirical geobarometer has definite potential use. However, it is strongly recommended that it be applied in a critical manner for the amphibolite facies range of P-T contitions (T=500-700°C, P=2-7 Kbar). The cordierite-anthophyllite compositional relationships outlined from natural assemblages can be used as a guide for future experimental studies on the Fe-Mg exchange between these two minerals. Factors that need experimental evaluation are: the effect of varying oxidation states on $K_D^{Fe\text{-}Mg}$; changes in $K_D^{Fe\text{-}Mg}$ with T at constant P and with P at constant T; assessment of ideality of Fe-Mg mixing; the effects of Mn substitution; and the effects of the hydration state of cordierite.

CHAPTER 6

SULFIDATION AND OXIDATION OF Fe-ANTHOPHYLLITE AND METAMORPHIC FLUID SPECIATION

"Do mineral assemblages in a rock control the composition of the coexisting fluid, do external reservoirs of fluid control the mineralogy of rocks with which they are in communication, or does some intermediate situation occur."
Rice and Ferry (1982), MSA, v. 10, P. 263

"During the progressive metamorphism of many carbonates and pelites, it may be more reasonable to assume that the mineralogy has controlled the composition of the fluid phase rather than the more commonly assumed converse. ... In iron bearing rocks the oxygen fugacity is ordinarily controlled by the mineralogy rather than being imposed externally and thus should not be regarded as an independent variable."
Greenwood (1975), Am. J. Sci., V. 275, p. 573

Introduction

The petrogenesis of cordierite-orthoamphibole rocks has always been controversial and hypotheses concerning their origin are summarized in Hudson and Harte (1985) and Schneiderman and Tracy (1991). Recent studies on this topic favor contrasting models to explain the formation of cordierite-orthoamphibole rocks having coronitic textures similar to those in the three terranes studied. Schneiderman and Tracy (1991) could not rule out systematic variations in fO_2-fS_2 to explain variations in cordierite, biotite and anthophyllite compositions, in rocks from Orijarvi, Finland; they argued on the basis of high variance mineral assemblages, that changes in mineral chemistry reflect variation in bulk rock compositions. However, these authors do not provide any bulk rock compositions to sustain their hypothesis, and as shown in Chapter 5, their most magnesian minerals coexist with magnetite-rutile-ilmenite, indicating a higher fO_2 than their other samples.

Arnold and Sandiford (1990) suggested that cordierite-orthoamphibole

rocks from Springton, South Australia, were formed from a syn-metamorphic potassium metasomatism (removal of K_2O) during high water/rock ratio interaction of high temperature advecting metamorphic fluid in the metapelites. Again, no bulk rock compositions are provided and these authors do not present detailed metamorphic mineral assemblages. Bristol and Froese (1989) have suggested that the displacement of metamorphosed altered rocks toward the F apex on an AKF diagram is best explained by a decrease in the Al/(Al+Fe+Mg) ratio due to addition of Fe and Mg during hydrothermal alteration. It has been demonstrated in Chapter 3, that mass balance calculations indicate large additions of Fe, Mg and minor additions of potassium to the cordierite-orthoamphibole rocks in the three terranes studied.

Hence, it is imperative to assess the role of the metamorphic fluid, internal versus external fO_2-fS_2 buffering during metamorphism, and the effect of varying bulk rock compositions, to properly explain variations in mineral compositions and decipher the appropriate mechanism controlling the formation of cordierite-orthoamphibole rocks.

Field studies

Numerous field oriented studies have dealt with the interaction of sulfide-oxide-silicate minerals during metamorphism. In general, these studies have shown that X_{Fe} variations of Fe-Mg silicates depend on the sulfide-oxide assemblages at fixed P-T conditions. Key studies are those of: Chinner (1960), Fullager et al. (1967), Froese (1969), Thompson (1972), Froese (1973), Bachinski (1976), Hutcheon, (1979), Ferry, (1981), Nesbitt (1982), Mohr and Newton (1983), Petersen (1986), Tracy and Robinson (1988), and

Zaleski et al. (1991). Many of the above studies have benefited from the graphical methods outlined by Froese (1971), more specifically $logfO_2$-$logfS_2$ diagrams to represent sulfide-oxide-silicate equilibria.

The systematics of sulfide-oxide-silicate equilibria associated with metamorphosed ore deposits has been outlined and summarized by Froese (1977) and Nesbitt (1986a, 1986b). In comparing metamorphic changes in host rock mineral assemblages at the Ducktown (Tenessee) and Geco (Ontario) massive sulfide deposits, Nesbitt (1986b) concluded that the nature of chemical interactions between ore components and wall rocks during metamorphism, can be predicted. He also noted that sulfide-oxide-silicate interactions can be quite variable depending on the petrologic characteristics of the ore and the host rocks. This is particularly important in the case of metamorphosed hydrothermal alteration zones, where a wide range of bulk rock compositions and fO_2-fS_2 conditions can occur. If the host rocks are petrologically homogeneous (e.g. Ducktown), symmetrical zoning in silicate-oxide-sulfide mineral assemblages and compositions can occur. Where the host rocks are heterogeneous (e.g. Geco), asymetrical zoning in mineral assemblages and compositions, may reflects intrinsic fO_2-fS_2 variations owing to changes in bulk rock compositions and differences in buffering capacity.

The three terranes choosen provide natural laboratories to study changes in anthophyllite composition as a function of oxide-sulfide assemblages, P-T conditions and bulk rock compositions.

Early experimental work

Experimental studies on the sulfidation and oxidation of silicates were initiated by Kullerud and Yoder (1963, 1964) and Kullerud (1965) who studied

the stability of a series of hydrous and anhydrous Fe and Pb bearing silicates and carbonates reacting with sulfur (fayalite, hedenbergite, almandine, ferrocordierite (sekianite), ferroanthophyllite, and siderite, smithsonite and cerussite). Very few experimental studies have been done since that time on sulfidation-oxidation reactions involving silicates.

Popp et al. (1977a) studied the stability of ferroanthophyllite and anthophyllite with changes in fO_2 (MH, QFM, NNO) between 600°-725°C at P_{fluid}=2Kbar. Popp et al. (1977b) examined the effects of sulfidation for the same Fe-Mg amphiboles over a range of T=650°-725°C at P_{fluid}=2 kbar, for fO_2-fS_2 conditions buffered by the assemblage pyrrhotite-magnetite (PM). A study of the sulfidation of synthetic biotites was made by Tso et al. (1979) at T=700°C and P_{fluid}=2kbar for fO_2-fS_2 buffered by PM. Spry and Scott (1986b) reported experimental data on gahnite-forming reactions involving oxidation and desulfurization of sphalerite for the range T=550°-650°C at P=5 kbar and T=650°-700°C at P=2 kbar, under fO_2-fS_2 fixed by the pyrite-pyrrhotite-magnetite (PPM) buffering assemblage. The stability of Fe-Mg chlorites as a function of fO_2, fS_2, P (2, 4.5, 5, 6 kbar) an T (575°, 600°, 625°C) was studied by Bryndzia and Scott (1987) under the PPM buffer.

MacRae (1973) carried out experiments which suggested that cordierite-anthophyllite rocks at the Gull Pond deposit, Newfoundland, could have been formed by sulfurization of basalt under contact metamorphic conditions. His experimental products were plagioclase, Mg-cordierite, diopside, Fe-sulfides, quartz, sphene and anhydrite for runs at T=700°C and P=1 kbar; he assumed that calcium would be removed in a natural system as $CaSO_4$. However, no anthophyllite was found in his run products, probably because Ca could not escape the system and favored the formation of diopside.

Furthermore, the pressure was perhaps not high enough to favor the formation of an amphibole at this temperature (700°C). However, it has also been suggested that these cordierite-anthophyllite rocks formed from the metamorphism of chlorite-rich hydrothermal assemblages (Upadhyay and Smitheringale, 1972; Bachinski, 1976). Internally controlled sulfidation reactions linked to the metamorphic transformation of pyrite to pyrrhotite plus sulfur were invoked by Bachinski (1976) to explain the low X_{Fe} of anthophyllite and cordierite.

Assessment of Experimental Data

In this section, anthophyllite compositions will be modeled using Popp et al's. (1977b) experimental data for peak P-T conditions and oxide-sulfide±arsenide assemblages outlined (Chapters 3 and 4) for the three terranes. This will allow a test of the applicability of the experimental data.

Oxidation-sulfidation of Fe-anthophyllite

The experimental investigation involving sulfidation (6.1) and oxidation (6.2) of Fe-anthophyllite were carried out by Popp et al. (1977b) at T=650-725°C, and P=2.07 kbar , where $P_{H_2O}=P_{tot}$.

$$Ath + 7/2\ S_2 = 7FeS + 8\ Qtz + H_2O + 7/2\ O_2 \qquad (6.1)$$

$$Fe\text{-}Ath + 7/2O_2 = 7/3\ Mt + 8\ Qtz + H_2O \qquad (6.2)$$

The magnetite-pyrrhotite $logfO_2$-$logfS_2$ boundary was recalculated from equilibrium (6.3), given below, using Popp's et al. (1977b) pyrrhotite compositions with Robie's et al. (1978) thermodynamic data for magnetite, and thermodynamic expressions for the pyrrhotite-sulfur vapor equilibrium from

Fig. 6.1. Assessment of Popp et al.'s (1977) experimental data on the sulfidation and oxidation of ferro-anthophyllite. A) Pyrrhotite-magnetite boundary in a $\log fO_2$-$\log fS_2$ diagram recalculated using Popp et al's. experimental data. The wide dashed line is from the experimental data of Tso et al. (1979) and is shown for comparison. The errors for the 700°C run are from Tso et al. (1979). B) and C) Plots of $\Delta G_r^{(T,1)}$ versus T for the sulfidation (B) and oxidation (C) of ferro-anthophyllite reactions, corrected to the experimental pressure of 2 kbar.

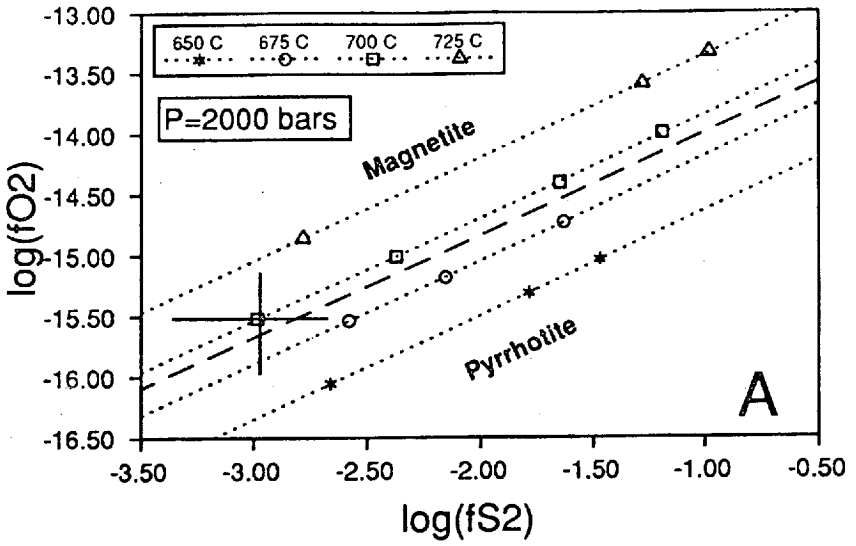
650 C
675 C
700 C
725 C
P=2000 bars
Magnetite
Pyrrhotite
A
log(fO2)
log(fS2)
-13.00
-13.50
-14.00
-14.50
-15.00
-15.50
-16.00
-16.50
-3.50
-3.00
-2.50
-2.00
-1.50
-1.00
-0.50

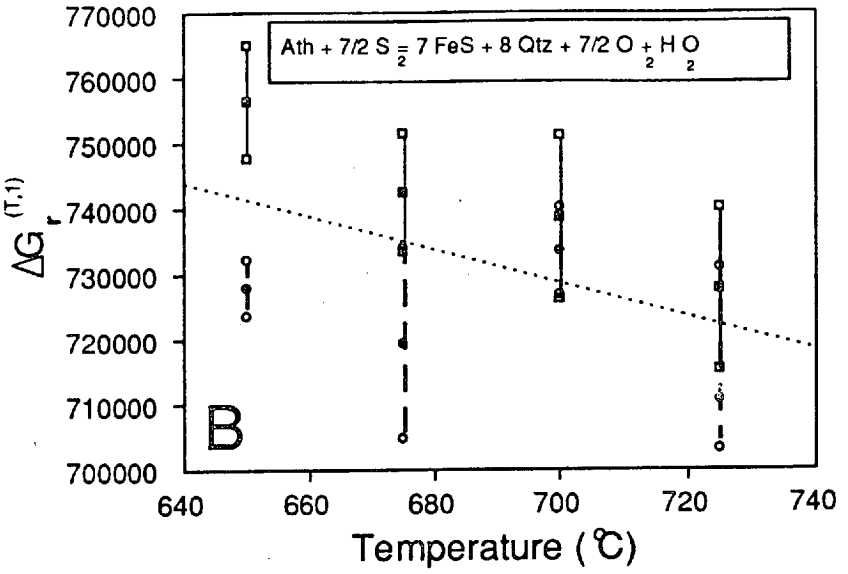
Ath + 7/2 S2 = 7 FeS + 8 Qtz + 7/2 O2 + H2O
B
ΔGr(T,1)
Temperature (°C)
770000
760000
750000
740000
730000
720000
710000
700000
640
660
680
700
720
740

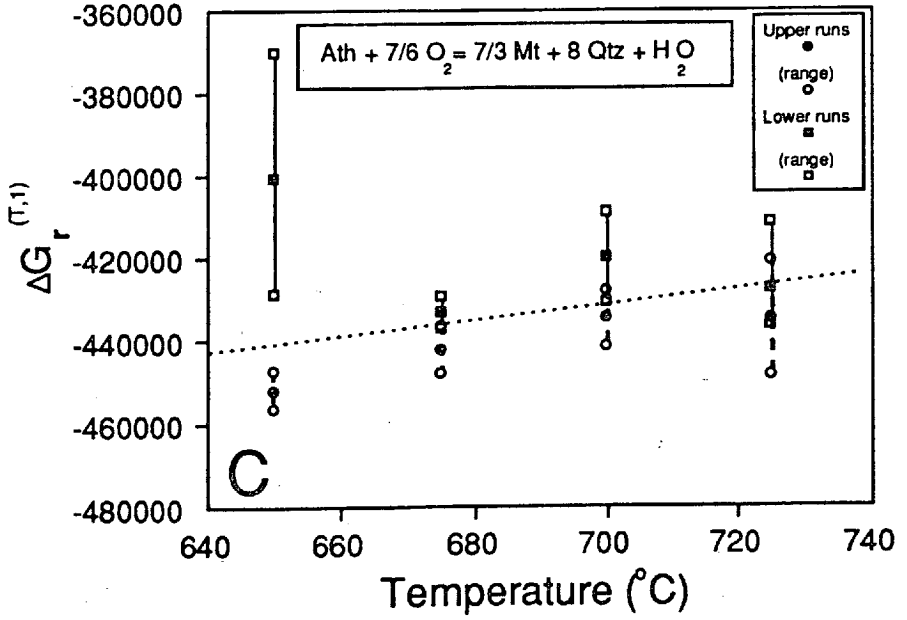
Ath + 7/6 O2 = 7/3 Mt + 8 Qtz + H2O
Upper runs
(range)
Lower runs
(range)
C
ΔGr(T,1)
Temperature (°C)
-360000
-380000
-400000
-420000
-440000
-460000
-480000
640
660
680
700
720
740

Froese and Gunter (1976).

$$Mt + 1/2\ S_2 = 3\ Po + 2\ O_2 \qquad (6.3)$$

A plot of the recalculated data is shown in figure (6.1A). The 700°C calculated boundary is in excellent agreement with that of Froese (1977) and Tso et al. (1979) (who used the magnetite data of Hewitt (1978)), both corrected to P=2 Kbar total presure. The variation in ΔG_r for reactions 6.1 and 6.2 for the ferroanthophyllite compositions and experimental temperature ranges used by Popp et al. (1977b) was calculated from:

$$\Delta G^{T,1}_{(6.1)} + \int_1^P \Delta V_s dP = -2.303\ RT[\log fH_2O + 7/2 \log fO_2 + 7\ \log a^{Po}_{FeS} - 7/2 \log fS_2 - \log a^{Fe\text{-}Ath}] \qquad (6.4)$$

$$\Delta G^{T,1}_{(6.2)} + \int_1^P \Delta V_s dP = -2.303\ RT[\log fH_2O - 7/6 \log fO_2 - \log a^{Fe\text{-}Ath}] \qquad (6.5)$$

where $\Delta G^{T,1}_{(r)}$ is the free energy change of the reaction at T (K), P=1bar, ΔV_s is the molar volume change of the solids, R if the gas constant (8.314 j/molK). The details on the pressure integral calculation are presented in *Appendix III*. The molar volume of ferroanthophyllite (27.87 J/bar) used is that given in Holland and Powell (1990). The experimental partial pressures of the gas species were calculated in the system H-O-S according to the ideal mixing scheme of Ohmoto and Kerrick (1977) assuming:

$$P_{tot} = \frac{fH_2}{\overline{\varphi H_2}} + \frac{fH_2O}{\overline{\varphi H_2O}} + \frac{fH_2S}{\overline{\varphi H_2S}} + \frac{fSO_2}{\overline{\varphi SO_2}} + \frac{fS_2}{\overline{\varphi S_2}} + \frac{fO_2}{\overline{\varphi O_2}} \qquad (6.6)$$

where φ is the fugacity coefficient for a gas species at the T and P of

interest. Poulson and Ohmoto (1989) showed that under high T and P conditions, fluids compositions modelled with ideal and non-ideal mixing are qualitatively the same and could not justify the use of the MRK equation. The sources of thermodynamic data are presented in a later section of this chapter. The calculated $\log fH_2O$ value for each experimental run was used in equations (6.4) and (6.5). The results, presented in figures 6.1B and 6.1C, indicate that the 650°C runs of Popp et al.(1977b) are poorly bracketed and apparently have not achieved equilibrium. Equilibrium must lie in the overlapping zones defined by the ranges of calculated $\Delta G_r^{T,1}$ for the upper (low X_{Fe}, high fO_2-fS_2) and lower (high X_{Fe}, low fO_2-fS_2) experimental runs.

The variations in $\Delta G_r^{T,1}$ with T for reactions 6.1 and 6.2 were regressed from the recalculated experimental data between 650-725°C of Popp et al. (1977b), assuming a linear relationship between $\Delta G_r^{T,1}$ and temperature:

$$\Delta G^{T,1}_{(6.1)} = [-208.58\ T(°C) + 877792] \pm 10000\ J/mol \qquad (6.7)$$

$$\Delta G^{T,1}_{(6.2)} = [148.36\ T(°C) - 532899] \pm 5000\ J/mol \qquad (6.8)$$

The errors are estimated from the maximum and minimum slopes.

Froese (1977) recalculated an average value of $\Delta G^{T,1}_{(6.1)} + \int_1^P \Delta V_s dP$ for the four best runs at T=700°C (98, 106, 108, 113) of Popp et al. (1977b). He determined values of 743677 J (177743 cal) and -426768 J (-102000 cal) for reaction (6.2), which are in good agreement with those obtained from equations (6.7) (740056 J or 176877 cal) and (6.8) (-426484 J or -101932 cal) when corrected to P=2 Kbar. Hence, although, as shown in Fig. 6.2, the overall experimental results are not well bracketed, they are the only ones available at this time and must be used as a first approximation and tested against natural assemblages.

Other oxidation and sulfidation reactions involving anthophyllite were

investigated thermodynamically by Popp et al. (1977b) in conjuction with the experimental results, and were used to map X_{Fe}^{Ath} in $\log(fO_2)$-$\log(fS_2)$ space under fixed P,T conditions.

$$\text{Fe-Ath} + 7/4O_2 = 7/2\ \text{Hem} + 8\ \text{Qtz} + H_2O \qquad (6.9)$$

$$\text{Fe-Ath} + 7S_2 = 7\ FeS_2 + 8\ \text{Qtz} + H_2O \qquad (6.10)$$

These have also been recalculated using the thermodynamic data for magnetite from Robie et al. (1978). The variation in free energy changes (ΔG) with temperature (at 1bar) for the sulfidation (6.1) and oxidation (6.2) reactions were extrapolated to peak temperatures in the three terranes using equations (6.7) and (6.8), assuming a linear down temperature relationship (Figs 6.1B,C). This allowed mapping of X_{Fe}^{Ath} isopleths in $\log(fO_2)$-$\log(fS_2)$ space for peak P-T conditions in each terrane (Fig. 6.2). The thermodynamic and equations used in constructing these diagrams (Fig. 6.2) are given in *Appendix III*.

Estimation of fO_2-fS_2 Conditions in the Three Terranes

Isopleths of X_{Fe}^{Ath} were calculated in $\log(fO_2)$-$\log(fS_2)$ space with oxide-sulfide boundaries. In sulfide bearing rocks, the metamorphic fluid can be described the system C-O-H-S. If graphite is present and P, T, fO_2 and fS_2 conditions are known for a given rock, the partial pressure of the gas species assuming ideal mixing can be calculated by solving a mass balance equation of involved equilibria (Ohmoto and Kerrick, 1977; Ferry, 1981; Poulson and Ohmoto, 1989; Hall et al., 1991). This allows fH_2O to be calculated, a value necessary to calculate the fO_2-fS_2 location of X_{Fe}^{Ath} isopleths. Unfortunately, graphite is absent in the cordierite-anthophyllite rocks in the three terranes, hence $a^{Graphite}<1$. The sulfur fugacity (fS_2) can be estimated from

Fig. 6.2. Ferro-anthophyllite stability on $logfO_2$-$logfS_2$ plots for the peak P-T conditions recorded in the three terranes. A) Atik Lake, B) Némiscau, C) Montauban. Gr=graphite. Graphite is stable below Gr Max. The ranges in pyrrhotite or sphalerite compositions are shown on the diagrams, and details are given in the inset.

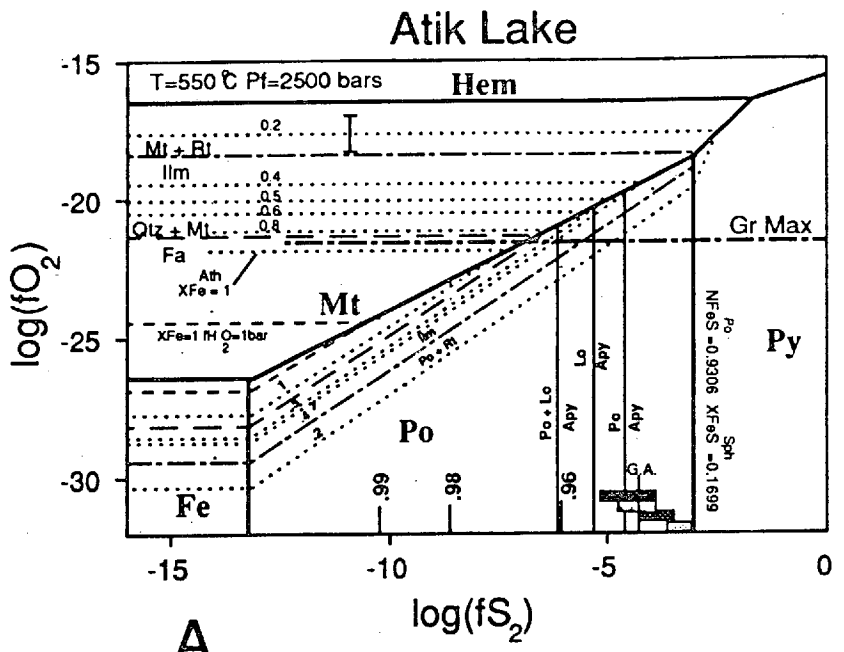
Atik Lake
T=550 C Pf=2500 bars
Hem
Mt + Rt
Ilm
Qtz + Mt
Fa
Ath
XFe = 1
Mt
XFe=1 fH2O=1bar
Po
Fe
Po + Lo
Apy
Lo
Apy
Po
Apy
G.A.
Gr Max
Py
NFeS = 0.9306 XFeS = 0.1691
log(fO2)
log(fS2)
A

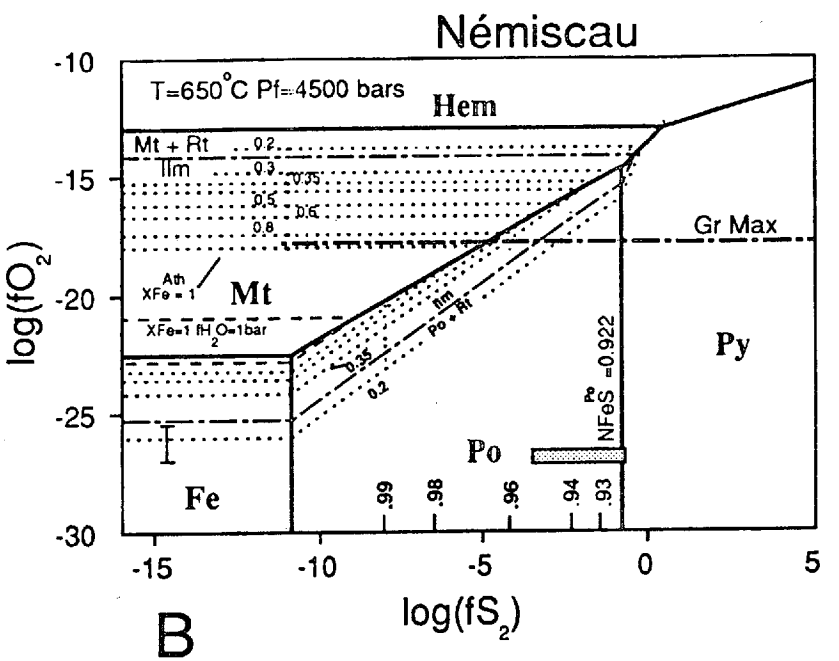
Némiscau
T=650°C Pf=4500 bars
Hem
Mt + Rt
Ilm
Ath
XFe = 1
Mt
XFe=1 fH2O=1bar
Po + Rt
Fe
Po
NFeS = 0.922
Gr Max
Py
log(fO2)
log(fS2)
B

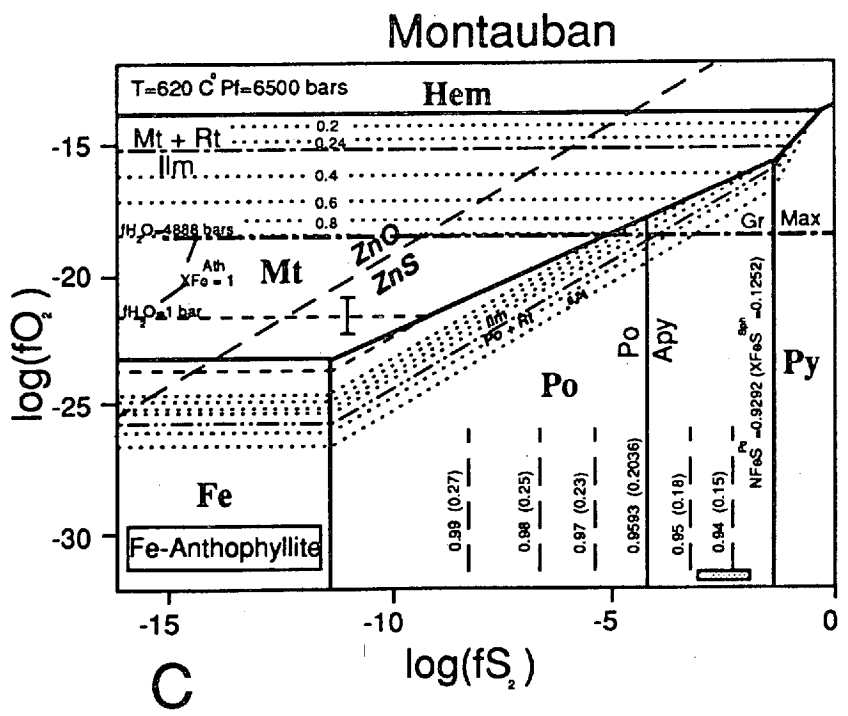
Montauban
T=620 C Pf=6500 bars
Hem
Mt + Rt
Ilm
fH2O=4888 bars
Ath
XFe = 1
Mt
ZnO
ZnS
fH2O=1 bar
Po + Rt
Po
Apy
Gr Max
Py
Fe
Fe-Anthophyllite
log(fO2)
log(fS2)
C

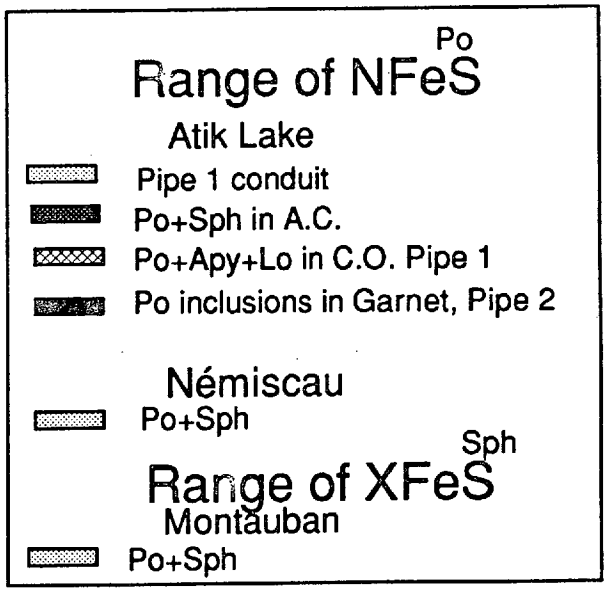
Range of NFeS Po
Atik Lake
Pipe 1 conduit
Po+Sph in A.C.
Po+Apy+Lo in C.O. Pipe 1
Po inclusions in Garnet, Pipe 2
Némiscau
Po+Sph
Range of XFeS Sph
Montauban
Po+Sph

sphalerite and arsenide compositions coexisting with pyrrhotite at P-T conditions of interest, but fO_2 and $a^{Graphite}$ are difficult or impossible to determine in a graphite absent-system. The only constraint on fO_2 is that graphite-absent rocks must have recorded $\log(fO_2)$ values higher than the maximum stability for graphite (for $X_{CO_2} = 1$, see GR MAX boundaries in Fig. 6.2). To circumvent the lack of data on fH_2O, two extreme cases were calculated, $P_{H_2O}=P_{total}$ and $P_{H_2O} \ll P_{total}$ (fH_2O from Burnham et al., 1969). The problem of metamorphic fluid speciation is addressed in detail in the next section. It can be seen from figure 6.2 that decreases in P_{H2O} contribute to a drastic diminution of the anthophyllite stability fields (compare X_{Fe} isopleths). The isopleths and reaction lines in figure (6.2) ought to be considered as zones (see estimated error bar).

Atik Lake

The modelling of fO_2-fS_2 equilibria under peak P-T conditions can be achieved for BIF, mineralized chert, and altered basalt by using the sulfide-oxide-arsenide assemblages and the X_{Fe} of grunerite and anthophyllite. The energetics of ferroanthophyllite do not differ greatly from those of grunerite (see thermodynamic database in Holland and Powell, 1990). It is well known that increases in fO_2 and fS_2 can induce lowering of XFe in Fe-Mg silicates through magnetite-, hematite- or pyrrhotite-forming reactions (Kullerud and Yoder, 1963; Froese, 1971; Popp et al, 1977; Tso et al, 1979; Nesbitt, 1982). This behavior is depicted by the anthophyllite X_{Fe} isopleths in figure 6.2A. Thus, the composition of grunerite and anthophyllite can be buffered by appropriate oxide, sulfide and arsenide assemblages, and vice versa. It is possible to test the validity of figure (6.2A) by comparing

amphibole compositions for various buffering assemblages.

The fO_2 in the grunerite-fayalite-quartz-magnetite BIF (U-18-04) was internally buffered near QFM, and both grunerite (X_{Fe}=0.97) and fayalite (X_{Fe}=0.99) are very Fe-rich. The calculated QFM boundary is at $\log(fO_2)$=-21.3 and falls between the X_{Fe}=1 and X_{Fe}=0.8 isopleths (Fig. 6.2A), for $P_{H_2O}=P_{total}$. The analysed grunerite composition is in good agreement with the predicted composition, considering the uncertainties involved. This suggests that grunerite in BIF was in equilibrium with a water rich fluid under peak P-T (2,5 Kbar, 550°C) conditions.

By contrast, grunerite coexisting with pyrrhotite and magnetite in BIF (U-23-01) has X_{Fe}=0.75. Under peak P-T conditions, the grunerite composition would have been buffered along the magnetite-pyrrhotite boundary above the QFM value. This is consistent with the calculated isopleths shown in figure 6.2, for a water-rich fluid. The grunerite composition with the lowest analysed X_{Fe} (0.36) is from a pyrrhotite-sphalerite-bearing mineralized chert (U-05-05).

Pyrrhotite composition and structure are known to easily reset during retrograde processes and have been judged unreliable in evaluating prograde conditions (Valley et al., 1990). The composition of quenched pyrrhotite has been used to calculate fS_2 (Barton and Skinner, 1967; Popp et al., 1977; Bryndzia et al. 1990) conditions during experimental runs. Pyrrhotite in altered basalts and mineralized chert at Atik Lake has a wide range in N_{FeS}^{Po} (0.914-0.955), with the core generally more Fe-rich than the rim. Values lower that N_{FeS}^{Po}=0.93 are obviously re-equilibrated. The ranges of calculated fS_2 from pyrrhotites is shown in figure 6.2A for various rock types. The altered basalts equilibrated in the range of $\log fO_2$= -19.5 to -21.2 and

$LogfS_2$=-4.6 to -5.3, whereas the mineralized chert recorded the highest $LogfO_2$ (≈-18) at $LogfS_2$ (≈-3.05), and necessitate a water-rich metamorphic fluid. The highest N^{Po}_{FeS} values are from inclusions of pyrrhotite coexisting with löllingite or arsenopyrite in garnet from alteration pipe 2. These values are believed to represent "frozen" compositions that have not re-equilibrated upon cooling. The overall range of pyrrhotite compositions above N^{Po}_{FeS}=0.93 is compatible with prograde fS_2 conditions Fig. 6.2A).

Pyrite-pyrrhotite is a common assemblage in the massive sulfide body together with mineralized chert and graphitic argillite. Carpenter (1974) reported that desulfidation of pyrite (Py-Po isograd) during regional metamorphism will begin near the biotite-in isograd for pelitic rocks. Pyrite porphyroblasts at Atik Lake are in all cases surrounded by pyrrhotite, and suggest that desulfidation of pyrite was a prograde sulfur-releasing mechanism, and an effective fS_2 internal buffer for Fe-Mg-Mn silicate assemblages in the mineralized chert and massive sulfide body.

The anthophyllite from altered basalts has XFe=0.48-0.52 and coexists with pyrrhotite-ilmenite (and may coexist with arsenopyrite, löllingite or pyrrhotite). The calculated X_{Fe}=0.4 and 0.5 isopleths fall well within the pyrrhotite-ilmenite field (Fig. 6.2A). In order for these isopleths to be in the range of fS_2 values indicated by the Po-Lo-Apy, Po-Lo and Apy-Po boundaries and within the pyrrhotite-ilmenite field, it is necessary that the anthophyllite was in equilibrium with a water-rich fluid. Pyrite was identified in only one sample of altered basalts (U-12); it was present in trace amounts and contained up to 0.68% Co and 0.75% Ni. Pyrrhotite plus coulsonite-rich magnetite and ilmenite is the dominant buffering assemblage in U-12 which has $X^{Gedrite}_{Fe}$=0.75. Gedrite X_{Fe} isopleths will parallel these of

anthophyllite, but are always slightly more Fe-rich. The oxidation-sulfidation of gedrite would involve an Al-rich phase, probably plagioclase, which would also account for the alkalies in the gedrite.

The effect of the incorporation of large amounts of vanadium in magnetite on the Po/Mt and Po/Mt/Py boundaries can be evaluated using the magnetite activity model of Stormer (1983). The activity of magnetite in U-12 is calculated to be 0.32, but this decrease from unity only contributes to a displacement of the boundaries down -0.24 $\log(fO_2)$ units. Local variations in fO_2-fS_2 in pipe 1 cordierite-orthoamphibole rocks are also indicated by the variation in spinel compositions (Bernier, 1990), the presence of sphene±ilmenite in somewhat altered basalt, and ilmenite alone in fresh samples (c.f. Spear, 1981). These variations are most likely inherent to bulk rock compositions and accompanied intrinsic variation in oxidation (sulfidation) states, and different buffering capacities.

Hence, it is evident that BIF, altered basalts and mineralized chert have mineral compositions reflecting internal buffering and a strong influence of bulk rock composition which excludes large influxes of fluids that would have homogenized mineral compositions during metamorphism.

Némiscau

The anthophyllites coexisting with ilmenite and pyrrhotite are in the range X_{Fe}=0.38-0.53 and and slightly overlap those with pyrrhotite-magnetite±pyrite (X_{Fe}=0.34-0.38), reflecting changes in fO_2-fS_2 under fixed peak P-T conditions (Fig. 6.2B). Pyrite porphyroblasts are present in the magnetite-pyrrhotite bearing cordierite-anthophyllite rocks and frequently associated with retrograde chlorite replacing cordierite. These

rocks most likely equilibrated near the PPM invariant point (log fO_2=-14.62, logfS_2=-0.783); the range of anthophyllite composition fall below the PPM inariant point, but is within the limits of the error bar. The low X_{Fe} anthophyllite lies along the Po-Mt boundary (LogfO_2≈-15 to -16, Log fS_2≈-1.4 to -2.2), whereas the more Fe-rich ones are within the ilmenite-pyrrhotite field at slightly lower logfO_2-logfS_2 values. The range of pyrrhotite compositions coexisting with minor sphalerite is outlined in figure 6.2B.

Montauban

Anthophyllite coexisting with pyrrhotite and rutile has an average X_{Fe}=0.24±0.05. The calculated X_{Fe}=0.24 isopleth falls within the pyrrhotite-rutile field (Fig. 6.2C) for P_{H_2O}=P_{tot}. A high water pressure is required to keep the 0.24 isopleth within this field (Fig. 6.2C), supporting the previous inference for a highly hydrated cordierite at peak P-T conditions. When the range of coexisting pyrrhotite and sphalerite compositions is considered with the 0.24 isopleth, a fairly well constrained range of logfO_2-logfS_2 (Fig. 6.2C) is defined where logfO_2 ranges from -16.4 to -18.5 and logfS_2 from -1.3 to -3.5.

Conclusion

Using the experimental data of Popp et al. (1977b), the sulfide-oxide mineral equilibria for the three terranes impose constraints on the range of logfO_2-logfS_2 values that are consistent with the X_{Fe}^{Ath} compositions of grunerite and anthophyllite only when P_{H_2O}≈P_{fluid} at peak P-T conditions. However, these calculations should be considered a first approximation. Estimates of the fugacity of water under peak P-T are needed to calculate

ferroanthophyllite sulfidation and oxidation equilibria and vice versa.

The nature of the fluid under peak metamorphic conditions is assessed in further detail in the following section.

Fluid Equilibria in the System C-O-H-S

Introduction

In this section the metamorphic fluid speciation in the system C-O-H-S will be assessed for cordierite-orthoamphibole rocks and related gneisses using the peak metamorphic P-T conditions outlined in Chapter 4. The question of internal buffering of the metamorphic fluid by mineral assemblages will be discussed.

The metamorphic fluid speciation can be modelled in the C-O-H-S system when fS_2 and fO_2 are known at P-T conditions of interest and graphite is present (Ohmoto and Kerrick, 1977; Ferry, 1981; Poulson and Ohmoto, 1989; Valley et al, 1990; Hall et al., 1991). For graphite absent-rocks, fluid speciation can only be modelled for various values of $a^{Graphite}<1$ because it is impossible to estimate it.

Fluid speciation as a function of fO_2 was calculated assuming an ideal mixing model and the equilibrium constant-mass balance technique of Ohmoto and Kerrick (1977). The computer program FLUICOHS (written by LRB) perform these calculations (see *Appendix* details). The scheme of Ohmoto and Kerrick (1977) was modified to include input of graphite activity ($a^{Graphite}=1$ for graphite present, $a^{Graphite}<1$ for graphite absent) and of $\log(fS_2)$ values. The pyrrhotite-pyrite equilibrium was modeled using equations of Froese and Gunter (1976), because the equilibrium constant of Huebner (1971) used by Ohmoto and Kerrick (1977) is erroneous and has led to underestimations of the H_2S, COS

Fig. 6.3. Plot of mole fractions of H_2O, CO_2, CH_4, and H_2S versus $\log fO_2$ for the metamorphic conditions in the Atik Lake terrane. A) Graphite-bearing system (a^C=1) at fS_2 defined by the PP buffer. B) Graphite absent system (a^C=0.1) at fS_2 define by the PP buffer. C) and D) Graphite absent system (a^C=0.1, and a^C=0.001, respectively) at fS_2 intermediate to the pyrrhotite-arsenopyrite and löllingite-arsenopyrite buffers. These plots can be regarded as sections for fixed values of fS_2 across the fO_2-fS_2 space in Fig. 6.2A.

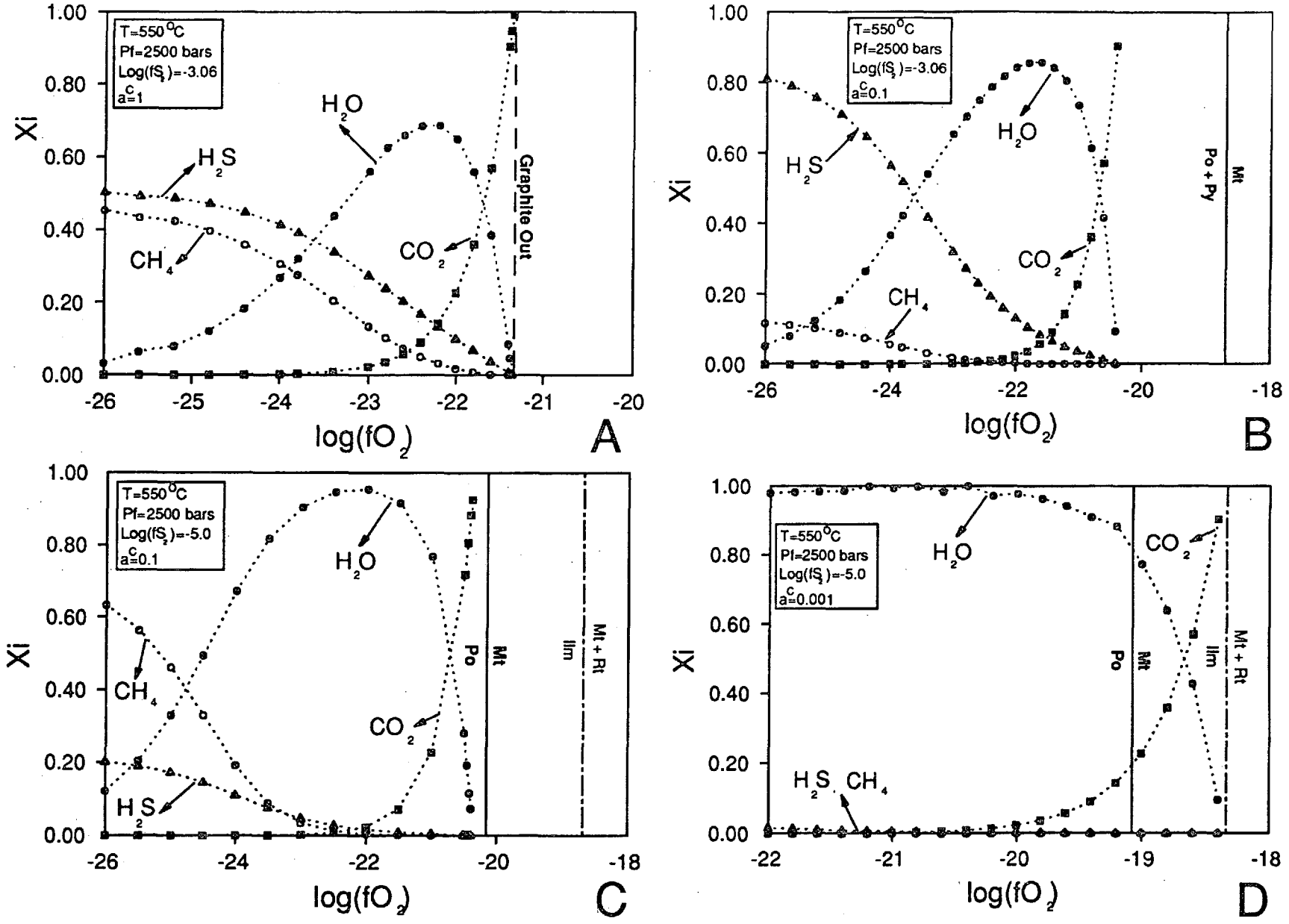
T=550°C
Pf=2500 bars
Log(fS2)=-3.06
ac=1
H2O
H2S
CH4
CO2
Graphite Out
Xi
log(fO2)
A
T=550°C
Pf=2500 bars
Log(fS2)=-3.06
ac=0.1
H2O
H2S
CH4
CO2
Po + Py
Mt
Xi
log(fO2)
B
T=550°C
Pf=2500 bars
Log(fS2)=-5.0
ac=0.1
H2O
CH4
CO2
H2S
Po
Mt
Ilm
Mt + Rt
Xi
log(fO2)
C
T=550°C
Pf=2500 bars
Log(fS2)=-5.0
ac=0.001
H2O
CO2
H2S, CH4
Po
Mt
Ilm
Mt + Rt
Xi
log(fO2)
D

and SO_2 mole fractions (Poulson and Ohmoto, 1989). The gas species fugacity coefficients are from the following sources: H_2O Burnham et al. (1969), CO_2 Mel'nik (1972), H_2S, CH_4, H_2, CO Ryzhenko and Volkov (1971). For SO_2 and COS, the activity coefficients were calculated using reduced temperature and pressure parameters with a Redlich-Kwong equation of state (program REDKWONG in *Appendix*). This was done because the reduced pressures for these gases are much larger than the range used by Ryzhenko and Volkov (1971) to derive their equations of state. The activity coefficients of S_2 and S_8 were taken to be 1 (Ohmoto and Kerrick, 1977).

Atik Lake

The graphitic argillite at Atik Lake is characterized by the presence of graphite, pyrite, pyrrhotite, rutile and ± arsenopyrite. Metamorphic fluid speciation at $\log(fS_2)$=-3.06 (Po/Py), $a^{Graphite}$=1 places the upper stability limit for graphite at $\log(fO_2)$=-21.30 for XCO_2=1 (Figs. 6.2A, 6.3A). The graphite maximum stability occurs at a $\log(fO_2)$ value slightly above that of QFM buffer ($\log(fO_2)$=-21.99) which is in good agreement with calculations of Poulson and Ohmoto (1989). There is not a good control on the oxidation state, which is necessary in order to have a fully constrained system for an evaluation of the fluid composition. However, since calcite is generally absent or occurs as an accessory phase, and muscovite, plagioclase and quartz are the dominant minerals in the graphitic argillite, it is reasonable to assume that the metamorphic fluid was water-rich. The maximum amount of H_2O (XH_2O=0.70) is obtained at $\log(fO_2)$=-22.3 (below QFM) with XH_2S=0.15, XCO_2=0.10 and XCH_4≈0.05 (Fig. 6.3A). Decreases in fO_2 can contribute to increases in XH_2S. This is of importance, as production of significant

amounts of H_2S fluids would favor the formation of sulfide complexes, and mobilization of ore metals may occur (Barnes, 1979; Poulson and Ohmoto, 1989). However, local variations in peak metamorphic fluid composition within the graphitic argillite cannot be ruled out.

Most studies on metamorphic fluid composition assessed the principal gas species present, but aqueous fluids can carry significant quantities of dissolved material, predominantly in the form of chloride complexes at moderate to high grades (c.f. Eugster, 1981; Haack et al., 1984; Yardley, 1985; Eugster, 1986). Thus chloride complexes may have played a significant role in mobilizing ore components during metamorphism.

The mineralized chert, which occurs between beds of graphitic argillite, does not contain graphite ($a^{Graphite}<1$). This is consistent with the presence of low-Fe grunerite ($XFe\leq0.36$) which indicates fO_2 conditions above the upper stability of graphite in a water-rich fluid (Fig. 6.2A). Pyrite-pyrrhotite-arsenopyrite, pyrite-pyrrhotite and pyrrhotite- arsenopyrite are common assemblages in the mineralized chert. Peak metamorphic fluid speciation was thus modeled at $\log(fS_2)=-3.06$ (Po/Py) and at a value of -5 which is intermediate to the Po/Apy and Po/Lo boundaries and $a^{Graphite}=0.1$ (Figs 6.3B,C). Any value of $a^{Graphite}$ lower than 1 could have been used as there is no way to estimate this parameter, and 0.1 is choosen strictly for a comparison basis with graphite-present fluid equilibria.

The main changes imposed by decreasing $a^{Graphite}$ to 0.1 are: 1) an increase in H_2S and a diminution of the amounts of carbon species, 2) an expansion of the H_2O field, and 3) an increase of the maximum XH_2O (0.90) accompanied by a shift in fO_2 ($LogfO_2=-21.8$). H_2O and H_2S become the dominant fluid species at a $LogfO_2$ value of about -21.5 (Fig. 6.3B). A decrease in fS_2

expands the field of dominance of H_2O (Fig. 6.3C) to a maximum XH_2O=0.95 at $LogfO_2$=-22. If a value of $a^{Graphite}$=0.001 is used at log(fS_2)=-5, then the domiant species will be H_2O and CO_2 at the pyrrhotite-magnetite boundary (Fig. 6.3D), and XH_2O will be close to unity at a $LogfO_2$ value of -20. The $a^{Graphite}$ will have a profound effect on the capacity of a metamorphic fluid to generate H_2S and contribute to mobilization of ore components. Because graphitic argillite is closely associated with the mineralized chert on Mistuhe Island, it is possible that $a^{Graphite}$ was much higher than 0.1. In this case a condition between those of figures 6.3A and B would occur.

The grunerite-magnetite-quartz banded iron formation along strike with the mineralized chert would require a water-rich fluid for it to be stable under peak metamorphic conditions. Very low fS_2 are conditions indicated by the absence of sulfides, and low XCO_2 suggested by the absence of carbonate and graphite.

The cordierite-orthoamphibole rocks and other altered basalt units are characterized by a range of buffering mineral assemblages and compositions. These occur in a single outcrop (e.g. pipe 1), which strongly favors local variations in metamorphic fluid compositions and strong bulk compositional control (c.f.. Hall et al., 1991). The constraints imposed by the dominant oxide-sulfide±arsenide assemblages (Po-Ilm, Po-Ilm-Mt and Po-Ilm-Apy-Po) and the composition of the orthoamphiboles and other coexisting Fe-Mg-silicates, explicitly implies a water-rich peak metamorphic fluid. A low activity of graphite at a relatively low log(fS_2)=-5 will favor water-rich fluids over a wide range of oxidation states (Figs 6.3C). These conclusions support the previous inferences on peak metamorphic fluid speciation in the altered basalts.

Fig. 6.4. T-XCO_2 multi-equilibrium diagram using reduced mineral activities derived from the microprobe analyses of calc-silicates in sample U-2C, Atik Lake. The plot is calculated for non-ideal mixing of CO_2-H_2O using GEO-CALC (Brown et al., 1988) for the system CaO-FeO-MgO-SiO_2-Al_2O_3-CO_2-H_2O. [Mineral abbreviations as in Chapter 1 except Gr=grossular, Py=pyrope, and Qz=quartz.]

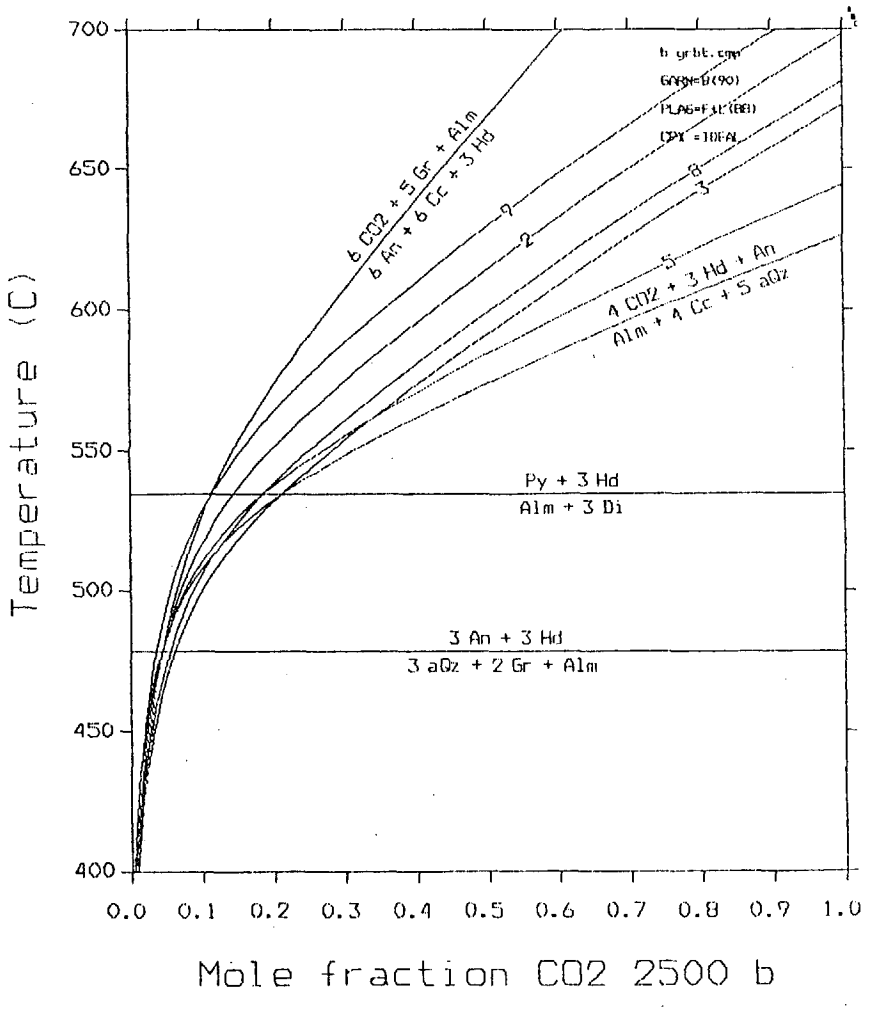

REACTION LIST (U02C)
Assemblages on the left are stable on the:
high side of the Y-axis variable, or the
high side of the X-axis variable for vertical reactions

1): 4 CO2 + 3 Hd + An = Alm + 4 Cc + 5 aQz

2): 2 CO2 + Gr = An + 2 Cc + aQz

3): 4 CO2 + 3 Di + An = 4 Cc + Py + 5 aQz

4): 3 An + 3 Hd = 3 aQz + 2 Gr + Alm

5): 6 CO2 + 3 Hd + Gr = Alm + 6 Cc + 6 aQz

6): 6 CO2 + 5 Gr + Alm = 6 An + 6 Cc + 3 Hd

7): Py + 3 Hd = Alm + 3 Di

8): 6 CO2 + Gr + 3 Di = 6 Cc + Py + 6 aQz

9): 6 CO2 + Py + 5 Gr = 6 An + 6 Cc + 3 Di

Multi-equilibrium calculations

The multi-equilibrium method outlined by Berman (1991) was applied on the Atik Lake pipe 1 wallrock calc-silicate assemblage (Table 4.1A, chapter 4) to estimate XCO_2 by generating a T-XCO_2 diagram (Fig. 6.4) at P=2 Kbar. Because calcite is present and sulfides are absent, it is likely that the metamorphic fluid was essentially a H_2O-CO_2 mixture. The estimated XCO_2 will represent a maximum value for other rock types with no calcite. Hornblende was left out because it is not part of the Berman (1988) thermodynamic database. All decarbonation reactions intersect the garnet-clinopyroxene thermometer (T=530°C) in a range of XCO_2=0.2-0.1, indicating that a water-rich metamorphic fluid was in equilibrium with the calc-silicate assemblage under peak P-T conditions. Hence, the earlier assumptions favoring a water-rich metamorphic fluid in equilibrium with the cordierite-orthoamphibole rocks mineral assemblages is validated. In the absence of graphite and calcite, and in the presence of sulfides and arsenides, H_2S might have been an important constituent.

In summary, the peak metamorphic fluid composition at Atik Lake was most likely internally buffered within the mineralized chert, BIF, altered basalts and alteration conduits. The contrasting arsenide and orthoamphibole compositions in altered basalts and mineralized chert is convincing evidence of the strong bulk compositional effect exerted on mineral equilibration during metamorphism. This is consistent with a low water-rock ratio regime, and internally controlled devolatilisation and oxidation-sulfidation reactions (Thompson, 1972, Rice and Ferry, 1982). However, it cannot be ruled out that some elements (Na, Ca, Mn etc...) were being exchanged with an external fluid at low water/rock ratios in a combination of buffering-infiltration

mechanisms. Only a tedious, rigourous and very detailed study of modal amounts of reacting phases combined with compositional data and evaluation of the progress of reactions at various scales (thin section, hand specimen, outcrop and regional) could solve this problem. It is evident that syn-peak metamorphic fluids in the graphitic argillite and mineralized chert were H_2S-bearing. Thus, local mobility of gold as $HAu(HS)_2$ may have taken place. Also, chloride complexes could have contribute to mobilize ore components. The gold deposition mechanism generally invoked implies sulfidation of grunerite. The gold would be deposited at the contact of pyrrhotite and grunerite, but none has been observed in this texture at Atik Lake.

Némiscau

Most of the above discussion on fluid speciation for Atik Lake applies to the Némiscau terrane, and a precise estimate of the metamorphic fluid composition could not be achieved for the same reasons. Calculated fluid compositions are shown in Table 6.1 for fixed values of $logfO_2$, and $a^{graphite}$ at $LogfS_2$ defined by Po/Py for a comparison basis. The speciation in the system C-O-H-S was calculated but the resulting Xi-$LogfO_2$ diagrams at various fS_2 and $a^{Graphite}$ values did not differ greatly from those for the Montauban rocks (see next section) and are not shown.

Table 6.1 Némiscau and Montauban Metamorphic Fluid Speciation

Némiscau (T=650°C, P=4.5 Kbar) Po/Py boundary, $logfS_2$=-0.78, $a^{graphite}$=0.1 $logfO_2$=-18.2	Montauban (T=620°C, P=6.5Kbar) Po/Py boundary, $logfS_2$=-2.26 $a^{graphite}$=0.1 $logfO_2$=-18.2
XH_2O=0.735	XH_2O=0.789
XCO_2=0.091	XCO_2=0.200
XH_2S=0.171	XH_2S=0.010
XH_2 =0.002	XH_2 =0.0004
XCH_4=0.0005	XCH_4=0.0001
XCOS=0.0009	XCOS=0.0001
XCO =0.0004	XCO =0.0003
XS_2 =0.00004	XS_2 =8.5×10^{-7}
XSO_2=7×10^{-7}	XSO_2=1.7×10^{-7}
XS_8 =1×10^{-8}	XS_8 =5.4×10^{-14}

Multi-equilibrium calculations

It turns out that the assemblages from the metapelitic samples V4811 and S30, for which P-T multi-equilibrium calculations were made in Chapter 4, also provide a means to estimate XCO_2 by plotting T-XCO_2 diagrams (Fig. 6.5) calculated with GEO-CALC for reduced mineral activities. A metamorphic fluid with XCO_2=0.55 was in equilibrium with the metapelitic mineral assemblage (V4811) under peak P-T conditions in the staurolite-andalusite zone. However, the same equilibria intersect at a much lower XCO_2 value of 0.1 for the metapelite S30 in the sillimanite zone. It can be inferred from these results that the metamorphic fluid in equilibrium with the cordierite-anthophyllite rocks in the Lac Voirdye area (sillimanite zone) was water-rich.

Fig. 6.5. T-XCO_2 multi-equilibrium diagrams using reduced mineral activities derived from the microprobe analyses in metapelite samples from Némiscau. A) V4811 from the andalusite-staurolite zone. B) S-30 from the sillimanite zone. The plots are calculated for non-ideal mixing of CO_2-H_2O using GEO-CALC (Brown et al., 1988), in the system K_2O-FeO-MgO-SiO_2-Al_2O_3-CO_2-H_2O. [Mineral abbreviations as in Chapter 1 except Ann=annite, Gr=grossular, Py=pyrope, and Qz=quartz.]

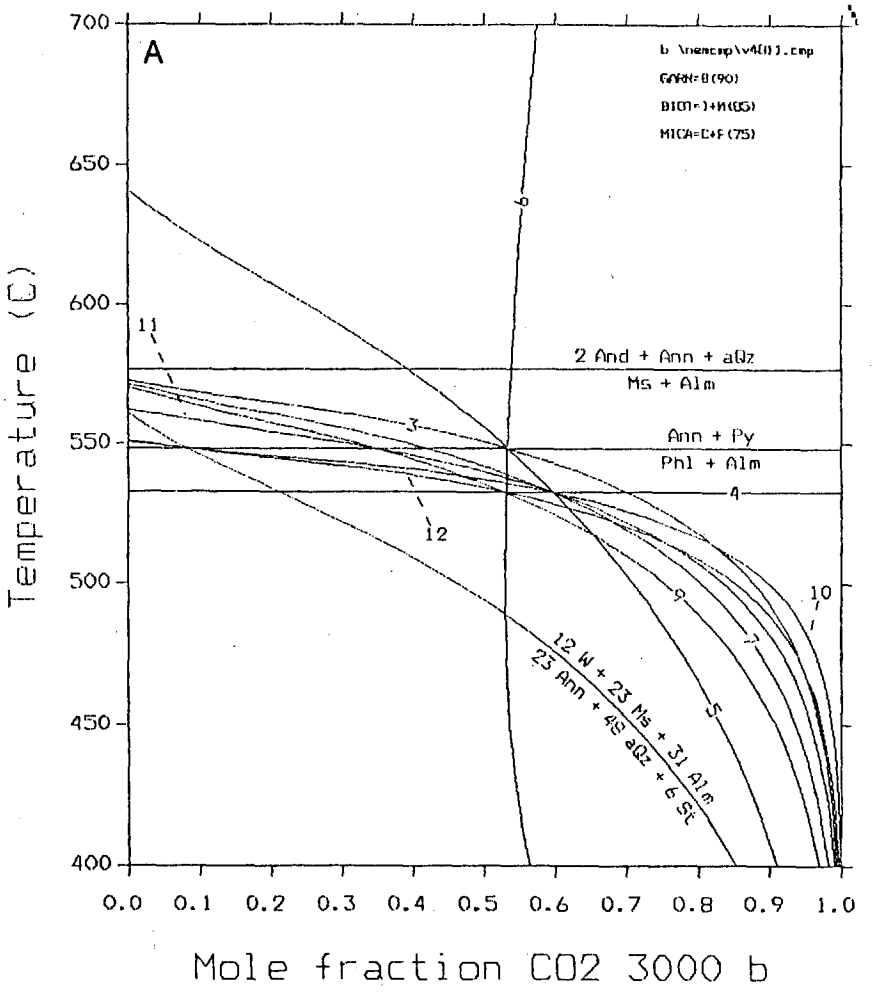

REACTION LIST (V4811)
Assemblages on the left are stable on the:
high side of the Y-axis variable, or the
high side of the X-axis variable for vertical reactions

1): Ann + Py = Phl + Alm

2): 2 And + Ann + aQz = Ms + Alm

3): 12 W + 25 Ann + 96 And = 17 Alm + 25 Ms + 6 St

4): Ms + Py = aQz + Phl + 2 And

5): 12 W + 17 Phl + 8 Ann + 96 And = 25 Ms + 17 Py + 6 St

6): 25 Ms + 25 Py + 6 St = 12 W + 25 Phl + 96 And + 8 Alm

7): 12 W + 8 Ann + 62 And = 8 Ms + 17 aQz + 6 St

8): 12 W + 23 Ms + 31 Alm = 23 Ann + 48 aQz + 6 St

9): 12 W + 46 And + 8 Alm = 25 aQz + 6 St

10): 12 W + 31 Py + 23 Ms + 8 Ann = 31 Phl + 48 aQz + 6 St

11): 12 W + 8 Py + 8 Ann + 46 And = 8 Phl + 25 aQz + 6 St

12): 12 W + 23 Py + 23 Ms + 8 Alm = 23 Phl + 48 aQz + 6 St

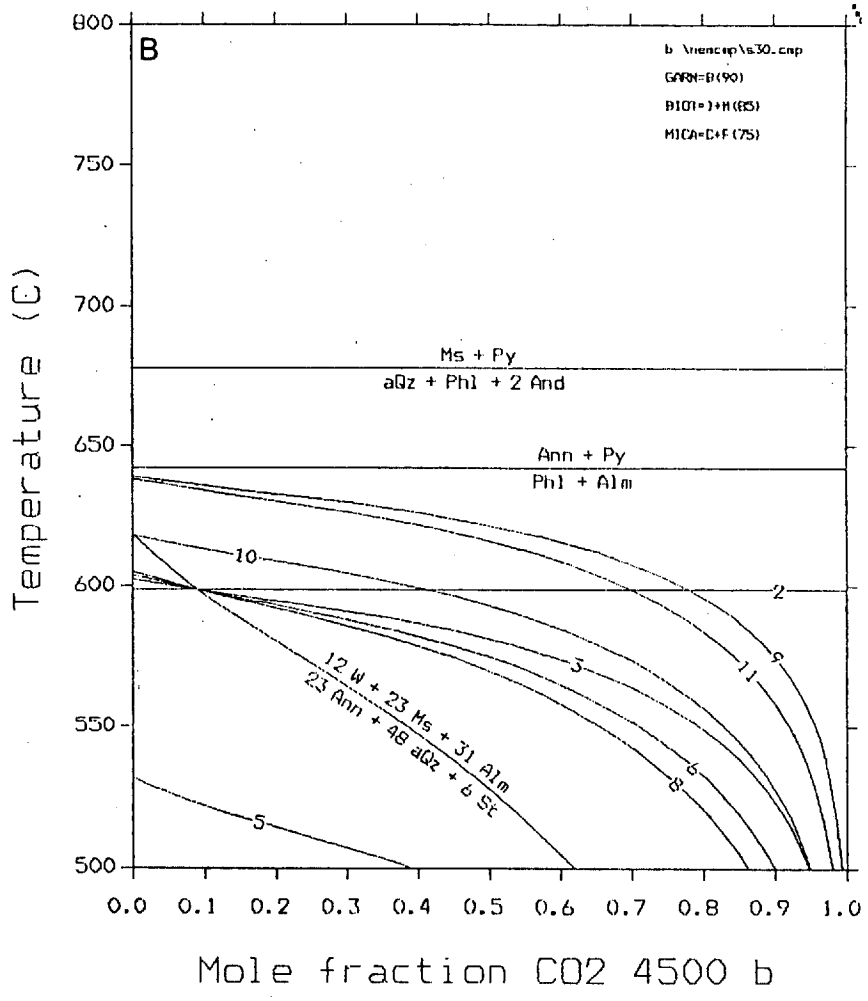

REACTION LIST (S-30)
Assemblages on the left are stable on the:
high side of the Y-axis variable, or the
high side of the X-axis variable for vertical reactions

1): Ann + Py = Phl + Alm

2): 2 And + Ann + aQz = Ms + Alm

3): 12 W + 25 Ann + 96 And = 17 Alm + 25 Ms + 6 St

4): Ms + Py = aQz + Phl + 2 And

5): 12 W + 17 Phl + 8 Ann + 96 And = 25 Ms + 17 Py + 6 St

6): 12 W + 25 Phl + 96 And + 8 Alm = 25 Ms + 25 Py + 6 St

7): 12 W + 8 Ann + 62 And = 8 Ms + 17 aQz + 6 St

8): 12 W + 23 Ms + 31 Alm = 23 Ann + 48 aQz + 6 St

9): 12 W + 46 And + 8 Alm = 25 aQz + 6 St

10): 12 W + 31 Py + 23 Ms + 8 Ann = 31 Phl + 48 aQz + 6 St

11): 12 W + 8 Py + 8 Ann + 46 And = 8 Phl + 25 aQz + 6 St

12): 12 W + 23 Py + 23 Ms + 8 Alm = 23 Phl + 48 aQz + 6 St

Montauban

At Montauban, graphite is absent from the mineral assemblages of the cordierite-anthophyllite rocks and adjacent gneisses, indicating that $a^{Graphite}<1$ (e.g. Valley et al., 1990). Because there are no assemblages limiting $a^{Graphite}$, calculations have been made using FLUICOHS for the conditions T=620°C, Pf=P=6.5 kbars and $a^{Graphite}$= 1 and 0.1. The calculations assuming the presence of graphite provide maximum values of carbon-bearing fluid species at a given fO_2 (Nesbitt and Essene, 1982; Valley et al., 1990). A value of $LogfS_2$= -2.26 corresponding to a sphalerite composition X_{FeS}^{Sph}=0.15 coexisting with pyrrhotite under peak metamorphic conditions was used in the calculations. Pyrrhotite is much less refractory than sphalerite and is known to reequilibrate during retrograde metamorphism (Nesbitt and Essene, 1982; Valley et al., 1990). The average sphalerite composition was used to back-calculate the composition of coexisting pyrrhotite X_{FeS}^{Po}=0.9323. The average pyrrhotite core compositions analysed by microprobe is 0.9304±0.0042, which is in good agreement with the calculated value.

The resulting mole fraction (Xi) of dominant fluid species (H_2O, CO_2, CH_4, H_2S) versus $LogfO_2$ diagrams are shown in figure 6.6. Figures 6.6A, B represent sections at a fixed $LogfS_2$ value in $LogfO_2$-$LogfS_2$ space (Fig. 6.1C). In comparing figures 6.6A ($a^{Graphite}$=1) with figure 6.6B ($a^{Graphite}$=0.1) it can be seen that the field of H_2O expands at higher $LogfO_2$ values at the expense of CO_2, whereas H_2S become the dominant species and oversteps CH_4 under more reduced conditions.

Multi-equilibrium calculation

Sample A-30 (St-Seymour, 1975) was used to estimate XCO_2 from the

Fig. 6.6. Plots of mole fractions of H_2O, CO_2, CH_4, and H_2S versus $\log fO_2$ for the metamorphic conditions in the Montauban terrane. A) Graphite-bearing system ($a^C=1$) at fS_2 defined by the pyrrhotite-sphalerite buffer for $X_{FeS}^{Sph}=0.15$. B) Graphite absent system ($a^C=0.1$) at the same fS_2 value as in (A). These plots are sections at fixed fS_2 values in fO_2-fS_2 space in Fig. 6.2C.

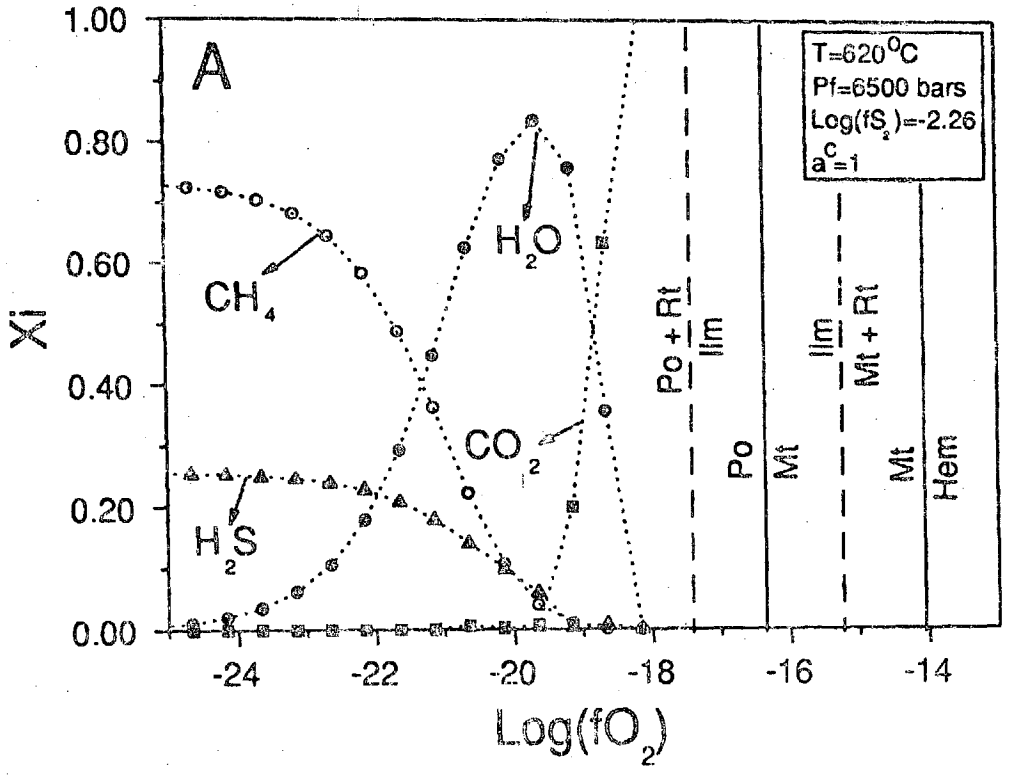
A
T=620°C
Pf=6500 bars
Log(fS2)=-2.26
ac=1
Xi
1.00
0.80
0.60
0.40
0.20
0.00
H2O
CH4
CO2
H2S
Po + Rt
Ilm
Po
Mt
Ilm
Mt + Rt
Mt
Hem
-24
-22
-20
-18
-16
-14
Log(fO2)

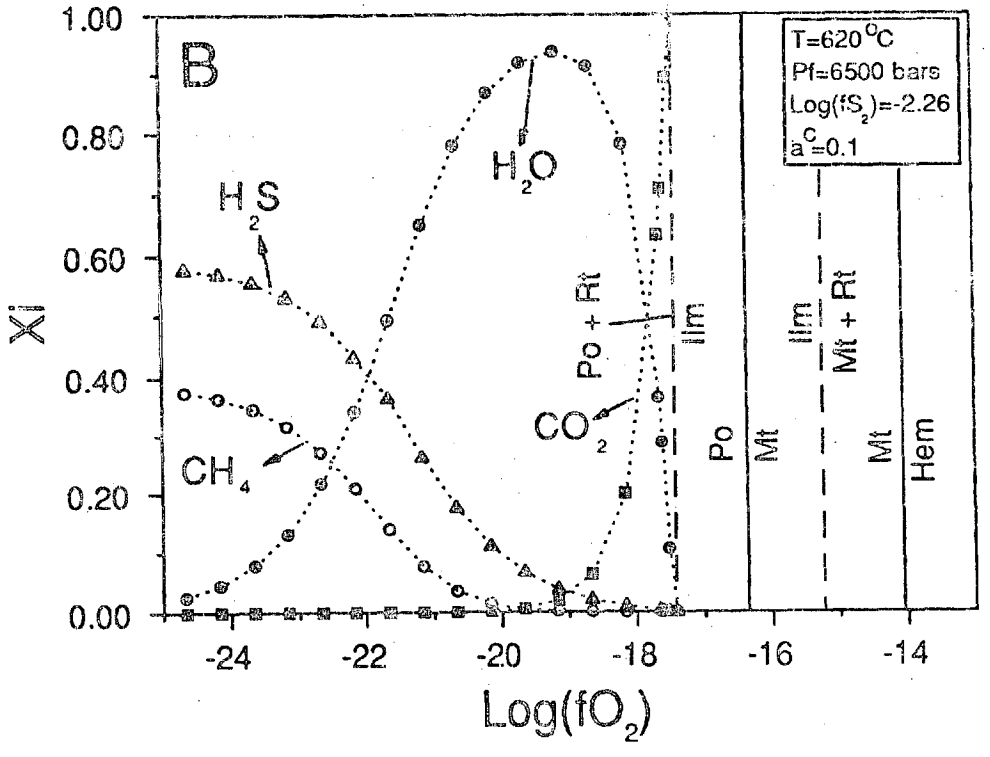
B
T=620°C
Pf=6500 bars
Log(fS2)=-2.26
ac=0.1
Xi
1.00
0.80
0.60
0.40
0.20
0.00
H2O
H2S
CH4
CO2
Po + Rt
Ilm
Po
Mt
Ilm
Mt + Rt
Mt
Hem
-24
-22
-20
-18
-16
-14
Log(fO2)

calc-silicate assemblage (tremolite, calcite, dolomite, sphene, diopside) which is most common in the massive sulfide host rocks. Rutile and quartz, with activites of 1, were added to the list of reactants to generate a T-XCO_2 diagram (Fig. 6.7). Because rutile is absent (a^{rutile}<1), the thermometer defined by reaction (4) (reaction list, Fig. 6.7) provides a maximum T estimate of 648°C at P=6.5 Kbar. The intersection of reactions 4 and 6 provides a maximum value of XCO_2=0.35. St-Seymour and MacLean (1984) reported the occurrence of the invariant assemblage calcite-dolomite-quartz-tremolite-diopside and concluded the the metamorphic fluid was CO_2-rich. However, it is clear from figure 6.7 that the metamorphic fluid was internally buffered under peak P-T conditions and was a water-rich H_2O-CO_2 fluid, dominant in the calc-silicate rocks.

These calculations support the earlier conclusion that a water rich fluid or conditions near $P_{H_2O}=P_{total}$ are necessary to have Mg-rich cordierite and anthophyllite coexisting with pyrrhotite and rutile. Furthermore, an $a^{Graphite}$ much lower than 0.1 (0.0001) is necessary to bring the maximum H_2O crest (Fig. 6.6B) towards a LogfO_2 value of -17.3 at LogfS_2=-2.26. Influxes of water-rich fluids could have come from the high T breakdown of Mg-rich chlorite through dehydration reactions in the north gold zone altered rocks, thus keeping XCO_2 to a low value in the calc-silicate rocks.

Conclusions

It can be concluded that under peak P-T conditions dominantly water-rich metamorphic fluids were in equilibrium with the mineral assemblages of the cordierite-orthoamphibole rocks in all three terranes. Calculated X_{Fe}^{Ath}

Fig. 6.7. $T\text{-}XCO_2$ multi-equilibrium diagram using reduced mineral activities derived from the microprobe analyses in a calc-silicate rock (Sample A-30; data from St-Seymour, 1976), Montauban. The plot is calculated for non-ideal mixing of CO_2-H_2O using GEO-CALC (Brown et al., 1988) in the system CaO-FeO-MgO-SiO_2-TiO_2-CO_2-H_2O. [Mineral abbreviations as in Chapter 1 except Sph=sphene (titanite), Do=dolomite, and Qz=quartz.]

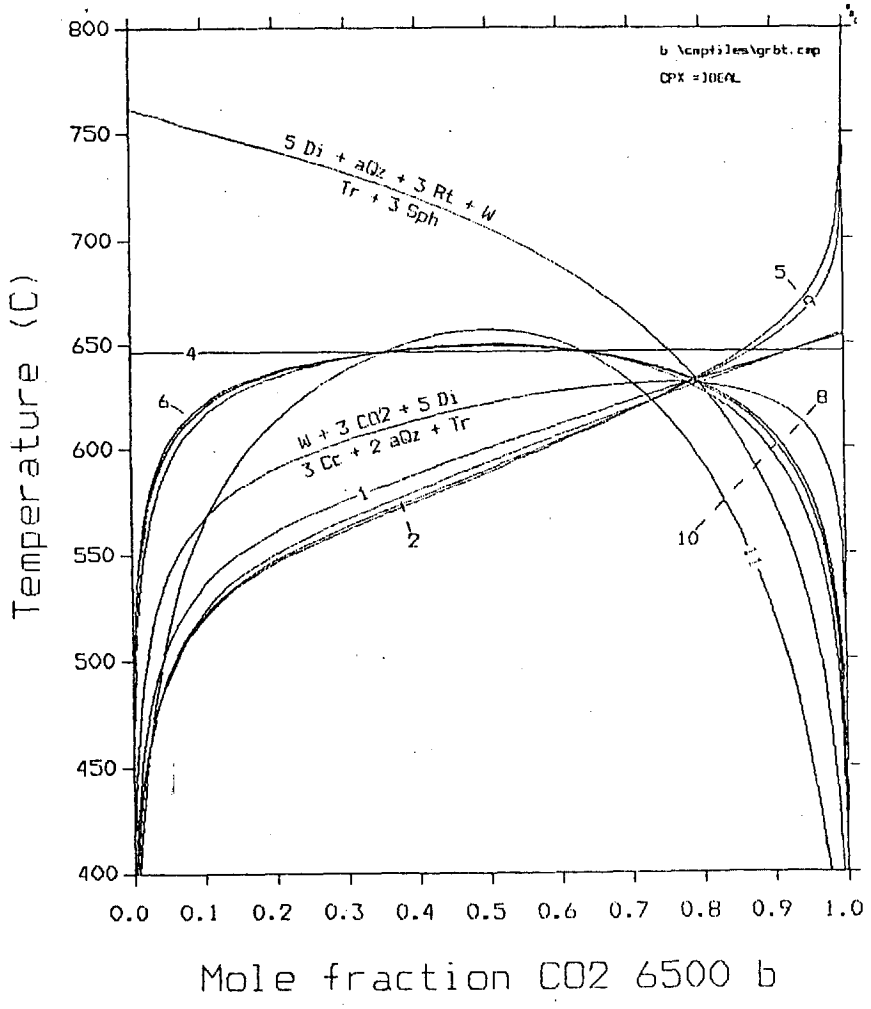

REACTION LIST (A-30)
Assemblages on the left are stable on the:
high side of the Y-axis variable, or the
high side of the X-axis variable for vertical reactions

1): 2 CO2 + Di = Do + 2 aQz

2): Sph + CO2 = Rt + aQz + Cc

3): W + 3 CO2 + 5 Di = 3 Cc + 2 aQz + Tr

4): 2 Rt + Di + 2 Cc = Do + 2 Sph

5): 7 CO2 + Tr + 3 Cc = 5 Do + 8 aQz + W

6): W + CO2 + Do + 4 Di = 3 Cc + Tr

7): 5 Di + aQz + 3 Rt + W = Tr + 3 Sph

8): W + CO2 + 2 Rt + 5 Di = Cc + 2 Sph + Tr

9): 10 CO2 + Tr + 3 Sph = 5 Do + 11 aQz + 3 Rt + W

10): 2 W + 2 CO2 + 6 Rt + 11 Di = Do + 6 Sph + 2 Tr

11): 5 Do + 8 Sph + CO2 + W = Tr + 8 Rt + 11 Cc

isopleths in fO_2-fS_2 space necessitate water-rich metamorphic fluids under peak P-T conditions for the three terranes. Results on the fluid speciation derived from FLUICOHS and the multi-equilibrium calculations were consistent, and also indicate a high XH_2O. Variations in fO_2-fS_2 were most likely internally controlled by variations in the altered rocks protoliths compositions. Solid-solution mineral buffering is an effective mechanism for neutralizing external changes imposed by low water/rock ratios externally controlled fO_2-fS_2 variations. Hypotheses involving syn-metamorphic metasomatism and large influxes of fluids for the origin of cordierite-gedrite rocks, such as proposed by Arnold and Sandiford (1991), are ruled out for these three terranes.

CHAPTER 7

SUMMARY AND CONCLUSIONS

Cordierite-orthoamphibole rocks in the three terranes are associated with contrasting styles of mineralization and exhibit knotenschiefer textures characteristic of post-tectonic crystallisation under mostly static metamorphism at or near peak P-T conditions. At Atik Lake, gold in sulfide-arsenopyrite-bearing chert is the dominant type of mineralization. Copper-nickel mineralization occur in the main lens of cordierite-anthophyllite rock at Némiscau which is associated with pyrrhotite-rich quartzites in amphibolite and quartzofeldspathic gneisses. Mineralization in both terranes are presently uneconomic. The polymetallic (Zn-Pb-Cu-Ag-Au) mineralization at Montauban is of two types, massive sulfides in calc-silicate rocks, and disseminated sulfides in cordierite-anthophyllite rocks and associated gneisses.

Major and trace element geochemistry, mass balance calculations, and log(Ratio) profiles indicate that these cordierite-orthoamphibole rocks in all three terranes are the metamorphosed equivalents of hydrothermally altered basalts and volcanogenic sediments (Atik Lake and Némiscau), ultramafic rock (Némiscau) and felsic volcanics (Montauban).

Geothermobarometric studies indicate that these cordierite-orthoamphibole rocks were formed under a wide range of P-T conditions covering a wide spectrum of the amphibolite- to near granulite-facies. The large range of bulk-rock compositions in the three terranes favored the development of aluminous mineral assemblages allowing various metamorphic reactions to occur. These have been useful in reconstructing the metamorphic evolution in each terrane.

Atik Lake

The protoliths of the cordierite-orthoamphibole rocks are hydrothermally altered tholeiitic basalts (MORB-type) theh form pipe-like zones stratigraphically below BIF and auriferous chert, and also volcanogenic sediments containing a high proportion of mafic component. Calculations indicate that both mass and volume losses of up to 25% occurred during hydrothermal alteration. These changes resulted from the addition of Fe, K, Rb and Ba, and the removal of Si, Ca, Na, Ca, Sr, ± Mg. The oxidation state of the altered basalts (low Fe^{3+}/Fe^{+2}) indicates that the mineralizing fluid was reduced.

The geothermobarometry revealed that peak P-T conditions were around T=550°C and P=2.5 kbar, which is corroborated by the presence of andalusite in the belt. The metamorphism of the aluminous alteration zones allowed the formation of cordierite-orthoamphibole (gedrite-anthophyllite) rocks and andalusite ± staurolite-bearing patches. Gedrite is observed only in the more Fe-rich aluminous altered basalts where garnet is also present. The volcanogenic metasediments are more potassic than the altered basalts and anthophyllite is the only amphibole.

The presence of prograde chlorite in the cordierite-orthoamphibole rocks is supported by consistent garnet-chlorite temperature estimates (T=553±36°C). The local mineral assemblage of quartz-chlorite-muscovite-biotite-cordierite indicates that biotite and cordierite formed from the prograde breakdown of a chlorite-sericite-quartz assemblage. Inclusions of chlorite, pyrrhotite, arsenopyrite, and löllingite in garnets are strong evidence for a premetamorphic origin for the mineralization and hydrothermal alteration. The presence of quartz-chlorite-sericite alteration indicates that the mineralizing fluid was slightly acidic. Residual enrichment of immobile

components (Al, Ti, Zr, Cr, Nb, and V) occurred throughout the altered rocks that have undergone mass loss. A direct consequence of this was the formation, during metamorphism, of vanadiferous zincian-chromian hercynite and coulsonite-rich magnetite in the altered basalts.

Mineral assemblages in the BIF and auriferous chert are indicative of the breakdown of grunerite and ferro-actinolite to produce fayalite and hedenbergite, respectively, at peak P-T conditions in the belt. The arsenopyrite in the cordierite-orthoamphibole rocks contains appreciable Co-Ni-Sb, whereas arsenopyrite in the auriferous chert contains no detectable concentrations of these elements. Löllingite and gersdorffite occur exclusively in the altered basalts. The contrasting arsenopyrite compositions suggest low-fluid rock ratios during metamorphism; their chemistry reflects the influence of the host rock-composition (Co-Ni-rich in basalt, Fe-rich in iron formation).

Némiscau

The cordierite-anthophyllite rocks were derived from three hydrothermally altered protoliths: 1) intermediate and low-Cr amphibolites having a MORB-type chemical signature, 2) high Cr-amphibolite, and 3) ultramafic rocks.

The intersection of the staurolite-out and andalusite-sillimanite isograds in the NE part of the Némiscau belt provides T and P estimates of ~600°C and ~3.0 kbar. The metamorphic gradient increases across the staurolite-out isograd toward the SW where staurolite relics are found as inclusions in garnet. The metamorphic conditions prevailing in the andalusite-staurolite zone were slightly lower than the above values. The cordierite-anthophyllite rocks formed within the sillimanite-zone where the

peak T-P conditions reached 650°C and 4.5 kbar. The disappearance of the andalusite-sillimanite and staurolite-out isograds at fault boundaries indicate large faults movements. The belt has undergone intensive shearing and retrograde metamorphism indicated by ubiquitous chlorite veinlets and intense sericitization of amphibolite near the Lac de la Hutte fault where a mineralized quartz vein was discovered during mineral exploration. Prograde metamorphism of quartz-chlorite-sericite assemblages in hydrothermally altered basalts and serpentinized ultramafic bodies resulted in the formation of the cordierite-anthophyllite±garnet and anthophyllite-cummingtonite-plagioclase rocks and anthophyllite-rich lenses. The protoliths of the various cordierite-anthophyllite rocks have successfully been identified using the log(Ratio) method.

Rare vanadiferous zincian-chromian hercynite similar to that at Atik Lake were found in a sample of cordierite-anthophyllite rock. Spinel is characteristic of the ultramafic rocks whereas gahnite rimming zincian-staurolite formed in a metapelite in the proximity of a zinc showing. Hence, spinel chemistry is a good petrogenetic indicator and a potential exploration tool in metamorphic terranes. The local availability of zinc allowed the stabilization of staurolite below the staurolite-out isograd, in the sillimanite zone.

Montauban

Nodular sillimanite gneiss and cordierite-anthophyllite rocks in the mine sequence at Montauban surround a mineralized quartzitic gneiss which formed the silicified core of a metamorphosed and deformed hydrothermal alteration zone associated with a massive sulfide ore deposit. The metal zoning is characterized by a Cu-Au anomaly in the central quartzitic gneiss,

which plunges gently south, parallel to the mineral lineation in the surrounding gneiss. Log(Ratio) profiles and mass balance calculations show that the rocks of the mine sequence were derived by hydrothermal alteration from surrounding quartzo-feldspathic gneisses which represent metamorphosed intermediate to felsic volcanics or volcaniclastic rocks. Mass changes in the mine sequence, except in quartzitic gneis, are marked by large losses of Si. Potassium was added in small amounts to most of the sequence, but was leached in the cordierite-anthophyllite rocks. All altered units recorded additions of Fe, Mg, Mn, Pb and Rb, and depletions in Ca, Na, Ba and Sr. The gain in Fe was largest in the central quartzitic gneiss, whereas Mg was enriched in the surrounding altered rocks.

Peak P-T conditions were estimated at ~620°C and ~6.5 kbar. The presence of kyanite surrounded by cordierite ± muscovite and biotite, and sillimanite indicate a P-T path transitional to the kyanite and sillimanite field; this is consistent with the above P-T values. The observed zonation in rock types at the north gold zone in the mine sequence resulted from metamorphism in the upper amphibolite facies of an alteration zone having a siliceous core surrounded successively by concentric zones of chlorite, chlorite-quartz and sericite ± chlorite ± quartz ± talc. The alteration zone has been transposed during ductile shearing. The availability of Zn and Mn allowed zincian staurolite, gahnite and garnet to be stabilized. The presence of porphyroblastic gahnite and Mn-rich garnet in the quartzitic gneiss, and vermicular gahnite rimming zincian staurolite (coronitic texture) in the cordierite-anthophyllite rock, was modeled in the system Fe-Mg-Zn-Mn-Al-Si-H-O-S as resulting from an overall increase in oxidation state during decompression.

The metamorphosed massive sulfide deposit and associated alteration zone

are volcanogenic in origin. They belong to a class of deposits that have formed in submarine calc-alkaline felsic volcanic rocks over a wide span of geologic time. They have many geological similarities with modern Kuroko-type deposits in Japan and, as the Mount Chalmers deposit in Australia.

Geothermobaromatric considerations

The chemistry of the orthoamphiboles in each of three terranes is consistent with the empirical solvus proposed by Spear (1980). The P-T estimates and ranges of bulk rock compositions suggest that the position of the solvus is not affected by pressure and X_{Fe}.

The study of Fe-Mg partitioning between cordierite and anthophyllite in the three terranes is consistent with data compiled from the literature, and indicates compositional changes involved in continuous reaction(s). The $K_D^{Fe\text{-}Mg}$ is slightly temperature dependent and definitly pressure dependent: it is relatively unaffected by the elements Zn and Mn, and thus provides a very useful geobarometer for metamorphosed alteration zones rocks.

The contrasting cordierite-orthoamphibole rock compositions and oxide-sulfide±arsenide fO_2-fS_2 buffering assemblages, allowed the usage of Popp et al. (1977b) experimental data to model the oxidation and sulfidation of ferro-anthophyllite at the peak P-T conditions for each terrane. The range of anthophyllite compositions is consistent with internal buffering, but necessitates a water-rich metamorphic fluid. The range in bulk rock compositions (Fe-rich at Atik Lake and Mg-rich at Montauban) is compatible with the breakdown of a chlorite-bearing hydrothermal assemblage at near peak P-T conditions, which provided an *in situ* syn-metamorphic water-rich fluid.

ORIGINAL CONTRIBUTIONS TO KNOWLEDGE

Major contributions

1) The study demonstrates that cordierite-orthoamphibole rocks are stable through a wide range of metamorphic conditions of at least 550-650°C and 2.5-6.5 kbar. The most Fe-rich rocks develop the cordierite-orthoamphibole assemblages at the lowest metamorphic conditions.

2) A new geobarometer based on Fe-Mg exchange between cordierite and anthophyllite has been developed. Unlike other geobarometers using ferromagnesian minerals, it is not measurably affected by Zn and Mn substitutions which significantly expand the stability fields of such other minerals as staurolite and garnet. It provides an additional tool to estimate pressure in metamorphic terranes containing these rocks.

3) A new method, the log(Ratio) diagram, was designed to identify altered rocks protoliths in metamorphic terranes. The potential of this method in complex stratigraphic sequence has been demonstrated.

4) The Popp et al. (1977) experimental data on oxidation-sulfidation of ferro-anthophyllite is, for the first time, thoroughly applied to natural mineral assemblages containing contrasting sulfide-oxide±arsenide fO_2-fS_2 buffers. The cordierite-anthophyllite rocks were buffered at or closely below the pyrite-pyrrhotite-magnetite triple point.

Other contributions

5) A rare case of crossing isograds (staurolite-out, andalusite-sillimanite) was mapped for the first time in the Némiscau belt.

6) Unusual vanadiferous zincian-chromian hercynite showing a wide range of composition has been reported for the first time in Canada. It was demonstrated that this spinel formed as a primary metamorphic mineral in

altered basalt under low-amphibolite facies metamorphism.

7) The breakdown of grunerite to fayalite + quartz has only been rarely observed in natural samples of iron formation and is reported for the first time in the Atik Lake belt.

RECOMMENDATIONS FOR FUTURE RESEARCH

A serious constraint in the interpretation of the paleo-tectonic settings in the three terranes studied in this thesis was the lack of detailed structural analysis available. There is a rising controversy regarding the origin of cordierite-anthophyllite rocks associated with lode-gold deposits, particularly regarding the timing of the mineralization, hydrothermal alteration and metamorphism (pre-metamorphic versus syn-metamorphic). Thus detailed metamorphic, fluid-inclusion, ore textures and age dating studies will be required. The lack of data on trace elements geochemistry in cordierite-anthophyllite rocks of probable sedimentary and evaporitic origins precluded the application of the log(Ratio) method on such rocks.

Experimental studies are required to provide information on the effect of varying oxidation states, T and P on $K_D^{Fe\text{-}Mg}$ for the cordierite-anthophyllite pair, and to assess the ideallity of Fe-Mg mixing and the substitution of Mn in these minerals, and the variability of the hydration state of cordierite, are also needed. The lack of experimental data on expanded chemical systems that would include Zn and Mn seriously limits the utilization of petrogenetic grids in the study of metamorphosed altered rocks associated with ore deposits. Finally, there are no available experimental data on the sulfidation and oxidation of cordierite and staurolite which are necessary to quantitatively assess the chemical variations in these minerals.

REFERENCES

Abbott, R.N., 1982, A petrogenetic grid for medium and high grade metabasites, Am. Mineral., v. 67, p. 865-876.

Abraham, K., and Schreyer, W., 1973, Petrology of a ferruginous hornfels from Riekensgluck, Harz Mountains, Germany, Contrib. Mineral. Petrol., v. 40, p. 275-292.

Afifi, A.M., and Essene,W.J., 1988, MINFILE: a microcomputer program for storage and manipulation of chemical data on minerals, Am. Mineral., v. 73, p. 446-448.

Aftabi, A., 1980, Polymetamorphism, textural relations and mineralogical changes in Archan massive sulfide deposits at the Garon Lake Mine, Matagami, Quebec. Unpub. Msc Thesis McGill University.

Akella, J., 1966, Calculation of material transport in some metasomatic processes, N. Jb. Miner. Abh., v. 104, p. 316-329.

Akella, J., and Winkler, H.G.F., 1966, Orthorhombic amphibole in some metamorphic reactions, Contr. Mineral. and Petrol., v. 12, p. 1-12.

Albee, A.L., 1965, A petrogenetic grid for the Fe-Mg silicates of pelitic schists, Am. J. Sci., v. 263, p. 512-536.

Albee, A.L., 1972, Metamorphism of pelitic schists: reaction relations of chloritoid and staurolite, Geol. Soc. Am. Bull., v. 83, p. 3249-3268.

Appleyard, E.C., and Guha, J., 1991, A special issue on applications of hydrothermal alteration studies to mineral exploration, Econo. Geol., v. 86, p. 461-485.

Aranovich, L.Y., and Podlesskii, K.K., 1983, The cordierite-garnet-silimanite-quartz equilibrium: experiments and applications. In Kinetics and Equilibrium in Mineral Reactions (S.K. Saxena, ed.). Springer-Verlag, New York.

Arnold, J., and Sandiford, M., 1990, Petrogenesis of cordierite-orthoamphibole assemblages from the Springton region, South Australia, Contrib. Mineral. Petrol., v. 106, p. 100-109.

Ashworth, J.R., 1975, The sillimanite zones of the Huntly-Portsoy area, northeast Scotland, Geol. Mag., v. 112, p. 113-136.

Atherton, M.P., 1968, The variation in garnet, biotite and chlorite composition in medium grade pelitic rocks from the Dalradian, Scotland, with Particular reference to the zonation in garnet, Contr. Mineral. Petrol., v. 18, p. 347-371.

Atkin, B.P., 1978, Hercynite as a breakdown product of staurolite from within the aureole of the Ardara pluton, Co., Donegal, Eire, Mineral. Mag., v. 42, p. 237-239.

Bachinski, D., 1976, Metamorphism of cupriferous iron sulfide deposits, Notre Dame Bay, Newfoundland, Econ. Geol., v. 71, p. 443-452.

Baker, J., Holland, T., and Powell, R., 1991, Isograds in internally buffered systems without solid solutions: principles and examples, Contrib. Mineral. Petrol., v. 106, p. 170-182.

Ball, D.G.A., and Robin, P.-Y.F., 1990, METPET: metamorphic petrology microcomputer programs, J. Metamorphic Geol., v. 8, p. 251-256.

Bancroft, J.A., 1915, Geology of a part of Montaubau and chavigny townships and of De Grondines seigniory, Dept. of Colonization, Mines and Fisheries, Mines Branch, Quebec, p. 109-151.

Barber, J.P., and Yardley, B.W.D., 1985, Conditions of high grade metmorphism in the Dalradian of Connemara, Ireland, J. Geol. Soc., London, v. 142, p. 87-96.

Barley, M.E., and Groves, D.I., 1990, Deciphering the tectonic evolution of Archaean Greenstone Belts: the importance of contrasting histories to the distribution of mineralization in the Yilgarn Craton, Western Australia, Precambrian Research, v. 46, p. 3-20.

Barnes, H.L., 1979, Solubilities of ore minerals, in Geochemistry of hydrothermal ore deposits, John Wiley & Sons, New York, p. 404-460.

Barrett, T.J., and MacLean, W.H., 1991, Chemical, mass, and oxygen isotope cheanges during extreme hydrothermal alteration of an Archean rhyolite, Noranda, Quebec, Econ. Geol., v. 86, p. 406-414.

Barsdell, M., and Berry, R.F., 1990, Origin and evolution of primitive Island Arc Ankaramites from Western Epi, Vanuatu, J. Petrol., v. 31, pt. 3, p. 747-777.

Barton, P.B., and Skinner, B.J., 1979, Sulfide mineral stabilities, in Barnes, H.L., ed., Geochemistry of hydrothermal ore deposits, John Wiley & sons, New York, p. 404-460.

Bayliss, P., 1969, Isomorphous substitution in synthetic cobaltite and ullmannite, Am. Mineral., v. 54, p. 426-430.

Beeson, R., 1978, The geochemistry of orthoamphiboles and coexisting cordierites and phlogopites from South Norway, Contr. Miner. Petrol., v. 66, p.5-14.

-------- 1988, Identification of cordierite-anthophyllite rock types associated with sulphide deposits of copper, lead and zinc, in Trans. Instn. Min. Metall. (sect. B: Appl. earth sci.), v. 97, p. B108-B115.

Berman, R.G., 1988, Internally-consistent thermodynamic data for minerals in the system Na_2O-K_2O-CaO-MgO-FeO-Fe_2O_3-Al_2O_3-SiO_2-TiO_2-H_2O-CO_2. J. Petrol., v. 29, p. 445-522.

-------- 1990, Mixing properties of Ca-Mg-Fe-Mn garnets, Am. Mineral., v. 75, p. 328-344.

-------- 1991, Thermobarometry using multi-equilibrium calculations: a new technique, with petrological applications, Can. Mineral., v. 29, p. 833-855.

Bernier, L.R., 1985, Géologie, minéralogie et pétrographie de la zone aurifère nord du gisement métamorphisé de Zn-Pb-Cu-Au-Ag de Montauban-les-Mines, Que., Unpub. M.Sc.A. thesis, Ecole Polytechnique de Montréal, Québec, 283 p.

-------- 1990, Vanadiferous zincian-chromian hercynite in a metamorphosed basalt-hosted alteration zone, Atik Lake, Manitoba, Can. Mineral., v. 28, p. 37-50.

-------- 1991, Proterozoic metamorphic evolution of the Montauban area, an insight on mineral equilibria in cordierite- anthophyllite rocks and the breakdown of zincian staurolite, Geol. Assoc. Canada / Mineralog. Assoc. Canada, Program with abstracts, v. 16, p. A10.

-------- 1992, Geometry and metamorphic evolution of an alteration zone associated with massive sulfide deposits, Montauban, Grenville Province, Quebec, Grenville Workshop, Quebec april 3-5 (Unpub.)

Bernier, L., Pouliot, G., and MacLean, W.H., 1987, Geology and metamorphism of the Montauban north gold zone: a metamorphosed polymetallic exhalative deposit, Grenville Province, Quebec, Econ. Geol., v. 82, p. 2076-2090.

Bernier, L.R., and MacLean, W.H., 1989, Auriferous chert, banded iron formation, and related volcanogenic hydrothermal alteration, Atik Lake, Manitoba, Can. J. Earth Sci., v. 26, p. 2676-2690.

Bérubé, M.A., 1982, La minéralogie appliquée au traitement des minerais, Can. Inst. Min. Metall., v. 75, no. 847, p. 121-131.

Best, M.G., 1982, Igneous and metamorphic petrology, W.H. Freeman and Company, San Francisco, 630 p.

Bird, G.W., and Fawcett, J.J., 1973, Stability relations of Mg-chlorite-muscovite and quartz between 5 and 10 kb water pressure, J. Petrol., v. 14, p. 415-428.

Bloomer, S.H., and Hawkins, J.W., 1987, Petrology and geochemistry of boninite series volcanic rocks from the Mariana trench, Contrib. Mineral. Petrol., v. 97, p. 361-377.

Boberski, C., and Schreyer, W., 1990, Synthesis and water contents of Fe^{2+}-bearing cordierites, Eur. J. Mineral., v. 2, p. 565-584.

Bohlen, S.R., Montana, A., and Kerrick, D.M., 1991, Precise determinations of the equilibria kyanite ⇌ sillimanite and kyanite ⇌ andalusite and a revised triple point for Al_2SiO_5 polymorphs, Am. Mineral., v. 76, p. 677-680.

Bristol, C.B., and Froese, E., 1989, Highly metamorphosed altered rocks associated with the Osborne Lake volcanogenic massive sulphide deposit, Snow Lake area, Manitoba, Can. Mineral., v. 27, p. 593-600.

Brown, T.H., Berman, R.G., and Perkins, E.H., 1988, GEØ-CALC: software package for calculation and display of pressure-temperature-composition phase diagrams using an IBM or compatible personal computer, Comput & Geosci., v. 14, p. 279-289.

Bruckmann-Benke, P., Chatterjee, N.D., and Aksyuk, M.A., 1988, Thermodynamic properties of $Zn(Al,Cr)_2O_4$ spinels at high temperatures and pressures, Contrib. Mineral. Petrol., v. 98, p. 91-96.

Bryndzia, L.T., and Scott, S.D., 1987, The composition of chlorite as a function of sulfur and oxygen fugacity: an experimental study, Am. J. Sci., v. 287, p. 50-76.

Bryndzia, L.T., Scott, S.D., and Spry, P.G., 1990, Sphalerite and hexagonal pyrrhotite geobarometer: correction in calibration and application, Econ. Geol., v. 85, p. 408-411.

Burnham, C.W., Holloway, J.R., and Davies, V.F., 1969, Thermodynamic properties of water to 1000°C and 10,000 bars, Geol. Soc. America Spec. Paper, v. 132, 96 p.

Card, K.D., 1990, A review of the Superior Province of the Canadian Shield, a product of Archean accretion, Precambrian Research, v. 48, p. 99-156.

Carmichael, D.M., 1969, On the mechanism of prograde metamorphic reactions in quartz-bearing pelitic rocks, Contr. Mineral. Petrol., v. 20, p. 244-267.

-------- 1990, Metamorphism, metasomatism, and Archean lode gold deposits, in Robert, F., Sheahan, P.A., and Green, S.B., eds, Greenstone gold and crustal evolution: NUNA conference volume, Geological Association of canada, p. 142-143.

-------- 1991, Univariant mixed-volatile reactions: pressure-temperature phase diagrams and reaction isograds, Can. Mineral., v. 29, p. 741-754.

Carmichael, I.S., 1974, Igneous petrology, McGraw-Hill, New York.

Carpenter, R.H., 1974, Pyrrhotite isograd in southeastern Tennessee and southwestern North Carolina, Geol. Soc. Am. Bull., v. 85, p. 451-456

Casselman, M.J., and Mioduszewska, B.M., 1982, The Bathurst Norsemines sulfide deposits, Hackett River, N.W.T., Geol. Assoc. Canada Spec. Paper 25, p. 365-402.

Chinner, G.A., 1960, Pelitic gneisses with varying ferrous/ferric ratios from Glen Clova, Angus, Scotland, J. Petrol., v. 1, pt. 2, p. 178-217.

Chinner, G.A., and Fox, J.S., 1974, The origin of cordierite-anthophyllite rocks in the Land's End aureole, Geol. Mag.,v.111, p. 397-408.

Chipera, S.J., and Perkins, D., 1988, Evaluation of biotite-garnet geothermometers: application to the English River subprovince, Ontario, Contrib. Mineral. Petrol., v. 98, p. 40-48.

Colvine, A.C., Fyon, J.A., Heather, K.B., Marmont, S., Smith, P.M., and Troop, D.G., Archean lode gold deposits in Ontario. Ontario Geological Survey, Miscellaneaous Paper 139, 136 p.

Connolly, J.A.D., and Trommsdorff, V., 1991, Petrogenetic grids for metacarbonate rocks: pressure-temperature phase-diagram projection for mixed-volatile systems, Contrib. Mineral. Petrol., v. 108, p. 93-105.

Cornell, D.H., Theart, H.F.J., and Humphreys, H.C., 1990, Dating a collision-related metamorphic cycle at Prieska copper mines, south Africa, in Spry, P.G., and Bryndzia, L.T., eds., Regional metamorphim of ore deposits and genetic implications, VSP, Utrecht, The Netherlands, p. 97-116.

Costa, U.R., Barnett, R.L., and Kerrich, R., 1983, The Mattagami Lake mine Archean Zn-Cu sulfide deposit, Quebec: hydrothermal coprecipitation of talc and sulfides in a sea-floor brine chemistry, Econ. Geol., v. 78, p. 1144-1203.

Cox, S.F., 1987, Flow mechanisms in sulphide minerals, Ore Geol. Rev., v. 2, p. 133-171.

Dallmeyer, R.D., 1974, The role of crystal structure in controlling the partitioning of Mg and Fe between coexisting garnet and biotite, Am. Mineral., v. 59, p. 201-203.

Damman,A.H., 1989, Hydrothermal orthoamphibole-bearing assemblages from the Gåsborn area, West Bergslagen, central Sweden, Am. Mineral., v. 74, p. 573-585.

de Rosen-Spence, A., 1969, Genèse des roches à cordiérite-anthophyllite des gisements cupro-zincifères de la région de Rouyn-Noranda, Québec, Canada, Can. J. Earth Sci., v. 6, p. 1339-1969.

Deb, M., 1980, Genesis and metamorphism of two stratiform massive sulfide deposits at Ambaji and Deri in the Precambrian of Western India, Econ. Geol., v. 75, p. 572-591.

Deb, M., and Sarkar, S.C., 1990, Proterozoic tectonic evolution and metallogenesis in the Aravallhi-Delhi orogenic complex, Northwestern India, Precambrian research, v. 46, p. 115-137.

Dell'Angelo, L.N., and Tullis, J., 1989, Fabric development in experimentally sheared quartzites, Tectonophysics, v. 169, p. 1-21.

deWit, M.J., and Ashwal, L.D., 1986, Workshop on tectonic evolution of greenstone belts. LPI Tech. Rpt. 86-10. Lunar and Planetary Institute, Houston, 227 p.

Dipple, G.M., Wintsch, R.P., and Andrews, M.S., 1990, Identification of the scales of differential element mobility in a ductile fault zone, J. Metamorphic Geol., v. 8, p. 645-661.

Dobbe, R.T.M., 1991, Ullmannite, cobaltian ullmannite and willyamite from Tunaberg, Bergslagen, central Sweden, Can. Mineral., v. 29, p. 199-205.

Dostal, J., and Strong, D.F., 1983, Trace-element mobility during low-grade metamorphism and silicification of basaltic rocks from Saint John, New Brunswick, Can. J. Earth Sci., v. 20, p. 431-435.

Douglas, R.J.W., 1979, Geology and mineral resources of Canada: economic geology series no 1, part 1. Geological Survey of Canada, p.145-151.

Dyar, M.D., 1990, Mössbauer spectra of biotite from metapelites, Am. Mineral., v. 75, p.656-666.

Dymek, R.F., and Smith, M.S., 1990, Geochemistry and origin of Archean quartz cordierite gneisses from the Godthåbsfjord region, West Greenland, contrib. Mineral. Petrol., v. 105, p. 715-730.

Edwards, L., and Essene, E.J., 1988, Pressure, temperature and C-O-H fluid fugacities across the amphibolite-granulite transition, northwest Adirondack Mountains, New York, J. Petrol., v. 29, pt. 1, p. 39-72.

Elliot-Meadows, S.R., and Appleyard, E.C., 1991, The alteration geochemistry and petrology of the Lar Cu-Zn deposit, Lynn Lake Area, Manitoba, Canada, Econ. Geol., v. 86, p. 486-505.

Ernst, W.G., 1966, Synthesis and stability relations of ferrotremolite, Am. J. Sci., v. 264, p. 37-65.

Eskola, P., 1914, On the petrology of the Orijärvi region in southwestern Finland, Comm. géol. Finlande Bull., no. 40, p. 1-279.

Essene, E.J., 1989, The current status of thermobarometry in metamorphic rocks, in Daly, j.S., Cliff, R.A., and Yardley, B.W.D., eds, Evolution of metamorphic belts. Geological Society Special Pub. no. 43, p. 1-44.

Etheridge, M.A., and Wall, V.J., 1983, The role of the fluid phase during regional metamorphism and deformation, J. Metamorphic Geol., v. 1, p. 205-226.

Eugster, H.P., 1981, Metamorphic solutions and reactions, in F.E. Wickman and D.T. Rickard, eds., Chemistry and geochemistry of solutions at high temperatures and pressures, Physics and Chemistry of the Earth, 13/14, p. 461-507. Pergamon Press, New York.

-------- 1986, Minerals in hot water, Am. Mineral., v. 71, p. 655-673.

Ferry, J.M., 1981, Petrology of graphitic sulfide-rich schists from south-central Maine: an example of desulfidation during prograde regional metamorphism, Am. Mineral., v. 66, p. 908-930.

Ferry, J.M., and Spear, F.S., 1978, Experimental calibration of the partitioning of Fe and Mg between biotite and garnet, Contrib. Mineral. Petrol., v. 66, p. 113-117.

Finlow-Bates, T., and Stumpfl, E.F., 1981, The behavior of the so-called immobile elements in hydrothermally altered rocks associated with volcanogenic submarine-exhalative ore deposits, Mineralium Deposita, v. 16, p. 319-328.

Fleming, P.D., and Fawcett, J.J., 1976, Upper stability of chlorite + quartz in the system MgO-FeO-Al_2O_3-SiO_2-H_2O at 2 kbars water pressure, Am. Mineral., v. 61, p. 1175-1193.

Fletcher, I.R., and Farquhar, R.M., 1982, The protocontinental nature and regional variability of the Central Metasedimentary Belt of the Grenville Province: lead isotope evidence, Can. Jour. Earth Sci., v. 19, p. 239-253.

Fonarev, V.I., Korolkov, G.Ya., and Dokina, T.N., 1976, Stability of the cummingtonite-quartz-magnetite association, Geochem. Internat., v. 13, p. 34-35.

-------- 1979, Cummingtonite + olivine + quartz association, Geochem. Internat., v. 16, p. 21-32.

Forbes, W.C., 1977, Stability relations of grunerite, $Fe_7Si_8O_{22}(OH)_2$, Am. J. Sci., v. 277, p. 735-749.

Foster, R.P., Fuber, F.M.W., Gilligan, J.M., and Green, D., 1986, Shamva gold mine, Zimbabwe: a product of calc-alkaline-linked exhalative, volcaniclastic, and epiclastic sedimentation in the Late Archean, in Keppie, D.J., Boyle, R.W., and Haynes, S.J., eds., Turbidite-hosted gold deposits. Geological Association of Canada, GAC Special paper 32, p. 41-66.

Fouquet, Y., and ten authors, 1991, Hydrothermal activity in the Lau Back-arc basin: sulfides and water chemistry, Geology, v. 19, p. 303-306.

Fowler, C.M.R., and Nisbet, E.G., 1988, Geotherms in the continental crust and metamorphism, in Short course on heat, metamorphism and tectonics, Mineralogical Association of Canada, v. 14, p. 34-50.

Franklin, J.M., Lydon, J.W., and Sangster, D.F., 1981, Volcanic-associated massive sulfide deposits, Econ. Geol. 75th Ann. V., p. 485-627.

Froese, E., 1969, Metamorphic rocks from the Coronation Mine and surrounding area, Canada Geol. Survey, Paper 68-5, p. 55-77.

-------- 1971, The graphical representation of sulfide-silicate phase equilibria, Econ. Geol., v. 66, p. 335-341.

-------- 1973, The oxidation of almandine and iron cordierite, Can. Mineral., v. 11, p. 991-1002.

-------- 1976, Applications of thermodynamics in metamorphic petrology, Canada Geol. Survey, Paper 75-43, 36 p.

-------- 1977, Oxidation and sulfidation reactions, in Greenwood, H.J., ed., Application of thermodynamics to petrology and ore deposits, Mineralog. Assoc. of Canada Short Course Handbook, v. 2, p. 84-98.

Froese, E., and Ashton, K.E., 1990, Alteration zones in the Kisseynew Gneisses of Saskatchewan, (Unpub. abstract).

Froese, E., and Gunter, A.E., 1976, A note on the pyrrhotite-sulfur vapor equilibrium, Econ. Geol., v. 71, 1589-1594.

Fullager, P.D.,, Brown, H.S., and Hagner, A.F., 1967, Geochemistry of wall rock alteration and the role of sulfurization in the formation of the Ore Knob sulfide deposit, Econ. Geol, v. 62, p. 798-825.

Gaál, G., 1990, Tectonic styles of early Proterozoic ore deposition in the Fennoscandian shield, Precambrian Research, v. 46, p. 83-114.

Galbreath, D.C., Duke, E.F., Papike, J.J., and Laul, J.C., 1988, Mass transfer during wall-rock alteration: an example from a quartz-graphite vein, Black Hills, South Dakota, Geochimica et Cosmochimica Acta, v. 52, p. 1905-1918.

Ganguly, J., and Kennedy, G.C., 1974, The energetics of natural garnet solid solution. 1. Mixing of the aluminosilicate endmembers, Contributions to Mineralogy and Petrology, v. 48, p. 137-148.

Ganguly, J., and Saxena, S.K., 1984, Mixing properties of aluminosilicate garnets: constraints from natural and experimental data and applications to geothermo-barometry, Am. Mineral., v. 69, p. 88-97.

-------- 1985, Mixing properties of aluminosilicate garnets: constraints from natural and experimental data and applications to geothermo-barometry: clarifications, Am. Mineral., v. 70, p. 1320.

Gilbert, M.C., Helz, R.T., Popp, R.K., and Spear, F.S., 1982, Experimental studies of amphibole stability, Rev. Mineral., v. 98, p. 229-353.

Goldman, D.S., and Albee, A.L., 1977, Correlation of Mg/Fe partitioning between garnet and biotite with $^{18}O/^{16}O$ partitioning between quartz and magnetite, Am. J. Sci., v. 277, p. 750-767.

Graham, C.M., and Powell, R., 1984, A garnet-hornblende geothermometer: calibration, testing, and application to the Pelona schist, southern California, J. Metamorph. Geol, v. 2, p. 13-31.

Grambling, J.A., and Williams, M.L., 1985, The effects of Fe^{3+} and Mn^{3+} on aluminum silicate phase relations in north-central New Mexico, USA, J. Petrol., v. 26, p. 324-354.

Grauch, R.I., 1988, Rare earth elements in metamorphic rocks, Rev. Mineralogy, v. 21, p. 147-167.

Gresens, R.L., 1967, Composition-volume relationships of metasomatism, Chem. Geol., v. 2, p. 47-55.

Grieve, R.A.F., and Fawcett, J.J., 1974, The stability of chloritoid below 10 kb PH_2O, Jour. Petrol., v. 15, p. 113-139.

Griffen, D.T., 1981, Synthetic Fe/Zn staurolites and the ionic radius of $^{IV}Zn^{2+}$, Am. Mineral., v. 66, p. 932-937.

Griffen, D.T., and Ribbe, P.H., 1973, The crystal chemistry of staurolite, Am. J. Sci., v. 273-A, p. 479-495.

Guidotti, C.V., 1970, The mineralogy and petrology of the transition from the lower to upper sillimanite zone in the Oquossoc area, Maine, J. of Petrol., v. 11, p. 277-336.

Haack, U., Heinrichs, H., Bonell, M., and Schneider, A., 1984, Loss of metals from pelites during regional metamorphism, Contrib Mineral. Petrol., v. 85, p. 116-132.

Haase, C.S., 1982, Metamorphic petrology of the Negaunee Iron Formation, Marquette district, northern Michigan: mineralogy, metamorphic reactions and phase equilibria, Econ. Geol., v. 77, p. 60-81.

Hackler, R.T., and Wood, B.J., 1989, Experimental determination of Fe and Mg exchange between garnet and olivine and estimation of Fe-Mg mixing properties in Garnet, A. Mineral., v. 74, p. 994-999.

Hall, B.V., 1982, Geology of the alteration pipe at the Amulet Upper A deposit, Noranda, Quebec, Can. Jour. Earth Sci., v. 19, p. 2060-2084.

Hall, D.L., Bodnar, R.J., and Craig J.R., 1991, Evidence for postentrapment diffusion of hydrogen into peak metamorphic fluid inclusions from the massive sufide deposits at Ducktown, Tennessee, Am. Mineral., v. 76, p. 1344-1355.

Hargreaves, R., 1978, Morphology and chemistry of early Precambrian metabasalt flows, Utik Lake, Manitoba, M.Sc. thesis, The University of Manitoba, Winnipeg.

Hargreaves, R., and Ayres, L.D., 1979, Morphology of Archean metabasalt flows, Utik Lake, Manitoba, Can. J. Earth Sci., v. 16, p. 1452-1466.

Harley, S.L., 1985, Paragenetic and mineral-chemical relationships in orthoamphibole-bearing gneisses from Enderby Land, east Antarctica: a record of Proterozoic uplift, J. Metamorphic Geol., v. 3, p. 179-200.

Hébert, C., and Gobeil, A., 1991, Province de Grenville: zones de favorabilité pour l'exploration minérale, principaux indices et producteurs (anciens et actuels), Ministère de l'Energie et des Ressources, Québec, PRO 91-08.

Hébert, C., and Nadeau, L., 1990, Nouvelles cibles d'exploration de sulfures polymétalliques (Zn, Cu, Pb, Au, Ag), Province de Grenville, région de Portneuf, Ministère de l'Energie et des Ressources, Québec, PRO 90-08.

Herzig, P.M., and Plüger, W.L., 1988, Exploration for hydrothermal activity near the Rodriguez Triple Junction, indian Ocean, Can. Mineral., v. 26, p. 721-736.

Hess, P.C., 1969, The metamorphic paragenesis of cordierite in pelitic rocks, Contr. Mineral. Petrol., v. 24, p. 191-207.

Hewitt, D.A., 1978, A redetermination of the fayalite-magnetite-quartz equilibrium between 650-850°C, Am. J. Sci., v. 278, p. 715-724.

Hickey R.L., Frey, F.A., and Gerlach, D.C., 1986, Multiple sources for basaltic arc rocks from the southern volcanic zone of the Andes (34°-41°): trace element and isotopic evidence for contributions from subducted oceanic crust, mantle and continental crust, J. Geophy. Res., v. 91, p. 5963-5983.

Hobbs, B.E., Means, W.D., and Williams, P.F., 1976, An outline of structural geology, New York, John Wiley & Sons, Inc., 571 p.

Hodges, K.V., and Spear, F.S., 1982, Geothermometry, geobarometry and the Al_2SiO_5 triple point at Mt. Moosilauke, New Hampshire, A. Mineral., v. 67, p. 1118-1134.

Hoffman, P.F., 1990, On accretion of granite-greenstone terranes, in Robert, F., Sheahan, P.A., and Green, S.B., eds., Greenstone gold and crustal evolution: NUNA conference volume, Geological Association of Canada, p. 32-45.

Hoinkes, G., 1986, Effect of grossular-content in garnet on the partitioning of Fe and Mg between garnet and biotite, Contrib. Mineral. Petrol., v. 92, p. 393-399.

Holdaway, M.J., and Lee, S.M., 1977, Fe-Mg cordierite stability in high grade pelitic rock based on experimental, theoretical and natural observations, Contr. Mineral. Petrol., v. 63, p. 175-198.

Holdaway, M.J., Dutrow, B.L., and Shore, P., 1986, A model of the crystal chemistry of staurolite, Am. Mineral., v. 71, p. 1142-1159.

Holdaway, M.J., Dutrow, B.L., and Hinton R.W., 1988, Devonian and Carboniferous metamorphism in west-central Maine: the muscovite-almandine geobarometer and the staurolite problem revisited, A. Mineral., v. 73, p. 20-47.

Holland, T.J.B., and Powell, R., 1990, An enlarged and updated internally consistent thermodynamic dataset with uncertainties and correlations: the system K_2O-Na_2O-CaO-MgO-MnO-FeO-Fe_2O_3-Al_2O_3-TiO_2-SiO_2-C-H_2-O_2, J. Metamorph. Geol., v. 8, p. 89-124.

Howard, K.J., and Fisk, M.R., 1988, Hydrothermal alumina-rich clays and boehmite on the Gorda Ridge, Geochim. Cosmochim. Acta 52, p. 2269-2279.

Hudson, N.F.C., and Harte, B., K_2O-poor, aluminous assemblages from the Buchan Dalradian, and the variety of orthoamphibole assemblages in aluminous bulk compositions in the amphibolite facies, Am. J. Sci., v. 285, p. 224-266.

Huebner, J.S., 1971, Buffering techniques for hydrostatic systems at elevated pressures, in Ulmer, G., ed., Research techniques for high pressure and high temperature, Springer-Verlag, New York, p. 173-177.

Huston, D.L., and Large, R.R., 1989, A chemical model for the concentration of gold in volcanogenic massive sulphide deposits, Ore Geol. Reviews, v. 4, p. 171-200.

Hutcheon, I., 1978, Calculation of metamorphic pressure using the sphalerite-pyrite-pyrrhotite equilibrium, Am. Mineral., v. 63, p. 87-95.

-------- 1979, Sulfide-oxide-silicate equilibria; Snow Lake, Manitoba, Am. J. Sci., v. 279, p. 643-665.

Hutcheon, I., Froese, E., and Gordon, T.M., 1974, The assemblage quartz-sillimanite-garnet-cordierite as an indicator of metamorphic conditions in the Daly Bay complex, NWT, Contrib. Mineral. Petrol., v. 44, p. 29-34.

Indares, A., and Martignole, J., 1985, Biotite-garnet geothermometry in the granulite facies: the influence of Ti and Al in biotite, A. Mineral., v. 70, p. 272-278.

James, R.S., Grieve, R.A.F., and Pauk, L., 1978, The petrology of cordierite-anthophyllite gneisses and associated mafic and pelitic gneisses at Manitouwadge, Ontario, Am. J. Sci., v. 278, p. 41-63.

Johannes, W., and Schreyer, W. 1981, Experimental introduction of CO_2 and H_2O into Mg-cordierite, Am. J. Sci., v. 281, p. 299-317.

Johnson, C.A., Rye, D.M., and Skinner, B.J., 1990, Petrology and stable isotope geochemistry of the metamorphosed Zinc-iron-manganese deposit at Sterling Hill, New Jersey, Econ. Geol., v. 85, p. 1133-1161.

Jourdain, V., Roy, D.W., and Simard, J.-M., 1987, Stratigraphy and structural analysis of the north gold zone at Montauban-les-mines, Quebec, CIM Bulletin, v. 80, no 906, p. 61-66.

Kamineni, D.C., 1975, Chemical Mineralogy of some cordierite-bearing rocks near Yellowknife, northwest territories, Canada, Contrib. Mineral. Petrol., v. 53, p. 293-310.

-------- 1979, Metasedimentary cordierite-gedrite rocks of Archean age near Yellowknife, Canada, Precambrian Research, v. 9, p. 289-301.

Kerrich, R., 1982, Geochemistry of gold deposits in the Abitibi Greeston belt, The Canadian Inst. of Mining and Metallurgy, special volume 27, 75 p.

Kerrick, D.M., 1987, Fribrolite in contact aureoles of Donegal, Ireland, Am. Mineral., v. 72, p. 240-254.

-------- 1988, Al_2SiO_5-bearing segregations in the Lepontine Alps, Switzerland: aluminum mobility in metapelites, Geology, v. 16, p. 636-640.

Kerrick, D.M., 1990, The Al_2SiO_5 polymorphs, Rev. Mineral., v. 22, 406 p.

Kerrick, D.M., and Speer, J.A., 1988, The role of minor element solid solution on the andalusite-sillimanite equilibrium in metapelites and peraluminous granitoids, Am. J. Sci., v. 288, p. 152-192.

King, H.F., 1958, Notes on ore occurrences in highly metamorphosed Precambrian rocks, Australisian Inst. Min. Metal., F.L. Stilwell Anniversary Volume, p. 143-167.

Klein, G. deV., and Lee, Y.I., 1984, A preliminary assessment of geodynamic controls on depositional systems and sandstone diagenesis in back-arc basins, western Pacific ocean, Tectonophysics, v. 102, p. 119-152.

Klemm, D., 1965, Synthesen und analysen in den dreiecksdiagrammen FeAsS-CoAsS-NiAsS und FeS_2-CoS_2-NiS_2, Neues Jahrbuch Für Mineralogie Abhandlungen, v. 103, p. 205-255.

Kohn, M.J., and Spear, F.S., 1989, Empirical calibration of geobarometers for the assemblage garnet + hornblende + plagioclase + quartz, Am. Mineral., v. 74, p. 77-84.

-------- 1990, Two new geobarometers for garnet amphibolites, with applications to southeastern Vermont, Am. Mineral., v. 75, p. 89-96.

Koziol, A.M., and Newton, R.C., 1988, Redetermination of the anorthite breakdown reaction and improvement of the plagioclasse-garnet-Al_2SiO_5-quartz geobarometer. Am. Mineral., v. 73, p. 216-233.

Kranidiotis, P., and MacLean, W.H., 1987, Systematics of chlorite alteration at the Phelps Dodge massive sulfide deposit, Matagami, Quebec, Econ. Geol., v. 82, p. 1898-1911.

Kretschmar, U., and Scott, S.D., 1976, Phase relations involving arsenopyrite in the system Fe-As-S and their application, Can. Mineral., v. 14, p. 364-386.

Kretz, R., 1983, Symbols for rock-forming minerals, Am. Mineral., v. 68, p. 277-279.

-------- 1990, Biotite and garnet compositional variation and mineral equilibria in Grenville gneisses of the Otter Lake area, Quebec, J. Metamorphic Geol., v. 8, p. 493-506.

Kullerud, G., 1965, Sulfide-carbonate reactions, Carnegie Instit. Washington, Year Book 64-65, p. 188-193.

Kullerud, G., and Yoder, H.S., 1963, Sulfide-silicate relations, Carnegie Inst. Washington Year Book 62, p. 215-218.

-------- 1964, Sulfide-lilicate relations, Carnegie Inst. Washington Year Book 63, p. 218-222.

Kurepin, V.A., 1985, H_2O and CO_2 contents of cordierite as an indicator of thermodynamic conditions of formation, Geochemistry International, v. 22, p.148-156.

Large, R.R., and Both, R.A., 1980, The volcanogenic sulfide ores at Mount Chalmers Eastern Queensland, Econ. Geol., v. 75, p. 992-1009.

Latvalahti, U., 1979, Cu-Zn-Pb ores in the Aijala-Orijarvi area, Southwest Finland, Econ. Geol., v. 74, p. 1035-1059.

Leake, B.E., 1978, Nomenclature of amphiboles, Am. Mineral., v. 63, p. 1023-1053.

Lieberman, J., and Petrakakis, K., 1991, TWEEQU thermobarometry: analysis of uncertainties and applications to granulites from western Alaska and Austria, Can. Mineral., v. 29, 857-887.

Lonker, S.W., 1981, The P-T-X relations of the cordierite-garnet-sillimanite-quartz equilibrium, Am. J. Sci., v. 281, p. 1056-1090.

Luff, W.M., Goodfellow, W.D., and Juras, S.J., 1992, Evidence for a feeder pipe and associated alteration at the Brunswick no. 12 massive-sulfide deposit, Explor. Mining Geol., v. 1, no. 2, p. 167-185.

MacLean, W.H., 1990, Mass change calculations in altered rock series, Mineral. deposita, v. 25, p. 44-49.

MacLean, W.H., and Kranidiotis, P., 1987, Immobile elements as monitors of mass transfer in hydrothermal alteration, Phelps Dodge massive sulfide deposit, Matagami, Quebec, Econ. Geol., v. 82, p. 951-952.

MacLean, W.H., St-Seymour, K., and Prabhu, M.K., 1982, Sr, Y, Zr, Nb, Ti and REE in Grenville amphibolite at Montauban-les-Mines, Quebec, Can. Jour. Earth Sci., v. 19, p. 633-644.

MacRae, N.D., 1974, Sulfurization of basalt under thermal metamorphic conditions to produce cordierite-bearing rocks, Can. J. Earth Sci., v. 11, p. 246-253.

Marshall, B., and Gilligan, L.B., 1987, An introduction to remobilization: information from ore-body geometry and experimental considerations, Ore Geol. Rev., v. 2, p. 87-131.

Martignole, J., and Sissi, J.-C., 1981, Cordierite-garnet-H_2O equilibrium: a geological thermometer, barometer and water fugacity indicator, Contrib. Mineral. Petrol., v. 77, p. 38-46.

Mathieson, N.A., and Hodgson, C.J., 1984, Alteration, mineralization, and metamorphism in the area of the East South "C" ore zone, 24th level of the Dickenson mine, Red Lake, northwestern Ontario, Can. J. Earth Sci., v. 21, p. 35-52.

Max, M.D., Rex, D., and Winchester, J.A., 1988, The Farnacht formation along the south side of the Clew bay fault zone, western Ireland: its chemistry and age of metamorphism, Geol. J., v. 23, p. 249-260.

McMullin, D.W., Berman, R.G., and Greenwood, H.J., 1991, Calibration of the SGAM thermobarometer for pelitic rocks using data from phase-equilibrium experiments and natural assemblages, Can. Mineral., v. 29, p. 889-908.

McPhail, D.C., Berman, R.G., and GreenWood, H.J., 1990, Experimental and theoretical constraints on aluminum substitution in magnesian chlorite, and a thermodynamic model for H_2O in magnesian cordierite, Can. Mineral., V. 28, p. 859-874.

Mel'nik, Y.P., 1972, Thermodynamic parameters of compressed gases and metamorphic reactions involving water and carbon dioxide, Geochem. Internat., v. 9, p. 419-426.

Milligan, G.C., and Take, W.F., 1954, Geology of the eastern Bear Lake area, Manitoba Department of Mines and Natural Resources, Publication 53-1.

Miyake, A., 1985, Zn-rich staurolite from the Uvete area, central Kenya, Mineral. Mag., v. 49, p. 573-578.

Miyano, T., and Klein, C., 1986, Fluid behavior and phase relations in the system Fe-Mg-Si-C-O-H: application to high grade metamorphism of iron-formations, Am. J. Sci., v. 286, p. 540-575.

Miyashiro, A., 1959, Calcium-poor garnet in relation to metamorphism, Geochimica et Cosmochimica Acta, v. 4, p. 179-208.

-------- 1973, Metamorphism and metamorphic belts, Allen and Unwin, Boston, 492 p.

Mohr, D.W., and Newton, R.C., 1983, Kyanite-staurolite metamorphism in sulfidic schists of the Anakeesta Formation, Great Smokey Mountains, North Carolina, Am. J. Sci., v. 283, p. 97-134.

Moore, J.M., 1986, Introduction: The Grenville Problem then and now, in Moore, J.M., Davidson, A., and Baer, A.J., eds., The Grenville Province, GAC Special Paper 31, p. 1-11.

Moore, J.M., and Reid, A.M., 1988, Implications of sphalerite inclusions in gahnite from the Namaqualand metamorphic complex, south Africa, Can. Mineral., v. 26, p. 293-300.

-------- 1989, A Pan-African zincian staurolite imprint on Namaqua quartz-gahnite-sillimanite assemblages, Mineral. Mag., v. 53, p. 63-70.

Morin, G., 1987, Gîtologie de la région de Montauban, Ministère de l'Energie et des ressources, Québec, MM-86-02.

Nadeau, L., and Corrigan, D., 1991, Preliminary notes on the geology of the St.Maurice tectonic zone, Grenville orogen, Quebec, Current Research, part E, Geol. Survey of Canada, Paper 91-1E, p. 245-255.

Nesbitt, B.E., 1982, Metamorphic sulfide-silicate equilibria in the massive sulfide deposits at Ducktown, Tennessee, Econ. Geol., v. 77, p. 364-378.

-------- 1986a, Oxide-sulfide-silicate equilibria associated with metamorphosed ore deposits. Part I: Theoretical considerations, Econ. Geol., v. 81, p. 831-840.

-------- 1986b, Oxide-sulfide-silicate equilibria associated with metamorphosed ore deposits. Part II: Pelitic and felsic volcanic terrains, Econ. Geol., v. 81, p. 831-840.

Nesbitt, B.E., and Essene, E.J., 1982, Metamorphic thermometry and barometry of a portion of the southern Blue Ridge province, Am. J. Sci., v. 282, p. 701-729.

Nesbitt, R.W., Sun, S.-S., and Purvis, A.C., 1979, Komatiites: geochemistry and genesis, Can. Mineral., v. 17, p. 165-186.

Newton, R.C., and Wood, B.J., 1979, Thermodynamics of water in cordierite and some petrologic consequences of cordierite as a hydrous phase, Contrib. Mineral. Petrol., v. 68, p. 391-405.

Newton, R.C., and Haselton, H.T., 1981, Thermodynamics of the garnet-plagioclase-Al_2SiO_5-quartz geobarometer, In Newton, R.C., Navrotsky, A., and Wood, B.J., eds., Thermodynamics of minerals and melts, Springer-Verlag, New York, p. 131-147.

O'Hara, K., 1988, Fluid flow and volume loss during mylonitization - an origin for phyllonite in an overthrust setting, North Carolina, USA, Tectonophysics, v. 156, p. 21-36.

O'Hara, K., and Blackburn, W.H., 1989, Volume-loss model for trace-element enrichments in mylonites, Geology, v. 17, p. 524-527.

Ohmoto, H., and Kerrick, D., 1977, Devolatilization quilibria in graphitic systems, Am. J. Sci., v. 277, p. 1013-1044.

O'Neil, J.J., and Osborne, F.F., 1939, La mine Tétreault, Montauban-les-Mines, comté de Portneuf, Ministère des Mines et des Pêcheries, Québec, RP-136.

Osborne, F.F., 1939, The Montauban mineralized zone, Quebec, Econ. Geol., v. 34, p. 712-726.

Pan, Y., and Fleet, M.E., 1991, Barian feldspar and barian-chromian muscovite from the Hemlo area, Ontario, Can. Mineral., v. 29, p. 481-498.

Patrick, B.E., and Evans, B.W., 1989, Metamorphic evolution of the Seward Peninsula Blueschist Terrane, J. Petrol., v. 30, pt 3, p. 531-555.

Pattison, D.R.M., 1989, P-T conditions and the influence of graphite on pelitic phase relations in the Ballachulish Aureole, Scotland, J. Petrol. v. 30, pt 5, p. 1219-1244.

Pattison, D., and Harte, B., 1985, A petrogenetic grid for pelites in the Ballachulish and other Scottish thermal aureoles, J. Geol. Soc. Lon., v. 142, p. 7-28.

Pearce, J.A., Harris, N.B., and Tindle, A.G., 1984, Trace element discrimination diagrams for the tectonic interpretation of granitic rocks, Jour. Petrol., v. 25, 956-983.

Perchuck, L.L., 1977, Thermodynamical control of metamorphic processes, in Energetics of Geological Processes, edited by Saxena, s.K. and Bhattacharji, S., Springer-Verlag, New York, p. 285-352.

-------- 1981, Correction of the biotite-garnet thermometer in case of the Mn ⇌ Mg + Fe isomorphism in garnet, Dokl. USSR AS 256, p. 38-41.

Perchuck, L.L., and Lavrent'eva, I.V., 1983, Experimental investigation of exchange equilibria in the system cordierite-garnet-biotite. In Kinetics and equilibria in mineral reactions. Edited by E.D. Saxena. Springer-Verlag, New York, Advances in Geochemistry, v. 3, p. 198-240.

Percival, J.A., Carmichael, D.M., Helmstaedt, H., 1982, A petrogenetic grid for calcium and alkali-dificient bulk compositions, Current Research, part A, Geol. Survey Canada v.82-1A, p. 169-173.

Peredery, W.V., 1966, Cordierite-anthophyllite rocks of Pike Lake Region, Quebec, east of James Bay, Unbpub. Thesis, McGill University.

Perkins, D., Essene, E.J., and Wall, V.J., 1987, THERMO: a computer program for calculation of mixed-volatile equilibria, Am. Mineral. v. 72, p. 446-447.

Petersen, E.U., 1986, Tin in volcanogenic massive sulfide deposits: an exemple from the Geco Mine, Manitouwadge District, Ontario, Canada, Econ. Geol., v. 81, p. 323-342.

Phinney, W.C., Morrison, D.A., and Maczuga, D.E., 1988, Anorthosites and related megacrystic units in the evolution of Archean crust, J. Petrol., v. 29, pt 6, p. 1283-1323.

Pollard, P.J., 1981, Hydrothermal tin-tungsten mineralization and origin of associated cordierite-anthophyllite rocks at Tommy Burns mine, north Queensland, Australia, Trans. Instn. Min. Metall. (sect. B: Appl. earth sci.), 90, p. B65-69.

Popp, R.K., Gilbert, M.C., and Craig, J.R., 1977a, Stability of Fe-Mg amphiboles with respect to oxygen fugacity, Am. Mineral., v. 62, p. 1-12.

-------- 1977b, Stability of Fe-Mg amphiboles with respect to sulfur fugacity, Am. Mineral., v. 62, p. 13-30.

Poulson, S.R., and Ohmoto, H., 1989, Devolatilization equilibria in graphite-pyrite-pyrrhotite bearing pelites with application to magma-pelite interaction, Contrib Mineral. Petrol., v. 101, p. 418-425.

Powell, R., and Holland, T., 1988, An internally consistent thermodynamic dataset with uncertainties and correlations: 3. Applications to geobarometry, worked examples and a computer program, J. Metamorphic Geol., v. 6, p. 173-204.

-------- 1990, Calculated mineral equilibria in the pelite system, KFMASH (K_2O-FeO-MgO-Al_2O_3-SiO_2-H_2O), Am. Mineral., v. 75, p. 367-380.

Prabhu, M.K., 1981, Geology geochemistry and genesis of Montauban lead-zinc deposits. Ph.D. thesis, McGill University, Montreal, P.Q., 271 p.

Prahbu, M.K., and Webber, G.R., 1984, Origin of quartzofeldspathic gneisses at Montauban-les-mines, Quebec, Can. Jour. Earth Sci., v. 21, p. 336-345.

Pyke, D.R., 1966, Geology of the Montauban-Colbert area, Champlain and Portneuf townships, Quebec Dept. Mines Geol. Report RP-545, 18 p.

Ramsay, C.R., and Davidson, L.R., 1974, Cordierite-anthophyllite rocks formed by isochemical regional metamorphism at Mary Kathleen, northwestern Queesland, Australia, Proceedings of the Royal Society of Queensland, v. 85, p. 43-55.

Reinhardt, J., 1987, Cordierite-anthophyllite rocks from north-west Queensland, Australia: metamorphosed magnesian pelites, J. Metamorphic Geol., v. 5, p. 451-472.

Riverin, G., and Hodgson, C.J. 1980, Wall-rock alteration at the Millenbach Cu-Zn mine, Noranda, Quebec, Econ. Geol., v. 75, p. 424-444.

Rivers, T., Martignole, J., Gower, C.F., and Davidson, A., 1989, New tectonic divisions of the Grenville province, southeast Canadian Shield, Tectonics, v. 8, p. 63-84.

Robert, F., Sheahan, P.A., and Green, S.B., eds, 1990, Greenstone gold and crustal evolution: NUNA conference volume, Geological association of Canada, Mineral Deposits Division, 252 p.

Roberts, R.G., and Reardon, E.J., 1978, Alteration and ore-forming processes at Mattagami Lake mine, Quebec, Can. Jour. Earth Sci., v. 15, p. 1-21.

Robie, R.A., Hemingway, B.S., and Fisher, J.R., 1978, Thermodynamic properties of minerals and related substances at 298.15 K and 1 bar (10^5 pascals) pressure and at higher temperatures, U.S. Geol. Survey Bull., v. 1452, 455 p.

Robinson, D.J., 1984, Silicate facies iron-formation and strata-bound alteration: tuffaceous exhalites derived by mixing-evidence from Mn garnet-stilpnomelane rocks at Redstone, Timmins, Ontario, Econ. Geol., v. 79, p. 1796-1817.

Robinson, D., 1987, Transition from diagenesis to metamorphism in extensional and collision settings, Geology, v. 15, p. 866-869.

Robinson, P., and Jaffe, H.W., 1969, Aluminous enclaves in gedrite-cordierite gneiss from southwestern New Hampshire, Am. J. Sci., v. 267, p. 389-421.

-------- 1971, Composition of the anthophyllite-gedrite series, comparisons of gedrite and hornblende and the anthophyllite-gedrite solvus, Am. Mineral., v. 56, p. 1005-1041.

Robinson, P., Spear, F.S., Schumacher, J.C., Laird, J., Klein, C., Evans, B.W., and Doolan, B.L., 1982, Phase relations of metamorphic amphiboles: natural occurrence and theory, in Veblen, D.R., and Ribbe, P.H., eds., Amphiboles: petrology and experimental phase relations. Reviews in Mineralogy, v. 9B, p. 159-182. - Miner. Soc. Am.

Rondot, J., 1978, Région de Saint-Maurice, Ministère des Richesses Naturelles, Quebec, DPV-594.

Ryzhenko, B.N., and Volkov, V.P., 1971, Fugacity coefficients of some gases in a broad range of temperatures and pressures, Geochemistry International, v. 8, p. 468-481.

Salje, E., 1986, Heat capacities and entropies of andalusite and sillimanite: the influence of fibrolitization on the phase diagram of the Al_2SiO_5 polymorphs, Am. Mineral., v. 71, p. 1366-1371.

Sangster, D.F., 1972, Precambrian volcanogenic massive sulfide deposits in Canada: a review, Geol. Surv. Canada Paper 72-22, 44 p.

Schneiderman, J.S., and Tracy, R.J., 1991, Petrology of orthoamphibole-cordierite gneisses from the Orijärvi area, southwest Finland, Am. Mineral., v. 76, p. 942-955.

Schreurs, J., and Westra, L., 1985, Cordierite-orthopyroxene rocks: the granulite facies equivalents of the Orijärvi cordierite-anthophyllite rocks in West Uusimaa, southwest Finland, Lithos, v. 18, p. 215-228.

Schumacher, J.C., 1988, Stratigraphy and geochemistry of the Ammonoosuc volcanics, central Massachusetts and southwestern New Hampshire, Am. J. Sci., v. 288, p. 619-663.

Schumacher, J.C., and Robinson, P., 1987, Mineral chemistry and metasomatic growth of aluminous enclaves in gedrite-cordierite-gneiss from soutwestern New Hampshire, U.S.A., Jour. Petrol., v. 28, p. 1033-1073.

Scott, S.D., 1973, Experimental calibration of the sphalerite geobarometer, Econ. Geol., v. 68, p. 466-474.

Secord, T.K. and Brown, P.E., 1986, Geology and geochemistry of the Ore Hill Zn-Pb-Cu massive sulfide deposit, Warren, New Hampshire, Econ. Geol., v. 81, p. 371-387.

Sharma, R.S., and MacRae, N.D., 1981, Paragenetic relations in gedrite-cordierite-staurolite-biotite-sillimanite-kyanite-gneisses at Ajitpura, Rajasthan, India, Contrib. Mineral. Petrol., v. 78, p. 48-60.

Sharp, Z.K., Essene, E.J., and Kelly, W.C., 1985, A re-examination of the arsenopyrite geothermometer: pressure considerations and applications to natural assemblages, Can. Mineral., v. 23, p. 517-534.

Slack, J.F., and Coad, P.R., 1989, Multiple hydrothermal and metamorphic events in the Kidd Creek volcanogenic massive sulphide deposit, Timmins, Ontario: evidence from tourmalines and chlorites, Can. J. Earth Sci., v. 26, p. 694-715.

Smith, J.R., 1956, Montauban-les-Mines area, Quebec Dept. Mines Geol. Rept. 65, 43 p.

Spear, F.S., 1978, Petrogenetic grid for amphibolites from the Post Pond and Ammonoosuc Volcanics, Carnegie Inst. Washington Year book 77, p. 805-808.

-------- 1980, The gedrite-anthophyllite solvus and the composition limits of orthoamphibole from the Post Pond Volcanics, Vermont, Am. Mineral., v. 65, p. 1103-1118.

-------- 1981, An experimental study of hornblende stability and compositional variability in amphibolite, Am. J. Sci., v. 281, p. 697-734.

-------- 1982, Phase equilibria of amphibolites from the Post Pond Volcanics, Mt. Cube Quadrangle, Vermont, Jour. Petrol., v. 23, p. 383-426.

-------- 1988, The Gibbs method and Duhem's theorem: the quantitative relationships among P, T, chemical potential, phase composition and reaction progress in igneous and metamorphic systems, Contrib. Mineral Petrol., v. 99, p. 249-256.

Spear, F.S., and Cheney, J.T., 1989, A petrogenetic grid for pelitic schists in the system SiO_2-Al_2O_3-FeO-MgO-K_2O-H_2O, Contrib. Mineral. Petrol., v. 101, p. 149-164.

Spear, F.S., and Rumble,D., 1986, Pressure, temperature and structural evolution of the Orfordville Belt, West-Central New Hampshire, J. Petrol., v. 27, p. 1071-1093.

Spear, F.S., and Schumacher, J.C., 1982, Origin of cordierite-anthophyllite rocks, Rev. Mineral., v. 98, p. 159-177.

Spry, A., 1969, Metamorphic textures. Pergamon Press Ltd, 350 p.

Spry, P.G., 1987, A sulphur isotope study of the Broken Hill deposit, New South Wales, Australia, Mineral Deposita, v. 22, p. 109-115.

Spry, P.G., and Scott, S.D., 1986a, Zincian spinel and staurolite as guides to ore in the Appalachians and Scandinavian Caledonides, Can. Mineral., v.24, p. 147-163.

-------- 1986b, The stability of zincian spinels in sulfide systems and their potential as exploration guides for metamorphosed massive sulfide deposit, Econ. Geol., v. 81, p. 1446-1463.

Stamatelopoulou-Seymour, K., 1975, Metamorphosed Pb-Zn deposits at Montauban, Quebec. M.Sc. thesis, McGill University, Montreal, P.Q., 230 p.

Stamatelopoulou-Seymour, K., and MacLean, W.H., 1977, The geochemistry of possible metavolcanic rocks and their relationship to mineralization at Montauban-les-Mines, Quebec, Can. Jour. Earth Sci., v. 14, p. 2440-2452.

-------- 1984, Metamorphosed volcanogenic ores at Montauban, Grenville Province, Quebec, Can. Mineral., v. 22, p. 595-604.

Stephens, M.B., Swinden, H.S., and Slack, J.F., Correlation of massive sulfide deposits in the Appalachian-Caledonian orogen on the basis of Paleotectonic setting, Econ. Geol., v. 79, p. 1442-1478.

Stoddard, E.F., 1979, Zinc-rich hercynite in high-grade metamorphic rocks: a product of the dehydration of staurolite, Am. Mineral., v. 67, p. 737-774.

Stoddard, E.F., and Miller,C.F., 1990, Chemistry and phase petrology of amphiboles and orthoamphibole-cordierite rocks, Old Woman Mountains, SE California, USA, Mineral. Mag., v. 54, p. 393-406.

Stormer, J.C., 1983, The effects of recalculation on estimates of temperature and oxygen fugacity from analyses of multicomponent iron-titanium oxides, Am. Mineral., v. 68, p. 586-594.

Studer, R.D., 1982, Geology of the Stall Lake copper deposit, Snow Lake, Manitoba, Canadian Inst. Min. Metall. Bull. 75, no. 837, p. 66-71.

Suffel, G.G., 1971, Metamorphism of massive sulphides at Manitouwadge, Ontario, Canada, Soc Mining Geol. Japan, Spec. Issue 3, p. 235-240.

Teng, L.S., and Lo, H.-J., 1985, Sedimentary sequences in the Island arc settings of the coastal range, eastern Taiwan, Acta Geologica Taiwanica, Science reports of the national Taiwan University, no. 23, p. 77-98.

Thompson, J.B., Jr., 1972, Oxides and sulfides in regional metamorphism of pelitic schists, Internat. Geol. Cong., 24th, Montreal, 1972, sec. 10, p. 27-35.

Thompson, A.B., 1976, Mineral reactions in pelitic rocks: II. Calculation of some P-T-X (Fe-Mg) phase relations, Am. J. Sci., v. 276, p. 425-454.

-------- 1981, The pressure-temperature (P,T) plane veiwed by geophysicists and petrologists, TERRA Cognita 1, p. 11-20.

Thurston, P.C., and Chivers, K.M., 1990, Secular variation in greenstone sequence development emphasizing Superior Province, Canada, Precamb. Res., v. 46, p. 21-58.

Tracy, R.J., 1982, Compositional zoning and inclusions in metamorphic minerals, Mineral. Soc. Am. Reviews in Mineralogy, v. 10, p. 355-397.

Tracy, R.J., and Robinson, P., 1979, Evolution of metamorphic belts: information from detailed petrologic studies, I.G.C.P. Blacksburg, Virginia, 189-195.

-------- 1988, Silicate-sulfide-oxide-fluid reactions in granulite-grade pelitic rocks, central Massachusetts, Am. J. Sci., v. 288-A, p. 45-74.

Trägårdh, J., 1988, Cordierite-mica-quartz schists in a Proterozoic volcanic iron ore-bering terrain, Riddarhyttan area, Bergslagen, Sweden, Geologie en Mijnbouw, v. 67, p. 397-409.

Treloar, P.J., Koistinen, T.J., and Bowes, D.R., 1981, Metamorphic development of cordierite-amphibole rocks and mica schists in the vicinity

of the Outokumpu ore deposit, Finland, Trans. Roy. Soc. Edinb., Earth Sci., v. 72, p. 201-215.

Treloar, P.J., and Putnis, A., 1982, Chemistry and microstructure of orthoamphiboles from cordierite-amphibole rocks at Outokumpu, North Karelia, Finland, Mineral. Mag., v. 45, p. 55-62.

Tso, J.L., Gilbert, M.C., and Craig, J.R., 1979, Sulfidation of synthetic biotites, Am. Mineral., v. 64, p. 304-316.

Tuisku, P., 1992, Contact zone interaction of metabasites with metapelites: amphibolite facies mineral assemblages, chemical profiles and their origin, the Puolankajärvi Formation, Finland, Lithos, v. 27, p. 279-300.

Tuisku, P., and Laajoki, K., 1990, Metamorphic and structural evolution of the Early Proterozoic Puolankajärvi Formation, Finland - II. The pressure-temperature-deformation-composition path, J. Metamorphic Geol., v. 8, p. 375-391.

Tuisku, P., Ruostesuo, P., and Häkkinen, A.-M., 1987, The metamorphic behaviour and petrogenetic significance of zinc in amphibolite facies, staurolite-bearing mica schists, Puolankajärvi Formation, central Finland, Geochimica et Cosmochimica Acta, v. 51, p. 1639-1650.

Upadhyay, H.D., and Smitheringale, W.G., 1972, Geology of the Gullbridge copper deposit, Newfoundland: volcanogenic sulfides in cordierite-anthphyllite rocks, Can. J. Earth Sci., v. 9, p. 1061-1073.

Urabe, T., Scott, S.D., and Hattori, K., 1983, A comparison of footwall-rock alteration and geothermal systems beneath some Japanese and Canadian volcanogenic massive sulfide deposits, Econ. Geol. Monograph 5, p. 345-364.

Valiquette, G., 1964, Géologie des régions du Lac des Montagnes et du Lac Lemare. Territoire de Mistassini. Thèse de doctorat, Univ. Laval, Québec.

Valiquette, G., 1975, Région de la rivière Némiscau. Ministère des richesses naturelles, Québec, Rap. Geol. 158, 156 p.

Vallance, T.G., 1967, Mafic rock alteration and isochemical development of some cordierite-anthophyllite rocks, Jour. Petrol., v. 8, p. 84-96.

Valley, J.W., Bohlen, S.R., Essene, E.J., and Lamb, W., 1990, Metamorphism in the Adirondacks: II. The role of fluids, J. Petrol., v. 31, pt 3, p. 555-596.

van Reenen, D.D., 1986, Hydration of cordierite and hypersthene and a description of the retrograde orthoamphibole isograd in the Limpopo belt, South Africa, Am. Mineral., v. 71, p. 900-915.

Vance, R.K., and Condie, K.C., 1987, Geochemistry of footwall alteration associated with the early Proterozoic United Verde massive sulfide deposit, Jerome, Arizona, Econ. Geol., v. 82, p. 571-586.

Vernon, R.H., 1979, Formation of late sillimanite by hydrogen metasomatism (base leaching) in some high-grade gneisses, Lithos, v. 12, p. 143-152.

-------- 1987, Growth and concentration of fibrous sillimanite related to heterogeneous deformation in K-feldspar-sillimanite metapelites, J. Metamorphic Geol., v. 5, p. 51-68.

Vivallo, W., 1985, The metamorphism of the supracrustal rocks at Gapenberg, south central Sweden, Geologiska Föreningens i Stockholm Förhandlingar, v. 106, pt. 3, p. 257-267.

Visser, D., and Senior, A., 1990, Aluminous reaction textures in orthoamphibole-bearing rocks: the pressure-temperature evolution of the high-grade Proterozoic of the Bamble sector, south Norway, J. Metamorphic Geol., v. 8, p. 231-246.

Vry, J.K., Brown, P.E., and Valley, J.W., 1990, Cordierite volatile content and the role of CO_2 in high-grade metamorphism, Am. Mineral., v. 75, p. 71-88.

Weber, W., 1974, Utik Lake - Bear Lake project. In Summary of Geological field work, 1974. Edited by R.F.J. Scoates. Manitoba Mineral Resources Division, Exploration and Geological Survey Branch, Geological Paper 2-74, p. 27-32.

-------- 1991, The Churchill-Superior Boundary Zone, southeast margin of the Trans-Hudson Orogen: a review, in Lewry, J.F. and Stauffer, M.R., eds., The Early Proterozoic Trans-Hudson Orogen of North America, Geological assocation of Canada, Special Paper 37, p. 41-55.

Weber, W., and Scoates, R.F.J., 1978, Archean and Proterozoic metamorphism in the northwestern Superior Province and along the Churchill - Superior boundary, Manitoba. In Metamorphism in the Canadian Shield. Edited by J.A. Fraser and W.W. Heywood. Geological Survey of Canada, Paper 78-10, p. 516.

Whitford, D.J., McPherson, W.P.A., and Wallace, D.B., Geochemistry of the host rocks of the volcanogenic massive sulfide deposit at Que River, Tasmania, Bull. Soc. Econ. Geol., v. 84, p. 1-21.

Williams, K.L., and Kullerud, G., 1968, The Ni-Sb-S system, Carnegie Inst. of Washington Yearbook 68, p. 270-273.

Williams, M.L., and Grambling, J.A., 1990, Manganese, ferric iron, and the equilibrium between garnet and biotite, Am Mineral., v. 75, p. 886-908.

Wilson, N.L., 1939, An investigation of the metamorphism of the Orijarvi type deposits at Montauban-les-mines, P.Q., Unpub. Ph.D., McGill, 163p.

Winchester, J.A., and Floyd, P.A., 1977, Geochemical discrimination of different magma series and their differentiation products using immobile elements, Chem. Geol., v. 20, p. 325-343.

Winchester, J.A., and Max, M.D., 1984, Element mobility associated with syn-metamorphic shear zones near Scotchport, NW Mayo, Ireland, J. Metamorphic Geol., v. 2, p. 1-11.

Winkler, H.G.F., 1979, Petrogenesis of metamorphic rocks, Springer-Verlag, New York, 348 p.

Wolter, H.U., and Seifert, F., 1984, Mineralogy and genesis of cordierite-anthophyllite rocks from the sulfide deposit of Falun, Sweden, Lithos, 17, p. 147-152.

Yardley, B.W.D., 1985, Apatite composition and the fugacities of HF and HCl in metamorphic fluids, Mineral. Mag., v. 49, p. 77-79.

Yund, R.A., 1962, The system Ni-As-S phase relations and mineralogical significance. Am. J. Sci., v. 260, p. 761-782.

Zaleski, E., Froese, E., and Gordon, T.M., 1991, Metamorphic petrology of Fe-Zn-Mg-Al alteration at the Linda volcanogenic massive sulfide deposit, Snow Lake, Manitoba, Can. Mineral, v. 29, p. 995-1017.

APPENDIX 1. SAMPLE LOCATIONS MAPS

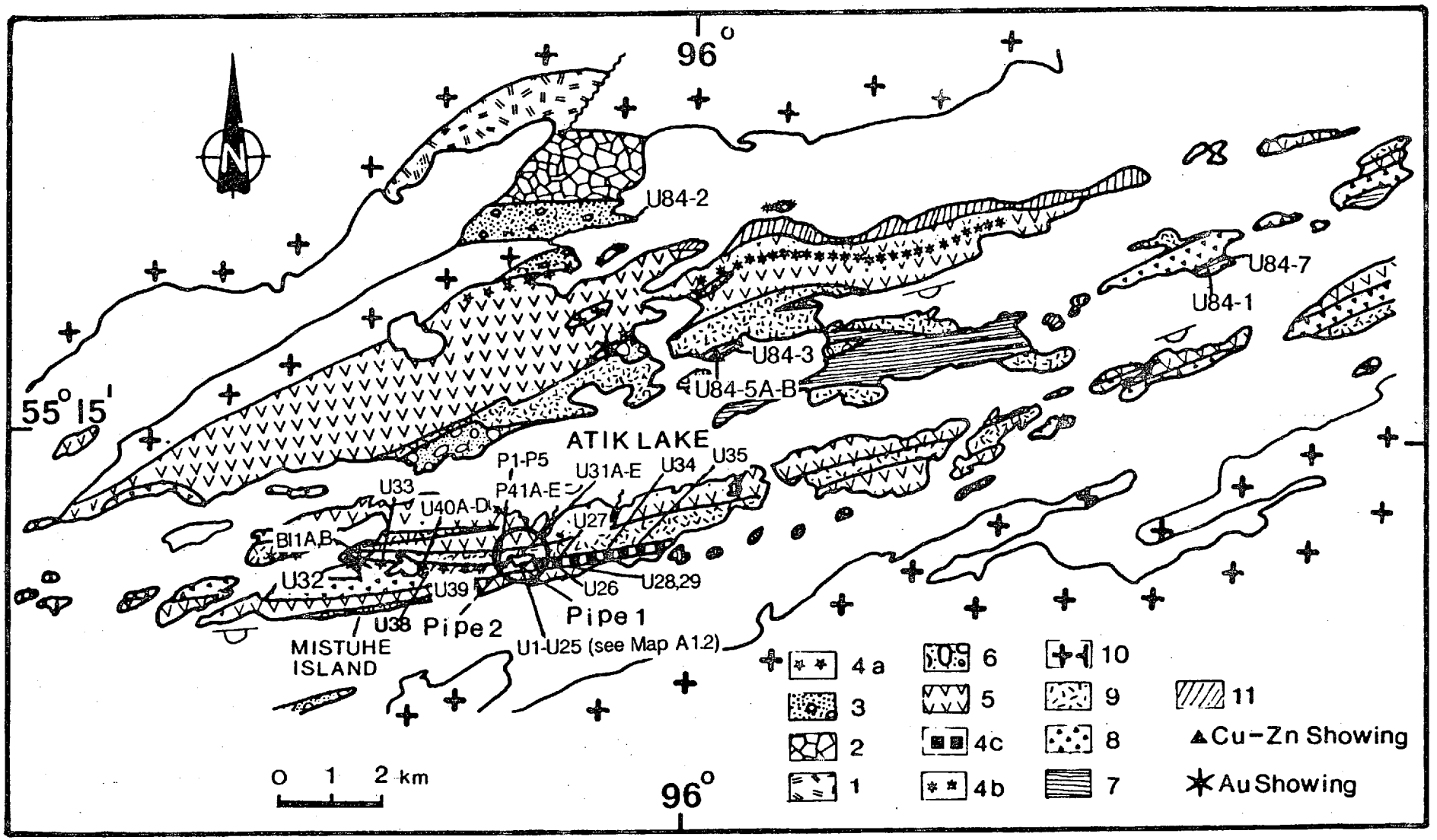

Map A1.1 Sample Locations, Atik Lake

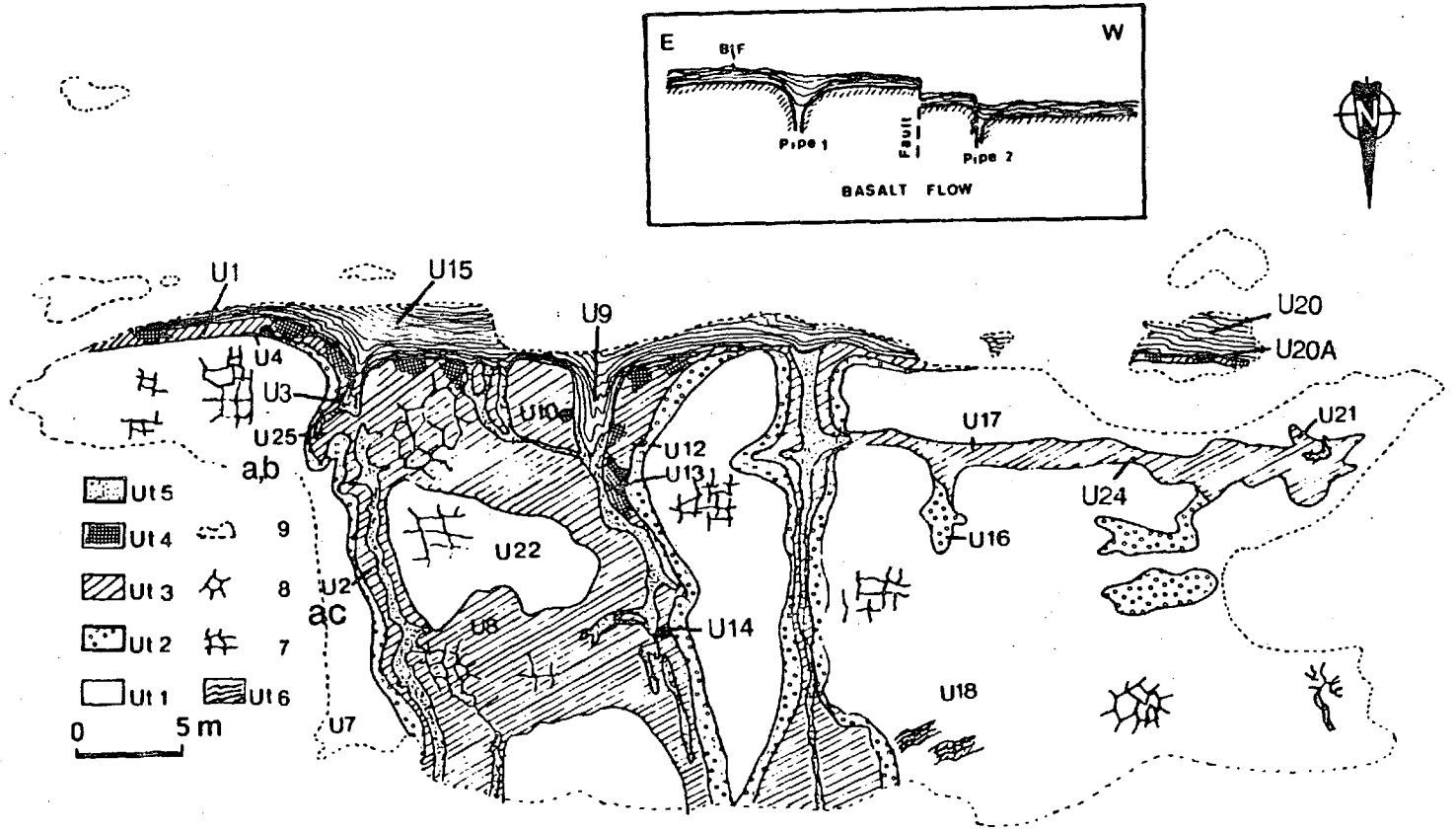

Map A1.2 Sample Locations in pipe-1, Atik Lake

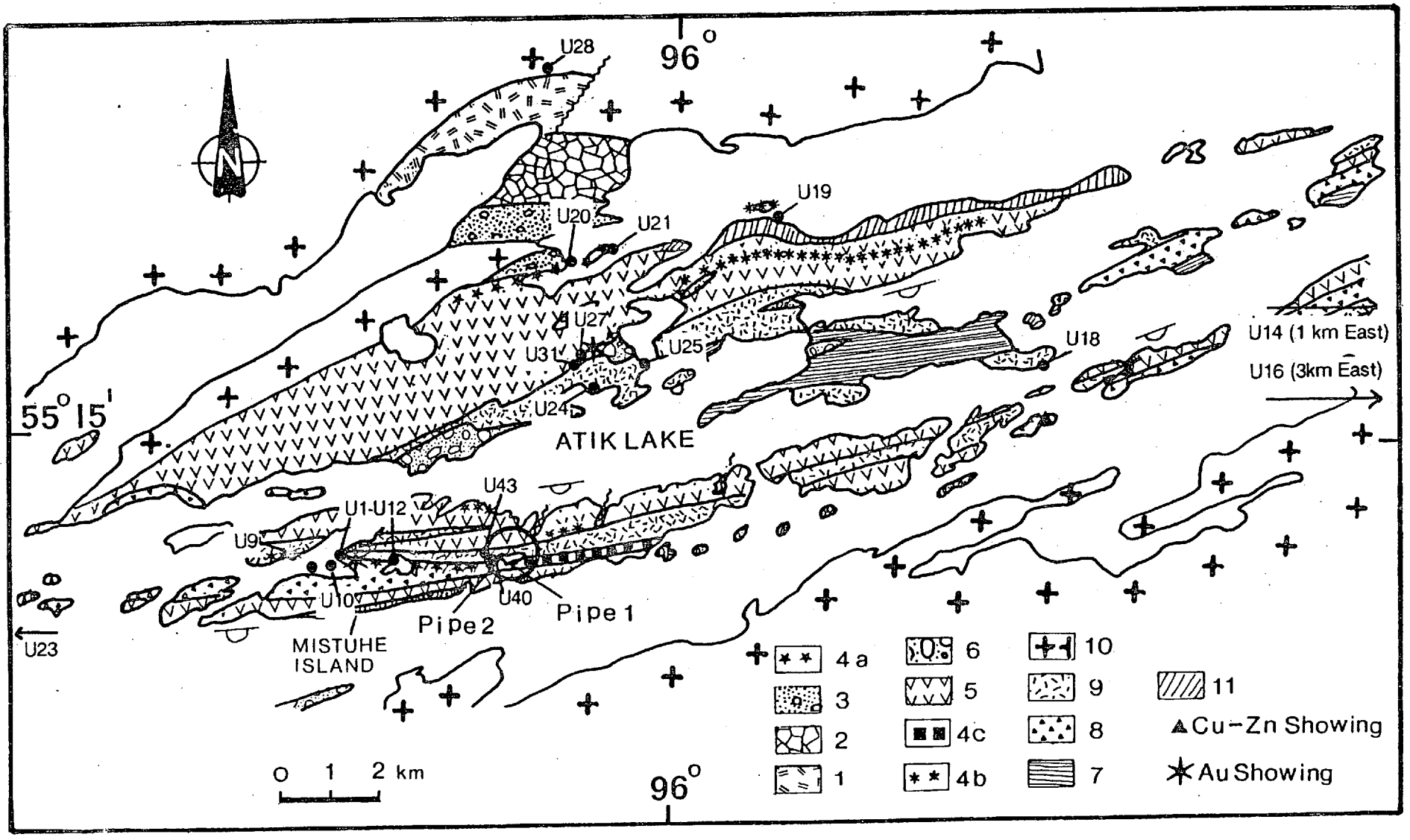

Map A1.3 Drill Sample Locations, Atik Lake

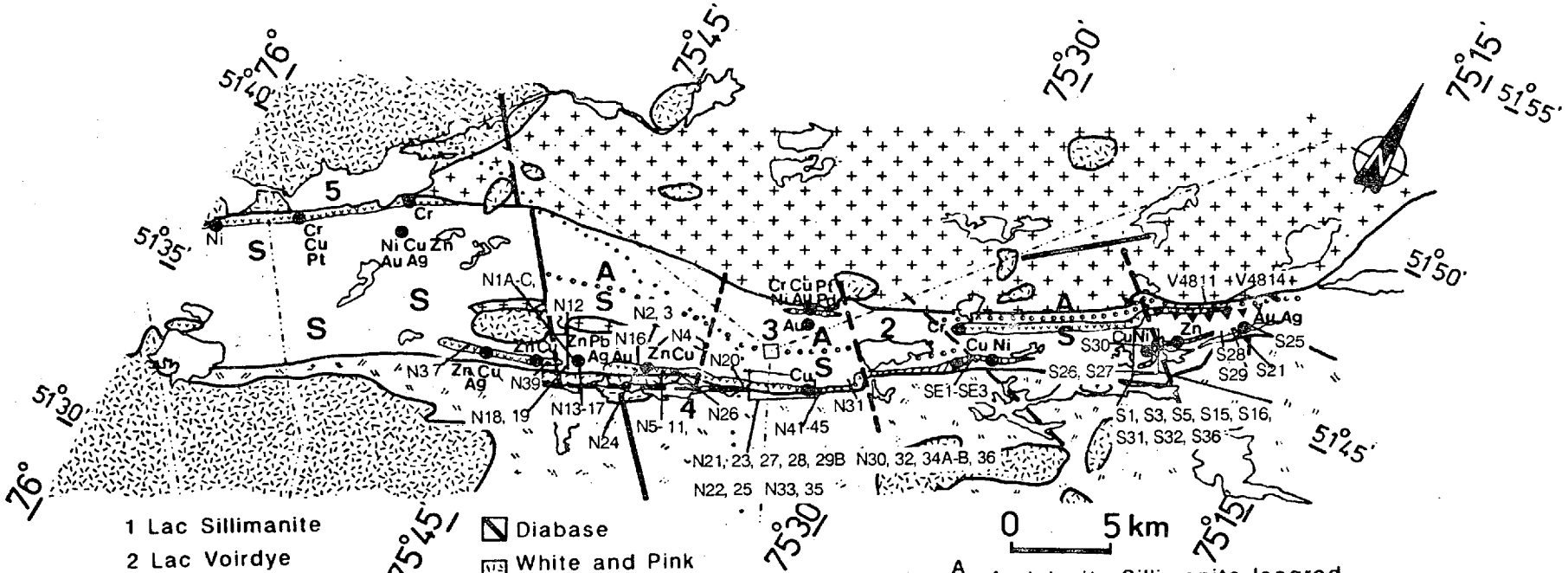

Map A2 Sample Locations, Nemiscau

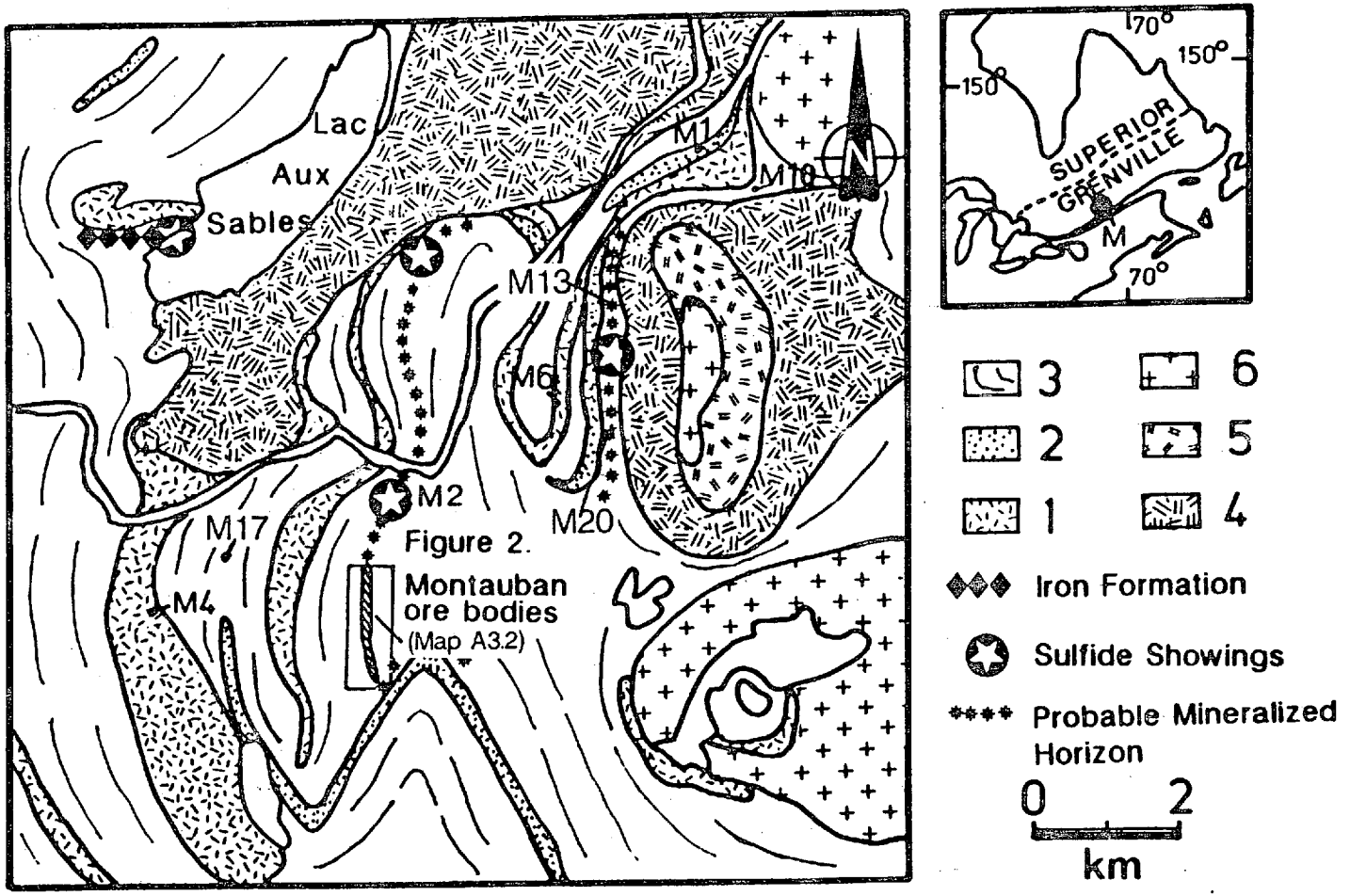

Map A3.1 Regional Sample Locations in Montauban

(Amphibolites and Metapelites)

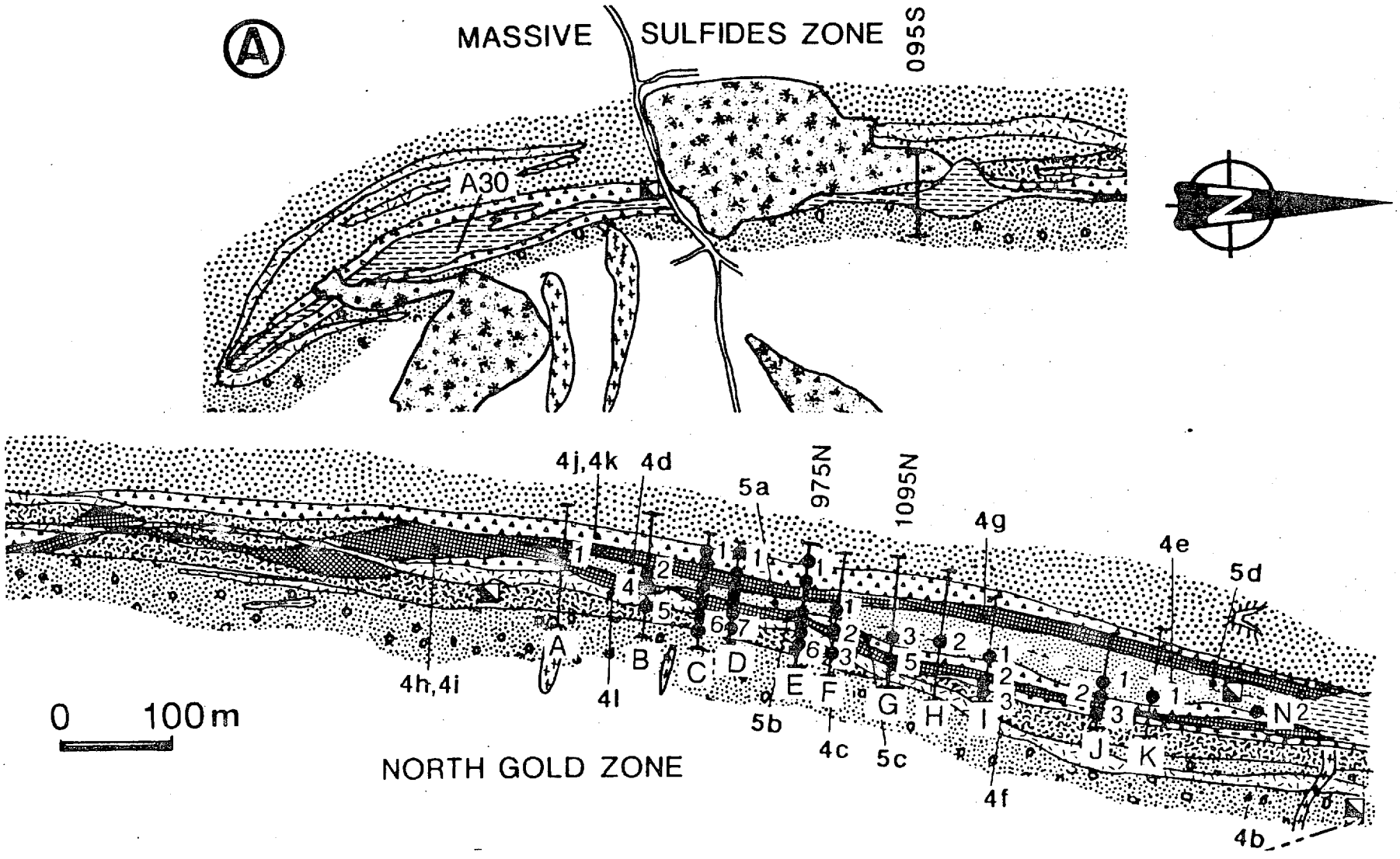

Map A3.2 Drill Sample Locations, Mine Sequence, Montauban

APPENDIX 2. ELECTRON MICROPROBE DATA FOR THE THREE TERRANES

ATIK LAKE

Actinolite and hornblende analyses, Atik Lake

	U2A-1	U2A-2	U2A-3	U2C-1	U-2C-2	U2C-3	-1-9-A	-1-9-B	-1-9-C	-1-9-D	-1-9-E	-1-9-F	U019G	U019H	U019I	U019J
SiO2	49.57	50.75	49.36	47.29	44.76	44.29	55.58	51.51	55.43	53.52	53.68	53.11	55.79	56.02	55.65	56.30
TiO2	0.04	-	0.05	0.21	0.44	0.35	0.07	0.21	0.01	-	0.06	0.06	0.04	0.05	0.03	0.04
Al2O3	2.19	1.00	1.04	5.70	10.65	11.62	0.76	1.80	-	0.63	0.75	0.22	0.58	0.84	0.42	0.61
Cr2O3	-	-	-	-	-	-	-	-	-	-	-	-	-	-	-	-
Fe2O3	0.00	0.00	-	-	-	-	0.00	-	0.00	-	0.00	-	-	-	0.01	0.02
FeO	30.93	29.94	33.96	27.54	23.49	22.90	11.33	10.69	11.40	10.67	16.74	15.57	11.51	10.11	11.51	11.82
MnO	1.54	1.29	2.86	0.79	0.63	0.51	3.29	2.76	3.19	2.81	3.93	3.24	3.15	2.87	2.27	2.80
MgO	5.96	5.55	4.49	5.18	5.60	5.49	18.30	16.05	17.59	17.52	13.45	13.48	16.75	17.37	15.89	16.00
ZnO	-	-	-	-	-	-	-	-	-	-	-	-	0.11	0.19	-	0.10
CaO	9.46	10.50	5.68	11.61	11.63	11.79	10.29	10.77	10.32	10.48	10.24	11.28	10.29	10.75	11.26	10.22
Na2O	0.39	0.41	0.34	0.37	0.58	0.52	0.41	0.53	0.07	0.20	0.36	0.32	0.13	0.12	0.05	0.03
K2O	-	-	-	0.13	0.27	0.28	-	-	-	-	-	-	0.03	0.05	0.02	0.03
H2O	1.95	1.95	1.88	1.94	1.96	1.96	2.13	2.00	2.09	2.05	2.05	2.02	2.10	2.11	2.08	2.10
Total	102.01	101.40	99.65	100.76	100.01	99.71	102.17	96.32	100.10	97.87	101.25	99.29	100.48	100.48	99.19	100.07
#Si IV	7.62	7.82	7.85	7.29	6.83	6.76	7.81	7.70	7.95	7.84	7.84	7.88	7.96	7.94	8.03	8.05
#Al IV	0.38	0.18	0.15	0.71	1.17	1.24	0.13	0.30	-	0.11	0.13	0.04	0.04	0.06	-	-
#Fe +3	-	0.00	-	-	-	-	0.00	-	0.00	-	0.00	-	-	-	-	-
#Ti IV	-	-	-	-	-	-	0.01	-	0.00	-	0.01	0.01	-	-	-	-
T site	8.00	8.00	8.00	8.00	8.00	8.00	7.95	8.00	7.95	7.95	7.98	7.93	8.00	8.00	8.03	8.05
#Al VI	0.02	-	0.05	0.32	0.75	0.85	-	0.02	-	-	-	-	0.06	0.09	0.07	0.10
#Fe +3	0.00	-	-	-	-	-	-	-	-	-	-	-	-	-	0.00	0.00
#Ti	0.00	-	0.01	0.02	0.05	0.04	-	0.02	-	-	-	-	0.00	0.01	0.00	0.00
#Cr	-	-	-	-	-	-	-	-	-	-	-	-	-	-	-	-
#Mg	1.36	1.28	1.07	1.19	1.27	1.25	3.84	3.58	3.76	3.83	2.93	2.98	3.56	3.67	3.42	3.41
#Fe +2	3.61	3.72	3.88	3.46	2.93	2.86	1.16	1.34	1.24	1.17	2.04	1.93	1.37	1.20	1.39	1.41
#Zn	-	-	-	-	-	-	-	-	-	-	-	-	0.00	0.02	-	0.01
#Mn	-	-	-	-	-	-	-	0.04	-	-	0.03	0.08	-	0.02	0.12	0.06
#Ca	-	-	-	-	-	-	-	-	-	-	-	-	-	-	-	-
M1,2,3	5.00	5.00	5.00	5.00	5.00	5.00	5.00	5.00	5.00	5.00	5.00	5.00	5.00	5.00	5.00	5.00
#Mg	-	-	-	-	-	-	-	-	-	-	-	-	-	-	-	-
#Fe +2	0.36	0.13	0.64	0.09	0.07	0.06	0.17	-	0.13	0.13	-	-	-	-	-	-
#Zn	-	-	-	-	-	-	-	-	-	-	-	-	0.01	-	-	-
#Mn	0.20	0.17	0.38	0.10	0.08	0.07	0.39	0.31	0.39	0.35	0.46	0.32	0.38	0.33	0.16	0.28
#Ca	1.44	1.70	0.97	1.81	1.85	1.87	1.44	1.69	1.49	1.52	1.54	1.68	1.57	1.63	1.74	1.56
#Na	-	-	0.01	-	-	-	-	-	-	-	-	-	0.03	0.03	0.01	0.01
M4 site	2.00	2.00	2.00	2.00	2.00	2.00	2.00	2.00	2.00	2.00	2.00	2.00	2.00	1.99	1.91	1.85
#Ca	0.12	0.03	-	0.11	0.05	0.05	0.11	0.04	0.10	0.13	0.06	0.12	-	-	-	-
#Na	0.12	0.12	0.09	0.11	0.17	0.15	0.11	0.15	0.02	0.06	0.10	0.09	0.00	-	-	-
#K	-	-	-	0.03	0.05	0.05	-	-	-	-	-	-	0.01	0.01	0.00	0.01
A site	0.23	0.16	0.09	0.24	0.28	0.26	0.22	0.19	0.12	0.18	0.16	0.21	0.01	0.01	0.00	0.01
#O	22.00	22.00	22.00	22.01	22.00	22.00	22.00	22.00	22.00	22.00	22.00	22.00	22.00	22.00	22.00	22.00
#OH	2.00	2.00	2.00	1.99	2.00	2.00	2.00	2.00	2.00	2.00	2.00	2.00	2.00	2.00	2.00	2.00
Charge	-	-4E-06	0.00	-5E-07	-3E-06	-1E-06	0.00	0.00	-	0.00	-	0.00	0.00	-1E-05	0.00	0.00

	U08SA	U08SB	U08SC	U08SD	U08SE	U035A	U035B	U057A	U22A	U272A	U272B	U231A	U231B
SiO2	54.01	53.49	54.17	54.66	54.82	54.51	55.08	41.93	44.42	54.69	55.35	49.73	50.93
TiO2	0.03	-	-	-	0.02	0.03	0.05	0.42	0.59	0.01	0.04	-	0.03
Al2O3	0.55	0.64	0.50	0.22	0.21	1.37	0.62	13.32	10.88	1.38	1.24	2.17	1.74
Cr2O3	-	-	-	-	-	-	-	-	-	-	-	-	-
Fe2O3	-	-	-	0.00	0.02	-	-	-	0.00	-	-	-	-
FeO	16.00	18.32	19.10	16.81	17.46	16.93	16.68	20.74	20.31	15.08	13.38	27.33	27.84
MnO	2.00	2.27	1.31	2.24	1.89	4.95	3.41	0.76	0.52	0.88	0.81	0.06	0.01
MgO	13.40	13.08	12.14	13.13	12.57	12.44	12.02	7.08	7.69	14.63	15.59	6.78	6.80
ZnO	0.13	0.05	0.10	0.05	0.15	0.14	0.20	4.12	-	0.12	0.07	0.07	0.15
CaO	11.65	10.38	10.47	11.84	11.86	9.24	11.18	11.58	11.82	12.49	12.37	11.50	11.07
Na2O	0.05	0.06	0.08	0.04	0.03	0.13	0.07	1.77	1.14	0.12	0.07	0.36	0.27
K2O	0.01	0.04	0.07	-	0.02	0.06	0.06	0.68	0.37	0.10	0.08	0.07	0.07
H2O	2.04	2.03	1.93	2.06	2.06	2.06	2.06	1.97	1.98	2.09	2.10	1.94	1.96
Total	99.87	100.36	99.87	101.05	101.11	101.86	101.43	104.37	99.72	101.59	101.10	100.01	100.87
#Si IV	7.93	7.88	8.01	7.96	7.99	7.91	8.00	6.26	6.73	7.83	7.88	7.67	7.77
#Al IV	0.07	0.11	-	0.04	0.01	0.09	-	1.74	1.27	0.17	0.12	0.33	0.23
#Fe +3	-	-	-	0.00	-	-	-	-	-	-	-	-	-
#Ti IV	-	-	-	-	-	-	-	-	-	-	-	-	-
T site	8.00	7.99	8.01	7.99	8.00	8.00	8.00	8.00	8.00	8.00	8.00	8.00	8.00
#Al VI	0.02	-	0.09	-	0.02	0.14	0.11	0.60	0.67	0.06	0.09	0.07	0.09
#Fe +3	-	-	-	-	0.00	-	-	-	0.00	-	-	-	-
#Ti	0.00	-	-	-	0.00	0.00	0.01	0.05	0.07	0.00	0.00	-	0.00
#Cr	-	-	-	-	-	-	-	-	-	-	-	-	-
#Mg	2.93	2.87	2.68	2.85	2.73	2.69	2.60	1.58	1.74	3.12	3.31	1.56	1.55
#Fe +2	1.96	2.13	2.24	2.05	2.13	2.05	2.03	2.59	2.53	1.81	1.59	3.37	3.36
#Zn	0.01	-	-	0.01	0.02	0.01	0.02	0.18	-	0.01	-	-	-
#Mn	0.06	-	-	0.10	0.10	0.09	0.24	-	-	-	-	-	-
#Ca	-	-	-	-	-	-	-	-	-	-	-	-	-
M1,2,3	5.00	5.00	5.00	5.00	5.00	5.00	5.00	5.00	5.00	5.00	5.00	5.00	5.00
#Mg	-	-	-	-	-	-	-	-	-	-	-	-	-
#Fe +2	-	0.13	0.13	-	-	-	-	-	0.05	-	0.00	0.15	0.19
#Zn	-	0.01	0.01	-	-	-	-	0.27	-	0.01	0.01	0.01	0.02
#Mn	0.18	0.28	0.16	0.18	0.13	0.51	0.18	0.10	0.07	0.11	0.10	0.01	0.00
#Ca	1.82	1.58	1.66	1.82	1.85	1.44	1.74	1.63	1.89	1.89	1.89	1.83	1.79
#Na	-	-	0.02	-	0.01	0.04	0.02	-	-	-	0.01	-	-
M4 site	2.00	2.00	1.98	2.00	1.99	1.99	1.94	2.00	2.00	2.00	2.00	2.00	2.00
#Ca	0.02	0.06	-	0.02	-	-	-	0.22	0.03	0.03	-	0.07	0.02
#Na	0.01	0.02	-	0.01	-	-	-	0.51	0.33	0.03	0.01	0.11	0.08
#K	0.00	0.01	0.01	-	0.00	0.01	0.01	0.13	0.07	0.02	0.01	0.01	0.01
A site	0.03	0.08	0.01	0.03	0.00	0.01	0.01	0.86	0.44	0.08	0.03	0.19	0.11
#O	22.00	22.00	22.10	22.00	22.00	22.01	22.00	22.04	22.00	22.00	22.00	22.00	22.00
#OH	2.00	2.00	1.90	2.00	2.00	1.99	2.00	1.96	2.00	2.00	2.00	2.00	2.00
Charge	0.00	0.00	0.00	0.00	0.00	-8E-06	-7E-06	0.00	0.00	-5E-06	0.00	-1E-06	0.00

Anthophyllite Analyses, Atik Lake

	U-2B-A	U-2B-B	U-2B-C	U-2B-D	U10A-A	U10A-B	U10A-C	U29B-A	U29B-B	U841A	U841B	U841C	U841D	U845A	U845B	U847A	U847B	U847C	U847D	U-08A	U-10A	U-24A	U-24D	U40C1	U40C2
SiO2	50.89	53.33	53.48	53.77	50.05	51.21	53.35	52.51	48.10	50.76	52.39	52.84	51.89	55.55	55.64	55.31	55.01	55.14	55.04	52.08	49.60	50.40	52.85	51.17	51.17
TiO2	0.10	0.04	0.05	0.05	0.09	0.06	0.03	0.09	0.06	0.08	0.03	0.02	0.08	0.03	-	0.05	0.01	0.03	0.05	0.03	0.08	0.06	0.06	0.04	-
Al2O3	3.84	2.15	1.53	1.47	7.37	5.43	1.68	4.01	8.89	6.21	3.46	2.48	3.94	1.26	1.15	1.68	1.44	1.97	1.89	3.27	6.87	5.57	2.81	3.87	3.80
Cr2O3	-	-	-	-	0.03	0.05	0.04	-	-	-	-	-	-	-	-	-	-	-	-	-	-	-	-	-	-
Fe2O3	-	-	-	-	-	0.01	-	-	0.02	0.03	-	-	-	-	-	-	-	-	0.01	-	-	-	0.01	0.00	-
FeO	27.13	27.41	27.52	26.41	26.07	26.36	26.38	26.70	27.27	25.94	25.85	26.23	25.75	21.24	21.75	20.81	21.12	20.48	20.85	26.46	26.23	26.24	26.44	26.22	26.13
MnO	0.31	0.27	0.31	0.22	0.34	0.35	0.51	0.15	0.28	0.89	0.81	0.84	1.01	0.64	0.63	0.47	0.58	0.64	0.70	0.37	0.62	0.47	0.44	0.14	0.18
MgO	14.67	15.29	15.32	15.83	13.67	14.26	15.53	15.35	13.02	14.21	15.31	15.45	15.03	20.28	19.80	19.83	19.89	19.80	19.90	15.39	13.05	14.32	15.33	14.91	14.78
ZnO	0.16	0.02	-	-	0.10	-	0.16	0.12	0.15	-	0.08	-	0.06	0.14	0.12	0.14	-	0.07	0.14	0.03	-	0.12	0.04	0.09	0.09
CaO	0.30	0.26	0.31	0.23	0.26	0.27	0.16	0.22	0.25	0.17	0.18	0.11	0.20	0.18	0.21	0.27	0.26	0.31	0.27	0.16	0.26	0.28	0.16	0.19	0.22
Na2O	0.35	0.19	0.02	0.22	0.61	0.35	0.12	0.21	0.73	0.58	0.32	0.16	0.32	0.11	0.11	0.11	0.13	0.16	0.17	0.27	0.70	0.47	0.12	0.38	0.31
K2O	-	-	-	-	-	-	-	-	-	0.01	0.08	0.01	-	-	-	0.03	0.01	-	0.01	0.01	-	0.01	-	-	-
H2O	2.01	2.04	2.03	2.04	2.04	2.04	2.03	2.06	2.03	2.05	2.04	2.03	2.03	2.11	2.11	2.10	2.09	2.10	2.11	2.03	2.01	2.02	2.04	2.01	2.00
Total	99.76	101.00	100.57	100.24	100.63	100.39	99.99	101.42	100.80	100.92	100.55	100.17	100.31	101.54	101.52	100.80	100.54	100.70	101.14	100.10	99.42	99.96	100.30	99.02	98.68
#Si IV	7.59	7.82	7.88	7.90	7.35	7.53	7.88	7.64	7.11	7.43	7.69	7.79	7.64	7.87	7.90	7.88	7.87	7.85	7.83	7.69	7.39	7.47	7.77	7.63	7.66
#Al IV	0.41	0.18	0.12	0.10	0.65	0.47	0.12	0.36	0.89	0.57	0.31	0.21	0.36	0.13	0.10	0.12	0.13	0.15	0.17	0.31	0.61	0.53	0.23	0.37	0.34
#Fe +3	-	-	-	-	-	-	-	-	-	-	-	-	-	-	-	-	-	-	-	-	-	-	-	-	-
#Ti IV	-	-	-	-	-	-	-	-	-	-	-	-	-	-	-	-	-	-	-	-	-	-	-	-	-
T site	8.00	8.00	8.00	8.00	8.00	8.00	8.00	8.00	8.00	8.00	8.00	8.00	8.00	8.00	8.00	8.00	8.00	8.00	8.00	8.00	8.00	8.00	8.00	8.00	8.00
#Al VI	0.26	0.19	0.14	0.15	0.62	0.47	0.17	0.33	0.66	0.51	0.29	0.22	0.32	0.08	0.09	0.16	0.11	0.18	0.14	0.26	0.60	0.44	0.26	0.32	0.33
#Fe +3	-	-	-	-	-	0.00	-	-	0.00	0.00	-	-	-	-	-	-	-	-	0.00	-	-	-	0.00	0.00	-
#Ti	0.01	0.00	0.01	0.01	0.01	0.01	0.00	0.01	0.01	0.01	0.00	0.00	0.01	0.00	-	0.01	0.00	0.00	0.01	0.00	0.01	0.01	0.01	0.00	-
#Cr	-	-	-	-	0.00	0.01	0.00	-	-	-	-	-	-	-	-	-	-	-	-	-	-	-	-	-	-
#Mg	3.26	3.34	3.36	3.47	2.99	3.13	3.42	3.33	2.87	3.10	3.35	3.39	3.30	4.28	4.19	4.21	4.24	4.20	4.22	3.39	2.90	3.16	3.36	3.32	3.30
#Fe +2	1.47	1.47	1.49	1.37	1.37	1.39	1.41	1.34	1.46	1.38	1.36	1.38	1.37	0.63	0.71	0.63	0.64	0.61	0.63	1.35	1.49	1.39	1.37	1.36	1.37
#Zn	-	-	-	-	-	-	-	-	-	-	-	-	-	-	-	-	-	-	-	-	-	-	-	-	-
#Mn	-	-	-	-	-	-	-	-	-	-	-	-	-	-	-	-	-	-	-	-	-	-	-	-	-
#Ca	-	-	-	-	-	-	-	-	-	-	-	-	-	-	-	-	-	-	-	-	-	-	-	-	-
M1,2,3	5.00	5.00	5.00	5.00	5.00	5.00	5.00	5.00	5.00	5.00	5.00	5.00	5.00	5.00	5.00	5.00	5.00	5.00	5.00	5.00	5.00	5.00	5.00	5.00	5.00
#Mg	-	-	-	-	-	-	-	-	-	-	-	-	-	-	-	-	-	-	-	-	-	-	-	-	-
#Fe +2	1.91	1.89	1.90	1.87	1.83	1.85	1.85	1.91	1.91	1.80	1.82	1.85	1.80	1.89	1.87	1.85	1.88	1.83	1.85	1.91	1.78	1.86	1.88	1.91	1.90
#Zn	0.02	0.00	-	-	0.01	-	0.02	0.01	0.02	-	0.01	-	0.01	0.01	0.01	0.01	-	0.01	0.01	0.00	-	0.01	0.00	0.01	0.01
#Mn	0.04	0.03	0.04	0.03	0.04	0.04	0.06	0.02	0.04	0.11	0.10	0.10	0.13	0.08	0.08	0.06	0.07	0.08	0.08	0.05	0.08	0.06	0.05	0.02	0.02
#Ca	0.03	0.04	0.05	0.04	0.04	0.04	0.03	0.03	0.04	0.03	0.03	0.02	0.03	0.02	0.03	0.04	0.04	0.05	0.04	0.03	0.04	0.04	0.03	0.03	0.04
#Na	-	0.03	0.01	0.06	0.08	0.06	0.03	0.02	-	0.06	0.05	0.03	0.03	-	0.01	0.03	0.01	0.04	0.01	0.01	0.10	0.03	0.03	0.03	0.04
M4 site	2.00	2.00	1.99	2.00	2.00	2.00	1.99	2.00	2.00	2.00	2.00	2.00	2.00	2.00	2.00	1.99	2.00	2.00	2.00	2.00	2.00	2.00	2.00	2.00	2.00
#Ca	0.02	-	-	-	-	-	-	-	0.00	-	-	-	-	0.01	-	-	-	-	-	-	-	-	-	-	-
#Na	0.10	0.02	-	-	0.09	0.04	-	0.04	0.21	0.10	0.05	0.02	0.06	0.03	0.02	-	0.03	0.00	0.03	0.06	0.10	0.11	-	0.08	0.05
#K	-	-	-	-	-	-	-	-	-	0.00	0.01	0.00	-	-	-	0.01	0.00	-	0.00	0.00	-	0.00	-	-	-
A site	0.12	0.02	-	-	0.09	0.04	-	0.04	0.21	0.10	0.06	0.02	0.06	0.04	0.02	0.01	0.03	0.00	0.03	0.07	0.10	0.11	-	0.08	0.05
#O	22.00	22.01	22.01	22.00	22.00	22.00	22.00	22.00	22.00	22.00	22.00	22.00	22.01	22.01	22.00	22.01	22.01	22.01	22.00	22.00	22.00	22.00	22.00	22.00	22.00
#OH	2.00	1.99	1.99	2.00	2.00	2.00	2.00	2.00	2.00	2.00	2.00	2.00	1.99	1.99	2.00	1.99	1.99	1.99	2.00	2.00	2.00	2.00	2.00	2.00	2.00
Charge	-4E-06	0.00	-1E-06	0.00	0.00	0.00	0.00	0.00	0.00	0.00	0.00	0.00	0.00	-8E-06	-2E-06	0.00	0.00	-8E-06	0.00	0.00	0.00	-1E-06	0.00	0.00	-3E-06

GEDRITE ANALYSES, ATIK LAKE

	U-12-A	U-12-B	U-14-A	U-14-B	U-14-C	U-14-D	U25B-A	U25B-B	U29B-A	U29B-B	U29B-C	U29B-D	U27B-E	U-08A	U-08B	U-08C	U-08D	U-17A	U-17B	U-17C
SiO2	39.27	40.82	41.90	42.37	41.88	41.85	45.61	46.55	42.83	42.71	45.08	47.07	42.21	43.23	43.41	44.10	44.00	43.00	44.77	46.01
TiO2	0.05	0.49	0.14	0.15	0.09	0.10	0.13	0.08	0.23	0.14	0.14	0.15	0.16	0.13	0.18	0.13	0.14	0.09	0.06	0.06
Al2O3	21.34	19.21	18.19	18.36	18.36	20.18	12.16	10.95	16.70	16.66	14.70	12.02	15.74	15.61	15.66	15.14	15.93	11.13	10.91	9.88
Cr2O3	-	-	-	-	-	-	-	-	-	-	-	-	-	-	-	-	-	-	-	-
Fe2O3	0.00	0.00	-	0.01	-	0.01	-	-	-	-	0.02	-	-	0.01	0.02	-	-	0.02	-	-
FeO	30.52	30.44	27.24	27.62	28.40	25.04	27.53	27.86	27.63	27.66	27.32	27.74	27.06	25.80	25.93	25.75	25.70	26.82	26.95	26.06
MnO	0.28	0.43	0.15	0.20	0.22	-	0.12	0.16	0.26	0.20	0.22	0.16	0.19	0.44	0.40	0.36	0.44	0.36	0.59	0.50
MgO	5.32	6.16	8.74	8.63	8.80	11.67	10.92	11.41	9.59	9.35	10.73	11.61	10.17	10.70	10.75	10.94	10.66	11.94	11.39	12.91
ZnO	0.09	-	0.12	0.14	0.21	-	0.07	0.06	0.04	0.07	0.09	0.04	0.02	0.16	0.08	0.04	0.02	-	0.03	0.11
CaO	0.24	0.32	0.39	0.39	0.35	0.04	0.36	0.39	0.42	0.41	0.42	0.31	0.34	0.44	0.41	0.38	0.44	0.25	0.75	0.23
Na2O	1.66	1.33	1.64	1.63	1.51	0.01	1.11	1.05	1.83	1.73	1.19	1.02	1.43	1.40	1.44	1.26	1.34	0.47	0.79	0.74
K2O	-	-	-	-	-	-	-	-	-	-	-	-	-	-	-	0.02	-	0.03	0.02	0.01
H2O	1.98	1.99	2.01	2.03	2.02	2.06	2.00	2.01	2.02	2.01	2.05	2.05	1.98	2.01	2.02	2.02	1.98	1.92	1.96	1.98
Total	100.75	101.19	100.52	101.53	101.84	100.96	100.01	100.52	101.55	100.94	101.96	102.17	99.30	99.93	100.30	100.14	100.65	96.03	98.22	98.49
#Si IV	5.94	6.14	6.25	6.26	6.20	6.09	6.82	6.93	6.34	6.36	6.60	6.87	6.38	6.45	6.45	6.54	6.50	6.72	6.84	6.96
#Al IV	2.06	1.86	1.75	1.74	1.80	1.91	1.18	1.07	1.66	1.64	1.40	1.13	1.62	1.55	1.55	1.46	1.50	1.28	1.16	1.04
#Fe +3	-	-	-	-	-	-	-	-	-	-	-	-	-	-	-	-	-	-	-	-
#Ti IV	-	-	-	-	-	-	-	-	-	-	-	-	-	-	-	-	-	-	-	-
T site	8.00	8.00	8.00	8.00	8.00	8.00	8.00	8.00	8.00	8.00	8.00	8.00	8.00	8.00	8.00	8.00	8.00	8.00	8.00	8.00
#Al VI	1.75	1.54	1.45	1.46	1.40	1.56	0.96	0.85	1.25	1.28	1.14	0.94	1.18	1.20	1.20	1.19	1.27	0.77	0.81	0.72
#Fe +3	0.00	0.00	-	0.00	-	0.00	-	-	-	-	0.00	-	-	0.00	0.00	-	-	0.00	-	-
#Ti	0.01	0.06	0.02	0.02	0.01	0.01	0.01	0.01	0.03	0.02	0.02	0.02	0.02	0.01	0.02	0.01	0.02	0.01	0.01	0.01
#Cr	-	-	-	-	-	-	-	-	-	-	-	-	-	-	-	-	-	-	-	-
#Mg	1.20	1.38	1.94	1.90	1.94	2.53	2.43	2.53	2.12	2.08	2.34	2.53	2.29	2.38	2.38	2.42	2.35	2.78	2.59	2.91
#Fe +2	2.04	2.02	1.59	1.62	1.65	0.90	1.59	1.61	1.61	1.63	1.50	1.52	1.51	1.41	1.40	1.37	1.37	1.43	1.59	1.36
#Zn	-	-	-	-	-	-	-	-	-	-	-	-	-	-	-	-	-	-	-	-
#Mn	-	-	-	-	-	-	-	-	-	-	-	-	-	-	-	-	-	-	-	-
#Ca	-	-	-	-	-	-	-	-	-	-	-	-	-	-	-	-	-	-	-	-
M1,2,3	5.00	5.00	5.00	5.00	5.00	5.00	5.00	5.00	5.00	5.00	5.00	5.00	5.00	5.00	5.00	5.00	5.00	5.00	5.00	5.00
#Mg	-	-	-	-	-	-	-	-	-	-	-	-	-	-	-	-	-	-	-	-
#Fe +2	1.82	1.81	1.80	1.79	1.87	2.15	1.85	1.86	1.81	1.82	1.84	1.87	1.91	1.81	1.82	1.82	1.81	2.08	1.85	1.93
#Zn	0.01	-	0.01	0.02	0.02	-	0.01	0.01	0.00	0.01	0.01	0.00	0.00	0.02	0.01	0.00	0.00	-	0.00	0.01
#Mn	0.04	0.05	0.02	0.03	0.03	-	0.02	0.02	0.03	0.03	0.03	0.02	0.02	0.06	0.05	0.05	0.06	0.05	0.08	0.06
#Ca	0.04	0.05	0.06	0.06	0.06	-	0.06	0.06	0.07	0.07	0.07	0.05	0.06	0.07	0.07	0.06	0.07	-	0.07	-
#Na	0.10	0.09	0.10	0.11	0.02	-	0.06	0.05	0.08	0.08	0.05	0.06	0.01	0.04	0.05	0.07	0.07	-	-	-
M4 site	2.00	2.00	2.00	2.00	2.00	2.15	2.00	2.00	2.00	2.00	2.00	2.00	2.00	2.00	2.00	2.00	2.00	2.12	2.00	2.01
#Ca	-	-	-	-	-	0.01	-	-	-	-	-	-	-	-	-	-	-	0.04	0.05	0.04
#Na	0.39	0.30	0.37	0.36	0.41	0.00	0.26	0.25	0.44	0.42	0.28	0.23	0.41	0.36	0.36	0.30	0.32	0.14	0.23	0.22
#K	-	-	-	-	-	-	-	-	-	-	-	-	-	-	-	0.00	-	0.01	0.00	0.00
A site	0.39	0.30	0.37	0.36	0.41	0.01	0.26	0.25	0.44	0.42	0.28	0.23	0.41	0.36	0.36	0.30	0.32	0.19	0.29	0.26
#O	22.00	22.00	22.00	22.00	22.01	22.00	22.01	22.00	22.01	22.00	22.00	22.00	22.00	22.00	22.00	22.00	22.05	22.00	22.00	22.00
#OH	2.00	2.00	2.00	2.00	1.99	2.00	1.99	2.00	1.99	2.00	2.00	2.00	2.00	2.00	2.00	2.00	1.95	2.00	2.00	2.00
Charge	-	-4E-06	-5E-06	0.00	0.00	0.00	0.00	0.00	-8E-06	-6E-06	0.00	-5E-06	-2E-07	0.00	0.00	-5E-06	-5E-06	0.00	-2E-06	0.00

	U-17D	U-17E	U-24A	U-24B	U-24C	U-31A	U-31B	U40C1	U40C2	U40C3	U40C4	U41C1	U41C2
SiO2	45.45	45.64	43.93	44.97	43.65	41.84	43.11	46.81	43.22	46.12	47.47	40.66	39.51
TiO2	0.12	0.10	0.14	0.13	0.15	0.11	0.11	0.07	0.11	0.12	0.17	0.16	0.12
Al2O3	11.65	11.92	15.56	14.24	16.03	16.29	15.50	11.54	14.58	10.82	10.93	19.32	20.35
Cr2O3	-	-	-	-	-	-	-	-	-	-	-	-	-
Fe2O3	-	-	-	-	0.01	-	-	0.02	-	0.02	-	-	0.01
FeO	27.21	26.37	25.80	26.20	25.47	26.67	26.55	26.20	26.23	25.67	26.04	30.33	31.05
MnO	0.51	0.43	0.54	0.56	0.56	0.31	0.28	0.15	0.17	0.16	0.14	0.48	0.38
MgO	11.32	11.76	10.57	10.95	10.32	9.00	9.45	12.00	11.16	12.02	12.19	5.35	5.14
ZnO	-	0.03	0.09	0.08	-	0.11	0.03	0.01	0.15	0.06	0.09	0.04	0.02
CaO	0.29	0.24	0.36	0.40	0.35	0.36	0.39	0.29	0.30	0.30	0.32	0.24	0.15
Na2O	0.88	0.94	1.42	1.33	1.50	1.38	1.35	1.20	1.24	1.09	0.99	1.53	1.77
K2O	0.02	0.02	-	0.01	0.01	0.03	0.39	0.02	0.03	0.02	-	0.01	0.02
H2O	1.99	2.00	2.02	2.03	2.02	1.96	1.98	2.03	1.99	1.99	2.03	1.97	1.97
Total	99.44	99.45	100.43	100.90	100.07	98.06	99.14	100.34	99.18	98.38	100.37	100.09	100.49
#Si IV	6.84	6.83	6.51	6.64	6.48	6.40	6.51	6.92	6.51	6.95	7.00	6.18	6.02
#Al IV	1.16	1.17	1.49	1.36	1.52	1.60	1.49	1.08	1.49	1.05	1.00	1.82	1.98
#Fe +3	-	-	-	-	-	-	-	-	-	-	-	-	-
#Ti IV	-	-	-	-	-	-	-	-	-	-	-	-	-
T site	8.00	8.00	8.00	8.00	8.00	8.00	8.00	8.00	8.00	8.00	8.00	8.00	8.00
#Al VI	0.90	0.94	1.23	1.12	1.29	1.33	1.27	0.93	1.10	0.88	0.90	1.65	1.67
#Fe +3	-	-	-	-	0.00	-	-	0.00	-	0.00	-	-	0.00
#Ti	0.01	0.01	0.02	0.01	0.02	0.01	0.01	0.01	0.01	0.01	0.02	0.02	0.01
#Cr	-	-	-	-	-	-	-	-	-	-	-	-	-
#Mg	2.54	2.62	2.34	2.41	2.28	2.05	2.13	2.64	2.51	2.70	2.68	1.21	1.17
#Fe +2	1.55	1.43	1.42	1.46	1.41	1.60	1.59	1.41	1.39	1.40	1.40	2.12	2.15
#Zn	-	-	-	-	-	-	-	-	-	-	-	-	-
#Mn	-	-	-	-	-	-	-	-	-	-	-	-	-
#Ca	-	-	-	-	-	-	-	-	-	-	-	-	-
M1,2,3	5.00	5.00	5.00	5.00	5.00	5.00	5.00	5.00	5.00	5.00	5.00	5.00	5.00
#Mg	-	-	-	-	-	-	-	-	-	-	-	-	-
#Fe +2	1.88	1.87	1.78	1.78	1.75	1.81	1.76	1.83	1.92	1.83	1.81	1.74	1.80
#Zn	-	0.00	0.01	0.01	-	0.01	0.00	0.00	0.02	0.01	0.01	0.00	0.00
#Mn	0.06	0.05	0.07	0.07	0.07	0.04	0.04	0.02	0.02	0.02	0.02	0.06	0.05
#Ca	0.05	0.04	0.06	0.06	0.06	0.06	0.06	0.05	0.05	0.05	0.05	0.04	0.02
#Na	0.01	0.03	0.09	0.08	0.12	0.08	0.14	0.11	-	0.09	0.11	0.16	0.12
M4 site	2.00	2.00	2.00	2.00	2.00	2.00	2.00	2.00	2.00	2.00	2.00	2.00	2.00
#Ca	-	-	-	-	-	-	-	-	0.00	-	-	-	-
#Na	0.25	0.24	0.32	0.30	0.31	0.33	0.26	0.24	0.36	0.23	0.17	0.29	0.40
#K	0.00	0.00	-	0.00	0.00	0.00	0.01	0.08	0.00	0.01	0.00	-	0.00	0.00
A site	0.25	0.24	0.32	0.30	0.31	0.33	0.34	0.24	0.37	0.23	0.17	0.29	0.41
#O	22.00	22.00	22.00	22.00	22.00	22.00	22.01	22.00	22.00	22.00	22.00	22.00	22.00
#OH	2.00	2.00	2.00	2.00	2.00	2.00	1.99	2.00	2.00	2.00	2.00	2.00	2.00
Charge	0.00	-5E-06	-1E-06	0.00	0.00	0.00	-7E-06	0.00	-3E-06	0.00	-1E-05	0.00	0.00

GRUNERITE ANALYSES, ATIK LAKE

	U-2-A	U-2-B	U-2-C	U1804	U1804B	U184C	U231A	U231B	U231C	U231D	U231E	U055A	U055B	U055C	U055D
SiO2	49.88	48.47	48.81	49.48	49.88	49.46	51.00	51.21	50.88	51.17	50.93	54.45	54.59	54.94	54.07
TiO2	-	0.05	-	-	-	0.02	-	0.01	0.01	-	-	0.04	0.02	0.06	0.07
Al2O3	0.10	0.12	0.67	0.11	0.11	0.12	0.09	0.13	0.10	0.08	0.12	0.49	0.43	0.50	0.69
Cr2O3	-	-	-	-	-	-	-	-	-	-	-	-	-	-	-
Fe2O3	-	0.00	-	-	0.03	-	0.00	-	0.01	0.02	0.00	-	0.01	-	0.01
FeO	38.69	38.94	38.62	47.45	47.86	48.40	39.91	39.46	39.00	39.86	40.24	20.53	20.87	19.87	20.48
MnO	3.22	3.36	3.41	0.07	0.09	0.06	0.09	0.03	0.03	0.07	0.07	5.13	5.34	4.71	4.57
MgO	5.11	5.26	4.46	0.12	0.08	0.10	6.94	6.42	6.98	6.61	6.22	15.48	15.41	15.50	15.25
ZnO	-	-	-	-	0.02	-	-	0.07	0.01	0.06	-	0.11	0.12	0.31	0.11
CaO	1.49	1.44	0.99	0.52	0.55	0.51	0.48	0.51	0.52	0.44	0.54	2.18	2.00	3.16	2.81
Na2O	0.27	0.46	0.54	0.06	0.10	0.10	0.01	-	0.07	0.06	0.06	0.08	0.06	0.08	0.08
K2O	-	-	-	-	0.01	0.04	0.01	-	0.01	0.02	0.03	0.04	-	-	0.01
H2O	1.88	1.86	1.85	1.82	1.84	1.83	1.91	1.90	1.90	1.91	1.90	2.04	2.05	2.06	2.04
Total	100.65	99.95	99.35	99.63	100.56	100.64	100.44	99.74	99.52	100.30	100.11	100.57	100.89	101.27	100.19
#Si IV	7.94	7.83	7.89	8.15	8.14	8.10	8.01	8.08	8.03	8.04	8.04	7.98	7.99	7.98	7.95
#Al IV	0.02	0.02	0.11	-	-	-	-	-	-	-	-	0.02	0.01	0.02	0.05
#Fe +3	-	0.00	-	-	-	-	-	-	-	-	-	-	-	-	-
#Ti IV	-	0.01	-	-	-	-	-	-	-	-	-	-	-	-	-
T site	7.96	7.85	8.00	8.15	8.14	8.10	8.01	8.08	8.03	8.04	8.04	8.00	8.00	8.00	8.00
#Al VI	-	-	0.02	0.02	0.02	0.02	0.02	0.02	0.02	0.01	0.02	0.07	0.06	0.06	0.07
#Fe +3	-	-	-	-	0.00	-	0.00	-	0.00	0.00	0.00	-	0.00	-	0.00
#Ti	-	-	-	-	-	0.00	-	0.00	0.00	-	-	0.00	0.00	0.01	0.01
#Cr	-	-	-	-	-	-	-	-	-	-	-	-	-	-	-
#Mg	1.21	1.27	1.08	0.03	0.02	0.02	1.62	1.51	1.64	1.55	1.46	3.38	3.36	3.37	3.34
#Fe +2	3.79	3.73	3.90	4.95	4.96	4.95	3.36	3.47	3.34	3.43	3.51	1.55	1.58	1.56	1.58
#Zn	-	-	-	-	-	-	-	-	-	-	-	-	-	-	-
#Mn	-	-	-	-	-	-	-	-	-	-	-	-	-	-	-
#Ca	-	-	-	-	-	-	-	-	-	-	-	-	-	-	-
M1,2,3	5.00	5.00	5.00	5.00	5.00	5.00	5.00	5.00	5.00	5.00	5.00	5.00	5.00	5.00	5.00
#Mg	-	-	-	-	-	-	-	-	-	-	-	-	-	-	-
#Fe +2	1.36	1.52	1.32	1.58	1.58	1.68	1.88	1.74	1.81	1.81	1.80	0.97	0.98	0.86	0.94
#Zn	-	-	-	-	0.00	-	-	0.01	0.00	0.01	-	0.01	0.01	0.03	0.01
#Mn	0.43	0.46	0.47	0.01	0.01	0.01	0.01	0.00	0.00	0.01	0.01	0.64	0.66	0.58	0.57
#Ca	0.20	0.02	0.17	0.09	0.10	0.09	0.08	0.09	0.09	0.07	0.09	0.34	0.31	0.49	0.44
#Na	-	-	0.04	0.02	0.03	0.03	0.00	-	0.02	0.02	0.02	0.02	0.02	0.02	0.02
M4 site	2.00	2.00	2.00	1.71	1.72	1.81	1.98	1.84	1.93	1.91	1.92	1.98	1.98	1.98	1.99
#Ca	0.05	0.23	-	-	-	-	-	-	-	-	-	-	-	-	-
#Na	0.08	0.14	0.13	-	-	-	-	-	-	-	-	-	-	-	-
#K	-	-	-	-	0.00	0.01	0.00	-	0.00	0.00	0.01	0.01	-	-	0.00
A site	0.13	0.38	0.13	-	0.00	0.01	0.00	-	0.00	0.00	0.01	0.01	-	-	0.00
#O	22.00	22.00	22.00	22.00	22.00	22.00	22.00	22.00	22.00	22.00	22.00	22.01	22.00	22.00	22.00
#OH	2.00	2.00	2.00	2.00	2.00	2.00	2.00	2.00	2.00	2.00	2.00	1.99	2.00	2.00	2.00
Charge	-	0.00	0.00	-9E-06	0.00	0.00	0.00	-3E-06	0.00	0.00	0.00	0.00	0.00	0.00	0.00

Garnet analyses, Atik Lake

	U25B-A	U25B-B	U29B-A	U29B-B	U31A-A	U31A-B	U31A-C	U211-A	U211-B	U211-C	U211-D
SiO2	38.28	37.92	38.11	38.37	37.92	37.83	38.26	36.62	36.22	36.38	36.28
TiO2	0.01	0.01	0.01	0.05	0.06	0.06	0.07	0.02	0.02	0.05	0.02
Al2O3	21.37	21.14	21.52	21.52	21.31	21.21	21.19	21.40	21.22	21.46	21.22
Cr2O3	-	-	-	-	-	-	-	0.02	0.03	0.06	-
Fe2O3	0.43	0.43	0.20	0.09	0.16	0.22	0.16	-	0.21	0.54	0.20
FeO	36.10	32.39	35.60	36.20	34.94	35.66	31.55	39.03	38.36	38.42	39.29
MnO	0.73	4.23	1.10	0.95	1.76	0.98	5.90	1.61	1.44	2.46	2.03
MgO	3.29	1.41	3.78	3.22	2.65	3.26	2.42	1.83	2.08	1.76	1.38
CaO	2.09	3.50	1.87	1.94	2.25	2.12	2.04	0.31	0.42	0.43	0.22
Total	102.30	101.03	102.19	102.34	101.05	101.34	101.59	100.84	100.00	101.56	100.64
#Si IV	6.00	6.00	5.98	6.00	6.00	6.00	6.00	5.92	5.90	5.85	5.90
#Al IV	-	-	0.02	-	-	-	-	0.08	0.10	0.15	0.10
T site	6.00	6.00	6.00	6.00	6.00	6.00	6.00	6.00	6.00	6.00	6.00
#Al VI	3.95	3.94	3.96	3.97	3.97	3.96	3.92	4.00	3.97	3.92	3.97
#Ti VI	0.00	0.00	0.00	0.01	0.01	0.01	0.01	0.00	0.00	0.01	0.00
#Cr	-	-	-	-	-	-	-	0.00	0.00	0.01	-
#Fe +3	0.05	0.05	0.02	0.01	0.02	0.03	0.02	-	0.03	0.07	0.02
O site	4.00	3.99	3.98	3.98	4.00	4.00	3.94	4.00	4.00	4.00	4.00
#Fe +2	4.73	4.29	4.67	4.73	4.62	4.73	4.14	5.28	5.22	5.17	5.35
#Mn +2	0.10	0.57	0.15	0.13	0.24	0.13	0.78	0.22	0.20	0.34	0.28
#Mg	0.77	0.33	0.88	0.75	0.63	0.77	0.57	0.44	0.50	0.42	0.33
#Ca	0.35	0.59	0.31	0.33	0.38	0.36	0.34	0.05	0.07	0.07	0.04
A site	5.95	5.78	6.02	5.94	5.87	5.99	5.83	5.99	6.00	6.00	6.00
#O	23.95	23.77	23.98	23.91	23.87	23.99	23.75	23.95	23.95	23.93	23.95

Garnet analyses, Atik Lake iron formations

	U313A	U313B	U019A	U019B	U019C	U019D	U035A	U055A	U055B	U055C	U057A	U057B
SiO2	38.69	37.26	38.00	38.31	38.48	38.36	38.44	38.44	38.06	37.78	38.69	38.82
TiO2	0.10	0.05	0.15	0.12	0.05	0.04	0.06	0.07	0.02	0.27	0.11	0.06
Al2O3	18.73	5.88	20.67	20.55	20.78	20.87	19.46	20.50	20.39	20.23	20.42	20.60
Cr2O3	-	-	-	-	-	-	-	-	-	-	-	-
Fe2O3	4.46	23.42	0.84	0.89	0.81	0.83	2.76	1.32	0.94	1.22	1.59	1.51
FeO	12.05	2.91	9.72	9.92	11.34	12.42	10.67	15.59	15.21	15.59	20.83	21.54
MnO	3.62	2.62	24.58	24.38	25.47	22.30	22.33	19.16	20.06	20.56	10.92	11.45
MgO	-	-	1.18	0.99	1.54	2.22	0.48	1.51	1.62	1.41	1.27	1.38
CaO	23.05	29.66	6.02	5.57	3.24	4.42	7.56	5.29	5.13	4.17	8.06	7.19
Total	100.70	101.80	101.16	100.73	101.71	101.46	101.76	101.88	101.83	101.23	101.89	102.55
#Si IV	6.00	6.00	6.00	6.00	6.00	6.00	6.00	6.00	6.00	6.00	6.00	6.00
#Al IV	-	-	-	-	-	-	0.00	0.00	-	-	-	-
T site	6.00	6.00	6.00	6.00	6.00	6.00	6.00	6.00	6.00	6.00	6.00	6.00
#Al VI	3.42	1.12	3.85	3.79	3.82	3.85	3.58	3.77	3.86	3.79	3.73	3.75
#Ti VI	0.01	0.01	0.02	0.01	0.01	0.00	0.01	0.01	0.00	0.03	0.01	0.01
#Cr	-	-	-	-	-	-	-	-	-	-	-	-
#Fe +3	0.52	2.84	0.10	0.10	0.10	0.10	0.32	0.16	0.11	0.15	0.19	0.18
O site	3.96	3.96	3.96	3.91	3.92	3.95	3.91	3.93	3.98	3.96	3.93	3.94
#Fe +2	1.56	0.39	1.28	1.30	1.48	1.62	1.39	2.04	2.01	2.07	2.70	2.78
#Mn +2	0.48	0.36	3.29	3.23	3.36	2.95	2.95	2.53	2.68	2.77	1.43	1.50
#Mg	-	-	0.28	0.23	0.36	0.52	0.11	0.35	0.38	0.33	0.29	0.32
#Ca	3.83	5.12	1.02	0.93	0.54	0.74	1.26	0.88	0.87	0.71	1.34	1.19
A site	5.87	5.87	5.87	5.70	5.74	5.84	5.72	5.80	5.93	5.88	5.77	5.79
#O	23.81	23.81	23.82	23.57	23.62	23.76	23.59	23.71	23.90	23.84	23.67	23.70

Garnet analyses, Atik Lake

	U842-A	U284-B	U284-C	U584-A	U584-B	U585-C	U-2B-A	U-2B-B	U-2B-C	U-2B-D	U-2C-A	U-2C-B	U-2C-C	U-2C-D	U-4-A	U-4-B	U-4-C	U-6-A	U-6-B	U10A-A
SiO2	38.05	38.37	38.33	37.51	37.73	38.15	38.61	38.31	37.97	37.54	38.52	38.15	38.62	39.01	38.17	37.89	37.13	36.09	36.60	37.78
TiO2	0.04	0.02	0.04	0.05	0.02	-	0.02	0.02	0.01	0.01	0.14	0.10	0.06	0.09	0.01	0.02	-	0.02	-	0.03
Al2O3	21.32	21.47	21.18	21.27	21.39	21.13	21.20	21.52	21.09	21.22	20.22	20.03	19.95	20.10	21.56	21.19	21.09	21.06	21.06	21.59
Cr2O3	-	-	-	-	-	-	-	-	-	-	-	-	-	-	-	-	-	-	-	0.08
Fe2O3	0.18	0.20	0.33	0.11	0.00	0.33	0.54	0.24	0.22	0.01	2.17	2.29	2.51	2.44	0.04	0.07	0.05	0.38	0.62	-
FeO	34.64	34.59	34.51	34.91	34.42	35.05	34.48	35.36	34.67	36.07	16.60	18.67	14.61	15.07	35.65	36.33	36.51	31.46	33.11	35.76
MnO	2.84	3.04	2.92	1.97	2.13	2.52	1.28	1.59	1.43	1.63	7.09	6.96	6.77	6.19	0.56	1.66	1.22	6.39	5.34	0.11
MgO	2.67	2.60	2.39	3.53	2.92	2.61	3.68	3.53	3.09	2.33	0.24	0.32	0.15	0.15	3.46	2.21	2.45	2.25	2.18	3.19
CaO	2.29	2.42	2.25	1.78	1.82	1.81	2.03	2.03	2.00	2.01	16.61	14.96	18.22	18.37	2.06	1.95	1.86	1.54	1.56	2.40
Total	102.03	102.71	101.95	101.13	100.43	101.60	101.84	102.60	100.48	100.82	101.59	101.48	100.89	101.42	101.50	101.32	100.32	99.20	100.46	100.94
#Si IV	6.00	6.00	6.00	5.96	5.99	6.00	6.00	6.00	6.00	6.00	6.00	6.00	6.00	6.00	6.00	6.00	5.99	5.90	5.91	5.97
#Al IV	0.00	-	-	0.04	0.01	-	-	0.00	-	-	-	-	0.00	-	-	-	0.01	0.10	0.09	0.03
T site	6.00	6.00	6.00	6.00	6.00	6.00	6.00	6.00	6.00	6.00	6.00	6.00	6.00	6.00	6.00	6.00	6.00	6.00	6.00	6.00
#Al VI	3.96	3.96	3.91	3.94	4.00	3.92	3.88	3.97	3.93	4.00	3.71	3.71	3.65	3.64	3.99	3.95	3.99	3.95	3.93	3.99
#Ti VI	0.00	0.00	0.00	0.01	0.00	-	0.00	0.00	0.00	0.00	0.02	0.01	0.01	0.01	0.00	0.00	-	0.00	-	0.00
#Cr	-	-	-	-	-	-	-	-	-	-	-	-	-	-	-	-	-	-	-	0.01
#Fe +3	0.02	0.02	0.04	0.01	0.00	0.04	0.06	0.03	0.03	0.00	0.25	0.27	0.29	0.28	0.00	0.01	0.01	0.05	0.07	-
O site	3.99	3.98	3.95	3.96	4.00	3.96	3.95	4.00	3.96	4.00	3.98	4.00	3.95	3.94	4.00	3.97	4.00	4.00	4.00	4.00
#Fe +2	4.57	4.52	4.52	4.64	4.57	4.61	4.48	4.63	4.58	4.82	2.16	2.46	1.90	1.94	4.69	4.81	4.92	4.30	4.47	4.72
#Mn +2	0.38	0.40	0.39	0.27	0.29	0.34	0.17	0.21	0.19	0.22	0.94	0.93	0.89	0.81	0.07	0.22	0.17	0.88	0.73	0.01
#Mg	0.63	0.61	0.56	0.84	0.69	0.61	0.85	0.82	0.73	0.56	0.06	0.08	0.03	0.03	0.81	0.52	0.59	0.55	0.53	0.75
#Ca	0.39	0.41	0.38	0.30	0.31	0.30	0.34	0.34	0.34	0.34	2.77	2.52	3.03	3.03	0.35	0.33	0.32	0.27	0.27	0.41
A site	5.96	5.94	5.84	6.04	5.86	5.86	5.84	6.00	5.84	5.94	5.93	5.98	5.86	5.81	5.92	5.89	6.00	6.00	6.00	5.90
#O	23.95	23.91	23.77	23.96	23.86	23.80	23.76	24.00	23.77	23.94	23.91	23.98	23.79	23.72	23.92	23.84	23.99	23.95	23.96	23.88

	U10A-B	U10A-C	U10A-D	U10B-A	U10B-B	U10B-C	U10B-D	U10B-E	U10B-F	U12A-A	U14-A	U14-B
SiO2	38.17	38.31	38.34	38.19	38.06	38.14	38.23	38.30	38.38	38.29	38.60	38.82
TiO2	0.01	0.07	0.03	0.05	0.21	0.10	0.01	-	0.06	-	0.03	0.06
Al2O3	21.83	21.83	21.81	21.69	21.65	21.59	21.80	21.39	21.21	21.38	21.70	21.53
Cr2O3	0.12	0.06	0.04	0.09	0.08	0.08	0.07	0.17	0.09	-	-	-
Fe2O3	0.00	-	0.00	0.00	-	0.00	-	0.07	0.21	0.61	0.21	0.61
FeO	35.30	35.42	35.34	36.11	35.43	35.10	35.91	35.74	35.32	38.29	37.26	36.38
MnO	0.62	0.64	2.03	1.48	1.85	1.78	0.36	0.46	2.53	1.27	0.86	0.91
MgO	3.93	3.78	2.87	2.82	2.68	2.57	3.46	3.42	2.40	2.27	3.14	2.35
CaO	2.10	2.30	2.17	1.67	1.78	1.76	2.07	2.27	1.99	1.73	1.94	1.82
Total	102.08	102.41	102.63	102.10	101.74	101.12	101.91	101.82	102.19	103.84	103.74	102.48
#Si IV	5.96	5.97	5.98	5.98	6.00	5.99	5.97	6.00	6.00	5.99	6.00	6.00
#Al IV	0.04	0.03	0.02	0.02	-	0.01	0.03	-	-	0.01	0.00	-
T site	6.00	6.00	6.00	6.00	6.00	6.00	6.00	6.00	6.00	6.00	6.00	6.00
#Al VI	3.98	3.98	3.99	3.98	4.02	3.98	3.99	3.95	3.91	3.93	3.97	3.92
#Ti VI	0.00	0.01	0.00	0.01	0.02	0.01	0.00	-	0.01	-	0.00	0.01
#Cr	0.01	0.01	0.00	0.01	0.01	0.01	0.01	0.02	0.01	-	-	-
#Fe +3	0.00	-	0.00	0.00	-	0.00	-	0.01	0.02	0.07	0.02	0.07
O site	4.00	4.00	4.00	4.00	4.06	4.00	4.00	3.98	3.95	4.00	4.00	4.00
#Fe +2	4.61	4.62	4.61	4.73	4.67	4.61	4.69	4.68	4.62	5.01	4.84	4.70
#Mn +2	0.08	0.08	0.27	0.20	0.25	0.24	0.05	0.06	0.34	0.17	0.11	0.12
#Mg	0.92	0.88	0.67	0.66	0.63	0.60	0.81	0.80	0.56	0.53	0.73	0.54
#Ca	0.35	0.38	0.36	0.28	0.30	0.30	0.35	0.38	0.33	0.29	0.32	0.30
A site	5.96	5.97	5.91	5.86	5.85	5.74	5.89	5.92	5.85	6.00	6.00	5.66
#O	23.94	23.96	23.90	23.86	23.95	23.74	23.88	23.89	23.78	24.00	24.00	23.67

CORDIERITE ANALYSES, ATIK LAKE

	U284-A	U284-B	U284-C	U-4-A	U-4-B	U584-A	U584-B	U-12-A	U-12-B	U29B-A
SiO2	45.84	48.00	47.85	48.86	49.58	48.66	48.71	49.84	49.87	48.52
TiO2	0.02	0.02	-	0.03	-	0.01	0.01	0.03	0.04	0.02
Al2O3	32.41	32.59	32.16	33.07	33.06	32.53	32.70	32.56	32.50	33.12
FeO	8.28	8.53	9.45	7.29	7.35	7.15	7.14	10.16	10.54	7.63
MnO	0.07	0.12	0.15	0.06	0.09	0.13	0.12	0.15	0.12	0.02
MgO	7.13	7.79	7.11	8.58	8.36	8.97	8.95	6.99	6.79	8.62
Na2O	0.40	0.48	0.40	0.39	0.41	0.12	0.15	0.17	0.10	0.19
Total	94.15	97.53	97.12	98.28	98.85	97.57	97.78	99.90	99.96	98.12
#Si+4	4.94	5.00	5.02	5.01	5.05	5.02	5.02	5.08	5.09	4.99
#Ti+4	0.00	0.00	-	0.00	-	0.00	0.00	0.00	0.00	0.00
#Al+3	4.12	4.00	3.98	4.00	3.97	3.96	3.97	3.91	3.91	4.01
#Fe+2	0.75	0.74	0.83	0.63	0.63	0.62	0.61	0.87	0.90	0.66
#Mn+2	0.01	0.01	0.01	0.01	0.01	0.01	0.01	0.01	0.01	0.00
#Mg+2	1.15	1.21	1.11	1.31	1.27	1.38	1.37	1.06	1.03	1.32
#Na+1	0.08	0.10	0.08	0.08	0.08	0.02	0.03	0.03	0.02	0.04
#TOTAL	11.04	11.05	11.03	11.03	11.00	11.01	11.01	10.97	10.96	11.02
#O-2	18.00	18.00	18.00	18.00	18.00	18.00	18.00	18.00	18.00	18.00

	U29B-B	U841A	U841B	U841C	U841D	U-17A	U-17B	U-17C	U-17D	U-24A
SiO2	48.74	49.18	49.83	49.65	49.75	47.41	48.20	48.85	48.47	49.32
TiO2	0.03	0.01	-	0.01	-	-	0.01	0.04	-	-
Al2O3	33.05	32.89	32.65	32.84	32.94	33.44	33.22	33.22	32.95	33.06
FeO	7.59	7.47	7.43	7.65	7.75	8.25	8.24	8.47	8.26	7.84
MnO	0.11	0.29	0.26	0.25	0.24	0.12	0.19	0.14	0.22	0.12
MgO	8.46	9.00	8.77	8.75	8.97	8.48	8.61	8.55	8.45	8.45
Na2O	0.30	0.20	0.25	0.12	0.13	0.17	0.08	0.15	0.24	0.19
Total	98.28	99.04	99.19	99.27	99.78	97.87	98.55	99.42	98.59	98.98
#Si+4	5.00	5.01	5.06	5.05	5.03	4.91	4.95	4.98	4.98	5.03
#Ti+4	0.00	0.00	-	0.00	-	-	0.00	0.00	-	-
#Al+3	4.00	3.95	3.91	3.93	3.93	4.08	4.02	3.99	3.99	3.97
#Fe+2	0.65	0.64	0.63	0.65	0.66	0.71	0.71	0.72	0.71	0.67
#Mn+2	0.01	0.03	0.02	0.02	0.02	0.01	0.02	0.01	0.02	0.01
#Mg+2	1.30	1.37	1.33	1.33	1.35	1.31	1.32	1.30	1.29	1.28
#Na+1	0.06	0.04	0.05	0.02	0.03	0.03	0.02	0.03	0.05	0.04
#TOTAL	11.02	11.03	11.01	11.00	11.02	11.06	11.04	11.04	11.05	11.00
#O-2	18.00	18.00	18.00	18.00	18.00	18.00	18.00	18.00	18.00	18.00

	U-24B	U40C1	U40C2	U40C3	U41C1	U41C2
SiO2	49.09	49.05	49.10	48.98	48.96	50.65
TiO2	0.04	0.01	0.03	0.02	-	0.02
Al2O3	32.93	32.08	32.07	32.11	31.98	32.07
FeO	7.75	8.00	7.75	7.51	11.27	10.77
MnO	0.09	0.06	0.08	0.02	0.10	0.11
MgO	8.83	8.65	8.64	8.53	6.12	6.28
Na2O	0.17	0.13	0.28	0.19	0.36	0.39
Total	98.90	97.98	97.95	97.36	98.79	100.29
#Si+4	5.01	5.06	5.06	5.07	5.08	5.15
#Ti+4	0.00	0.00	0.00	0.00	-	0.00
#Al+3	3.96	3.90	3.90	3.92	3.91	3.85
#Fe+2	0.66	0.69	0.67	0.65	0.98	0.92
#Mn+2	0.01	0.01	0.01	0.00	0.01	0.01
#Mg+2	1.34	1.33	1.33	1.32	0.95	0.95
#Na+1	0.03	0.03	0.06	0.04	0.07	0.08
#TOTAL	11.02	11.01	11.02	10.99	11.00	10.96
#O-2	18.00	18.00	18.00	18.00	18.00	18.00

Clinopyroxene analyses, Atik Lake

	U2CA	U2CB	U2CC	U2CD	U2CE	U2CF	U2CG	U2CH	U32A	U32B
SiO2	51.11	50.85	50.49	50.53	50.56	50.95	50.50	50.70	53.32	54.03
TiO2	0.01	0.05	0.02	0.06	0.02	0.01	0.01	0.01	-	-
Al2O3	0.25	0.23	0.13	0.16	0.22	0.22	0.25	0.30	0.31	0.20
Cr2O3	-	-	-	-	-	-	-	-	-	-
Fe2O3	-	-	0.30	-	0.03	0.08	0.31	0.23	-	-
FeO	19.88	19.73	20.69	20.90	19.42	19.14	19.50	19.69	7.41	7.33
MnO	1.23	1.25	1.32	1.42	1.36	1.42	1.21	1.27	1.86	2.26
NiO	-	-	-	-	-	-	-	-	-	-
MgO	5.74	5.63	5.09	5.08	5.81	5.97	5.82	5.60	12.59	12.84
CaO	22.58	22.67	22.72	22.45	22.60	22.83	22.65	22.91	24.19	24.03
Na2O	0.01	0.05	0.04	0.04	0.08	0.10	0.06	0.07	0.04	0.07
K2O	-	-	-	-	-	-	-	-	-	-
Total	100.81	100.46	100.80	100.64	100.09	100.72	100.31	100.78	99.72	100.76
#Si IV	2.01	2.00	1.99	2.00	2.00	2.00	1.99	1.99	2.01	2.01
#Al IV	-	-	0.01	0.00	0.00	0.00	0.01	0.01	-	-
T site	2.01	2.00	2.00	2.00	2.00	2.00	2.00	2.00	2.01	2.01
#Al VI	0.01	0.01	-	0.01	0.01	0.01	0.00	0.01	0.01	0.01
#Ti	0.00	0.00	0.00	0.00	0.00	0.00	0.00	0.00	-	-
#Cr	-	-	-	-	-	-	-	-	-	-
#Fe +3	-	-	0.01	-	0.00	0.00	0.01	0.01	-	-
#Fe +2	0.65	0.65	0.68	0.69	0.64	0.63	0.64	0.65	0.23	0.23
#Mn +2	0.04	0.04	0.04	0.05	0.05	0.05	0.04	0.04	0.06	0.07
#Ni	-	-	-	-	-	-	-	-	-	-
#Mg	0.34	0.33	0.30	0.30	0.34	0.35	0.34	0.33	0.71	0.71
#Ca	0.95	0.96	0.96	0.95	0.96	0.96	0.96	0.96	0.98	0.96
#Na	0.00	0.00	0.00	0.00	0.01	0.01	0.00	0.01	0.00	0.01
#K	-	-	-	-	-	-	-	-	-	-
M1,M2	1.99	2.00	2.00	2.00	2.00	2.00	2.00	2.00	1.99	1.99
#O	6.01	6.01	6.00	6.00	6.00	6.00	6.00	6.00	6.01	6.02
Charge	0.03	0.02	0.00	0.00	-	-	-	-	0.03	0.03

	U32C	U272A	U272B	U272C	U272D	U313A	U313B	U313C	U313D
SiO2	52.45	52.97	52.55	52.57	53.80	48.90	49.50	49.06	48.48
TiO2	0.01	-	-	-	0.01	0.03	0.03	0.05	0.01
Al2O3	0.35	0.74	0.33	0.33	0.25	0.60	0.42	0.53	0.56
Cr2O3	-	-	-	-	-	-	-	-	-
Fe2O3	0.03	-	-	-	-	0.48	-	0.42	1.07
FeO	11.24	11.16	13.14	12.83	8.30	25.57	25.94	25.11	26.49
MnO	1.92	1.36	1.21	1.20	0.87	1.10	1.08	1.03	1.26
NiO	-	-	-	-	-	-	-	-	-
MgO	10.26	11.25	9.88	10.02	12.97	1.85	1.86	2.27	0.86
CaO	24.21	23.25	23.41	23.32	24.06	21.79	22.06	21.96	22.10
Na2O	0.05	0.15	0.09	0.06	0.04	0.13	0.10	0.08	0.08
K2O	-	-	-	-	-	-	-	-	-
Total	100.52	100.88	100.61	100.33	100.30	100.45	100.99	100.51	100.91
#Si IV	1.99	1.99	2.00	2.01	2.01	1.98	2.00	1.98	1.97
#Al IV	0.01	0.01	-	-	-	0.02	0.00	0.02	0.03
T site	2.00	2.00	2.00	2.01	2.01	2.00	2.00	2.00	2.00
#Al VI	0.01	0.03	0.01	0.01	0.01	0.01	0.02	0.01	-
#Ti	0.00	-	-	-	0.00	0.00	0.00	0.00	0.00
#Cr	-	-	-	-	-	-	-	-	-
#Fe +3	0.00	-	-	-	-	0.01	-	0.01	0.03
#Fe +2	0.36	0.35	0.42	0.41	0.26	0.87	0.87	0.85	0.90
#Mn +2	0.06	0.04	0.04	0.04	0.03	0.04	0.04	0.04	0.04
#Ni	-	-	-	-	-	-	-	-	-
#Mg	0.58	0.63	0.56	0.57	0.72	0.11	0.11	0.14	0.05
#Ca	0.99	0.94	0.96	0.95	0.96	0.95	0.95	0.95	0.96
#Na	0.00	0.01	0.01	0.00	0.00	0.01	0.01	0.01	0.01
#K	-	-	-	-	-	-	-	-	-
M1,M2	2.00	2.00	2.00	1.99	1.99	2.00	2.00	2.00	2.00
#O	6.00	6.00	6.01	6.01	6.02	6.00	6.00	6.00	6.00
Charge	-1E-06	0.01	0.01	0.03	0.03	-1E-06	0.00	-1E-06	0.00

Plagioclase Analyses, Atik Lake

	I-1-A	I-1-B	U-2B-A	U-2B-B	U-2B-C	U-2C-A	U-2C-B	U-6-A	U-6-B	U-14-A
SiO2	68.51	63.81	58.10	57.79	58.05	44.46	45.77	52.27	55.88	49.43
Al2O3	20.39	18.91	25.59	25.83	25.71	34.63	33.78	30.33	28.07	32.86
CaO	0.04	-	8.38	8.47	8.18	19.05	18.49	13.60	10.72	16.06
K2O	1.66	11.86	0.02	0.03	0.02	-	0.02	0.02	0.04	0.02
Na2O	10.39	2.27	6.31	6.11	6.27	0.36	0.89	3.33	4.81	2.19
TOTAL	100.98	96.85	98.40	98.23	98.23	98.50	98.95	99.55	99.52	100.56
#Si+4	2.98	2.99	2.63	2.62	2.63	2.08	2.13	2.38	2.52	2.24
#Al+3	1.04	1.04	1.37	1.38	1.37	1.91	1.85	1.63	1.49	1.76
#Ca+2	0.00	-	0.41	0.41	0.40	0.96	0.92	0.66	0.52	0.78
#K	0.09	0.71	0.00	0.00	0.00	-	0.00	0.00	0.00	0.00
#Na+1	0.87	0.21	0.55	0.54	0.55	0.03	0.08	0.29	0.42	0.19
#TOTAL	4.99	4.95	4.96	4.96	4.96	4.98	4.99	4.96	4.95	4.98
#O-2	8.00	8.00	8.00	8.00	8.00	8.00	8.00	8.00	8.00	8.00

	U-14-B	U-14-C	U25B-A	U25B-B	U29B-A	U29B-B	U31A-A	U31A-B	U10A-A	U10A-B
SiO2	50.54	46.77	49.83	46.77	54.55	55.10	46.38	47.55	46.13	45.66
Al2O3	32.42	34.18	30.65	33.28	29.10	27.53	33.66	33.15	34.33	35.04
CaO	15.10	17.96	18.02	17.04	12.23	9.84	17.02	16.65	17.75	17.86
K2O	0.02	0.02	0.28	0.03	0.01	0.04	0.01	0.02	-	0.01
Na2O	2.72	1.33	2.16	1.64	4.74	5.73	1.47	1.78	1.44	1.12
TOTAL	100.80	100.26	100.94	98.76	100.63	98.24	98.54	99.15	99.65	99.69
#Si+4	2.28	2.14	2.27	2.17	2.45	2.52	2.16	2.20	2.13	2.11
#Al+3	1.72	1.85	1.65	1.82	1.54	1.48	1.85	1.80	1.87	1.90
#Ca+2	0.73	0.88	0.88	0.85	0.59	0.48	0.85	0.82	0.88	0.88
#K	0.00	0.00	0.02	0.00	0.00	0.00	0.00	0.00	-	0.00
#Na+1	0.24	0.12	0.19	0.15	0.41	0.51	0.13	0.16	0.13	0.10
#TOTAL	4.98	4.99	5.01	4.99	4.99	4.99	4.99	4.98	5.00	4.99
#O-2	8.00	8.00	8.00	8.00	8.00	8.00	8.00	8.00	8.00	8.00

	U10A-C	U10B-A	U10B-B	U10B-C	U10B-D	U10B-E	U10B-F	21-1-A	21-1-B	U-22-A
SiO2	49.71	46.49	46.28	47.21	45.52	49.44	45.91	64.53	66.11	47.27
Al2O3	31.75	35.11	34.50	33.59	35.32	33.35	34.78	21.21	21.03	32.10
CaO	14.60	18.10	17.66	16.73	18.45	16.90	17.96	1.40	1.42	16.73
K2O	0.02	0.02	-	0.01	-	-	0.02	-	0.02	-
Na2O	3.12	1.25	1.44	2.02	1.05	1.71	1.18	10.41	10.20	1.97
TOTAL	99.20	100.97	99.88	99.56	100.34	101.40	99.85	97.55	98.78	98.07
#Si+4	2.28	2.12	2.13	2.17	2.09	2.23	2.11	2.90	2.92	2.21
#Al+3	1.72	1.88	1.87	1.82	1.91	1.77	1.89	1.12	1.10	1.77
#Ca+2	0.72	0.88	0.87	0.83	0.91	0.82	0.89	0.07	0.07	0.84
#K	0.00	0.00	-	0.00	-	-	0.00	-	0.00	-
#Na+1	0.28	0.11	0.13	0.18	0.09	0.15	0.11	0.91	0.87	0.18
#TOTAL	5.00	5.00	5.00	5.00	5.00	4.96	4.99	4.99	4.96	5.00
#O-2	8.00	8.00	8.00	8.00	8.00	8.00	8.00	8.00	8.00	8.00

	U-22-B	U-22-C	U845A	U847A	U847B	U-08A	U-24A
SiO2	47.57	55.72	60.97	61.03	60.92	51.72	46.45
Al2O3	32.43	26.72	24.29	24.24	24.35	29.64	33.77
CaO	16.85	10.54	6.46	6.21	6.43	12.50	17.64
K2O	0.01	0.06	0.04	0.06	0.04	0.06	0.01
Na2O	1.93	5.81	7.78	8.25	8.07	4.35	1.33
TOTAL	98.79	98.85	99.54	99.79	99.81	98.27	99.20
#Si+4	2.21	2.54	2.72	2.72	2.71	2.38	2.15
#Al+3	1.77	1.43	1.28	1.27	1.28	1.61	1.84
#Ca+2	0.84	0.51	0.31	0.30	0.31	0.62	0.88
#K	0.00	0.00	0.00	0.00	0.00	0.00	0.00
#Na+1	0.17	0.51	0.67	0.71	0.70	0.39	0.12
#TOTAL	4.99	5.00	4.98	5.00	5.00	5.01	4.99
#O-2	8.00	8.00	8.00	8.00	8.00	8.00	8.00

Chlorite Analyses, Atik Lake

	U-4-A	U-4-B	U-4-C	U-4-D	U-4-E	U-4-F	U-4-G	U-4-H	U-4-I	U-4-J
SiO2	26.29	24.60	25.06	25.51	25.53	25.64	25.20	25.68	25.37	24.90
TiO2	0.09	0.04	0.08	0.06	0.03	0.12	0.13	0.09	0.14	0.13
Al2O3	20.84	22.48	21.94	24.03	24.26	24.01	23.77	23.57	23.33	24.22
Fe2O3	-	0.00	-	0.00	0.00	0.00	-	0.00	0.00	-
FeO	22.73	24.37	23.26	21.21	19.90	21.48	20.70	23.05	22.66	22.74
MnO	0.05	0.06	-	0.06	-	0.06	0.09	0.09	0.03	0.04
MgO	15.86	14.21	15.24	17.33	17.75	16.99	17.30	16.08	16.42	16.15
CaO	-	-	0.03	-	-	0.01	-	0.05	0.03	-
Na2O	0.02	0.04	0.03	-	-	-	0.01	0.01	0.03	-
K2O	-	0.04	0.01	0.03	0.05	-	-	-	0.01	-
H2O	11.33	11.19	11.24	11.75	11.74	11.76	11.64	11.74	11.67	11.66
Total	97.21	97.03	96.89	99.98	99.26	100.07	98.84	100.36	99.69	99.84
#Si IV	2.78	2.64	2.67	2.60	2.61	2.62	2.60	2.63	2.61	2.56
#Al IV	1.22	1.36	1.33	1.40	1.39	1.38	1.40	1.37	1.39	1.44
T site	4.00	4.00	4.00	4.00	4.00	4.00	4.00	4.00	4.00	4.00
#Al VI	1.38	1.47	1.43	1.49	1.53	1.50	1.49	1.48	1.45	1.50
#Ti	0.01	0.00	0.01	0.00	0.00	0.01	0.01	0.01	0.01	0.01
#Fe +3	-	0.00	-	0.00	0.00	0.00	-	0.00	0.00	-
#Fe +2	2.01	2.18	2.07	1.81	1.70	1.83	1.78	1.97	1.95	1.96
#Mn +2	0.00	0.01	-	0.01	-	0.01	0.01	0.01	0.00	0.00
#Mg	2.50	2.27	2.42	2.64	2.70	2.58	2.66	2.46	2.52	2.48
#Ca	-	-	0.00	-	-	0.00	-	0.01	0.00	-
#Na	0.00	0.01	0.01	-	-	-	0.00	0.00	0.01	-
#K	-	0.01	0.00	0.00	0.01	-	-	-	0.00	-
O site	5.91	5.95	5.95	5.95	5.94	5.93	5.95	5.93	5.95	5.95
#O	10.00	10.00	10.00	10.00	10.00	10.00	10.00	9.98	9.98	9.99
#OH	8.00	8.00	8.00	8.00	8.00	8.00	8.00	8.02	8.02	8.01
Charge	0.00	0.00	0.00	-1E-06	0.00	-	-	-	-	0.00

	U10A-A	U10A-B	U10A-C	U10A-D	U10A-E	U10A-F	U10B-A	U10B-B	U10B-C	U10B-D
SiO2	25.34	25.52	25.46	24.92	25.55	25.60	25.87	26.00	24.53	25.28
TiO2	0.02	0.07	0.06	0.05	0.06	0.10	0.04	0.05	0.10	0.08
Al2O3	23.27	22.82	23.19	22.85	22.91	23.19	22.25	22.81	22.71	23.22
Fe2O3	-	-	0.00	0.00	0.00	-	0.00	-	0.00	0.00
FeO	23.86	23.27	22.80	23.48	24.09	23.16	24.53	25.12	23.72	24.63
MnO	0.04	0.09	0.09	0.07	0.14	0.08	0.03	0.02	0.04	0.01
MgO	15.76	16.41	16.42	15.27	15.60	15.73	15.55	14.97	14.60	15.17
CaO	-	0.01	0.02	0.06	0.01	-	0.02	0.15	1.39	0.06
Na2O	-	0.04	-	0.07	0.02	0.02	-	0.03	-	-
K2O	-	-	0.02	0.08	-	0.01	0.01	-	0.03	0.01
H2O	11.59	11.63	11.62	11.38	11.58	11.59	11.58	11.65	11.35	11.58
Total	99.88	99.86	99.68	98.23	99.96	99.48	99.88	100.80	98.47	100.04
#Si IV	2.62	2.64	2.63	2.62	2.65	2.65	2.68	2.68	2.59	2.62
#Al IV	1.38	1.36	1.37	1.38	1.35	1.35	1.32	1.32	1.41	1.38
T site	4.00	4.00	4.00	4.00	4.00	4.00	4.00	4.00	4.00	4.00
#Al VI	1.46	1.41	1.45	1.46	1.44	1.48	1.40	1.45	1.42	1.46
#Ti	0.00	0.01	0.00	0.00	0.00	0.01	0.00	0.00	0.01	0.01
#Fe +3	-	-	0.00	0.00	0.00	-	0.00	-	0.00	0.00
#Fe +2	2.06	2.01	1.97	2.07	2.09	2.00	2.13	2.16	2.10	2.14
#Mn +2	0.00	0.01	0.01	0.01	0.01	0.01	0.00	0.00	0.00	0.00
#Mg	2.43	2.53	2.53	2.40	2.41	2.43	2.40	2.30	2.30	2.34
#Ca	-	0.00	0.00	0.01	0.00	-	0.00	0.02	0.16	0.01
#Na	-	0.01	-	0.01	0.00	0.00	-	0.01	-	-
#K	-	-	0.00	0.01	-	0.00	0.00	-	0.00	0.00
O site	5.96	5.97	5.96	5.97	5.96	5.93	5.95	5.94	5.99	5.95
#O	10.00	9.99	10.00	10.01	10.00	10.00	9.99	10.00	10.00	9.99
#OH	8.00	8.01	8.00	7.99	8.00	8.00	8.01	8.00	8.00	8.01
Charge	0.00	-	0.00	0.00	-	-	-	-	-	-

	U10B-E	U-14-A	U-14-B	U-14-C	U25B-A	U25B-B	U31A-A	U31A-B	U31A-C	U192A	U847A
SiO2	25.56	25.27	26.62	25.77	24.99	26.32	25.47	25.39	25.63	29.68	27.36
TiO2	0.11	0.14	0.09	0.08	0.10	0.12	0.18	0.09	0.10	0.02	0.06
Al2O3	23.08	22.86	22.53	23.08	22.70	21.32	22.74	22.58	22.91	20.63	22.17
Fe2O3	0.00	-	-	-	0.00	-	-	-	-	0.00	-
FeO	24.28	26.00	22.69	23.68	25.83	26.73	23.41	23.40	23.18	11.33	16.47
MnO	0.05	0.01	0.04	0.05	0.01	-	0.04	-	0.06	1.16	0.10
MgO	15.18	14.41	17.00	16.24	14.32	13.49	15.94	15.72	15.36	24.92	22.21
CaO	0.02	0.06	0.03	-	0.11	0.08	0.03	0.02	0.04	0.01	0.03
Na2O	-	0.02	0.02	0.02	0.14	0.01	0.01	0.01	0.02	-	-
K2O	0.02	-	-	-	0.06	0.13	-	0.01	-	-	0.10
H2O	11.58	11.51	11.78	11.69	11.43	11.74	11.54	11.46	11.50	12.28	12.07
Total	99.88	100.28	100.80	100.61	99.69	99.94	99.36	98.68	98.80	100.03	100.57
#Si IV	2.65	2.63	2.71	2.64	2.62	2.75	2.65	2.66	2.67	2.90	2.72
#Al IV	1.35	1.37	1.29	1.36	1.38	1.25	1.35	1.34	1.33	1.10	1.28
T site	4.00	4.00	4.00	4.00	4.00	4.00	4.00	4.00	4.00	4.00	4.00
#Al VI	1.47	1.44	1.41	1.43	1.43	1.37	1.43	1.44	1.49	1.27	1.31
#Ti	0.01	0.01	0.01	0.01	0.01	0.01	0.01	0.01	0.01	0.00	0.00
#Fe +3	0.00	-	-	-	0.00	-	-	-	-	0.00	-
#Fe +2	2.10	2.26	1.93	2.03	2.27	2.34	2.03	2.05	2.02	0.92	1.37
#Mn +2	0.00	0.00	0.00	0.00	0.00	-	0.00	-	0.01	0.10	0.01
#Mg	2.34	2.24	2.58	2.48	2.24	2.10	2.47	2.45	2.39	3.63	3.29
#Ca	0.00	0.01	0.00	-	0.01	0.01	0.00	0.00	0.00	0.00	0.00
#Na	-	0.00	0.00	0.00	0.03	0.00	0.00	0.00	0.00	-	-
#K	0.00	-	-	-	0.01	0.02	-	0.00	-	-	0.01
O site	5.93	5.96	5.94	5.96	5.99	5.85	5.95	5.95	5.92	5.92	5.99
#O	10.00	10.01	10.00	10.00	10.00	9.82	10.01	10.00	10.00	10.01	10.01
#OH	8.00	7.99	8.00	8.00	8.00	8.18	7.99	8.00	8.00	7.99	7.99
Charge	-	-	-	0.00	-	-	-	0.00	-	-	-

Biotite Analyses, Atik Lake

	U284-A	U284-B	U284-C	U284-D	U584-A	U584-B	U584-C	U584-D	U584-E	U584-F	U-2B-A	U-2B-B	U-2B-C	U-2B-D	U-04-A	U-04-B	U-04-C	U-04-D	U-04-E	U-6B-A	U-6B-B	U-6B-C	U10A-A	U10A-B	U10A-C
SiO2	35.50	27.12	32.38	34.05	35.97	36.33	36.13	36.32	36.26	34.53	34.67	37.59	36.92	35.29	34.94	33.47	36.60	35.71	35.06	35.00	35.13	35.39	32.68	36.48	36.78
TiO2	1.97	1.64	1.66	1.77	1.38	1.52	1.40	1.41	0.66	1.45	1.13	1.48	1.57	1.59	1.65	1.36	1.71	1.80	1.65	1.64	1.67	1.62	1.76	1.77	1.66
Al2O3	19.70	35.54	21.66	19.80	19.45	19.07	18.90	19.29	19.36	19.37	18.99	17.97	18.36	17.99	19.43	12.85	20.11	19.91	20.00	19.13	19.02	19.12	19.03	17.48	17.71
Cr2O3	-	-	-	-	-	-	-	-	-	-	-	-	-	-	0.32	0.27	0.22	0.46	0.42	-	-	-	0.29	0.30	0.35
Fe2O3	-	-	0.00	-	-	0.00	0.00	-	-	-	-	-	-	0.00	-	0.00	0.00	0.00	-	-	-	0.00	-	-	-
FeO	21.96	17.19	22.22	21.58	16.94	17.18	17.84	16.97	17.37	18.85	20.14	18.80	19.32	19.46	16.97	18.69	16.12	17.81	17.68	20.66	21.52	21.13	21.26	18.72	18.77
MnO	0.05	0.03	0.02	0.04	0.01	-	0.01	0.03	0.03	0.03	0.04	-	-	0.02	0.05	0.03	-	0.03	-	0.03	0.07	0.15	-	0.01	0.01
MgO	7.84	6.26	7.94	7.73	10.32	11.07	11.47	11.39	11.17	11.77	12.78	11.70	10.58	10.38	11.00	12.85	11.32	10.66	11.24	8.23	7.78	7.86	12.16	11.23	11.70
CaO	-	0.14	0.03	0.01	0.12	0.05	-	0.03	-	-	0.02	0.05	0.03	0.03	0.05	0.01	0.01	-	0.01	0.02	0.02	-	0.03	0.01	-
Na2O	0.18	0.17	0.31	0.29	0.15	0.17	0.20	0.17	0.19	0.10	0.07	0.18	0.12	0.09	0.17	0.12	0.22	0.11	0.15	0.19	0.17	0.16	0.07	0.16	0.16
K2O	10.13	7.85	8.88	9.82	8.94	9.23	9.01	9.06	9.48	9.87	8.67	9.32	9.28	9.29	9.99	8.32	9.05	8.42	9.66	9.48	9.67	9.15	8.08	9.41	9.40
H2O	3.96	4.05	3.87	3.87	3.92	3.97	3.97	3.98	4.00	3.92	3.95	4.04	4.00	3.88	3.90	3.92	4.03	3.98	3.92	3.87	3.88	3.88	3.86	3.96	4.01
Total	101.29	99.99	98.97	98.96	97.20	98.59	98.93	98.65	98.52	99.89	100.46	101.13	100.18	98.02	98.47	91.89	99.39	98.89	99.79	98.25	98.93	98.46	99.22	99.53	100.55
#Si IV	5.37	4.02	5.02	5.28	5.50	5.49	5.45	5.47	5.49	5.24	5.22	5.57	5.54	5.45	5.33	5.53	5.44	5.38	5.28	5.42	5.43	5.46	5.03	5.52	5.50
#Al IV	2.63	3.98	2.98	2.72	2.50	2.51	2.55	2.53	2.51	2.76	2.78	2.43	2.46	2.55	2.67	2.47	2.56	2.62	2.72	2.58	2.57	2.54	2.97	2.48	2.50
#Fe IV	-	-	-	-	-	-	-	-	-	-	-	-	-	-	-	-	-	-	-	-	-	-	-	-	-
#Ti IV	-	-	-	-	-	-	-	-	-	-	-	-	-	-	-	-	-	-	-	-	-	-	-	-	-
T site	8.00	8.00	8.00	8.00	8.00	8.00	8.00	8.00	8.00	8.00	8.00	8.00	8.00	8.00	8.00	8.00	8.00	8.00	8.00	8.00	8.00	8.00	8.00	8.00	8.00
#Al VI	0.88	2.22	0.97	0.90	1.00	0.88	0.82	0.90	0.94	0.70	0.59	0.71	0.78	0.72	0.82	0.03	0.97	0.91	0.83	0.91	0.89	0.94	0.48	0.63	0.62
#Ti VI	0.22	0.18	0.19	0.21	0.16	0.17	0.16	0.16	0.08	0.17	0.13	0.16	0.18	0.18	0.19	0.17	0.19	0.20	0.19	0.19	0.19	0.19	0.20	0.20	0.19
#Cr	-	-	-	-	-	-	-	-	-	-	-	-	-	-	0.04	0.04	0.03	0.05	0.05	-	-	-	0.04	0.04	0.04
#Fe +3	-	-	0.00	-	-	0.00	0.00	-	-	-	-	-	-	0.00	-	0.00	0.00	0.00	-	-	-	0.00	-	-	-
#Fe +2	2.78	2.13	2.88	2.80	2.17	2.17	2.25	2.14	2.20	2.39	2.54	2.33	2.42	2.51	2.17	2.58	2.00	2.24	2.23	2.67	2.78	2.73	2.73	2.37	2.35
#Mn +2	0.01	0.00	0.00	0.01	0.00	-	0.00	0.00	0.00	0.00	0.01	-	-	0.00	0.01	0.00	-	0.00	-	0.00	0.01	0.02	-	0.00	0.00
#Mg	1.77	1.38	1.83	1.79	2.35	2.49	2.58	2.56	2.52	2.66	2.87	2.58	2.37	2.39	2.50	3.16	2.51	2.39	2.52	1.90	1.79	1.81	2.79	2.53	2.61
O site	5.65	5.91	5.88	5.69	5.68	5.72	5.81	5.76	5.74	5.92	6.13	5.79	5.75	5.80	5.72	5.98	5.70	5.80	5.81	5.68	5.67	5.69	6.24	5.77	5.81
#Ca	-	0.02	0.00	0.00	0.02	0.01	-	0.00	-	-	0.00	0.01	0.00	0.00	0.01	0.00	0.00	-	0.00	0.00	0.00	-	0.00	0.00	-
#Na	0.05	0.05	0.09	0.09	0.04	0.05	0.06	0.05	0.06	0.03	0.02	0.05	0.03	0.03	0.05	0.04	0.06	0.03	0.04	0.06	0.05	0.05	0.02	0.05	0.05
#K	1.95	1.48	1.76	1.94	1.74	1.78	1.74	1.74	1.83	1.91	1.67	1.76	1.78	1.83	1.94	1.75	1.72	1.62	1.86	1.87	1.91	1.80	1.59	1.82	1.79
A site	2.01	1.55	1.85	2.03	1.81	1.84	1.79	1.80	1.89	1.94	1.69	1.82	1.82	1.86	2.00	1.79	1.78	1.65	1.90	1.93	1.96	1.85	1.61	1.86	1.84
#O	20.01	20.00	20.00	20.00	20.00	20.00	20.00	20.00	19.96	20.04	20.03	20.01	20.00	20.01	20.03	19.68	20.00	20.00	20.06	20.00	20.00	20.00	20.04	20.00	20.00
#OH	3.99	4.00	4.00	4.00	4.00	4.00	4.00	4.00	4.04	3.96	3.97	3.99	4.00	3.99	3.97	4.32	4.00	4.00	3.94	4.00	4.00	4.00	3.96	4.00	4.00

	U-14-C	U-14-D	U25B-A	U25B-B	U29B-A	U29B-B	U31A-A	U31A-B	U31A-C	U841A	U841B	U841C	U841D	U845A	U845B	U847A	U847B	U-08A	U-08B	U-08C	U10B-A	U10B-B	U-12-A	U-14-A	U-14-B
SiO2	36.78	37.06	35.50	36.50	36.70	36.65	36.18	36.78	35.37	35.89	37.33	37.60	36.90	37.72	38.42	39.58	38.57	37.23	37.04	35.53	37.24	42.35	33.52	36.26	36.73
TiO2	1.88	1.74	1.64	1.56	1.32	1.60	1.38	1.30	1.34	1.32	1.35	1.33	1.37	1.46	1.66	1.31	1.59	1.40	1.40	1.32	1.33	1.05	1.36	1.40	1.54
Al2O3	17.83	17.80	17.67	17.52	17.48	18.77	19.48	17.39	18.37	19.54	18.66	18.82	18.31	16.67	15.88	15.71	16.57	17.72	17.45	17.82	20.81	17.84	19.28	18.36	17.94
Cr2O3	-	-	-	-	-	-	-	-	-	-	-	-	-	-	-	-	-	-	-	-	0.53	0.54	-	-	-
Fe2O3	-	0.00	0.00	-	0.00	0.00	-	-	0.00	-	0.00	0.00	-	-	-	-	0.00	-	-	0.00	0.00	0.00	-	-	-
FeO	19.43	20.31	19.84	20.04	19.08	17.57	17.85	18.16	19.14	17.96	17.42	17.41	18.35	14.95	14.22	14.07	13.87	17.95	18.40	20.55	14.92	15.64	22.00	20.51	20.07
MnO	-	0.01	-	-	-	0.08	0.01	-	0.08	0.11	0.05	0.10	0.06	-	-	0.04	0.06	0.02	-	0.02	-	-	0.01	-	0.01
MgO	10.63	11.08	10.67	10.57	11.97	11.14	11.27	11.47	12.35	11.42	11.90	11.32	11.33	15.36	15.86	16.15	16.38	11.82	9.32	12.30	11.21	11.07	8.45	10.77	10.81
CaO	0.02	0.02	0.10	0.04	0.01	-	0.01	-	0.01	0.07	-	-	0.01	0.04	0.01	0.08	0.10	0.01	0.02	0.05	0.01	0.06	0.09	0.04	0.04
Na2O	0.06	0.08	0.27	0.62	0.04	0.11	0.13	0.12	0.09	0.31	0.22	0.20	0.19	0.11	0.07	0.10	0.07	0.12	0.09	0.05	0.19	0.10	0.04	0.13	0.17
K2O	9.42	9.43	9.49	9.28	8.50	8.93	9.18	8.67	8.98	9.04	9.66	9.55	9.38	8.83	9.23	9.16	9.10	9.16	9.32	9.13	9.28	6.75	9.09	9.02	9.08
H2O	3.98	4.33	3.89	3.96	3.96	3.98	3.90	3.93	3.95	3.99	4.05	4.04	3.99	4.04	4.06	4.11	4.11	3.99	3.98	1.98	4.06	4.12	3.78	3.98	3.99
Total	100.03	101.86	99.07	100.09	99.06	98.83	99.39	97.82	99.68	99.65	100.64	100.37	99.89	99.18	99.41	100.31	100.42	99.42	97.02	98.75	99.58	99.52	97.62	100.47	100.38
#Si IV	5.54	5.48	5.44	5.52	5.55	5.52	5.44	5.61	5.35	5.39	5.53	5.58	5.53	5.60	5.68	5.77	5.62	5.59	5.71	5.59	5.49	6.11	5.27	5.46	5.52
#Al IV	2.46	2.52	2.56	2.48	2.45	2.48	2.56	2.39	2.65	2.61	2.47	2.42	2.47	2.40	2.32	2.23	2.38	2.41	2.29	2.41	2.51	1.89	2.73	2.54	2.48
#Fe IV	-	-	-	-	-	-	-	-	-	-	-	-	-	-	-	-	-	-	-	-	-	-	-	-	-
#Ti IV	-	-	-	-	-	-	-	-	-	-	-	-	-	-	-	-	-	-	-	-	-	-	-	-	-
T site	8.00	8.00	8.00	8.00	8.00	8.00	8.00	8.00	8.00	8.00	8.00	8.00	8.00	8.00	8.00	8.00	8.00	8.00	8.00	8.00	8.00	8.00	8.00	8.00	8.00
#Al VI	0.70	0.58	0.63	0.65	0.66	0.85	0.89	0.74	0.62	0.84	0.79	0.87	0.77	0.51	0.44	0.48	0.47	0.73	0.88	0.89	1.11	1.15	0.84	0.71	0.70
#Ti VI	0.21	0.19	0.19	0.18	0.15	0.18	0.16	0.15	0.15	0.15	0.15	0.15	0.15	0.16	0.18	0.14	0.17	0.16	0.16	0.16	0.15	0.11	0.16	0.16	0.17
#Cr	-	-	-	-	-	-	-	-	-	-	-	-	-	-	-	-	-	-	-	-	0.06	0.06	-	-	-
#Fe +3	-	0.00	0.00	-	0.00	0.00	-	-	0.00	-	0.00	0.00	-	-	-	-	0.00	-	-	0.00	0.00	0.00	-	-	-
#Fe +2	2.45	2.51	2.54	2.54	2.41	2.21	2.24	2.32	2.42	2.25	2.16	2.16	2.30	1.85	1.76	1.72	1.69	2.25	2.37	2.70	1.84	1.89	2.89	2.58	2.52
#Mn +2	-	0.00	-	-	-	0.01	0.00	-	0.01	0.01	0.01	0.01	0.01	-	-	0.00	0.01	0.00	-	0.00	-	-	0.00	-	0.00
#Mg	2.39	2.44	2.44	2.38	2.70	2.50	2.53	2.61	2.78	2.56	2.63	2.50	2.53	3.40	3.49	3.51	3.56	2.65	2.14	2.88	2.46	2.38	1.98	2.42	2.42
O site	5.75	5.73	5.80	5.75	5.92	5.76	5.82	5.81	5.99	5.82	5.74	5.70	5.77	5.93	5.88	5.85	5.91	5.79	5.56	6.63	5.62	5.60	5.87	5.87	5.82
#Ca	0.00	0.00	0.02	0.01	0.00	-	0.00	-	0.00	0.01	-	-	0.00	0.01	0.00	0.01	0.02	0.00	0.00	0.01	0.00	0.01	0.02	0.01	0.01
#Na	0.02	0.02	0.08	0.18	0.01	0.03	0.04	0.04	0.03	0.09	0.06	0.06	0.06	0.03	0.02	0.03	0.02	0.03	0.03	0.02	0.05	0.03	0.01	0.04	0.05
#K	1.81	1.78	1.86	1.79	1.64	1.72	1.76	1.69	1.73	1.73	1.83	1.81	1.79	1.67	1.74	1.70	1.69	1.75	1.83	1.83	1.75	1.24	1.82	1.73	1.74
A site	1.83	1.81	1.95	1.98	1.65	1.75	1.80	1.72	1.76	1.83	1.89	1.87	1.85	1.71	1.76	1.75	1.73	1.79	1.86	1.86	1.80	1.28	1.85	1.78	1.80
#O	20.00	19.73	20.02	20.00	20.01	20.00	20.09	20.00	20.02	20.01	20.00	20.00	20.01	20.00	20.00	20.00	20.00	20.00	19.91	21.92	20.01	20.03	20.04	20.00	20.00
#OH	4.00	4.27	3.98	4.00	3.99	4.00	3.91	4.00	3.98	3.99	4.00	4.00	3.99	4.00	4.00	4.00	4.00	4.00	4.09	2.08	3.99	3.97	3.96	4.00	4.00
Charge	0.00	-2E-06	-2E-06	0.00	-2E-06	-3E-06	-	0.00	0.00	0.00	-	-2E-06	0.00	-5E-07	0.00	0.00	-1E-06	0.00	-1E-06	0.00	0.00	-1E-06	0.00	0.00	-5E-07

MUSCOVITE ANALYSES, ATIK LAKE

	I-1-A	I-1-B	I-1-C	I-1-D	I-1-E	U-4-A	U-4-B	U-4-C	U-4-D	U-4-E
SiO2	46.49	46.22	47.65	52.30	52.30	47.22	47.79	46.93	47.41	43.07
TiO2	0.78	0.41	1.38	0.88	0.88	0.04	0.02	0.04	0.13	0.78
Al2O3	31.60	33.51	31.83	29.51	29.51	37.68	37.51	37.21	36.81	34.26
Cr2O3	-	-	-	-	-	0.02	-	0.04	0.02	0.08
Fe2O3	-	0.00	-	-	0.00	0.05	0.06	-	-	0.01
FeO	1.68	1.76	1.39	0.88	0.87	0.80	0.94	1.12	1.16	5.74
MnO	-	-	-	-	-	-	0.01	0.01	0.02	0.05
MgO	1.83	1.26	1.74	1.16	1.15	0.62	0.70	0.85	0.80	2.63
CaO	0.07	-	0.00	-	-	0.01	-	0.01	-	-
Na2O	0.13	0.44	0.30	0.12	0.12	0.78	0.76	0.81	0.77	0.69
K2O	10.23	9.77	10.34	9.21	9.21	9.69	8.75	9.75	9.54	9.23
H2O	4.51	4.52	4.52	4.60	4.60	4.62	4.63	4.61	4.61	4.45
Total	97.32	97.89	99.16	98.66	98.65	101.54	101.18	101.38	101.27	100.99
#Si IV	6.36	6.26	6.38	6.91	6.91	6.12	6.18	6.11	6.17	5.80
#Al IV	1.64	1.74	1.62	1.09	1.09	1.88	1.82	1.89	1.83	2.20
#Fe IV	-	-	-	-	-	-	-	-	-	-
#Ti IV	-	-	-	-	-	-	-	-	-	-
T site	8.00	8.00	8.00	8.00	8.00	8.00	8.00	8.00	8.00	8.00
#Al VI	3.45	3.62	3.40	3.50	3.50	3.88	3.90	3.82	3.81	3.24
#Ti VI	0.08	0.04	0.14	0.09	0.09	0.00	0.00	0.00	0.01	0.08
#Cr	-	-	-	-	-	0.00	-	0.00	0.00	0.01
#Fe +3	-	0.00	-	-	0.00	0.01	0.01	-	-	0.00
#Fe +2	0.19	0.20	0.16	0.10	0.10	0.09	0.10	0.12	0.13	0.65
#Mn +2	-	-	-	-	-	-	0.00	0.00	0.00	0.01
#Mg	0.37	0.25	0.35	0.23	0.23	0.12	0.13	0.16	0.16	0.53
O site	4.10	4.11	4.05	3.92	3.92	4.10	4.14	4.12	4.11	4.51
#Ca	0.01	-	0.00	-	-	0.00	-	0.00	-	-
#Na	0.03	0.12	0.08	0.03	0.03	0.20	0.19	0.20	0.19	0.18
#K	1.78	1.69	1.77	1.55	1.55	1.60	1.44	1.62	1.58	1.59
A site	1.83	1.81	1.84	1.58	1.58	1.80	1.63	1.83	1.78	1.77
#O	20.00	20.00	20.00	20.00	20.00	20.01	20.01	20.00	20.00	20.00
#OH	4.00	4.00	4.00	4.00	4.00	3.99	3.99	4.00	4.00	4.00
Charge	-	-	0.00	0.00	-	0.00	0.00	0.00	0.00	0.00

	U-4-F	U-4-G	U-4-H	U-4-I	U192A	U192B	U40C1
SiO2	47.48	47.24	47.17	46.42	50.35	49.89	50.27
TiO2	0.04	0.13	0.06	0.07	0.04	0.02	-
Al2O3	37.39	37.03	36.25	36.16	31.17	32.82	32.91
Cr2O3	-	0.01	0.04	-	-	-	-
Fe2O3	0.03	0.03	0.03	-	0.05	0.03	0.03
FeO	1.03	0.84	1.03	0.93	0.91	0.85	1.25
MnO	-	0.01	-	-	0.06	0.06	0.02
MgO	0.68	0.46	0.63	0.46	1.73	1.62	0.74
CaO	0.01	-	0.01	0.03	-	0.01	0.17
Na2O	0.81	0.81	0.67	0.73	0.40	0.39	0.55
K2O	9.67	9.64	8.85	8.73	10.55	11.13	9.65
H2O	4.63	4.59	4.54	4.53	4.53	4.59	4.57
Total	101.76	100.78	99.28	98.06	99.80	101.41	100.15
#Si IV	6.15	6.17	6.23	6.20	6.66	6.51	6.59
#Al IV	1.85	1.83	1.77	1.80	1.34	1.49	1.41
#Fe IV	-	-	-	-	-	-	-
#Ti IV	-	-	-	-	-	-	-
T site	8.00	8.00	8.00	8.00	8.00	8.00	8.00
#Al VI	3.85	3.87	3.86	3.90	3.51	3.56	3.68
#Ti VI	0.00	0.01	0.01	0.01	0.00	0.00	-
#Cr	-	0.00	0.00	-	-	-	-
#Fe +3	0.00	0.00	0.00	-	0.01	0.00	0.00
#Fe +2	0.11	0.09	0.11	0.10	0.10	0.09	0.14
#Mn +2	-	0.00	-	-	0.01	0.01	0.00
#Mg	0.13	0.09	0.12	0.09	0.34	0.32	0.14
O site	4.10	4.06	4.12	4.10	3.97	3.98	3.96
#Ca	0.00	-	0.00	0.00	-	0.00	0.02
#Na	0.20	0.21	0.17	0.19	0.10	0.10	0.14
#K	1.60	1.61	1.49	1.49	1.78	1.85	1.61
A site	1.80	1.81	1.66	1.68	1.88	1.95	1.78
#O	20.00	20.00	20.00	19.96	20.01	20.00	20.00
#OH	4.00	4.00	4.00	4.04	3.99	4.00	4.00
Charge	-2E-06	0.00	0.00	0.04	-1E-06	-1E-06	-

Vanadiferous zincian-chromian hercynite analyses, Atik Lake

	A10A	A10B	A10C	A10D	A10E	A10F	A10G	A10H	A10I	A10J	A10BF	A10BG	A10BH	A10BI	A10BJ	A10BK	A10BL	A10BM	A04A	A04B
SiO2	0.05	0.07	0.09	0.03	0.07	0.12	0.07	0.08	0.10	0.06	0.09	0.10	0.10	0.07	0.03	0.04	0.09	0.12	0.13	0.14
TiO2	-	-	-	-	-	-	-	-	-	-	-	-	-	-	-	-	-	-	0.09	0.06
Al2O3	46.31	44.33	44.18	45.84	42.37	40.93	42.75	41.46	41.42	45.31	34.19	32.81	35.68	40.22	41.32	39.94	40.34	38.53	44.98	47.08
Cr2O3	12.72	14.86	14.21	13.62	16.30	17.76	15.56	17.13	18.01	13.59	23.78	24.29	22.74	17.41	16.85	17.47	17.30	19.33	13.43	10.94
V2O3	1.43	1.51	1.51	1.56	1.60	1.47	1.63	1.69	1.60	1.55	3.11	3.36	3.14	3.11	3.17	3.19	3.01	3.16	1.56	1.51
Fe2O3	-	-	-	-	-	-	0.63	0.29	-	0.07	-	0.78	-	-	-	-	-	-	-	-
FeO	26.57	25.68	26.21	27.15	27.44	26.62	27.82	28.46	28.89	27.80	27.61	28.23	27.14	28.14	27.26	27.04	28.42	27.69	24.96	23.05
MgO	1.53	1.26	1.35	1.38	1.28	1.11	1.33	1.08	1.10	1.54	0.80	0.81	0.77	1.18	1.20	1.17	1.22	1.08	1.25	1.23
MnO	0.10	0.12	0.04	0.10	0.09	0.07	-	0.06	0.18	0.15	-	-	0.08	-	-	-	-	0.01	-	-
ZnO	10.19	9.37	9.89	9.83	8.58	8.46	9.23	8.60	7.86	9.30	7.55	7.29	7.96	7.89	7.81	7.59	7.43	6.77	12.94	14.36
Total	98.90	97.20	97.48	99.51	97.73	96.54	99.02	98.85	99.16	99.37	97.13	97.67	97.61	98.02	97.64	96.44	97.81	96.69	99.34	98.37
#Si+4	0.00	0.00	0.00	0.00	0.00	0.00	0.00	0.00	0.00	0.00	0.00	0.00	0.00	0.00	0.00	0.00	0.00	0.00	0.00	0.00
#Ti+4	-	-	-	-	-	-	-	-	-	-	-	-	-	-	-	-	-	-	0.00	0.00
#Al+3	1.67	1.63	1.62	1.65	1.57	1.54	1.56	1.53	1.52	1.63	1.32	1.27	1.36	1.50	1.53	1.50	1.50	1.45	1.63	1.71
#Cr+3	0.31	0.37	0.35	0.33	0.40	0.45	0.38	0.42	0.44	0.33	0.61	0.63	0.58	0.43	0.42	0.44	0.43	0.49	0.33	0.27
#V	0.04	0.04	0.04	0.04	0.04	0.04	0.04	0.04	0.04	0.04	0.08	0.09	0.08	0.08	0.08	0.08	0.08	0.08	0.04	0.04
#Fe+3	-	-	-	-	-	-	0.01	0.01	-	0.00	-	0.02	-	-	-	-	-	-	-	-
#Fe+2	0.68	0.67	0.68	0.69	0.72	0.71	0.72	0.74	0.75	0.71	0.75	0.77	0.73	0.74	0.72	0.72	0.75	0.74	0.64	0.59
#Mg+2	0.07	0.06	0.06	0.06	0.06	0.05	0.06	0.05	0.05	0.07	0.04	0.04	0.04	0.06	0.06	0.06	0.06	0.05	0.06	0.06
#Mn+2	0.00	0.00	0.00	0.00	0.00	0.00	-	0.00	0.00	0.00	-	-	0.00	-	-	-	-	0.00	-	-
#Zn+2	0.23	0.22	0.23	0.22	0.20	0.20	0.21	0.20	0.18	0.21	0.18	0.18	0.19	0.18	0.18	0.18	0.17	0.16	0.29	0.33
#TOTAL	2.99	2.98	2.99	2.99	2.99	2.99	3.00	3.00	3.00	3.00	2.99	3.00	2.99	2.99	2.98	2.99	2.99	2.98	3.00	2.99
#O-2	4.00	4.00	4.00	4.00	4.00	4.00	4.00	4.00	4.00	4.00	4.00	4.00	4.00	4.00	4.00	4.00	4.00	4.00	4.00	4.00

	A10K	A10L	A10M	A10N	A10O	A10BA	A10BB	A10BC	A10BD	A10BE	A04C	A04D	A04E	A04F	A04G	A04H	A04I	A04J	A04K	A04L
SiO2	0.06	0.07	0.06	0.10	0.11	0.05	0.13	0.09	0.09	0.07	0.16	0.15	0.77	0.04	0.11	0.07	0.07	0.08	0.06	0.23
TiO2	-	-	-	-	-	-	-	-	-	-	0.06	0.04	0.04	0.03	0.04	-	0.13	0.12	0.04	0.23
Al2O3	45.75	44.78	43.69	45.28	37.47	32.35	34.97	31.58	41.18	40.88	47.98	47.99	41.56	46.54	48.23	46.80	52.47	49.08	54.44	50.01
Cr2O3	12.87	13.84	14.70	13.10	20.52	24.18	23.02	23.87	17.32	17.59	10.51	10.47	13.26	12.07	10.51	11.63	6.38	9.24	5.05	8.36
V2O3	1.46	1.42	1.52	1.38	3.79	4.25	3.19	4.54	2.90	2.92	1.38	1.32	1.81	1.31	1.27	1.40	1.79	1.99	1.79	2.04
Fe2O3	0.44	1.03	1.07	0.89	-	1.22	0.19	2.08	-	-	-	-	0.31	-	-	-	-	0.08	-	-
FeO	27.63	28.23	28.18	27.63	25.86	29.39	28.84	29.26	27.51	26.58	23.77	23.29	23.42	23.89	23.47	24.91	21.17	22.98	19.93	21.34
MgO	1.74	1.58	1.62	1.61	0.96	0.79	0.88	0.74	1.19	1.21	1.32	1.33	1.07	1.59	1.65	1.51	2.14	1.80	2.05	1.80
MnO	0.17	0.14	0.10	0.10	0.05	-	-	-	-	0.04	-	-	-	-	-	-	-	-	0.01	-
ZnO	9.20	8.92	8.58	9.54	9.14	6.10	7.16	6.15	8.61	8.69	14.64	14.76	13.23	12.95	14.24	12.79	17.20	15.63	17.07	16.91
Total	99.32	100.01	99.52	99.63	97.90	98.33	98.38	98.31	98.80	97.98	99.82	99.35	95.47	98.42	99.52	99.11	101.35	101.00	100.44	100.92
#Si+4	0.00	0.00	0.00	0.00	0.00	0.00	0.00	0.00	0.00	0.00	0.00	0.00	0.02	0.00	0.00	0.00	0.00	0.00	0.00	0.01
#Ti+4	-	-	-	-	-	-	-	-	-	-	0.00	0.00	0.00	0.00	0.00	-	0.00	0.00	0.00	0.01
#Al+3	1.64	1.61	1.58	1.63	1.41	1.24	1.33	1.22	1.51	1.51	1.71	1.72	1.58	1.69	1.72	1.69	1.81	1.73	1.87	1.75
#Cr+3	0.31	0.33	0.36	0.32	0.52	0.62	0.59	0.62	0.43	0.44	0.25	0.25	0.34	0.29	0.25	0.28	0.15	0.22	0.12	0.20
#V	0.04	0.03	0.04	0.03	0.10	0.11	0.08	0.12	0.07	0.07	0.03	0.03	0.05	0.03	0.03	0.03	0.04	0.05	0.04	0.05
#Fe+3	0.01	0.02	0.02	0.02	-	0.03	0.00	0.05	-	-	-	-	0.01	-	-	-	-	0.00	-	-
#Fe+2	0.70	0.72	0.72	0.71	0.69	0.80	0.78	0.80	0.72	0.70	0.60	0.59	0.63	0.61	0.59	0.64	0.52	0.57	0.49	0.53
#Mg+2	0.08	0.07	0.07	0.07	0.05	0.04	0.04	0.04	0.06	0.06	0.06	0.06	0.05	0.07	0.07	0.07	0.09	0.08	0.09	0.08
#Mn+2	0.00	0.00	0.00	0.00	0.00	-	-	-	-	0.00	-	-	-	-	-	-	-	-	0.00	-
#Zn+2	0.21	0.20	0.19	0.21	0.22	0.15	0.17	0.15	0.20	0.20	0.33	0.33	0.31	0.29	0.32	0.29	0.37	0.34	0.37	0.37
#TOTAL	3.00	3.00	3.00	3.00	2.98	2.99	3.00	2.99	2.99	2.99	2.99	2.99	2.99	2.99	2.99	3.00	2.99	3.00	2.98	2.99
#O-2	4.00	4.00	4.00	4.00	4.00	4.00	4.00	4.00	4.00	4.00	4.00	4.00	4.00	4.00	4.00	4.00	4.00	4.00	4.00	4.00

	A08A	A08B	A08C	A08D	A08E	A08F	A08G	A08H	A12A	A12B
SiO2	0.13	0.06	0.09	0.09	0.35	0.10	0.10	0.18	0.07	0.08
TiO2	0.02	0.03	0.09	0.04	0.04	0.03	0.04	0.05	0.10	0.06
Al2O3	41.69	43.47	36.43	36.45	39.58	38.87	38.85	39.56	38.74	40.03
Cr2O3	16.18	14.86	16.72	17.13	17.00	17.28	18.99	17.74	16.13	14.79
V2O3	1.30	1.23	5.72	5.59	3.07	3.14	1.50	1.42	2.66	2.65
Fe2O3	1.28	1.36	2.00	1.14	-	-	-	-	4.14	3.34
FeO	27.06	26.60	29.61	29.48	26.96	26.77	27.78	26.97	33.61	33.46
MgO	1.34	1.47	0.75	0.73	0.93	0.82	1.05	1.07	0.86	0.96
MnO	-	-	-	-	-	-	-	-	-	-
ZnO	10.02	10.97	7.19	7.10	9.86	9.35	8.49	8.97	3.32	3.20
Total	99.02	100.05	98.60	97.75	97.79	96.36	96.80	95.96	99.63	98.57
#Si+4	0.00	0.00	0.00	0.00	0.01	0.00	0.00	0.01	0.00	0.00
#Ti+4	0.00	0.00	0.00	0.00	0.00	0.00	0.00	0.00	0.00	0.00
#Al+3	1.53	1.57	1.38	1.39	1.48	1.48	1.47	1.51	1.43	1.48
#Cr+3	0.40	0.36	0.42	0.44	0.43	0.44	0.48	0.45	0.40	0.37
#V	0.03	0.03	0.15	0.14	0.08	0.08	0.04	0.04	0.07	0.07
#Fe+3	0.03	0.03	0.05	0.03	-	-	-	-	0.10	0.08
#Fe+2	0.71	0.68	0.79	0.80	0.72	0.72	0.75	0.73	0.88	0.88
#Mg+2	0.06	0.07	0.04	0.04	0.04	0.04	0.05	0.05	0.04	0.04
#Mn+2	-	-	-	-	-	-	-	-	-	-
#Zn+2	0.23	0.25	0.17	0.17	0.23	0.22	0.20	0.21	0.08	0.07
#TOTAL	3.00	3.00	3.00	3.00	2.99	2.99	3.00	3.00	3.00	3.00
#O-2	4.00	4.00	4.00	4.00	4.00	4.00	4.00	4.00	4.00	4.00

	A12C	A12D	A12E	A12F	A17A	A17B	A17C	A17D	A17E	A17F	A17G	A17H	A17I	A17J	A17K	A17L
SiO2	0.08	0.06	0.04	0.07	0.14	0.13	0.20	0.03	0.07	0.09	0.13	0.06	0.09	0.16	0.10	0.47
TiO2	0.08	0.19	0.09	0.12	0.13	0.15	0.15	0.10	0.13	0.11	0.09	0.09	0.06	0.16	0.05	0.10
Al2O3	39.01	37.59	36.28	36.52	31.41	29.29	28.79	29.95	29.64	29.05	31.70	33.53	33.47	33.08	33.16	33.50
Cr2O3	15.54	16.16	17.02	16.69	23.74	25.27	25.97	25.71	25.38	25.10	22.89	22.42	22.09	22.66	23.52	23.24
V2O3	2.71	3.40	3.28	3.35	2.16	2.07	2.16	2.69	2.63	2.53	1.91	2.02	2.09	1.91	1.07	1.03
Fe2O3	2.49	3.71	4.77	3.92	4.30	3.93	4.26	4.36	4.75	5.05	4.51	3.96	3.88	4.01	3.63	2.72
FeO	32.73	33.81	33.61	33.55	31.17	31.01	31.31	32.14	31.76	31.13	31.40	31.01	31.28	31.35	31.39	31.03
MgO	0.85	0.67	0.63	0.61	0.51	0.44	0.39	0.51	0.55	0.56	0.54	0.60	0.63	0.57	0.62	0.81
MnO	-	-	-	-	-	-	-	-	-	-	-	-	-	-	-	-
ZnO	3.51	2.74	2.98	2.73	4.97	4.20	4.20	3.92	4.05	4.26	4.36	5.56	5.05	5.15	4.78	4.69
Total	97.00	98.33	98.70	97.56	98.53	96.49	97.43	99.41	98.96	97.88	97.53	99.25	98.64	99.05	98.32	97.59
#Si+4	0.00	0.00	0.00	0.00	0.00	0.00	0.01	0.00	0.00	0.00	0.00	0.00	0.00	0.01	0.00	0.02
#Ti+4	0.00	0.00	0.00	0.00	0.00	0.00	0.00	0.00	0.00	0.00	0.00	0.00	0.00	0.00	0.00	0.00
#Al+3	1.47	1.41	1.37	1.39	1.21	1.16	1.13	1.15	1.15	1.14	1.23	1.28	1.28	1.26	1.27	1.29
#Cr+3	0.39	0.41	0.43	0.43	0.61	0.67	0.69	0.66	0.66	0.66	0.60	0.57	0.57	0.58	0.61	0.60
#V	0.07	0.09	0.08	0.09	0.06	0.06	0.06	0.07	0.07	0.07	0.05	0.05	0.05	0.05	0.03	0.03
#Fe+3	0.06	0.09	0.11	0.10	0.11	0.10	0.11	0.11	0.12	0.13	0.11	0.10	0.09	0.10	0.09	0.07
#Fe+2	0.88	0.90	0.90	0.90	0.85	0.87	0.88	0.88	0.87	0.87	0.87	0.84	0.85	0.85	0.85	0.85
#Mg+2	0.04	0.03	0.03	0.03	0.02	0.02	0.02	0.02	0.03	0.03	0.03	0.03	0.03	0.03	0.03	0.04
#Mn+2	-	-	-	-	-	-	-	-	-	-	-	-	-	-	-	-
#Zn+2	0.08	0.06	0.07	0.06	0.12	0.10	0.10	0.09	0.10	0.10	0.11	0.13	0.12	0.12	0.11	0.11
#TOTAL	3.00	3.00	3.00	3.00	3.00	3.00	3.00	3.00	3.00	3.00	3.00	3.00	3.00	3.00	3.00	2.99
#O-2	4.00	4.00	4.00	4.00	4.00	4.00	4.00	4.00	4.00	4.00	4.00	4.00	4.00	4.00	4.00	4.00

Ilmenite analyses, Atik Lake

	U08A	U12A	U12B	U12C	U12D	U12E	U12F	U12G	U17A	U17B	U17C	U17D	U17E	U17F
FeO	44.80	44.32	44.17	43.98	43.95	44.41	45.16	44.96	44.87	45.45	44.53	44.32	44.49	45.39
Fe2O3	0.81	-	-	2.50	-	-	-	-	-	1.02	1.69	1.20	-	-
MgO	0.30	0.07	0.04	0.12	0.32	0.05	0.03	0.13	0.17	0.17	0.08	0.11	0.16	0.20
V2O3	3.63	3.08	3.57	2.92	4.19	3.97	3.23	3.64	2.80	2.89	2.81	2.74	3.72	3.38
Cr2O3	0.12	0.05	0.13	0.24	0.16	0.07	0.04	0.13	0.63	0.10	0.07	0.10	0.09	0.06
MnO	0.32	0.22	0.22	0.29	0.49	0.58	0.51	0.38	0.56	0.54	0.45	0.48	0.69	0.59
TiO2	50.69	50.39	50.45	49.21	49.89	50.58	50.80	49.87	50.63	51.42	50.12	49.76	51.27	51.46
Total	100.67	98.13	98.58	99.26	99.00	99.66	99.77	99.11	99.66	101.59	99.75	98.71	100.42	101.08
#Fe+2	1.88	1.90	1.89	1.87	1.87	1.88	1.91	1.92	1.90	1.89	1.89	1.90	1.86	1.89
#Fe+3	0.03	-	-	0.10	-	-	-	-	-	0.04	0.06	0.05	-	-
#Mg+2	0.02	0.01	0.00	0.01	0.02	0.00	0.00	0.01	0.01	0.01	0.01	0.01	0.01	0.01
#V	0.15	0.13	0.15	0.12	0.17	0.16	0.13	0.15	0.11	0.12	0.11	0.11	0.15	0.14
#Cr+3	0.00	0.00	0.01	0.01	0.01	0.00	0.00	0.01	0.03	0.00	0.00	0.00	0.00	0.00
#Mn+2	0.01	0.01	0.01	0.01	0.02	0.02	0.02	0.02	0.02	0.02	0.02	0.02	0.03	0.02
#Ti+4	1.91	1.94	1.94	1.88	1.91	1.92	1.93	1.91	1.93	1.92	1.91	1.91	1.93	1.93
#TOTAL	4.00	3.99	3.99	4.00	4.00	3.99	4.00	4.01	4.00	4.00	4.00	4.00	3.99	4.00
#O-2	6.00	6.00	6.00	6.00	6.00	6.00	6.00	6.00	6.00	6.00	6.00	6.00	6.00	6.00

Magnetite analyses, Atik Lake

	U12A	U12B	U12C	U12D
FeO	31.91	32.50	31.84	33.31
Fe2O3	39.41	36.63	38.62	34.13
ZnO	0.13	-	0.10	0.11
Al2O3	2.39	2.51	2.30	2.23
MgO	-	-	-	0.02
V2O3	16.64	17.12	16.95	16.97
SiO2	0.09	0.09	0.09	0.11
Cr2O3	6.94	7.05	7.01	7.11
MnO	0.02	0.11	0.04	-
TiO2	0.82	1.56	0.86	2.79
Total	98.35	97.57	97.81	96.78
#Fe+2	1.02	1.04	1.02	1.07
#Fe+3	1.13	1.05	1.11	0.99
#Zn+2	0.00	-	0.00	0.00
#Al+3	0.11	0.11	0.10	0.10
#Mg+2	-	-	-	0.00
#V	0.51	0.53	0.52	0.52
#Si+4	0.00	0.00	0.00	0.00
#Cr+3	0.21	0.21	0.21	0.22
#Mn+2	0.00	0.00	0.00	-
#Ti+4	0.02	0.04	0.02	0.08
#TOTAL	3.00	3.00	3.00	3.00
#O-2	4.00	4.00	4.00	4.00

Olivine analyses, Atik Lake

	U184A	U184B	U184C
SiO2	33.16	31.85	30.96
Al2O3	-	0.02	-
TiO2	-	0.02	-
FeO	66.48	65.88	69.02
MnO	0.11	0.18	0.12
MgO	0.06	0.04	0.01
ZnO	0.05	0.04	0.05
CaO	0.07	0.04	0.03
Na2O	0.02	0.25	0.13
TOTAL	99.95	98.32	100.32
#Si+4	1.09	1.07	1.03
#Al+3	-	0.00	-
#Ti+4	-	0.00	-
#Fe+2	1.82	1.85	1.92
#Mn+2	0.00	0.01	0.00
#Mg+2	0.00	0.00	0.00
#Zn+2	0.00	0.00	0.00
#Ca+2	0.00	0.00	0.00
#Na+1	0.00	0.02	0.01
#TOTAL	2.92	2.94	2.97
#O-2	4.00	4.00	4.00

Tourmaline analyses, Atik Lake

	I-1A-1	I-1A-2	I-1A-3	I-1A-4	I-1A-5	I-1A-6	U-04-1	U-04-2	-21-1A	-21-1B
NA2O	1.98	2.18	2.01	1.92	2.04	1.84	1.28	1.16	1.94	1.94
MGO	8.90	10.55	8.77	8.48	8.55	7.84	6.28	7.12	4.14	4.12
AL2O3	35.18	34.83	33.48	35.03	35.75	34.80	31.09	29.63	33.17	32.75
SIO2	38.08	38.65	38.12	38.83	38.02	37.91	35.70	35.84	35.85	35.46
CAO	0.92	1.20	1.10	0.84	0.74	0.62	1.00	1.76	0.29	0.27
FEO	1.85	1.18	4.16	3.74	3.53	3.79	6.19	6.23	10.48	11.21
MNO	-	-	-	-	-	-	-	-	-	-
TIO2	-	-	-	-	-	-	0.30	0.73	0.70	0.60
TOTAL	86.91	88.59	87.64	88.84	88.63	86.80	81.84	82.46	86.57	86.36

	-21-1C	-21-1D
NA2O	1.93	2.05
MGO	4.74	5.25
AL2O3	34.16	33.39
SIO2	36.12	36.08
CAO	0.14	0.25
FEO	9.10	8.56
MNO	0.06	-
TIO2	0.36	0.63
TOTAL	86.61	86.22

Arsenopyrite analyses, Atik Lake

SAMPLE	As	Fe	S	CO	NI	SB	TOT
UBI1A	0.325	0.314	0.335	0.007	0.008	0.004	0.995
	0.317	0.322	0.348	0.005	0.000	0.003	0.993
	0.324	0.315	0.338	0.008	0.004	0.004	0.992
	0.320	0.316	0.339	0.008	0.008	0.005	0.995
	0.332	0.307	0.333	0.007	0.011	0.005	0.995
	0.316	0.326	0.344	0.005	0.003		0.995
	0.328	0.322	0.329	0.006	0.009		0.994
	0.329	0.334	0.327	0.002	0.001		0.993
	0.335	0.331	0.325	0.002	0.000		0.993
	0.334	0.314	0.330	0.009	0.008		0.994
	0.335	0.314	0.331	0.007	0.008		0.994
	0.326	0.321	0.334	0.004	0.009		0.994
	0.318	0.322	0.346	0.009	0.000		0.995
POLY	0.311	0.343	0.346				1.000
	0.357	0.325	0.318				1.000
	0.350	0.332	0.318				1.000
	0.346	0.331	0.323				0.999
	0.355	0.321	0.324				1.000
	0.342	0.322	0.337				1.000
	0.335	0.337	0.328				1.000
	0.342	0.322	0.337				1.000
BI1B	0.321	0.336	0.341				0.999
POLY	0.325	0.337	0.337				1.000
	0.329	0.335	0.336				1.000
	0.327	0.336	0.337				1.000
U32	0.321	0.317	0.358				0.996
	0.319	0.313	0.362				0.995
U0805	0.337	0.314	0.337	0.001	0.005		0.994
	0.312	0.320	0.362	0.001	0.000		0.995
	0.317	0.318	0.360	0.000	0.001		0.995
	0.337	0.316	0.338	0.000	0.003		0.994
	0.346	0.315	0.329	0.001	0.002		0.994
	0.313	0.316	0.366	0.001	0.000		0.996
U3104	0.335	0.315	0.345	0.000	0.001		0.995
	0.337	0.319	0.337	0.000	0.001		0.994
	0.317	0.320	0.359	0.000	0.000		0.996
	0.336	0.318	0.340	0.000	0.001		0.994
	0.334	0.316	0.344	0.000	0.001		0.995
	0.312	0.320	0.364	0.000	0.000		0.996
	0.318	0.321	0.356	0.000	0.000		0.995
U2702	0.332	0.333	0.327	0.000	0.001		0.993
	0.332	0.335	0.325	0.000	0.001		0.993
	0.334	0.332	0.325	0.000	0.001		0.993
	0.330	0.332	0.331	0.000	0.001		0.993
	0.332	0.334	0.326	0.000	0.001		0.993
U0305	0.322	0.331	0.340	0.000	0.000		0.994
	0.315	0.328	0.352	0.000	0.000		0.995
	0.336	0.332	0.322	0.001	0.002		0.993
	0.317	0.334	0.343	0.000	0.000		0.994
	0.335	0.332	0.325	0.000	0.001		0.993
	0.337	0.332	0.322	0.000	0.002		0.993
POLY	0.358	0.330	0.312				1.000
	0.347	0.340	0.314				1.000
	0.343	0.335	0.313				0.990
	0.351	0.333	0.316				1.000
	0.355	0.333	0.313				1.000
	0.359	0.331	0.309				1.000
	0.350	0.337	0.313				1.000
	0.344	0.334	0.322				1.000
U0109	0.338	0.352	0.310				1.000
POLY	0.347	0.336	0.318				1.000
	0.347	0.339	0.314				1.000
	0.344	0.335	0.321				1.000
	0.348	0.335	0.317				1.000
	0.346	0.336	0.318				1.000
	0.347	0.337	0.316				1.000
	0.348	0.334	0.319				1.000
	0.347	0.334	0.319				1.000
	0.340	0.333	0.327				1.000
U38	0.309	0.319	0.368	0.001	0.000	0.000	0.997
	0.301	0.328	0.368	0.000	0.000	0.000	0.996
	0.300	0.327	0.368	0.001	0.000	0.001	0.996
	0.307	0.325	0.362	0.001	0.001	0.000	0.996
	0.301	0.322	0.372	0.001	0.000	0.001	0.997
	0.336	0.333	0.327	0.003	0.000		0.999
	0.335	0.330	0.331	0.002	0.001		0.999
U0506	0.350	0.331	0.319				1.000
	0.356	0.343	0.301				1.000
	0.356	0.331	0.312				1.000
	0.356	0.331	0.313				1.000
	0.347	0.337	0.316				1.000
	0.360	0.331	0.309				1.000
U-04	0.345	0.287	0.322	0.027	0.012	0.002	0.995
U-10A	0.322	0.319	0.347	0.005	0.001	0.001	0.995
	0.326	0.319	0.336	0.011	0.002	0.001	0.994
U43B	0.362	0.275	0.297	0.036	0.019	0.005	0.994
	0.337	0.298	0.322	0.026	0.008	0.003	0.994
	0.334	0.300	0.326	0.023	0.008	0.003	0.995
	0.352	0.285	0.310	0.030	0.015	0.003	0.994
	0.374	0.260	0.283	0.041	0.030	0.006	0.994
	0.365	0.281	0.292	0.036	0.020		0.993
	0.355	0.290	0.306	0.029	0.013		0.994
	0.343	0.304	0.313	0.025	0.009		0.994
	0.337	0.300	0.321	0.023	0.013		0.995
	0.354	0.297	0.300	0.030	0.012		0.993
	0.369	0.279	0.290	0.038	0.017		0.993
U10B	0.358	0.285	0.317	0.020	0.015		0.995
	0.344	0.296	0.327	0.013	0.015		0.995
	0.350	0.287	0.316	0.018	0.024		0.995
	0.330	0.316	0.333	0.000	0.015		0.994
	0.313	0.330	0.349	0.000	0.002		0.995
	0.330	0.313	0.334	0.001	0.018		0.995
	0.361	0.288	0.299	0.027	0.019		0.994
	0.356	0.293	0.303	0.027	0.016		0.994
	0.346	0.294	0.317	0.026	0.011		0.995
	0.404	0.271	0.278	0.024	0.014	0.002	0.992
	0.341	0.290	0.331	0.009	0.023	0.002	0.996
	0.350	0.279	0.322	0.019	0.023	0.002	0.996
	0.306	0.331	0.356	0.000	0.000	0.002	0.995
	0.308	0.325	0.361	0.001	0.000	0.001	0.996
	0.318	0.313	0.352	0.002	0.009	0.001	0.996
	0.315	0.324	0.355	0.000	0.002	0.000	0.995
FEAS.9S.	0.300	0.333	0.367				1.000
FEASS	0.333	0.333	0.333				0.999
FeAsS.85	0.383	0.333	0.283				1.000
STD555	0.335	0.323	0.332	0.005	0.002	0.002	1.000

Löllingite analyses, Atik Lake

SAMPLE	As	Fe	S	CO	NI	SB	TOT
theor	0.667	0.333	0.000				1.000
U-04	0.624	0.193	0.023	0.041	0.095	0.003	1.000
	0.622	0.196	0.021	0.040	0.096	0.003	1.000
	0.618	0.197	0.020	0.041	0.099	0.003	1.000
	0.619	0.189	0.018	0.044	0.106	0.003	1.000
	0.632	0.193	0.012	0.038	0.099	0.003	0.999
	0.620	0.178	0.022	0.058	0.098	0.004	1.000
	0.624	0.188	0.022	0.047	0.094	0.004	1.000
	0.618	0.163	0.024	0.065	0.106	0.005	1.000
	0.620	0.180	0.021	0.051	0.102	0.005	0.999
U-10A	0.625	0.180	0.019	0.032	0.119	0.003	0.999
	0.626	0.179	0.019	0.032	0.119	0.004	1.000
	0.621	0.191	0.019	0.053	0.092	0.002	0.999
	0.625	0.190	0.019	0.049	0.094	0.002	1.000
	0.618	0.190	0.022	0.030	0.113	0.005	1.000
U-10B	0.626	0.188	0.017	0.044	0.099	0.004	1.000
	0.623	0.187	0.022	0.044	0.098	0.005	1.000
	0.618	0.188	0.023	0.045	0.101	0.004	1.000
	0.623	0.186	0.020	0.044	0.102	0.004	1.000
	0.618	0.185	0.023	0.044	0.104	0.005	0.999
	0.634	0.171	0.025	0.045	0.100	0.005	1.000
	0.621	0.184	0.023	0.046	0.102	0.004	1.000
	0.625	0.184	0.020	0.044	0.101	0.005	1.000
	0.623	0.186	0.020	0.045	0.101	0.003	1.000
U-43B	0.612	0.194	0.031	0.043	0.095	0.005	1.000
	0.621	0.186	0.020	0.050	0.098	0.004	1.000
	0.624	0.207	0.019	0.047	0.081	0.002	1.002
U-43D	0.621	0.197	0.021	0.064	0.069	0.005	1.000
	0.618	0.199	0.020	0.066	0.069	0.005	1.000
	0.623	0.197	0.019	0.007	0.068	0.005	0.940

Gersdorffite analyses

SAMPLE							
U-10B	0.356	0.090	0.324	0.062	0.172	0.003	1.000
	0.363	0.087	0.314	0.059	0.179	0.003	1.000
	0.366	0.088	0.316	0.059	0.174	0.003	1.000

Ullmanite analyses

UBI1A	0.021	0.012	0.333	0.006	0.314	0.332	1.000
	0.018	0.014	0.346	0.003	0.309	0.325	0.996

Staurolite analyses, Atik Lake

Sample	U12A	U12B	U12C	U12D
SiO2	26.500	27.070	28.250	28.410
TiO2	0.450	0.420	0.430	0.450
Al2O3	53.970	53.670	53.530	54.020
Fe2O3*	1.173	1.176	1.189	1.198
FeO*	12.515	12.032	13.300	13.092
MnO	0.100	0.070	0.060	0.090
MgO	1.290	1.260	1.300	1.260
ZnO	0.660	0.570	0.730	0.690
H2O*	1.814	1.923	1.468	1.573
Total	98.471	98.191	100.258	100.783
Stoichiometry				
Si	7.507	7.650	7.894	7.876
AlIV	0.493	0.350	0.106	0.124
AlVI	17.530	17.530	17.530	17.530
Fe+3	0.250	0.250	0.250	0.250
Mn	0.024	0.017	0.014	0.021
Fe+2	0.226	0.233	0.236	0.229
Ti+4	0.096	0.089	0.090	0.094
Fe+2	2.739	2.610	2.873	2.806
Mg	0.545	0.531	0.541	0.521
Zn	0.138	0.119	0.151	0.141
Tet site	3.517	3.349	3.655	3.562
H+	3.427	3.633	2.775	2.973
O	48.000	48.000	48.000	48.000

NÉMISCAU

ANTHOPHYLLITE ANALYSES, NÉMISCAU

	S32AC	S32AR	S32R1	S32R2	N14AC	N14AR	N14BC	N14CC	N22C	N22R	S32BC	S32BR	S32CC	S36C1	S36C2	N16A	N16B	N20C1	N20C2	N26C1	SE3AR	SE3BC	SE3BR
SiO2	54.71	54.17	54.44	54.15	52.96	53.57	53.61	53.86	53.34	53.01	54.25	54.90	54.25	55.04	54.75	54.00	54.53	53.82	51.31	55.27	55.33	54.20	51.97
TiO2	0.03	0.03	0.05	0.02	0.09	0.02	0.06	0.03	0.05	0.03	0.06	0.06	0.07	0.03	-	0.07	0.08	0.08	0.19	0.06	0.05	0.02	0.06
Al2O3	0.67	0.96	0.96	1.00	3.06	2.59	2.89	2.48	1.48	1.52	1.91	0.99	1.35	1.48	2.07	1.89	2.03	4.81	8.54	1.67	6.06	2.74	5.45
Cr2O3	0.04	0.03	0.04	-	0.18	0.14	0.20	0.20	0.03	0.01	-	-	-	-	-	-	-	-	-	-	-	-	-
Fe2O3	-	-	0.01	-	-	-	-	-	-	-	0.02	-	-	0.01	-	0.13	0.01	0.00	-	-	-	0.00	-
FeO	25.04	24.75	25.18	24.63	23.95	24.53	23.66	24.60	25.19	24.90	24.84	24.96	24.94	22.11	21.45	24.78	24.76	19.94	19.54	24.13	17.75	19.65	19.54
MnO	0.85	0.71	0.81	0.76	0.29	0.27	0.33	0.32	0.56	0.48	0.67	0.75	0.77	0.89	0.79	0.41	0.39	0.23	0.24	0.53	0.64	0.93	0.73
MgO	17.02	16.59	16.65	16.66	16.75	17.13	16.66	17.52	16.59	16.66	16.61	16.87	16.81	19.27	18.70	17.22	16.71	19.14	17.89	17.08	18.55	20.75	19.37
ZnO	-	0.10	0.15	-	0.14	0.06	0.07	0.03	-	-	0.09	0.03	0.03	0.02	0.02	0.20	0.11	0.03	0.15	0.05	-	0.05	0.06
CaO	0.48	0.60	0.43	0.46	0.30	0.30	0.30	0.28	0.36	0.34	0.97	0.50	0.68	0.23	0.21	0.32	0.42	0.44	0.40	0.35	0.31	0.24	0.40
Na2O	0.04	0.04	0.05	0.02	0.30	0.24	0.30	0.25	0.10	0.09	0.14	0.06	0.08	-	0.11	0.36	0.22	0.46	0.94	0.26	0.40	0.28	0.60
K2O	-	-	-	0.02	-	0.02	0.01	-	0.01	-	0.02	0.03	-	-	-	0.02	-	0.01	-	-	-	-	-
H2O	2.06	2.04	2.06	2.04	2.05	2.07	2.06	2.08	2.03	2.02	2.08	2.07	2.06	2.10	2.08	2.09	2.08	2.12	2.12	2.09	2.15	2.11	2.09
Total	100.94	100.02	100.83	99.76	100.07	100.94	100.15	101.65	99.74	99.06	101.66	101.22	101.04	101.18	100.18	101.49	101.34	101.08	101.32	101.49	101.24	100.97	100.27
#Si IV	7.95	7.94	7.93	7.95	7.73	7.76	7.79	7.75	7.86	7.85	7.83	7.95	7.88	7.86	7.87	7.80	7.86	7.61	7.25	7.93	7.70	7.70	7.45
#Al IV	0.05	0.06	0.07	0.05	0.27	0.24	0.21	0.25	0.14	0.15	0.17	0.05	0.12	0.14	0.13	0.20	0.14	0.39	0.75	0.07	0.30	0.30	0.55
#Fe +3	-	-	-	-	-	-	-	-	-	-	-	-	-	-	-	-	-	-	-	-	-	-	-
#Ti IV	-	-	-	-	-	-	-	-	-	-	-	-	-	-	-	-	-	-	-	-	-	-	-
T site	8.00	8.00	8.00	8.00	8.00	8.00	8.00	8.00	8.00	8.00	8.00	8.00	8.00	8.00	8.00	8.00	8.00	8.00	8.00	8.00	8.00	8.00	8.00
#Al VI	0.07	0.11	0.09	0.12	0.25	0.20	0.29	0.17	0.11	0.12	0.16	0.11	0.11	0.11	0.22	0.12	0.21	0.41	0.68	0.21	0.70	0.15	0.37
#Fe +3	-	-	0.00	-	-	-	-	-	-	-	0.00	-	-	0.00	-	0.01	0.00	0.00	-	-	-	0.00	-
#Ti	0.00	0.00	0.01	0.00	0.01	0.00	0.01	0.00	0.01	0.00	0.01	0.01	0.01	0.00	-	0.01	0.01	0.01	0.02	0.01	0.01	0.00	0.01
#Cr	0.00	0.00	0.00	-	0.02	0.02	0.02	0.02	0.00	0.00	-	-	-	-	-	-	-	-	-	-	-	-	-
#Mg	3.69	3.63	3.62	3.65	3.64	3.70	3.61	3.76	3.64	3.68	3.57	3.64	3.64	4.10	4.01	3.71	3.59	4.04	3.77	3.65	3.85	4.39	4.14
#Fe +2	1.24	1.26	1.28	1.23	1.07	1.08	1.07	1.05	1.23	1.20	1.26	1.24	1.24	0.78	0.77	1.15	1.19	0.54	0.53	1.13	0.45	0.45	0.49
#Zn	-	-	-	-	-	-	-	-	-	-	-	-	-	-	-	-	-	-	-	-	-	-	-
#Mn	-	-	-	-	-	-	-	-	-	-	-	-	-	-	-	-	-	-	-	-	-	-	-
#Ca	-	-	-	-	-	-	-	-	-	-	-	-	-	-	-	-	-	-	-	-	-	-	-
M1,2,3	5.00	5.00	5.00	5.00	5.00	5.00	5.00	5.00	5.00	5.00	5.00	5.00	5.00	5.00	5.00	5.00	5.00	5.00	5.00	5.00	5.00	5.00	5.00
#Mg	-	-	-	-	-	-	-	-	-	-	-	-	-	-	-	-	-	-	-	-	-	-	-
#Fe +2	1.80	1.77	1.79	1.79	1.85	1.89	1.80	1.91	1.87	1.89	1.74	1.78	1.79	1.86	1.81	1.85	1.80	1.82	1.78	1.76	1.62	1.88	1.85
#Zn	-	0.01	0.02	-	0.02	0.01	0.01	0.00	-	-	0.01	0.00	0.00	0.00	0.00	0.02	0.01	0.00	0.02	0.01	-	0.01	0.01
#Mn	0.10	0.09	0.10	0.09	0.04	0.03	0.04	0.04	0.07	0.06	0.08	0.09	0.09	0.11	0.10	0.05	0.05	0.03	0.03	0.06	0.08	0.11	0.09
#Ca	0.07	0.09	0.07	0.07	0.05	0.05	0.05	0.04	0.06	0.05	0.15	0.08	0.11	0.03	0.03	0.05	0.06	0.07	0.06	0.05	0.05	0.00	0.06
#Na	0.01	0.01	0.01	0.01	0.05	0.03	0.08	0.00	0.00	-	0.02	0.02	0.01	-	0.03	0.03	0.06	0.09	0.12	0.07	0.11	-	-
M4 site	1.99	1.98	1.99	1.97	2.00	2.00	1.98	2.00	2.00	2.00	2.00	1.97	2.00	2.00	1.97	2.00	1.98	2.00	2.00	1.96	1.85	2.00	2.00
#Ca	-	-	-	-	-	-	-	-	-	0.00	-	-	-	0.01	-	-	-	-	-	-	-	0.03	0.01
#Na	-	-	-	-	0.03	0.04	-	0.06	0.02	0.03	0.02	-	0.01	-	-	0.07	-	0.04	0.14	-	-	0.08	0.17
#K	-	-	-	0.00	-	0.00	0.00	-	0.00	-	0.00	0.01	-	-	-	0.00	-	0.00	-	-	-	-	-
A site	-	-	-	0.00	0.03	0.05	0.00	0.06	0.03	0.03	0.02	0.01	0.01	0.01	-	0.07	-	0.04	0.14	-	-	0.11	0.17
#O	22.00	22.01	22.00	22.00	22.00	22.00	22.00	22.00	22.01	22.00	22.00	22.00	22.00	22.00	22.01	21.99	22.00	22.00	22.00	22.00	22.00	22.00	22.00
#OH	2.00	1.99	2.00	2.00	2.00	2.00	2.00	2.00	1.99	2.00	2.00	2.00	2.00	2.00	1.99	2.01	2.00	2.00	2.00	2.00	2.00	2.00	2.00
Charge	-1E-05	0.00	0.00	-1E-06	-8E-06	-8E-06	-2E-06	-2E-06	0.00	-8E-06	0.00	0.00	-9E-06	0.00	0.00	0.01	0.00	0.00	-7E-06	0.00	-	-	-

	N26C2	N32C	N32I	N32R	N35AC	N35AR	N35BC	N35BR	N35CC	N35CR	N39C	N39R	SE1C	SE1R	SE1AC	SE1AR	SE2C	SE2R	SE2I	SE3AC
SiO2	55.24	48.58	53.55	44.45	48.88	52.68	52.85	52.27	53.13	53.03	53.95	54.08	52.95	53.86	52.83	52.18	50.38	54.75	52.77	54.77
TiO2	0.05	0.10	0.05	0.14	0.07	0.04	0.06	0.04	0.05	0.08	0.05	0.02	0.09	0.05	0.06	0.06	0.10	0.02	0.02	0.09
Al2O3	1.46	9.06	1.97	15.29	7.87	3.82	2.41	3.19	2.58	2.44	1.65	1.85	4.07	3.37	5.41	5.44	6.74	1.52	3.02	3.32
Cr2O3	-	0.09	0.02	0.13	0.13	0.14	0.07	2.04	0.08	0.06	0.07	0.13	-	-	-	-	0.03	0.02	-	-
Fe2O3	0.00	-	0.02	-	0.00	0.02	0.03	-	-	-	-	0.02	-	-	-	0.00	-	-	-	-
FeO	24.61	24.82	25.33	24.25	25.43	25.36	25.08	24.54	24.44	24.61	24.88	24.82	18.85	18.85	20.55	20.78	19.05	19.88	19.52	19.18
MnO	0.53	0.25	0.30	0.29	0.52	0.53	0.52	0.45	0.51	0.46	0.47	0.46	0.68	0.73	0.86	0.78	0.80	0.97	0.88	0.62
MgO	17.04	14.08	17.03	12.06	14.21	16.15	16.84	16.47	16.44	15.85	16.85	16.95	19.88	20.34	18.78	18.69	19.05	20.99	20.55	20.19
ZnO	0.19	0.01	0.02	-	-	-	0.01	0.05	0.08	0.07	0.02	0.15	0.01	-	0.03	-	0.10	-	-	-
CaO	0.34	0.30	0.17	0.41	0.23	0.19	0.17	0.26	0.24	0.44	0.33	0.41	0.34	0.29	0.41	0.38	0.46	0.19	0.32	0.35
Na2O	0.23	0.81	0.08	1.45	0.63	0.32	0.17	0.27	0.18	0.16	0.06	0.04	0.51	0.37	0.57	0.70	0.83	0.11	0.34	0.39
K2O	-	0.01	-	-	-	-	-	0.01	-	-	-	-	-	-	-	-	0.02	0.01	0.03	0.01
H2O	2.09	2.04	2.06	2.04	2.03	2.07	2.05	2.04	2.04	2.03	2.05	2.07	2.08	2.10	2.11	2.10	2.07	2.10	2.07	2.12
Total	101.78	100.15	100.60	100.51	100.00	101.32	100.25	101.63	99.77	99.23	100.38	101.00	99.46	99.96	101.61	101.11	99.63	100.56	99.52	101.04
#Si IV	7.93	7.14	7.80	6.53	7.22	7.64	7.74	7.58	7.79	7.83	7.87	7.84	7.61	7.69	7.49	7.45	7.28	7.81	7.62	7.73
#Al IV	0.07	0.86	0.20	1.47	0.78	0.36	0.26	0.42	0.21	0.17	0.13	0.16	0.39	0.31	0.51	0.55	0.72	0.19	0.38	0.27
#Fe +3	-	-	-	-	-	-	-	-	-	-	-	-	-	-	-	-	-	-	-	-
#Ti IV	-	-	-	-	-	-	-	-	-	-	-	-	-	-	-	-	-	-	-	-
T site	8.00	8.00	8.00	8.00	8.00	8.00	8.00	8.00	8.00	8.00	8.00	8.00	8.00	8.00	8.00	8.00	8.00	8.00	8.00	8.00
#Al VI	0.17	0.71	0.14	1.17	0.59	0.29	0.16	0.13	0.24	0.25	0.15	0.16	0.30	0.26	0.39	0.37	0.42	0.06	0.13	0.28
#Fe +3	0.00	-	0.00	-	0.00	0.00	0.00	-	-	-	-	0.00	-	-	-	0.00	-	-	-	-
#Ti	0.01	0.01	0.01	0.02	0.01	0.00	0.01	0.00	0.01	0.01	0.01	0.00	0.01	0.01	0.01	0.01	0.01	0.00	0.00	0.01
#Cr	-	0.01	0.00	0.02	0.02	0.02	0.01	0.23	0.01	0.01	0.01	0.01	-	-	-	-	0.00	0.00	-	-
#Mg	3.64	3.08	3.70	2.64	3.13	3.49	3.68	3.56	3.59	3.49	3.66	3.66	4.26	4.33	3.97	3.98	4.10	4.46	4.42	4.25
#Fe +2	1.18	1.19	1.15	1.16	1.26	1.19	1.15	1.08	1.15	1.25	1.17	1.16	0.43	0.41	0.63	0.65	0.46	0.47	0.44	0.46
#Zn	-	-	-	-	-	-	-	-	-	-	-	-	-	-	-	-	-	-	-	-
#Mn	-	-	-	-	-	-	-	-	-	-	-	-	-	-	-	-	-	-	-	-
#Ca	-	-	-	-	-	-	-	-	-	-	-	-	-	-	-	-	-	-	-	-
M1,2,3	5.00	5.00	5.00	5.00	5.00	5.00	5.00	5.00	5.00	5.00	5.00	5.00	5.00	5.00	5.00	5.00	5.00	5.00	5.00	5.00
#Mg	-	-	-	-	-	-	-	-	-	-	-	-	-	-	-	-	-	-	-	-
#Fe +2	1.78	1.86	1.94	1.82	1.89	1.88	1.92	1.90	1.84	1.79	1.86	1.85	1.83	1.84	1.81	1.83	1.84	1.90	1.92	1.80
#Zn	0.02	0.00	0.00	-	-	-	0.00	0.01	0.01	0.01	0.00	0.02	0.00	-	0.00	-	0.01	-	-	-
#Mn	0.06	0.03	0.04	0.04	0.07	0.07	0.06	0.06	0.06	0.06	0.06	0.06	0.08	0.09	0.10	0.09	0.10	0.12	0.11	0.07
#Ca	0.05	0.05	0.02	0.06	0.04	0.03	0.01	0.04	0.04	0.07	0.05	0.06	0.05	0.04	0.06	0.06	0.05	-	-	0.05
#Na	0.06	0.06	-	0.08	0.01	0.02	-	-	0.05	0.05	0.02	0.01	0.03	0.03	0.02	0.01	-	-	-	0.07
M4 site	1.98	2.00	2.00	2.00	2.00	2.00	2.00	2.00	2.00	1.97	1.99	2.00	2.00	2.00	2.00	2.00	2.00	2.02	2.02	2.00
#Ca	-	-	0.01	-	-	-	0.02	0.00	-	-	-	-	-	-	-	-	0.02	0.03	0.05	-
#Na	-	0.17	0.02	0.33	0.17	0.07	0.05	0.08	0.00	-	-	-	0.11	0.07	0.13	0.18	0.23	0.03	0.10	0.04
#K	-	0.00	-	-	-	-	-	0.00	-	-	-	-	-	-	-	-	0.00	0.00	0.01	0.00
A site	-	0.18	0.03	0.33	0.17	0.07	0.06	0.08	0.00	-	-	-	0.11	0.07	0.13	0.18	0.26	0.06	0.15	0.04
#O	22.00	22.00	22.00	22.00	22.00	22.00	22.00	22.03	22.00	22.00	22.01	22.00	22.01	22.00	22.00	22.00	22.01	22.00	22.01	22.00
#OH	2.00	2.00	2.00	2.00	2.00	2.00	2.00	1.97	2.00	2.00	1.99	2.00	1.99	2.00	2.00	2.00	1.99	2.00	1.99	2.00
Charge	0.00	0.00	0.00	0.00	0.00	0.00	0.00	0.00	-3E-06	-4E-06	0.00	0.00	0.00	0.00	-5E-06	0.00	-2E-07	-3E-06	-6E-06	0.00

BIOTITE ANALYSES, NÉMISCAU

	S5C	S5R	S14AC	S14AR	S14BC	S14BR	S16AC	S16AR	S16BC	S16BR	S30AC	S30AR	S30BC	S30BR	S32AC	S32AR	S32BC	S32BR	S32CC	S32CR
SiO2	36.34	35.83	36.02	36.79	36.50	36.72	36.52	36.82	35.86	36.42	35.75	35.61	36.50	36.58	37.25	34.22	37.15	34.57	36.41	36.62
TiO2	1.60	1.93	1.86	1.93	1.85	1.81	2.25	2.28	1.10	0.81	1.84	1.89	1.37	1.17	1.90	1.87	2.12	2.13	1.92	2.34
Al2O3	19.67	19.54	17.20	17.47	16.55	17.04	20.26	20.51	22.98	19.81	19.40	19.80	19.42	19.78	17.41	17.44	17.18	17.53	17.61	17.67
Cr2O3	-	-	-	-	-	-	-	-	-	-	-	-	-	-	0.11	0.12	0.15	0.14	0.05	0.13
Fe2O3	-	0.00	0.00	0.00	-	-	-	-	-	-	0.00	-	0.00	0.00	0.00	0.00	0.00	-	0.00	0.00
FeO	19.68	19.71	17.66	17.74	17.46	17.09	19.48	19.08	18.87	20.64	17.11	17.14	17.45	16.75	16.89	17.10	17.10	17.39	17.05	17.31
MnO	0.03	0.03	0.09	0.05	0.02	0.07	0.04	0.02	-	0.04	-	0.05	0.03	0.05	0.05	0.04	0.01	0.05	0.07	0.06
MgO	9.78	9.93	12.00	12.47	13.41	13.15	8.64	8.48	8.83	8.75	10.36	10.32	11.01	11.09	12.90	12.68	12.68	12.89	12.42	12.49
CaO	0.03	-	0.06	0.06	0.03	0.01	0.01	0.07	0.03	0.01	0.06	0.04	0.03	0.01	0.03	0.04	-	-	0.02	0.04
Na2O	0.21	0.19	0.10	0.12	0.21	0.18	0.17	0.13	0.13	0.11	0.10	0.09	0.06	0.09	0.25	0.21	0.23	0.18	0.18	0.20
K2O	9.76	9.67	9.63	9.45	8.93	9.55	9.29	9.16	9.21	9.27	8.96	9.13	8.89	9.24	9.32	9.44	9.42	9.45	9.48	9.39
H2O	4.01	4.00	3.93	4.00	3.97	3.99	3.86	3.84	3.89	3.91	3.93	3.94	3.98	3.99	4.03	4.02	4.02	4.07	3.98	4.02
Total	101.11	100.83	98.55	100.08	98.93	99.61	100.52	100.39	100.90	99.77	97.51	98.01	98.74	98.75	100.14	97.18	100.06	98.40	99.19	100.27
#Si IV	5.43	5.37	5.49	5.51	5.52	5.51	5.46	5.50	5.31	5.52	5.45	5.41	5.49	5.49	5.54	5.29	5.54	5.28	5.49	5.46
#Al IV	2.57	2.63	2.51	2.49	2.48	2.49	2.54	2.50	2.69	2.48	2.55	2.59	2.51	2.51	2.46	2.71	2.46	2.72	2.51	2.54
#Fe IV	-	-	-	-	-	-	-	-	-	-	-	-	-	-	-	-	-	-	-	-
#Ti IV	-	-	-	-	-	-	-	-	-	-	-	-	-	-	-	-	-	-	-	-
T site	8.00	8.00	8.00	8.00	8.00	8.00	8.00	8.00	8.00	8.00	8.00	8.00	8.00	8.00	8.00	8.00	8.00	8.00	8.00	8.00
#Al VI	0.89	0.82	0.58	0.59	0.46	0.53	1.04	1.10	1.33	1.05	0.94	0.96	0.94	1.00	0.59	0.47	0.56	0.44	0.62	0.57
#Ti VI	0.18	0.22	0.21	0.22	0.21	0.20	0.25	0.26	0.12	0.09	0.21	0.22	0.16	0.13	0.21	0.22	0.24	0.24	0.22	0.26
#Cr	-	-	-	-	-	-	-	-	-	-	-	-	-	-	0.01	0.01	0.02	0.02	0.01	0.02
#Fe +3	-	0.00	0.00	0.00	-	-	-	-	-	-	0.00	-	0.00	0.00	0.00	0.00	0.00	-	0.00	0.00
#Fe +2	2.46	2.47	2.25	2.22	2.21	2.15	2.44	2.38	2.34	2.61	2.18	2.18	2.20	2.10	2.10	2.21	2.13	2.22	2.15	2.16
#Mn +2	0.00	0.00	0.01	0.01	0.00	0.01	0.01	0.00	-	0.01	-	0.01	0.00	0.01	0.01	0.01	0.00	0.01	0.01	0.01
#Mg	2.18	2.22	2.73	2.78	3.02	2.94	1.93	1.89	1.95	1.98	2.36	2.34	2.47	2.48	2.86	2.92	2.82	2.94	2.79	2.78
O site	5.70	5.73	5.79	5.81	5.90	5.83	5.66	5.63	5.74	5.74	5.69	5.70	5.76	5.72	5.79	5.85	5.77	5.86	5.79	5.79
#Ca	0.00	-	0.01	0.01	0.00	0.00	0.00	0.01	0.00	0.00	0.01	0.01	0.00	0.00	0.00	0.01	-	-	0.00	0.01
#Na	0.06	0.06	0.03	0.03	0.06	0.05	0.05	0.04	0.04	0.03	0.03	0.03	0.02	0.03	0.07	0.06	0.07	0.05	0.05	0.06
#K	1.86	1.85	1.87	1.80	1.72	1.83	1.77	1.74	1.74	1.79	1.74	1.77	1.71	1.77	1.77	1.86	1.79	1.84	1.82	1.79
A site	1.92	1.90	1.91	1.85	1.79	1.88	1.82	1.79	1.78	1.82	1.78	1.80	1.73	1.80	1.85	1.93	1.86	1.90	1.88	1.85
#O	20.01	20.00	20.00	20.01	20.00	20.00	20.15	20.18	20.15	20.05	20.00	20.01	20.00	20.00	20.00	19.85	20.00	19.85	20.00	20.00
#OH	3.99	4.00	4.00	3.99	4.00	4.00	3.85	3.82	3.85	3.95	4.00	3.99	4.00	4.00	4.00	4.15	4.00	4.15	4.00	4.00
Charge	0.00	0.00	0.00	-	0.00	0.00	0.00	0.00	0.00	0.00	0.00	0.00	-2E-06	-	-1E-06	0.00	-	0.00	-1E-06	0.00

	S32DC	S32DR	S32EI	V11AC	V11AR	V11BC	V14AC	V14AR	V14BC	V14BR	N14AC	N14AR	N14BC	N14BR	N14CC	N14CR	N22AC	N22AR	N22BC	N22BR
SiO2	36.74	36.20	36.74	36.41	35.34	36.19	35.18	35.28	35.50	35.71	35.47	36.36	36.65	36.76	36.44	37.38	36.74	36.60	36.36	35.63
TiO2	2.08	2.25	1.55	1.16	1.33	1.31	1.72	1.96	1.45	1.52	1.37	1.41	1.40	1.45	1.63	1.74	1.58	1.67	1.65	1.65
Al2O3	17.18	17.60	17.43	18.89	18.70	19.20	19.69	18.40	20.59	19.46	17.90	17.94	16.86	16.86	17.23	17.30	17.92	18.00	18.32	18.10
Cr2O3	0.13	0.12	0.06	-	-	-	-	0.11	0.07	0.05	0.36	0.34	0.81	0.82	0.56	0.69	-	-	0.06	0.07
Fe2O3	-	-	-	0.00	0.00	0.00	0.00	0.00	-	-	-	0.00	0.00	0.00	-	-	-	-	0.00	0.00
FeO	17.55	17.60	19.16	21.92	21.99	21.04	22.09	21.83	21.07	21.49	16.93	17.42	18.67	18.70	17.06	16.76	18.39	18.42	17.76	18.48
MnO	0.05	0.02	0.09	-	-	-	0.01	-	0.02	0.01	0.05	0.07	0.02	0.02	0.04	0.11	0.01	0.06	0.05	-
MgO	12.70	12.54	11.99	9.35	8.98	9.24	9.33	9.12	8.99	8.87	13.77	12.77	11.76	11.98	13.02	12.62	12.43	12.49	12.63	12.52
CaO	-	0.02	0.03	0.07	0.01	0.06	-	0.13	-	0.04	0.02	-	-	0.02	-	0.05	-	-	-	-
Na2O	0.26	0.23	0.17	0.17	0.08	0.18	0.19	0.14	0.26	0.22	0.06	0.06	0.05	0.06	0.08	0.08	0.24	0.39	0.29	0.24
K2O	9.50	9.45	9.33	9.03	9.23	9.32	9.63	9.46	9.33	9.44	8.16	8.84	9.67	9.58	9.64	9.97	8.98	8.83	8.85	8.50
H2O	4.01	4.00	4.00	3.98	3.91	3.97	3.99	3.93	4.00	3.97	3.95	3.99	3.97	3.97	3.99	4.04	4.01	4.02	4.01	3.97
Total	100.20	100.03	100.55	100.98	99.57	100.51	101.83	100.36	101.28	100.78	98.04	99.20	99.86	100.22	99.69	100.74	100.30	100.48	99.98	99.16
#Si IV	5.49	5.43	5.51	5.48	5.42	5.46	5.28	5.38	5.32	5.39	5.38	5.47	5.54	5.53	5.48	5.55	5.48	5.46	5.43	5.38
#Al IV	2.51	2.57	2.49	2.52	2.58	2.54	2.72	2.62	2.68	2.61	2.62	2.53	2.46	2.47	2.52	2.45	2.52	2.54	2.57	2.62
#Fe IV	-	-	-	-	-	-	-	-	-	-	-	-	-	-	-	-	-	-	-	-
#Ti IV	-	-	-	-	-	-	-	-	-	-	-	-	-	-	-	-	-	-	-	-
T site	8.00	8.00	8.00	8.00	8.00	8.00	8.00	8.00	8.00	8.00	8.00	8.00	8.00	8.00	8.00	8.00	8.00	8.00	8.00	8.00
#Al VI	0.52	0.54	0.58	0.83	0.80	0.87	0.77	0.68	0.95	0.86	0.58	0.65	0.54	0.53	0.53	0.58	0.64	0.62	0.66	0.61
#Ti VI	0.23	0.25	0.17	0.13	0.15	0.15	0.19	0.22	0.16	0.17	0.16	0.16	0.16	0.16	0.18	0.19	0.18	0.19	0.19	0.19
#Cr	0.02	0.01	0.01	-	-	-	-	0.01	0.01	0.01	0.04	0.04	0.10	0.10	0.07	0.08	-	-	0.01	0.01
#Fe +3	-	-	-	0.00	0.00	0.00	0.00	0.00	-	-	-	0.00	0.00	0.00	-	-	-	-	0.00	0.00
#Fe +2	2.20	2.21	2.40	2.76	2.82	2.65	2.77	2.78	2.64	2.71	2.15	2.19	2.36	2.35	2.14	2.08	2.30	2.30	2.22	2.34
#Mn +2	0.01	0.00	0.01	-	-	-	0.00	-	0.00	0.00	0.01	0.01	0.00	0.00	0.01	0.01	0.00	0.01	0.01	-
#Mg	2.83	2.80	2.68	2.10	2.05	2.08	2.09	2.07	2.01	2.00	3.11	2.86	2.65	2.69	2.92	2.79	2.77	2.78	2.81	2.82
O site	5.81	5.82	5.86	5.82	5.82	5.75	5.83	5.78	5.77	5.75	6.04	5.91	5.81	5.83	5.84	5.74	5.88	5.88	5.89	5.96
#Ca	-	0.00	0.00	0.01	0.00	0.01	-	0.02	-	0.01	0.00	-	-	0.00	-	0.01	-	-	-	-
#Na	0.08	0.07	0.05	0.05	0.02	0.05	0.06	0.04	0.08	0.06	0.02	0.02	0.01	0.02	0.02	0.02	0.07	0.11	0.08	0.07
#K	1.81	1.81	1.78	1.73	1.81	1.79	1.85	1.84	1.78	1.82	1.58	1.70	1.86	1.84	1.85	1.89	1.71	1.68	1.69	1.64
A site	1.89	1.88	1.84	1.79	1.83	1.86	1.90	1.90	1.86	1.89	1.60	1.71	1.88	1.86	1.87	1.92	1.78	1.79	1.77	1.71
#O	20.00	20.00	20.00	20.01	20.00	20.00	20.00	20.00	20.00	20.00	20.00	20.00	20.00	20.01	20.00	20.00	20.01	20.00	20.00	20.00
#OH	4.00	4.00	4.00	3.99	4.00	4.00	4.00	4.00	4.00	4.00	4.00	4.00	4.00	3.99	4.00	4.00	3.99	4.00	4.00	4.00
Charge	0.00	-1E-06	0.00	-	0.00	0.00	-1E-06	-5E-07	-1E-06	0.00	0.00	-	-	-2E-06	0.00	-	-5E-07	0.00	0.00	0.00

	N22CC	N22CI	N22DC	N22DR	N32AC	N32AR	N32BC	N32BR	N35AC	N35AR	N35BC	N35BR	N35CC	N35CR	N38AC	N38AI	N38BC	N38BR	N38CC	N38CR
SiO2	36.20	35.78	36.95	36.98	36.64	36.03	37.01	35.38	35.43	36.06	36.16	36.20	37.21	36.90	33.77	34.14	34.49	34.73	35.81	35.34
TiO2	2.17	1.65	1.88	1.92	1.13	1.47	1.42	1.17	1.31	1.51	1.52	1.54	1.25	1.34	1.40	1.11	1.44	1.93	1.54	1.72
Al2O3	18.03	17.96	18.30	18.67	18.36	18.24	18.04	18.70	17.68	19.43	18.04	18.10	17.94	18.41	20.29	20.48	20.06	20.44	19.74	19.57
Cr2O3	0.07	0.11	-	0.06	0.17	0.17	0.18	0.09	0.23	0.17	0.20	0.18	0.02	0.04	0.03	-	0.06	0.08	0.03	0.05
Fe2O3	-	-	0.00	0.00	0.00	0.00	0.00	0.00	-	-	-	-	0.00	-	-	-	-	-	-	0.00
FeO	18.01	18.74	18.27	16.80	18.03	17.76	17.02	18.46	19.43	16.95	18.43	17.83	17.30	17.36	21.44	21.24	21.73	20.43	21.22	20.70
MnO	0.04	0.11	-	0.08	0.04	0.06	0.08	0.05	0.05	0.09	0.09	0.09	0.06	0.04	0.05	0.03	0.09	0.03	0.05	0.08
MgO	12.06	12.99	12.01	12.20	12.75	12.59	8.66	13.03	13.42	13.16	11.84	12.44	12.16	11.90	8.94	8.67	8.51	8.24	8.45	8.48
CaO	-	0.03	-	-	-	-	-	-	0.05	-	-	0.63	-	-	-	-	-	-	-	0.01
Na2O	0.26	0.13	0.45	0.41	0.12	0.14	0.14	0.08	0.13	0.10	0.15	0.11	0.22	0.15	0.10	0.13	0.14	0.12	0.25	0.13
K2O	8.92	7.88	9.08	9.00	9.15	8.60	9.36	8.71	8.68	8.34	8.36	7.29	8.56	8.48	9.31	9.74	9.63	9.78	9.09	9.18
H2O	3.99	3.98	4.04	4.04	4.02	3.98	4.02	3.99	3.95	4.04	3.96	3.97	3.99	3.98	3.89	3.90	3.92	3.93	3.85	3.91
Total	99.75	99.36	100.98	100.16	100.41	99.04	95.93	99.66	100.36	99.85	98.75	98.38	98.71	98.60	99.22	99.44	100.07	99.71	100.03	99.17
#Si IV	5.43	5.38	5.48	5.48	5.46	5.43	5.73	5.32	5.33	5.35	5.47	5.46	5.59	5.55	5.20	5.25	5.27	5.29	5.43	5.40
#Al IV	2.57	2.62	2.52	2.52	2.54	2.57	2.27	2.68	2.67	2.65	2.53	2.54	2.41	2.45	2.80	2.75	2.73	2.71	2.57	2.60
#Fe IV	-	-	-	-	-	-	-	-	-	-	-	-	-	-	-	-	-	-	-	-
#Ti IV	-	-	-	-	-	-	-	-	-	-	-	-	-	-	-	-	-	-	-	-
T site	8.00	8.00	8.00	8.00	8.00	8.00	8.00	8.00	8.00	8.00	8.00	8.00	8.00	8.00	8.00	8.00	8.00	8.00	8.00	8.00
#Al VI	0.62	0.57	0.67	0.75	0.68	0.67	1.02	0.64	0.46	0.75	0.69	0.68	0.77	0.82	0.88	0.95	0.89	0.97	0.97	0.93
#Ti VI	0.24	0.19	0.21	0.21	0.13	0.17	0.17	0.13	0.15	0.17	0.17	0.17	0.14	0.15	0.16	0.13	0.17	0.22	0.18	0.20
#Cr	0.01	0.01	-	0.01	0.02	0.02	0.02	0.01	0.03	0.02	0.02	0.02	0.00	0.00	0.00	-	0.01	0.01	0.00	0.01
#Fe +3	-	-	0.00	0.00	0.00	0.00	0.00	0.00	-	-	-	-	0.00	-	-	-	-	-	-	0.00
#Fe +2	2.26	2.36	2.26	2.08	2.25	2.24	2.20	2.32	2.44	2.10	2.33	2.25	2.17	2.18	2.76	2.73	2.78	2.60	2.69	2.65
#Mn +2	0.01	0.01	-	0.01	0.01	0.01	0.01	0.01	0.01	0.01	0.01	0.01	0.01	0.01	0.01	0.00	0.01	0.00	0.01	0.01
#Mg	2.70	2.91	2.65	2.70	2.83	2.83	2.00	2.92	3.01	2.91	2.67	2.80	2.72	2.67	2.05	1.99	1.94	1.87	1.91	1.93
O site	5.84	6.05	5.80	5.76	5.91	5.93	5.42	6.03	6.10	5.97	5.90	5.93	5.82	5.83	5.87	5.80	5.79	5.68	5.76	5.72
#Ca	-	0.00	-	-	-	-	-	-	0.01	-	-	0.10	-	-	-	-	-	-	-	0.00
#Na	0.08	0.04	0.13	0.12	0.03	0.04	0.04	0.02	0.04	0.03	0.04	0.03	0.06	0.04	0.03	0.04	0.04	0.04	0.07	0.04
#K	1.71	1.51	1.72	1.70	1.74	1.65	1.85	1.67	1.67	1.58	1.61	1.40	1.64	1.63	1.83	1.91	1.88	1.90	1.76	1.79
A site	1.78	1.56	1.85	1.82	1.77	1.69	1.89	1.69	1.71	1.61	1.66	1.54	1.71	1.67	1.86	1.95	1.92	1.94	1.83	1.83
#O	20.01	20.01	20.01	20.00	20.01	20.00	19.85	20.00	20.04	20.00	20.00	20.01	20.00	20.01	20.00	20.00	20.00	20.00	20.10	20.01
#OH	3.99	3.99	3.99	4.00	3.99	4.00	4.15	4.00	3.96	4.00	4.00	3.99	4.00	3.99	4.00	4.00	4.00	4.00	3.90	3.99
Charge	0.00	0.00	0.00	-1E-06	-1E-06	-	-2E-06	-3E-06	0.00	0.00	0.00	0.00	-5E-06	0.00	-	0.00	0.00	-	0.00	0.00

	N39AC	N39AR	N39BC	N39BR	N39CC	N39CR	SE1AC	SE1AR	SE1BC	SE3C	SE3R	S36	N16A	N16B	N20	S3AC	S3AR	S3BC	S3BR
SiO2	36.85	36.59	35.98	36.69	37.25	34.63	38.54	39.23	39.22	40.36	39.33	38.72	33.84	36.07	37.61	34.49	35.36	34.63	35.26
TiO2	1.62	1.56	1.45	1.60	1.51	1.28	0.93	0.88	1.00	0.99	1.07	1.47	1.00	1.20	1.04	1.99	2.05	2.10	2.11
Al2O3	18.04	17.79	17.89	17.91	18.84	18.08	16.85	17.12	16.49	16.63	17.27	17.11	19.60	17.51	16.93	18.88	18.45	19.05	19.08
Cr2O3	0.66	0.79	0.26	0.61	0.52	0.63	-	-	-	-	-	-	-	-	-	0.04	0.06	0.06	0.04
Fe2O3	-	-	0.00	-	-	0.00	-	0.00	-	0.00	0.00	0.00	0.00	0.00	-	0.00	-	-	-
FeO	16.84	16.81	17.97	17.61	16.11	19.84	13.60	14.95	12.63	11.92	12.41	14.33	20.40	18.36	12.81	17.07	17.48	15.55	15.62
MnO	0.05	0.07	0.06	0.08	0.05	0.08	0.10	0.05	0.09	0.08	0.07	0.07	0.08	0.06	0.05	0.50	0.50	0.41	0.35
MgO	13.34	12.81	12.70	12.60	13.24	12.85	15.79	16.22	17.70	17.60	16.72	14.74	14.23	12.68	16.92	13.53	12.15	12.98	12.34
CaO	-	0.03	0.03	0.02	-	0.04	0.03	0.07	0.01	-	0.05	0.01	0.02	0.04	0.07	0.01	-	-	0.01
Na2O	0.12	0.13	0.08	0.12	0.23	0.10	0.32	0.22	0.25	0.63	0.26	0.16	0.02	0.11	0.14	0.13	0.09	0.36	0.20
K2O	8.89	8.89	8.93	9.02	8.95	8.53	8.18	8.29	8.62	7.80	8.38	9.11	8.41	8.94	8.59	8.42	9.60	9.22	10.08
H2O	4.05	4.00	3.96	4.02	4.08	3.98	4.04	4.15	4.01	4.18	4.13	4.08	3.92	3.93	4.02	3.97	3.97	3.95	3.97
Total	100.46	99.47	99.31	100.28	100.78	100.04	98.38	101.18	100.02	100.19	99.69	99.80	100.52	98.90	98.18	99.03	99.71	98.31	99.06
#Si IV	5.46	5.48	5.43	5.47	5.47	5.24	5.70	5.67	5.70	5.79	5.70	5.68	5.11	5.47	5.58	5.21	5.33	5.25	5.32
#Al IV	2.54	2.52	2.57	2.53	2.53	2.76	2.30	2.33	2.30	2.21	2.30	2.32	2.89	2.53	2.42	2.79	2.67	2.75	2.68
#Fe IV	-	-	-	-	-	-	-	-	-	-	-	-	-	-	-	-	-	-	-
#Ti IV	-	-	-	-	-	-	-	-	-	-	-	-	-	-	-	-	-	-	-
T site	8.00	8.00	8.00	8.00	8.00	8.00	8.00	8.00	8.00	8.00	8.00	8.00	8.00	8.00	8.00	8.00	8.00	8.00	8.00
#Al VI	0.60	0.62	0.61	0.61	0.73	0.47	0.64	0.58	0.52	0.60	0.65	0.64	0.42	0.60	0.54	0.56	0.61	0.66	0.71
#Ti VI	0.18	0.18	0.16	0.18	0.17	0.15	0.10	0.10	0.11	0.11	0.12	0.16	0.11	0.14	0.12	0.23	0.23	0.24	0.24
#Cr	0.08	0.09	0.03	0.07	0.06	0.08	-	-	-	-	-	-	-	-	-	0.00	0.01	0.01	0.00
#Fe +3	-	-	0.00	-	-	0.00	-	0.00	-	0.00	0.00	0.00	0.00	0.00	-	0.00	-	-	-
#Fe +2	2.08	2.10	2.27	2.19	1.98	2.51	1.68	1.81	1.53	1.43	1.50	1.76	2.58	2.33	1.59	2.15	2.21	1.97	1.97
#Mn +2	0.01	0.01	0.01	0.01	0.01	0.01	0.01	0.01	0.01	0.01	0.01	0.01	0.01	0.01	0.01	0.06	0.06	0.05	0.04
#Mg	2.94	2.86	2.86	2.80	2.90	2.90	3.48	3.49	3.83	3.76	3.61	3.23	3.20	2.87	3.74	3.04	2.73	2.93	2.77
O site	5.90	5.86	5.93	5.87	5.84	6.11	5.91	5.98	6.01	5.90	5.89	5.80	6.33	5.95	5.99	6.06	5.86	5.86	5.75
#Ca	-	0.00	0.00	0.00	-	0.01	0.00	0.01	0.00	-	0.01	0.00	0.00	0.01	0.01	0.00	-	-	0.00
#Na	0.03	0.04	0.02	0.03	0.07	0.03	0.09	0.06	0.07	0.18	0.07	0.05	0.01	0.03	0.04	0.04	0.03	0.11	0.06
#K	1.68	1.70	1.72	1.71	1.68	1.65	1.54	1.53	1.60	1.43	1.55	1.71	1.62	1.73	1.63	1.62	1.85	1.78	1.94
A site	1.71	1.74	1.75	1.75	1.74	1.68	1.64	1.60	1.67	1.60	1.63	1.75	1.63	1.77	1.68	1.66	1.87	1.89	2.00
#O	20.00	20.01	20.02	20.00	20.00	19.98	20.01	20.00	20.12	20.00	20.01	20.01	20.05	20.02	20.02	20.00	20.01	20.00	20.01
#OH	4.00	3.99	3.98	4.00	4.00	4.02	3.99	4.00	3.88	4.00	3.99	3.99	3.95	3.98	3.98	4.00	3.99	4.00	3.99
Charge	0.00	0.00	-5E-07	0.00	0.00	-	0.00	0.00	0.00	-3E-06	0.00	-1E-06	-	-5E-07	0.00	0.00	-	0.00	-

Chlorite analyses, Némiscau

	S16	NE1A	NE1B	NE1C	NE1D	N14A	N14B	N32A	N35A	N35B	N35C	N38A	N38B	N38C	SE1A	SE1B
SiO2	29.77	26.44	26.58	26.93	26.88	27.15	26.15	38.19	25.73	25.72	27.67	29.04	28.76	31.08	30.41	22.94
TiO2	0.66	0.02	-	-	-	0.49	0.33	-	0.08	0.05	0.03	0.44	0.20	0.38	0.02	-
Al2O3	23.21	21.48	21.90	22.82	22.43	22.14	22.39	24.13	22.88	23.67	23.12	19.25	20.32	19.88	14.63	27.75
Fe2O3	0.00	-	0.00	-	0.00	0.00	-	-	-	-	-	-	0.00	0.00	-	-
FeO	22.63	20.49	20.25	20.79	20.05	20.05	19.65	15.36	21.39	22.01	21.07	25.82	27.42	22.83	31.69	27.99
MnO	0.03	1.06	1.07	1.01	0.95	0.07	0.10	0.08	0.05	0.08	0.10	0.07	0.10	0.04	0.15	0.18
MgO	9.24	17.98	18.03	18.45	18.72	17.59	18.67	7.56	17.88	17.14	17.25	10.91	12.08	12.44	12.06	10.95
CaO	0.11	-	-	0.01	-	0.55	0.03	0.34	0.03	-	0.04	-	0.03	0.02	0.09	0.03
Na2O	0.07	-	-	-	0.02	0.02	0.02	0.04	0.02	0.02	0.02	0.02	-	0.08	0.01	0.01
K2O	3.06	0.01	-	-	-	0.02	-	0.47	0.03	0.03	0.26	2.95	0.82	2.47	0.02	-
H2O	11.68	11.62	11.70	12.00	11.89	11.82	11.73	12.32	11.70	11.77	11.97	11.35	11.59	11.75	11.25	11.55
Total	100.46	99.10	99.53	102.01	100.94	99.90	99.07	98.49	99.79	100.49	101.53	99.85	101.32	100.97	100.33	101.40
#Si IV	3.06	2.73	2.72	2.69	2.71	2.76	2.68	3.72	2.64	2.62	2.77	3.07	2.98	3.17	3.24	2.38
#Al IV	0.94	1.27	1.28	1.31	1.29	1.24	1.32	0.28	1.36	1.38	1.23	0.93	1.02	0.83	0.76	1.62
T site	4.00	4.00	4.00	4.00	4.00	4.00	4.00	4.00	4.00	4.00	4.00	4.00	4.00	4.00	4.00	4.00
#Al VI	1.86	1.34	1.37	1.38	1.37	1.41	1.38	2.48	1.40	1.46	1.50	1.46	1.45	1.56	1.08	1.78
#Ti	0.05	0.00	-	-	-	0.04	0.03	-	0.01	0.00	0.00	0.03	0.02	0.03	0.00	-
#Fe +3	0.00	-	0.00	-	0.00	0.00	-	-	-	-	-	-	0.00	0.00	-	-
#Fe +2	1.94	1.77	1.74	1.74	1.69	1.70	1.68	1.25	1.83	1.88	1.76	2.28	2.37	1.95	2.82	2.43
#Mn +2	0.00	0.09	0.09	0.09	0.08	0.01	0.01	0.01	0.00	0.01	0.01	0.01	0.01	0.00	0.01	0.02
#Mg	1.41	2.77	2.75	2.75	2.81	2.66	2.85	1.10	2.73	2.60	2.57	1.72	1.86	1.89	1.92	1.69
#Ca	0.01	-	-	0.00	-	0.06	0.00	0.04	0.00	-	0.00	-	0.00	0.00	0.01	0.00
#Na	0.01	-	-	-	0.00	0.00	0.00	0.01	0.00	0.00	0.00	0.00	-	0.02	0.00	0.00
#K	0.40	0.00	-	-	-	0.00	-	0.06	0.00	0.00	0.03	0.40	0.11	0.32	0.00	-
O site	5.70	5.97	5.95	5.96	5.96	5.88	5.95	4.94	5.98	5.96	5.89	5.90	5.82	5.77	5.85	5.92
#O	10.00	10.00	10.00	9.99	10.01	9.99	9.99	10.00	10.00	10.00	10.01	10.00	10.00	10.00	10.01	10.00
#OH	8.00	8.00	8.00	8.01	7.99	8.01	8.01	8.00	8.00	8.00	7.99	8.00	8.00	8.00	7.99	8.00
Charge	-	-	0.00	-	-	-	-	0.00	0.00	0.00	0.00	0.00	0.00	-1E-06	-	-

Clinopyroxene analyses, Némiscau

	N2AC	N2AR	NABC	N2BR
SiO2	49.34	49.47	50.14	49.91
TiO2	0.02	0.03	-	0.03
Al2O3	0.40	0.33	0.31	0.34
Cr2O3	0.02	-	-	-
Fe2O3	-	-	-	0.09
FeO	19.89	19.04	18.32	18.80
MnO	1.21	1.20	0.91	0.95
NiO	-	-	-	-
MgO	4.39	4.80	5.67	5.46
CaO	22.99	23.21	23.58	23.58
Na2O	-	-	-	-
K2O	-	-	-	-
Total	98.26	98.08	98.93	99.16
#Si IV	2.00	2.00	2.00	1.99
#Al IV	-	-	0.00	0.01
T site	2.00	2.00	2.00	2.00
#Al VI	0.02	0.02	0.01	0.01
#Ti	0.00	0.00	-	0.00
#Cr	0.00	-	-	-
#Fe +3	-	-	-	0.00
#Fe +2	0.67	0.64	0.61	0.63
#Mn +2	0.04	0.04	0.03	0.03
#Ni	-	-	-	-
#Mg	0.27	0.29	0.34	0.32
#Ca	1.00	1.01	1.01	1.01
#Na	-	-	-	-
#K	-	-	-	-
M1,M2	2.00	2.00	2.00	2.00
#O	6.01	6.01	6.01	6.00
Charge	0.02	0.02	0.01	-1E-06

Muscovite analyses, Némiscau

	S30	V11A
SiO2	45.66	46.67
TiO2	0.15	0.40
Al2O3	35.81	29.77
Cr2O3	-	-
Fe2O3	-	-
FeO	1.43	6.09
MnO	-	-
MgO	0.37	3.21
CaO	0.01	0.08
Na2O	1.60	0.15
K2O	8.96	8.61
H2O	4.46	4.42
Total	98.45	99.40
#Si IV	6.13	6.33
#Al IV	1.87	1.67
#Fe IV	-	-
#Ti IV	-	-
T site	8.00	8.00
#Al VI	3.80	3.09
#Ti VI	0.02	0.04
#Cr	-	-
#Fe +3	-	-
#Fe +2	0.16	0.69
#Mn +2	-	-
#Mg	0.07	0.65
O site	4.05	4.47
#Ca	0.00	0.01
#Na	0.42	0.04
#K	1.53	1.49
A site	1.95	1.54
#O	20.01	20.00
#OH	3.99	4.00
Charge	0.00	0.00

Cordierite analyses, Némiscau

	S30A	S30B	S30C	S30D	N32AC	N32AR	N32BC	N32BR	N32CC	N32CR	N39CC	N39CR	SE1C	SE1R	SE1AR	SE1AC	SE1BC	SE1BR	SE2C	SE2R
SiO2	47.74	48.48	48.40	48.59	47.08	49.24	48.71	50.26	48.82	48.98	49.56	49.54	50.32	50.00	50.09	50.53	50.51	50.47	49.04	49.22
TiO2	-	0.02	-	0.01	-	0.02	-	-	-	0.01	0.03	0.02	-	-	-	0.02	-	0.01	-	0.04
Al2O3	32.65	33.05	32.58	32.82	31.34	33.10	32.79	31.14	33.44	33.08	33.41	33.55	33.13	32.72	33.46	33.13	33.37	33.28	33.47	33.22
FeO	8.75	8.50	7.06	7.54	6.88	6.83	6.51	6.21	6.51	6.50	6.85	6.89	3.65	3.86	4.39	4.27	4.50	4.56	4.31	4.37
MnO	0.08	0.10	0.09	0.10	0.10	0.09	0.03	0.06	0.06	0.08	0.12	0.11	0.11	0.10	0.18	0.09	0.18	0.16	0.12	0.15
ZnO	0.33	0.13	0.14	0.10	-	-	-	-	-	-	0.01	-	0.07	0.06	-	-	0.10	-	0.04	0.05
MgO	7.86	8.13	8.39	7.79	9.39	8.74	8.28	8.49	8.64	8.66	9.04	9.23	10.85	10.69	10.80	10.66	10.79	10.75	11.01	11.05
CaO	0.06	0.02	0.03	-	0.03	0.02	0.03	0.04	0.02	0.02	0.03	0.02	0.01	0.01	0.01	0.02	0.03	0.01	0.03	-
Na2O	0.74	0.28	0.34	0.38	1.18	0.62	0.96	1.36	0.78	0.74	0.35	0.44	0.13	0.20	0.34	0.32	0.27	0.22	0.25	0.23
K2O	0.13	0.02	0.01	-	-	-	-	-	0.01	-	0.02	-	-	0.02	-	0.15	0.01	0.03	-	-
Total	98.34	98.73	97.04	97.33	96.00	98.66	97.31	97.56	98.28	98.07	99.42	99.80	98.27	97.66	99.27	99.19	99.76	99.49	98.27	98.33
#Si+4	4.96	4.98	5.03	5.04	4.97	5.02	5.03	5.17	5.00	5.02	5.01	5.00	5.07	5.07	5.02	5.06	5.04	5.05	4.97	4.98
#Ti+4	-	0.00	-	0.00	-	0.00	-	-	-	0.00	0.00	0.00	-	-	-	0.00	-	0.00	-	0.00
#Al+3	3.99	4.00	3.99	4.01	3.90	3.98	3.99	3.78	4.03	4.00	3.98	3.99	3.93	3.91	3.95	3.91	3.92	3.92	4.00	3.96
#Fe+2	0.76	0.73	0.61	0.65	0.61	0.58	0.56	0.53	0.56	0.56	0.58	0.58	0.31	0.33	0.37	0.36	0.38	0.38	0.37	0.37
#Mn+2	0.01	0.01	0.01	0.01	0.01	0.01	0.00	0.01	0.01	0.01	0.01	0.01	0.01	0.01	0.02	0.01	0.02	0.01	0.01	0.01
#Zn+2	0.03	0.01	0.01	0.01	-	-	-	-	-	-	0.00	-	0.01	0.00	-	-	0.01	-	0.00	0.00
#Mg+2	1.22	1.25	1.30	1.20	1.48	1.33	1.28	1.30	1.32	1.32	1.36	1.39	1.63	1.62	1.61	1.59	1.61	1.60	1.66	1.67
#Ca+2	0.01	0.00	0.00	-	0.00	0.00	0.00	0.00	0.00	0.00	0.00	0.00	0.00	0.00	0.00	0.00	0.00	0.00	0.00	-
#Na+1	0.15	0.06	0.07	0.08	0.24	0.12	0.19	0.27	0.15	0.15	0.07	0.09	0.03	0.04	0.07	0.06	0.05	0.04	0.05	0.05
#K	0.02	0.00	0.00	-	-	-	-	-	0.00	-	0.00	-	-	0.00	-	0.02	0.00	0.00	-	-
#TOTAL	11.13	11.04	11.02	11.00	11.20	11.05	11.06	11.07	11.07	11.05	11.03	11.05	10.98	10.99	11.04	11.02	11.02	11.01	11.06	11.05
#O-2	18.00	18.00	18.00	18.00	18.00	18.00	18.00	18.00	18.00	18.00	18.00	18.00	18.00	18.00	18.00	18.00	18.00	18.00	18.00	18.00

	N35AC	N35AR	N35BC	N35BR	N35CC	N35CR	N39AC	N39AR	N39BC	N39BR	SE3AC	SE3AR	SE3BC	SE3BR
SiO2	48.47	48.08	48.15	48.42	48.76	49.50	49.34	49.52	49.55	49.31	49.60	49.69	50.54	50.00
TiO2	0.03	-	-	0.01	-	-	-	-	-	0.01	-	-	-	0.02
Al2O3	33.02	32.77	33.15	33.14	33.11	33.40	33.68	33.46	33.53	33.39	33.17	32.95	33.01	32.87
FeO	6.91	7.05	6.59	6.57	6.65	6.25	6.77	7.08	6.89	6.74	4.24	4.01	3.88	3.98
MnO	0.06	0.13	0.13	0.07	0.07	0.09	0.12	0.10	0.13	0.19	0.13	0.11	0.16	0.12
ZnO	0.09	-	-	0.05	0.08	0.07	-	0.04	0.01	-	0.01	-	-	-
MgO	8.70	8.68	8.20	8.51	8.65	8.91	9.13	8.97	9.14	9.19	10.83	10.76	10.93	10.83
CaO	0.02	0.01	0.03	0.03	0.02	-	0.02	0.04	0.01	0.01	0.04	0.01	0.04	0.02
Na2O	0.59	0.48	1.17	0.90	0.51	0.46	0.30	0.42	0.29	0.34	0.23	0.25	0.19	0.27
K2O	-	-	-	-	0.01	-	0.01	-	-	-	0.02	0.01	0.01	-
Total	97.89	97.20	97.42	97.70	97.86	98.68	99.37	99.63	99.55	99.18	98.27	97.79	98.76	98.11
#Si+4	4.99	4.99	4.98	4.99	5.01	5.03	4.99	5.01	5.01	5.00	5.02	5.04	5.07	5.06
#Ti+4	0.00	-	-	0.00	-	-	-	-	-	0.00	-	-	-	0.00
#Al+3	4.01	4.01	4.04	4.03	4.01	4.00	4.02	3.99	3.99	3.99	3.95	3.94	3.90	3.92
#Fe+2	0.60	0.61	0.57	0.57	0.57	0.53	0.57	0.60	0.58	0.57	0.36	0.34	0.33	0.34
#Mn+2	0.01	0.01	0.01	0.01	0.01	0.01	0.01	0.01	0.01	0.02	0.01	0.01	0.01	0.01
#Zn+2	0.01	-	-	0.00	0.01	0.01	-	0.00	0.00	-	0.00	-	-	-
#Mg+2	1.34	1.34	1.27	1.31	1.33	1.35	1.38	1.35	1.38	1.39	1.63	1.63	1.64	1.63
#Ca+2	0.00	0.00	0.00	0.00	0.00	-	0.00	0.00	0.00	0.00	0.00	0.00	0.00	0.00
#Na+1	0.12	0.10	0.23	0.18	0.10	0.09	0.06	0.08	0.06	0.07	0.05	0.05	0.04	0.05
#K	-	-	-	-	0.00	-	0.00	-	-	-	0.00	0.00	0.00	-
#TOTAL	11.06	11.06	11.11	11.09	11.04	11.01	11.03	11.04	11.03	11.04	11.03	11.01	10.99	11.01
#O-2	18.00	18.00	18.00	18.00	18.00	18.00	18.00	18.00	18.00	18.00	18.00	18.00	18.00	18.00

Spinels analyses, Némiscau

	N8739A	N8739B	N8739C	N8739D	N8739E	N8739F	N8739G	N8739H	N8739I	N8739J
SiO2	0.04	0.10	0.29	0.23	0.61	0.25	0.17	0.28	1.07	2.15
TiO2	0.06	0.11	0.12	0.02	0.04	0.08	0.07	0.05	0.04	0.05
Al2O3	31.78	31.71	32.69	32.54	32.38	33.23	32.50	31.77	32.10	32.73
Cr2O3	27.44	26.90	27.37	27.08	27.56	27.55	27.02	26.95	27.10	27.16
V2O3	1.14	1.69	1.12	1.12	1.24	1.14	1.20	1.00	1.14	0.98
Fe2O3	1.61	1.51	0.46	0.25	0.52	-	1.14	1.17	0.16	-
FeO	29.14	29.65	29.25	28.60	28.89	28.93	29.06	28.14	28.73	26.31
MgO	0.89	1.50	1.53	1.25	1.11	1.16	1.34	0.99	1.10	1.62
MnO	0.33	0.02	0.10	0.15	0.37	0.10	0.15	0.07	0.06	0.07
ZnO	6.37	4.88	5.52	6.27	6.58	6.33	5.98	7.07	6.75	9.18
Total	98.80	98.07	98.45	97.51	99.30	98.77	98.63	97.49	98.25	100.25
#Si+4	0.00	0.00	0.01	0.01	0.02	0.01	0.01	0.01	0.03	0.07
#Ti+4	0.00	0.00	0.00	0.00	0.00	0.00	0.00	0.00	0.00	0.00
#Al+3	1.22	1.22	1.25	1.25	1.23	1.26	1.24	1.23	1.23	1.22
#Cr+3	0.71	0.69	0.70	0.70	0.70	0.70	0.69	0.70	0.69	0.68
#V	0.03	0.04	0.03	0.03	0.03	0.03	0.03	0.03	0.03	0.02
#Fe+3	0.04	0.04	0.01	0.01	0.01	-	0.03	0.03	0.00	-
#Fe+2	0.79	0.81	0.79	0.78	0.78	0.78	0.79	0.77	0.78	0.69
#Mg+2	0.04	0.07	0.07	0.06	0.05	0.06	0.06	0.05	0.05	0.08
#Mn+2	0.01	0.00	0.00	0.00	0.01	0.00	0.00	0.00	0.00	0.00
#Zn+2	0.15	0.12	0.13	0.15	0.16	0.15	0.14	0.17	0.16	0.21
#TOTAL	3.00	3.00	3.00	3.00	2.99	2.99	3.00	3.00	2.99	2.97
#O-2	4.00	4.00	4.00	4.00	4.00	4.00	4.00	4.00	4.00	4.00

	N8739J	N8739K	n87391	S31A	S31B	S31C	S31D	S-30AR	S-30AC	S30BR	S-30CR
SiO2	0.42	0.14	0.11	0.08	0.01	0.04	0.02	0.05	0.31	0.09	0.03
TiO2	0.07	0.12	0.19	0.01	-	0.02	0.02	0.01	0.03	-	-
Al2O3	31.46	32.58	32.27	57.98	61.34	60.45	61.43	57.08	56.56	57.05	56.68
Cr2O3	27.49	26.71	26.85	5.67	2.71	2.72	2.37	-	-	-	-
V2O3	1.08	0.97	1.07	-	0.08	0.02	0.04	-	-	-	-
Fe2O3	1.13	1.87	1.81	2.45	2.84	2.97	2.74	1.48	1.98	1.59	1.45
FeO	27.61	30.68	30.76	17.89	16.38	16.59	16.76	19.51	18.35	18.80	18.44
MgO	0.90	1.66	1.55	14.81	16.12	15.86	15.93	1.89	2.08	1.86	1.96
MnO	0.07	0.08	0.05	0.30	0.38	0.30	0.34	0.03	0.04	0.09	0.06
ZnO	8.11	3.75	3.78	0.10	0.26	0.12	0.20	20.39	21.34	21.25	21.09
Total	98.34	98.56	98.44	99.29	100.12	99.09	99.85	100.44	100.69	100.73	99.71
#Si+4	0.01	0.00	0.00	0.00	0.00	0.00	0.00	0.00	0.01	0.00	0.00
#Ti+4	0.00	0.00	0.00	0.00	-	0.00	0.00	0.00	0.00	-	-
#Al+3	1.21	1.24	1.23	1.83	1.89	1.88	1.90	1.97	1.94	1.96	1.97
#Cr+3	0.71	0.68	0.69	0.12	0.06	0.06	0.05	-	-	-	-
#V	0.03	0.03	0.03	-	0.00	0.00	0.00	-	-	-	-
#Fe+3	0.03	0.05	0.04	0.05	0.06	0.06	0.05	0.03	0.04	0.03	0.03
#Fe+2	0.76	0.83	0.83	0.40	0.36	0.37	0.37	0.48	0.45	0.46	0.45
#Mg+2	0.04	0.08	0.07	0.59	0.63	0.62	0.62	0.08	0.09	0.08	0.09
#Mn+2	0.00	0.00	0.00	0.01	0.01	0.01	0.01	0.00	0.00	0.00	0.00
#Zn+2	0.20	0.09	0.09	0.00	0.01	0.00	0.00	0.44	0.46	0.46	0.46
#TOTAL	2.99	3.00	3.00	3.00	3.00	3.00	3.00	3.00	3.00	3.00	3.00
#O-2	4.00	4.00	4.00	4.00	4.00	4.00	4.00	4.00	4.00	4.00	4.00

Plagioclase analyses, Némiscau

	S5C	S5R	S32C	S32R	S32BC	S32BR	V11AC	V11AR	V11BC	V11BR
SiO2	52.26	55.12	45.11	45.24	45.74	45.43	62.77	63.24	62.61	62.78
Al2O3	30.08	28.12	35.01	34.67	34.61	34.91	23.73	23.44	24.07	23.45
CaO	13.14	11.38	18.52	18.65	18.36	18.67	5.56	5.46	5.66	5.47
K2O	0.04	0.07	-	0.01	-	-	0.07	0.05	0.08	0.04
Na2O	3.93	5.17	0.87	0.95	0.84	0.92	8.15	8.07	8.04	8.28
TOTAL	99.45	99.86	99.51	99.52	99.55	99.93	100.28	100.26	100.46	100.02
#Si+4	2.38	2.49	2.09	2.10	2.11	2.10	2.77	2.79	2.76	2.78
#Al+3	1.61	1.50	1.91	1.89	1.88	1.90	1.23	1.22	1.25	1.22
#Ca+2	0.64	0.55	0.92	0.93	0.91	0.92	0.26	0.26	0.27	0.26
#K	0.00	0.00	-	0.00	-	-	0.00	0.00	0.00	0.00
#Na+1	0.35	0.45	0.08	0.09	0.08	0.08	0.70	0.69	0.69	0.71
#TOTAL	4.99	4.99	5.00	5.00	4.98	5.00	4.97	4.95	4.96	4.97
#O-2	8.00	8.00	8.00	8.00	8.00	8.00	8.00	8.00	8.00	8.00

	V14C	V14R	N14AC	N14AR	N14BC	N14BR	N39AC	N39AR	N39B	N39B2
SiO2	63.15	63.91	56.01	55.61	52.17	55.77	51.65	53.43	53.03	52.47
Al2O3	23.40	23.43	27.14	27.62	30.88	27.75	30.17	28.58	30.19	30.70
CaO	5.17	4.99	9.45	9.69	13.18	10.42	13.03	11.79	12.57	13.23
K2O	0.05	0.06	0.05	0.03	0.01	0.05	0.01	0.01	0.01	-
Na2O	8.52	8.54	6.45	6.20	3.97	6.06	4.40	5.23	4.64	4.30
TOTAL	100.29	100.93	99.10	99.15	100.21	100.05	99.26	99.04	100.44	100.70
#Si+4	2.78	2.80	2.54	2.52	2.36	2.51	2.36	2.44	2.39	2.36
#Al+3	1.22	1.21	1.45	1.48	1.65	1.47	1.63	1.54	1.60	1.63
#Ca+2	0.24	0.23	0.46	0.47	0.64	0.50	0.64	0.58	0.61	0.64
#K	0.00	0.00	0.00	0.00	0.00	0.00	0.00	0.00	0.00	-
#Na+1	0.73	0.72	0.57	0.54	0.35	0.53	0.39	0.46	0.41	0.38
#TOTAL	4.97	4.96	5.02	5.01	4.99	5.02	5.02	5.02	5.01	5.01
#O-2	8.00	8.00	8.00	8.00	8.00	8.00	8.00	8.00	8.00	8.00

	S32	S36A	S36B	N16A	N16B	N20A	N20B
SiO2	46.20	53.06	52.15	53.14	54.53	47.46	47.74
Al2O3	34.62	29.64	30.56	29.89	29.01	33.35	33.21
CaO	18.45	12.26	13.35	12.74	11.67	16.50	16.56
K2O	0.01	0.03	0.02	0.03	0.08	-	0.01
Na2O	0.78	4.28	3.54	4.28	4.84	1.72	1.91
TOTAL	100.06	99.27	99.62	100.08	100.13	99.03	99.43
#Si+4	2.12	2.41	2.37	2.40	2.46	2.19	2.20
#Al+3	1.87	1.59	1.64	1.59	1.54	1.82	1.80
#Ca+2	0.91	0.60	0.65	0.62	0.56	0.82	0.82
#K	0.00	0.00	0.00	0.00	0.00	-	0.00
#Na+1	0.07	0.38	0.31	0.38	0.42	0.15	0.17
#TOTAL	4.98	4.98	4.97	4.99	4.99	4.98	4.99
#O-2	8.00	8.00	8.00	8.00	8.00	8.00	8.00

Garnet analyses, Némiscau

	S5C	S5R	S14AC	S14AR	S14BC	S14BR	S16AC	S16AR	S16BC	S16BR	S32CC	S32CR	S32C1	S32C2	S32DC	S32DR	S32I1	S32I2	V11AC	V11AR
SiO2	38.61	39.10	37.93	38.15	37.95	37.82	37.30	37.28	37.34	37.36	37.77	38.01	37.88	37.61	38.76	38.62	38.28	38.47	38.59	38.80
TiO2	0.04	-	-	0.02	0.03	0.03	0.01	0.05	0.01	0.02	-	0.03	0.02	0.03	0.03	0.05	0.04	0.05	-	0.01
Al2O3	21.85	21.60	21.07	21.47	21.01	20.75	20.90	20.58	20.83	20.88	20.99	20.91	20.61	20.43	21.72	21.78	21.80	21.76	21.90	21.52
Cr2O3	-	-	-	0.04	0.05	0.03	0.02	0.04	0.01	-	0.06	0.11	-	0.07	0.04	-	0.04	0.10	-	-
Fe2O3	0.00	0.24	0.60	0.11	0.83	0.71	0.28	0.40	0.14	0.15	0.27	0.39	0.37	0.69	0.25	0.05	0.00	-	-	0.66
FeO	33.08	34.75	29.44	30.82	31.73	30.85	34.56	35.81	34.75	35.36	29.38	29.29	28.36	28.71	28.68	30.66	31.27	30.89	37.60	37.48
MnO	2.56	1.93	1.68	3.31	2.90	3.05	1.57	1.82	1.67	1.81	3.33	4.48	4.17	4.15	3.35	3.84	4.48	4.16	0.83	0.93
MgO	3.97	3.48	4.88	3.84	3.82	3.66	3.23	2.50	3.29	2.72	4.20	3.33	3.54	3.52	4.84	3.50	2.79	3.08	2.83	2.23
CaO	1.82	1.75	2.66	2.75	3.47	3.15	1.16	1.26	1.24	1.52	3.31	3.59	3.12	3.41	3.56	3.53	3.76	4.01	1.20	1.13
Total	101.93	102.85	98.26	100.51	101.79	100.05	99.03	99.74	99.28	99.82	99.31	100.14	98.07	98.62	101.22	102.04	102.46	102.52	102.95	102.76
#Si IV	6.00	6.00	6.00	6.00	5.96	6.00	6.00	6.00	6.00	6.00	6.00	6.00	6.00	6.00	6.00	6.00	5.98	6.00	5.99	6.00
#Al IV	0.00	0.00	-	-	0.04	-	-	-	-	-	-	-	-	-	-	0.00	0.02	-	0.01	0.00
T site	6.00	6.00	6.00	6.00	6.00	6.00	6.00	6.00	6.00	6.00	6.00	6.00	6.00	6.00	6.00	6.00	6.00	6.00	6.00	6.00
#Al VI	4.00	3.91	3.93	3.98	3.86	3.88	3.96	3.90	3.94	3.95	3.93	3.89	3.85	3.84	3.96	3.99	3.99	4.00	4.00	3.92
#Ti VI	0.00	-	-	0.00	0.00	0.00	0.00	0.01	0.00	0.00	-	0.00	0.00	0.00	0.00	0.01	0.00	0.01	-	0.00
#Cr	-	-	-	0.00	0.01	0.00	0.00	0.01	0.00	-	0.01	0.01	-	0.01	0.00	-	0.00	0.01	-	-
#Fe +3	0.00	0.03	0.07	0.01	0.10	0.08	0.03	0.05	0.02	0.02	0.03	0.05	0.04	0.08	0.03	0.01	0.00	-	-	0.08
O site	4.00	3.93	4.00	4.00	3.96	3.97	4.00	3.96	3.96	3.97	3.97	3.95	3.89	3.94	4.00	4.00	4.00	4.02	4.00	4.00
#Fe +2	4.30	4.46	3.89	4.05	4.17	4.09	4.65	4.82	4.67	4.75	3.90	3.87	3.76	3.83	3.71	3.98	4.08	4.03	4.88	4.85
#Mn +2	0.34	0.25	0.23	0.44	0.39	0.41	0.21	0.25	0.23	0.25	0.45	0.60	0.56	0.56	0.44	0.51	0.59	0.55	0.11	0.12
#Mg	0.92	0.80	1.15	0.90	0.90	0.87	0.77	0.60	0.79	0.65	0.99	0.78	0.84	0.84	1.12	0.81	0.65	0.72	0.66	0.51
#Ca	0.30	0.29	0.45	0.46	0.58	0.54	0.20	0.22	0.21	0.26	0.56	0.61	0.53	0.58	0.59	0.59	0.63	0.67	0.20	0.19
A site	5.85	5.79	5.72	5.86	6.04	5.90	5.84	5.89	5.90	5.91	5.91	5.86	5.68	5.81	5.86	5.89	5.96	5.96	5.85	5.67
#O	23.86	23.70	23.72	23.86	23.97	23.86	23.84	23.83	23.85	23.87	23.86	23.79	23.52	23.72	23.86	23.89	23.95	23.99	23.84	23.67

	S26A	S26B	S30AC	S30AR	S30BC	S30BR	S32AC	S32AR	S32R1	S32R2	V11BC	V11BR	V14AC	V14AR	V14BC	V14BR	N2AC	N2AR	N2BC	N2BR
SiO2	37.43	37.28	38.16	38.09	37.63	36.89	37.98	38.05	37.87	38.01	38.84	38.95	37.78	37.74	37.96	37.55	38.32	38.54	38.56	38.31
TiO2	0.01	-	0.02	0.02	0.01	0.08	0.04	0.06	-	0.04	-	-	0.05	0.03	0.01	0.02	0.31	0.27	0.23	0.23
Al2O3	20.33	20.41	21.62	21.29	20.50	20.64	20.83	21.18	20.81	20.48	21.42	21.32	21.81	21.82	21.71	21.90	17.36	17.16	17.49	17.32
Cr2O3	-	-	-	-	0.06	0.07	0.14	0.04	0.06	0.10	-	-	0.03	0.03	0.04	0.03	0.02	0.02	0.01	0.01
Fe2O3	0.88	0.63	-	0.38	0.42	0.20	0.44	0.03	0.41	0.78	0.22	0.33	0.00	0.00	0.00	0.00	6.37	6.76	6.33	6.48
FeO	12.87	12.75	33.87	33.31	33.48	34.20	27.36	29.37	28.62	28.52	36.92	37.25	37.84	37.98	37.86	37.87	2.49	2.23	2.65	2.28
MnO	24.12	24.21	1.70	1.50	1.67	1.68	3.25	3.83	4.06	3.48	0.96	0.84	0.87	0.79	0.85	0.86	1.23	1.23	1.34	1.30
MgO	3.20	3.12	4.12	3.81	3.73	3.33	4.94	3.87	3.74	3.94	2.88	2.75	2.96	2.71	2.84	2.72	0.05	0.03	0.05	0.78
CaO	0.45	0.41	0.88	0.94	0.80	1.14	3.68	3.30	3.57	3.55	1.17	1.07	1.10	1.00	0.97	1.05	32.64	32.76	32.39	32.61
Total	99.29	98.81	100.37	99.34	98.30	98.23	98.66	99.73	99.14	98.90	102.41	102.51	102.44	102.10	102.24	102.00	98.79	99.00	99.05	99.32
#Si IV	6.00	6.00	6.00	6.00	6.00	6.00	6.00	6.00	6.00	6.00	6.00	6.00	5.95	5.94	5.97	5.92	6.00	6.00	6.00	5.96
#Al IV	-	-	-	-	-	-	-	0.00	0.00	-	-	-	0.05	0.06	0.03	0.08	0.00	-	-	0.04
T site	6.00	6.00	6.00	6.00	6.00	6.00	6.00	6.00	6.00	6.00	6.00	6.00	6.00	6.00	6.00	6.00	6.00	6.00	6.00	6.00
#Al VI	3.84	3.87	4.01	3.95	3.85	3.96	3.88	3.94	3.89	3.81	3.90	3.87	3.99	3.99	3.99	3.99	3.20	3.15	3.21	3.13
#Ti VI	0.00	-	0.00	0.00	0.00	0.01	0.00	0.01	-	0.00	-	-	0.01	0.00	0.00	0.00	0.04	0.03	0.03	0.03
#Cr	-	-	-	-	0.01	0.01	0.02	0.00	0.01	0.01	-	-	0.00	0.00	0.00	0.00	0.00	0.00	0.00	0.00
#Fe +3	0.11	0.08	-	0.05	0.05	0.02	0.05	0.00	0.05	0.09	0.03	0.04	0.00	0.00	0.00	0.00	0.75	0.79	0.74	0.76
O site	3.95	3.95	4.01	4.00	3.91	4.00	3.95	3.95	3.94	3.92	3.93	3.91	4.00	4.00	4.00	4.00	3.99	3.97	3.98	3.92
#Fe +2	1.73	1.72	4.45	4.39	4.46	4.65	3.61	3.87	3.79	3.76	4.77	4.80	4.98	5.00	4.98	5.00	0.33	0.29	0.34	0.30
#Mn +2	3.27	3.30	0.23	0.20	0.23	0.23	0.43	0.51	0.54	0.47	0.13	0.11	0.12	0.11	0.11	0.11	0.16	0.16	0.18	0.17
#Mg	0.76	0.75	0.97	0.89	0.89	0.81	1.16	0.91	0.88	0.93	0.66	0.63	0.69	0.64	0.67	0.64	0.01	0.01	0.01	0.18
#Ca	0.08	0.07	0.15	0.16	0.14	0.20	0.62	0.56	0.61	0.60	0.19	0.18	0.19	0.17	0.16	0.18	5.48	5.46	5.40	5.43
A site	5.84	5.84	5.79	5.64	5.71	5.89	5.84	5.85	5.83	5.76	5.75	5.72	5.98	5.91	5.92	5.93	5.98	5.92	5.93	6.08
#O	23.77	23.76	23.81	23.64	23.58	23.89	23.77	23.78	23.74	23.64	23.64	23.58	23.95	23.89	23.91	23.89	23.98	23.90	23.91	23.95

	N14AC	N14AR	N14BC	N14BR	N22AC	N22AR	N22BC	N22I	N22R1	N22R1
SiO2	37.93	37.65	37.62	37.86	37.94	37.59	38.17	38.03	37.85	37.85
TiO2	0.01	0.02	0.01	-	-	0.04	0.06	0.01	0.02	0.02
Al2O3	21.00	20.84	20.87	20.37	21.89	21.66	21.61	21.72	21.53	21.53
Cr2O3	0.02	0.10	0.10	0.29	0.04	0.07	0.05	0.06	0.07	0.07
Fe2O3	0.29	0.16	0.18	0.65	-	0.00	0.04	0.10	0.04	0.04
FeO	30.82	30.53	30.91	30.85	32.73	33.68	32.13	33.27	33.16	33.16
MnO	2.64	1.92	1.61	1.72	2.00	2.22	3.54	2.21	2.25	2.25
MgO	4.63	4.82	5.06	4.44	4.08	3.68	4.15	4.23	4.03	4.03
CaO	2.00	2.15	1.94	2.08	2.21	2.23	2.33	2.10	2.19	2.19
Total	99.34	98.19	98.30	98.26	100.89	101.18	102.08	101.73	101.14	101.14
#Si IV	6.00	6.00	6.00	6.00	5.95	5.95	5.97	5.96	5.98	5.98
#Al IV	-	-	-	-	0.05	0.05	0.03	0.04	0.02	0.02
T site	6.00	6.00	6.00	6.00	6.00	6.00	6.00	6.00	6.00	6.00
#Al VI	3.92	3.91	3.92	3.80	4.00	3.99	3.95	3.98	3.98	3.98
#Ti VI	0.00	0.00	0.00	-	-	0.01	0.01	0.00	0.00	0.00
#Cr	0.00	0.01	0.01	0.04	0.00	0.01	0.01	0.01	0.01	0.01
#Fe +3	0.03	0.02	0.02	0.08	-	0.00	0.00	0.01	0.00	0.00
O site	3.95	3.95	3.96	3.92	4.00	4.00	3.97	4.00	4.00	4.00
#Fe +2	4.08	4.07	4.12	4.09	4.29	4.46	4.20	4.36	4.38	4.38
#Mn +2	0.35	0.26	0.22	0.23	0.27	0.30	0.47	0.29	0.30	0.30
#Mg	1.09	1.15	1.20	1.05	0.95	0.87	0.97	0.99	0.95	0.95
#Ca	0.34	0.37	0.33	0.35	0.37	0.38	0.39	0.35	0.37	0.37
A site	5.86	5.84	5.87	5.72	5.88	6.00	6.03	6.00	6.00	6.00
#O	23.79	23.76	23.81	23.60	23.86	23.98	23.97	23.98	23.99	23.99

	N22R2	N32AC	N32AR	N32BC	N32BR	N35AC	N35AR	N35BC	N35BR	N38AC	N38AR	N38BC	N38BR	N38CC	N38CR	N39AC	N39AR	N39BC	N39BR
SiO2	38.15	38.13	38.23	38.17	38.49	38.26	37.66	38.26	38.11	37.33	37.24	37.37	37.27	37.15	36.94	36.99	36.86	36.58	36.84
TiO2	0.02	0.02	-	-	-	-	0.02	-	0.02	0.03	-	-	-	-	0.01	-	0.03	-	0.02
Al2O3	21.77	21.93	21.89	20.72	21.21	21.86	21.93	21.86	21.59	21.23	20.81	21.11	21.11	21.03	20.90	20.89	20.92	20.81	20.81
Cr2O3	-	0.02	0.02	0.10	0.02	0.01	-	0.04	0.07	-	0.04	0.01	0.05	0.04	0.04	0.07	0.07	0.02	0.05
Fe2O3	-	-	0.00	0.32	0.26	0.24	0.44	-	0.00	0.00	0.36	0.03	0.00	0.00	0.00	0.45	0.30	0.14	0.24
FeO	33.03	33.78	33.88	32.48	32.95	31.98	32.78	32.14	32.43	35.90	35.01	35.50	35.92	35.76	36.54	32.34	33.63	31.31	33.22
MnO	2.19	1.12	1.22	0.67	1.27	2.10	2.59	2.28	2.29	1.02	1.12	1.09	1.28	1.14	1.37	2.28	2.28	2.67	2.16
MgO	3.84	4.39	4.17	3.94	4.20	5.06	4.31	4.74	4.15	2.96	2.83	2.83	2.58	2.62	2.18	4.61	3.88	4.54	3.82
CaO	2.26	1.98	1.97	2.23	2.08	2.30	2.13	2.17	2.07	1.25	1.29	1.31	1.01	1.27	1.27	2.03	2.02	1.99	1.98
Total	101.26	101.37	101.38	98.63	100.48	101.80	101.85	101.49	100.73	99.72	98.70	99.25	99.22	99.01	99.25	99.66	99.99	98.06	99.14
#Si IV	5.98	5.96	5.97	6.00	6.00	5.96	5.90	5.97	5.99	5.98	6.00	6.00	5.99	6.00	6.00	5.92	5.91	5.94	5.95
#Al IV	0.02	0.04	0.03	-	-	0.04	0.10	0.03	0.01	0.02	-	-	0.01	0.00	0.00	0.08	0.09	0.06	0.05
T site	6.00	6.00	6.00	6.00	6.00	6.00	6.00	6.00	6.00	6.00	6.00	6.00	6.00	6.00	6.00	6.00	6.00	6.00	6.00
#Al VI	4.00	4.00	4.00	3.84	3.90	3.97	3.95	4.00	3.99	4.00	3.95	3.99	3.99	3.99	3.99	3.85	3.86	3.92	3.91
#Ti VI	0.00	0.00	-	-	-	-	0.00	-	0.00	0.00	-	-	-	-	0.00	-	0.00	-	0.00
#Cr	-	0.00	0.00	0.01	0.00	0.00	-	0.00	0.01	-	0.01	0.00	0.01	0.01	0.01	0.01	0.01	0.00	0.01
#Fe +3	-	-	0.00	0.04	0.03	0.03	0.05	-	0.00	0.00	0.04	0.00	0.00	0.00	0.00	0.05	0.04	0.02	0.03
O site	4.00	4.00	4.00	3.89	3.93	4.00	4.00	4.00	4.00	4.00	4.00	4.00	4.00	4.00	4.00	3.92	3.91	3.94	3.95
#Fe +2	4.33	4.41	4.42	4.27	4.30	4.16	4.29	4.20	4.26	4.81	4.72	4.77	4.83	4.83	4.96	4.33	4.51	4.25	4.49
#Mn +2	0.29	0.15	0.16	0.09	0.17	0.28	0.34	0.30	0.30	0.14	0.15	0.15	0.17	0.16	0.19	0.31	0.31	0.37	0.30
#Mg	0.90	1.02	0.97	0.92	0.98	1.17	1.01	1.10	0.97	0.71	0.68	0.68	0.62	0.63	0.53	1.10	0.93	1.10	0.92
#Ca	0.38	0.33	0.33	0.38	0.35	0.38	0.36	0.36	0.35	0.21	0.22	0.23	0.17	0.22	0.22	0.35	0.35	0.35	0.34
A site	5.90	5.92	5.89	5.66	5.79	6.00	6.00	5.96	5.89	5.87	5.77	5.82	5.80	5.83	5.90	6.08	6.09	6.06	6.05
#O	23.88	23.90	23.87	23.49	23.68	23.98	23.95	23.95	23.88	23.87	23.77	23.82	23.79	23.83	23.89	23.92	23.91	23.94	23.95

Recalculated analyses — Staurolite

Sample	V11AR	V11AC	V11AR2	V11AR3	V11BR	V11BC
SiO2	27.28	27.51	28.06	28.27	28.25	27.88
TiO2	0.44	0.51	0.52	0.48	0.45	0.46
Al2O3	54.79	53.96	54.34	54.11	54.22	53.84
Fe2O3*	1.20	1.19	1.20	1.20	1.20	1.19
FeO*	13.75	13.85	13.36	13.29	14.10	13.83
MnO	0.04	0.04	0.00	0.05	0.06	0.06
MgO	1.56	1.60	1.44	1.42	1.22	1.41
ZnO	0.16	0.30	0.17	0.27	0.44	0.34
H2O*	1.59	1.38	1.62	1.59	1.46	1.44
Total	100.81	100.34	100.71	100.68	101.40	100.45
Stoichiometry						
Si	7.58	7.71	7.78	7.84	7.82	7.79
AlIV	0.42	0.29	0.22	0.16	0.18	0.21
AlVI	17.53	17.53	17.53	17.53	17.53	17.53
Fe+3	0.25	0.25	0.25	0.25	0.25	0.25
Mn	0.01	0.01	0.00	0.01	0.01	0.01
Fe+2	0.24	0.24	0.25	0.24	0.24	0.24
Ti+4	0.09	0.11	0.11	0.10	0.09	0.10
Fe+2	2.96	3.01	2.85	2.84	3.03	3.00
Mg	0.65	0.67	0.59	0.59	0.50	0.59
Zn	0.03	0.06	0.03	0.06	0.09	0.07
Tet site	3.73	3.84	3.58	3.59	3.72	3.75
H+	2.94	2.55	3.00	2.95	2.71	2.67
O	48.00	48.00	48.00	48.00	48.00	48.00

Recalculated analyses — Staurolite

Sample	V11CR1	V11CR2	V11CC1	V11CC2	V14AR	V14AC	V14BC
SiO2	28.62	27.96	27.73	28.01	27.72	28.33	28.61
TiO2	0.40	0.48	0.41	1.03	0.53	0.49	0.48
Al2O3	53.31	53.79	53.32	53.32	54.74	53.49	53.91
Fe2O3*	1.19	1.19	1.18	1.18	1.20	1.19	1.20
FeO*	13.30	13.42	14.08	13.98	13.53	14.02	12.92
MnO	0.06	0.09	0.03	0.04	0.05	0.05	0.03
MgO	1.66	1.57	1.62	1.92	1.12	1.74	1.34
ZnO	0.36	0.12	0.25	0.29	0.33	0.18	0.43
H2O*	1.39	1.50	1.28	0.87	1.73	1.21	1.65
Total	100.29	100.12	99.90	100.63	100.95	100.70	100.57
Stoichiometry							
Si	7.99	7.81	7.81	7.87	7.67	7.91	7.92
AlIV	0.01	0.19	0.19	0.13	0.33	0.09	0.08
AlVI	17.53	17.53	17.53	17.53	17.53	17.53	17.53
Fe+3	0.25	0.25	0.25	0.25	0.25	0.25	0.25
Mn	0.01	0.02	0.01	0.01	0.01	0.01	0.01
Fe+2	0.24	0.23	0.24	0.24	0.24	0.24	0.24
Ti+4	0.08	0.10	0.09	0.22	0.11	0.10	0.10
Fe+2	2.87	2.91	3.08	3.04	2.89	3.04	2.75
Mg	0.69	0.65	0.68	0.80	0.46	0.72	0.55
Zn	0.07	0.02	0.05	0.06	0.07	0.04	0.09
Tet site	3.72	3.69	3.89	4.13	3.53	3.90	3.49
H+	2.57	2.77	2.38	1.61	3.20	2.24	3.05
O	48.00	48.00	48.00	48.00	48.00	48.00	48.00

Recalculated analyses

Sample	V14BR	V14CC	S30AC	S30AR	S30BC	S30BR	S30CC
SiO2	28.36	28.46	28.36	27.96	26.89	28.22	27.02
TiO2	0.49	0.44	0.30	0.38	0.43	0.31	0.48
Al2O3	54.42	54.03	54.29	53.72	55.84	54.19	55.08
Fe2O3*	1.20	1.20	1.20	1.19	1.21	1.20	1.20
FeO*	13.15	13.47	10.69	11.42	10.95	11.40	10.81
MnO	0.03	0.01	0.06	0.09	0.13	0.02	0.07
MgO	1.49	1.59	1.18	1.23	1.38	1.22	1.35
ZnO	0.18	0.28	2.28	2.31	3.10	2.42	3.24
H2O*	1.64	1.48	2.00	1.70	1.83	1.77	1.76
Total	100.96	100.96	100.36	100.00	101.77	100.75	101.01
Stoichiometry							
Si	7.83	7.88	7.84	7.82	7.40	7.82	7.50
AlIV	0.17	0.12	0.16	0.18	0.60	0.18	0.50
AlVI	17.53	17.53	17.53	17.53	17.53	17.53	17.53
Fe+3	0.25	0.25	0.25	0.25	0.25	0.25	0.25
Mn	0.01	0.00	0.01	0.02	0.03	0.00	0.02
Fe+2	0.24	0.25	0.24	0.23	0.22	0.25	0.23
Ti+4	0.10	0.09	0.06	0.08	0.09	0.06	0.10
Fe+2	2.79	2.87	2.23	2.44	2.30	2.40	2.28
Mg	0.61	0.66	0.49	0.51	0.57	0.50	0.56
Zn	0.04	0.06	0.47	0.48	0.63	0.50	0.66
Tet site	3.54	3.68	3.25	3.51	3.59	3.46	3.60
H+	3.05	2.74	3.70	3.16	3.40	3.29	3.26
O	48.00	48.00	48.00	48.00	48.00	48.00	48.00

Recalculated analyses

Sample	S30CR	S30DR	S30DC	S30ER	S30EC	S30FR	S30FC
SiO2	28.50	28.19	26.80	26.26	27.33	27.35	26.72
TiO2	0.08	0.43	0.38	0.51	0.47	0.64	0.43
Al2O3	55.51	54.39	54.93	53.89	54.00	54.04	53.20
Fe2O3*	1.22	1.20	1.19	1.17	1.18	1.18	1.16
FeO*	10.31	11.40	11.28	11.28	10.12	11.01	11.56
MnO	0.13	0.06	0.11	0.06	0.08	0.04	0.09
MgO	1.36	1.43	1.28	1.84	2.10	1.90	2.06
ZnO	2.95	2.16	2.34	3.70	2.66	2.54	3.51
H2O*	2.06	1.70	1.90	1.21	1.59	1.42	1.01
Total	102.12	100.96	100.21	99.92	99.54	100.13	99.74
Stoichiometry							
Si	7.75	7.80	7.47	7.47	7.67	7.67	7.63
AlIV	0.25	0.20	0.53	0.53	0.33	0.33	0.37
AlVI	17.53	17.53	17.53	17.53	17.53	17.53	17.53
Fe+3	0.25	0.25	0.25	0.25	0.25	0.25	0.25
Mn	0.03	0.01	0.03	0.01	0.02	0.01	0.02
Fe+2	0.22	0.24	0.22	0.24	0.23	0.24	0.23
Ti+4	0.02	0.09	0.08	0.11	0.10	0.13	0.09
Fe+2	2.12	2.40	2.41	2.45	2.14	2.34	2.53
Mg	0.55	0.59	0.53	0.78	0.88	0.79	0.88
Zn	0.59	0.44	0.48	0.78	0.55	0.53	0.74
Tet site	3.28	3.52	3.50	4.11	3.67	3.80	4.24
H+	3.82	3.14	3.53	2.25	2.95	2.63	1.87
O	48.00	48.00	48.00	48.00	48.00	48.00	48.00

Ilmenite analyses, Némiscau

	S14A	S14B	S14C	S14D	S16	S32	V4811	N14	N32A	N32B
FeO	37.20	22.53	40.28	41.60	45.77	45.90	44.97	43.68	45.16	45.18
Fe2O3	18.19	50.25	7.65	6.61	-	-	3.49	2.01	0.61	2.07
MgO	0.64	0.28	0.77	0.12	0.07	0.12	0.17	0.02	0.09	0.15
V2O3	-	-	-	-	-	-	-	-	-	-
Cr2O3	0.06	0.21	0.05	0.05	-	0.03	-	-	0.15	0.05
MnO	0.37	0.35	0.29	0.57	0.32	1.06	0.10	0.97	0.85	0.58
TiO2	43.00	25.84	50.59	50.12	51.44	52.38	50.42	53.31	51.17	51.17
Total	99.46	99.46	99.63	99.07	97.60	99.49	99.15	99.99	98.03	99.20
#Fe+2	1.59	0.98	1.69	1.76	1.98	1.95	1.92	1.83	1.95	1.92
#Fe+3	0.70	1.97	0.29	0.25	-	-	0.13	0.08	0.02	0.08
#Mg+2	0.05	0.02	0.06	0.01	0.01	0.01	0.01	0.00	0.01	0.01
#V	-	-	-	-	-	-	-	-	-	-
#Cr+3	0.00	0.01	0.00	0.00	-	0.00	-	-	0.01	0.00
#Mn+2	0.02	0.02	0.01	0.02	0.01	0.05	0.00	0.04	0.04	0.03
#Ti+4	1.65	1.01	1.90	1.91	2.00	2.00	1.93	2.01	1.98	1.96
#TOTAL	4.00	4.00	3.95	3.96	4.00	4.00	4.00	3.95	4.00	4.00
#O-2	6.00	6.00	6.00	6.00	6.00	6.00	6.00	6.00	6.00	6.00

	N39A	N39B	N39C	N39D	N39E	S32B
FeO	45.65	44.34	45.22	45.46	44.79	44.05
Fe2O3	-	1.48	0.30	-	1.90	-
MgO	0.07	0.10	0.05	0.08	0.09	0.32
V2O3	0.78	0.56	0.33	0.45	0.19	-
Cr2O3	0.13	0.03	0.07	0.03	-	-
MnO	1.27	1.40	1.54	1.41	0.62	1.19
TiO2	52.50	51.07	52.08	52.55	50.69	52.04
Total	100.40	98.98	99.59	99.98	98.28	97.60
#Fe+2	1.92	1.89	1.92	1.92	1.93	1.90
#Fe+3	-	0.06	0.01	-	0.07	-
#Mg+2	0.01	0.01	0.00	0.01	0.01	0.02
#V	0.03	0.02	0.01	0.02	0.01	-
#Cr+3	0.01	0.00	0.00	0.00	-	-
#Mn+2	0.05	0.06	0.07	0.06	0.03	0.05
#Ti+4	1.98	1.96	1.99	1.99	1.96	2.01
#TOTAL	4.00	4.00	4.00	4.00	4.00	3.99
#O-2	6.00	6.00	6.00	6.00	6.00	6.00

Magnetite analyses, Némiscau

	S31	SE1	SE3
FeO	30.65	31.01	31.43
Fe2O3	68.48	68.81	68.17
ZnO	0.02	-	-
Al2O3	0.02	0.09	0.19
MgO	0.06	-	-
V2O3	0.01	-	-
SiO2	0.13	0.01	0.04
Cr2O3	-	-	-
MnO	0.06	0.03	-
TiO2	-	0.01	0.05
Total	99.43	99.96	99.88
#Fe+2	0.99	1.00	1.01
#Fe+3	1.99	1.99	1.98
#Zn+2	0.00	-	-
#Al+3	0.00	0.00	0.01
#Mg+2	0.00	-	-
#V	0.00	-	-
#Si+4	0.01	0.00	0.00
#Cr+3	-	-	-
#Mn+2	0.00	0.00	-
#Ti+4	-	0.00	0.00
#TOTAL	3.00	3.00	3.00
#O-2	4.00	4.00	4.00

Tourmaline analyses, Némiscau

	S3AC	S3AR	S3BR	S3BC	S21	S30A	S30B	N39A	N39B	SE1A
SiO2	35.93	36.01	36.34	35.24	36.25	40.62	39.60	42.24	41.22	37.45
TiO2	0.96	0.85	0.65	0.61	0.83	0.04	0.01	0.03	0.03	-
Al2O3	34.43	33.99	33.35	34.39	33.88	33.59	34.70	30.09	24.42	24.47
Cr2O3	0.06	0.02	0.08	0.16	0.02	-	-	-	-	-
FeO	4.30	4.20	4.16	3.91	8.32	5.69	6.32	6.52	10.22	16.68
MnO	0.05	0.10	0.07	0.13	-	0.02	0.01	0.10	0.04	0.16
MgO	7.30	7.39	7.67	7.47	5.69	2.36	0.59	6.64	9.67	9.39
CaO	1.00	1.02	0.28	1.18	1.15	0.15	0.01	0.36	0.08	0.20
Na2O	1.74	1.78	2.10	1.82	1.36	0.06	0.04	0.05	0.47	0.08
K2O	0.06	0.04	-	0.02	0.03	0.19	0.26	0.39	1.57	0.07
Total	85.83	85.40	84.70	84.93	87.53	82.72	81.54	86.42	87.72	88.50

	SE1B
SiO2	36.52
TiO2	0.02
Al2O3	23.84
Cr2O3	-
FeO	17.54
MnO	0.23
MgO	9.05
CaO	0.15
Na2O	-
K2O	0.05
Total	87.40

MONTAUBAN

ANTHOPHYLLITE ANALYSES, MONTAUBAN

	MQ12A	C322AC	C322AR	C322BC	C322CC	E24AC	E24BC	E24CC	E24DC	J215AC	J215BC	J215CC	J215CR	G315AC	G315BC	G315CC	D211A	D211B	D211C	D211D
SiO2	53.57	54.41	53.93	54.20	53.31	54.85	54.86	54.70	51.78	57.24	56.90	57.82	56.93	56.14	55.01	54.65	56.00	56.03	55.28	55.00
TiO2	0.06	0.06	0.06	0.06	0.09	0.09	0.08	0.07	0.11	0.01	0.03	0.05	0.04	0.05	0.04	0.09	-	0.02	0.02	0.02
Al2O3	4.23	4.12	3.84	3.61	5.07	3.07	2.53	2.83	4.69	1.59	1.75	1.77	1.81	2.77	3.27	4.05	1.94	1.89	1.96	1.95
Fe2O3	-	-	0.02	-	0.00	0.02	-	-	0.02	-	-	-	0.02	-	0.00	-	-	-	-	0.01
FeO	17.24	16.00	15.94	15.58	16.12	16.63	16.42	16.83	17.05	12.24	12.08	11.51	11.37	13.42	13.09	12.82	15.22	15.62	14.90	15.49
MnO	0.98	1.75	1.63	1.53	1.55	1.54	2.77	2.10	1.32	1.02	1.04	1.07	0.83	2.86	2.79	2.73	1.91	1.61	1.87	1.60
MgO	20.50	21.89	22.13	22.11	20.84	21.50	21.23	21.47	21.71	25.62	25.85	26.48	26.10	23.23	23.39	23.34	22.31	22.46	22.54	22.44
ZnO	-	0.17	0.13	0.11	0.20	0.09	0.24	0.14	0.15	0.17	0.05	0.19	0.27	0.11	0.27	0.09	-	0.14	0.07	0.09
CaO	0.38	0.37	0.38	0.32	0.36	0.37	0.34	0.33	0.34	0.48	0.40	0.47	0.50	0.38	0.40	0.46	0.32	0.28	0.31	0.29
Na2O	0.39	0.38	0.30	0.30	0.49	0.22	0.20	0.32	0.42	0.06	0.06	0.08	0.10	0.19	0.21	0.34	0.12	0.08	0.06	0.12
K2O	-	-	-	-	0.01	-	-	-	0.40	-	-	-	-	-	0.02	-	0.01	0.01	0.01	-
H2O	2.10	2.14	2.13	2.12	2.12	2.13	2.12	2.12	2.10	2.18	2.17	2.21	2.18	2.16	2.15	2.15	2.13	2.13	2.11	2.11
Total	99.45	101.29	100.48	99.94	100.16	100.51	100.79	100.91	100.09	100.61	100.33	101.65	100.14	101.31	100.64	100.72	99.96	100.27	99.13	99.12
#Si IV	7.64	7.60	7.60	7.65	7.54	7.73	7.75	7.71	7.40	7.87	7.84	7.84	7.84	7.77	7.67	7.60	7.88	7.87	7.84	7.82
#Al IV	0.36	0.40	0.40	0.35	0.46	0.27	0.25	0.29	0.60	0.13	0.16	0.16	0.16	0.23	0.33	0.40	0.12	0.13	0.16	0.18
#Fe +3	-	-	-	-	-	-	-	-	-	-	-	-	-	-	-	-	-	-	-	-
#Ti IV	-	-	-	-	-	-	-	-	-	-	-	-	-	-	-	-	-	-	-	-
T site	8.00	8.00	8.00	8.00	8.00	8.00	8.00	8.00	8.00	8.00	8.00	8.00	8.00	8.00	8.00	8.00	8.00	8.00	8.00	8.00
#Al VI	0.35	0.28	0.24	0.26	0.39	0.24	0.17	0.18	0.19	0.13	0.12	0.13	0.13	0.22	0.21	0.27	0.20	0.18	0.17	0.15
#Fe +3	-	-	0.00	-	0.00	0.00	-	-	0.00	-	-	-	0.00	-	0.00	-	-	-	-	0.00
#Ti	0.01	0.01	0.01	0.01	0.01	0.01	0.01	0.01	0.01	0.00	0.00	0.01	0.00	0.01	0.00	0.01	-	0.00	0.00	0.00
#Mg	4.36	4.56	4.65	4.65	4.39	4.52	4.47	4.51	4.63	4.87	4.87	4.87	4.86	4.77	4.78	4.72	4.68	4.70	4.77	4.76
#Fe +2	0.29	0.15	0.11	0.08	0.21	0.23	0.35	0.30	0.17	-	-	-	-	-	-	-	0.12	0.12	0.06	0.09
#Zn	-	-	-	-	-	-	-	-	-	-	-	-	-	-	-	-	-	-	-	-
#Mn	-	-	-	-	-	-	-	-	-	-	-	-	-	-	-	-	-	-	-	-
#Ca	-	-	-	-	-	-	-	-	-	-	-	-	-	-	-	-	-	-	-	-
M1,2,3	5.00	5.00	5.00	5.00	5.00	5.00	5.00	5.00	5.00	5.00	5.00	5.00	5.00	5.00	5.00	5.00	5.00	5.00	5.00	5.00
#Mg	-	-	-	-	-	-	-	-	-	0.38	0.43	0.48	0.49	0.02	0.08	0.12	-	-	-	-
#Fe +2	1.77	1.72	1.77	1.76	1.70	1.73	1.59	1.69	1.87	1.41	1.39	1.31	1.31	1.55	1.53	1.49	1.67	1.72	1.71	1.75
#Zn	-	0.02	0.01	0.01	0.02	0.01	0.03	0.01	0.02	0.02	0.01	0.02	0.03	0.01	0.03	0.01	-	0.01	0.01	0.01
#Mn	0.12	0.21	0.19	0.18	0.19	0.18	0.33	0.25	0.16	0.12	0.12	0.12	0.10	0.34	0.33	0.32	0.23	0.19	0.22	0.19
#Ca	0.06	0.05	0.02	0.05	0.05	0.06	0.05	0.05	-	0.07	0.05	0.07	0.07	0.06	0.04	0.06	0.05	0.04	0.05	0.04
#Na	0.05	-	-	0.00	0.04	0.02	-	-	-	0.01	-	-	0.00	0.02	-	-	0.03	0.02	0.02	0.00
M4 site	2.00	2.00	2.00	2.00	2.00	2.00	2.00	2.00	2.04	2.00	2.00	2.00	2.00	2.00	2.00	2.00	1.98	1.99	2.00	2.00
#Ca	-	0.00	0.03	-	-	-	0.00	0.00	0.05	-	0.01	0.00	-	-	0.02	0.01	-	-	-	-
#Na	0.05	0.10	0.08	0.08	0.09	0.04	0.05	0.09	0.12	0.01	0.02	0.02	0.02	0.03	0.06	0.09	-	-	0.00	0.03
#K	-	-	-	-	0.00	-	-	-	0.07	-	-	-	-	-	0.00	-	0.00	0.00	0.00	-
A site	0.05	0.10	0.12	0.08	0.09	0.04	0.06	0.09	0.24	0.01	0.03	0.02	0.02	0.03	0.08	0.10	0.00	0.00	0.00	0.03
#O	22.00	22.00	22.00	22.00	22.00	22.00	22.00	22.01	22.00	22.00	22.01	22.00	22.00	22.01	22.00	22.00	22.00	22.01	22.00	22.00
#OH	2.00	2.00	2.00	2.00	2.00	2.00	2.00	1.99	2.00	2.00	1.99	2.00	2.00	1.99	2.00	2.00	2.00	1.99	2.00	2.00
Charge	0.00	0.00	0.00	-3E-06	0.00	0.00	-5E-07	0.00	0.00	0.00	0.00	-7E-07	0.00	-2E-06	0.00	0.00	-3E-06	-5E-06	-3E-06	0.00

Biotite analyses, Montauban

	MQ1IC	MQ1IR	MQ1AR	MQ1AC	MQ1BR	MQ1CR	MQGAR	MQ6AC	MQ6BC	MQ10I1	MQ10I2	MQ10AC	MQ10BC	MQ10CC	MQ10CR	MQ1013	MQ12AR	MQ12AC	MQ12BC	MQ12CR	MQ12CC	MQ12DR	E32AC	E32AR	E32AI	C322AC	C322AR	C322BC	E24AC	E24BC
SiO2	37.45	37.27	36.62	35.30	36.76	36.28	36.08	35.97	35.50	35.93	35.06	34.46	34.79	35.44	35.28	34.87	39.85	39.51	39.63	39.61	40.26	39.43	37.55	37.50	36.92	40.56	40.88	39.93	39.79	40.68
TiO2	2.14	2.10	1.99	1.60	2.03	1.92	2.93	2.81	2.85	3.94	4.30	3.55	3.43	3.18	3.20	3.51	0.83	0.77	0.94	1.06	0.63	1.24	1.54	1.52	1.53	0.89	0.95	1.12	1.09	1.10
Al2O3	17.79	17.97	18.11	18.00	17.98	17.95	16.31	16.44	16.38	19.40	18.39	18.94	19.43	20.59	19.04	19.82	18.11	17.96	18.36	17.69	17.42	17.45	17.20	17.11	17.38	17.70	17.73	16.94	17.63	17.48
Fe2O3	-	-	0.01	0.21	0.07	0.00	0.02	0.07	0.08	-	-	-	-	-	-	-	-	0.03	0.22	0.06	-	0.06	0.05	0.07	-	-	0.02	-	0.04	0.03
FeO	16.90	18.55	18.46	20.38	18.43	17.92	22.69	22.60	22.19	19.81	22.07	23.37	22.62	22.24	23.10	20.89	9.53	9.28	9.61	9.72	6.89	9.40	17.14	17.47	16.96	7.54	7.44	8.21	10.53	10.26
MnO	0.03	0.05	-	0.01	-	0.01	0.15	0.11	0.16	0.06	0.07	0.06	0.08	-	0.03	0.05	0.07	0.03	0.07	0.05	0.02	0.05	0.04	0.04	-	0.13	0.12	0.08	0.19	0.25
MgO	13.14	11.61	11.42	10.62	11.43	11.48	9.19	9.06	9.11	8.16	7.56	6.60	6.50	6.15	6.93	7.05	18.41	18.38	18.36	18.07	20.82	18.36	13.16	12.96	12.87	19.77	20.13	19.94	18.74	18.67
CaO	0.03	-	-	-	-	-	-	-	-	-	-	-	-	-	-	-	-	0.01	-	-	-	-	-	-	-	0.03	0.02	0.03	0.02	-
Na2O	0.43	0.19	0.22	0.18	0.23	0.19	0.09	0.14	0.13	0.08	0.13	0.09	0.11	0.09	0.07	0.20	0.59	0.56	0.51	0.59	-	0.52	0.29	0.26	0.32	0.49	0.49	0.54	0.29	0.37
K2O	9.22	10.00	9.78	9.24	9.92	9.71	9.94	9.71	9.92	9.35	9.11	9.06	9.13	8.82	9.03	9.80	8.47	8.48	8.42	8.49	8.32	8.55	9.31	9.34	9.14	8.26	8.42	8.40	8.42	8.60
H2O	4.08	4.06	4.01	3.90	4.01	3.97	3.94	3.92	3.89	4.02	3.96	3.91	3.93	3.98	3.95	3.94	4.21	4.17	4.19	4.17	4.22	4.16	4.03	4.02	3.99	4.24	4.27	4.20	4.22	4.26
Total	101.21	101.80	100.62	99.44	100.87	99.43	101.34	100.83	100.21	100.75	100.65	100.04	100.02	100.49	100.63	100.13	100.07	99.17	100.31	99.51	98.58	99.22	100.32	100.29	99.11	99.61	100.47	99.39	100.96	101.70
#Si IV	5.51	5.51	5.47	5.40	5.49	5.48	5.49	5.49	5.46	5.38	5.33	5.30	5.33	5.36	5.37	5.31	5.68	5.68	5.64	5.69	5.74	5.68	5.58	5.58	5.55	5.74	5.74	5.70	5.65	5.72
#Al IV	2.49	2.49	2.53	2.60	2.51	2.52	2.51	2.51	2.54	2.62	2.67	2.70	2.67	2.64	2.63	2.69	2.32	2.32	2.36	2.31	2.26	2.32	2.42	2.42	2.45	2.26	2.26	2.30	2.35	2.28
#Fe IV	-	-	-	-	-	-	-	-	-	-	-	-	-	-	-	-	-	-	-	-	-	-	-	-	-	-	-	-	-	-
#Ti IV	-	-	-	-	-	-	-	-	-	-	-	-	-	-	-	-	-	-	-	-	-	-	-	-	-	-	-	-	-	-
T site	8.00	8.00	8.00	8.00	8.00	8.00	8.00	8.00	8.00	8.00	8.00	8.00	8.00	8.00	8.00	8.00	8.00	8.00	8.00	8.00	8.00	8.00	8.00	8.00	8.00	8.00	8.00	8.00	8.00	8.00
#Al VI	0.59	0.64	0.66	0.64	0.65	0.67	0.41	0.45	0.43	0.80	0.62	0.73	0.83	1.03	0.79	0.86	0.72	0.72	0.72	0.68	0.66	0.64	0.59	0.59	0.63	0.69	0.67	0.55	0.60	0.62
#Ti VI	0.24	0.23	0.22	0.18	0.23	0.22	0.34	0.32	0.33	0.44	0.49	0.41	0.39	0.36	0.37	0.40	0.09	0.08	0.10	0.11	0.07	0.13	0.17	0.17	0.17	0.09	0.10	0.12	0.12	0.12
#Fe +3	-	-	0.00	0.02	0.01	0.00	0.00	0.01	0.01	-	-	-	-	-	-	-	-	0.00	0.02	0.01	-	0.01	0.01	0.01	-	-	0.00	-	0.00	0.00
#Fe +2	2.08	2.29	2.31	2.61	2.30	2.26	2.89	2.88	2.85	2.48	2.80	3.01	2.90	2.81	2.94	2.66	1.14	1.11	1.14	1.17	0.82	1.13	2.13	2.18	2.13	0.89	0.87	0.98	1.25	1.21
#Mn +2	0.00	0.01	-	0.00	-	0.00	0.02	0.01	0.02	0.01	0.01	0.01	0.01	-	0.00	0.01	0.01	0.00	0.01	0.01	0.00	0.01	0.01	0.01	-	0.02	0.01	0.01	0.02	0.03
#Mg	2.88	2.56	2.54	2.42	2.54	2.58	2.08	2.06	2.09	1.82	1.71	1.51	1.48	1.39	1.57	1.60	3.91	3.94	3.89	3.87	4.42	3.94	2.91	2.88	2.88	4.17	4.21	4.24	3.97	3.91
O site	5.79	5.73	5.74	5.87	5.73	5.74	5.74	5.74	5.73	5.56	5.63	5.67	5.62	5.58	5.67	5.53	5.86	5.86	5.89	5.84	5.98	5.85	5.82	5.82	5.82	5.87	5.87	5.91	5.96	5.89
#Ca	0.00	-	-	-	-	-	-	-	-	-	-	-	-	-	-	-	-	0.00	-	-	-	-	-	-	-	0.00	0.00	0.00	0.00	-
#Na	0.12	0.05	0.06	0.05	0.07	0.06	0.03	0.04	0.04	0.02	0.04	0.03	0.03	0.03	0.02	0.06	0.16	0.16	0.14	0.16	-	0.15	0.08	0.08	0.09	0.13	0.13	0.15	0.08	0.10
#K	1.73	1.88	1.87	1.80	1.89	1.87	1.93	1.89	1.95	1.79	1.77	1.78	1.78	1.70	1.75	1.90	1.54	1.55	1.53	1.56	1.51	1.57	1.76	1.77	1.75	1.49	1.51	1.53	1.52	1.54
A site	1.86	1.94	1.93	1.86	1.96	1.93	1.96	1.93	1.99	1.81	1.80	1.80	1.82	1.73	1.77	1.96	1.70	1.71	1.67	1.72	1.51	1.72	1.85	1.85	1.85	1.63	1.64	1.68	1.61	1.64
#O	20.00	20.00	20.00	20.02	20.01	20.00	20.00	20.01	20.01	19.98	19.99	19.99	19.99	19.99	19.99	20.00	20.00	20.00	20.02	20.01	19.99	20.01	20.01	20.01	20.00	20.00	20.00	20.00	20.00	20.00
#OH	4.00	4.00	4.00	3.98	3.99	4.00	4.00	3.99	3.99	4.02	4.01	4.01	4.01	4.01	4.01	4.00	4.00	4.00	3.98	3.99	4.01	3.99	3.99	3.99	4.00	4.00	4.00	4.00	4.00	4.00
Charge	0.00	0.00	0.00	0.00	0.00	-1E-06	-1E-06	0.00	0.00	0.02	0.01	0.01	0.01	0.01	0.01	0.00	0.00	0.00	0.00	-3E-06	0.01	0.00	-	0.00	0.00	0.00	0.00	0.00	0.00	0.00

	E24CC	G315AC	C522A	C522B	D211A	D211B	C27AR	C27AC	C27BR	C27BC	C27CR	C27CC	K16A	K16B
SiO2	39.53	40.89	40.04	41.05	40.13	40.58	38.22	37.34	38.07	37.51	38.29	37.38	38.46	38.77
TiO2	1.24	1.37	0.69	1.12	1.32	1.32	0.64	0.61	0.87	0.89	1.24	1.17	0.71	0.66
Al2O3	17.36	17.83	20.16	18.69	16.59	16.70	19.71	19.50	19.37	19.92	19.36	19.38	20.20	20.40
Fe2O3	0.03	0.01	-	-	0.04	0.05	-	-	0.00	0.01	-	-	-	-
FeO	10.30	7.21	4.60	4.35	7.87	7.68	12.46	12.64	13.17	12.50	12.14	12.10	10.77	10.81
MnO	0.28	0.22	0.27	0.22	0.11	0.13	-	0.07	0.08	-	0.05	-	0.21	0.24
MgO	17.73	20.58	20.33	20.78	19.09	19.12	15.98	16.38	15.80	15.79	15.42	14.98	15.53	15.71
CaO	-	0.04	0.02	0.03	-	-	-	-	-	-	-	-	0.01	0.03
Na2O	0.35	0.59	0.50	0.41	0.46	0.40	0.60	0.51	0.57	0.49	0.58	0.57	0.34	0.34
K2O	8.62	8.31	9.14	8.93	8.78	8.50	8.63	7.96	8.45	8.61	8.42	8.61	9.02	9.01
H2O	4.16	4.31	4.29	4.30	4.16	4.18	4.16	4.11	4.15	4.13	4.14	4.07	4.14	4.18
F	-	-	0.39	0.26	-	-	-	-	-	-	-	-	0.12	0.26
Cl	-	-	0.03	0.04	-	-	-	-	-	-	-	-	0.07	0.04
O=F	-	-	0.16	0.11	-	-	-	-	-	-	-	-	0.05	0.11
O=Cl	-	-	0.01	0.01	-	-	-	-	-	-	-	-	0.02	0.01
Total	99.60	101.36	100.29	100.06	98.55	98.65	100.40	99.12	100.53	99.85	99.64	98.26	99.51	100.33
#Si IV	5.69	5.69	5.59	5.72	5.78	5.81	5.51	5.45	5.50	5.45	5.55	5.51	5.56	5.56
#Al IV	2.31	2.31	2.41	2.28	2.22	2.19	2.49	2.55	2.50	2.55	2.45	2.49	2.44	2.44
#Fe IV	-	-	-	-	-	-	-	-	-	-	-	-	-	-
#Ti IV	-	-	-	-	-	-	-	-	-	-	-	-	-	-
T site	8.00	8.00	8.00	8.00	8.00	8.00	8.00	8.00	8.00	8.00	8.00	8.00	8.00	8.00
#Al VI	0.64	0.61	0.91	0.80	0.59	0.63	0.86	0.81	0.80	0.85	0.86	0.88	1.00	1.01
#Ti VI	0.13	0.14	0.07	0.12	0.14	0.14	0.07	0.07	0.09	0.10	0.14	0.13	0.08	0.07
#Fe +3	0.00	0.00	-	-	0.00	0.01	-	-	0.00	0.00	-	-	-	-
#Fe +2	1.24	0.84	0.54	0.51	0.95	0.92	1.50	1.54	1.59	1.52	1.47	1.49	1.30	1.30
#Mn +2	0.03	0.03	0.03	0.03	0.01	0.02	-	0.01	0.01	-	0.01	-	0.03	0.03
#Mg	3.81	4.27	4.23	4.32	4.10	4.08	3.43	3.56	3.40	3.42	3.33	3.29	3.35	3.36
O site	5.86	5.89	5.79	5.77	5.80	5.80	5.87	5.99	5.90	5.89	5.80	5.79	5.76	5.77
#Ca	-	0.01	0.00	0.00	-	-	-	-	-	-	-	-	0.00	0.00
#Na	0.10	0.16	0.14	0.11	0.13	0.11	0.17	0.14	0.16	0.14	0.16	0.16	0.10	0.09
#K	1.58	1.47	1.63	1.59	1.61	1.55	1.59	1.48	1.56	1.59	1.56	1.62	1.66	1.65
A site	1.68	1.64	1.77	1.70	1.74	1.66	1.76	1.63	1.72	1.73	1.72	1.78	1.76	1.75
#O	20.00	20.00	19.82	19.88	20.00	20.01	20.00	20.00	20.00	20.00	20.00	20.00	19.93	19.87
#OH	4.00	4.00	4.00	4.00	4.00	3.99	4.00	4.00	4.00	4.00	4.00	4.00	3.99	4.00
#F	-	-	0.17	0.11	-	-	-	-	-	-	-	-	0.05	0.12
#Cl	-	-	0.01	0.01	-	-	-	-	-	-	-	-	0.02	0.01
Charge	0.00	0.00	0.18	0.12	0.00	-1E-06	0.00	0.00	-	0.00	0.00	0.00	0.07	0.13

CHLORITE ANALYSES, MONTAUBAN

	MT1	C211
SiO2	27.90	29.75
TiO2	0.07	0.21
Al2O3	23.82	15.57
Fe2O3	0.00	0.00
FeO	9.90	26.32
MnO	0.09	0.28
MgO	25.59	16.71
CaO	-	0.09
Na2O	-	0.14
K2O	-	0.40
H2O	12.35	11.45
F	0.11	-
Cl	0.01	-
O=F	0.05	-
O=Cl	0.00	-
Total	99.79	100.92
#Si IV	2.70	3.09
#Al IV	1.30	0.91
T site	4.00	4.00
#Al VI	1.42	0.99
#Ti	0.01	0.02
#Fe +3	0.00	0.00
#Fe +2	0.80	2.28
#Mn +2	0.01	0.02
#Mg	3.70	2.58
#Ca	-	0.01
#Na	-	0.03
#K	-	0.05
O site	5.93	5.99
#O	10.00	10.00
#OH	7.96	8.00
#F	0.03	-
#Cl	0.00	-
Charge	0.00	-

MUSCOVITE ANALYSES, MONTAUBAN

	MQ10	C522A	C522B	C332A	C332B	I326
SiO2	46.12	47.44	47.91	46.27	46.82	46.85
TiO2	0.94	-	0.02	0.22	0.19	0.77
Al2O3	34.71	36.96	36.90	32.34	32.59	36.95
Fe2O3	0.02	0.07	-	-	-	-
FeO	1.43	-	0.03	0.15	0.19	0.59
MnO	0.03	0.12	0.30	-	-	-
MgO	0.62	0.30	0.38	6.55	6.63	2.41
CaO	-	0.80	0.80	-	-	-
Na2O	0.33	0.14	0.67	0.18	0.28	0.02
K2O	10.90	9.35	9.01	9.13	9.81	8.92
H2O	4.48	4.54	4.57	4.55	4.53	4.58
F	-	-	0.27	-	-	-
Cl	-	-	0.05	-	-	-
O=F	-	-	0.11	-	-	-
O=Cl	-	-	0.01	-	-	-
Total	99.58	99.72	100.79	99.39	101.04	101.09
#Si IV	6.17	6.22	6.23	6.13	6.13	6.06
#Al IV	1.83	1.78	1.77	1.87	1.87	1.94
#Fe IV	-	-	-	-	-	-
#Ti IV	-	-	-	-	-	-
T site	8.00	8.00	8.00	8.00	8.00	8.00
#Al VI	3.64	3.93	3.89	3.19	3.15	3.70
#Ti VI	0.09	-	0.00	0.02	0.02	0.07
#Fe +3	0.00	0.01	-	-	-	-
#Fe +2	0.16	-	0.00	0.02	0.02	0.06
#Mn +2	0.00	0.01	0.03	-	-	-
#Mg	0.12	0.06	0.07	1.29	1.29	0.47
O site	4.03	4.01	4.00	4.52	4.49	4.30
#Ca	-	0.11	0.11	-	-	-
#Na	0.09	0.04	0.17	0.05	0.07	0.01
#K	1.86	1.56	1.49	1.54	1.64	1.47
A site	1.95	1.71	1.78	1.59	1.71	1.48
#O	20.00	20.03	19.91	20.00	20.00	20.00
#OH	4.00	3.97	3.96	4.00	4.00	4.00
#F	-	-	0.11	-	-	-
#Cl	-	-	0.01	-	-	-
Charge	0.00	-2E-02	0.09	0.00	0.00	0.00

CORDIERITE ANALYSES, MONTAUBAN

	MQ12AC	MQ12AR	C322AC	C322AR	C322BC	C522AC	J215AC	J215BC	J215CC	G315AC
SiO2	49.43	49.33	49.61	49.30	49.49	50.02	50.47	50.05	50.44	49.91
TiO2	0.01	-	0.02	-	-	0.03	-	-	-	0.01
Al2O3	32.75	33.13	32.23	32.92	32.83	33.03	32.05	33.76	33.69	33.32
FeO	3.63	3.42	3.14	3.33	3.07	1.67	1.94	1.91	1.90	2.38
MnO	0.18	0.16	0.30	0.28	0.24	0.49	0.16	0.12	0.09	0.46
ZnO	-	-	0.22	-	-	0.06	0.03	-	0.23	0.06
MgO	10.73	10.97	11.02	11.19	11.22	12.32	12.44	12.47	12.55	11.92
CaO	0.01	0.03	0.01	0.07	0.01	0.01	0.03	0.02	0.01	0.02
Na2O	0.35	0.30	0.39	0.37	0.40	0.18	0.17	0.18	0.19	0.31
K2O	-	-	-	0.04	-	-	-	-	-	-
Total	97.09	97.34	96.94	97.50	97.26	97.81	97.29	98.51	99.10	98.39
#Si+4	5.05	5.02	5.07	5.01	5.04	5.03	5.10	5.00	5.01	5.01
#Ti+4	0.00	-	0.00	-	-	0.00	-	-	-	0.00
#Al+3	3.94	3.97	3.88	3.95	3.94	3.92	3.82	3.97	3.94	3.94
#Fe+2	0.31	0.29	0.27	0.28	0.26	0.14	0.16	0.16	0.16	0.20
#Mn+2	0.02	0.01	0.03	0.02	0.02	0.04	0.01	0.01	0.01	0.04
#Zn+2	-	-	0.02	-	-	0.00	0.00	-	0.02	0.00
#Mg+2	1.63	1.66	1.68	1.70	1.70	1.85	1.87	1.86	1.86	1.78
#Ca+2	0.00	0.00	0.00	0.01	0.00	0.00	0.00	0.00	0.00	0.00
#Na+1	0.07	0.06	0.08	0.07	0.08	0.04	0.03	0.03	0.04	0.06
#K	-	-	-	0.01	-	-	-	-	-	-
#TOTAL	11.02	11.02	11.02	11.05	11.04	11.02	11.01	11.03	11.03	11.05
#O-2	18.00	18.00	18.00	18.00	18.00	18.00	18.00	18.00	18.00	18.00

	G315BC	MT1A	MT1B	MT1C	C522A	C522B	C522C	C522D	D211A	D211B	F419
SiO2	49.76	50.50	50.97	50.40	50.87	50.66	50.18	50.92	49.81	49.74	50.11
TiO2	0.01	0.01	0.05	-	0.03	0.01	-	-	-	0.05	0.06
Al2O3	33.61	33.19	34.00	33.49	33.31	33.29	33.56	33.52	33.04	32.58	32.69
FeO	2.55	3.43	2.82	2.83	1.51	1.45	1.46	1.46	2.93	2.97	3.25
MnO	0.46	0.31	0.29	0.27	0.37	0.52	0.44	0.47	0.18	0.09	0.39
ZnO	0.05	0.05	0.04	-	0.07	0.17	0.03	-	0.01	0.03	0.05
MgO	11.64	11.11	11.59	11.52	12.26	11.99	12.13	11.87	11.50	11.42	10.89
CaO	0.01	-	0.02	0.02	-	0.02	0.01	-	0.02	-	-
Na2O	0.27	0.26	0.28	0.28	0.19	0.17	0.20	0.16	0.30	0.34	-
K2O	-	-	-	-	-	-	-	-	-	-	-
Total	98.36	98.86	100.06	98.81	98.61	98.28	98.01	98.40	97.79	97.22	97.44
#Si+4	5.00	5.06	5.03	5.04	5.07	5.07	5.03	5.08	5.03	5.06	5.08
#Ti+4	0.00	0.00	0.00	-	0.00	0.00	-	-	-	0.00	0.00
#Al+3	3.98	3.92	3.96	3.95	3.91	3.92	3.96	3.94	3.94	3.90	3.91
#Fe+2	0.21	0.29	0.23	0.24	0.13	0.12	0.12	0.12	0.25	0.25	0.28
#Mn+2	0.04	0.03	0.02	0.02	0.03	0.04	0.04	0.04	0.02	0.01	0.03
#Zn+2	0.00	0.00	0.00	-	0.01	0.01	0.00	-	0.00	0.00	0.00
#Mg+2	1.74	1.66	1.71	1.72	1.82	1.79	1.81	1.76	1.73	1.73	1.65
#Ca+2	0.00	-	0.00	0.00	-	0.00	0.00	-	0.00	-	-
#Na+1	0.05	0.05	0.05	0.05	0.04	0.03	0.04	0.03	0.06	0.07	-
#K	-	-	-	-	-	-	-	-	-	-	-
#TOTAL	11.04	11.01	11.01	11.02	11.00	10.99	11.01	10.97	11.03	11.02	10.96
#O-2	18.00	18.00	18.00	18.00	18.00	18.00	18.00	18.00	18.00	18.00	18.00

Garnite analyses, Montauban

	MT1A	MT1B	D211A	D211B	K16A	K16B	K16C	I24A	I24B	I2BC	I23BR	I23CR	I23DR	F419AR	F419BR	F419CR	F419DR	E624	E624BR	D211AR
SiO2	0.01	0.03	0.32	-	0.04	0.07	0.05	0.09	0.03	0.01	0.02	0.02	0.01	0.04	0.04	0.02	0.01	0.02	0.06	0.02
TiO2	0.01	-	-	0.01	0.01	-	-	0.01	-	-	0.08	0.01	0.04	0.01	0.02	-	0.03	-	0.02	0.05
Al2O3	60.19	60.53	59.78	60.42	59.76	59.61	60.13	60.08	60.10	60.19	60.74	60.41	60.82	60.20	60.12	60.38	61.25	60.51	60.33	60.39
Cr2O3	-	-	-	-	-	-	-	-	-	-	-	-	-	-	-	-	-	0.03	-	-
Fe2O3	-	-	-	-	-	-	-	-	-	-	-	-	-	-	-	-	-	-	0.10	-
FeO	6.88	7.32	6.77	6.94	6.33	6.07	5.91	8.06	7.83	7.13	6.47	6.33	5.60	7.49	7.43	7.48	7.58	8.41	8.96	6.43
MnO	0.17	0.19	0.24	0.17	0.16	0.25	0.31	0.36	0.32	0.30	0.26	0.24	0.17	0.25	0.23	0.27	0.22	0.13	0.14	0.21
MgO	4.33	4.32	4.47	4.35	2.78	2.81	2.66	4.18	4.19	4.12	4.29	4.11	4.26	4.53	4.11	4.25	4.65	4.44	4.97	4.19
ZnO	27.92	27.82	27.47	27.16	29.31	30.57	30.80	25.70	25.90	27.12	28.58	29.39	29.54	27.01	27.81	27.85	26.36	26.06	24.78	28.24
Total	99.51	100.22	99.05	99.05	98.39	99.41	99.87	98.51	98.38	98.87	100.44	100.51	100.44	99.53	99.76	100.25	100.10	99.60	99.36	99.53
#Si+4	0.00	0.00	0.01	-	0.00	0.00	0.00	0.00	0.00	0.00	0.00	0.00	0.00	0.00	0.00	0.00	0.00	0.00	0.00	0.00
#Ti+4	0.00	-	-	0.00	0.00	-	-	0.00	-	-	0.00	0.00	0.00	0.00	0.00	-	0.00	-	0.00	0.00
#Al+3	2.04	2.03	2.03	2.04	2.06	2.04	2.05	2.04	2.05	2.04	2.04	2.03	2.04	2.03	2.03	2.03	2.04	2.04	2.03	2.04
#Cr+3	-	-	-	-	-	-	-	-	-	-	-	-	-	-	-	-	-	0.00	-	-
#Fe+3	-	-	-	-	-	-	-	-	-	-	-	-	-	-	-	-	-	-	0.00	-
#Fe+2	0.17	0.17	0.16	0.17	0.15	0.15	0.14	0.19	0.19	0.17	0.15	0.15	0.13	0.18	0.18	0.18	0.18	0.20	0.21	0.15
#Mn+2	0.00	0.00	0.01	0.00	0.00	0.01	0.01	0.01	0.01	0.01	0.01	0.01	0.00	0.01	0.01	0.01	0.01	0.00	0.00	0.01
#Mg+2	0.19	0.18	0.19	0.19	0.12	0.12	0.11	0.18	0.18	0.18	0.18	0.17	0.18	0.19	0.18	0.18	0.20	0.19	0.21	0.18
#Zn+2	0.59	0.59	0.58	0.58	0.63	0.66	0.66	0.55	0.55	0.58	0.60	0.62	0.62	0.57	0.59	0.59	0.55	0.55	0.52	0.60
#TOTAL	2.98	2.98	2.98	2.98	2.97	2.98	2.97	2.98	2.98	2.98	2.98	2.98	2.98	2.98	2.98	2.98	2.98	2.98	2.98	2.98
#O-2	4.00	4.00	4.00	4.00	4.00	4.00	4.00	4.00	4.00	4.00	4.00	4.00	4.00	4.00	4.00	4.00	4.00	4.00	4.00	4.00

	MT2AR	MT2AC	MT2BR	MT2C	E326	E326B	I18AR	I18AC	I18BR	I23A	D211BR	D211CR
SiO2	0.03	-	0.01	0.01	-	0.01	0.05	0.01	0.03	0.05	0.04	0.01
TiO2	0.03	0.02	0.01	0.04	-	-	-	0.03	0.02	-	0.03	-
Al2O3	60.47	60.70	59.92	60.28	60.99	61.03	60.95	61.38	60.80	61.25	60.06	60.17
Cr2O3	-	-	-	-	-	0.05	-	-	-	-	-	-
Fe2O3	-	-	-	-	0.58	0.38	-	-	0.11	-	-	-
FeO	7.85	7.84	7.33	6.54	4.78	4.82	6.96	7.68	6.64	6.05	6.55	6.66
MnO	0.22	0.12	0.18	0.16	0.38	0.37	0.14	0.23	0.13	0.17	0.16	0.21
MgO	4.69	4.73	4.07	4.25	4.43	4.44	4.09	4.49	3.95	4.08	4.03	4.36
ZnO	26.77	26.41	27.48	29.09	28.05	28.27	28.21	26.17	28.96	28.53	28.53	28.09
Total	100.06	99.82	99.00	100.37	99.21	99.37	100.40	99.99	100.64	100.13	99.40	99.50
#Si+4	0.00	-	0.00	0.00	-	0.00	0.00	0.00	0.00	0.00	0.00	0.00
#Ti+4	0.00	0.00	0.00	0.00	-	-	-	0.00	0.00	-	0.00	-
#Al+3	2.03	2.04	2.04	2.03	2.05	2.05	2.04	2.05	2.04	2.05	2.04	2.04
#Cr+3	-	-	-	-	-	0.00	-	-	-	-	-	-
#Fe+3	-	-	-	-	0.01	0.01	-	-	0.00	-	-	-
#Fe+2	0.19	0.19	0.18	0.16	0.11	0.11	0.17	0.18	0.16	0.14	0.16	0.16
#Mn+2	0.01	0.00	0.00	0.00	0.01	0.01	0.00	0.01	0.00	0.00	0.00	0.01
#Mg+2	0.20	0.20	0.18	0.18	0.19	0.19	0.17	0.19	0.17	0.17	0.17	0.19
#Zn+2	0.56	0.55	0.59	0.61	0.59	0.60	0.59	0.55	0.61	0.60	0.61	0.60
#TOTAL	2.98	2.98	2.98	2.98	2.97	2.97	2.98	2.97	2.98	2.97	2.98	2.98
#O-2	4.00	4.00	4.00	4.00	4.00	4.00	4.00	4.00	4.00	4.00	4.00	4.00

Garnet analyses, Montauban

	MQ1AR	MQ1AC	MQ1BR	MQ1BC	MQ1CR	MQ1CC	MQ1DR	MQ4AC	MQ4AR	MQ4BC
SiO2	38.80	38.94	38.97	38.63	38.49	38.40	38.60	37.14	37.50	37.49
TiO2	-	0.06	0.03	0.01	-	0.01	-	0.05	0.05	0.09
Al2O3	21.49	21.76	21.34	21.39	21.56	21.38	21.40	20.67	20.85	20.91
Cr2O3	-	-	-	-	-	-	-	-	-	-
Fe2O3	0.30	0.12	0.55	0.43	0.25	0.35	0.35	0.71	0.56	0.31
FeO	32.56	32.82	32.15	31.53	32.99	32.20	32.17	25.32	25.74	25.29
MnO	1.71	1.65	1.57	2.12	1.72	1.72	1.73	6.70	6.89	6.69
MgO	3.46	4.41	4.12	4.39	4.02	4.37	4.13	0.25	0.23	0.22
CaO	3.75	2.77	3.14	3.02	3.07	2.67	3.10	9.70	9.19	9.41
Total	102.07	102.53	101.87	101.52	102.10	101.10	101.48	100.54	101.01	100.41
#Si IV	6.00	6.00	6.00	6.00	6.00	6.00	6.00	5.96	6.00	6.00
#Al IV	0.00	-	-	-	-	-	-	0.04	0.00	-
T site	6.00	6.00	6.00	6.00	6.00	6.00	6.00	6.00	6.00	6.00
#Al VI	3.92	3.95	3.87	3.92	3.96	3.94	3.92	3.87	3.92	3.94
#Ti VI	-	0.01	0.00	0.00	-	0.00	-	0.01	0.01	0.01
#Cr	-	-	-	-	-	-	-	-	-	-
#Fe +3	0.03	0.01	0.06	0.05	0.03	0.04	0.04	0.09	0.07	0.04
O site	3.95	3.97	3.94	3.97	3.99	3.98	3.96	3.96	4.00	3.99
#Fe +2	4.21	4.23	4.14	4.10	4.30	4.21	4.18	3.40	3.44	3.38
#Mn +2	0.22	0.22	0.20	0.28	0.23	0.23	0.23	0.91	0.93	0.91
#Mg	0.80	1.01	0.95	1.02	0.93	1.02	0.96	0.06	0.05	0.05
#Ca	0.62	0.46	0.52	0.50	0.51	0.45	0.52	1.67	1.57	1.61
A site	5.85	5.91	5.81	5.89	5.97	5.90	5.88	6.04	6.00	5.96
#O	23.78	23.88	23.72	23.84	23.96	23.87	23.82	23.96	24.00	23.95

	MQ10AC	MQ10I1	MQ10I2	MQ10BR	MQ10BC	MQ12AC	MQ12AR	MQ12BR	MQ12BC	MQ12CR
SiO2	38.07	38.05	38.15	37.73	37.66	39.37	38.80	38.83	38.90	38.71
TiO2	0.01	0.02	0.03	0.01	-	-	0.02	-	-	0.01
Al2O3	21.47	21.43	21.54	21.56	21.57	22.08	22.04	22.09	21.87	21.77
Cr2O3	-	-	-	-	-	-	-	-	-	-
Fe2O3	0.09	0.04	0.03	0.00	-	0.08	-	-	0.10	0.06
FeO	35.72	36.31	36.27	35.96	36.04	25.32	26.71	26.46	24.64	25.74
MnO	3.46	3.47	3.05	3.15	3.50	5.27	5.23	5.54	5.58	5.43
MgO	2.19	2.13	1.99	2.14	2.18	7.06	6.03	6.05	7.09	6.46
CaO	1.16	1.22	1.26	1.28	1.24	2.50	2.42	2.44	2.55	2.43
Total	102.17	102.67	102.32	101.83	102.19	101.68	101.25	101.41	100.73	100.61
#Si IV	6.00	6.00	6.00	5.97	5.97	6.00	5.99	5.99	6.00	6.00
#Al IV	-	0.00	-	0.03	0.03	-	0.01	0.01	-	-
T site	6.00	6.00	6.00	6.00	6.00	6.00	6.00	6.00	6.00	6.00
#Al VI	3.99	3.98	3.99	4.00	4.00	3.97	4.00	4.00	3.98	3.98
#Ti VI	0.00	0.00	0.00	0.00	-	-	0.00	-	-	0.00
#Cr	-	-	-	-	-	-	-	-	-	-
#Fe +3	0.01	0.00	0.00	0.00	-	0.01	-	-	0.01	0.01
O site	4.00	3.99	4.00	4.00	4.00	3.98	4.00	4.00	3.99	3.99
#Fe +2	4.71	4.79	4.77	4.76	4.78	3.23	3.45	3.41	3.18	3.34
#Mn +2	0.46	0.46	0.41	0.42	0.47	0.68	0.68	0.72	0.73	0.71
#Mg	0.51	0.50	0.47	0.51	0.52	1.60	1.39	1.39	1.63	1.49
#Ca	0.20	0.21	0.21	0.22	0.21	0.41	0.40	0.40	0.42	0.40
A site	5.88	5.96	5.86	5.91	5.97	5.92	5.92	5.93	5.96	5.95
#O	23.88	23.94	23.86	23.90	23.96	23.88	23.91	23.92	23.94	23.92

	MQ4BR	MQ4CC	MQ4CR	MQ6AR	MQ6AC	MQ6BR	MQ6BC	MQ6CR	MQ6CC	MQ10AR
SiO2	37.78	37.13	37.36	38.47	37.30	38.43	37.72	37.23	37.52	37.85
TiO2	0.03	0.01	0.02	-	0.05	0.05	0.04	-	0.02	-
Al2O3	20.66	20.79	20.76	21.55	21.06	21.24	21.32	21.11	20.94	21.47
Cr2O3	-	-	-	-	-	-	-	-	-	-
Fe2O3	0.81	0.54	0.65	0.29	0.53	0.38	0.03	0.05	0.32	-
FeO	24.07	24.62	24.72	27.42	27.21	26.99	27.41	26.66	26.77	37.15
MnO	6.39	6.26	6.10	6.74	6.64	6.69	6.46	6.49	6.37	2.63
MgO	0.23	0.24	0.22	1.87	1.96	1.68	1.77	1.59	1.78	1.86
CaO	10.46	10.49	10.56	6.42	6.21	6.39	6.30	6.65	6.36	0.97
Total	100.43	100.08	100.39	102.76	100.96	101.85	101.05	99.79	100.08	101.93
#Si IV	6.00	5.97	5.99	6.00	5.94	6.00	5.99	5.99	6.00	5.99
#Al IV	-	0.03	0.01	-	0.06	-	0.01	0.01	-	0.01
T site	6.00	6.00	6.00	6.00	6.00	6.00	6.00	6.00	6.00	6.00
#Al VI	3.87	3.91	3.91	3.96	3.89	3.91	3.99	3.99	3.95	4.00
#Ti VI	0.00	0.00	0.00	-	0.01	0.01	0.00	-	0.00	-
#Cr	-	-	-	-	-	-	-	-	-	-
#Fe +3	0.10	0.07	0.08	0.03	0.06	0.04	0.00	0.01	0.04	-
O site	3.97	3.97	3.99	4.00	3.96	3.96	4.00	4.00	3.99	4.00
#Fe +2	3.20	3.31	3.31	3.58	3.62	3.52	3.64	3.59	3.58	4.92
#Mn +2	0.86	0.85	0.83	0.89	0.90	0.88	0.87	0.88	0.86	0.35
#Mg	0.05	0.06	0.05	0.43	0.47	0.39	0.42	0.38	0.42	0.44
#Ca	1.78	1.81	1.81	1.07	1.06	1.07	1.07	1.15	1.09	0.16
A site	5.89	6.03	6.01	5.97	6.04	5.87	6.00	6.00	5.96	5.88
#O	23.84	23.97	23.99	23.97	23.95	23.81	24.00	24.00	23.94	23.87

	MQ12CC	MQ12I	B41AR	B41AC	B41BR	B41BC	B41CR	B41CC	E32AR	E32AC
SiO2	38.84	38.82	38.89	39.14	38.89	38.91	39.09	38.66	38.24	38.63
TiO2	-	0.01	0.02	0.08	0.03	0.04	0.02	0.05	-	0.02
Al2O3	21.87	21.78	21.71	21.60	22.00	21.38	21.50	21.36	21.70	21.30
Cr2O3	-	-	-	-	-	-	-	-	-	-
Fe2O3	0.16	0.02	0.34	0.35	-	0.67	0.47	0.51	-	0.59
FeO	24.63	26.12	31.25	28.58	31.69	28.58	31.29	28.46	30.33	29.26
MnO	5.35	5.27	1.25	2.14	1.37	2.60	1.47	2.53	1.52	3.82
MgO	6.88	6.24	4.00	3.08	3.45	3.07	3.37	3.15	3.77	2.98
CaO	2.45	2.47	5.18	7.27	5.21	7.05	5.18	6.98	4.96	5.51
Total	100.18	100.73	102.64	102.24	102.64	102.30	102.39	101.70	100.52	102.11
#Si IV	6.00	6.00	6.00	6.00	6.00	6.00	6.00	6.00	5.99	6.00
#Al IV	-	-	-	-	0.00	0.00	-	-	0.01	-
T site	6.00	6.00	6.00	6.00	6.00	6.00	6.00	6.00	6.00	6.00
#Al VI	3.98	3.97	3.95	3.90	4.00	3.89	3.89	3.91	4.00	3.90
#Ti VI	-	0.00	0.00	0.01	0.00	0.00	0.00	0.01	-	0.00
#Cr	-	-	-	-	-	-	-	-	-	-
#Fe +3	0.02	0.00	0.04	0.04	-	0.08	0.05	0.06	-	0.07
O site	4.00	3.97	3.99	3.95	4.00	3.97	3.95	3.97	4.00	3.97
#Fe +2	3.18	3.38	4.03	3.66	4.09	3.69	4.02	3.69	3.97	3.80
#Mn +2	0.70	0.69	0.16	0.28	0.18	0.34	0.19	0.33	0.20	0.50
#Mg	1.58	1.44	0.92	0.70	0.79	0.71	0.77	0.73	0.88	0.69
#Ca	0.41	0.41	0.86	1.19	0.86	1.16	0.85	1.16	0.83	0.92
A site	5.87	5.91	5.97	5.84	5.92	5.90	5.83	5.92	5.89	5.91
#O	23.87	23.87	23.96	23.77	23.92	23.85	23.75	23.88	23.89	23.87

	E32BR	E32BC	E32CR	E32CC	G511AC	G511AR	G511BC	G511BR	G513AR	G513AC
SiO2	38.27	38.19	38.98	38.68	37.69	38.07	37.56	37.26	39.30	38.94
TiO2	-	0.02	0.01	0.04	0.03	0.01	0.04	0.02	-	0.10
Al2O3	21.10	20.17	20.70	20.95	21.42	21.40	21.10	21.69	21.51	21.29
Cr2O3	-	-	-	-	-	-	-	0.02	-	-
Fe2O3	0.92	1.68	1.56	0.84	0.00	0.25	0.19	0.95	0.68	0.80
FeO	31.44	28.92	30.54	28.88	27.34	31.12	28.26	30.89	29.87	25.12
MnO	1.57	1.77	1.49	2.15	4.09	2.62	3.06	2.45	2.85	5.47
MgO	3.62	3.75	3.71	3.71	2.35	2.83	2.39	3.07	3.05	2.01
CaO	5.02	5.28	5.01	5.45	7.37	5.30	7.29	5.28	5.83	9.02
Total	101.94	99.78	102.00	100.70	100.28	101.60	99.89	101.64	103.09	102.75
#Si IV	5.99	6.00	6.00	6.00	5.99	5.99	6.00	5.86	6.00	6.00
#Al IV	0.01	-	-	-	0.01	0.01	0.00	0.14	-	-
T site	6.00	6.00	6.00	6.00	6.00	6.00	6.00	6.00	6.00	6.00
#Al VI	3.88	3.73	3.76	3.83	4.00	3.96	3.97	3.88	3.87	3.87
#Ti VI	-	0.00	0.00	0.00	0.00	0.00	0.00	0.00	-	0.01
#Cr	-	-	-	-	-	-	-	0.00	-	-
#Fe +3	0.11	0.20	0.18	0.10	0.00	0.03	0.02	0.11	0.08	0.09
O site	3.99	3.94	3.94	3.93	4.00	4.00	4.00	4.00	3.95	3.97
#Fe +2	4.12	3.80	3.93	3.75	3.63	4.10	3.77	4.06	3.81	3.24
#Mn +2	0.21	0.24	0.19	0.28	0.55	0.35	0.41	0.33	0.37	0.71
#Mg	0.84	0.88	0.85	0.86	0.56	0.66	0.57	0.72	0.69	0.46
#Ca	0.84	0.89	0.83	0.91	1.25	0.89	1.25	0.89	0.95	1.49
A site	6.01	5.80	5.80	5.79	5.99	6.00	6.00	6.00	5.83	5.90
#O	23.99	23.71	23.71	23.69	23.99	23.99	24.00	23.93	23.75	23.86

	G513BR	G513BC	G519AC	G519BC	I35AR	I35AC	I35BC	I37AR	I37AC	I37BC
SiO2	38.94	39.33	38.31	38.39	38.80	39.24	38.92	38.38	38.42	38.75
TiO2	0.01	0.04	0.01	0.01	-	0.04	0.05	0.01	0.02	0.06
Al2O3	21.29	21.51	21.54	21.48	21.55	21.48	21.41	20.49	21.76	21.74
Cr2O3	-	-	-	-	-	-	-	-	-	-
Fe2O3	0.80	0.66	0.28	0.22	0.27	0.69	0.76	1.53	0.00	0.10
FeO	25.12	25.33	30.56	30.72	31.71	31.21	31.31	30.60	31.16	30.93
MnO	5.47	5.59	2.70	2.77	1.21	1.32	1.28	1.02	1.25	1.05
MgO	2.01	1.89	3.08	3.03	3.50	3.65	3.65	3.82	3.64	4.08
CaO	9.02	8.90	5.61	5.11	5.84	5.30	5.37	5.01	5.39	5.20
Total	102.66	103.25	102.09	101.73	102.88	102.93	102.75	100.86	101.64	101.91
#Si IV	6.00	6.00	5.99	6.00	6.00	6.00	6.00	6.00	6.00	6.00
#Al IV	-	-	0.01	-	0.00	-	-	-	0.00	-
T site	6.00	6.00	6.00	6.00	6.00	6.00	6.00	6.00	6.00	6.00
#Al VI	3.87	3.87	3.96	3.96	3.93	3.87	3.89	3.78	4.00	3.97
#Ti VI	0.00	0.00	0.00	0.00	-	0.00	0.01	0.00	0.00	0.01
#Cr	-	-	-	-	-	-	-	-	-	-
#Fe +3	0.09	0.08	0.03	0.03	0.03	0.08	0.09	0.18	0.00	0.01
O site	3.96	3.95	3.99	3.98	3.96	3.95	3.98	3.96	4.00	3.99
#Fe +2	3.24	3.23	3.99	4.02	4.10	3.99	4.04	4.00	4.07	4.01
#Mn +2	0.71	0.72	0.36	0.37	0.16	0.17	0.17	0.14	0.17	0.14
#Mg	0.46	0.43	0.72	0.71	0.81	0.83	0.84	0.89	0.85	0.94
#Ca	1.49	1.45	0.94	0.86	0.97	0.87	0.89	0.84	0.90	0.86
A site	5.90	5.84	6.01	5.94	6.03	5.86	5.93	5.87	5.98	5.95
#O	23.84	23.76	23.99	23.92	23.97	23.80	23.91	23.80	23.98	23.93

	I37BR	I37CR	I37CC	C27AR	C207AC	C27BC	C27BR
SiO2	38.51	38.66	38.72	38.49	38.66	38.64	38.34
TiO2	0.02	-	0.05	0.03	0.01	-	0.02
Al2O3	21.59	21.79	21.84	22.40	22.09	22.20	21.86
Cr2O3	-	-	-	-	-	-	-
Fe2O3	0.06	0.01	0.05	0.16	0.00	-	-
FeO	31.08	31.63	31.46	31.44	30.76	30.77	30.89
MnO	1.07	1.13	1.69	2.69	2.95	2.96	2.87
MgO	3.60	3.69	3.23	5.84	5.82	5.88	5.61
CaO	5.29	4.94	5.37	1.63	1.67	1.64	1.60
Total	101.22	101.85	102.40	102.68	101.96	102.09	101.19
#Si IV	6.00	6.00	6.00	5.92	5.98	5.96	5.98
#Al IV	-	-	-	0.08	0.02	0.04	0.02
T site	6.00	6.00	6.00	6.00	6.00	6.00	6.00
#Al VI	3.96	3.99	3.99	3.98	4.00	4.00	4.00
#Ti VI	0.00	-	0.01	0.00	0.00	-	0.00
#Cr	-	-	-	-	-	-	-
#Fe +3	0.01	0.00	0.01	0.02	0.00	-	-
O site	3.97	3.99	4.00	4.00	4.00	4.00	4.00
#Fe +2	4.05	4.11	4.08	4.04	3.98	3.97	4.03
#Mn +2	0.14	0.15	0.22	0.35	0.39	0.39	0.38
#Mg	0.84	0.85	0.75	1.34	1.34	1.35	1.30
#Ca	0.88	0.82	0.89	0.27	0.28	0.27	0.27
A site	5.91	5.93	5.94	6.00	5.98	5.98	5.98
#O	23.87	23.91	23.94	23.96	23.97	23.96	23.97

HORNBLENDE ANALYSES, MONTAUBAN

	MQ4AR	MQ4AC	MQ4BR	MQ4BC	MQ4CR	MQ4CC	MQ6AC	MQ6AR	MQ6BR	MQ6BC	MQ6CC	MQ6CR	B41AR	B41AR	B41BR	B41BC	B41CR	B41CC	E32AR	E32AC	G511AR	G511AC	G511BR	G511BC	G511CR	G511CC
SiO2	38.75	38.37	38.07	37.29	38.48	38.08	42.41	42.32	41.52	41.46	41.66	40.80	45.75	45.27	45.89	46.34	45.39	44.16	45.42	45.36	42.83	43.69	41.47	43.44	43.86	43.57
TiO2	0.64	0.69	0.56	0.89	0.78	0.92	0.68	0.68	0.66	0.82	0.68	0.68	0.53	0.80	0.69	0.52	0.52	0.82	0.64	0.71	0.80	0.90	0.33	0.73	0.94	0.86
Al2O3	13.75	13.40	14.32	13.52	13.80	13.25	13.17	13.49	13.69	12.91	13.13	13.72	13.23	13.24	12.54	12.23	12.72	12.95	13.37	12.78	13.15	13.22	15.87	12.84	13.38	13.48
Cr2O3	0.01	0.02	-	-	-	-	-	-	-	-	-	-	-	-	-	-	-	-	-	-	-	-	-	0.04	-	-
Fe2O3	-	-	-	0.01	-	-	-	-	-	-	0.02	0.01	-	-	-	-	-	-	-	-	-	-	-	-	-	-
FeO	28.53	29.18	28.37	29.79	29.34	29.28	21.59	21.30	21.03	21.00	20.74	21.71	16.02	16.51	16.30	16.94	16.07	16.52	15.94	16.36	18.26	19.58	19.58	17.81	17.87	18.84
MnO	0.45	0.49	0.42	0.45	0.45	0.45	0.43	0.40	0.46	0.41	0.33	0.36	0.10	0.15	0.08	0.13	0.12	0.11	0.10	0.08	0.25	0.20	0.13	0.22	0.20	0.22
MgO	1.73	1.73	1.57	1.71	1.66	1.71	7.19	7.04	6.67	6.97	6.92	6.38	10.34	9.96	10.72	10.41	10.23	9.73	10.35	10.86	9.11	8.77	7.15	8.98	9.17	8.38
ZnO	-	0.04	0.12	0.03	0.08	0.07	0.10	0.03	-	-	-	-	-	0.09	-	-	0.07	-	0.04	-	-	-	-	0.06	-	0.02
CaO	10.87	10.72	10.77	10.78	10.89	10.68	11.19	11.17	10.98	10.96	11.28	11.01	11.59	11.20	11.47	10.63	10.87	11.13	11.09	10.53	11.02	10.95	11.24	11.02	11.10	10.95
Na2O	1.52	1.48	1.38	1.37	1.56	1.60	1.45	1.49	1.52	1.49	1.37	1.56	1.15	1.07	1.11	1.08	1.06	1.20	1.16	1.18	1.53	1.53	1.78	1.67	1.52	1.55
K2O	1.92	1.97	1.98	2.02	2.00	1.96	0.82	0.82	0.85	0.82	0.72	0.86	0.35	0.40	0.41	0.37	0.35	0.51	0.36	0.41	0.47	0.47	0.49	0.44	0.47	0.57
H2O	1.87	1.86	1.86	1.85	1.88	1.86	1.98	1.98	1.95	1.94	1.95	1.94	2.06	2.05	2.06	2.05	2.03	2.01	2.05	2.04	1.99	2.01	1.99	1.99	2.02	2.01
Total	100.04	99.95	99.42	99.71	100.92	99.86	101.01	100.72	99.33	98.78	98.80	99.03	101.12	100.74	101.27	100.70	99.43	99.14	100.52	100.31	99.41	101.32	100.03	99.24	100.53	100.45
#Si IV	6.19	6.17	6.13	6.05	6.13	6.14	6.41	6.40	6.37	6.40	6.41	6.31	6.65	6.62	6.67	6.77	6.70	6.58	6.63	6.65	6.45	6.47	6.25	6.53	6.50	6.49
#Al IV	1.81	1.83	1.87	1.95	1.87	1.86	1.59	1.60	1.63	1.60	1.59	1.69	1.35	1.38	1.33	1.23	1.30	1.42	1.37	1.35	1.55	1.53	1.75	1.47	1.50	1.51
#Fe +3	-	-	-	-	-	-	-	-	-	-	-	-	-	-	-	-	-	-	-	-	-	-	-	-	-	-
#Ti IV	-	-	-	-	-	-	-	-	-	-	-	-	-	-	-	-	-	-	-	-	-	-	-	-	-	-
T site	8.00	8.00	8.00	8.00	8.00	8.00	8.00	8.00	8.00	8.00	8.00	8.00	8.00	8.00	8.00	8.00	8.00	8.00	8.00	8.00	8.00	8.00	8.00	8.00	8.00	8.00
#Al VI	0.78	0.71	0.84	0.63	0.72	0.66	0.75	0.80	0.85	0.75	0.80	0.81	0.91	0.90	0.82	0.87	0.91	0.86	0.93	0.85	0.78	0.78	1.06	0.81	0.84	0.86
#Fe +3	-	-	-	0.00	-	-	-	-	-	-	0.00	0.00	-	-	-	-	-	-	-	-	-	-	-	-	-	-
#Ti	0.08	0.08	0.07	0.11	0.09	0.11	0.08	0.08	0.08	0.10	0.08	0.08	0.06	0.09	0.08	0.06	0.06	0.09	0.07	0.08	0.09	0.10	0.04	0.08	0.10	0.10
#Cr	0.00	0.00	-	-	-	-	-	-	-	-	-	-	-	-	-	-	-	-	-	-	-	-	-	0.00	-	-
#Mg	0.41	0.41	0.38	0.41	0.39	0.41	1.62	1.59	1.53	1.60	1.59	1.47	2.24	2.17	2.32	2.27	2.25	2.16	2.25	2.37	2.04	1.94	1.61	2.01	2.03	1.86
#Fe +2	3.73	3.79	3.71	3.85	3.79	3.82	2.55	2.53	2.55	2.55	2.53	2.64	1.79	1.84	1.79	1.81	1.78	1.89	1.75	1.70	2.08	2.18	2.29	2.09	2.03	2.18
#Zn	-	-	-	-	-	-	-	-	-	-	-	-	-	-	-	-	-	-	-	-	-	-	-	-	-	-
#Mn	-	-	-	-	-	-	-	-	-	-	-	-	-	-	-	-	-	-	-	-	-	-	-	-	-	-
#Ca	-	-	-	-	-	-	-	-	-	-	-	-	-	-	-	-	-	-	-	-	-	-	-	-	-	-
M1,2,3	5.00	5.00	5.00	5.00	5.00	5.00	5.00	5.00	5.00	5.00	5.00	5.00	5.00	5.00	5.00	5.00	5.00	5.00	5.00	5.00	5.00	5.00	5.00	5.00	5.00	5.00
#Mg	-	-	-	-	-	-	-	-	-	-	-	-	-	-	-	-	-	-	-	-	-	-	-	-	-	-
#Fe +2	0.09	0.13	0.10	0.19	0.11	0.13	0.18	0.16	0.14	0.16	0.14	0.17	0.15	0.18	0.19	0.26	0.21	0.17	0.20	0.31	0.22	0.25	0.17	0.15	0.18	0.17
#Zn	-	0.00	0.01	0.00	0.01	0.01	0.01	0.00	-	-	-	-	-	0.01	-	-	0.01	-	0.00	-	-	-	-	-	0.01	-	0.00
#Mn	0.06	0.07	0.06	0.06	0.06	0.06	0.06	0.05	0.06	0.05	0.04	0.05	0.01	0.02	0.01	0.02	0.02	0.01	0.01	0.01	0.03	0.03	0.02	0.03	0.03	0.03
#Ca	1.85	1.80	1.82	1.74	1.82	1.80	1.76	1.78	1.80	1.79	1.82	1.78	1.80	1.75	1.79	1.66	1.72	1.78	1.73	1.65	1.75	1.73	1.81	1.78	1.76	1.75
#Na	-	-	-	-	-	-	-	-	-	-	-	-	0.03	0.04	0.01	0.06	0.05	0.03	0.05	0.03	-	-	-	0.04	0.03	0.05
M4 site	2.00	2.00	2.00	2.00	2.00	2.00	2.00	2.00	2.00	2.00	2.00	2.00	2.00	2.00	2.00	2.00	2.00	2.00	2.00	2.00	2.00	2.00	2.00	2.00	2.00	2.00
#Ca	0.01	0.05	0.03	0.13	0.04	0.04	0.05	0.03	0.01	0.03	0.04	0.04	-	-	-	-	-	-	-	-	0.03	0.01	0.00	-	-	-
#Na	0.47	0.46	0.43	0.43	0.48	0.50	0.42	0.44	0.45	0.45	0.41	0.47	0.29	0.27	0.30	0.25	0.25	0.31	0.28	0.31	0.45	0.44	0.52	0.45	0.40	0.40
#K	0.39	0.40	0.41	0.42	0.41	0.40	0.16	0.16	0.17	0.16	0.14	0.17	0.06	0.07	0.08	0.07	0.07	0.10	0.07	0.08	0.09	0.09	0.09	0.08	0.09	0.11
A site	0.87	0.91	0.87	0.98	0.93	0.94	0.64	0.62	0.63	0.63	0.59	0.68	0.36	0.34	0.38	0.31	0.32	0.41	0.35	0.38	0.56	0.54	0.62	0.53	0.49	0.50
#O	22.01	22.01	22.00	22.00	22.00	22.00	22.00	22.00	22.00	22.00	22.00	22.00	22.00	22.00	22.00	22.00	22.00	22.00	22.00	22.01	22.00	22.01	22.00	22.00	22.00	22.00
#OH	1.99	1.99	2.00	2.00	2.00	2.00	2.00	2.00	2.00	2.00	2.00	2.00	2.00	2.00	2.00	2.00	2.00	2.00	2.00	1.99	2.00	1.99	2.00	2.00	2.00	2.00
Charge	-1E-05	-8E-06	0.00	0.00	0.00	-2E-06	0.00	0.00	-1E-06	0.00	0.00	0.00	-3E-06	-8E-06	-8E-06	-5E-06	-8E-06	-1E-05	-5E-06	0.00	0.00	0.00	0.00	-5E-06	-1E-06	-1E-06

	G513AR	G513AC	G513IN	G513BC	G519AC	G519BC	I35AR	I35AC	I35BC	I37AC	I37AC	I37AC2	I37AR2	I37BR	I37BC	I37CR	I37CC	E32BR	E32BC	E32CR	E32CC
SiO2	44.67	44.06	44.33	45.13	43.11	44.30	44.71	44.51	45.88	44.80	44.76	44.33	44.61	44.75	44.27	45.18	44.85	45.31	44.81	44.98	45.57
TiO2	0.85	0.87	1.00	0.57	0.87	0.79	0.59	0.47	0.65	0.55	0.43	0.49	0.60	0.53	0.67	0.65	0.55	0.65	0.60	0.77	0.64
Al2O3	13.24	13.25	12.69	12.45	13.73	13.02	13.29	14.27	11.98	12.73	13.48	13.28	14.03	13.50	13.30	13.56	14.10	11.82	13.09	13.30	13.01
Cr2O3	-	-	-	-	-	-	-	-	-	-	-	-	-	-	-	-	-	-	-	-	-
Fe2O3	-	-	-	-	-	-	0.00	-	-	-	0.02	0.00	-	0.02	0.02	-	-	-	-	-	-
FeO	17.68	18.20	20.15	19.05	18.93	19.02	17.09	16.79	17.88	16.96	15.99	16.82	15.67	15.12	16.48	15.98	15.36	17.90	16.08	16.32	16.85
MnO	0.23	0.20	0.30	0.26	0.22	0.22	0.15	0.09	0.12	0.08	0.11	0.05	0.04	0.05	0.07	0.06	0.07	0.16	0.18	0.11	0.19
MgO	9.06	8.89	8.02	8.66	8.23	8.92	9.66	9.07	10.47	10.18	10.35	10.41	10.26	10.69	10.33	10.48	10.39	10.68	10.18	10.09	10.28
ZnO	0.12	-	0.18	-	0.08	0.09	0.09	0.03	0.10	0.01	0.03	-	0.05	-	0.01	-	0.09	0.12	0.05	0.03	-
CaO	11.08	11.16	11.22	11.44	10.89	11.06	10.66	10.79	9.75	10.07	10.42	10.35	11.06	11.20	10.90	10.64	11.04	9.81	11.27	11.06	10.68
Na2O	1.42	1.39	1.04	1.15	1.70	1.57	1.39	1.71	1.34	1.31	1.24	1.16	1.41	1.32	1.29	1.23	1.35	1.13	1.29	1.26	1.29
K2O	0.50	0.52	0.72	0.32	0.52	0.46	0.39	0.45	0.40	0.35	0.35	0.33	0.36	0.36	0.38	0.65	0.36	0.38	0.39	0.39	0.36
H2O	2.03	2.02	2.02	2.03	2.00	2.03	2.03	2.03	2.04	2.01	2.03	2.02	2.04	2.04	2.03	2.05	2.05	2.02	2.03	2.04	2.05
Total	100.88	100.56	101.67	101.06	100.28	101.48	100.05	100.21	100.61	99.05	99.21	99.24	100.13	99.58	99.75	100.48	100.21	99.98	99.97	100.35	100.92
#Si IV	6.58	6.53	6.57	6.66	6.45	6.53	6.60	6.56	6.74	6.66	6.62	6.58	6.54	6.58	6.55	6.60	6.56	6.70	6.61	6.60	6.65
#Al IV	1.42	1.47	1.43	1.34	1.55	1.47	1.40	1.44	1.26	1.34	1.38	1.42	1.46	1.42	1.45	1.40	1.44	1.30	1.39	1.40	1.35
#Fe +3	-	-	-	-	-	-	-	-	-	-	-	-	-	-	-	-	-	-	-	-	-
#Ti IV	-	-	-	-	-	-	-	-	-	-	-	-	-	-	-	-	-	-	-	-	-
T site	8.00	8.00	8.00	8.00	8.00	8.00	8.00	8.00	8.00	8.00	8.00	8.00	8.00	8.00	8.00	8.00	8.00	8.00	8.00	8.00	8.00
#Al VI	0.88	0.85	0.78	0.83	0.87	0.80	0.92	1.04	0.81	0.90	0.97	0.90	0.97	0.93	0.87	0.94	0.99	0.77	0.88	0.90	0.89
#Fe +3	-	-	-	-	-	-	0.00	-	-	-	0.00	0.00	-	0.00	0.00	-	-	-	-	-	-
#Ti	0.09	0.10	0.11	0.06	0.10	0.09	0.07	0.05	0.07	0.06	0.05	0.05	0.07	0.06	0.07	0.07	0.06	0.07	0.07	0.08	0.07
#Cr	-	-	-	-	-	-	-	-	-	-	-	-	-	-	-	-	-	-	-	-	-
#Mg	1.99	1.96	1.77	1.91	1.84	1.96	2.13	1.99	2.29	2.26	2.28	2.30	2.24	2.34	2.28	2.28	2.27	2.36	2.24	2.21	2.24
#Fe +2	2.04	2.09	2.34	2.20	2.20	2.15	1.89	1.92	1.83	1.79	1.70	1.74	1.72	1.67	1.78	1.70	1.69	1.81	1.82	1.81	1.80
#Zn	-	-	-	-	-	-	-	-	-	-	-	-	-	-	-	-	-	-	-	-	-
#Mn	-	-	-	-	-	-	-	-	-	-	-	-	-	-	-	-	-	-	-	-	-
#Ca	-	-	-	-	-	-	-	-	-	-	-	-	-	-	-	-	-	-	-	-	-
M1,2,3	5.00	5.00	5.00	5.00	5.00	5.00	5.00	5.00	5.00	5.00	5.00	5.00	5.00	5.00	5.00	5.00	5.00	5.00	5.00	5.00	5.00
#Mg	-	-	-	-	-	-	-	-	-	-	-	-	-	-	-	-	-	-	-	-	-
#Fe +2	0.14	0.17	0.16	0.15	0.17	0.19	0.22	0.15	0.37	0.32	0.28	0.35	0.20	0.19	0.26	0.25	0.19	0.41	0.16	0.20	0.25
#Zn	0.01	-	0.02	-	0.01	0.01	0.01	0.00	0.01	0.00	0.00	-	0.01	-	0.00	-	0.01	0.01	0.01	0.00	-
#Mn	0.03	0.03	0.04	0.03	0.03	0.03	0.02	0.01	0.01	0.01	0.01	0.01	0.00	0.01	0.01	0.01	0.01	0.02	0.02	0.01	0.02
#Ca	1.75	1.77	1.78	1.81	1.75	1.75	1.69	1.70	1.53	1.60	1.65	1.64	1.74	1.77	1.73	1.67	1.73	1.56	1.78	1.74	1.67
#Na	0.07	0.04	0.00	0.01	0.05	0.02	0.06	0.13	0.07	0.06	0.05	-	0.05	0.04	0.00	0.08	0.06	0.00	0.03	0.05	0.05
M4 site	2.00	2.00	2.00	2.00	2.00	2.00	2.00	2.00	2.00	2.00	2.00	2.00	2.00	2.00	2.00	2.00	2.00	2.00	2.00	2.00	2.00
#Ca	-	-	-	-	-	-	-	-	-	-	-	0.00	-	-	-	-	-	-	-	-	-
#Na	0.34	0.36	0.30	0.32	0.44	0.43	0.34	0.36	0.31	0.32	0.30	0.33	0.35	0.34	0.37	0.27	0.32	0.32	0.34	0.31	0.31
#K	0.09	0.10	0.14	0.06	0.10	0.09	0.07	0.08	0.07	0.07	0.07	0.06	0.07	0.07	0.07	0.12	0.07	0.07	0.07	0.07	0.07
A site	0.43	0.46	0.43	0.38	0.54	0.51	0.41	0.44	0.38	0.38	0.37	0.40	0.42	0.41	0.44	0.39	0.39	0.39	0.41	0.38	0.38
#O	22.01	22.00	22.00	22.00	22.00	22.00	22.00	22.00	22.00	22.01	22.00	22.00	22.00	22.00	22.00	22.00	22.00	22.01	22.00	22.00	22.00
#OH	1.99	2.00	2.00	2.00	2.00	2.00	2.00	2.00	2.00	1.99	2.00	2.00	2.00	2.00	2.00	2.00	2.00	1.99	2.00	2.00	2.00
Charge	0.00	-1E-06	0.00	0.00	0.00	-6E-06	0.00	0.00	0.00	0.00	0.00	0.00	-5E-07	0.00	0.00	-6E-06	-2E-06	0.00	-2E-06	0.00	-7E-06

Plagioclase analyses, Montauban

	MQ1AC	MQ1AR	MQ1BR	MQ1BC	MQ4AC	MQ4AR	MQ4BC	MQ4BR	MQ4CC	MQ4CR
SiO2	54.86	55.05	54.98	54.43	63.25	62.82	63.11	64.13	63.65	63.27
Al2O3	29.03	29.06	28.40	28.42	23.98	23.51	23.94	23.45	23.34	23.85
CaO	11.33	11.31	10.78	11.04	4.44	4.25	4.60	4.19	4.09	4.24
K2O	0.04	0.03	0.05	0.04	0.21	0.20	0.18	0.17	0.19	0.19
Na2O	5.19	5.12	5.41	5.12	8.07	8.88	7.71	7.99	8.86	7.56
TOTAL	100.45	100.57	99.62	99.05	99.95	99.66	99.54	99.93	100.13	99.11
#Si+4	2.46	2.47	2.49	2.48	2.79	2.78	2.79	2.82	2.80	2.80
#Al+3	1.54	1.53	1.51	1.52	1.24	1.23	1.25	1.21	1.21	1.24
#Ca+2	0.54	0.54	0.52	0.54	0.21	0.20	0.22	0.20	0.19	0.20
#K	0.00	0.00	0.00	0.00	0.01	0.01	0.01	0.01	0.01	0.01
#Na+1	0.45	0.44	0.47	0.45	0.69	0.76	0.66	0.68	0.76	0.65
#TOTAL	5.00	4.99	5.00	4.99	4.94	4.99	4.92	4.92	4.97	4.91
#O-2	8.00	8.00	8.00	8.00	8.00	8.00	8.00	8.00	8.00	8.00

	MQ6AR	MQ6AC	MQ6BR	MQ6BC	B41AR	B41AC	B41BR	B41BC	B41CR	B41CC
SiO2	60.12	60.30	59.25	59.20	46.13	46.63	46.77	46.23	46.52	46.67
Al2O3	25.33	24.97	25.14	25.14	34.39	33.37	33.39	33.36	33.81	33.02
CaO	7.06	6.64	6.92	6.85	17.85	17.49	17.24	17.73	17.32	17.82
K2O	0.06	0.10	0.08	0.10	0.01	-	0.01	-	0.03	0.03
Na2O	7.71	7.45	7.61	7.66	1.12	1.38	1.55	1.26	1.59	1.30
TOTAL	100.28	99.46	99.00	98.95	99.50	98.87	98.96	98.58	99.27	98.84
#Si+4	2.67	2.69	2.67	2.67	2.13	2.16	2.17	2.15	2.15	2.17
#Al+3	1.33	1.31	1.33	1.33	1.87	1.83	1.82	1.83	1.84	1.81
#Ca+2	0.34	0.32	0.33	0.33	0.88	0.87	0.86	0.89	0.86	0.89
#K	0.00	0.01	0.00	0.01	0.00	-	0.00	-	0.00	0.00
#Na+1	0.66	0.65	0.66	0.67	0.10	0.12	0.14	0.11	0.14	0.12
#TOTAL	5.00	4.98	5.00	5.00	4.98	4.98	4.99	4.99	5.00	4.99
#O-2	8.00	8.00	8.00	8.00	8.00	8.00	8.00	8.00	8.00	8.00

	E32AC	E32AR	E32BC	E32BR	E32CC	E32CR	G511AC	G511AR	G511BC	G511BI
SiO2	57.42	53.38	59.70	55.67	56.85	57.31	58.53	59.27	58.04	58.76
Al2O3	26.16	29.72	24.53	26.59	26.74	26.69	24.98	25.66	26.11	26.58
CaO	8.78	12.49	6.79	9.73	9.44	8.45	6.56	7.37	7.89	8.19
K2O	0.04	0.03	0.06	0.01	0.03	0.24	0.06	0.02	0.07	0.05
Na2O	6.65	4.29	7.91	6.17	6.30	6.43	7.79	7.17	7.06	7.03
TOTAL	99.05	99.91	98.99	98.17	99.36	99.12	97.92	99.49	99.17	100.61
#Si+4	2.60	2.41	2.69	2.55	2.57	2.59	2.66	2.65	2.61	2.61
#Al+3	1.39	1.58	1.30	1.43	1.42	1.42	1.34	1.35	1.39	1.39
#Ca+2	0.43	0.61	0.33	0.48	0.46	0.41	0.32	0.35	0.38	0.39
#K	0.00	0.00	0.00	0.00	0.00	0.01	0.00	0.00	0.00	0.00
#Na+1	0.58	0.38	0.69	0.55	0.55	0.56	0.69	0.62	0.62	0.61
#TOTAL	5.00	4.98	5.01	5.01	5.00	4.99	5.01	4.98	5.00	5.00
#O-2	8.00	8.00	8.00	8.00	8.00	8.00	8.00	8.00	8.00	8.00

	G511BR	G511CR	G511CC	G513AR	G513AC	G513I1	G513I2	G519AC	G519BC	I35AC
SiO2	62.13	59.20	58.29	51.97	53.54	45.58	46.08	59.17	59.92	56.80
Al2O3	23.99	26.11	26.45	29.97	28.29	33.27	33.65	25.57	25.17	27.11
CaO	5.41	7.58	8.16	13.77	12.18	18.17	18.14	7.26	6.94	9.36
K2O	0.06	0.07	0.07	0.03	0.03	-	0.01	0.04	0.02	0.03
Na2O	8.59	6.99	6.97	3.72	4.44	1.10	1.07	7.41	7.69	6.12
TOTAL	100.18	99.95	99.94	99.46	98.48	98.12	98.95	99.45	99.74	99.42
#Si+4	2.75	2.64	2.61	2.37	2.46	2.14	2.14	2.65	2.67	2.56
#Al+3	1.25	1.37	1.39	1.61	1.53	1.84	1.84	1.35	1.32	1.44
#Ca+2	0.26	0.36	0.39	0.67	0.60	0.91	0.90	0.35	0.33	0.45
#K	0.00	0.00	0.00	0.00	0.00	-	0.00	0.00	0.00	0.00
#Na+1	0.74	0.60	0.60	0.33	0.39	0.10	0.10	0.64	0.67	0.53
#TOTAL	5.00	4.98	5.00	4.99	4.98	4.99	4.99	5.00	5.00	4.99
#O-2	8.00	8.00	8.00	8.00	8.00	8.00	8.00	8.00	8.00	8.00

	I35AR	I35BC	I37AR	I37AC	I37BR	I37BC	I37CR	I37CC	C522A	C522B
SiO2	58.36	57.04	53.27	54.85	56.44	54.39	47.78	47.39	45.50	45.47
Al2O3	26.28	27.12	30.13	27.72	27.61	28.21	32.45	33.03	34.66	35.08
CaO	8.51	9.07	13.08	10.35	9.05	10.60	16.38	16.10	18.64	19.18
K2O	0.04	0.03	0.03	0.03	0.01	0.04	0.01	0.02	0.03	0.03
Na2O	6.74	6.28	4.03	5.63	6.24	5.31	2.09	2.17	0.83	0.70
TOTAL	99.93	99.54	100.54	98.58	99.35	98.55	98.71	98.71	99.66	100.46
#Si+4	2.61	2.57	2.40	2.50	2.54	2.48	2.22	2.20	2.10	2.09
#Al+3	1.39	1.44	1.60	1.49	1.47	1.52	1.77	1.80	1.89	1.90
#Ca+2	0.41	0.44	0.63	0.51	0.44	0.52	0.81	0.80	0.92	0.94
#K	0.00	0.00	0.00	0.00	0.00	0.00	0.00	0.00	0.00	0.00
#Na+1	0.58	0.55	0.35	0.50	0.55	0.47	0.19	0.20	0.07	0.06
#TOTAL	4.99	4.99	4.98	5.00	4.99	4.99	4.99	5.00	4.99	4.99
#O-2	8.00	8.00	8.00	8.00	8.00	8.00	8.00	8.00	8.00	8.00

K-feldspar analyses, Montauban

	MQ10A	MQ10B
SiO2	64.51	64.46
Al2O3	18.68	18.53
CaO	-	-
K2O	15.71	15.86
Na2O	1.09	1.14
TOTAL	99.99	99.99
#Si+4	2.98	2.98
#Al+3	1.02	1.01
#Ca+2	-	-
#K	0.93	0.94
#Na+1	0.10	0.10
#TOTAL	5.02	5.03
#O-2	8.00	8.00

Staurolite analyses, Montauban

Sample	D-2-11-1 CORE	D-2-11-2 RIM	D-2-11-4 RIM	D-2-11-6 RIM	D-2-11-8 RIM	D-2-11-10 RIM	MM094-4 CORE
SiO2	28.29	27.74	27.95	28.10	27.92	28.12	27.68
TiO2	0.47	0.47	0.67	0.58	0.63	0.35	0.65
Al2O3	53.91	54.16	54.44	54.43	54.58	54.96	54.57
Fe2O3*	1.20	1.19	1.20	1.20	1.20	1.21	1.20
FeO*	6.44	6.53	6.39	6.20	6.67	6.40	5.75
MnO	0.46	0.48	0.48	0.58	0.50	0.59	0.88
MgO	3.01	2.70	2.75	2.62	2.78	2.66	2.96
ZnO	3.68	4.00	4.11	4.02	4.22	4.20	3.58
H2O*	1.72	1.82	1.73	1.87	1.66	1.91	1.85
Total	99.17	99.09	99.72	99.59	100.16	100.39	99.12
Stoichiometry							
Si	7.86	7.73	7.75	7.78	7.73	7.73	7.68
AlIV	0.14	0.27	0.25	0.22	0.27	0.27	0.32
AlVI	17.53	17.53	17.53	17.53	17.53	17.53	17.53
Fe+3	0.25	0.25	0.25	0.25	0.25	0.25	0.25
Mn	0.11	0.11	0.11	0.14	0.12	0.14	0.21
Fe+2	0.14	0.14	0.14	0.11	0.13	0.11	0.04
Ti+4	0.10	0.10	0.14	0.12	0.13	0.07	0.14
Fe+2	1.36	1.38	1.34	1.32	1.41	1.36	1.29
Mg	1.25	1.12	1.14	1.08	1.15	1.09	1.22
Zn	0.76	0.82	0.84	0.82	0.86	0.85	0.73
Tet site	3.46	3.43	3.46	3.34	3.55	3.37	3.38
H+	3.18	3.38	3.21	3.46	3.07	3.54	3.44
O	48.00	48.00	48.00	48.00	48.00	48.00	48.00

Staurolite analyses, Montauban

Sample	MM094-4 RIM	C-2-7-3 RIM	C-2-7-6 RIM	C-2-7-10 CORE	C-2-7-11 CORE	C-2-7-12 RIM	C-2-7-16 RIM
SiO2	27.53	28.04	27.94	27.29	27.97	27.96	28.02
TiO2	0.64	0.23	0.21	0.22	0.21	0.28	0.35
Al2O3	54.49	53.54	53.24	53.41	54.12	53.62	53.84
Fe2O3*	1.19	1.19	1.18	1.17	1.19	1.19	1.19
FeO*	5.79	10.11	10.29	9.82	9.96	10.05	10.25
MnO	0.80	0.16	0.06	0.14	0.15	0.21	0.04
MgO	2.96	2.43	2.46	2.42	2.56	2.40	2.50
ZnO	3.91	1.53	1.69	1.71	1.86	1.98	1.63
H2O*	1.80	1.69	1.61	1.77	1.68	1.60	1.61
Total	99.11	98.92	98.68	97.96	99.70	99.29	99.43
Stoichiometry							
Si	7.66	7.85	7.86	7.72	7.78	7.83	7.82
AlIV	0.34	0.15	0.14	0.28	0.22	0.17	0.18
AlVI	17.53	17.53	17.53	17.53	17.53	17.53	17.53
Fe+3	0.25	0.25	0.25	0.25	0.25	0.25	0.25
Mn	0.19	0.04	0.01	0.03	0.04	0.05	0.01
Fe+2	0.06	0.21	0.24	0.22	0.21	0.20	0.24
Ti+4	0.13	0.05	0.04	0.05	0.04	0.06	0.07
Fe+2	1.28	2.16	2.19	2.11	2.10	2.15	2.15
Mg	1.23	1.01	1.03	1.02	1.06	1.00	1.04
Zn	0.80	0.32	0.35	0.36	0.38	0.41	0.34
Tet site	3.45	3.54	3.61	3.53	3.59	3.62	3.60
H+	3.34	3.14	2.98	3.28	3.11	2.97	2.99
O	48.00	48.00	48.00	48.00	48.00	48.00	48.00

Staurolite analyses, Montauban

Sample	E-6-24-1 RIM	E-6-24-1 RIM	E-6-24-3 RIM	F419-2 RIM	F419-4 RIM	F419-6 CORE	F419-7 RIM
SiO2	27.38	27.72	28.61	27.97	27.71	28.44	28.43
TiO2	0.47	0.18	0.36	0.78	0.78	0.69	0.67
Al2O3	54.71	54.16	53.96	54.01	54.18	53.59	54.03
Fe2O3*	1.20	1.19	1.20	1.19	1.19	1.19	1.20
FeO*	6.88	6.53	7.04	6.66	6.62	6.54	7.10
MnO	0.34	0.36	0.36	0.64	0.69	0.61	0.64
MgO	2.91	3.01	3.13	2.73	2.69	2.88	2.81
ZnO	4.85	4.38	3.84	4.04	4.08	3.79	4.12
H2O*	1.56	1.76	1.54	1.55	1.59	1.55	1.42
Total	100.30	99.29	100.04	99.58	99.53	99.27	100.41
Stoichiometry							
Si	7.61	7.73	7.92	7.79	7.73	7.92	7.88
AlIV	0.39	0.27	0.08	0.21	0.27	0.08	0.12
AlVI	17.53	17.53	17.53	17.53	17.53	17.53	17.53
Fe+3	0.25	0.25	0.25	0.25	0.25	0.25	0.25
Mn	0.08	0.09	0.08	0.15	0.16	0.14	0.15
Fe+2	0.17	0.16	0.17	0.10	0.09	0.11	0.10
Ti+4	0.10	0.04	0.07	0.16	0.16	0.14	0.14
Fe+2	1.43	1.36	1.46	1.45	1.46	1.42	1.55
Mg	1.21	1.25	1.29	1.13	1.12	1.19	1.16
Zn	1.00	0.90	0.78	0.83	0.84	0.78	0.84
Tet site	3.73	3.55	3.62	3.58	3.58	3.53	3.69
H+	2.90	3.26	2.86	2.88	2.95	2.88	2.63
O	48.00	48.00	48.00	48.00	48.00	48.00	48.00

Staurolite analyses, Montauban

SAMPLE	F419-9 RIM	F419-11 CORE	F419-12 RIM	F419-14 RIM	F419-15 RIM
SiO2	28.15	28.65	28.03	28.12	27.97
TiO2	0.63	0.57	0.65	0.58	0.49
Al2O3	54.25	53.54	54.34	53.82	54.99
Fe2O3*	1.20	1.19	1.20	1.19	1.21
FeO*	6.90	6.83	7.14	6.70	6.71
MnO	0.57	0.58	0.63	0.56	0.61
MgO	2.78	3.00	2.61	2.67	2.56
ZnO	4.25	3.77	4.22	3.96	3.77
H2O*	1.53	1.47	1.54	1.67	1.92
Total	100.26	99.59	100.34	99.27	100.23
Stoichiometry					
Si	7.80	7.97	7.77	7.84	7.69
AlIV	0.20	0.03	0.23	0.16	0.31
AlVI	17.53	17.53	17.53	17.53	17.53
Fe+3	0.25	0.25	0.25	0.25	0.25
Mn	0.13	0.14	0.15	0.13	0.14
Fe+2	0.12	0.11	0.10	0.12	0.11
Ti+4	0.13	0.12	0.14	0.12	0.10
Fe+2	1.48	1.48	1.55	1.44	1.44
Mg	1.15	1.24	1.08	1.11	1.05
Zn	0.87	0.77	0.86	0.82	0.77
Tet site	3.63	3.61	3.63	3.49	3.35
H+	2.83	2.73	2.86	3.10	3.56
O	48.00	48.00	48.00	48.00	48.00

APPENDIX III

Geothermobarometers used in chapted 4

A) Garnet-plagioclase-hornblende geothermobarometers

Temperature estimates based on Fe-Mg cation exchange were obtained using Graham and Powell geothermometer (reaction 5):

$$T\ (^{\circ}K) = \frac{2880 + 3280X_{Ca}^{grt}}{\ln(K_D) + 2.426} \quad \text{where } K_D = \frac{X_{Alm}\ XMg^{Hbl}}{X_{Prp}\ X_{Fe}^{Hbl}}$$

The pressures were calculated using GRHBPLTP, a basic program that I wrote using the above Graham and Powell (1984) geothermometer in conjunction with Kohn and Spear (1989, 1990) geobarometers.

Kohn and Spear (1989) Model I

Reaction (6)

$$P^1_{Mg} = [120593 + T(10.3 + 8.314\ln(K_2))]/14.81 \text{ (bars)}$$

$$K_2 = \frac{a^2_{Grs}\ a_{Prp}\ a^3_{Prg}\ a_{Qtz}}{a^6_{An}\ a^3_{Ab}\ a^3_{Tr}}$$

Reaction (7)

$$P^1_{Fe} = [117993 + T(47.8 + 8.314\ln(K_3))]/11.29 \text{ (bars)}$$

$$K_3 = \frac{a^2_{Grs}\ a_{Alm}\ a^3_{Fe\text{-}Prg}\ a_{Qtz}}{a^6_{An}\ a^3_{Ab}\ a^3_{Fe\text{-}Act}}$$

$$a_{Fe\text{-}Prg} = a_{Prg} = 16(X^{Al}_{T1})^2\ (X^{Si}_{T1})^2\ X^{Na}_{A}$$

$$a_{Fe\text{-}act} = a_{Tr} = (X^{Si}_{T1})^4\ X^{A}_{\square}$$

$$a_{Prp} = \{X_{Prp}\exp[(13800-6.28T)\ (X^2_{Grs}+X_{Alm}X_{Grs}+X_{Grs}X_{Sps})/RT]\}^3$$

$$a_{Grs} = \{X_{Grs}\exp[(13800-6.28T)\ (X^2_{Prp}+X_{Alm}X_{Prp}+X_{Prp}X_{Sps})/RT]\}^3$$

$$a_{Alm} = \{X_{Alm}\exp[(13800-6.28T)\ (-X_{Prp}X_{Grs})/RT]\}^3$$

$$a_{An} = X_{An}\exp[(610.34/T)-0.3837]$$

$$a_{Ab} = X_{Ab}$$

Kohn and Spear (1989) Model II

Reaction (6)

$$P^2_{Mg} = [44724 + T(51.9 + 8.314\ln(K_2))]/9.19 \text{ (bars)}$$

Reaction (7)

$$P^2_{Fe} = [-4948 + T(81.8 + 8.314\ln(K_3))]/9.52 \text{ (bars)}$$

K_2 and K_3 as in model I but with the following amphiboles activity models:

$$a_{Prg} = 4X^{Al}_{M2}\, X^{Mg}_{M2}\, X^{Na}_{A}$$

$$a_{Fe\text{-}Prg} = 4X^{Al}_{M2}\, X^{Fe}_{M2}\, X^{Na}_{A}$$

$$a_{Tr} = (X^{Mg}_{M2})^2\, X^{A}_{\square}$$

$$a_{Fe\text{-}act} = (X^{Fe}_{M2})^2\, X^{A}_{\square}$$

Kohn and Spear (1990)

Reaction (8)

$$P^4_{Mg} = [79507 + T(29.1 + 8.314\ln(K_4))]/10.99 \text{ (bars)}$$

$$K_4 = \frac{a^2_{Grs}\; a_{Prp}\; a^3_{Tsch}\; a^6_{Qtz}}{a^6_{An}\; a^3_{Tr}}$$

$$a_{Tsch} = (256/27)\, X^{Al}_{T1}\, (X^{Si}_{T1})^3\, [Mg/(Mg+Fe)]$$

$$a_{Tr} = (X^{Si}_{T1})^4\, [Mg/(Mg+Fe)]^2$$

Reaction (9)

$$P^2_{Fe} = [35327 + T(56.04 + 8.314\ln(K_5))]/11.91 \text{ (bars)}$$

$$K_5 = \frac{a^2_{Grs}\; a_{Alm}\; a^3_{Fe\text{-}Tsch}\; a^6_{Qtz}}{a^6_{An}\; a^3_{Fe\text{-}Act}}$$

$$a_{Fe\text{-}Tsch} = (256/27)\, X^{Al}_{T1}\, (X^{Si}_{T1})^3\, [Fe/(Mg+Fe)]$$

$$a_{Tr} = (X^{Si}_{T1})^4\, [Fe/(Mg+Fe)]^2$$

For all above equations, T is in Kelvin, R=8.314 J/(mol K). For the details concerning mole fractions and sites occupancies

calculations, the reader is refered to Appendix 1 in Kohn and Spear (1989) and Table 1 in Kohn and Spear (1990).

B. Garnet-Biotite geothermometers

Details for calculations of temperatures estimates using various geothermometers based on Fe-Mg exchange reaction (3) 2) are as follows:

Emperical Calibration

Thompson (1976)

$$T^{\circ}C = \frac{2739.646 + 0.234(P-1)(bars)}{1.56 - \ln K_D} - 273$$

Experimental calibrations

Ferry and Spear (1978)

$$T^{\circ}C = \frac{2089 + .0096P(bars)}{0.782 - \ln K_D} - 273$$

$$K_D = (Mg/Fe)^{Grt}/(Mg/Fe)^{Bt}$$

Perchuck (1981)

$$T^{\circ}C = \left[\frac{3660}{2.57 - \ln K_D} - 252.25(X_{Sps} - .035)\right] - 273$$

Perchuck and Lavrent'eva (1983)

$$T^{\circ}C = \frac{7843.7 - 0.0246(P-6000)(bars)}{5.6999 - 1.987 \ln K_D} - 273$$

Ferry and Spear's clones

Correction for Ca

Newton and Haselton (1981)

This geothermometer is based on Ferry and Spear (1978) calibration with the grossular activity and partial molar volume models of Newton and Haselton (1981).

$$TK = \frac{2089 + .00956P(bars) + (1661-0.755T(K))X_{Grs}}{0.782 - \ln K_D}$$

Hoinkes (1986)

$$T°C = \frac{2089 + 0.00956P(bars)}{0.782 - \ln K_D - 2.978X_{Grs} + 5.906X^2} - 273$$

Corrections for Ca and Mn

Pigage and Greenwood (1982)

Pigage and Greenwood applied Ganguly (1979) garnet activity models to the Ferry and Spear (1978) geothermometer.

$$T°C = \frac{1586X_{Grs} + 1308X_{Sps} + 2089 - 914 + 0.00956P(bars)}{0.782 - \ln K_D} - 273$$

Hodges and Spear (1982)

$$TK = \frac{2089 + 0.00956P(bars) + A + B}{0.782 - \ln K_D} - 273$$

where $A = (3300 - 1.5TK)(X^2_{Grs} + X_{Alm}X_{Grs} + X_{Sps}X_{Grs} + X_{Prp}X_{Grs})$

$B = W_{MgMn}(X^2_{Sps} + X_{Sps}X_{Grs} + X_{Sps}X_{Alm} + X_{Prp}X_{Sps})$ cal/mol

W_{MgMn} = a value between 0 and 3500 cal/mol inclusively.

The above expression has to be solved through successive iteration for T at pressure of interest, because the activity model for grossular is temperature dependant.

Ganguly and Saxena (1984, 1985)

$$T°C = \frac{A + 1511(X_{Grs} + X_{Sps}) + 2089 - 914 + 0.00956P(bars)}{0.782 - \ln K_D} - 273$$

where $A = W_{FeMg}(X_{Alm} - X_{Prp})$

$W_{FeMg} = 835[X_{Prp}/(X_{Alm}+X_{Prp})] + 10460[X_{Alm}/(X_{Alm}+X_{Prp})]$

Williams and Grambling (1990) model 3

$$T^{\circ}C=\left[\frac{-17369 - 79.5P + 0.8W_{FeMg} - W_{FeMg}(X_{Alm}-X_{Prp}) - 12550X_{Grs}}{8.3143(\ln K_D - 0.894)} - \frac{8230X_{Sps}}{8.3143(\ln K_D - 0.894)}\right] - 273, \quad \text{where P is in kbars}$$

C. Garnet-chlorite geothermometer

Patrick and Evans (1989)

$$T(K) = \frac{55841 + 0.212P\ (bars) + 4950A}{10.76 - 15R\ln K_D + 225}$$

$$A= (X^2Grs + XAlm\ XGrs + XPrp\ XGrs + XSps\ XGrs)$$

$$K_D = (Mg/Fe)^{Grt}/(Mg/Fe)^{Chl}$$

D. Garnet-cordierite geothermobarometers

The temperature and pressure estimates based on reactions (7) and (8) (Table 3) have been obtained from the following equations:

Emperical geothermometer

Thompson (1976)

$$T^{\circ}C= \frac{-2725 + 0.0155(P-1)\ (bars)}{\ln K_D + 0.896} - 273$$

$$K_D= (Fe/Mg)^{Grt}/(Fe/Mg)^{Crd}$$

Experimental geothermometer

Perchuck and Lavrent'eva (1983)

$$T^{\circ}C= \frac{3020 + 0.018P(bars)}{\ln K_D + 1.287} - 273$$

Emperical geobarometer

Thompson (1976)

$$P_{Mg} = [-T(K)\ (-6\ln K_{Mg} + 12.982) + 30324.5]/1.909$$

$$K_{Mg} = (X_{Mg}^{Grt}/X_{Mg}^{Crd})$$

$$P_{Fe} = [-T(K)\ (-6\ln K_{Fe} + 7.601) + 13994.6]/1.956$$

$$K_{Fe} = (X_{Fe}^{Grt}/X_{Fe}^{Crd})$$

Experimental geobarometer

Aranovich and Podlesskii (1983) (for hydrous cordierite)

$$P_{Mg} = [-1.98726\ T(K)\ \ln K_D + 1201 + 3.62(K)]/0.452 \text{ (bars)}$$

$$K_{Mg} = (X_{Mg}^{Crd}/X_{Mg}^{Grt})$$

$$P_{Fe} = [(-1.98726\ T(K)\ \ln K_D) + 4933 + 6.29(K)]/0.487 \text{ (bars)}$$

$$K_{Fe} = (X_{Fe}^{Crd}/X_{Fe}^{Grt})$$

E. Garnet-plagioclase-Al_2SiO_5-quartz geobarometer

Pressure estimates based on reaction (10) (Table 4) were obtained using the following equations:

$P = [-\Delta G^{\circ}_{(10)} - 8.3144\ T(K)\ \ln(a_{Grs}/a^{3}_{An})]/\Delta\bar{V}_{(10)}$ (bars), based on Newton and Haselton (1981).

$\Delta G^{\circ}_{(10)} = -P^{\circ}_{Ky}(-6.210)$, from Koziol and Newton (1988).

$P^{\circ}_{Ky} = 22.80T(^{\circ}C) - 1093$, from Koziol and Newton (1988).

$\Delta\bar{V}_{(10)} = (8.824 + 2.269 + \bar{V}_{Grs}) - 30.225$ (j/bar)

$\bar{V}_{Grs} = A - CX^2_{Prp} + D\ (1 + (ZX_{Prp}/F))\ \exp(-Z^2/2)$

where A=125.24

$$C = \frac{-0.512X_{Prp} - 1.482X_{Alm}}{(X_{Prp} + X_{Alm})}$$

$$D = \frac{-0.418X_{Prp} - 8.293X_{Alm}}{(X_{Prp} + X_{Alm})}$$

$$E = \frac{-0.940X_{Prp} + 0.914X_{Alm}}{(X_{Prp} + X_{Alm})}$$

$$F = \frac{0.083X_{Prp} + 0.066X_{Alm}}{(X_{Prp} + X_{Alm})}$$

$$Z = \frac{X_{Prp} - E}{F}$$

$$a_{Grs} = [X_{Grs} \exp\{(13800-6.28T)\ (X^2_{Prp} + X_{Alm}X_{Prp} + X_{Prp}X_{Sps})/RT\}]^3$$

$$a_{An} = X_{An}(1+X_{An})^2 \ /\ 4\exp\{((1-X_{An})^2/\ RT)\ (8585 + 39330X_{An})\}$$

where R=8.3143 (j/mol K) and T is in Kelvin.

F. Pyrrhotite-sphalerite geobarometer

The composition of sphalerite have been calculated when coexisting with pyrrhotite and pyrite at 620°C and 6.5 Kbars, and with various pyrrhotite compositons within the pyrrhotite-rutile fO_2-fS_2 field.

From the work of Toulmin and Barton (1964) and Froese and Gunter (1976), equations (F1) and (F2) can be solved simultaneously for a value of X^{Po}_{FeS} (thus, $\log(fS_2)$) that will satisfy both equations. The program FROGUN2 was written for that purpose.

$$FeS^{Po} + 1/2S_2 = FeS_2 \quad (F1)$$

$$\square S^{Po} = 1/2\ S_2^{vapor} \quad (F2)$$

The thermodynamic for reactions (F1) and (F2) is as follows:

Reaction (F1)

$$\Delta G^{T,1}_{(F1)} = -153862.416 + 150.649\ T(K) \quad (J/mol)$$

$$\Delta G^{T,1}_{(F1)} = RT(\ln(a^{Po}_{FeS}) + 1/2\ \ln(fS_2)),\ \text{where } a_{Py} = 1.$$

$$\Delta G^{T,P}_{(F1)} = \Delta G^{T,1}_{(E1)} + \int_1^P (\Delta V^{(F1)}_{solids}\ dP)$$

Reaction (F2)

$$\Delta G^{T,1}_{(F2)} = -242529.744 + 145.704\ T(K) \quad (J/mol)$$

$$\Delta G^{T,1}_{(F2)} = RT(-1/2\ \ln(fS_2)) + \ln(1-X^{Po}_{FeS}) + \ln(\gamma_{\square S}))$$

$$\Delta G^{T,P}_{(F2)} = \Delta G^{T,1}_{(E2)} + \int_1^P (\Delta V^{(F2)}_{solids}\ dP)$$

$$RT\ln(\gamma_{\square S}) = (2\overline{G}^{ex}_{FeS} - \overline{G}^{ex}_{\square S})X^2_{FeS} + 2(\overline{G}^{ex}_{\square S} - \overline{G}^{ex}_{FeS})X^3_{FeS}$$

where $\overline{G}^{ex}_{FeS} = -592299.592 + 530.636T(K)$ (j/mol)

and $\overline{G}^{ex}_{\square S} = -392923.624 + 247.902T(K)$ (j/mol)

The activity of pyrrhotite is defined as:

$$a^{Po}_{FeS} = (X\ \gamma)^{Po}_{FeS}$$

where;

$$\gamma^{Po}_{FeS} = \exp[\{(2\overline{G}^{ex}_{\square S} - \overline{G}^{ex}_{FeS})(1-X^{Po}_{FeS})^2 + 2(\overline{G}^{ex}_{FeS} - \overline{G}^{ex}_{\square S})(1-X_{FeS})^3\}/RT]$$

Thus, knowing fS_2, a^{Po}_{FeS}, and X^{Po}_{FeS} for pyrrhotite coexisting with pyrite at T and P of interest, we can calculate X^{Sph}_{FeS} for sphalerite coexisting with pyrrhotite and pyrite (reaction 21) using Hutcheon (1978) equations:

$$\Delta G^{o}_{(21)} = [999.976 + 3.515T\ (K)]\ (j/mol)$$

$$\Delta G^{o}_{(21)} = [-RT\ln(a^{Sph}_{FeS} - a^{Po}_{FeS}) - \int_1^P \Delta V_s\, dP]\ (j/mol)$$

$$RT\ln(\gamma^{Sph}_{FeS}) = (2\overline{G}^{ex}_{ZnS} - \overline{G}^{ex}_{FeS})X^{Sph^2}_{ZnS} + 2(\overline{G}^{ex}_{FeS} - \overline{G}^{ex}_{ZnS})X^{Sph^3}_{ZnS}$$

$$RT\ln(\gamma^{Sph}_{ZnS}) = (2\overline{G}^{ex}_{FeS} - \overline{G}^{ex}_{ZnS})X^{Sph^2}_{FeS} + 2(\overline{G}^{ex}_{ZnS} - \overline{G}^{ex}_{FeS})X^{Sph^3}_{FeS}$$

where $\overline{G}^{ex}_{ZnS} = [2.685T\ (K) + 0.0548P\ (bars)]\ (j/bar)$

$\overline{G}^{ex}_{FeS} = [4.8451T\ (K) + 0.0544P\ (bars)]\ (j/bar)$

The composition of sphalerite (X^{Sph}_{FeS}) coexisting with varying pyrrhotite compositions (thus varying fS_2 within the divariant pyrrhotite-rutile field $\log(fO_2)$-$\log(fS_2)$) can be calculated from reaction (21) using the progams FROGUN2 and ACTCOEF.

The pressure integral

The pressure integral of equations (F1), (F2), (21) and for other reactions was solved by using thermal expansivity and compressibility data (Table) in Scott (1973).

The pressure integral was solved by integrating the area under the curve such that:

$$\int_1^P \Delta Vs \; dP = \frac{(\Delta Vs^{T,1} + \Delta Vs^{T,P})}{2} \times (P-1)$$

$$\text{where} \quad \Delta V_s^{T,P} = \Delta V_s^o + \Delta V_s^o \left(\frac{\Delta \alpha_1^T + \Delta \beta_P^{298}}{100} \right)$$

$$\text{and} \quad \Delta V_{T,1} = \left(\frac{\Delta \alpha_1^T \times \Delta V_s^o}{100} \right) + \Delta V_s^o$$

The volume change of a reaction is expressed by:

$$\Delta V_s = (\sum(V)_{Products} - \sum(V)_{Reactants}) \quad (j/bar)$$

The thermal expansion change of a reaction is expressed by:

$$\Delta \alpha_{1\ bar}^T = \left(\frac{\Delta V_s^{T,1} - \Delta V_s^o}{\Delta V_s^o} \right) \times 100$$

where $\alpha^{pyrite} = 0.004T - 0.310$ (Skinner, 1966)

$\alpha^{troilite} = 0.0064T + 1.740$ (Taylor, 1970)

$\alpha^{sphalerite} = 0.0028T - 0.2058$ (Skinner, 1966)

and T is in degree Celsius.

The compressibility change of a reaction is expressed by:

$$\Delta \beta_P^{298} = \left(\frac{\Delta V_s^{298,P} - V_s^o}{\Delta V_s^o} \right) \times 100$$

where $\beta^{pyrite} = -0.069P$ (Kbars)

$\beta^{troilite} = -0.12P$ (Kbars)

$\beta^{sphalerite} = -0.13P$ (Kbars)

APPENDIX 4. GWBASIC SOURCE CODES

ACTCOEF

```
5 REM ACTCOEF
6 CLS
10 PRINT "PROGRAM TO CALCULATE FeS, ZnS ACTIVITIES COEFFICIENTS OF SPHALERITI
15 PRINT "AT ANY P-T OF INTEREST."
20 PRINT "WHAT IS THE TEMPERATURE IN DEGREE CENTIGRADE?"
30 PRINT "T=     ":INPUT T
40 T=T+273
50 PRINT "WHAT IS THE PRESSURE IN BARS?"
60 PRINT "P=     ":INPUT P
70 PRINT "WHAT WILL BE THE INCREMENT INTERVAL FOR XFeS: (EX: 001, 002, 05)"
80 PRINT "II=":INPUT II
90 X=(1/II)+1
100 DIM A(X,8)
105 REM GZN=EXCESS FREE ENERGY OF ZNS AND GFE=EXC. FREE EN. FES
110 GZN=.642*T+.0131*P
120 GFE=1.158*T+.0131*P
130 XFES=1+II:XZNS=0
140 FOR I=0 TO X:XFES=XFES-II
145 CLS:PRINT "NOW CALCULATING"
150 XZNS=1-XFES
160 A(I,1)=XFES
170 A(I,4)=XZNS
180 XFES2=XFES^2
190 XFES3=XFES^3
200 XZNS2=XZNS^2
210 XZNS3=XZNS^3
220 A(I,2)=((2*GZN-GFE)*XZNS2+2*XZNS3*(GFE-GZN))/(T*1.987)
230 A(I,3)=EXP(A(I,2))
240 A(I,5)=((2*GFE-GZN)*XFES2+2*(GFE-GZN)*XZNS3)/(T*1.987)
250 A(I,6)=EXP(A(I,5))
251 A(I,7)=XFES*A(I,3)
252 A(I,8)=XZNS*A(I,6)
260 NEXT I
270 CLS
280 PRINT " DO YOU WANT TO DISPLAY THE DATA? YES=Y NO=N"
290 INPUT A$
300 IF ASC(A$)=78 THEN GOTO 420 ELSE
310 PRINT "   XFES   lnacFeS   acFeS   XZnS   lnacZnS   acZnS   AFES   AZNS"
320
PRINT"*****************************************************************"
330 FOR I=1 TO X-1
340 FOR J=1 TO 8
350 PRINT USING "  ##.###";A(I,J);
360 NEXT J
370 PRINT "      "
380 NEXT I
390 PRINT
400 PRINT "T=";T;"K";"   P=";P;" BARS";"  INCREMENT:";II;
410 PRINT
420 PRINT "DO YOU WANT A PRINT OUT OF THE DATA? YES=Y NO=N"
```

```
430 INPUT B$
440 IF ASC(B$)=78 THEN GOTO 560
450 LPRINT "   XFES   lnacFeS  acFeS   XZnS   lnacZnS  acZnS   AFES   AZNS"
460
LPRINT"*************************************************************************"
470 FOR I=1 TO X-1
480 FOR J=1 TO 8
490 LPRINT USING "  ##.###";A(I,J);
500 NEXT J
510 LPRINT "      "
520 NEXT I
530 LPRINT
540 LPRINT "T=";T;"K";"   P=";P;" BARS";"  INCREMENT:";II;
550 LPRINT
560 PRINT "DO YOU WANT TO DO OTHER CALCULATIONS? YES=Y NO=N"
570 INPUT C$
580 IF ASC(C$)=78 THEN END ELSE GOTO 5
```

BTGRTEM

```
100 REM BTGRTEM
110 DIM G(6,6):DIM B(6,6):DIM V$(20)
120 CLS
160 LOCATE 10,11:COLOR 6,7:PRINT "BIOTITE-GARNET GEOTHERMOMETRY, WRITTEN BY
LOUIS R. BERNIER 1989"
170 LOCATE 12,30 :PRINT"McGILL UNIVERSITY"
185 INPUT A$:CLS:COLOR 7,0
190 LOCATE 2,2:PRINT "THE FOLLOWING GEOTHERMOMETERS (BIT-GRT) ARE USED:"
200 LOCATE 4,2:PRINT "FERRY & SPEAR 1978 (TFS); THOMPSON 1976 (TT); GANGULY
1979 (TG); PERCHUCK 1981 (TP); PIGAGE & GREENWOOD 1982 (TPG); PERCHUCK &
LAVRENT'EVA 1983 (TPL)."
203 LOCATE 6,2:PRINT "NEWTON & HASELTON 1981 (TNH); GANGULY & SAXENA 1984
(TGS); HOINKES 1986 (TH); WILLIAMS AND GRAMBLING 1990 (TWG)."
205 LOCATE 10,5:PRINT"ENTER GARNET CATIONS DATA: FE2, FE3, MG, CA, MN."
210 J=1 :FOR I=1 TO 5: INPUT G(I,J):NEXT I
211 XTOT=G(1,1)+G(2,1)+G(3,1)+G(4,1)+G(5,1)
215
XALM=G(1,1)/XTOT:XAN=G(2,1)/XTOT:XPY=G(3,1)/XTOT:XGR=G(4,1)/XTOT:XSP=G(5,1)/XT
OT
220 G(1,2)=XPY/XALM:CLS
225 LOCATE 10,5:PRINT "ENTER BIOTITE CATIONS DATA: ON WHAT SI+AL6 BASIS?
(4,8..)"
230 INPUT N:C=3*N/4
240 LOCATE 12,5:PRINT "ENTER SI, ALTOT, TI, FE, MG, MN"
250 J=1:FOR I=1 TO 6:INPUT B(I,J):NEXT I:B(1,2)=(B(1,1)+B(2,1)-N)/C:
260 B(2,2)=B(1,2)+B(3,1)+B(4,1)+B(5,1)+B(6,1)
270
XAL6=B(1,2):XTIB=B(3,1)/B(2,2):XFEB=B(4,1)/B(2,2):XMGB=B(5,1)/B(2,2):XMNB=B(6,
1)/B(2,2)
280 B(3,2)=XMGB/XFEB
290 KD=G(1,2)/B(3,2)
295 PRINT:INPUT "ENTER PRESSURE OF INTEREST (BARS)?";P
300 REM CALCULATE FERRY SPEAR T
310 TFS=(2089+.00956*P)/(.782-LOG(KD))-273
```

```
400 REM CALCULATE THOMPSON T
410 TT=(2739.646+.0234*(P-1))/(1.56-LOG(KD))-273
500 REM CALCULATE GANGULY 1979 T
510 TG=(1586*XGR+1308*XSP+2089+.00956*P)/(.78198-LOG(KD))-273
600 REM CALCULATE PERCHUCK 1981 T
610 TP=3650/(2.57-LOG(KD))+252.25*(XSP-.035)-273
800 REM CALCULATE PERCHUCK & LAVRENT'EVA T USING DV F & S 1978
810 TPLFS=(7843.7-.0577*(P-6000))/(5.699-1.987*LOG(KD))-273
820 TPL=(7843.7-.0246*(P-6000))/(5.699-1.987*LOG(KD))-273
900 REM CALCULATE NEWTON & HASELTON T
905 TX=TFS+273:TY=T+273:TZ=T+273
910 TNH=((1661-.755*TX)*XGR+2089+.00956*P)/(.782-LOG(KD))
920 LOCATE 20,5:PRINT "TNH="TNH
930 LOCATE 20,20:PRINT "GUESS T AS TFS="TX
940 IF ABS(TNH-TX)<=1 THEN TNH=TNH-273 ELSE TX=(TX+TNH)/2:GOTO 910
1000 REM CALCULATE GANGULY AND SAXENA T
1005 WFEMG=(835*XPY/(XPY+XALM)+10460*XALM/(XPY+XALM))/8.3143
1010
TGS=(WFEMG*(XALM-XPY)+1511*(XGR+XSP)+2089-914+.00956*P)/(.782-LOG(KD))-273
1020 REM CALCULATE HODGES & SPEAR 1982 T
1021 PRINT:INPUT "ENTER WMG-MN VALUE (0-3500)";WMGMN
1025 TY=TFS+273
1030
THS=(2089+.00956*P+(3300-1.5*TY)/1.987*(XGR^2+XALM*XGR+XGR*XSP+XPY*XGR)+WMGMN/
1.987*(XSP^2+XGR*XSP+XALM*XSP+XPY*XSP))/(.782-LOG(KD))
1035 LOCATE 20,5:PRINT "THS="THS
1040 LOCATE 20,20:PRINT "GUESS T AS TFS="TY
1045 IF ABS(THS-TY)<=1 THEN THS=THS-273 ELSE TY=(TY+THS)/2:GOTO 1030
1050 REM CALCULATE HOINKES 1986 T
1060
TH=(2089+.00956*P)/(.7821-LOG(KD)-2.978*XGR*(844/TY)+5.906*XGR^2*(844/TY)^2)
1070 LOCATE 20,5:PRINT " TH=";TH
1080 LOCATE 20,20:PRINT "GUESS TAS TFS IN K";TY
1085 IF ABS (TH-TY)<=1 THEN TH=TH-273 ELSE TY=(TY+TH)/2:GOTO 1060
1100 REM CALCULATE WILLIAM & GRAMBLING 1990 T
1102 WFSGS=9660: WFSWH=1960
1105 WGS=835*(XPY/(XPY+XALM))+10460*(XALM/(XPY+XALM))
1110 WHW=695*(XPY/(XPY+XALM))+2115*(XALM/(XPY+XALM))
1200
TWG2=(-17369-79.5*(P/1000)+.8*WFSGS-WGS*(XALM-XPY)-12550*XGR-18975*XSP)/(8.314
3*(LOG(KD)-.782+LOG(.9)))-273
1300
TWG3=(-17369-79.5*(P/1000)+.8*WFSHW-WHW*(XALM-XPY)-12550*XGR-8230*XSP)/(8.3143
*(LOG(KD)-.782+LOG(.9)))-273
2000 CLS: PRINT "READY TO PRINT RESULTS, PLEASE ENTER A SAMPLE NAME +
LOCATION"
2010 INPUT V$
2020 LPRINT V$:LPRINT
2030 LPRINT "DATA FOR GARNET:"
2040 LPRINT "FE2="G(1,1);"  FE3=";G(2,1);"  MG=";G(3,1);"  CA=";G(4,1)
2050 LPRINT "MN=";G(5,1)
2060 LPRINT "XFE2=";XALM;"  XFE3=";XAN;"  XMG=";XPY;"  XCA=";XGR
2070 LPRINT "XMN=";XSP;"  MG/FE=";G(1,2);"  XCa+XMn=";XGR+XSP
3000 LPRINT
3010 LPRINT "DATA FOR BIOTITE:"
```

```
3020 LPRINT "SI=";B(1,1);"  ALTOT=";B(2,1);"  AL6=";B(1,2)*C
3030 LPRINT "TI=";B(3,1);"  FE=";B(4,1);"  MG=";B(5,1);"  MN=";B(6,1)
3040 LPRINT "XAL6=";XAL6;"  XTI=";XTIB;"  XFE=";XFEB
3050 LPRINT "XMG=";XMGB;"          MG/FE=";B(3,2)
4000 LPRINT: LPRINT "KD=";KD;"     LN(KD)=";LOG(KD)
4500 LPRINT: LPRINT "RESULTS FOR BIOTITE-GARNET GEOTHERMOMETRY AT P=";P;"BAI
5000 LPRINT "FERRY AND SPEAR 1978 T=";TFS
5100 LPRINT "THOMPSON 1976 T=";TT
5200 LPRINT "GANGULY 1979/ PIGAGE & GREENWOOD 1982 T=";TG
5300 LPRINT "PERCHUCK 1981 T=";TP
5500 LPRINT "PERCHUCK & LAVRENT'EVA 1983 (F&S DV) T=";TPLFS
5550 LPRINT "PERCUCK & LAVRENT'EVA 1983 T=";TPL
5600 LPRINT "NEWTON & HASELTON 1981 T=";TNH
5700 LPRINT "GANGULY AND SAXENA 1984 T=";TGS
5750 LPRINT "HODGES & SPEAR 1982 ASSUMING WMG-MN=";WMGMN;" T=";THS
5800 LPRINT "HOINKES 1986 T=";TH
5805 LPRINT "WILLIAMS & GRAMBLING 1990"
5810 LPRINT "WITH WMG-FE OF GANGULY AND SAXENA 1984 T=";TWG2
5820 LPRINT "WITH WMG-FE OF HACKLER & WOOD 1989     T=";TWG3
6000 CLS:PRINT "DO YOU WANT TO DO THE CALCULATION WITH AN OTHER PRESSURE
6100 INPUT Z$: IF ASC(Z$)=89 THEN INPUT "P=";P:GOTO 300 ELSE
6200 CLS:PRINT "DO YOU WANT TO DO ANOTHER CALCULATION? (Y,N)"
6300 INPUT T$:IF ASC(T$)=89 THEN LPRINT:LPRINT:GOTO 120 ELSE END
6500 END
```

FLUICOHS

```
10 REM "FLUICOHS"
20 PRINT "PROGRAM TO CALCULATE MOLE FRACTIONS OF CO2, H2O, CO, H2, "
30 PRINT "CH4, SO2, COS, H2S, S2, S8 IN AN IDEAL MIXING MODEL BASED ON"
40 PRINT "OHMOTO AND KERRICK (1977) PAPER, AT P-T OF INTEREST FOR A GIVEN fS:
50 PRINT "VALUE CORRESPONDING TO A PYRRHOTITE OR SPHALERITE COMPOSITION (
60 PRINT "PYRITE-PYRRHOTITE BOUNDARY.  NECESSARY INPUT INFORMATION IS:"
70 PRINT "FUGACITY COEFFICIENT OF THE GAS SPECIES (H2O=BURHAM ET AL. 1969,
CO2, SO2, H2S, CH4, H2=RYAHNKO AND VOLKOV 1971, CO, COS, S2, S8=REDKWONG."
75 PRINT "THE PROGRAM PERFORM THE CALCULATION FOR A RANGE OF LOGfO2"
76 PRINT "FOR GRAPHITE PRESENT; a=1.0, FOR GRAPHITE ABSCENT, A<1 (.5, .1
ETC.)"
77 PRINT:COLOR 15: PRINT "WRITTEN BY LOUIS BERNIER, MCGILL UNIVERSITY, 1991"
78 PRINT: COLOR 7:PRINT "IS GRAPHITE PRESENT? Y OR N":INPUT A$
79 IF ASC(A$)=89 THEN AC=1: LPRINT " GRAPHITE IS PRESENT, AC=";AC ELSE PRINT
"INPUT ACTIVITY OF GRAPHITE":INPUT AC :LPRINT "GRAPHITE IS ABSCENT, AC=";AC
80 PRINT
85 DIM T(2) :DIM F(10): CL=2.3026
90 PRINT "WHAT ARE THE T(C) AND P(BARS) OF INTEREST?"
100 FOR I=1 TO 2: INPUT T(I): NEXT I
101 T=T(1)+273.15:PATM=T(2)*.9869: PF=T(2):CLS
105 PRINT "INPUT FUGACITY COEFFICIENTS FOR GAS AT P-T IN THE FOLLOWING ORD
106 PRINT "CO2, H2O, SO2, H2S, CH4, H2, CO, COS, S2, S8"
110 FOR J=1 TO 10:INPUT F(J): NEXT J
140 PRINT "WHAT IS THE RANGE OF LOGfO2 OF INTEREST? (EX: -12 -24)"
150 PRINT "INPUT FIRST VALUE OF LOGFO2:": INPUT LFO2A
160 PRINT "INPUT LAST VALUE OF LOGFO2:": INPUT LFO2B
```

```
170 PRINT "WHAT WILL BE THE INCREMENT INTERVAL FOR LOGfO2? (EX:2, 1, .05)"
180 PRINT "II=":INPUT II
190 X=(LFO2A-LFO2B)/II+1: DIM A(X,12)
200 PRINT "INPUT THE LOGfS2 OF INTEREST?": INPUT LFS2
210 FS2=EXP(CL*LFS2):LPRINT "LOGFS2=";LFS2
220 LKB=20586/T+.0421+.028*(PATM-1)/T :KB=EXP(CL*LKB)
230 LKC=14751/T-4.535: KC=EXP(CL*LKC)
240 LKD=12510/T-.979*LOG(T)/CL+.483: KD=EXP(CL*LKD)
250 LKE=41997!/T+.719*LOG(T)/CL-2.404
260 LKF=18929/T-3.783: KF=EXP(CL*LKF)
270 LKG=4731/T-4.338: KG=EXP(CL*LKG)
280 LKH=-8117/T+.188*LOG(T)/CL-.352: KH=EXP(CL*LKH)
290 LKI=21446/T-24.43: KI=EXP(CL*LKI)
300 REM CALCULATIONS OF GAS MOLE FRACTIONS AT VARIOUS  LOGfO2
310 FOR I=1 TO X
320 A(I,1)=LFO2A :FO2=EXP(CL*A(I,1))
330 K2=KB*FO2*AC/(F(1)*PF)
340 K3=F(1)/(KC*F(7)*FO2^.5)
350 K4=F(2)/(KD*F(6)*FO2^.5)
360 LK5=LOG(F(1))/CL+2*LOG(F(2))/CL+2*LOG(PF)/CL-LKE-LOG(F(5))/CL-2*A(I,1)
365 K5=EXP(CL*LK5)
370 K6=KF*FO2*FS2^.5/(F(3)*PF)
380 K7=KG*F(7)*FS2^.5/F(8)
390 K8=KH*F(2)*FS2^.5/(F(4)*FO2^.5)
400 K9=FS2/(F(9)*PF)
410 K10=KI*FS2^4/(F(10)*PF)
420 LFO2A=LFO2A-II
440 A(I,2)=K2: A(I,3)=K2*K3: A(I,6)=K6: A(I,7)=(K7*K3*K2)
450 A(I,9)=K9: A(I,10)=K10
460 A=K2*K5:B=K4+K8+1
470 C=K2+K2*K3+K6+K2*K3*K7+K9+K10-1
480 A(I,11)=(-B+(B^2-4*A*C)^.5)/(2*A)
490 A(I,4)=A(I,11)*K4: A(I,5)=A(I,11)^2*K2*K5: A(I,8)=A(I,11)*K8
500 NEXT I
600 CLS
610 PRINT "DO YOU WANT TO DISPLAY THE RESULTS? Y OR N"
620 INPUT Z$
630 IF ASC(Z$)=78 THEN GOTO 730
640 PRINT "T="T(1); "C";"  PFLUID=PTOT=";T(2);" BARS";"  INCREMENT:";II;
650 FOR I=1 TO X
655 PRINT
660 PRINT "LOGFO2=";A(I,1)
670 PRINT "XCO2=";A(I,2);"     XCO=";A(I,3)
675 PRINT "XH2=";A(I,4);"     XCH4=";A(I,5)
680 PRINT "XSO2=";A(I,6);"     XCOS=";A(I,7)
690 PRINT "XH2S=";A(I,8);"     XS2=";A(I,9)
700 PRINT "XS8=";A(I,10);"     XH2O=";A(I,11)
705 PRINT:PRINT
710 NEXT I:PRINT "    "
730 PRINT "DO YOU WANT A PRINT OUT? Y OR N": INPUT B$
740 IF ASC(B$)=78 THEN GOTO 850
750 LPRINT "T="T(1); "C";"  PFLUID=PTOT=";T(2);" BARS";"  INCREMENT:";II;
760 FOR I=1 TO X
765 LPRINT
770 LPRINT "LOGFO2=";A(I,1)
```

```
780 LPRINT "XCO2=";A(I,2);"     XCO=";A(I,3)
785 LPRINT "XH2=";A(I,4);"     XCH4=";A(I,5)
790 LPRINT "XSO2=";A(I,6);"     XCOS=";A(I,7)
800 LPRINT "XH2S=";A(I,8);"     XS2=";A(I,9)
810 LPRINT "XS8=";A(I,10);"     XH2O=";A(I,11)
815 LPRINT:LPRINT
820 NEXT I:LPRINT "    "
850 CLS
925  PRINT "DO YOU WANT ANOTHER LOGFS2 VALUE? (Y OR N)"
928 INPUT D$
930 IF ASC(D$)=89 THEN LFO2A=LFO2B+(X-1)*II:GOTO 200 ELSE
1000 END
```

FROGUN

```
10 PRINT "PROGRAM TO CALCULATE aFeS Po  (FROESE & GUNTER 1976)"
15 PRINT "WRITTEN BY LOUIS BERNIER 1989"
20 INPUT V:CLS
25 GEXF=0:GEXS=0:ACOEFES=0
30 PRINT "INPUT T (C) OF INTEREST": INPUT T:T=T+273
40 PRINT "INPUT NFeS Po": INPUT NFP :XFP=NFP/(2-NFP):RT=1.987*T
42 PRINT "INPUT PRESSURE INTEGRAL (CAL)":INPUT PRI
45 DG=-57966!+34.824*T
50 GEXF= -141563!+126.824*T
55 GEXS=-93911!+59.25*T
56 ACOES=((2*GEXF-GEXS)*XFP^2+2*(GEXS-GEXF)*XFP^3)/RT
57 AS=EXP(ACOES)*(1-XFP)
60 ACOEFES=((2*GEXS-GEXF)*(1-XFP)^2 + 2*(GEXF-GEXS)*(1-XFP)^3)/RT
70 AFESPO=EXP(ACOEFES)
75 LGFS2=(DG-RT*LOG(AS)+PRI)/(-.5*RT*2.303)
76 PRINT "NFES=";NFP;"    XFES=";XFP;"    PRESSURE INTEGRAL=";PRI
80 PRINT "ACTIVITY FeS Po AT T=  ";T-273;"  IS:  ";AFESPO*XFP
90 PRINT "LOGFS2= ";LGFS2
96 LPRINT "NFES=";NFP;"    XFES=";XFP;"    PRESSURE INTEGRAL=";PRI
100 LPRINT "ACTIVITY FeS Po AT T=  ";T-273;"  IS:  ";AFESPO*XFP
110 LPRINT "LOGFS2= ";LGFS2
120 LPRINT
122 LPRINT
```

GBPALTP

```
10 REM GBPALTP
15 DIM G(6,6):DIM B(6,6):DIM P(3):DIM V$(20)
25 SCREEN 9:CLS
100 LOCATE 9,11:COLOR 6,7:PRINT "GAR-BT-PL-ALSIL GEOTHERMO-BAROMETRY (HODGE
SPEAR 82 AND NEWTON & HASELTON 81)"
200 LOCATE 12,22:PRINT "WRITTEN BY LOUIS BERNIER 1989":COLOR 7,1
201 INPUT W$:CLS
205 LOCATE 10,5:PRINT "ENTER GARNET CATIONS DATA: FE2, FE3, MG, CA, MN"
210 J=1:FOR I=1 TO 5: INPUT G(I,J):NEXT I
211 XTOT=G(1,1)+G(2,1)+G(3,1)+G(4,1)+G(5,1)
215
```

```
XALM=G(1,1)/XTOT:XAND=G(2,1)/XTOT:XPY=G(3,1)/XTOT:XGR=G(4,1)/XTOT:XSP=G(5,1)/X
TOT
220 G(1,2)=XPY/XALM:CLS
225 LOCATE 10,5:PRINT "ENTER BIOTITE CATIONS DATA: ON WHAT SI+AL6 BASIS?
(4,8...)"
230 INPUT N:C=3*N/4
240 LOCATE 12,5: PRINT "ENTER SI, ALTOT, TI, FE, MG, MN"
250 J=1:FOR I=1 TO 6: INPUT B(I,J):NEXT I:B(1,2)=(B(1,1)+B(2,1)-N)/C
260 B(2,2)=B(1,2)+B(3,1)+B(4,1)+B(5,1)+B(6,1)
270
XAL6=B(1,2):XTIB=B(3,1)/B(2,2):XFEB=B(4,1)/B(2,2):XMGB=B(5,1)/B(2,2):XMNB=B(6,
1)/B(2,2)
280 B(3,2)=XMGB/XFEB
290 KD=G(1,2)/B(3,2):CLS
300 LOCATE 10,5:PRINT "ENTER PLAGIOCLASE CATION DATA, CA, NA, K"
310 YTOT=0:FOR J=1 TO 3:INPUT P(J):YTOT=YTOT+P(J):NEXT J
320 XAN=P(1)/YTOT:XAB=P(2)/YTOT:CLS
345 REM CALCULATION OF PARTIAL MOL. VOL. GROSSULAR IN J/B
346 AV=125.24:CV=((XPY*-.5120001)+(XALM*-1.482))/(XPY+XALM)
347 DV=((XPY*-.418)+(XALM*-8.293))/(XPY+XALM)
348 EV=((XPY*.94)+(XALM*.914))/(XPY+XALM)
349 FV=((XPY*.083)+(XALM*.066))/(XPY+XALM):ZV=(XPY-EV)/FV
350 VGR=(AV-CV*XPY^2+DV*(1+(ZV*XPY)/FV)*EXP(-ZV^2/2))/10
360 DVK=(8.824001+2.269+VGR)-(3*10.075)
365 DVS=(9.965999+2.269+VGR)-(3*10.075)
550 PRINT :INPUT "ENTER GUESS T FOR ITERATION";TY
555 PRINT:INPUT "GUESS PRESSURE IN BARS P=";PX
560 TX=TY+273
600 PRINT: INPUT "ENTER WMG-MN VALUE (0-3500)";WMGMN
650 CLS
660 REM CALCULATE T-P BY ITERATION FOR KYANITE AS ALSILICATE.
700
THS=(2089+.00956*PX+(3300-1.5*TX)/1.987*(XGR^2+XALM*XGR+XGR*XSP+XPY*XGR)+WMGM
/1.987*(XSP^2+XGR*XSP+XALM*XSP+XPY*XSP))/(.782-LOG(KD))
701 PK=(-2.1+.0232*(THS-273))*1000:DGK=-PK*-6.594
702 AGR=XGR*EXP((13800-6.28*THS)*(XPY^2+XALM*XPY+XPY*XSP)/(8.3413*THS))
703 AAN=XAN*(1+XAN^2)/4*EXP(((1-XAN)^2/(1.987*THS))*(2050+9392*XAN))
710 PNHK=(-DGK-8.3144*THS*LOG(AGR^3/AAN^3))/DVK
800 LOCATE 5,5:PRINT "THS=";THS-273:LOCATE 5,20:PRINT "GUESS T=";TX-273
810 LOCATE 7,5:PRINT "GUESS P IN BAR=";PX:LOCATE 7,35:PRINT "PNHK=";PNHK
900 IF ABS(PNHK-PX)<=10 THEN T=THS-273:P=PNHK ELSE
TX=(TX+THS)/2:PX=(PNHK+PX)/2:GOTO 700
905 REM CALCULATE T-P BY ITERATION USING SILLIMANITE AS ALSIL.
910
THS2=(2089+.00956*PX+(3300-1.5*TX)/1.987*(XGR^2+XALM*XGR+XGR*XSP+XPY*XGR)+WMGM
N/1.987*(XSP^2+XGR*XSP+XALM*XSP+XPY*XSP))/(.782-LOG(KD))
912 AGR=XGR*EXP((13800-6.28*THS2)*(XPY^2+XALM*XPY+XPY*XSP)/(8.3413*THS2))
914 AAN=XAN*(1+XAN^2)/4*EXP(((1-XAN)^2/(1.987*THS2))*(2050+9392*XAN))
920 PS=(-1.17+.0238*(THS2-273))*1000:DGS=-PS*-5.452
930 PNHS=(-DGS-8.3144*THS2*LOG(AGR^3/AAN^3))/DVS
950 LOCATE 10,5:PRINT "THS=";THS2-273:LOCATE 10,20:PRINT "GUESS T=";TX-273
960 LOCATE 12,5:PRINT "GUESS P IN BAR=";PX:LOCATE 12,35:PRINT "PNHS=";PNHS
990 IF ABS(PNHS-PX)<=10 THEN T=THS2-273 ELSE
TX=(TX+THS2)/2:PX=(PNHS+PX)/2:GOTO 910
3000 PRINT:INPUT "ENTER SAMPLE #";V$:LPRINT V$
```

```
3010 LPRINT:LPRINT "DATA FOR GARNET:"
3012 LPRINT "FE2=";G(1,1);"  FE3=";G(2,1);"  MG=";G(3,1);"  CA=";G(4,1)
3014 LPRINT "MN=";G(5,1)
3016 LPRINT "XALM=";XALM;"  XAND=";XAND;"  XPY=";XPY;"  XGR=";XGR
3018 LPRINT "XSP=";XSP;"  MG/FE=";G(1,2);"  XCA+XMN=";XGR+XSP
3020 LPRINT "ACTIVITY OF GROSSULAR AGR=";AGR:LPRINT
3030 LPRINT "DATA OF BIOTITE:"
3040 LPRINT "SI=";B(1,1);"  ALTOT=";B(2,1);"  AL6=";B(1,2)*C
3050 LPRINT "TI=";B(3,1);"  FE=";B(4,1);"  MG=";B(5,1);"  MN=";B(6,1)
3060 LPRINT "XAL6=";XAL6;"  XTI=";XTIB;"  XFE=";XFEB
3070 LPRINT "XMG=";XMGB;"  MG/FE=";B(3,2)
3075 LPRINT:LPRINT "KDBT-GR=";KD;"  LNKD=";LOG(KD)
3080 LPRINT: LPRINT "DATA OF PLAGIOCLASE:"
3090 LPRINT "XAN=";XAN;"  XAB=";XAB;"  XK=";P(3)/YTOT
3095 LPRINT "ACTIVITY OF ANORTHITE AAN=";AAN
3100 LPRINT "HODGES & SPEAR T ASUMING WMGMN=";WMGMN;"
T=";((THS-273)+(THS2-273))/2
3200 LPRINT "PRESSURE (GRT-BT-KY-PL-QTZ) PNHK=";P
3210 LPRINT "PRESSURE (GRT-BT-SIL-PL-QZ) PNHS=";PNHS
3510 CLS:PRINT "DO YOU WANT TO INPUT ANOTHER WMG-MN VALUE?"
3520 INPUT Z$: IF ASC(Z$)=89 THEN INPUT "WMGMN=";WMGMN:GOTO 650 ELSE
3600 CLS: PRINT "DO YOU WANT ANOTHER CALCULATION (Y,N)?"
3700 INPUT T$:IF ASC(T$)=89 THEN LPRINT :LPRINT:GOTO 100 ELSE END
4000 END
```

GRCDTP

```
100 REM GRCDTP
110 DIM G(5):DIM C(3):DIM V$(20)
120 SCREEN 8:CLS
130 LOCATE 10,20:COLOR 7,0:PRINT "GARNET-CORDIERITE GEOTHERMOBAROMETRY"
140 LOCATE 12,20:PRINT "WRITTEN BY LOUIS R. BERNIER, 1989"
150 LOCATE 14,30: PRINT "MCGILL UNIVERSITY":COLOR 7,0
160 INPUT A$:CLS
170 LOCATE 2,2:PRINT "THIS PROGRAM USES GARNET-CORDIERITE DATA AND CALCUL
USING THE THOMPSON (1976) AND PERCHUCK AND LAVRENT'EVA (1983) EXPRESSIONS
200 LOCATE 10,5:PRINT "ENTER GARNET CATION DATA: FE2, FE3, MG, CA, MN:
210 XTOT=0:FOR I=1 TO 5: INPUT G(I):XTOT=XTOT+G(I):NEXT I
220 XALM=G(1)/XTOT:XAN=G(2)/XTOT:XPY=G(3)/XTOT:XGR=G(4)/XTOT:XSP=G(5)/XTOT
300 CLS:LOCATE 10,5: PRINT "ENTER CORDIERITE CATION DATA: FE, MG, MN"
310 YTOT=0: FOR J=1 TO 3: INPUT C(J):YTOT=YTOT+C(J): NEXT J
320 XFE=C(1)/YTOT:XMG=C(2)/YTOT:XMN=C(3)/YTOT
330 KD=(XALM*XMG)/(XFE*XPY)
332 KDMG=XPY/XMG:KDFE=XALM/XFE
335 CLS:LOCATE 10,5:PRINT "GUESS PRESSURE P=":INPUT P
340 REM THOMPSON TEMP WITH NO P CORRECTION (.0155(P-1))
341 PX=P
350 TT=2725/(LOG(KD)+.896)
355 TTP=(2725+.0155*(PX-1))/(LOG(KD)+.896)
357 PTMG=(-TTP*(-6*LOG(KDMG)+12.982)+30324.3)/1.909
359 LOCATE 10,5:PRINT "PTMG=";PTMG:LOCATE 11,1:PRINT "     P=";PX
360 IF ABS(PTMG-PX)<=10 THEN TTMG=TTP ELSE PX=(PX+PTMG)/2:GOTO 355
361 PX=P
```

```
362 TTP=(2725+.0155*(PX-1))/(LOG(KD)+.896)
363 PTFE=(-TTP*(-6*LOG(KDFE)+7.601)+13994.6)/1.9558
365 LOCATE 12,5:PRINT "PTFE=";PTFE:LOCATE 13,5:PRINT "P=";PX
368 IF ABS(PTFE-PX)<=10 THEN TTFE=TTP ELSE PX=(PX+PTFE)/2:GOTO 362
370 REM PERCHUCK AND LAVRET'EVA TEMP WITH NO P CORRECTION (.O18P)
371 PY=P
372 TPL=3020/(LOG(KD)+1.287)
374 TPLP=(3020+.018*PY)/(LOG(KD)+1.287)
380 PAPMG=(-1.98726*TPLP*LOG(1/KDMG)+1201+3.62*TPLP)/.45213
382 LOCATE 10,30:PRINT "PAPMG=";PAPMG:LOCATE 11,30:PRINT "P=";PY
384 IF ABS(PAPMG-PY)<=10 THEN TPLFE=TPLP ELSE PY=(PY+PAPMG)/2:GOTO 374
400 PY=P
402 TPLP=(3020+.018*PY)/(LOG(KD)+1.287)
404 PAPFE=(-1.98726*TPLP*LOG(1/KDFE)-4933+6.288*TPLP)/.487
410 LOCATE 12,30:PRINT "PAPFE=";PAPFE:LOCATE 13,30:PRINT "P=";PY
412 IF ABS(PAPFE-PY)<=10 THEN TPLMG=TPLP ELSE PY=(PY+PAPFE)/2:GOTO 402
500 LOCATE 20,5:PRINT "READY TO PRINT RESULTS, SET PRINTER ON, ENTER SAMPLE
510 INPUT V$
520 LPRINT V$:LPRINT
530 LPRINT "DATA FOR GARNET:"
540 LPRINT "FE2="G(1);"  FE3=";G(2);"  MG=";G(3);"  CA=";G(4);"  MN=";G(5)
550 LPRINT "XALM=";XALM;"  XAN=";XAN;"  XPY=";XPY;"  XGR=";XGR
560 LPRINT "XSP=";XSP;"  MG/FE=";XPY/XALM;
600 LPRINT:LPRINT "DATA FOR CORDIERITE"
610 LPRINT "FE=";C(1);"  MG=";C(2);"  MN=";C(3)
615 LPRINT"XFE=";XFE;"  XMG=";XMG;"  XMN=";XMN;"  Mg/Fe=";XMG/XFE
620 LPRINT:LPRINT "KD=";KD;"  LNKD=";LOG(KD)
622 LPRINT "KDFE=";KDFE;"  LN(KDFE)=";LOG(KDFE)
624 LPRINT "KDMG=";KDMG;"  LN(KDMG)=";LOG(KDMG)
640 LPRINT:LPRINT "THOMPSON 1976 AT P=0, T=";TT-273
642 LPRINT "THOMPSON (1976) T AT P, TFE=";TTFE-273;"  TMG=";TTMG-273
645 LPRINT "THOMPSON (1976) P, PFE=";PTFE;"  PMG=";PTMG
660 LPRINT "PERCHUCK-LAVRENTEVA 1983 T AT P=0, T=";TPL-273
662 LPRINT "PERCHUCK-LAVRENTEVA 1983 T AT P, TFE=";TPLFE-273;"
TMG=";TPLMG-273
665 LPRINT "ARANOVICH-PODLESSKII (1983) P, PFE=";PAPFE;"  PMG=";PAPMG
700 CLS:PRINT "DO YOU WANT TO DO AN OTHER CALCULATION? (Y,N)"
800 INPUT T$:IF ASC(T$)=89 THEN LPRINT:LPRINT:GOTO 120 ELSE END
```

GRHBTP

```
1000 REM GRHBTP3 (1989-1990)
1100 DIM G(5):DIM P(3): DIM H(10):DIM V$(20)
1200 CLS
1300 LOCATE 10,20:COLOR 6,7:PRINT "GARNET-HORNBLENDE GEOTHERMOBAROMETRY'
1310 LOCATE 12,16:PRINT "WRITTEN BY LOUIS R. BERNIER , OCTOBER 1989."
1400 LOCATE 14,30:PRINT "McGILL UNIVERSITY":COLOR 7,0
1410 INPUT A$:CLS
1500 LOCATE 2,2:PRINT "THIS PROGRAM USES COMPOSITIONAL DATA FROM THE
ASSEMBLAGE GARNET, HORNBLENDE, PLAGIOCLASE AND QUARTZ AND CALCULATE T US
THE EXPRESSION OF GRAHAM AND POWELL (1984) AND CALCULATE PRESSURES USING TH
MODELS OF KOHN ANDSPEAR (1989-90)
1600 LOCATE 10,5:PRINT "ENTER GARNET CATIONS DATA: FE2, FE3, MG, CA, MN."
```

```
1610 XTOT=0:FOR I=1 TO 5: INPUT G(I):XTOT=XTOT+G(I):NEXT I
1630 XALM=G(1)/XTOT:XAND=G(2)/XTOT:XPY=G(3)/XTOT:XGR=G(4)/XTOT:XSP=G(5)/XTOT
1640 MF=XPY/XALM:CLS
1700 LOCATE 10,5:PRINT "ENTER PLAGIOCLASE CATIONS DATA: CA, NA, K"
1710 YTOT=0:FOR J=1 TO 3: INPUT P(J):YTOT=YTOT+P(J):NEXT J
1730 XAN=P(1)/YTOT:XAB=P(2)/YTOT:CLS
1800 LOCATE 10,5:PRINT "ENTER HORNBLENDE CATIONS DATA ON A SI+AL6 BASIS OF 8
1900 LOCATE 12,5:PRINT "ENTER SI, AL, TI, FE2, FE3, MG, MN, CA, NA, K"
2000 ZTOT=0:FOR K=1 TO 10: INPUT H(K):ZTOT=ZTOT+H(K):NEXT K
2100 SIT1=H(1)-4:ALT1=8-H(1)
2200 ALM2=H(1)+H(2)-8:TIM2=H(3):FE3M2=H(5)
2300 FE2M2=(2-(ALM2+TIM2+FE3M2))*H(4)/(H(4)+H(6))
2400 MGM2=(2-(ALM2+TIM2+FE3M2))*H(6)/(H(6)+H(4))
2500 NAA=ZTOT-H(10)-15
2600 VACA=1-NAA-H(10)
2700 XSIT1=SIT1/4:XALT1=ALT1/4:XNAA=NAA:XVACA=VACA
2800 XALM2=ALM2/2:XFEM2=FE2M2/2:XMGM2=MGM2/2
3000 REM CALCULATE TEMPERATURE GRAHAM & POWELL 1984
3100 KD=(XALM/XPY)/(H(4)/H(6))
3200 TK=(2880+3280*XGR)/(LOG(KD)+2.426):TC=TK-273
3500 REM CALCULATE GARNET ACTIVITIES (H&S 1982)
3600 APY=(XPY*EXP((13800-6.28*TK)*(XGR^2+XALM*XGR+XGR*XSP)/(8.3143*TK)))^3
3700 AGR=(XGR*EXP((13800-6.28*TK)*(XPY^2+XALM*XPY+XPY*XSP)/(8.3413*TK)))^3
3800 AALM=(XALM*EXP((13800-6.28*TK)*(-XPY*XGR)/(8.3143*TK)))^3
4000 REM CALCULATE PLAGIOCLASE ACTIVITIES
4100 AAN=XAN*EXP((610.34/TK)-.3837):AAB=XAB
4500 REM CALCULATE HORNBLENDE ACTIVITIES
4510 REM MODEL 1
4600 APRG1=16*XALT1^2*XSIT1^2*XNAA:ATR1=XSIT1^4*XVACA
4700 AFEPRG1=16*XALT1^2*XSIT1^2*XNAA:AFEACT1=XSIT1^4*XVACA
5000 REM CALCULATE MODEL-1 K'S
5100 KMG1=AGR^2*APY*APRG1^3/(AAN^6*AAB^3*ATR1^3)
5200 KFE1=AGR^2*AALM*AFEPRG1^3/(AAN^6*AAB^3*AFEACT1^3)
6000 REM CALCULATE PRESSURES WITH MODEL 1
6100 PMG1=(-120593!+TK*(-10.3-8.314*LOG(KMG1)))/-14.81
6200 PFE1=(-117993!+TK*(47.8-8.314*LOG(KFE1)))/-11.29
6500 REM MODEL-2
7000 APRG2=4*XALM2*XMGM2*XNAA:ATR2=XMGM2^2*XVACA
7100 AFEPRG2=4*XALM2*XFEM2*XNAA:AFEACT2=XFEM2^2*XVACA
7200 KMG2=AGR^2*APY*APRG2^3/(AAN^6*AAB^3*ATR2^3)
7300 KFE2=AGR^2*AALM*AFEPRG2^3/(AAN^6*AAB^3*AFEACT2^3)
7400 PMG2=(-44724!+TK*(-51.9-8.314*LOG(KMG2)))/-9.189999
7500 PFE2=(4948+TK*(-81.76-8.314*LOG(KFE2)))/-9.520001
7550 REM MODEL TSERM-TREM 1990
7600 ATSCH=9.481499*XALT1*XSIT1^3*H(6)/(H(4)+H(6))
7610 ATREM=XSIT1^4*(H(6)/(H(4)+H(6)))^2
7620 AFETSCH=9.481499*XALT1*XSIT1^3*H(4)/(H(4)+H(6))
7630 AFEACT=XSIT1^4*(H(4)/(H(4)+H(6)))^2
7640 KMG=AGR^2*APY*ATSCH^3/(AAN^6*ATREM^3)
7650 KFE=AGR^2*AALM*AFETSCH^3/(AAN^6*AFEACT^3)
7700 PMG=(79507!+TK*(29.14+8.3144*LOG(KMG)))/10.988
7750 PFE=(35327!+TK*(56.09+8.3144*LOG(KFE)))/11.906
8000 CLS:PRINT "READY TO PRINT RESULTS, INPUT SAMPLE NAME, LOCATION ETC..."
8010 INPUT V$:LPRINT V$:LPRINT
8020 LPRINT "DATA FOR GARNET"
```

```
8030 LPRINT "FE2=";G(1);"  FE3=";G(2);"  MG=";G(3);"  CA=";G(4);"  MN=";G(5)
8050 LPRINT "XFE2=";XALM;"  XFE3=";XAND;"  XMG=";XPY
8060 LPRINT "XCA=";XGR;"  XMN=";XSP
8070 LPRINT "aPY=";APY;"  aALM=";AALM;"  aGR=";AGR
9000 LPRINT:LPRINT "DATA FOR PLAGIOCLASE"
9010 LPRINT "CA=";P(1);"  NA=";P(2);"  K=";P(3)
9020 LPRINT "XAn=";XAN;"  XAb=";XAB
9030 LPRINT "aAn=";AAN;"  aAb=";AAB
9100 LPRINT:LPRINT "DATA FOR HORNBLENDE"
9200 LPRINT "  SI    AL    TI    FE    FE3   MG    MN    CA    NA    K    "
9300 FOR K=1 TO 10:LPRINT USING " #.###";H(K);:NEXT K
9400 LPRINT:LPRINT "XSiT1=";XSIT1;" XAlT1=";XALT1;" XNaA=";XNAA;"
XVACA=";XVACA
9500 LPRINT "XAlM2=";XALM2;"  XFeM2=";XFEM2;"  XMgM2=";XMGM2
9510 LPRINT "MODEL 1 HORNBLENDE ACTIVITIES"
9520 LPRINT
"aPrg1=";APRG1;"aTr1=";ATR1;"aFe-Prg1=";AFEPRG1;"aFe-Act1=";AFEACT1
9530 LPRINT "ATSCH=";ATSCH;"  ATREM=";ATREM;"  AFETSCH=";AFETSCH;"
AFEACT=";AFEACT
9540 LPRINT
"aPrg2=";APRG2;"aTr2=";ATR2;"aFe-Prg2=";AFEPRG2;"aFe-Act2=";AFEACT2
9600 LPRINT:LPRINT "TEMPERATURE CALCULATED WITH GRAHAM & POWELL (1984)"
9610 LPRINT "KD=";KD;"  T=";TC
9620 LPRINT:LPRINT "PRESSURES CALCULATED WITH MODEL 1 KOHN & SPEAR (1989)
9630 LPRINT "KMg1=";KMG1;"  KFe1=";KFE1;"  PMg1=";PMG1;"  PFe1=";PFE1
9640 LPRINT "PRESSURES USING MODEL 2"
9650 LPRINT "KMG2=";KMG2;"  KFE2=";KFE2;"  PMG2=";PMG2;"  PFE2=";PFE2
9700 LPRINT:LPRINT "PRESSURES CALCULATED WITH KOHN & SPEAR 1990"
9710 LPRINT "KMG=";KMG;"  KFE=";KFE;"  PMG=";PMG;"  PFE=";PFE
12000 CLS:PRINT "DO YOU WANT TO INPUT A NEW SET OF DATA? (Y,N)"
13000 INPUT T$:IF ASC(T$)=89 THEN LPRINT:LPRINT:GOTO 1200 ELSE END
14000 END
```

POLOAPY

```
10 REM PO-LO/APY
12 PRINT "INPUT NFES GUESS VALUE 1 OR SMALLER":INPUT NFES
15 DIM N(2,1):DIM A$(3):I=0:R=8.314:FL=2.303:J=0
20 PRINT "WHAT ARE THE T (C) AND P(BARS) OF INTEREST?"
30 PRINT "T=":INPUT T:PRINT "P=":INPUT P: T=T+273
40 PRINT "WHAT ARE THE PRESSURE INTEGRALS (J) OF THE FOLLOWING REACTION
50 PRINT "A)vacS in Po=1/2 S2v B)2FeAs2+2FeS+S2=4FeAsS
60 PRINT "FOR EACH REACTION INPUT REACTION LABEL (EX:A) THEN DVS(P-1)"
65 FOR I=1 TO 2
70 PRINT "REACTION LABEL:":INPUT A$(I):PRINT "DVs(P-1)=":INPUT N(I,1)
85 NEXT I
90 LPRINT "CALCULATION OF LOGS2 FOR THE PO-LO/APY BOUNDARY AT T=";T-273;"
P=";P;"BARS"
100 LPRINT "REACTION    DVs(P-1)=PRESSURE INTEGRAL"
110 FOR I=1 TO 2
115 LPRINT "     ";A$(I);"          ";N(I,1)
120 NEXT I
130 INPUT "ENTER aFeAsS=";AFEASS
```

```
180 GFC=(-69900!+55.6*T)*4.184
190 LPRINT "THE FREE ENERGY OF FORMATION AT T FOR REACTION B IS";GFC;"JOULES
200 GFB=(-57966!+34.824*T)*4.184
210 LPRINT "THE FREE ENERGY OF FORMATION FOR REACTION A AT T IS ";GFB;"JOULES
220 CLS:PRINT "TO CALCULATE THE PO/PY BOUNDARY, ONE HAS TO FIND A NFES PO T
 WILL SATISFY BOTH EQUATION A AND B. THIS CAN BE DONE BY USING THE EXCESS
PARTIALMOLAR FREE ENERGY AT INFINITE DILUTION MODELS OF FROESE AND GUNTER,
1976."
230 GEXFES=(-141563!+126.825*T)*4.184
240 GEXS=(-93911!+59.25*T)*4.184
250 PRINT "STARTING ITERATION PROCESS"
260 CLS:PRINT "CALCULATING NOW, BE PATIENT"
270 XFES=-NFES/(NFES-2)
280 RTLACS=(2*GEXFES-GEXS)*XFES^2+(2*(GEXS-GEXFES)*XFES^3)
290 RTLACFES=(2*GEXS-GEXFES)*(1-XFES)^2+2*(GEXFES-GEXS)*(1-XFES)^3
300 LNFS2=(-GFB-N(1,1)+(R*T*LOG(1-XFES))+RTLACS)/(.5*R*T)
305 LGFS2=LNFS2/FL
308 AFES=EXP(RTLACFES/(R*T))*XFES
310 GFC1=-4*R*T*LOG(AFEASS)+R*T*LNFS2+2*R*T*LOG(AFES)-N(2,1)
316 ACS=EXP(RTLACS/(R*T)):ACFES=EXP(RTLACFES/(R*T))
318 PRINT "GFC=";GFC
319 PRINT "GFC1=";GFC1
320 IF ABS(GFC-GFC1)<=50 THEN LPRINT "THE POLO/APY BOUNDARY IS AT
LOGFS2=";LGFS2:ELSE NFES=NFES-.0001:GOTO 260
325 LPRINT "   XFES   NFES   ACS   ACFES   AFES   AFEASS"
326 LPRINT USING "##.####"; XFES; NFES; ACS; ACFES;AFES;AFEASS
330 PRINT "DO YOU WANT TO DO OTHER CALCULATION FOR A NEW T?"
340 INPUT X$
350 IF ASC(X$)=78 THEN END ELSE LPRINT: PRINT "T=?":INPUT T: T=T+273: GOTO 130
360 END
```

POPY

```
10 REM PO/PY
12 PRINT "INPUT NFES GUESS VALUE 1 OR SMALLER":INPUT NFES
15 DIM N(3,1):DIM A$(3):I=0:R=8.314:FL=2.303:J=0
20 PRINT "WHAT ARE THE T (C) AND P(BARS) OF INTEREST?"
30 PRINT "T=":INPUT T:PRINT "P=":INPUT P: T=T+273
40 PRINT "WHAT ARE THE PRESSURE INTEGRALS (J) OF THE FOLLOWING REACTIONS ?"
50 PRINT "A)Fe+1/2S2=FeS B)vacS in Po=1/2 S2v C)FeS +1/2 S2=FeS2"
60 PRINT "FOR EACH REACTION INPUT REACTION LABEL (EX:A) THEN DVS(P-1)"
65 FOR I=1 TO 3
70 PRINT "REACTION LABEL:":INPUT A$(I):PRINT "DVs(P-1)=":INPUT N(I,1)
85 NEXT I
90 LPRINT "CALCULATION OF LOGS2 FOR THE PO/PY BOUNDARY AT T=";T-273;"
P=";P;"BARS"
100 LPRINT "REACTION   DVs(P-1)=PRESSURE INTEGRAL"
110 FOR I=1 TO 3
115 LPRINT "    ";A$(I);"          ";N(I,1)
120 NEXT I
130 PRINT"CALCULATION OF THE Fe/PO BOUNDARY"
140 GFA=(-35910!+12.56*T)*4.184
150 LPRINT "FREE ENERGY OF REACTION A AT T IS:";GFA;"JOULES"
```

```
160 LFS=(-GFA-N(1,1))*2/(-R*T*FL)
170 LPRINT "THE LOGFS2 FOR THE FE-PO BOUNDARY IS:";LFS
180 GFC=(-36774!+36.006*T)*4.184
190 LPRINT "THE FREE ENERGY OF FORMATION AT T FOR REACTION C IS";GFC;"JOULES
200 GFB=(-57966!+34.824*T)*4.184
210 LPRINT "THE FREE ENERGY OF FORMATION FOR REACTION B AT T IS";GFB;"JOULES
220 CLS:PRINT "TO CALCULATE THE PO/PY BOUNDARY, ONE HAS TO FIND A NFES PO T
 WILL SATISFY BOTH EQUATION B AND C. THIS CAN BE DONE BY USING THE EXCESS
PARTIALMOLAR FREE ENERGY AT INFINITE DILUTION MODELS OF FROESE AND GUNTER,
1976."
230 GEXFES=(-141563!+126.825*T)*4.184
240 GEXS=(-93911!+59.25*T)*4.184
250 PRINT "STARTING ITERATION PROCESS"
260 CLS:PRINT "CALCULATING NOW, BE PATIENT"
270 XFES=-NFES/(NFES-2)
280 RTLACS=(2*GEXFES-GEXS)*XFES^2+(2*(GEXS-GEXFES)*XFES^3)
290 RTLACFES=(2*GEXS-GEXFES)*(1-XFES)^2+2*(GEXFES-GEXS)*(1-XFES)^3
300 LNFS2=(-GFB-N(2,1)+(R*T*LOG(1-XFES))+RTLACS)/(.5*R*T)
305 LGFS2=LNFS2/FL
308 AFES=EXP(RTLACFES/(R*T))*XFES
310 GFC1=R*T*LOG(AFES)+(R*T*LNFS2/2)-N(3,1)
316 ACS=EXP(RTLACS/(R*T)):ACFES=EXP(RTLACFES/(R*T))
318 PRINT "GFC=";GFC
319 PRINT "GFC1=";GFC1
320 IF ABS(GFC-GFC1)<=50 THEN LPRINT "THE PO/PY BOUNDARY IS AT
LOGFS2=";LGFS2:ELSE NFES=NFES-.0001:GOTO 260
325 LPRINT "   XFES   NFES   ACS   ACFES    AFES"
326 LPRINT USING "##.####"; XFES; NFES; ACS; ACFES;AFES
330 PRINT "DO YOU WANT TO DO OTHER CALCULATION FOR A NEW T?"
340 INPUT X$
350 IF ASC(X$)=78 THEN END ELSE LPRINT: PRINT "T=?":INPUT T: T=T+273: GOTO 130
360 END
```

REDKWONG

```
5 REM REDKWONG
10 PRINT "PROGRAM TO CALCULATE COMPRESSIBILITY (Z), MOLAR VOLUME"
20 PRINT "AND FUGACITY COEFFICIENT FOR PURE SPECIES USING THE"
30 PRINT "REDLICH-KWONG EQUATION AND A POLYNOMIAL EXPRESSION TO"
40 PRINT "SOLVE FOR (Z) USING THE NEWTON'S METHOD."
50 PRINT
60 PRINT "REDUCED T (Tr) AND P(Pr) ARE ALSO CALCULATED."
70 PRINT "SO THAT GENERAL GAZ TABLES CAN BE USED IF AVAILABLE."
90 PRINT
100 PRINT "THE CRITICAL TEMPERATURE AND PRESSURE OF THE SPECIE OF "
110 PRINT "INTEREST AS TO BE KNOWN IN ORDER TO PERFORM THESE CALCULATION
120 PRINT "TO ANY P-T OF INTEREST."
130 PRINT
135 DIM A$(20):R=83.1441:Z=0:F1=0:ZF=0
140 PRINT "ENTER THE NAME OF THE FLUID OF INTEREST"
160 INPUT A$
170 PRINT "WHAT IS THE CRITICAL T IN KELVIN?"
180 PRINT "Tc=":INPUT TC
```

```
190 PRINT "WHAT IS THE CRITICAL P IN ATM?"
200 PRINT "PC=":INPUT PC
210 PRINT "WHAT IS THE TEMPERATURE OF INTEREST (CELSIUS)?
220 PRINT "T=":INPUT T
230 PRINT "WHAT IS THE PRESSURE OF INTEREST IN BARS?"
240 PRINT "P=":INPUT P:PA=P
250 T=T+273.15:PC=PC*1.01325
260 TR=T/TC:PR=P/PC
270 A=.4275*R^2*TC^2.5/PC
280 B=.0866*R*TC/PC
290 B2=B/(R*T)
300 A2=A/(R^2*T^2.5)
310 X1=-1
320 X2=B2*P*(A2/B2-B2*P-1)
330 X3=(-A2/B2)*(B2*P)^2
340 PRINT "WHAT IS THE STARTING GUESS Z VALUE?"
350 PRINT "Z=":INPUT Z
355 C=0
360 F=Z^3+(X1*Z^2)+(X2*Z)+X3
370 DF=(3*Z^2)+(2*X1*Z)+X2
380 Z1=Z-F/DF:ZX=Z1-Z
390 IF ABS(ZX)<.000001 THEN ZF=Z1 ELSE C=C+1:Z=Z1:F1=F:PRINT "F=";F;"
DF=";DF;" Z=";Z;" C=";C:GOTO 360
400 V=(ZF*R*T)/P
410 PRINT "NUMBERS OF ITERATIONS IS :";C
420 PRINT "DO YOU WANT TO INPUT A NEW GUESS Z VALUE? Y OR N"
430 INPUT B$
440 IF ASC(B$)=78 THEN ELSE GOTO 340
540 PRINT "THE FUGACITY COEFFICIENT IS:"
550 LNFC=ZF-1-LOG(ZF-B2*PA)-A2/B2*LOG(1+B2*PA/ZF)
560 FC=EXP(LNFC)
570 PRINT "FC=";FC;
572 CLS
575 PRINT "THE RESULTS WILL NO BE PRINTED"
580 LPRINT "DATA FOR: ",A$,
585 LPRINT
590 LPRINT "CRITICAL POINT DATA ARE: TC=";TC-273.15;"C";"  PC=";PC;"bars"
610 LPRINT
620 LPRINT "DATA AT: T=";T-273.15;"C";"  P=";P;"bars";"  Z=";ZF;"
V=";V;"cm3";
630 LPRINT
640 LPRINT "REDUCED TEMPERATURE Tr=T/Tc IS : ";TR;
645 LPRINT
650 LPRINT "REDUCED PRESSURE Pr=P/Pc IS: ";PR;
655 LPRINT
660 LPRINT "FUGACITY COEFFICIENT IS: ";FC;"bars";
665 LPRINT:LPRINT "":LPRINT ""
670 CLS:PRINT "DO YOU WANT TO DO THIS AGAIN FOR A NEW SPECIE? Y=YES N=NO"
680 INPUT D$
690 IF ASC(D$)=89 THEN A$="":GOTO 140 ELSE END
```